University of Southampton Research Repository

University of Southampton

Faculty of Medicine

Clinical and Experimental Sciences

Cellular Immunometabolism and Regulation of Mitochondrial Efficiency –
Healthy Ageing Across the Life Course

by

Marie Strickland

ORCID ID 0000-0002-1922-8457

Thesis for the degree of Doctor of Philosophy

January 2020

University of Southampton

<u>Abstract</u>

Faculty of Medicine

Clinical and Experimental Sciences

Thesis for the degree of Doctor of Philosophy

Cellular Metabolism and Regulation of Mitochondrial Efficiency –

Healthy Ageing Across the Life Course

by

Marie Strickland

As part of an ageing society understanding the science behind the ageing process is paramount in lightening the burden of age-related diseases such as cancer, diabetes and cardiovascular disease. Extending the number of years lived disease-free is of great importance in alleviating the detrimental effect ageing populations have on the medical and social sectors. Mitochondria are referred to as the powerhouse of the cell, providing energy and controlling metabolism for normal cellular function. However, mitochondrial dysfunction throughout the ageing process has been highlighted as one of the hallmarks of ageing, alongside senescence of the immune system. The aim of this study was to analyse mitochondrial dysfunction and metabolic efficiency in the context of ageing using both murine and human models of ageing. The murine models used within the study have previously been observed to have shortened lifespan due to low-grade chronic inflammation and senescence. For the human models, naïve T cells and senescent terminal effector T cells as well as peripheral blood from individuals partaking in the Singapore Longitudinal Ageing Study were analysed. This study utilised several methods to analyse metabolism and mitochondrial structure of immune cells, including advanced microscopy techniques, flow cytometry, cell sorting and live-cell metabolic analysis. This study established a variety of parameters contributing to mitochondrial dysfunction in each of the models tested. Mice with low-grade chronic inflammation showed reduced flexibility of mitochondrial structure in the bone marrow compared to wild-type mice alongside alterations in immune cell compartmentalisation in the spleen associated with a reduction in mitochondrial membrane potential of these cells, a marker of mitochondrial function. Mice with increased levels of senescence showed a similar phenomenon of reduced mitochondrial membrane potential as well as reductions in mitochondrial mass. These changes affected both the innate and adaptive arms of the immune system in these mice. In humans, measuring mitochondrial parameters associated with the development of senescence in CD4+ T cell populations, increased mitochondrial membrane potential was identified with the formation of memory which was

reduced in senescent cells. Despite conservation of some glucose transporter proteins, alterations in the control of mitochondrial network dynamics were observed resulting in decreased optic atrophy 1 (Opa1) expression following the formation of memory which was further reduced upon senescence. Finally, comparison of peripheral blood cell metabolism between young and old individuals revealed a reduction in maximal respiration rate with age in humans. This effect did not result in alterations in adenosine triphosphate production as increased glucose uptake was observed in peripheral blood cells with age. Subsequent analysis of resident immune cells populations revealed an age-associated increase in mitochondrial mass in both innate and adaptive immune cells. Taken together these results point towards mitochondrial dysfunction. In conclusion, mitochondrial dysfunction in ageing was attributed to alterations in mitochondrial mass and membrane potential as well as Opa1 expression within the models used for this study. Therefore, it is proposed that mitochondrial dysfunction is involved in the ageing process of mice and humans and excessive mitochondrial dysfunction is associated with shortened lifespan.

Table of Contents

Table of Tables

Table of Tables

Table of Figures

Table of Figures

Table of Figures

Table of Figures

Table of Figures

Research Thesis: Declaration of Authorship

Print name: Marie Strickland

Title of thesis: Cellular Immunometabolism and Regulation of Mitochondrial Efficiency – Healthy Ageing Across the Life Course

I declare that this thesis and the work presented in it are my own and has been generated by me as the result of my own original research.

I confirm that:

1. This work was done wholly or mainly while in candidature for a research degree at this University;
2. Where any part of this thesis has previously been submitted for a degree or any other qualification at this University or any other institution, this has been clearly stated;
3. Where I have consulted the published work of others, this is always clearly attributed;
4. Where I have quoted from the work of others, the source is always given. With the exception of such quotations, this thesis is entirely my own work;
5. I have acknowledged all main sources of help;
6. Where the thesis is based on work done by myself jointly with others, I have made clear exactly what was done by others and what I have contributed myself;
7. Parts of this work have been published as:

Strickland, M., Yacoubi-Loueslati, B., Bouhaouala-Zahar, B., Pender, S.L.F. & Larbi, A. Relationships between ion channels, mitochondrial functions and inflammation in human ageing. *Frontiers in Physiology* (2019) Volume 10, Issue MAR, DOI: 10.3389/fphys.2019.00158

Wong, G., Strickland, M. & Larbi, A. Changes in T-cell homeostasis and vaccine responses in old age. *Interdisciplinary Topics in Geronontology and Geriatrics* (2020) Volume 43 Page 36-55, DOI: 10.1159/000504487

Kared, H., Tan, S.W., Lau, M.C., Chevrier, M. *et al.* Immunological history governs human stem cell memory CD4 heterogeneity via the Wnt signalling pathway. *Nature Communications* (2020) Volume 11 Issue 821, DOI: 10.1038/s41467-020-14442-6

Signature: Date:

Acknowledgements

First of all, I wish to express my appreciation to my supervisor's Dr Sylvia Pender, Dr Anis Larbi, Dr Dave Johnston and Professor Peter Smith for the invaluable opportunity this PhD has offered me. My supervisory team has been fantastic and the wealth of knowledge they offered me has been invaluable during the development of this thesis. Individually, I would like to thank Dr Sylvia Pender: for her support and guidance over the last three years, without whom this thesis would not have been possible. Dr Dave Johnston: for imparting your knowledge of microscopy, helping me design assays and showing me the ropes of electron microscopy sample processing. Dr Peter Smith: for helping me to figure out the complexity of metabolism and the vital role of mitochondria within the cell. My supervisors at The University of Southampton have been fantastic and have supported me through every speed bump over the past 3 years. A special thanks goes to Dr Anis Larbi for providing me the opportunity to develop part of this work at the Singapore Immunology Network (SIgN). Your team is amazing, and I have learnt so much from both them and you. Flow cytometry has been integral in developing this thesis and I now feel confident enough to take this technique and the others you taught me into my next research role.

I am grateful for the Vice Chancellor Scholarship (University of Southampton) and to the A*STAR Research Attachment Program (ARAP; Singapore) that funded this project.

A sincere thanks go to Dr Hassen Kared, Dr Glenn Wong (for getting my English sense of humour), Crystal Tan and Salanne Lee for teaching me everything I needed to know and providing me with excellent advice for my experiments. My gratitude also goes to Dr Weili Xu, Ivy Low, Janice Tan, Michelle Chua, Dr Anteneh Mehari, Esther Mok, Wilson How, Seri Mustafah, Joni Chong, Shu Wen Tan, Neo Shiyong and Dr Yanxia Lu for making the lab a fun place to be on a daily basis and for laughing at my use of chopsticks. I would also like to thank Goh Wah Ing and Graham Wright from the A*STAR Imaging Platform for helping with the super-resolution microscopy experiment. I would like to thank my lab mates from Clinical and Experimental Sciences, Rebecca Holding, Dr Tim Biggs, Olivia Lee, Rachel Meadows and Ahmad Alzahrani for providing me with tea, cake and excellent distraction during my time in Southampton and Eileen Li for her help processing confocal microscopy images. Additionally, I would like to thank the BRF and the rest of the BIU staff for their help, particularly Patricia Goggin for running all my samples on the 3view system.

Moving to Singapore was the biggest highlight of my PhD and the memories and friends I met there will continue with me until I am as aged as the subjects in my study. There are too many dear friends to mention here but you all know who you are. Special thanks go to Ann, Em, Elizabeth, Lauren and Megan for putting up with my endless complaints about science which never goes to plan and the lack of seasons. My non-science friends

Acknowledgements

back in the UK have also been a lifeline allowing me to escape to normal whenever I need it. Cheers to Lucy, Suzy and Matt for always being there for me and pointing out when I'm being a nerd and to Rachel for your never-wavering support and friendship over these past few years despite the distance between us.

Finally, I would like to thank my family for always being there and helping me through the pressure which this PhD has put on me. To my mum, dad, brother and soon to be sister-in-law I will forever be grateful for the love and support you have given me over the course of this PhD and for providing me with the ultimate distraction every evening and weekend. It is only with your unwavering encouragement that I was able to complete and write this thesis. Thank you for trying to understand what I've been doing the last three years.

Definitions and Abbreviations

ABBREVIATION	DEFINITION
2DG	2-deoxy-D-glucose
2DG6P	2-deoxy-D-glucose-6-phosphate
3D-SIM	3 dimensional structured illumination microscopy
α-MEM	Alpha minimal essential medium
A*STAR	Agency for Science Technology and Research
AA	Antimycin A
ADAM17	Tumor necrosis factor-α-converting enzyme
ADP	Adenosine diphosphate
Af	AlexaFluor
AMD	Age-related macular degeneration
AMPK	Adenosine monophosphate-activated protein kinase
ANOVA	Analysis of variance
Apc	Allophycocyanin
APC	Antigen-presenting cell
APE-1	Apurinic/apyrimidinic endonuclease 1
ApoE	Apolipoprotein E
ARF	Alternate reading frame
ATP	Adenosine triphosphate
ATPase	Adenosine triphosphate synthase
AWERB	Animal welfare and ethics review board
β-actin	Beta actin
β-gal	Beta galactosidase
BCR	B cell receptor
BMC	Bone marrow mononuclear cell
BRF	Biological research facility
BSA	Bovine serum albumin
BV	Brilliant violet
C57	C57BL/6J
CCL	CC chemokine ligand
cDNA	Complementary deoxyribose nucleic acid
CM	Central memory
CMV	Cytomegalovirus
CO_2	Carbon dioxide
CPT	Cell preparation tube
CR	Caloric restriction
Ct	Cycle threshold
CTLA-4	Cytotoxic T-lymphocyte-associated protein 4

Definitions and Abbreviations

Cy	Cyanine
CyTOF	Mass cytometry time of flight
CXCL	Chemokine ligand
CXCR	Chemokine receptor
Daf-2	Dauer formation 2
DAMP	Damage-associated molecular pattern
DC	Dendritic cell
DENV	Dengue virus
DEPC	Diethyl pyrocarbonate
DMSO	Dimethyl sulfoxide
DNA	Deoxyribose nucleic acid
Dnm1L	Dynamin-1-like protein
Drp1	Dynamin-related protein 1
ECAR	Extracellular acidification rate
ECM	Extracellular matrix
EDTA	Ethylenediaminetetraacetic acid
ELISA	Enzyme-linked immunosorbent assay
ELSA	English Longitudinal Study of Ageing
EM	Effector memory
ERK	Extracellular signal-related kinase
ETC	Electron transport chain
FACS	Fluorescence-activated cell sorting
$FADH_2$	Flavin adenine dinucleotide hydroquinone
FAO	Fatty acid oxidation
FAS	Fatty acid synthesis
FBS	Fetal bovine serum
FCCP	Carbonyl cyanide-4-(trifluoromethoxy)phenylhydrazone
Fis1	Fission protein 1
FITC	Fluorescein isothiocyanate
FOXO	Forkhead box
FSC	Forward scatter
GLUT	Glucose transporter
Glut1	Glucose transporter 1
GO	Gene ontology
GSH	Glutathione
GSSG	Oxidised glutathione
GTP	Guanosine-5'-triphosphate
GZB	Granzyme B
H^+	Proton
H_2O_2	Hydrogen peroxide
HFD	High fat diet

HIF-1α	Hypoxia-inducible factor-1 alpha
HIV	Human immunodeficiency virus
HLA-DR	Human leukocyte antigen – DR isotype
HRP	Horseradish peroxidase
HSC	Haematopoietic stem cell
I-A/I-E	Major histocompatibility complex Class II
IACUC	Institutional Animal Care and Use Committee
IFNγ	Interferon gamma
IGF-1	Insulin-like growth factor 1
Ig	Immunoglobulin
IL	Interleukin
ILC	Innate cells of lymphoid lineage
INK4	Inhibitor of cyclin-dependent kinase 4
JAK	Janus kinase
KLRG1	Killer cell lectin-like receptor subfamily G member 1
KO	Tissue inhibitor of matrix metalloproteinase 3 knock-out mouse
Lck	Lymphocyte-specific protein tyrosine kinase
LCMV	Lymphocytic choriomeningitis
LP	Long pass filter
MACS	Magnetic-activated cell sorting
MAPK	Mitogen-activated protein kinase
mDC	Myeloid dendritic cell
MFI	Mean fluorescent index
Mfn1	Mitofusin 1
Mfn2	Mitofusin 2
MHC	Major histocompatibility complex
miRNA	microRNA
mRNA	Messenger ribonucleic acid
MMP	Matrix metalloproteinases
MSC	Mesenchymal stem cell
mtDNA	Mitochondrial deoxyribose nucleic acid
MTG	MitoTracker Green
mTOR	Mammalian target of rapamycin
NAD+	Oxidised nicotinamide adenine dinucleotide
NADH	Reduced nicotinamide adenine dinucleotide
NADPH	Nicotinamide adenine dinucleotide phosphate
NF-κB	Nuclear factor kappa-light-chain-enhancer of activated B cells
NHS	National health service
NK	Natural killer
NLRP3	Nod-like receptor family pyrin domain containing 3
NO	Nitric oxide

Definitions and Abbreviations

O_2	Oxygen
OCR	Oxygen consumption rate
Opa1	Optic atrophy 1
OXPHOS	Oxidative phosphorylation
PAMP	Pathogen-associated molecular pattern
PBMC	Peripheral blood mononuclear cell
PBS	Phosphate buffered saline
PCR	Polymerase chain reaction
PD-1	Programmed cell death protein 1
pDC	Plasmacytoid dendritic cell
PDL	Poly-D-lysine
PE	Phycoerythrin
Pen	Penicillin
PIPES	Piperazine-N, N'-bis(2-ethanesulfonic acid)
PI3K	Phosphoinositide 3-kinase
PFD	Pseudoinflammatory Fundus Dystrophy
PMA	Phorbol 12-myristate 13-acetate
PMT	Photomultiplier tube
PP	Polypropylene
PPP	Pentose phosphate pathway
PRR	Pattern recognition receptor
RBC	Red blood cell
RIG-I	Retinoic acid-inducible gene I
RLU	Relative luminescent unit
RNA	Ribonucleic acid
ROI	Region of interest
ROS	Reactive oxygen species
Rot	Rotenone
RPMI	Rosewell Park Memorial Institute
RT-qPCR	Reverse transcription real-time quantitative polymerase chain reaction
SAM	Senescence-accelerated mice
SAMP	Senescence-accelerated mice prone
SAMR	Senescence-accelerated mice resistant
SASP	Senescence-associated secretory phenotype
SBF-SEM	Serial block-face scanning electron microscopy
SEM	Scanning electron microscopy
SFD	Sorsby's Fundus Dystrophy
SHP-1	Src homology region 2 domain-containing phosphatase-1
SigF	Siglec F
SIgN	Singapore Immunology Network
SIM	Structure illumination Microscopy

SIRT1	Sirtuin 1
SLAS	Singapore longitudinal ageing study
SLAS II	Singapore longitudinal ageing study cohort II
SOD	Superoxide dismutase
SPF	Specific pathogen free
SRC	Spare respiratory capacity
SSC	Side scatter
STAT	Signal transducer and activator of transcription protein family
Strep	Streptomycin
TCR	T cell receptor
TEM	Transmission electron microscopy
TEMRA	Terminal effector memory T cell re-expressing CD45RA
TGF-β	Transforming growth factor beta
Th2	T helper 2
Timp3	Tissue inhibitor of matrix metalloproteinase 3
TLR	Toll-like receptor
TMB	3,3',5,5'-Tetramethylbenzidine
TMRE	Tetramethylrhodamine, Ethyl Ester, Perchlorate
TMRM	Tetramethylrhodamine, Methyl Ester, Perchlorate
TNF-α	Tumour necrosis factor alpha
TOM20	Translocase outer mitochondrial membrane 20
UK	United Kingdom
WHO	World Health Organisation
WT	Wild-type C57BL/6J mouse

Chapter 1   Introduction

1.1   Ageing

1.1.1   Population restructuring and global ageing

Due to worldwide success in treating childhood disease and reducing mortality in old age, today most people can expect to live to the age of 60 years and often beyond. However, whilst life expectancy has increased dramatically over the last 100 years fertility rates have been steadily declining (Figure 1.1). Due to this the global population is currently undergoing massive restructuring, termed global ageing. In 2015 the World Health Organisation (WHO) produced their latest report on human ageing. The main finding from this report was that the percentage of people aged over 60 years will increase from 12% to 22% of the global population by 2050 (World Health Organization, 2015). This trend is currently being observed in many Westernised nations including France, Sweden, the United Kingdom (UK) and Japan where the percentage of the population aged over 60 years has already reached 20%. Other countries such as the United States, China and Brazil will see the proportion of this population rise to 1 in 5 before the end of 2050 (Figure 1.2).
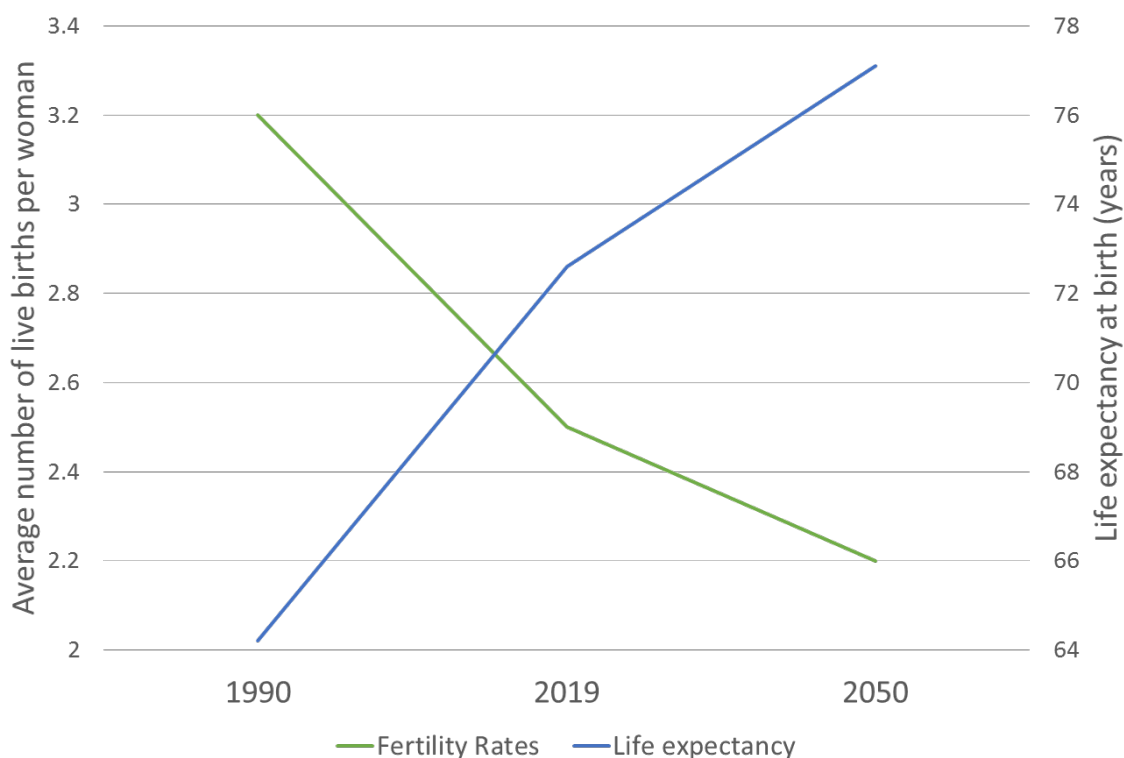
Figure 1.1   Comparison of global fertility rates and life expectancy from 1990 to 2050 (Adapted from (United Nations, 2019))
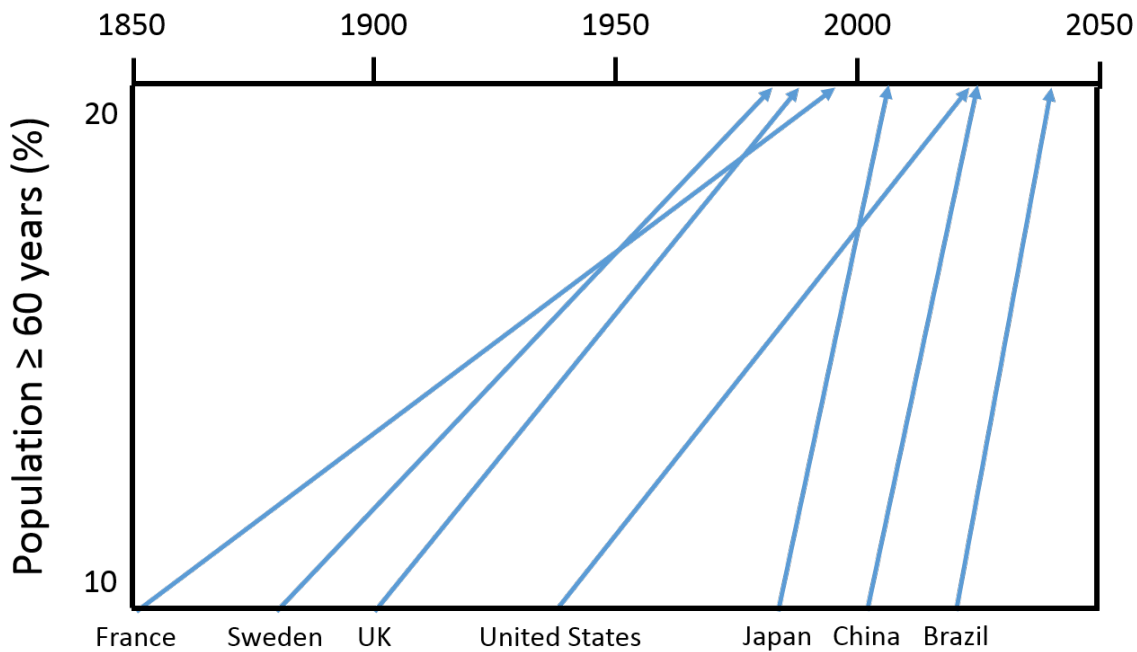
Figure 1.2   Rate of growth of the 60 years old and over age demographic from 10% to 20% of the total population (Adapted from (Geneva: World Health Organization, 2015))

Due to its complexity ageing is particularly hard to define and has been a cause for debate among scientists for many years. Put simply, ageing can be defined as the development of structural and functional decline with the passing of time. This decline causes a loss of adaption with age due to a non-linear time-progressive decline in physical, mental and functional abilities. This has been linked to decreasing pressure on natural selection with increasing age. However, loss of function and adaption are difficult to measure in organisms and often involve invasive techniques. Therefore, chronological age remains the mainstay for categorising ageing. In line with other studies described in this introduction, individuals aged 65 years and over have been termed 'older' within this study. Moreover, ageing is the greatest known risk factor for the development of disease, including:

- Atherosclerosis and cardiovascular disease
- Cancer
- Neurodegenerative diseases and Alzheimer's disease
- Type 2 diabetes
- Osteoporosis and osteoarthritis
- Cataracts and macular degenerative disease
- Chronic lower respiratory disease

Of the 150,000 people which die each day due to natural causes, around 66% (100,000) of these are attributed to age-related disease (de Grey Aubrey, 2007). This causation is even higher in Westernised nations, where age-related diseases contribute to 90% of deaths. Therefore,

understanding what influences health and vitality has become an important factor in ageing research.

Both the UK and Singapore expect to see major demographic shifts in population structure over the next decade. Children born currently in the UK and Singapore can expect to have a lifespan of 83.1 years and 81.2 years of age, respectively (World Health Organization, 2016). Population restructuring will see over 70% of population growth in the UK fall within the over 60 years age category, increasing from 14.9 to 21.9 million between 2014 and 2039 (Leeson, 2014). The latest population data release for the UK in 2018, states that 18% of the UK population is currently aged 65 years and over, almost one in five people (Office for National Statistics, 2018). This figure is projected to reach ~24% by the year 2036, whilst the percentage of the population aged 85 years and over could total 4% (Office for National Statistics, 2018). Further improvements in healthcare and lifestyle mean that life expectancy at birth will increase from 82.8 years to 86.6 years for females and from 79.1 years to 83.7 years for males between 2015 and 2036 (Office for National Statistics, 2018).

In Singapore the age demographic aged 65 years and over has quadrupled between 1970 and 2015, increasing from 3% to 13% of the total population (Figure 1.3) (Ministry of Health, 2016). This figure is expected to double again by the year 2030 with one in four Singaporeans aged 65 years or over (Ministry of Health, 2016). These population changes are not limited to the UK and Singapore. This degree of population ageing is expected to occur across the European Union and in other industrialised Asian countries, putting further strain on global economy.
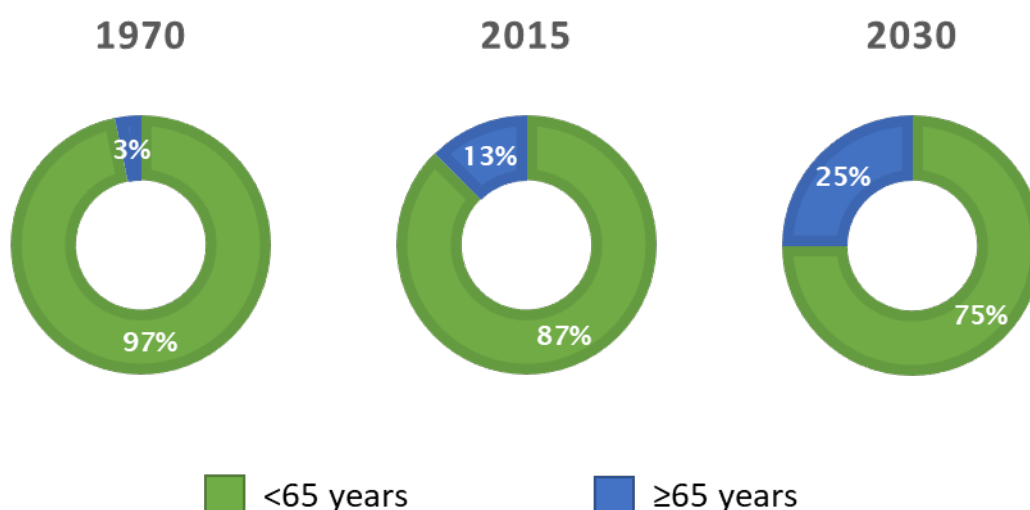
Figure 1.3   Projected growth of the Singaporean population aged 65 years and over from 1970 to 2030 as a percentage of the total population (Adapted from (Ministry of Health, 2016))

Chapter 1

1.1.2   Social impact

Living longer can have an incredibly positive impact on society particularly during this time of global ageing. Contributing to society through remaining in the workforce, mentoring younger people and acting as consumers can have both a positive impact on society and increase the well-being of the elderly through continued social engagement. However, this positive impact is dependent on the health status of the ageing population.

More than two-fifths of National Health Service (NHS) funding is spent on people over the age of 65 years in the UK (Age UK, 2019). In 2018 £109 billion of this funding came from the Department of Health and Social Care budget, leaving £16 billion for spending on social care, training and infrastructure. Acute conditions, such as the common cold and infections, have seen an increase in the number of hospital admissions since 2013 particularly in older age groups (Age UK, 2019). These conditions should not usually require hospital admission and represent the shortfall in primary care services and their inability to meet current demand. Due to this the number of people presenting at emergency rooms has steadily been increasing along with triage waiting times in the elderly.

In 2018 more than 1 in 7 older people required help with one or more essential daily activities, such as going to the bathroom, making a cup of tea or buying groceries. A total of £21.7 billion was spent on adult social care in 2017/2018, which has been steadily declining over the past decade. This supply of funding is not enough to keep up with the growth of the older population. Spending per capita fell by 17.5% in the older population between 2011 to 2018 (Age UK, 2019) whilst cost per capita has steadily been increasing. The gap in spending and the cost of care is expected to reach £6.1 billion by 2030. This shortfall is increasingly being met by the older populations and the family members supporting them.

These issues are also prevalent in Singapore. A 2016 report stated that healthcare costs stand at $5 billion. By 2030 this cost is expected to rise to $49 billion, with costs per capita rising from $8,196 to $37,427 (Tai, 2016). The Singaporean government has recently put together an action plan for investing an additional $3 billion on supporting healthy ageing, with $200 million of this budget expected to be set aside for improving ageing research (Ministry of Health, 2016).

1.1.3   Healthy ageing

In recent years there has been a significant shift in global health priorities. Previous efforts focused on reducing mortality rates in younger generations which has been successful worldwide. However, these populations are now becoming older and focus has shifted to helping people age in a healthy way and increase the quality of the extra years recent health advances have awarded us. Currently

healthy life expectancy, the number of years expected to be lived disease-free, stands at 73.9 years in Singapore and 71.4 years in the UK (World Health Organization, 2016).

"Healthy ageing… is the process of developing and maintaining the functional ability that enables well-being in older age"

World Health Organization, World Report on Ageing and Health, 2015 (Geneva: World Health Organization, 2015)

Figure 1.4 shows several trajectories in functional capacity which can occur with age. The blue line represents the ideal trajectory, maintenance of functional capacity which suddenly declines just before death. The orange line represents a second trajectory whereby functional capacity is maintained before premature death. The third trajectory follows the grey line, a period of reduced functional capacity in mid-life is followed by a period of recovery prior to sudden functional decline at death. There is the possibility for this period of reduced functional capacity to plateau prior to sudden decline (yellow line). Finally, the green line represents a trajectory following gradual reduced functional decline throughout the lifetime. This trajectory is commonplace today, with the elderly suffering from a multitude of age-related diseases which affect their independence and quality of life.

Understanding healthy ageing is a complex issue as it integrates well-being within numerous areas of life. This includes but is not limited to; physiological factors such as ageing at the biological level and environmental factors including social and psychological status which all affect intrinsic capacity. The diversity of health seen in individuals of the same chronological age is influenced by these trajectories. As shown in Figure 1.5, individuals of the same chronological age can exhibit varying degrees of health. The most healthy individuals (following the blue trajectory from Figure 1.4) experience a far greater health span than less healthy individuals (following the green trajectory from Figure 1.4), despite having the same lifespan. This highlights the importance in undertaking a life course approach to understanding ageing and the diversity between older members of the population.

"This represents a significant shift from previous global health priorities, where the emphasis was often on reducing mortality at younger ages. Instead, the focus of the strategy is on the extra years that these interventions now allow us to enjoy."

World Health Organization, Global Strategy and Action Plan on Global Ageing and Health, 2017 (Geneva: World Health Organization, 2017)
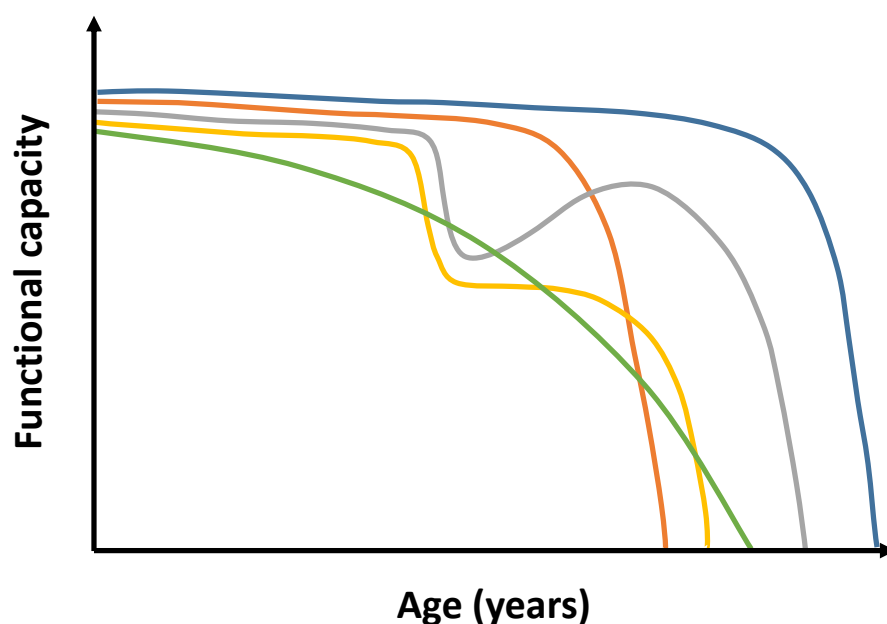
Figure 1.4   Possible trajectories of functional capacity during ageing showing an optimal (blue) and less optimal (orange) healthy ageing trajectory, interrupted ageing trajectories with (grey) and without (yellow) recovery and a steadily declining trajectory (green). (Adapted from (Geneva: World Health Organization, 2015))

The top conditions noted to affect health span include musculoskeletal and neurological disorders, cardiovascular disease and diabetes (World Health Organization, 2016). All these diseases increase in prevalence with age, affecting up to 90% of the population over the age of 65 years. Current research is focusing on understanding why some individuals become more burdened by disease than others during their lifetime. Understanding this issue will be paramount in providing better guidance, treatment and support for the older population.
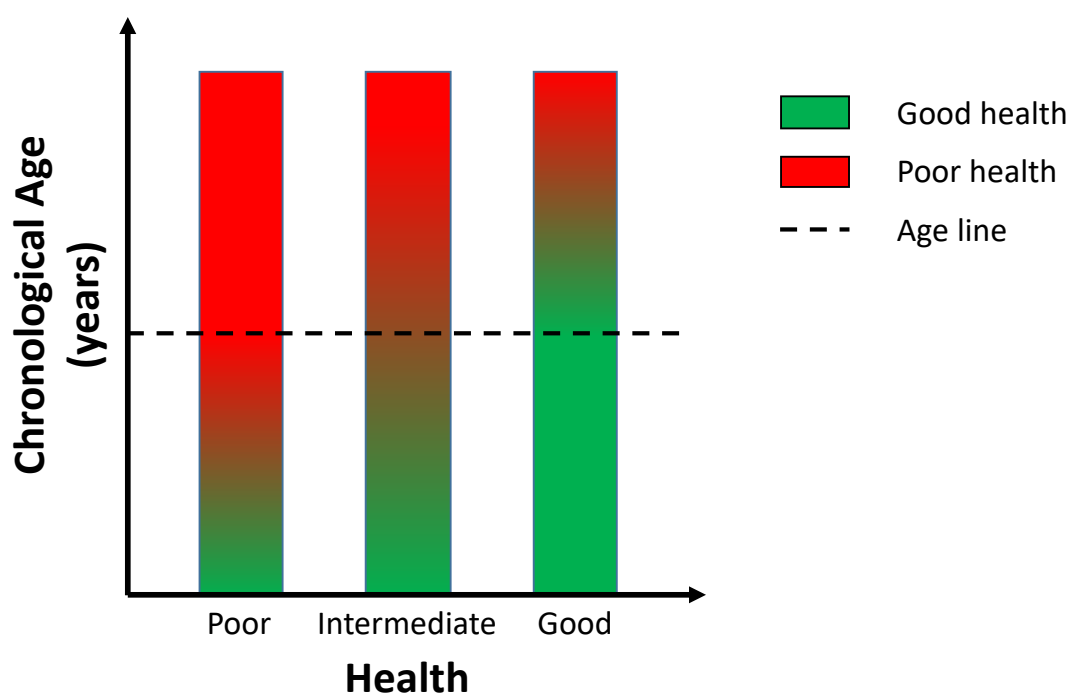
Figure 1.5   Effect of poor and good health on health status during ageing and the variability between individuals of the same age

1.1.3.1   Promoting healthy ageing

In 2017 the World Health Organization (WHO) released their vision, goals and strategic objectives for supporting healthy ageing in 2020 (Table 1.1). The report highlights that healthy ageing is not just the absence of disease but focuses instead on functional ability.

Table 1.1   World Health Organization action plan on healthy ageing taken from (Geneva: World Health Organization, 2017)

VISION	A WORLD IN WHICH EVERYONE CAN LIVE A LONG AND HEALTHY LIFE
Strategic objectives	1. Commitment to action on Healthy Ageing in every country 2. Developing age-friendly environments 3. Aligning health systems to the needs of older populations 4. Developing sustainable and equitable systems for providing long-term care (home, communities and institutions) 5. Improving measurement, monitoring and research on Healthy Ageing
Action plan 2016-2020 Goals	1. Five years of evidence-based action to maximise functional ability that reaches every person 2. By 2020, establish evidence and partnerships necessary to support a Decade of Healthy Ageing from 2020 to 2030

Chapter 1

The health issues that affect the older population are either preventable or can be delayed by improving the guidelines surrounding healthy ageing. This has involved increasing healthy behaviours not just during retirement, but across the life course. The strategy developed by WHO integrates the sustainable development goals produced in 2016 (World Health Organization, 2016). Changes in population structure result in alterations in social positions that require psychosocial growth and environments that require improvement for those with limited functional capacity. Each of the five strategic objectives has three priority areas for action.

1) Objective 1: Commitment to action on healthy ageing in every country

   a) National frameworks for action on healthy ageing: Focus on building relationships between the government, healthcare providers, academics and the general population to ensure people live long and healthy lives. Develop national and regional strategies and policies to address ageing and health.

   b) Strengthen national capacity to produce evidence-based policies: Increase awareness of the main findings from ageing research to improvement healthcare and the local environment in a cost-effective manner.

   c) Combat ageing and improve understanding: Remove restrictive social constructs with a negative view of ageing to foster personal growth and productivity of these populations, as well as including these groups in society.

2) Objective 2: Developing age-friendly environments

   a) Foster autonomy: Develop the ability to make lifestyle choices in the older population to improve well-being regardless of gender and functional capacity. Improve social and financial resources for these populations to meet basic needs and to support decision-making.

   b) Enable engagement: Increase participation of the older population into general society, by increasing access to facilities and community groups.

   c) Promote multi-sectoral action: Build relationships between the government, local councils and general population to improve local services and meet these goals.

3) Objective 3: Aligning health systems to the needs of older populations

   a) Orient health systems around functional capacity: Improve collection and recording of health data to improve health trajectory projections. Review the availability of medicines and assistive devices required to improve functional capacity and increase quality of life in the older population.

   b) Develop affordable access to person-centred quality healthcare: Develop comprehensive personalised care plans to provide support across healthcare sectors. Fund further research

and drug development for age-related diseases to improve functional capacity and self-management of healthcare needs.

c) Ensure sustainability in the healthcare workforce: Improve training, deployment and management of healthcare staff and increase knowledge of dealing with the older population and age-related diseases.

4) Objective 4: Developing sustainable and equitable systems for long-term care

a) Establish a sustainable long-term care system: Identify the key barriers to improving long-term care systems and develop guidance with a focus on building communities and social networks aligned to population needs.

b) Build caregiver workforce and improve support: Improve the training and support of caregivers and improve the value of the workforce in society.

c) Ensure quality of person-centred long-term care: Allow caregivers the opportunity to provide care and support the functional capacity and well-being of the older population. Provide condition-specific services to increase caregiver support and management of disease.

5) Objective 5: Improve measurement, monitoring and research on healthy ageing

a) Agree on ways to measure and monitor healthy ageing: Produce a common approach for metrics, biological markers, data collection methods and reporting approaches across the board. Integrate this knowledge to inform ageing and functional capacity trajectories.

b) Strengthen research capacities and incentives: Develop collaborations for voluntary knowledge exchange, resulting in better provision of assistive devices and medicines. Include the older populations in pharmaceutical and bioengineering research to foster improvements in health care.

c) Synergise evidence on healthy ageing: Foster more research to help develop political, social, biological and environmental aspects of ageing. Use ageing trajectories to improve these systems and improve the well-being of the older population.

1.1.4 Biology of ageing

The biology of ageing is a complex issue. Ageing occurs at both the biological level and physiological level in organisms as part of a multi-systemic process. The accumulation of several factors influences biological ageing over time leading to decreases in physiological capacity, an increase in disease development and a decline in functional capacity. This research into ageing has been hampered by the fact that ageing is contributed to by a variety of factors and is not linked to one single disease. The classification of ageing as a disease has been debated for centuries (Bulterijs et al., 2015), however as ageing does not have a specific cause it is hard to place within this category.

Rather ageing is characterised by a multi-systemic group of pathologies which are collectively seen with increasing age.

1.1.4.1   Theories of ageing

Over 300 theories of ageing have been postulated since ageing research began highlighting the multifaceted nature of the ageing process. However, deciphering these theories into the causes and effects of ageing has been difficult. In order to aid understanding of these concepts, a seminal paper "The hallmarks of ageing" written by López-Otín *et al* was published in 2013 (López-Otín et al., 2013). This article summarised the nine major contributors to ageing which are the most widely accepted and studied in modern ageing research. Despite being published over 6 years ago these hallmarks are still highly regarded today. This section will summarise each of the nine hallmarks of ageing.

- **Genomic instability:** The accumulation of cellular and genetic damage over time is widely regarded as a general cause of ageing. Throughout our lifetime both nuclear and mitochondrial deoxyribonucleic acid (DNA) are subjected to exogenous and endogenous damage, resulting in their disruption. Although the majority of this damage is repaired in a timely manner, some mutations arising from replication errors, reactive oxygen species (ROS) damage and biological agents can accumulate over time (Sohal et al., 1994, Yehuda et al., 2001). Mutations arising from damage such as DNA mis-match repair, non-homologous end joining and adduct formation are highly diverse and rarely conserved between ageing individuals. Mouse models with increased mutation rates caused by defective DNA repair mechanisms typically exhibit drastically shortened life span and humans with premature ageing diseases, such as Werner syndrome and Progeria, display elements of genomic instability (Yamagata et al., 1998, Liu et al., 2005a, McCord et al., 2013), although these syndromes only recapitulate some aspects of ageing. DNA mutations, including single nucleotide polymorphisms, chromosomal aneuploidy and gene copy number variations have long been associated with ageing, from model organisms to humans (Lee et al., 1999, Kujoth et al., 2005). These mutations result in dysfunctional cells which contribute to the loss of cellular fitness observed within ageing and diseased tissues. Ineffective DNA repair mechanisms contribute to lifespan deficiencies in model organisms, mice and premature ageing syndromes. Mutations within mitochondrial DNA co-exist with wild-type mitochondrial genomes throughout our lifetime. Mouse models which lack the mitochondrial DNA proofreading enzyme, DNA polymerase γ (Vermulst et al., 2008, Joseph et al., 2013) exhibit many aspects of the natural ageing process, from hair loss to sarcopenia, during their premature ageing and drastically shortened lifespan (Joseph et al.,

2013, Trifunovic et al., 2004). Interestingly these mice simulate many of the other ageing hallmarks, including stem cell exhaustion and mitochondrial dysfunction (Trifunovic et al., 2004).

- **Telomere attrition:** Telomeres are susceptible to age-related attrition due to the lack of DNA polymerase ability to bind to the terminal ends of nuclear DNA. Telomerase is a special enzyme which can add nucleotide bases to the terminal ends of chromosomes in order to protect them (Harrington, 2003). However telomerase activity is often lost following differentiation from stem cells (Sharma et al., 1995). Once telomeres reach a critical level cells are no longer able to divide and become either senescent or undergo apoptosis resulting in degeneration and disease appearance over time. Decreased telomerase activity has been observed in both mice and humans with age, alongside the development of degenerative and inflammatory disease such as fibrosis and anaemia (Harley et al., 1990, Alder et al., 2008, Rudolph et al., 1999, Yamaguchi et al., 2005). Various mouse models have shown that telomere length is directly related to organismal lifespan, with shortened telomeres and reduced telomerase activity in mice reducing lifespan by up to 13-24% (Rudolph et al., 1999, Bernardes de Jesus et al., 2012). This effect has previously been revealed in humans through meta-analysis (Bischoff et al., 2006).

- **Epigenetic alterations:** The epigenomes of cells continuously change over time in order to control gene expression and cell functionality. Epigenetic markers associated with ageing include increases in H4K16 acetylation and trimethylation of H4K20 and H3K4, H3K9 methylation has been also shown to be reduced with age alongside H3K27 trimethylation (Dang et al., 2009, Shumaker et al., 2006, Han et al., 2012, Greer and Shi, 2012, Kawakami et al., 2009, Kuzumaki et al., 2010). Disruption of histone methylation in nematodes and flies, as well as histone demethylases in *C. elegans*, extends longevity (Greer et al., 2010). Although the reasons behind this still remain unclear, it is believed that perturbation of pathways under the control of these genetic modifications affect the ageing process (reviewed in (D'Aquila et al., 2013)). For example, epigenetic modification of the insulin/insulin-like growth factor-1 (IGF-1) pathway has been implicated in the development of diabetes and other age-related diseases in humans (Jin et al., 2011).

- **Loss of proteostasis:** Maintaining proteostasis involves a variety of mechanisms for protein degradation and quality control to maintain function of the proteome. These systems prevent the aggregation and accumulation of misfolded or damaged proteins, however this protein maintenance system has been shown to be altered with age (Ben-Zvi et al., 2009,

Demontis and Perrimon, 2010, Schneider et al., 2015). Unrestrained accumulation of misfolded and damaged proteins results in the development of age-related diseases. These include the accumulation of amyloid beta and alpha-synuclein in neurodegenerative conditions such as Alzheimer's and Parkinson's disease (reviewed in (Morawe et al., 2012, Bosco et al., 2011)). Heat shock proteins are intimately involved within the stress-response pathway to unfolded proteins. Numerous animal models, including mice, show reduced longevity when deficient in heat shock proteins (Walker and Lithgow, 2003, Gifondorwa et al., 2007). Both the ubiquitin-proteasome and autophagy-lysosome protein degradation systems are deteriorated with ageing which contributes to dysregulated proteostasis (Carrard et al., 2002, Gray et al., 2003, Cuervo et al., 2005). In accordance with this, restoration of autophagic processes including chaperone-mediated autophagy has been shown to increase health span in aged mice (Zhang and Cuervo, 2008).

- **Dysregulated nutrient sensing:** Dysregulated nutrient sensing in mammalian cells generally involves the insulin/IGF-1 axis which plays a role in the development of Type 2 diabetes (Junnila et al., 2013). This pathway responds to glucose levels in the microenvironment and regulates signalling pathways which have been previously implicated in ageing. This includes the mammalian target of rapamycin (mTOR) pathway, adenosine monophosphate-activated protein kinase (AMPK) pathway and the Sirtuin protein family pathway (Anisimov, 2003, Wang et al., 2018, Lemieux et al., 2005, Mazucanti et al., 2015). Many components of the insulin/IGF-1 axis have been implicated in ageing across model organisms and are involved in enhancing lifespan following caloric restriction (CR) (Masoro, 2005, Fontana et al., 2008). Decreased insulin/IGF-1 signalling extends longevity in mice. However, growth hormone and IGF-1 levels are reduced with ageing as a response to cellular damage (reviewed in (Berryman et al., 2008)). Downregulation of mTOR and upregulation of AMPK and Sirtuins extend longevity by employing a diverse range of pathways. The manipulation of these proteins affects how nutrients are metabolised by the mitochondria enhancing the metabolic response and protection from some aspects of ageing in model organisms, ageing mice and humans (López-Otín et al., 2013).

- **Cellular senescence:** Irreversible cell growth arrest, also known as cellular senescence, is a major hallmark of ageing resulting in increased beta-galactosidase (β-Gal) activity, altered gene expression and dysregulated protein processing (Kurz et al., 2000). Senescence can be induced by a number of factors including but not limited to, oxidative stress, oncogene activation and genomic instability (Kurz et al., 2004). The first studied inducer of senescence was telomere shortening, however DNA damage and expression of the *INK4/ARF* (inhibitor

of cyclin-dependent kinase 4/alternate reading frame) locus with age can prompt cellular senescence (Hirosue et al., 2012, Di Micco et al., 2006). The *INK4/ARF* locus contains three tumour suppressor genes (*INK4A, INK4B* and *ARF*) which act to coordinate Retinoblastoma protein and p53 dependent inhibition of cell-cycle progression (Sherr, 2012). Expression of the *INK4/ARF* locus is the gene most robustly correlated with human ageing and age-related pathologies. These include cardiovascular disease, Type 2 diabetes and Alzheimer's disease (Matheu et al., 2009, Burd et al., 2010, González-Navarro et al., 2013, Popov and Gil, 2010). The clearance of senescent cells requires an intact cell replacement system in order to maintain tissue homeostasis, involving the replication of neighbouring cells and differentiation of stem and progenitor cells to replace the old. However, both the removal of senescent cells and the differentiation of stem cells are repressed with age (Wagner et al., 2009). The senescence-associated secretory phenotype (SASP) contributes to the development of age-related pathologies including neuronal degradation, cancer and frailty (Salminen et al., 2011, Cahu et al., 2012, Xu et al., 2015). SASP is enriched with pro-inflammatory cytokines and matrix metalloproteinases (MMPs), which contribute to ageing by affecting proliferation, inflammation and tissue repair (Salminen et al., 2011, van Deursen, 2014). The appearance of senescence and chronic inflammation with age forms the basis of many of the murine models employed in ageing research.

- **Stem cell exhaustion:** Over time tissues exhibit a decline in their regenerative potential, due to the exhaustion of stem cells. Haematopoietic stem cells (HSCs) are one of the most affected by the ageing process (Chen et al., 2003). HSCs derived from aged mice show drastically reduced cycling than those derived from young mice (Chen et al., 1999, Liang et al., 1998). This reduced cycling is correlated with the appearance of DNA damage and increased *INK4/ARF* locus expression. This links stem cell exhaustion to senescence and genetic instability respectively, alongside telomere shortening (Rossi et al., 2007, Liu et al., 2011). Exhaustion of HSCs may lead to senescence of the immune system, termed immunosenescence, and relates to the gradual deterioration of the immune system brought on by natural ageing. Whilst this aspect of stem cell exhaustion theory focuses on senescence, excessive proliferation of stem cells has been shown to be detrimental to the ageing process in flies (Boyle et al., 2007, Castilho et al., 2009). This highlights the fact that stem cell exhaustion and subsequent senescence is a cause of ageing rather than uncontrolled induction of senescence itself, as stem cells employ quiescence to maintain their vitality and regenerative capacity (Wilson et al., 2008).

- **Altered intercellular communication:** Increased inflammation is one attribute of altered intercellular communication which contributes to organismal ageing, termed "inflamm-ageing". Inflamm-ageing results from a variety of factors including but not limited to SASP, tissue damage and immunosenescence, contributing to Type 2 diabetes and atherosclerosis development (reviewed in (Franceschi et al., 2007)). Overactivation of the nuclear factor-kappa beta (NF-κB) inflammatory pathway has been implicated in inflamm-ageing through transcriptional profiling of aged tissues, including mouse HSCs and human fibroblasts (Salminen et al., 2008, Chambers et al., 2007, Kriete et al., 2008). These studies showed upregulation of the NF-κB cascade with ageing and increased nuclear localisation of the p65 NF-κB isoform. Nuclear localisation was increased from 3% to 71% in HSCs between 2 months and 22 months of age in mice (Chambers et al., 2007). Extensive communication between tissues occurs within mammalian organisms and inflammation in one tissue can affect distant tissues through the secretion of systemic factors (Zhang et al., 2012, Franceschi and Campisi, 2014). Parabiosis experiments also show this effect, where joining the circulation of young and old mice demonstrates that systemic factors derived from young mice can extend the health span of the old (Katsimpardi et al., 2014). This pioneering experiment by Katsimpardi *et al* (Katsimpardi et al., 2014) demonstrated that vascularisation of the neural stem cell niche and rates of neurogenesis were increased in the older of the parasymbiotic pair, ameliorating cognitive declines seen with age in these mice.

- **Mitochondrial dysfunction:** Mitochondrial dysfunction and improper regulation of mitochondrial biogenesis have been highlighted as a hallmark of ageing (Liu et al., 2002). Mitochondrial biogenesis and functionality are uniquely linked with the Sirtuin protein family which shields against mitochondrial dysfunction and age-associated disease (Van de Ven et al., 2017). The onset of age-related pathologies has been well-linked to mitochondrial dysfunction, including cardiovascular disease, Alzheimer's disease, diabetic kidney disease and Parkinson's disease among others (Lesnefsky et al., 2001, Reddy and Beal, 2008, Qi et al., 2017, Abou-Sleiman et al., 2006). Throughout the ageing process, the efficiency of the mitochondrial electron transport chain weakens, reducing the amount of adenosine triphosphate (ATP) production and increasing electron leakage and ROS production. Telomerase-deficiency in mice has been shown to impact mitochondrial biogenesis by downregulating the master regulator of mitochondrial production, peroxisome proliferator-activated receptor gamma coactivator proteins 1 alpha and beta. Decline in mitochondrial mass and reduced telomerase activity have been shown in wild-type mice with normal ageing (Birch et al., 2018, Baek et al., 2019, Sanderson and Simon,

2017). The free-radical theory of ageing highlights the production of ROS with age which cause progressive cellular damage, including that of the mitochondria which are more susceptible due to their close proximity (Kowaltowski and Vercesi, 1999). This damage reduces the efficiency of the electron transport chain (ETC) further, increasing ROS output and causing more damage in a never-ending cycle (Zorov et al., 2000). Over time this causes mitochondrial dysfunction and cells undergo apoptosis causing degeneration and the development of age-related disease (Kujoth et al., 2005). In fact, ROS have been implicated in the development of numerous age-related diseases. Recent findings and reviews on the role of ROS in disease pathogenesis are detailed in Table 1.2. Similarly the production of ROS has been shown to be increased with ageing in rat heart and increased anti-oxidant expression has been observed in Type 2 diabetic patients and obese rodents (Valerio et al., 2006, Petrosillo et al., 2009, Avila et al., 2012, Hartman et al., 2014). Despite the original evidence for the clear role of ROS in the ageing process, recent evidence has in fact shed light on a beneficial role for ROS in increasing longevity in worms, flies and mice (Wang et al., 2003, Lee et al., 2010). Antioxidant defence mechanisms have been shown to have limited effects on longevity (Ristow, 2014). In support of this Pérez et al. (2009) showed that genetic overexpression of catalase and two variants of superoxide dismutase (SOD), copper-zinc SOD and manganese SOD, are not sufficient to extend lifespan in male mice compared to wild-type controls (Pérez et al., 2009). However, previous evidence from Schreiner *et al.* suggests that overexpression of catalase localised to the mitochondria is enough to extend maximum lifespan by up to 5.5 months, delaying the development of age-related cardiac and optical pathology (Schriner et al., 2005). These developments have confused the causal role of ROS in accelerating the ageing process. Recent studies have suggested that ROS production is not an indication of cognitive decline in Alzheimer's disease (Desler et al., 2015).

Table 1.2   Age-related diseases associated with reactive oxygen species (ROS) production

AGE-RELATED PATHOLOGY	REFERENCE
ALZHEIMER'S DISEASE	(Ahmad et al., 2017, Cheignon et al., 2017, Ramachandran et al., 2016)
PARKINSON'S DISEASE	(Campolo et al., 2016, Casili et al., 2017, Pavshintcev et al., 2017)
CARDIOVASCULAR DISEASE	(Xia et al., 2017, Kietzmann et al., 2017, Abid and Sellke, 2016)
ATHEROSCLEROSIS	(Dorighello et al., 2017, Nowak et al., 2017, Yang et al., 2017)
CANCER	(Durand and Storz, 2017, Rey et al., 2016, Bousquet et al., 2017)
DIABETES	(Dong et al., 2016, Newsholme et al., 2016, Alves-Lopes et al., 2016)
MACULAR DEGENERATIVE DISEASE	(Kaarniranta et al., 2019, Chen et al., 2018, Bellezza, 2018)

1.1.5   Models for studying ageing

1.1.5.1   *C. elegans* and *Drosophila*

Model organisms provide one of the basic tools for biological research and, due to our in-depth knowledge of their genetics, they provide an ideal basis for studying complex conditions such as ageing. Model organisms such as *Caenorhabditis elegans* and *Drosophila melanogaster* are readily available and cheap to maintain. These organisms make ideal model systems for ageing research due to their relatively short lifespan and easy manipulation of their genetic make-up.

The nematode *C. elegans* has been used widely in biological research since the details of its genetics were studied by Sydney Brenner in 1974 (Brenner, 1974). Since then, *C. elegans* research has been pivotal in deciphering the pathways involved in programmed cell death, control of gene expression, testing methodology for genome cloning and DNA sequencing. Early studies for ageing research in *C. elegans* focused on measuring lifespan and longevity and this measurement remains the mainstay for ageing research today. The first experiments conducted into modulators of lifespan in *C. elegans,* by Klass in 1977 (Klass, 1977), revealed the importance of metabolic rate and CR in controlling lifespan by regulating temperature and food intake. This research has highlighted the implications of metabolism in ageing. Subsequent mapping of organisms with altered lifespan

identified a single genetic locus, *age-1* (Friedman and Johnson, 1988). With the introduction of health span research, *C. elegans* studies have begun measuring rate of movement, fitness and stress levels as parameters of health span. In 1993, mutation of a second gene was shown to confer lifespan extension in *C. elegans* mutants (Kenyon et al., 1993). This gene originally named *dauer formation-2* (*daf-2*) was shown to double the lifespan of *C. elegans* when mutated, which required the activity of a second gene *daf-16*. Subsequent research has identified these genes as key players in the insulin/IGF- 1 signalling pathway (Table 1.3). The role of these genes and components in regulating lifespan and longevity have since been confirmed in *D. melanogaster* and genome wide-wide association studies in humans (Deelen et al., 2013, Clancy et al., 2001, Tatar et al., 2001).

Table 1.3   Components of the insulin/IGF-1 pathway encoded by genes implicated in lifespan extension in *C. elegans*

C. ELEGANS GENE	COMPONENT
age-1	Phosphoinositide 3-kinase (PI3K) catalytic subunit
daf-2	IGF-1 receptor
daf-16	Forkhead box (FOXO) transcription factor

More than 50% of *Drosophila* genes have homologs in humans and 715 known human disease genes have homologs in *Drosophila* (Reiter et al., 2001). Many of these disease genes are implicated in the pathogenesis of age-related disease, such as amyloid precursor protein in Alzheimer's disease (Luo et al., 1992). Measurement of lifespan forms the basis of studying genetic and environmental effects on ageing in flies. Studies in *Drosophila* formed the preliminary experimental evidence for the free radical theory of ageing and have aided our understanding of the effects of CR on lifespan. The induction of oxidative stress in flies has shown that long-lived mutants are more resistant to oxidative stress than those with a shorter lifespan (Arking et al., 1991). However, studies reporting no increase in oxidative stress in long-lived mutants have formed scientific opposition to the free radical theory of ageing (Force et al., 1995). *D. melanogaster* presents a unique opportunity for studying additional parameters of ageing due to their greater complexity than *C. elegans*. Health span can be easily measured by assessing mobility, sleep patterns and cognitive function in *Drosophila*, parameters too complex to be studied in *C. elegans*. A reduction in locomotor function in *Drosophila* has been associated with ageing (reviewed in (Iliadi and Boulianne, 2010)). Due to its increased complexity *Drosophila* has been utilised as a model system to study the effects of immunosenescence and inflammation in ageing (McCarroll et al., 2004). Flies show increased innate

immune responses with age in a similar manner to humans and have been instrumental in the discovery of dysregulated innate immune signalling in the intestine (Guo et al., 2014). This dysregulation has been associated with increased NF-κB signalling with advancing age resulting in a trade-off between immunity and longevity (Guo et al., 2014, Libert et al., 2006).

1.1.5.2 Murine studies

1.1.5.2.1 Tissue inhibitor of metalloproteinase 3 knock-out (*Timp3$^{-/-}$*) mice

Tissue inhibitor of metalloproteinase 3 (TIMP3) is one of the natural inhibitors of matrix metalloproteinases (MMPs) a group of peptidases involved in degrading the extracellular matrix (ECM). TIMP3 is the only member of the TIMP family which is localised to the ECM and has the widest range of MMP targets. These targets include MMP-1, MMP-2, MMP-3, MMP-7, MMP-9, MMP-13, MMP-14 and MMP-15. TIMP3 forms a complex with MMPs and irreversibly inactivates them by binding to their catalytic region. TIMP3 expression is tightly regulated to the G1 stage of the cell cycle and is involved in processes such as cell cycle progression and cellular senescence (Wick et al., 1994).

Loss of the *TIMP3* gene in humans has been linked to the development of Sorsby's Fundus Dystrophy (SFD) and Pseudoinflammatory Fundus Dystrophy (PFD) which causes symptoms of age-related macular degeneration (AMD). Other than being involved with ECM maintenance, TIMP3 has been shown to modulate angiogenesis by inhibiting vascular endothelial factor binding to its receptor (Qi et al., 2003). This mechanism is involved in the pathogenesis of SFD and PFD. The relationship between TIMP3 and ageing is largely understudied, however TIMP3 expression has been shown to increase with age in most tissues and is associated with AMD in the elderly population (Kamei and Hollyfield, 1999, Macgregor et al., 2009).

The *Timp3$^{-/-}$* mouse model was developed by the Khokha group at the University of Toronto in 2001 (Leco et al., 2001). These mice develop spontaneous air space enlargement in the lung from 2 weeks after birth which progresses with age. This process has been attributed to enhanced degradation of collagen and disorganisation of collagen fibrils in the alveoli (Leco et al., 2001). Ageing of *Timp3$^{-/-}$* mice has been shown to increase the development of arthritis (Sahebjam et al., 2007). Through these disease processes *Timp3$^{-/-}$* mice have been shown to accelerate inflammation as a result of increased pro-inflammatory tumor necrosis factor-alpha (TNF-α) processing by the tumour necrosis factor alpha-converting enzyme (ADAM17) (Sahebjam et al., 2007), as Timp3 acts as an inhibitor of ADAM17. Due to increased processing of TNF-α in the liver, *Timp3$^{-/-}$* mice present with decreased liver regeneration following partial hepatectomy and dysregulated innate immunity characterised

by enhanced TNF-α processing and elevated serum levels of interleukin 6 (IL-6) due to chronic liver inflammation (Mohammed et al., 2004, Smookler et al., 2006).

Female *Timp3*$^{-/-}$ mice bred on a C57BL/6J background, typically display a lifespan of 50 weeks within the laboratory at Southampton compared to a lifespan of 2 years for female wild-type C57BL/6J mice (data not shown). Low-grade chronic inflammation is prevalent in human ageing, age-related disease and chronic inflammatory conditions (reviewed in (Franceschi et al., 2007, Franceschi and Campisi, 2014)). Therefore, *Timp3*$^{-/-}$ mice represent an ideal model for studying inflammation in the context of ageing and the development of age-related diseases.

1.1.5.2.2 Senescence-accelerated mice (SAM) model

The senescence-accelerated mouse (SAM) strains were developed by Takeda *et al.* in 1981. By out-breeding AKR/J mice with another unknown albino mouse strain a series of five senescence prone (SAMP) and three senescence resistant (SAMR) strains were developed (Takeda et al., 1981). SAMP mice are characterised by a tripled senescence score compared to SAMR strains. Senescence scores are based on hair loss, loss of reactivity, increased skin coarseness and lordokyphosis of the spine (Takeda et al., 1981). The SAMP strains have a shortened lifespan of 9.7 months which is 40% shorter than that observed for SAMR strains of 16.3 months (Takeda et al., 1994). Subsequent in-breeding of the SAMP and SAMR strains and out-breeding with other strains led to the development of thirteen SAMP and four SAMR strains by 1997, each carrying their own series of genetic mutations (Takeda et al., 1997). The SAM strains all show different pathobiological phenotypes associated with accelerated ageing. The main three phenotypes observed within each strain are summarised in Table 1.4. Ensuing reports have suggested that SAM strains can now live longer than originally believed due to genetic deviations from the original strains. Studies on SAMP8 mice have been conducted up to 18 months of age (Nakahara et al., 1998). Traditionally SAMR were designed to be utilised as controls for the SAMP strains. However, due to the costs of maintaining SAMR strains, the C57BL/6 strain can be interchanged as a model of normal ageing for SAMP mouse strains (Hasegawa-Ishii et al., 2016, Lok et al., 2013, Teramoto et al., 1995). Very few differences between SAMR1 and C57BL/6 mice have been observed, even in terms of their metabolism (Liu et al., 2017).

Table 1.4   Pathobiological phenotypes observed in senescence-accelerated mouse (SAM) strains (Adapted from (Takeda et al., 1997))

STRAIN	MAIN PHENOTYPES		
SAMP1	Senile amyloidosis	Contracted kidney	Impaired immune response
SAMP2	Senile and secondary amyloidosis	Contracted kidney	Impaired immune response
SAMP3	Degenerative joint disease		
SAMP6	Senile osteoporosis	Secondary amyloidosis	
SAMP7	Lymphoblastic lymphoma	Senile amyloidosis	
SAMP8	Learning and memory deficits	Impaired immune response	
SAMP9	Cataracts	Lymphoblastic lymphoma	Senile amyloidosis
SAMP10	Brain atrophy	Learning and memory deficits	
SAMP11	Contracted kidney	Senile amyloidosis	
SAMR1	Lymphoma	Histiocytic sarcoma	Ovarian cyst
SAMR4	Lymphoma	Histiocytic sarcoma	
SAMR5	Colitis		

SAM strains are extremely useful tools for conducting ageing research as they allow for studies of normal ageing, senescence and pathogenesis of age-related disease. The SAMP6 and SAMP8 strains are one of the most utilised strains in ageing research, as they recapitulate age-related diseases observed in humans. This includes osteoporosis in the case of SAMP6 mice and sarcopenia and Alzheimer's disease in the SAMP8 strain (Chang et al., 2019, Azuma et al., 2018, Akiguchi et al., 2017). Indicators of sarcopenia include decreased gastrocnemius muscle mass and cross-sectional area compared to SAMR1 mice, alongside decreased grip strength (Chang et al., 2019). Other than senescence the SAMP mouse strains are subject to other factors which accelerate ageing including decreased autophagy, inflammation, oxidative stress and mitochondrial dysfunction (Morley et al., 2012, Ma et al., 2011, Eckert et al., 2013, Jiang et al., 2014).

Due to observations of impaired immune responses in SAMP strains, these animals are regularly used for studying ageing of the immune system. Even the SAMR1 strain shows reductions in splenocyte proliferation, decreased proportions of helper T cells, suppressor T cells and B cells with age (Wang et al., 2016). The immunosenescence observed within these mice influences the

cytokine profile, switching towards a pro-inflammatory environment at 24 months of age compared to 12 months of age. This modulation of the pro-inflammatory cytokine profile with age has been observed in SAMP8 mice as a result of altered macrophage polarisation (Karuppagounder et al., 2016). The appearance of immune system dysfunction has been linked to increased ROS production and altered nutrient sensing pathway signalling in the bone marrow of SAMP10 mice (Li et al., 2016). Decreases in the number of naïve B cells and increased lymphocyte recruitment and activation have been observed in SAMP8 mice with age (Cortegano et al., 2017, Miró Martí et al., 2017).

1.1.5.3 Human studies

Longitudinal studies of human ageing are cumbersome, could take up to 120 years to complete and are hampered by excessive drop-out rates. Because of these issues, studies covering the entirety of the human life course are unpractical. Several countries have begun developing their own short-term longitudinal studies following the elderly population. These include the Singapore Longitudinal Ageing Study (SLAS), English Longitudinal Study of Ageing (ELSA), Berlin Ageing Study, United States Normative Ageing Study and Netherlands Maastrict Ageing Study (Baltes and Mayer, 2001, Bell et al., 1972, Jolles et al., 1995, Lu et al., 2016, Steptoe et al., 2012). These studies have been able to look at associations between the hallmarks of ageing and the development of age-related disease in this population. The main findings from the SLAS and ELSA studies are:

- **Singapore longitudinal ageing study (SLAS):** The SLAS follows over 6,000 participants from 5 districts in the South East region of Singapore aged 55 years and over which commenced in 2003. This study has implicated type 2 diabetes and metabolic syndrome in the development of mild cognitive impairment and the progression of dementia (Ng et al., 2016, Feng et al., 2013, Ho et al., 2008). Social factors have been investigated using the SLAS cohort. Tze Pin Ng *et al.* have shown that living in solitude significantly increases mortality risk independent of health status (Ng et al., 2015b). Work at the Singapore Immunology Network (SIgN) has linked T cell senescence and inflammation with both frailty and cognitive decline within the elderly population (Ng et al., 2015a, Lu et al., 2016, Gao et al., 2016). Other groups investigating frailty in the SLAS cohort have found relationships with age, type 2 diabetes, arthritis, poor perceptions of health and C reactive protein, a marker of inflammation (Cheong et al., 2019). Antioxidant vitamins A, C and E have been linked to increased health within ageing Singaporeans (Ng et al., 2014).

- **English longitudinal study of ageing (ELSA):** The ELSA consists of a representative multi-centre cohort of over 11,000 English residents aged 50 years or over which commenced in

2002. This study has been instrumental in linking healthy ageing with increased physical activity. An 8 year study following 3,454 ELSA participants, moderate or vigorous activity at least once per week was associated with healthy ageing as measured by disease status, physical impairment, depression and cognitive impairment (Hamer et al., 2014). Those who implemented an exercise regime or remained active during the course of the study were found to have improved health parameters. Similar relationships to those observed in the SLAS have been found in the ELSA cohort regarding social isolation, cognitive function and cardiovascular disease risk (Shankar et al., 2013, Valtorta et al., 2018). Associations between quality of life and age have been observed within ELSA participants which are dependent on psychological, socioeconomic and health parameters (Zaninotto et al., 2009).

As an alternative model normal human cells can be aged using cell culture systems. Human cells can typically divide up to 50 times before reaching the Hayflick limit and undergoing senescence (Hayflick and Moorhead, 1961). Non-invasive techniques for isolating cells from the skin and blood are useful in generating short-term ageing studies of specific cell types. Studies of ageing of human fibroblasts using these systems are the most common in ageing research. Early studies aided in identifying telomere length, telomerase activity and dysregulated proteostasis as hallmarks of ageing (Goldstein et al., 1976, Allsopp et al., 1992). Recent progress has been made in identifying altered transcriptomes and proteomes in aged cells *in vitro* as well as the induction of stress responses (Fleischer et al., 2018, Tan et al., 2018, Rattan et al., 2018). However, cell culture techniques do not fully recapitulate the complexity of the ageing process seen in human systems.

1.2   Cellular metabolism

Metabolism within organisms has three main goals. These are to convert fuel into energy for cellular processes, convert fuel to metabolites for generating proteins, lipids and nucleic acid for cellular growth and to eliminate metabolic waste. At the cellular level metabolism consists of both energy-releasing catabolic and energy-consuming anabolic processes which break down and synthesise metabolic components respectively. These systems are organised into a multitude of complex metabolic pathways which run in parallel and feed into one another. Catabolic processes often release energy which can be used for anabolism and vice-versa. All of these pathways require a series of enzymes which regulate the flux of metabolites through these pathways and sustain metabolism within a variety of microenvironments. This allows switching between metabolic pathways depending on nutrient availability.

The components involved in metabolism have a variety of roles within the cell. Amino acids which join together to make proteins form enzymes which are central for metabolism, generate the

cytoskeleton and are important in cellular signalling, immune responses and the cell cycle. Lipids make up both intracellular and extracellular biological membranes, whilst carbohydrates store and transport energy. Finally, nucleotides are involved in generating new genetic material during division and are required for gene expression.

1.2.1 Mitochondria

Mitochondria are known as the powerhouse of the cell as they produce the majority of energy required for cellular processes, this energy is called adenosine triphosphate (ATP). In order to produce energy intermediates derived from the catabolism of carbohydrates, proteins and lipids are fed into the Krebs cycle, also known as the citric acid or tricarboxylic acid cycle. This aspect of metabolism occurs within the matrix of the mitochondrion and was first discovered by Hans Krebs and William Johnson in 1937 (Krebs and Johnson, 1937). The Krebs cycle is summarised in Figure 1.6. The aim of the Krebs cycle is conversion of oxidised nicotinamide adenine dinucleotide (NAD+) into its reduced form (NADH). Alongside NADH the Krebs cycle produces the energy-containing compounds guanosine-5'-triphosphate (GTP) and flavin adenine dinucleotide hydroquinone ($FADH_2$). This cycle requires the input of acetyl-CoA generated by glycolysis, proteolysis and the oxidation of fatty acids as discussed in Section 1.2.2 Catabolism. The Krebs cycle continuously oxidises acetyl-CoA during the cycle generating CO_2 as a waste product. The oxidation of acetyl-CoA is performed by eight enzymes resulting in the production of CO_2 and water. The reaction catalysed by each of Krebs enzymes has been reviewed extensively elsewhere (Kornberg, 2000, Akram, 2014). NADH and $FADH_2$ are utilised by the electron transport chain (ETC) in order to fuel ATP production.

The ETC utilises a series of reactions to produce the majority of cellular ATP through a process called oxidative phosphorylation (OXPHOS). The inner mitochondrial membrane acts as the site of ETC and utilises proton (H^+) pumping into the intermembrane space as shown in Figure 1.7. H^+ pumping is accomplished by a series of reduction and oxidation reactions that transfer electrons from Complex I to Complex IV of the ETC. Details of the ETC have been reviewed extensively elsewhere (Guo et al., 2018, Zhao et al., 2019). Briefly, Complexes I and II accept electrons from NADH and $FADH_2$ respectively and pass them sequentially down the ETC to coenzyme Q, Complex III, Cytochrome *c* and Complex IV. The electrochemical gradient produced as a result of H^+ pumping, known as mitochondrial membrane potential, drives the synthesis of ATP by ATP synthase (ATPase; Complex V). Due to electron leakage the ETC is the main source of superoxide free-radical generation within the cell. This leakage has previously been linked to the biology of ageing as discussed in Section 1.1.4.1 Theories of ageing.
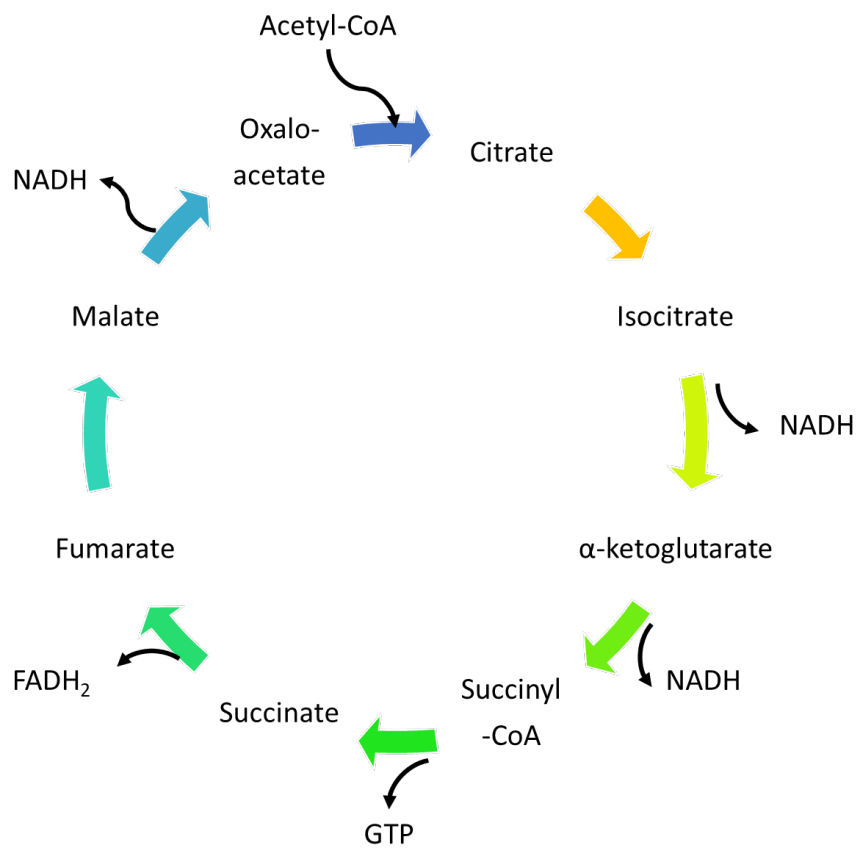
Figure 1.6   The Krebs cycle oxidises acetyl-CoA derived from carbohydrates, fats and proteins into reduced nicotinamide adenine dinucleotide (NADH), guanosine-5'-triphosphate (GTP) and flavin adenine dinucleotide hydroquinone (FADH$_2$) for use in the electron transport chain
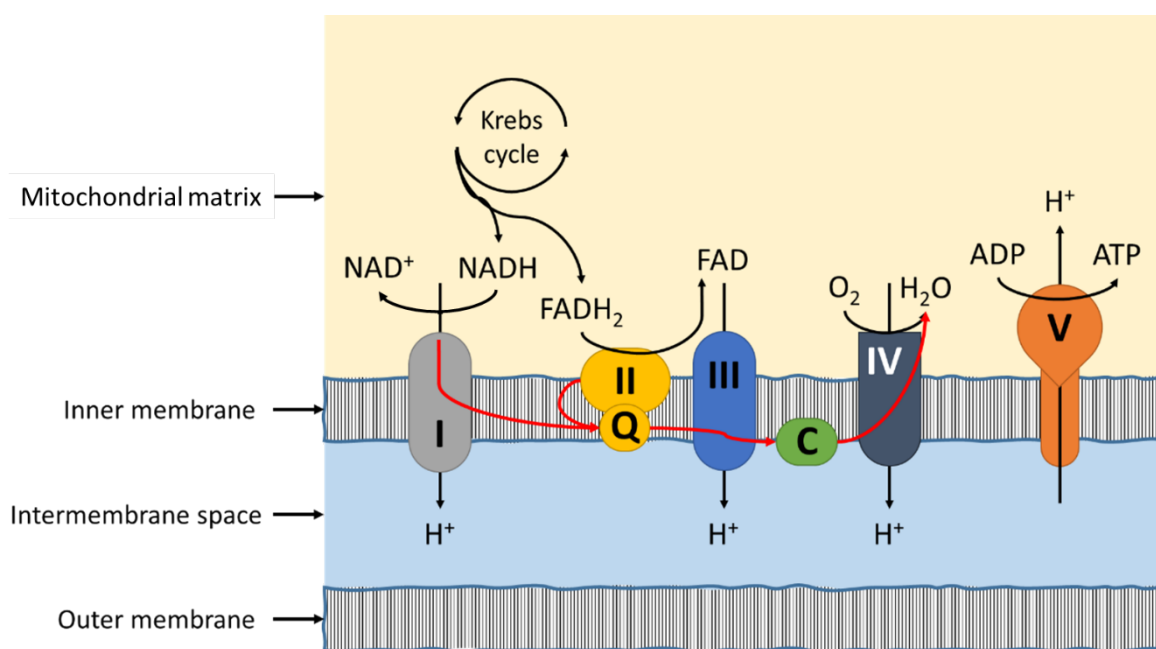
Figure 1.7   Components of the electron transport chain showing the location of ETC complexes I-V on the inner mitochondrial membrane. Intermediates derived from the Krebs cycle buffer the transfer of protons (H^+) into the intermembrane space. Red arrows show the flow of electrons through complexes I-IV. (Q=Coenzyme Q; C=Cytochrome c)

1.2.2   Catabolism

The breakdown of glucose, proteins and fats produces ATP through catabolic processes. The transport and breakdown of each of these macronutrients is described in detail below.

- **Glycolysis:** Glucose is transported into the cell by transmembrane proteins called glucose transporters (GLUTs). There are several classes of GLUTs, however the most well characterised and highly expressed are GLUT1-4. All cells express GLUTs however the most well-conserved transporter is GLUT1 which sustains basal glucose uptake in response to extracellular glucose availability (Mueckler et al., 1985, Galochkina et al., 2019). After transport into the cell glucose is converted into glucose-6-phosphate by hexokinase thus beginning the glycolytic pathway summarised in Figure 1.8. Briefly, glucose-6-phosphate is converted to pyruvate through a series of chemical reactions. Pyruvate is then transported into the mitochondria and converted to Acetyl-CoA by pyruvate dehydrogenase for use in the Krebs cycle (Figure 1.9). Glycolysis on its own produces 2 molecules of ATP per glucose molecule and can produce energy independently of OXPHOS in a process called aerobic glycolysis.

Hexokinase	• Glucose-6-phosphate
Glucose-6-phosphate isomerase	• Fructose-6-phosphate
Phosphofructokinase-1	• Fructose 1,6-biphosphate
Fructose-biphosphate aldolase	• Dihydroxy-acetone phosphate
Triosephosphate isomerase	• 2x Glyceraldehyde 3-phosphate
Glyceraldehyde-3-phosphate dehydrogenase	• 2x 1,3-Biphospho-glycerate
Phosphoglycerate kinase	• 2x 3-Phospho-glycerate
Phosphoglycerate mutase	• 2-Phospho-glycerate
Phosphopyruvate hydratase	• Phospho-enolpyruvate
Pyruvate kinase	• Pyruvate

Figure 1.8   Reactions in the glycolytic pathway showing the enzymes (right panel) and their products (left panel) which is used to fuel the next step
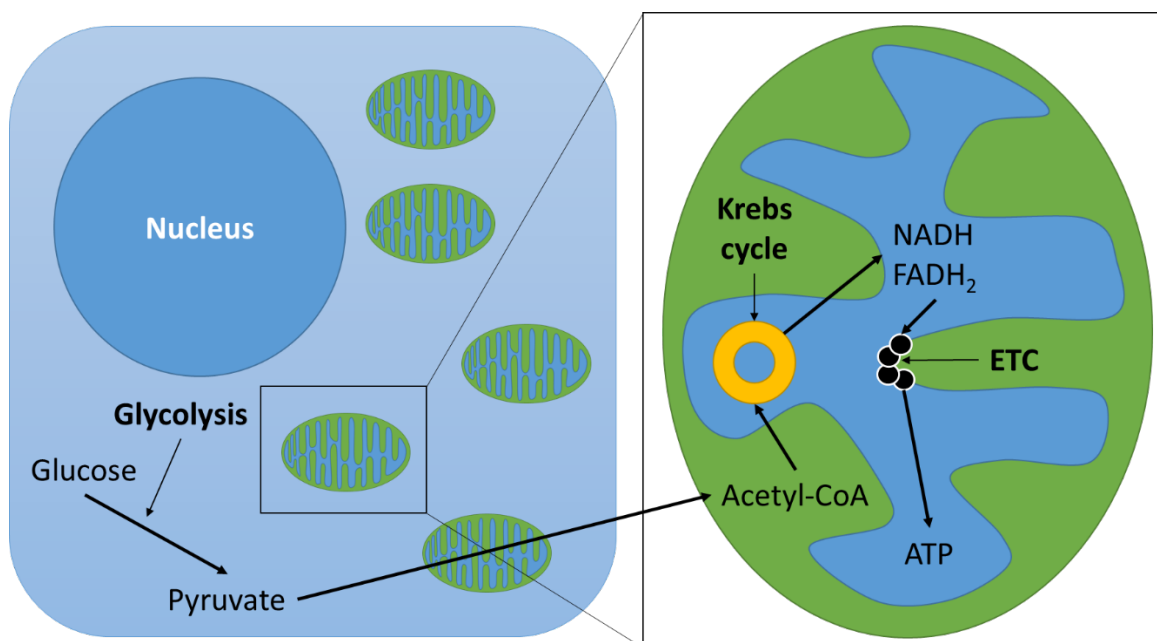
Figure 1.9   Role of glucose in fuelling mitochondrial ATP production integrating glycolysis to produce pyruvate, conversion to acetyl-coA in the mitochondria and its use in the Krebs cycle to produce NADH and $FADH_2$ fuelling the electron transport chain

- **Proteins:** Proteins are catabolised by specific enzymes called proteases which break proteins into their constituent amino acids. Glucogenic amino acids and ketogenic amino acids can be synthesised into pyruvate molecules and acetyl-CoA respectively to fuel the Krebs cycle (Munro, 2012). Glucogenic amino acids include alanine, cysteine, glycine, serine and threonine; whilst ketogenic amino acids such as phenylalanine, leucine and lysine undergo ketone oxidation. Alternately metabolic intermediates from other amino acids can enter the Krebs cycle directly. For examples, glutamine and tyrosine aid synthesis of α-ketoglutarate and fumarate respectively. The role of protein metabolism in ageing has been reviewed recently (Soultoukis and Partridge, 2016).

- **Fatty acids:** The catabolism of fatty acids is performed in a process termed fatty acid oxidation or β-oxidation (Schulz, 1991). β-oxidation generates acetyl-CoA for entry into the Krebs cycle as well as $FADH_2$ and NADH intermediates to drive the ETC. Fatty acids are typically oxidised within the mitochondria, however long chain fatty acids can be metabolised in peroxisomes. Fatty acids are transported into the cell using specific transport proteins called solute carriers. Once inside the cell, fats must be taken up by the mitochondria which involves carnitine shuttles. The main carnitine shuttle used to transport fatty acids into the mitochondria is carnitine palmitoyltransferase 1 which localises to both the inner and outer mitochondrial membranes (Schlaepfer et al., 2014).

1.2.3   Mitochondria and ageing

"The accumulation of dysfunctional mitochondria has been implicated in ageing, but a deeper understanding of mitochondrial dynamics and mitophagy during ageing is missing"

(Rana et al., 2017)

Mitochondrial dysfunction has been hailed as both a marker and foundation for ageing for many years. However, mild mitochondrial distress can have beneficial effects on longevity in model organisms *Drosophila melanogaster* (Owusu-Ansah et al., 2013, Copeland et al., 2009), *Caenorhabditis elegans* (Dillin et al., 2002, Liu et al., 2005b) and *Saccharomyces cerevisiae* (Kirchman et al., 1999), through the process of mitohormesis. Therefore, the current role for mitochondrial dysfunction in ageing is under debate. Here recent research into the varying roles of mitochondria in ageing will be examined, from their life-hindering to life-extending effects and their influence on health span.

Inhibition of glycolysis by 2-deoxy-D-glucose (2DG) treatment or glucose withdrawal, impacts upon the lifespan of *C. elegans*. By increasing the reliance of these organisms on mitochondrial respiration and β-oxidation by activating the metabolic regulator AMPK, the lifespan of *C. elegans* was increased by transiently increasing ROS production and oxidative stress. Surprisingly, pre-treatment of *C. elegans* with anti-oxidants prior to 2DG treatment, diminished the extension of lifespan. This highlights the fine balance between mitochondrial stress and anti-oxidant capacity. This finding has been recently observed in *D. melanogaster* (Owusu-Ansah et al., 2013). Independently of their ability to produce ROS, which may both help and hinder ageing, mitochondrial dysfunction can contribute to the ageing process through a variety of mechanisms. These include: increasing apoptotic signalling, triggering inflammation and impacting on cellular signalling (reviewed in (López-Otín et al., 2013)).

Ageing-related diseases such as cardiovascular disease can have a profound effect on the metabolism of distant organs. For example, Derlet *et al.* (Derlet et al., 2016) studied the effect of cardiac health on the metabolism of bone marrow mononuclear cells (BMC), which have recently been introduced as a pioneering treatment for chronic heart failure. Assessing BMC in healthy patients, those with acute myocardial infarction and chronic heart failure, showed that BMC from patients in cardiac failure have significantly reduced basal and maximal respiration compared to those from healthy subjects alongside reduced colony formation. Concurrently, BMC derived from patients following acute myocardial infarction showed increased basal and maximal rates of glycolysis compared to healthy controls (Derlet et al., 2016).

Whilst the life extending effects of CR have been well-studied, the effects of CR on health span extension are less well-known although overall CR appears to attenuate the onset of age-related disease. For example, McKiernan *et al* and Colman *et al* have shown that CR increases disease-free health span in rhesus monkeys, delaying the onset of sarcopenia (muscle wastage) and other age-related diseases (Colman et al., 2009, McKiernan et al., 2011, McKiernan et al., 2012). CR also reduced the incidence of diabetes, cancer, cardiovascular disease and neurodegenerative disease (Colman et al., 2009). Strikingly, no animals under CR developed diabetes or pre-diabetic symptoms through-out Colman *et al*'s longitudinal study, and showed consistent benefits to metabolic function (Colman et al., 2009). Defects in mitochondrial function were observed from mid-life in the vastus lateralis of these rhesus monkeys prior to the onset of sarcopenia, an effect reversed by CR (Pugh et al., 2013). Overall, rhesus monkeys were shown to have 3 times higher rate of death from an age-related cause when fed a normal diet compared to those under CR.

1.3   The immune system, immunometabolism and ageing

The immune system protects against disease by responding to pathogens such as bacteria, viruses and parasites and removing cancerous cells. In order to protect against disease, the immune system must first be able to discriminate between these pathogens and the organisms own healthy cells. There are two main arms of the immune response: the innate and adaptive systems, which work in synergy to neutralise pathogens. The innate immune system response to pathogens is non-specific and is conserved within many organisms, whilst the adaptive immune response is pathogen-specific and found only in vertebrates. In this section, cells of the immune system and their immunometabolism during ageing will be discussed. These cells are summarised in Figure 1.10 (Metcalf, 2007). Increased susceptibility to infection, autoimmunity and vaccine failure in the elderly have been linked to deterioration and exhaustion of the immune system with age (Martelli, 2017). These changes will be introduced in this section alongside their contribution towards immune-senescence in the elderly. Cells contained within both the innate and adaptive arms of the immune system will be discussed, with a focus on the cell types studied within this work.
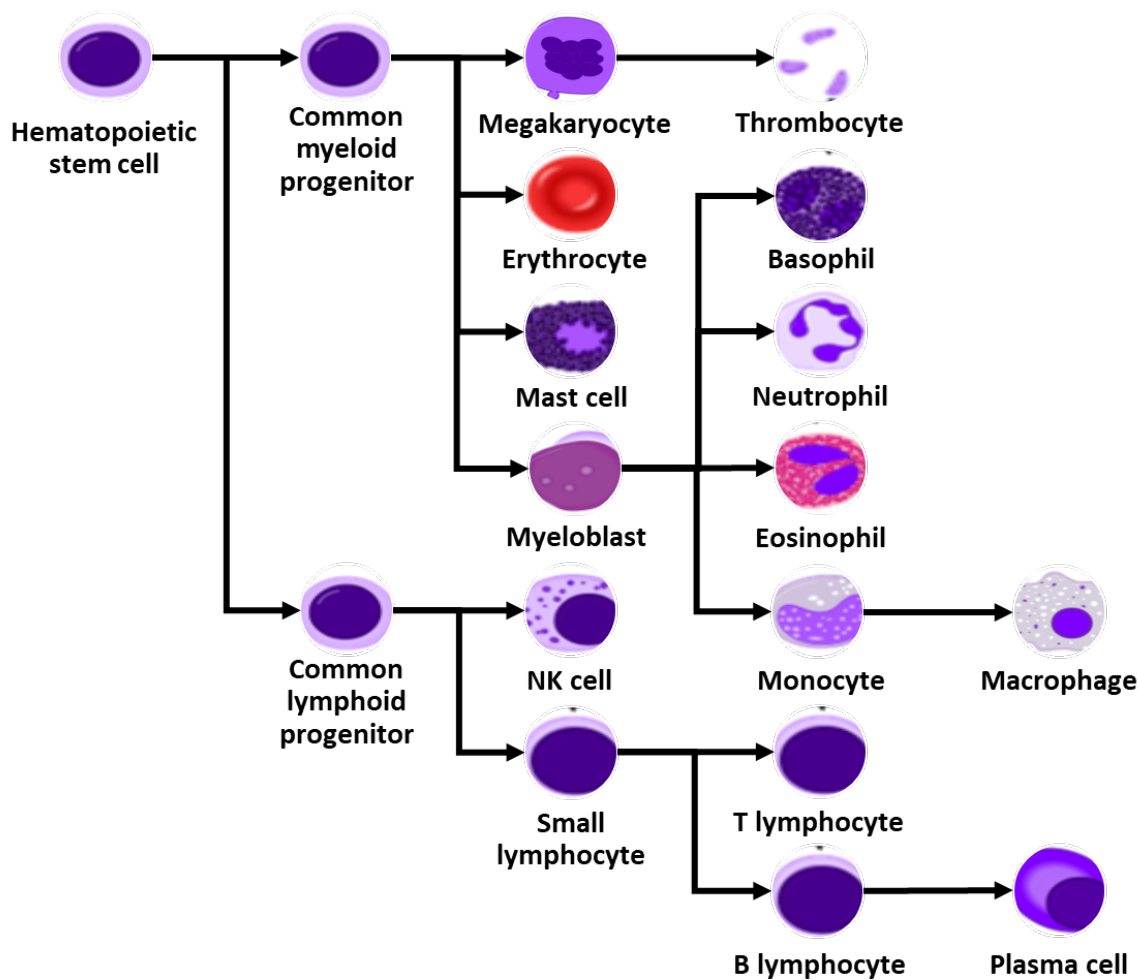
Figure 1.10   Immune cell lineages from hematopoietic stem cell to common myeloid and lymphoid progenitors to form cells of the innate and adaptive immune systems (adapted from (Metcalf, 2007))

Following activation immune cells require high levels of anabolism in order to produce inflammatory mediators, such as cytokines, and for proliferation in the case of the adaptive immune system. In order to achieve this high level of anabolism, immune cells have been shown to undergo the Warburg effect. This was originally attributed cancer cells which require high levels of anabolism to grow and proliferate (Warburg, 1956). The Warburg effect describes the predominant use of glycolysis by cancer cells where the end-product pyruvate is not used to produce acetyl-CoA for the Krebs cycle to fuel OXPHOS. Instead pyruvate is metabolised to lactate. This effect occurs despite the presence of sufficient oxygen and is commonly called aerobic glycolysis. The use of glycolysis in this manner allows cells to produce key intermediates for the pentose phosphate pathway (PPP) and nucleotide biosynthesis. The use of aerobic glycolysis by the immune system has been well-reviewed within the past decade and immunometabolism has become a hot topic within the immunology community (Ganeshan and Chawla, 2014, Jung et al., 2019). Only recently has the role of immunometabolism been contemplated in health, ageing and disease.

1.3.1 Innate immune system

The innate immune response provides the first-line defence against pathogens which enter the body. Cells contained within the innate arm of the immune response typically identify pathogens using pattern recognition receptors (PRRs) on their cell surface. PRRs detect both pathogen-associated molecular patterns (PAMPs) and damage-associated molecular patterns (DAMPs) that are expressed on the surface of pathogens or released from damaged or dead cells respectively. By identifying PAMPs and DAMPs the innate immune system can clear pathogens and damaged cells from the organism. The innate immune system is made up of many different cell types, each of which will be discussed in turn.

1.3.1.1 Monocytes

Monocytes are derived from bone marrow precursors and circulate in the blood (Figure 1.10). A large pool of monocytes resides within the spleen, which migrate towards sites of inflammation following infection (Swirski et al., 2009). Monocytes patrol the blood looking for signs of infection and have the ability to cross into tissue and differentiate into tissue-resident macrophages. Monocyte subsets can be distinguished by their cell surface expression of Ly6C in mice and the expression of CD14 and CD16 in humans. Ly6C+ or CD14+ monocytes, known as classical monocytes, represent those that are able to cross the epithelium whilst Ly6C- or CD16+ monocytes, known as non-classical monocytes, remain within the blood (Ingersoll et al., 2010). There is however a third subset of monocytes which express both CD16 and CD14 in humans, these have been termed intermediate monocytes.

Maturation of monocytes is induced by tissue alterations at the site of infection which is often accompanied by increased inflammation (Jakubzick et al., 2017). Following entry into the tissue monocytes upregulate C-C chemokine receptor type 7 (CCR7) and major histocompatibility complex (MHC) Class II molecules to facilitate migration (Zigmond et al., 2012, Sponaas et al., 2009). Following maturation into macrophages, these cells can engulf microorganisms and clear cellular debris from infected tissue. Upon activation macrophages release high levels of the pro-inflammatory cytokines IL-1β, IL-6, TNF-α and nitric oxide (NO) (Serbina et al., 2003, Kim et al., 2011). These TNF-α and NO-producing macrophages are involved in clearing infected tissues (reviewed in (Shi and Pamer, 2011)). Following pathogen clearance, it has been shown that pro-inflammatory monocytes can switch towards an anti-inflammatory phenotype to aid tissue repair (Arnold et al., 2007). Anti-inflammatory monocytes release IL-10 and transforming growth factor beta (TGF-β).

Chapter 1

Monocytes have the ability to induce adaptive immune responses by acting as antigen-presenting cells (APCs) due to their ability to differentiate into monocyte-derived dendritic cells (DCs) under certain conditions (Jakubzick et al., 2013, Leon et al., 2007). Monocyte-derived DCs have the ability to migrate to the lymph nodes following antigen uptake due to their CCR7 expression (Tamoutounour et al., 2013). Once in the lymph node these cells have been shown to induce both helper CD4+ T cell responses and cytotoxic CD8+ T cell responses in a TNF-α-dependent manner, eliciting increased interferon gamma (IFNγ) responses from these cells (Langlet et al., 2012, Flores-Langarica et al., 2011, Cheong et al., 2010, Kuhn et al., 2015).

During the differentiation of monocytes to macrophages and monocyte-derived DCs, new mitochondria are created in a process called mitochondrial biogenesis (Zaccagnino et al., 2012, Daigneault et al., 2010, Sonoda et al., 2007). Following stimulation monocytes and macrophages both use glucose as the main source of energy production (Ganeshan and Chawla, 2014, Newsholme et al., 1986). Markers of glycolysis are increased three-fold in monocytes stimulated with *Mycobacterium tuberculosis*, substantially decreasing the oxidative to glycolytic metabolic ratio (Lachmandas et al., 2016). This glycolytic switch is regulated by mTOR activity. Production of TNF-α within human monocytes and macrophages has recently been shown to be dependent on glycolytic metabolism (Millet et al., 2016). Interestingly, ROS generation by mitochondria plays a large role in the killing of intracellular pathogens in macrophages (Sonoda et al., 2007). Following phagocytosis mitochondria are recruited to the phagolysosome and contribute to bactericidal activity following toll-like receptor (TLR) signalling (West et al., 2011, Arnoult et al., 2009). Mitochondrial ROS production is required for the maturation of inflammasomes in macrophages, involved in the production and release of IL-1β (Zhou et al., 2011). Whilst the pro-inflammatory action of macrophages and monocytes is dependent on glycolytic metabolism, it would appear that anti-inflammatory actions are mediated by fatty acid oxidation (FAO) (Vats et al., 2006, Odegaard et al., 2007, Mills and O'Neill, 2016).

Increased numbers of non-classical monocytes have previously been shown with age (Pence and Yarbro, 2018, Hearps et al., 2012). Simultaneous increases in intermediate monocytes have been detected with age in humans, although not within all studies (Pence and Yarbro, 2018, Hearps et al., 2012). In line with this data, ageing is associated with increased markers of innate immune activation including soluble CD163 and the chemokine ligand (CXCL)-10 in plasma. Non-classical monocytes have been shown to produce more pro-inflammatory cytokines following stimulation and as a result of senescence, so increased numbers may be responsible in part for the increased levels of IL-6 and TNF-α observed with age (Cros et al., 2010, Bruunsgaard et al., 2003, Leng et al., 2011, Ong et al., 2018). Concurrently numbers of classical monocytes have been shown to decrease with age through linear regression analysis (Hearps et al., 2012).

In terms of monocyte function, ageing has been shown to both impair and enhance pro-inflammatory cytokine production in response to TLR1/2 and TLR4 stimulation respectively (Hearps et al., 2012, Van Duin et al., 2007, Nyugen et al., 2010, Cros et al., 2010). This suggests that altered monocyte function with age is specific to the source of stimulation. Enhanced production of pro-inflammatory cytokines following TLR4 stimulation was not associated with increased phagocytosis however, which was shown to be reduced with age in classical and intermediate monocytes (Hearps et al., 2012). Ageing has not been shown to affect the phagocytotic ability of monocyte-derived DCs however, particularly in regards to *Candida albicans* (Nascimento et al., 2015).

The involvement of monocytes in health and disease has been reviewed extensively elsewhere (Karlmark et al., 2012, Narasimhan et al., 2019). However, the relationships between monocytes and age-related disease such as atherosclerosis, Alzheimer's disease and cancer progression should be noted. Both non-classical and intermediate monocytes have previously been implicated in the development of cardiovascular disease and the autoimmunity of rheumatoid arthritis (Shantsila et al., 2011, Tsukamoto et al., 2017). Some effects of the ageing process on monocyte metabolism have previously been observed. For example, Pence and Yarbro found that classical monocytes derived from individuals aged 60-80 years had reduced mitochondrial maximal respiratory capacity and spare capacity than young controls aged 18-35 years (Pence and Yarbro, 2018). No alterations in glycolytic metabolism were observed with age in this study. Classical monocytes have been shown to retain mitochondrial mass and membrane potential with age in human studies (Pence and Yarbro, 2018), however their transcriptional profile has been shown to be altered. Reynolds *et al* found that both mitochondrial ribosomal and oxidative genes were differentially expressed with ageing in classical monocytes (Reynolds et al., 2015).

1.3.1.2 Neutrophils

Neutrophils are the most abundant type of phagocyte and embody up to 70% of circulating leukocytes (Dancey et al., 1976). Like monocytes and the majority of white blood cells, neutrophils develop in the bone marrow before entering the circulation. The main functions of neutrophils are phagocytosis and degranulation in order to kill microorganisms, however they produce cytokines and are involved with the resolution of inflammation (Nauseef and Borregaard, 2014, Tecchio and Cassatella, 2016, Greenlee-Wacker, 2016). Neutrophils are characterised by their nuclei, which have a lobulated morphology, as well as their cell surface expression of chemokine receptor (CXCR)2 and TLR4 (Rosales, 2018). Mature neutrophils contain antimicrobial enzymes stored in the form of granules which degrade and kill invading pathogens (Hager et al., 2010).

Following infection, neutrophils exit the circulation and enter tissues during activation by a series of integrins (Hajishengallis and Chavakis, 2013). Once in the tissue neutrophils mobilise their

granules which contain NADPH oxidase and other associated factors to clear bacterial and fungal infections. In order to mobilise their neutrophils must first be activated by PAMPs through their PRRs and phagocytose the pathogen. Granules are then delivered to the phagosome (Ley et al., 2018). Neutrophils have the ability to activate macrophages through their expression of TLR2-5/7-9 (Tsuda et al., 2004). Following pathogenic clearance, neutrophils undergo apoptosis and are cleared by surrounding macrophages. This triggers an anti-inflammatory response involving IL-23 and IL-17 leading to the resolution of inflammation (Stark et al., 2005).

According to research neutrophils contain very few mitochondria and derive the majority of their energy from glycolysis (Rodríguez-Espinosa et al., 2015). Following stimulation neutrophils dramatically upregulate expression of GLUT1 and increase their rate of glycolysis (Rodríguez-Espinosa et al., 2015). The formation of neutrophil extracellular traps is entirely glucose dependent, requires mTOR signalling and flux through the PPP (McInturff et al., 2012, Azevedo et al., 2015). The PPP is involved in the production of NADPH for the activity of NADPH oxidase, rendering mitochondria negligible in supporting neutrophil functions (Azevedo et al., 2015). However, neutrophil differentiation in the bone marrow requires the generation of fatty acids (Riffelmacher et al., 2017). These fatty acids support mitochondrial respiration and ATP production, proving the reliance of these cells on FAO during their generation.

Research has found that non-stimulated release of ROS and NO can be up to 38% higher in human neutrophils in individuals aged 65 years and over compared to younger controls (Nogueira-Neto et al., 2016). As CD11b is upregulated on the surface of neutrophils with age, which homes neutrophils to the vasculature, it is believed that increased ROS production by these cells may contribute towards vasculature damage and the development of atherosclerosis. In fact, increased oxidative stress and neutrophils numbers have already been observed in atherosclerotic plaques of aged mice (Wang et al., 2017). Analysis of neutrophils derived from aged individuals with increased frailty scores has suggested that neutrophils exist in a state of basal activation and show defects in maturation (Verschoor et al., 2015). This effect is thought to occur due to increased circulating levels of TNF-α with age associated with inflamm-ageing.

1.3.1.3 Dendritic cells (DCs)

After development in the bone marrow and exit into the circulation, DCs home to tissues where they have the potential for high phagocytic activity (Banchereau et al., 2000). DCs are recruited to sites of inflammation much the same as other immune cells, by the production of chemokines (McWilliam et al., 1996, McWilliam et al., 1994). At this stage DCs are referred to as immature, even as they phagocytose pathogens in order to capture antigen. Following antigen capture DCs migrate to the lymph nodes and present their antigen to CD4+ helper T cells where they mature. It is through

this purpose that DCs are referred to as APCs. DCs express high levels of MHC Class II, CD80 and CD86, which are required for engaging T cell responses (Steinman et al., 1999, Dudek et al., 2013).

Two types of DC exist within the circulation, plasmacytoid DCs (pDC) which mainly process viral particles and myeloid DCs (mDC) (Villani et al., 2017, Guilliams et al., 2016). pDCs are defined by CD141 and CD8a expression in humans and mice respectively, whilst mDCs are identified by CD1c and CD11c expression. Many subdivisions have recently been identified within the pDC and mDC populations but are beyond the scope of this study (Villani et al., 2017).

Activation of DCs through their TLRs induces a switch from OXPHOS to glycolysis (Krawczyk et al., 2010, Pantel et al., 2014). Immature DCs typically undergo active OXPHOS whilst mature DCs switch to glycolysis following pathogen sensing (Wculek et al., 2019). Monocyte-derived DCs show increased mitochondrial mass, higher ATP production and higher oxygen consumption rate (OCR) than monocytes (Zaccagnino et al., 2012). This has been observed in differentiated pDCs and mDCs (Krawczyk et al., 2010, Kratchmarov et al., 2018, Chougnet et al., 2015). Hypoxia-inducible factor-1 alpha (HIF-1α) is a key regulator of glycolytic metabolism in DCs downstream of the phosphoinositide 3-kinase (PI3K)/mTOR pathway, which induces both glycolytic and oxidative metabolic pathways (Wculek et al., 2019, Sathaliyawala et al., 2010).

The differentiation of DCs from monocytes involves the PI3K/mTOR pathway and the control of lipid metabolism, causing the activation of anabolic fatty acid synthesis (FAS) pathways (Szatmari et al., 2007, Gogolak et al., 2006). Simultaneously the activation of pDCs and mDCs following pathogen sensing requires FAS mediated by upregulation of glycolytic pathways and metabolic energy into the PPP (Scheffler et al., 2014, O'neill and Pearce, 2016, Thwe et al., 2017). The production of NO is increased using these pathways which dampens metabolic flux through the Krebs cycle and ETC, supporting the production of more NO, ROS and pro-inflammatory DC functions (Ryan and O'Neill, 2017, Everts et al., 2012). Disruption of the glycolytic pathway in DCs impairs their ability to engage CD4+ and CD8+ T cell responses (Everts et al., 2014, de Lima Thomaz et al., 2018).

DCs change their inflammatory profile with age, contributing towards a pro-inflammatory environment (Agrawal et al., 2017). A decrease in the number of pDCs has previously been observed with age whilst mDC numbers remain stable (Jing et al., 2009, Panda et al., 2010). However, both the mDC and pDC subsets have been reported to show functional defects with age (Panda et al., 2010). pDCs show a decrease in IFNγ following stimulation by west nile virus and influenza virus (Qian et al., 2011, Sridharan et al., 2011, Jing et al., 2009). On the other hand, mDCs show significant reductions in TNF-α, IL-6 and IL-12 production following stimulation with TLR agonists (Panda et al., 2010, Della Bella et al., 2007). The ability of DCs to engage T cell responses is decreased with age. Following DC stimulation, T cells from elderly individuals show reduced production of IFNγ and

Granzyme B (GZB) from CD4+ and CD8+ T cells respectively (Prakash et al., 2014, Briceño et al., 2016). Previous research has linked this age-related dysfunction to mitochondrial dysfunction in humans, reflected in reduced mitochondrial membrane potential, ATP production and OXPHOS, alongside increased ROS production (Chougnet et al., 2015).

1.3.1.4 Basophils and eosinophils

Basophils and eosinophils exist in low numbers in the circulation, however these cell arise in the bone marrow and exist in higher numbers in the spleen (Uciechowski and Rink, 2018). Basophils are known for their role in allergic responses, whilst eosinophils are involved in parasitic defence as well as allergic responses.

The granules contained within basophils contain high levels of histamine which is released in response to Immunoglobulin (Ig)E and TLR2/4 signalling (Steiner et al., 2016, Ishizaka et al., 1970, Sabroe et al., 2002). IgE stimulation causes signalling through the PI3K pathway, resulting in the production of a number of pro-inflammatory cytokines in response to allergic pathogens including IL-4, IL-13, IL-6 and TNF-α (Mukai et al., 2005, Kepley et al., 1998). Basophils are involved in mounting T helper 2 (Th2) cell responses to infection by generating IL-4 and IL-13 (van Beek et al., 2013, Moore et al., 2009). Basophil activation has been implicated in B cell responses to infection, including *Streptococcus* (Chen et al., 2009, Denzel et al., 2008). IL-5 is a key cytokine for the proliferation and priming of eosinophils (Wen and Rothenberg, 2016). Eosinophils are recruited to sites of infection by local Th2 cells which produce both IL-5 and IL-13 chemokines (Munitz et al., 2008). Eosinophils then induce further Th2 and effector T cell recruitment to the site (Jacobsen et al., 2008, Shen et al., 2003). Like basophils, eosinophils are capable of acting as APCs to induce Th2 responses, as they express MHC class II, CD80 and CD86 (Shi et al., 2000).

Van Beek *et al.* found that basophils become more pronounced with age in mice, whilst other groups have found relationships between basophil numbers and autoimmunity (Van Beek et al., 2018, Charles et al., 2010, Warde, 2010). Previously, Bochner *et al.* found that basophils reduce expression of CD11b following stimulation, which is involved in basophil adhesion (Bochner et al., 1990). Comparing asthmatic patients aged 60 years and over and aged under 30, has shown that both neutrophil and eosinophils numbers increase with age in humans, however these changes have not been observed in mice (Busse et al., 2017).

Very limited information is known about the metabolic requirements of basophils and eosinophils. As these cells form part of the granulocyte family alongside neutrophils, it is plausible that these cells may have similar metabolic requirements. In fact eosinophil differentiation and IL-4 expression have been linked to glycolysis, whilst a role for fatty acid metabolism has been observed in these

cells (Marques-Mejias et al., 2019, Arita, 2016, Ochkur et al., 2019). In addition, manipulation of glycolytic metabolism has been linked to basophil allergic responses. Increases in glycolysis in response to activation have been shown to occur through HIF-1α signalling as described for DCs (Sumbayev et al., 2009, Sumbayev et al., 2012).

1.3.1.5   Natural killer (NK) cells

Within humans, NK cells can be classified into three subclasses depending on their expression of CD56 and CD16. CD56+CD16+ (cytotoxic) NK cells are terminally differentiated, whilst CD56+CD16- (inflammatory) and CD56-CD16+ (regulatory) NK cells are immature cytokine-secreting cells which are poorly proliferative and cytotoxic respectively (Martelli, 2017). In mice, NK cells can be identified by their varying expression of CD27 and CD11b along the NK cell maturation pathway (CD27+CD11b-: immature, CD27+CD11b+: mid-maturation, CD27-CD11b+: mature) (Martelli, 2017). Whilst NK cells were originally considered to be myeloid cells, more recent research has identified them as innate cells of lymphoid lineage (ILCs) due to their production of IFNγ (Artis and Spits, 2015).

NK cells use either granule exocytosis or death receptor ligation to kill their target cells (Smyth et al., 2005). Granule exocytosis involves the secretion of cytotoxic molecules including perforin and GZB by cytotoxic NK cells, which form pores in the cell membrane of the target cell and activate caspase mediated apoptosis (Thiery et al., 2011, Goping et al., 2003). Death receptor ligation involves upregulation of Fas ligand and TNF-related apoptosis-inducing ligand on the surface of NK cells following cytokine stimulation and activating signals (Lavrik et al., 2005). These interact with molecules on the surface of the target cell to induce a similar mechanism of caspase-mediated apoptosis involving caspase 3. Regulatory NK cells act in a different manner, following activating signals these cells secrete high levels of TNF-α, IFNγ and several members of the interleukin family (2/5/10/13) to promote DC maturation, T cell function and the APC ability of macrophages (Vitale et al., 2005).

With age a decrease in number of mature (CD27-CD11b+) NK cells has been observed in mice, characterised by reduced expression of maturation markers such as killer cell lectin-like receptor subfamily G member 1 (KLRG1) (Beli et al., 2014, Martelli, 2017). This effect has been attributed to antagonistic IL-15 signalling (Chiu et al., 2013, Nair et al., 2015). Analysis of NK populations in humans have previously shown mixed results, however research within the Larbi group has identified accumulation of inflammatory and regulatory NK cells with age, with a particular increase in cells expressing CD57 as a marker of terminal differentiation (Martelli, 2017). These results have been corroborated by other groups (Hayhoe et al., 2010, Solana et al., 2006, Campos et al., 2014).

NK cell functions have been reported to be reduced with age, including their ability to induce NK maturation (Solana et al., 2012, Hazeldine and Lord, 2013).

1.3.2 Adaptive immune system

The adaptive immune system can form memory after the first encounter with a pathogen. This leads to an enhanced response to subsequent encounters. The adaptive immune system relies upon proper presentation of antigens and activation by cells of the innate immune response. This process takes much longer to initiate an immune response than the innate immune system, however following the acquisition of memory immune responses can occur rapidly.

1.3.2.1 T cells

T cells consist of both CD4+ T helper cells and CD8+ cytotoxic T cells. CD4+ T cells release a variety of cytokines to aid the function and activation of cells such as B cells, whilst CD8+ T cells use perforins and granzymes to induce apoptosis in infected and damaged cells, much in the same way as NK cells. Several other populations of T cell exist, including regulatory T cells which are involved in self-tolerance and gamma/delta T cells which have been less well studied (Martelli, 2017).

T cell precursors are first generated in the bone marrow before moving to the thymus for maturation into CD4+ and CD8+ T cells. Maturation of T cells begins with T cell receptor (TCR) rearrangement to increase the T cell repertoire and to remove T cells reactive to self-MHC molecules (Godfrey et al., 1994, Salam et al., 2013). Following maturation T cells are released from the thymus into the circulation and patrol the lymph nodes and spleen. Successful immune responses are dependent on engagement and activation of the TCR by foreign peptides loaded on MHC molecules of APCs (Figure 1.11). A successful response requires co-stimulatory signals and is mediated by CD28 via engagement with CD80/86 on APCs. Downstream of TCR/CD28 activation a number of signalling pathways are activated, including the mitogen-activated protein kinase/extracellular-signal-regulated kinase (MAPK/ERK) and PI3K which lead to the nuclear translocation of NF-κB and IL-2 to induce effector functions and expansion (Acuto and Michel, 2003). Populations induced as a result of TCR/CD28 stimulation include effector T cells and memory T cells resulting in cytotoxic and helper T cell responses to infection and the formation of memory following contraction (Salam et al., 2013). Memory cells are able to generate fast and efficient responses to pathogens which have been previously encountered and are characterised by increased IFNγ, perforin and granzyme levels (Sallusto et al., 2004). Central memory (CM) T cells are the most long-lived subset as they have the greatest proliferative capacity. Effector memory (EM) T cells on the other hand have a lower proliferative capacity and are shorter lived but have a greater range of effector functions (Gaber et al., 2015).

Diminishing numbers of naïve T cells were originally thought to occur through involution of the thymus with age (Busse and Mathur, 2010, Bains et al., 2009). Reduced numbers of naïve CD8+ T cells in the circulation is a well-accepted marker of immune ageing in adults (Whiting et al., 2015). However, thymic involution does not track changes in naïve T cell numbers, beginning within the first years of life with complete involution by 50 years of age. Maintenance of the T cell pool through these ages is therefore thought to occur through homeostatic proliferation of circulating T cells (Min, 2018, Goronzy and Weyand, 2019). Homeostatic proliferation is driven by low-level IL-15/7 and IL-2 stimulation of the TCR in CD8+ and CD4+ T cells respectively (van der Geest et al., 2015). The loss of CD28 expression on the surface of T cells with age is striking leading to altered co-stimulatory activity of these cells (Weng et al., 2009).

Repeated antigenic stimulation of T cells may contribute to immune senescence in the elderly by leading to T cell exhaustion and replicative senescence (Martelli, 2017). Chronic antigen stimulation occurs through chronic infections such as cytomegalovirus (CMV), human immunodeficiency virus (HIV) and hepatitis B and C viruses. T cell exhaustion is linked to increased expression of CD45RO, loss of CD27/CD28 and upregulation of inhibitory T cell receptors such as programmed cell death protein 1 (PD-1) and cytotoxic T-lymphocyte-associated protein 4 (CTLA-4) (Martelli, 2017, Blackburn et al., 2009). Blockage of PD-1 and CTLA-4 have previously been shown to partially reverse exhaustion by blocking inhibitory effects of T cell function (Barber et al., 2006, Sakuishi et al., 2010). Replicative senescence of T cells has been associated with the Hayflick limit as discussed in Section 1.1.5.3 Human studies relating to human fibroblast culture. T cells cultured over long periods of time begin to express cell cycle inhibitors, such as p21 and p16, which are both markers of senescence (Liu et al., 2009). Alongside this markers of SASP become apparent with replicative senescence, characterised by expression of IL-6 and TNF-α from CD8+ T cells (Coppe et al., 2010, Parish et al., 2009).

Age-related diseases can have a profound effect on the T cell population profile. Patients suffering from Parkinson's disease have a significantly reduced percentage of T effector memory cell re-expressing CD45RA (TEMRA) cells, with increased expression of the activation marker CD28 within the CD8^{+} population compared to age-matched controls (Williams-Gray et al., 2018). Strikingly, changes within the CD4+ population were not observed. A longitudinal study of TCR diversity in 6 individuals spanning 20 years concluded that there is a significant reduction in CD8^{+} TCR diversity and an increase in clonality which is not observed within the CD4^{+} T cell compartment (Yoshida et al., 2017). This data suggests that the CD8+ and CD4+ T cell populations age differently.

Throughout their development T cells dynamically switch between periods of quiescence and activation. This switching requires a high level of metabolic flexibility and adaptation in order to

meet the metabolic requirements of the cell. When they are first released from the thymus following maturation both CD4+ and CD8+ T cells prioritise oxidative phosphorylation and fatty acid oxidation to generate ATP. These metabolic pathways along with IL-7 signalling, support naïve T cells within peripheral blood and during homeostatic proliferation. TCR and co-stimulatory signalling activates these quiescent T cells and invokes a programme of anabolic growth for the accrual of biomass. Engaging anabolism marks the engagement of aerobic glycolysis, generating intermediates for proliferation and cell growth during clonal expansion. TCR and co-stimulatory signalling promotes the activation of mTOR, the master switch between oxidative phosphorylation and glycolysis, and enhances PI3K activation resulting in the phosphorylation of Akt to further promote mTOR activity (Le Page et al., 2018).

Deletion of Glut1 specifically within T cells dramatically impairs CD4+ T cell activation, expansion and survival (Macintyre et al., 2014), whilst CD8+ T cells with Glut1 deletion show reduced functional capacity (Jacobs et al., 2008, Cham et al., 2008). Previous data indicates that there are many metabolic differences between naïve, memory and effector T cells (van der Windt et al., 2013, van der Windt et al., 2012). Whilst naïve and memory T cells utilise OXPHOS in their quiescent state, effector cells tend to utilise glycolysis and reduce their mitochondrial mass. Memory T cells on the other hand have been shown to maintain their high levels of mitochondrial mass to support re-activation following secondary stimulation (Everts et al., 2012, van der Windt et al., 2013).

1.3.2.2   B cells

B cells have the ability to produce a diverse set of antibodies which are indispensable for proper functioning of the immune system (Cooper, 2015). B cells are first generated in the bone marrow, arising from pro-B-cells to form pre-B-cells and finally immature B cells. These immature B cells then exit the bone marrow before reaching maturity in the circulation (Ma et al., 2019). During their generation and maturation B cells develop a diverse range of B cell receptors (BCR) which are essential for host defence (Hoffman et al., 2016). Following antigen binding B cells integrate signalling from the BCR and helper T cells to become activated (Figure 1.11). B cells produce five different types of antibody: IgM, IgD, IgG, IgA and IgE. These antibodies act in three different ways to kill pathogens, by neutralising the target, activating innate immune responses by binding to Fc receptors or activating the classical complement pathway (Hoffman et al., 2016).

In mice, ageing is associated with a decline in the production of immature B cells from the bone marrow, although the number of B cells in the periphery tends to remain stable in humans (Blanco et al., 2018, Zharhary, 1988, Akkaya et al., 2018). As with T cells, B cells have the propensity to produce SASP markers following chronic stimulation which requires activation of AMPK and NF-κB (Frasca et al., 2017). Impaired humoral responses are characteristic of ageing alongside an

increased tendency for autoimmunity (Ma et al., 2019). B cells contribute to this phenomenon by producing autoantibodies (Grubeck-Loebenstein et al., 2009).

Mitogen- and antigen-stimulated B cells upregulate GLUT1 and their rate of glycolysis following activation of the PI3K pathway (Caro-Maldonado et al., 2014, Akkaya et al., 2018). A subset of pro-inflammatory B cells accumulates in the blood with age in humans which have been shown to produce autoantibodies (Frasca et al., 2019, Colonna-Romano et al., 2009). The appearance of these cells is associated with increased glucose utilisation and aerobic glycolysis to support their function with age, whilst these cells have minimal metabolic requirements in young individuals. These cells require the production of ROS and AMPK signalling to sustain their metabolic function (Frasca et al., 2019).
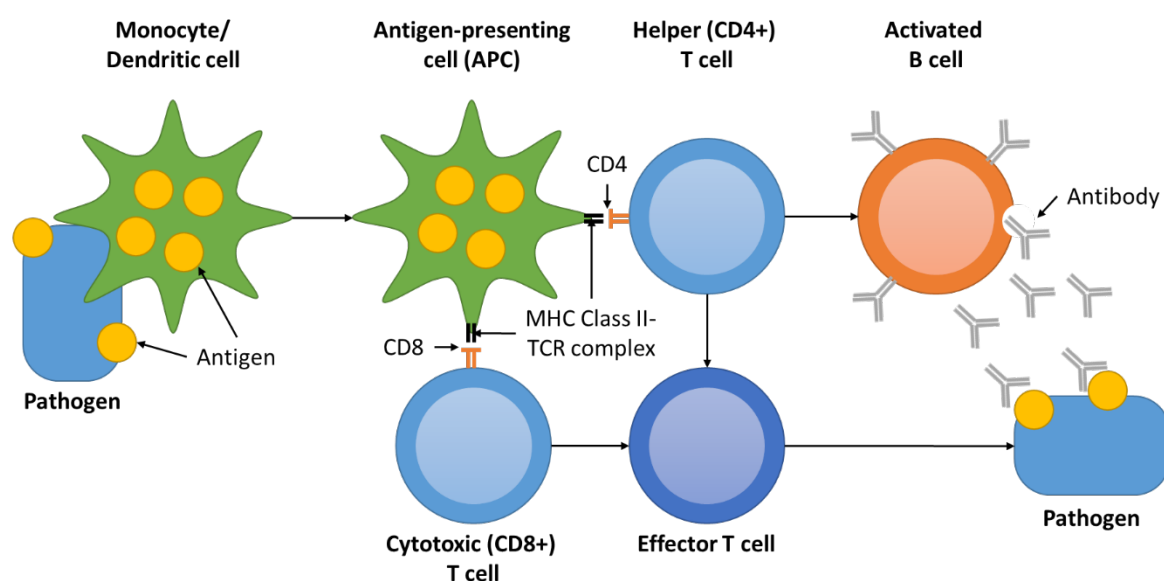
Figure 1.11 Summary of immune cell interactions involved in activating the adaptive immune response showing the interactions between pathogen and antigen presenting cells (APCs) such as monocytes and dendritic cells and their presentation of antigen to helper (CD4+) and cytotoxic (CD8+) T cells to mediate pathogen immobilisation and the production of antibody by B cells

1.4   Unmet needs in ageing research

Today there are still many unmet needs in ageing research, the first of which is to fully understand the ageing process. The ageing process is greatly complex and is contributed to by a wide range of biological and environmental factors. Whilst theories of ageing including mitochondrial dysfunction and immune-senescence have been well-studied separately, there is currently a major lack of research studying their relationship in the context of ageing. The current priorities for healthy ageing discussed in 1.1.3.1 Promoting healthy ageing, highlight the need to improve research in order to establish evidence-based practices for improving quality of life in the elderly population.

Studying immune-senescence is of clear importance as elderly individuals are particularly susceptible to developing infections and show reduced vaccine responses. Due to this immune-senescence is often associated with higher mortality in the elderly. Immune-senescence encompasses changes in the immune system which occur with age and can vary from decreases in the production of immune cells to alterations in their function, which affect the individuals ability to respond to infection and identify malignant cells. Aging not only increases the senescence of adaptive immune cells but also affects the ability of innate immune cells to produce pro-inflammatory and anti-inflammatory cytokines, often resulting in low-grade chronic inflammation (Aw et al., 2007). Immune-senescence has been a hot topic over the last decade or so and several routes for intervention have been suggested by scientists to improve the health span of ageing individuals (Aiello et al., 2019). However, the links between immune-senescence and the immunometabolism of these cells has yet to be studied. The metabolism of immune cells is central to innate and adaptive immune regulation and the ability to neutralise pathogens as discussed in Section 1.3 The immune system, immunometabolism and ageing. It is hoped that by developing research within these areas, new evidence-based practices can be added to the Healthy Ageing Action Plan (Geneva: World Health Organization, 2017). By studying alterations in the immune system and the metabolic landscape across the life course, researchers will be able to better understand the relationships between these factors and begin to unravel the complexity of ageing which has hampered research to date.

Besides studying the theories of ageing in a conjoined manner, research on ageing and the environment could be developed further. Research in this area will help to inform healthcare providers and carers of 'ideal' healthy ageing strategies. Whilst several aspects of the environment and the development of age-related disease have been well-studied, there is still room for improvement in understanding the role of environmental factors in extending health span. For example, the links between smoking, UV exposure and cancer have been known for some time, whereas the relationship between caloric restriction and health span in elderly humans remains

largely unknown. The effects of the surrounding environment on frailty and quality of life have also been well-studied but have not yet encompassed providing supportive environments for the elderly population to foster independence.

Much of the ageing research performed in humans to date has had a disease-specific focus. However, a shift towards studying the effects of ageing on a broader spectrum may be beneficial in developing better interventions to cultivate healthy ageing and extend health span. This work will involve studying the theories of ageing within individuals of differing health status in order to inform researchers and health care providers of what aspects are related to ageing and those that are related to disease development. By better understanding these mechanisms in both animal models and human studies, we may be able to reach the milestones set out in the Healthy Ageing Action Plan. Whilst animal models are important for studying ageing in the short term, more emphasis must be placed on utilising human studies as these will produce findings which are more translatable to the clinic.

Many of the treatments available for the elderly population are for disease management and improving quality of life. However, these interventions do not prevent the onset of disease or impact upon health span. There is a huge unmet clinical need in delaying the development of age-related diseases and allowing the elderly population to contribute actively in society. Whilst several interventional strategies which address this balance have been put forward, their use has been difficult to analyse clinically. For example, antioxidants and caloric restriction have been difficult to study as their clinical endpoints take many years to become evident. Better development of ageing biomarkers for measuring the outcomes of these interventions will help to accelerate this process. The successful development of ageing interventions will rely heavily on integrating findings from the identification of molecular targets/pathways, compound synthesis and testing effects in laboratory animals and human clinical trials. This places further emphasis on facilitating interaction and collaboration between investigators to improve ageing research.

Increasing understanding of the ageing process and developing better interventions is paramount for addressing the rapid growth of the ageing population and its impact on society. As discussed in Section 1.1.1, Population restructuring and global ageing are accelerating and the time available to study ageing is quickly decreasing. Delaying and/or reversing the ageing process will be necessary in the near future but must first be backed by adequate understanding of ageing and anti-ageing mechanisms. Once the central pathways involved in ageing are known, they can be used to fully inform the development of ageing therapies and long-lasting interventions can be established to benefit society.

1.5   Study aims

The aim of the study described in this thesis was to characterise mitochondrial dysfunction during the ageing process in both murine and human models of ageing, focusing on age-related immune cell dysfunction within the spleen, bone marrow and blood. It was hypothesised that mitochondrial dysfunction would accumulate with ageing, decreasing immune cell production and reducing their functionality. Ultimately, this work aims to expand the current knowledge of mitochondrial dysfunction during healthy ageing and examine its impact on the immune system. It is anticipated that this work will lead to novel insights in age-related dysfunction of the immune system.

The overall objectives of this study are as follows and forms the main aim of each of the result chapters contained within this thesis:

- To analyse mitochondrial dysfunction in the spleen and bone marrow immune cell compartments of C57BL/6J and $Timp3^{-/-}$ mice across the life course;
- To investigate age-related immune cell dysfunction in the spleen and bone marrow of C57BL/6J, SAMP6 and SAMP8 mouse strains by analysing mitochondria and metabolism;
- To determine mitochondrial programming in CD4+ T cell subsets during senescence, including naïve, central memory (CM), effector memory (EM) and terminal effector memory T cell re-expressing CD45RA (TEMRA) cells; and
- To examine mitochondrial dysfunction in peripheral blood mononuclear cells (PBMCs) derived from young and older donors by analysing mitochondrial parameters in PBMCs and immune cells.

Chapter 2   Materials and methods

2.1   Donors and sample preparation

2.1.1   Animal studies

2.1.1.1   Ethical approval

2.1.1.1.1   *Timp3*$^{-/-}$ study

Tissue inhibitor of metalloproteinase 3 knock-out (*Timp3*$^{-/-}$) mice were a kind gift from Professor Hideaki Nagase from the Kennedy Institute of Rheumatology in Oxford, UK. The mice were originated from Professor Rama Khoka's laboratory in Toronto. Female C57BL/6J wild-type control and female *Timp3*$^{-/-}$ mice bred on a C57BL/6J background were bred and maintained at the Biomedical Research Facility, University of Southampton in accordance with Home Office Procedures and Regulations and approved by the local Animal Welfare and Ethics Review Board (AWERB). Mice were maintained under a 12 hour light/dark cycle at a constant temperature of 22°C with autoclaved food and water available *ad libitum*. Mice were culled by Schedule 1 methods at 6 weeks, 15 weeks, 40 weeks and 72 weeks of age. Bone marrow and spleen were isolated from these mice for the purposes of this study.

2.1.1.1.2   Senescence-accelerated mouse (SAM) study

C57BL/6J (C57), SAMP6 and SAMP8 mice were housed under specific pathogen free (SPF) conditions in individually ventilated cages. Mice were bred and maintained in-house according to local Agency for Science, Technology and Research (A*STAR) Biological Resource Centre procedures. Mice were provided with standard food and water *ad libitum.* The study was approved by the A*STAR institutional animal care and use committee (IACUC) in Singapore. Mice were killed by euthanasia with CO_2.

2.1.1.2   Isolation of cells for animal studies

Bone marrow was removed from mouse femurs for analysis. After removal the tibia was cleaned of remaining muscle tissue before processing. To retrieve bone marrow cells, the bone heads were trimmed, and the bone marrow flushed into cell culture medium using a 1ml syringe and 23G needle into a 15ml falcon tube (ThermoFisher, MA). Cells were centrifuged at 1,500rpm for 5 minutes at 4°C and washed twice with cell culture medium prior to use in downstream assays. For splenocyte isolation the spleen was removed from mice and transferred into phosphate buffered

saline (PBS). The spleen was mechanically dissociated using the head of a 20ml syringe plunger into PBS and cells collected in a 15ml falcon tube. Red blood cells (RBC) were lysed by the addition of 1ml RBC lysis buffer (ThermoFisher, MA) and incubated for 5 minutes. Cells were centrifuged at 1,500rpm for 5 minutes at 4°C and washed twice with cell culture medium prior to use in downstream assays. Cells were counted manually with a haemocytometer and viability assessed by trypan blue exclusion (Sigma-Aldrich, MO).

2.1.2 Human studies

2.1.2.1 Ethical approval

2.1.2.1.1 CD4+ T cell study

Peripheral blood mononuclear cells (PBMCs) were isolated from whole blood donated by healthy adult volunteers and provided by the Blood Donation Centre, Health Sciences Authority in Singapore. The study was approved by the National University of Singapore-Institution Review Board 04-140 and all participants gave written informed consent.

2.1.2.1.2 Singapore Longitudinal Ageing Study (SLAS)

Blood was collected from elderly individuals recruited to the Singapore Longitudinal Ageing Study cohort II (SLAS II). The SLAS is a community-based long-term epidemiological study of ageing and health formed of Singaporean residents. SLAS II consists of elderly individuals of over 60 years of age. The study was approved by the National University of Singapore-Institution Review Board 04-140 and all participants gave written informed consent. Healthy, young volunteers were recruited from the Singapore Immunology Network (SIgN) and all participants gave written informed consent.

2.1.2.2 Isolation of cells for CD4+ T cell study (Chapter 5)

Whole blood was diluted 1:5 with PBS before layering 30ml over 20ml Ficoll-Paque™ (GE Healthcare, Singapore). The gradient was centrifuged at 20°C for 20 minutes at 400xg without a brake resulting in five layers. The cloudy PBMC-containing layer between the upper plasma and lower Ficoll layers (see Figure 2.1) was removed from each tube. PBMCs were washed twice with PBS and centrifuged at 1500rpm for 5 minutes at 4°C. Live cells were identified via trypan-blue exclusion and counted using a haemocytometer.
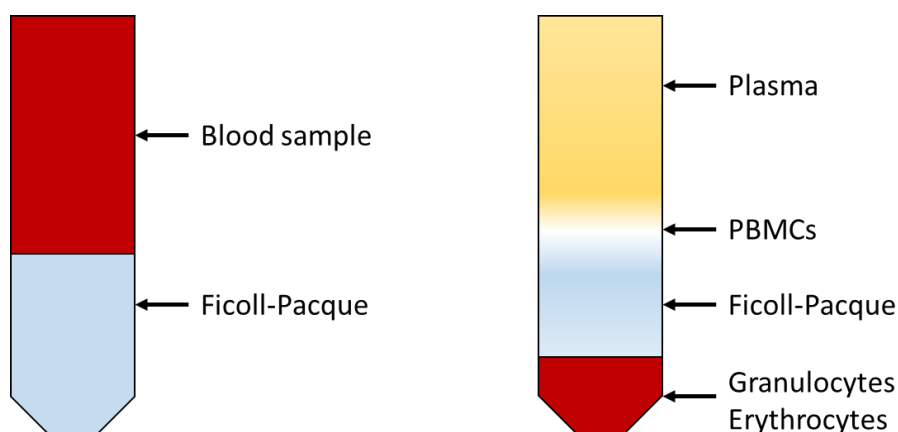
Figure 2.1   Isolation of PBMCs from blood using density separation prior to (left panel) and following (right panel) centrifugation and separation into plasma, PBMC, Ficoll-Pacque and Granulocyte/Erythrocyte layers

2.1.2.3   Isolation of cells for Singapore Longitudinal Ageing Study (SLAS) (Chapter 6)

The SLAS aims to investigate ageing by looking at biomedical, healthcare, psychological, lifestyle and behavioural data to generate information and guide clinical practice for elderly individuals. Donors within each group were matched for gender and cytomegalovirus (CMV) status.

Blood was drawn into 8ml Vacutainer® cell preparation tube (CPT)™ Mononuclear cell preparation tubes containing 0.1M sodium heparin (Becton Dickinson, NJ). Filled CPT tubes were centrifuged at 1650rpm for 20 minutes without a brake to separate the whole blood constituents as seen in Figure 2.2. Plasma was removed and PBMCs were collected using a Pasteur pipette. Following collection, PBMCs were washed twice with PBS and cryopreserved in liquid nitrogen in fetal bovine serum (FBS) containing 10% dimethyl sulfoxide (DMSO). The day of the experiment PBMCs were thawed and washed twice with PBS containing 10% FBS. Recovery and viability were tested using trypan blue exclusion and a haemocytometer.
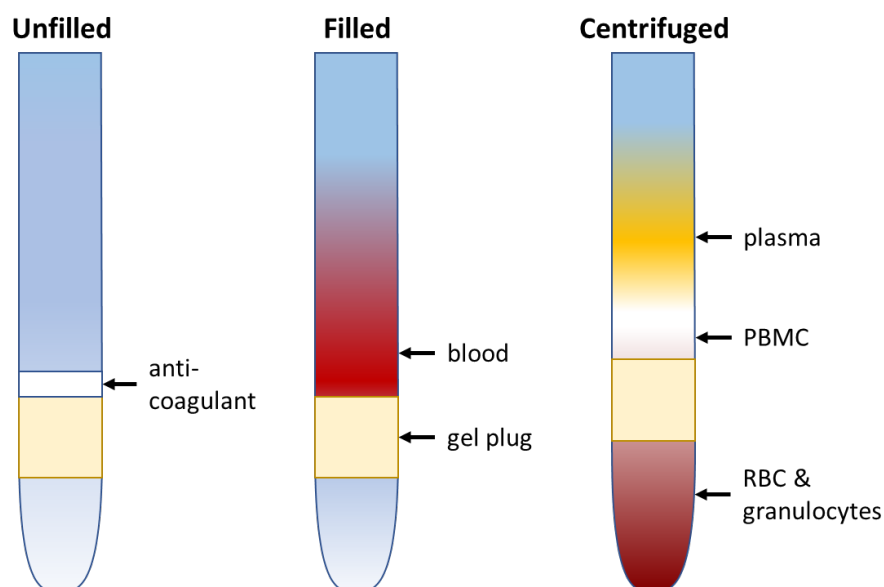
Figure 2.2   Separation of PBMCs whole blood using CPT tube showing empty CPT (left), after blood draw (middle) and after centrifugation (right) and separation into plasma, peripheral blood mononuclear cell (PBMC) and red blood cell (RBC) and granulocyte layers

2.1.3   Cell culture and tissue storage

All cell culture experiments were performed in humidified incubators at a controlled temperature of 37˚C with 5% CO_2. The details of the cell culture systems used in this study are contained within the experimental chapters.

For cryopreservation, PBMCs were pelleted by centrifugation and resuspended in FBS containing 10% DMSO (Kanto Kagaku, Singapore) at a density of ~50 million cells/ml and aliquoted into 2.5ml cryotubes designed for liquid nitrogen storage (ThermoFisher, MA). Cells were frozen at a controlled rate of 1˚C per minute to -80˚C using a MrFrosty™ (ThermoFisher, MA) containing isopropanol (GE Healthcare, IL). After a minimum of six hours at -80˚C, cryotubes were transferred to liquid nitrogen for long-term storage. Cryopreserved cells were thawed to room temperature before resuspending in 10ml medium pre-warmed to 37˚C to ensure maximal survival. DMSO was removed by washing the samples twice with medium and centrifugation at 1500rpm for 5 minutes before cells were used in downstream experiments. Cell viability was assessed by trypan blue exclusion and cells were counted using a haemocytometer prior to use.

2.2   Microscopy

2.2.1   Transmission electron microscopy (TEM)

Compared to traditional light microscopy, transmission electron microscopy (TEM) uses an electron beam which has a much shorter wavelength of 2.5pm which can image much smaller objects such as atoms or the internal structure of mitochondria. The first TEMs were constructed in the 1930s allowing for 100,000x magnification of samples. More advanced TEMs have advanced this further and can now magnify samples up to 30 million times.

TEMs consist of a tungsten filament or lanthanum hexaboride electron emission source as shown in Figure 2.3, which requires a high voltage of up to 300kV. The electron gun then controls and accelerates the beam of electrons through a series of electrostatic plates. The series of condenser lenses then focus the electron beam to the desired location and shape for the sample. After passing (transmission) through the sample, the beam is then pass through an objective lens and magnified onto the charge coupled detector. A vacuum system fitted to the TEM minimises the collision of electrons with other materials such as gas which affect the beam path.

In the case of biological research, samples are stained with a variety of heavy metals against cellular structures of interest. These heavy metals disrupt the flow of electrons through thin sample sections (<100nm) into different beam amplitudes and electron phases. These beam alterations are then detected within the microscope to provide high contrast at high levels of resolution. The resulting greyscale imaging can then be analysed with image processing techniques.
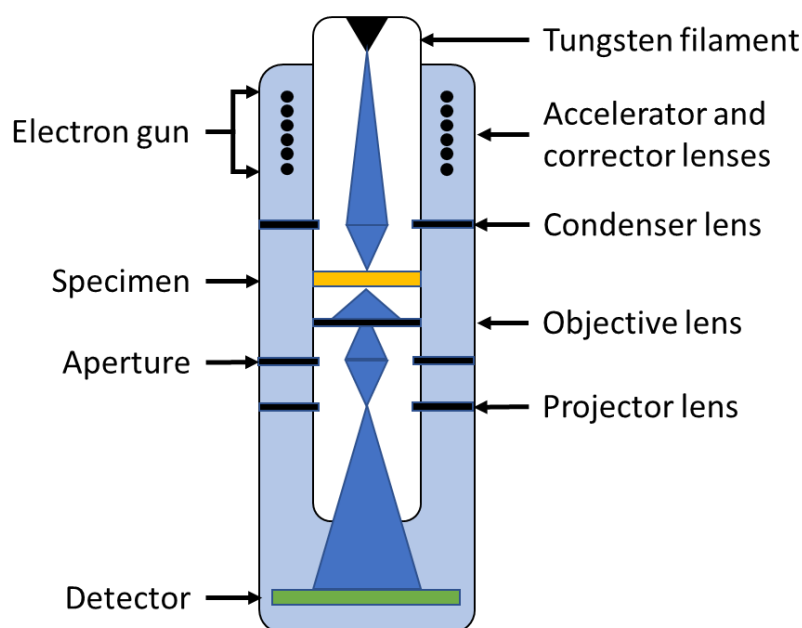
Figure 2.3   Components within a transmission electron microscope showing the placement of the tungsten filament, accelerator and corrector lens containing electron gun, condenser lens, specimen and detection lenses

Cells were flushed into 1ml of 3% glutaraldehyde 4% formaldehyde in 0.1M piperazine-N, N'-bis(2-ethanesulfonic acid) (PIPES) buffer (pH=7.2) and stored overnight at 4˚C for full fixation. To encapsulate the cells for staining, 500µl of bone marrow cells were layered over one drop of 5% sodium alginate gel and centrifuged at 16,000x*g* for 5 minutes at room temperature. The gel was hardened by incubation with 0.1M calcium chloride for 20 minutes at room temperature and cut into 1mm^3 sections for staining. The staining procedure for electron microscopy is detailed in Table 2.1. All steps were performed at room temperature unless otherwise stated. The final embedding step and curing was performed in an embedding capsule with a truncated cone tip (TAAB Laboratories Equipment Ltd, UK). After embedding, blocks were trimmed down to an observable region of interest (ROI) containing cellular material into a trapezoid shape using a razor blade to facilitate section ribboning. The block face was shaved using a glass knife until smooth. Three 500nm thick sections were then cut and placed on glass slides for toluidine blue staining and observed under the microscope for orientation and cellular density. Using a fresh glass knife thin 50-100nm sections were cut and mounted onto copper/palladium grids for TEM. The details of TEM imaging are listed within the experimental chapters.

Table 2.1   Staining procedure for electron microscopy

SOLUTION	SUPPLIER	PURPOSE	INCUBATION
0.1M PIPES (pH=7.2)	Sigma-Aldrich, MO	Wash	5 minutes
0.1M PIPES (pH=7.2)	Sigma-Aldrich, MO	Wash	5 minutes
2% Osmium tetroxide 1.5% potassium ferrocyanide	Sigma-Aldrich, MO	Lipids, sarcoplasmic reticulum and glycogen	1 hour on ice
0.1M PIPES (pH=7.2)	Sigma-Aldrich, MO	Wash	5 minutes
0.1M PIPES (pH=7.2)	Sigma-Aldrich, MO	Wash	5 minutes
Thiocarbohydrazide	Sigma-Aldrich, MO	Carbohydrates	20 minutes
0.1M PIPES (pH=7.2)	Sigma-Aldrich, MO	Wash	5 minutes
0.1M PIPES (pH=7.2)	Sigma-Aldrich, MO	Wash	5 minutes
2% Osmium tetroxide	Sigma-Aldrich, MO	Lipid staining	30 minutes
0.1M PIPES (pH=7.2)	Sigma-Aldrich, MO	Wash	5 minutes
0.1M PIPES (pH=7.2)	Sigma-Aldrich, MO	Wash	5 minutes
2% Uranyl acetate	Sigma-Aldrich, MO	Lipids and proteins	1 hour
0.1M PIPES (pH=7.2)	Sigma-Aldrich, MO	Wash	5 minutes
0.1M PIPES (pH=7.2)	Sigma-Aldrich, MO	Wash	5 minutes
Walton's lead aspartate solution	Sigma-Aldrich, MO	Proteins and glycogen	30 minutes
30% Ethanol	Sigma-Aldrich, MO	Dehydration	10 minutes
50% Ethanol	Sigma-Aldrich, MO	Dehydration	10 minutes
70% Ethanol	Sigma-Aldrich, MO	Dehydration	10 minutes
95% Ethanol	Sigma-Aldrich, MO	Dehydration	10 minutes
Absolute ethanol	Sigma-Aldrich, MO	Dehydration	20 minutes
Absolute ethanol	Sigma-Aldrich, MO	Dehydration	20 minutes
Acetonitrile	Sigma-Aldrich, MO	Dehydration	20 minutes
50% acetonitrile 50% Spurr resin	Sigma-Aldrich, MO	Embedding	Overnight
Spurr resin	Sigma-Aldrich, MO	Embedding	6 hours
Spurr resin	Sigma-Aldrich, MO	Embedding	18 hours at 60˚C

2.2.2   Serial block face scanning electron microscopy (SBF-SEM)

Scanning electron microscopy (SEM) differs to TEM in that instead of passing the electron beam through the sample, SEM scans the electron beam across the sample surface and detects the electrons which bounce back with a detector. This technique allows you to see the surface of biological samples in detail, although with slightly less resolution than TEM at ~5nm. Serial-block face SEM (SBF-SEM) couples this technique with an in-built ultramicrotome allowing the internal structure of samples such as cells to be imaged at the nanometer level. SBF-SEM conducts sequential imaging of the block face whilst the ultramicrotome equipped with a diamond knife cuts a section as little as 25nm thick. This generates a three dimensional view through the sample in the X, Y and Z planes. The resulting images can then be segmented and reconstructed to provide 3 dimensional data.

Samples for SBF-SEM were prepared using the same staining method as described above in Section 2.2.1 Transmission electron microscopy (TEM) to confirm their suitability for the technique. Suitable blocks were cut into $0.5cm^3$ cubes containing the ROI and mounted on a Gatan 3view pin using epoxy glue and cured for 18 hours at 60˚C. The block was then trimmed and polished again using a fresh glass knife. Samples were coated with gold/palladium to facilitate electron dispersion.

2.2.3   Confocal microscopy

Confocal microscopy was first developed in the 1960s, but laser point beam scanning was not developed until the 1980s by White and Amos at the Laboratory of Molecular Biology in Cambridge (White et al., 1987). Confocal microscopy is a technique used to increase the optical resolution of traditional wide-field fluorescence microscopy. Confocal microscopy uses a spatial pinhole to increase contrast and filter out-of-focus light from the captured image as seen in Figure 2.4. Imaging in the z-plane then allows for reconstruction of a series of 2 dimensional images into 3 dimensions. Confocal microscopy uses a pinhole to focus on a small section of the sample and then scanned across the sample using mirrors to increase optical resolution to 0.5μm. Whilst TEM is an excellent technique for imaging the ultrastructure of fixed cells and tissues. Confocal microscopy can be used for imaging live or fixed cells and tissue stained with fluorescent dyes against structures of interest.
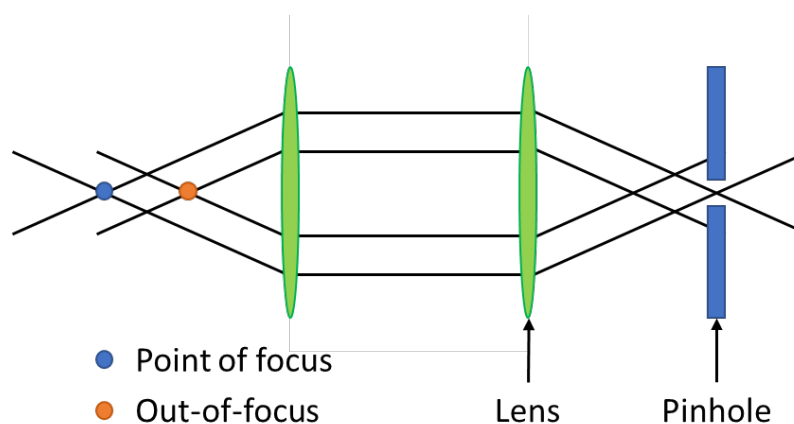
Figure 2.4   Components of the pinhole system in a confocal microscope for removing out-of-focus light and increasing optical resolution

Cells were transferred to a 96 well U-bottom plate (ThermoFisher, MA) for staining. After centrifugation at 1,500rpm for 5 minutes at 4°C, cells were resuspended in 200µl medium containing 150nM MitoTracker Green (MTG; ThermoFisher, MA) and 25nM Tetramethylrhodamine Ethyl Ester (TMRE; Sigma-Aldrich, MO). Cells were stained with 2µg/ml Hoechst 33342 (Sigma-Aldrich, MO). Cells were stained for a minimum of 2 hours in a humidified incubator at 37°C with 5% CO_2. Following staining cells were transferred to the wells of an 8 well µ-plate (ibidi, Germany) and an additional 100µl of staining medium added.

2.2.4   Super-resolution microscopy

Light microscopy techniques are limited by the Abbe limit, the lowest resolution of light at 250nm, new microscopy techniques have been developed to break this limit. These techniques have been termed super-resolution microscopy. As small mitochondria can sit right on this 250nm limit, super-resolution microscopy is useful for imaging organelles such as this as well as smaller particles including viruses and proteins down to 1nm. Many super-resolution microscopy techniques exist, however structured illumination microscopy (SIM) was utilised for this study. SIM uses Moiré patterns and the Fourier transform to increase resolution to 100nm in the xy plane and 250nm in the z plane as shown in Figure 2.5. Patterned illumination is used to excite the sample and transferred through several orientations to produce Moiré patterns as shown in Figure 2.6. These patterns are then processed using the specialised Fourier transform for a resolution of 100-130nm in the xy plane and 250nm in the z plane.
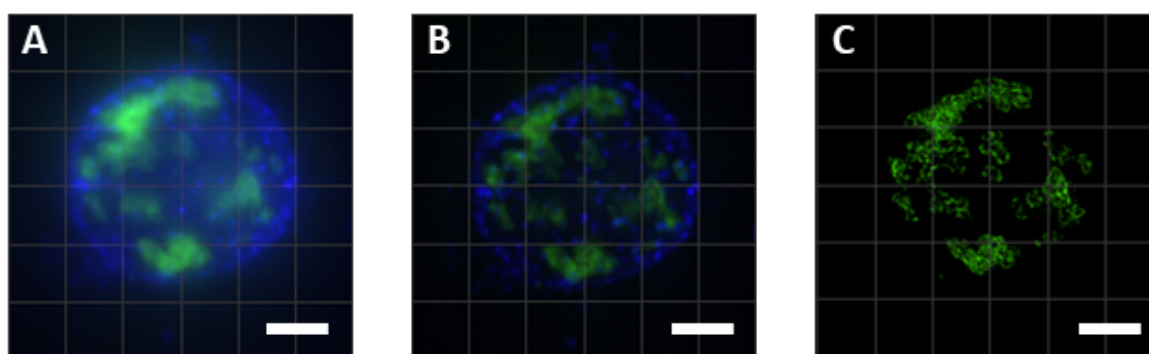
Figure 2.5   Comparison of super-resolution structured illumination microscopy with widefield microscopy showing (A) widefield image (B) deconvoluted widefield image and (C) SIM of mitochondria (scale=2µm; blue=nucleus, green=mitochondria)
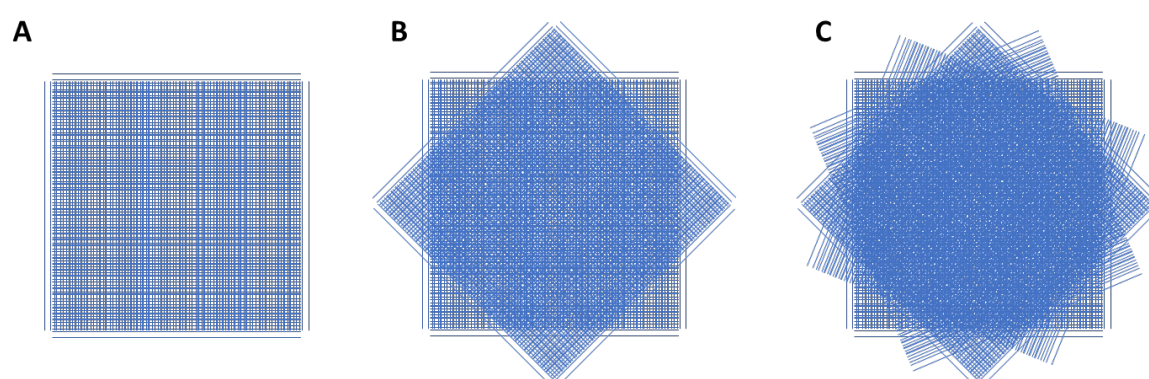
Figure 2.6   Moiré effect used for pattern illumination in SIM showing (A) 2 angles (B) 4 angles and (C) 8 angles of pattern rotation

Cells were transferred to 1.5ml Eppendorf tubes and washed twice with PBS using centrifugation at 1500 rpm for 5 minutes at 4˚C. Samples were then fixed and permeabilised with Cytofix/Cytoperm (Beckton Dickinson, NJ) for 20 minutes at 4˚C before washing twice with Permwash (Beckton Dickinson, NJ). Cells were stained with 1:50 dilution of translocase outer mitochondrial membrane 20 (TOM20) Rabbit immunoglobulin (Ig)G antibody (ProteinTech Group, IL) in 50µl Permwash and incubated for 1 hour at room temperature. Cells were washed twice again with permwash before incubating with 1:500 dilution of Goat anti-rabbit antibody conjugated to AlexaFluor (Af) 488 (Abcam, UK) for a further hour at room temperature. After another wash step cells were incubated with Hoechst-33528 (SigmaAldrich, MO) at 1:1000 dilution in Permwash, before final washing. Stained cells were mounted on 22mm square #1.5H high-performance coverslips (Paul Marienfeld, Germany) in Vectashield® H-1000 (Vector Laboratories, CA). Cells were imaged using a DeltaVision OMX inverted microscopy using 3D structured illumination microscopy (3D-SIM) technology (GE Healthcare, IL) and a 100X oil immersion objective lens. Samples were imaged by Goh Wah Ing from the A*STAR Institute of Medical Biology Imaging Platform. A comparison of the microscopy techniques used within this study is shown in Table 2.2.

Table 2.2   Comparison of microscopy techniques used within this study

MODALITY	RESOLUTION XY, Z	PROBES	ACQUISITION TIME	POST-PROCESSING
CONFOCAL	500nm, 800nm	Fluorescent	Minutes	Deconvolution if necessary
SIM	100nm, 250nm	Fluorescent	Seconds	Fourier transform
TEM	2.5pm, 50nm	Heavy metal	Milliseconds	NA
SBF-SEM	5nm, 25nm	Heavy metal	Milliseconds	Segmentation

2.3   Reverse transcription real-time quantitative polymerase chain reaction (RT-qPCR)

RT-qPCR combines the two techniques of reverse transcribing ribonucleic acid (RNA) to complementary deoxyribose nucleic acid (DNA) (cDNA) and amplification of these transcripts through polymerase chain reaction (PCR). Combining these techniques allows for the analysis of gene expression. Total ribonucleic acid was isolated from mice by flushing tissues into 1ml of TRIzol (ThermoFisher, MA) using a 23G needle. Samples were stored at 4˚C for 1 hour to facilitate digestion before homogenisation using pipette tips of decreasing size. The samples were incubated for 5 minutes at room temperature before adding 200µl chloroform (Sigma-Aldrich, MO), vortexing for 15 seconds and incubated for 3 minutes at room temperature to precipitate RNA. Samples were then centrifuged at 12,000xg for 30 minutes at 4˚C, separating the TRIzol into an aqueous, interphase and organic layers containing RNA, DNA and protein/lipid respectively. The aqueous phase was added to 500µl of 2-propanol (Sigma-Aldrich, MO), incubated for 10 minutes on ice and centrifuged at 12,000xg for 15 minutes at 4˚C. The RNA pellet was washed twice with 75% ethanol in diethyl pyrocarbonate (DEPC)-treated water (Primer Design, UK) and left to air-dry before resuspension in 10µl DEPC-treated water. RNA concentration was determined at an absorbance of 230nm using a NanoDrop 1000 (ThermoFisher, MA).

200ng RNA was reverse transcribed to cDNA using a High Capacity RNA-to-cDNA kit (ThermoFisher, MA) according to manufacturer's instructions. Briefly, 200ng RNA was diluted in 9µl DEPC-treated water before the addition of 11µl cDNA reaction buffer containing 10 parts reaction buffer to one-part reaction enzyme. The reaction was incubated at 37˚C for 1 hour and stopped by heating to 95˚C for 5 minutes, prior to storage at 4˚C for 10 minutes using a PTC-240 Tetrad 2 ThermoCycler

(BioRad, CA). cDNA samples were dilute with 180µl DEPC-treated water and stored at -20˚C until use.

Primers were diluted to a concentration of 10µM with PrecisionPLUS MasterMix (Primer Design, UK) containing SYBR green detection reagent to a concentration of 2.5µg/ml. 4.5µl of cDNA was loaded into each well along with 5.5µl of primer-master mix solution. Samples were run in duplicate in 384-well PCR plate format. The plate was centrifuged at 1,000rpm for 2 minutes before performing analysis.

2.4 Luciferase assays

Luciferase assays utilise luciferin as a reporter for molecules of interest, such as adenosine triphosphate (ATP), hydrogen peroxide (H_2O_2) or glucose. These assays work by adding a pro-luciferin substrate to the assay, which is converted to luciferin through enzyme dependent conversion. Examples include glutathione S-transferase or reductase which utilises the reduction of NADH→NAD or NADPH→NADP. Following the production of luciferin, light is emitted upon the introduction of the luciferase which converts luciferin to light as shown in Figure 2.7. As the light produced does not require excitation there is minimal autofluorescence and high sensitivity.
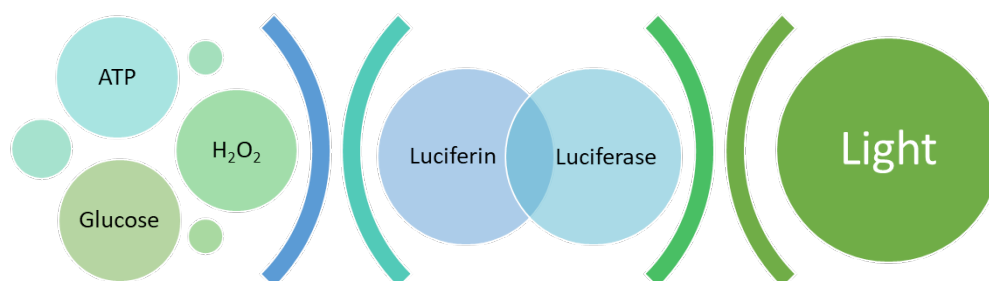
Figure 2.7   Generation of light as reporter molecule in a luciferase assays showing (A) ATP, H_2O_2 or glucose conversion of pro-luciferin to luciferin and processing by luciferase to produce light in the absence of external excitation

2.4.1   Adenosine triphosphate production

Cells were plated at a density of 10,000 cells per well in 96-well black opaque-walled plates (ThermoFisher, MA). Adenosine triphosphate (ATP) production was measured using the CellTiter-Glo® 2.0 Assay (Promega Corporation, WI), according to manufacturer's instructions. Briefly, CellTiter-Glo® 2.0 reagent was thawed to room temperature and mixed by inversion. Following treatment, 100µl CellTiter-Glo® 2.0 reagent was added to the cell culture medium and mixed for 2

minutes on an orbital shaker to induce cell lysis. The plate was left to stabilise for 10 minutes at room temperature before luminescence was recorded. Control wells were measured to determine background luminescence. A total of four repeats for each sample were used per assay condition.

2.4.2   Glutathione anti-oxidation system

Cells were plated at a density of 10,000 cells per well in 96-well white opaque-walled plates (ThermoFisher, MA). Total glutathione (GSH+GSSG) and oxidised glutathione (GSSG) were measured using the GSH/GSSG-Glo™ Assay (Promega, WI), according to manufacturer's instructions. Samples were plated in triplicate for each GSH+GSSG and GSSG measurement. Wells containing no cells were used as a control. Cells were grown overnight prior to conducting the assay. Cell medium was discarded and 50µl per well of total glutathione assay reagent or oxidised glutathione reagent was added to each well. The plate was then shaken for 5 minutes using the MixMate microplate shaker (Eppendorf, Germany). 50µl luciferin generation reagent was added to all wells before briefly shaking again for 10 seconds. Finally, 100µl luciferin detection reagent was added and incubated for 15 minutes at room temperature before luminescence detection.

2.4.3   Glucose uptake

Cells were plated at a density of 10,000 cells per well in 96-well white opaque-walled plates (ThermoFisher, MA). Glucose uptake was measured according to manufacturer's instructions using the Glucose Uptake-Glo™ Assay (Promega, WI). Wells containing no cells and no stop buffer were used as controls. Cells were plated in triplicate for each experiment. Briefly, the cell medium was removed, cells were washed twice with PBS and 50µl of 1mM 2-deoxy-D-glucose (2DG) was added to wells. The plate was shaken for 10 seconds and incubated for 30 minutes at room temperature. Next 25µl stop buffer was added to the wells followed by 25µl neutralisation buffer and shaken for 10 seconds between each addition. Finally, 100µl 2-deoxy-D-glucose-6-phosphate (2DG6P) detection reagent was added to the wells before incubation for 1 hour at room temperature and measurement of luminescence.

2.4.4   Hydrogen peroxide (H_2O_2) production

Cells were plated at a density of 20,000 cells per well in 96-well white opaque-walled plates (ThermoFisher, MA). Cells were plated in triplicate for each experiment. Medium without cells plus control or test compound was used to determine background luminescence. H_2O_2 production was measured using the reactive oxygen species (ROS)-Glo™ H_2O_2 Assay (Promega, WI), according to manufacturer's instructions. Briefly, 20µl H_2O_2 substrate solution was added to each well for the

treatment time or a minimum of 6 hours. Following treatment 100µl ROS-Glo™ detection solution was added to each well and incubated for 20 minutes at room temperature before measurement of luminescence.

2.4.5   Glucose concentration

Cells were plated at a density of 10,000 cells per well in 96-well U-bottom plates (ThermoFisher, MA). Cells were plated in triplicate for each experiment. Control wells containing medium only and PBS only were used as a control. 5µl medium was removed and transferred to another 96-well U-bottom plate containing 95µl PBS per well. Samples were then further diluted 4-fold in PBS for a final 100-fold dilution. 50µl diluted sample was transferred to a 96-well white opaque-walled plate (ThermoFisher, MA) for analysis. 50µl glucose detection reagent was added to each sample before the plate was shaken for 1 minute using the MixMate plate shaker (Eppendorf, Germany). Finally, the plate was incubated for 60 minutes at room temperature before recording luminescence.

2.5   Flow cytometry and cell sorting

2.5.1   Flow cytometry

Flow cytometers have five main components, which allow for high-throughput quantification of fluorescence on a single-cell basis. As shown in Figure 2.8, these components include the following:

1. Flow cell – a single-cell suspension and sheath fluid pass through the flow cell to align cells in single file for measurement
2. Measuring system – lasers excite the fluorophores which have stained each cell, the emission wavelengths of these fluorophores then pass through a series of dichromatic mirror (long pass) and band pass filters unique to each fluorophore
3. Detector – photomultiplier tubes (PMTs) convert the analogue signal to a digital signal for amplification
4. Amplification system – the PMTs then amplify the digital fluorophore signals on a logarithmic scale to be processed by the computer
5. Computer for analysis – the computer records the data produced by the flow cytometer and gating decisions can be made to analyse cell populations of interest

This process is termed sample acquisition. Modern flow cytometers can contain up to 10 lasers and 50 detection parameters in the BD FACSymphony™ system (Becton Dickinson, NJ). Spectral overlap between fluorescent markers limits the detection of multiple fluorophores in other instruments. However, flow cytometers use colour compensation to minimise spectral overlap into other

detectors. This process measures the spill over from each fluorophore into other detectors by acquiring single-stained samples. This highly complex compensation then allows for multiparameter acquisition for analysing large of numbers of parameters in large cell samples. Flow cytometers will happily run at acquisition rates up to 6,000 events per second, allowing for high-throughput measurement of cells.
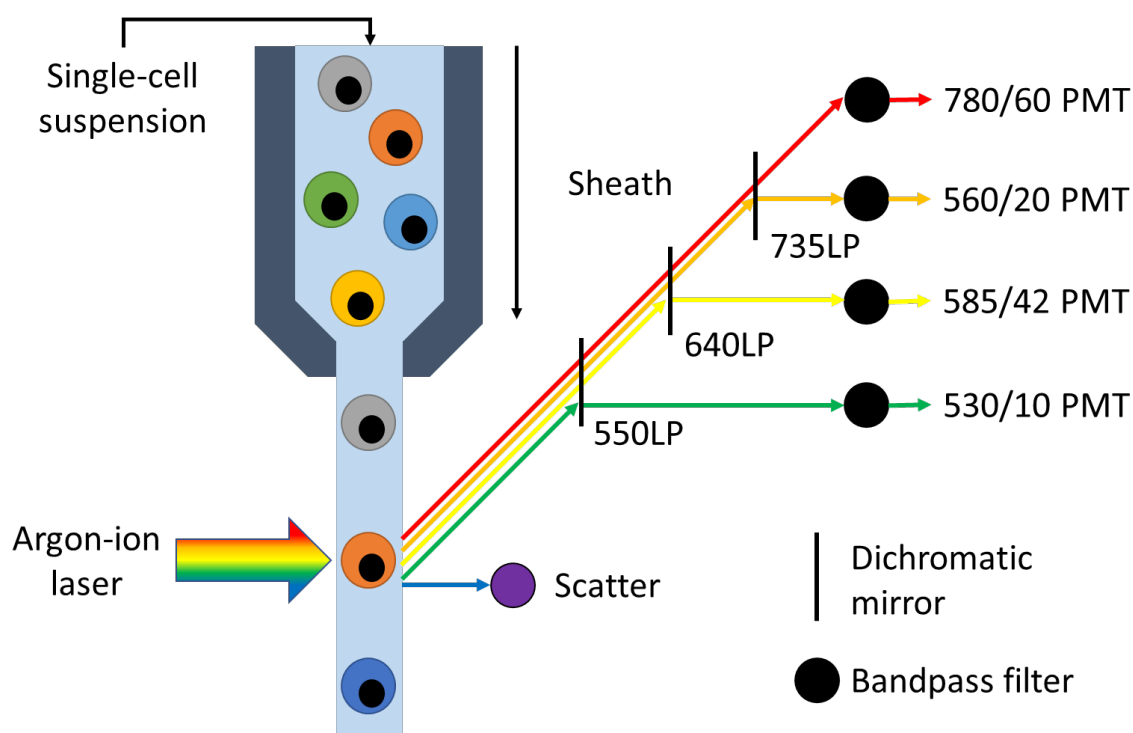
Figure 2.8   Components of a flow cytometry system showing application of a single-cell suspension to the cytometer and the flow of sheath fluid to create a stream of single cells for interrogation by the laser. Fluorescent measurements are made via amplification of the signal by photomultiplier tubes and a series of filters. LP=long pass filter, PMT=photomultiplier tube (Adapted from (Shapiro, 2005))

All cells can be identified by unique signatures of markers present on the cell surface. During flow cytometry staining and acquisition cells can be identified by staining for these markers and multiplexing these with other dyes for viability, mitochondria or intracellular protein expression. Therefore, flow cytometry is an excellent technique for studying the metabolic landscape of immune cells within both murine and human tissue in a high-throughput manner.

2.5.1.1   Cell surface staining

Cells were processed for flow cytometry after being transferred into a 96-well U-bottom plate (ThermoFisher, MA). PBMCs were washed and resuspended in fluorescence-activated cell sorting (FACS) buffer containing 95% PBS, 5% FBS and 5mM ethylenediaminetetraacetic acid (EDTA; ThermoFisher, MA). All following centrifugation steps were performed at 1500rpm at 4°C for 5

minutes. After washing cells were resuspended in a surface marker staining mix (detailed within each chapter) and incubated at room temperature for 20 minutes. Cells were washed twice following surface staining.

2.5.1.2   Live cell mitochondrial staining

Following cell surface staining, cells were incubated for a minimum of 2 hours in cell culture medium containing 150nM MTG (ThermoFisher, MA) and either 25nM TMRE (Sigma-Aldrich, MO) or 25nM Tetramethylrhodamine Methyl Ester (TMRM; Sigma-Aldrich, MO). Cells were incubated at 37°C with 5% CO_2 to facilitate dye infiltration into the cell. Following staining cells were transferred to 5ml polypropylene (PP) tubes for acquisition.

2.5.1.3   Intracellular protein staining

Cells were permeabilised via treatment with 100µl Cytofix/Cytoperm (Becton Dickson, MJ) for 20 minutes at 4°C. Cells were washed twice with Permwash (Becton Dickson, MJ) following permeabilisation. Cell were then incubated with a primary antibody (detailed within each chapter) against the protein of interest diluted in Permwash for 30 minutes at room temperature. Cells were washed twice with Permwash. Where required, cells were then incubated with secondary antibody (detailed within each chapter) against the primary antibody of interest diluted in Permwash for 30 minutes at room temperature. Following staining cells were collected in 5ml polypropylene tubes in 200µl FACS buffer for acquisition.

2.5.2   Fluorescence-activated cell sorting (FACS)

FACS utilises a similar technique to flow cytometry by staining the surface markers of cells of interest. Instead of utilising a constant flow stream, FACS break this stream into droplets each containing a single cell as seen in Figure 2.9A. Following acquisition, a charge is then applied to each droplet for sorting purposes as shown in Figure 2.9B. The cytometer applies the charges used for sorting based off the gating strategy applied during computational analysis. FACS requires complicated set-up for breaking the stream into droplets containing singular cells and the drop time required before applying charge to the droplets. FACS typically sorts cells with high purity of up to 99.9% in a high-throughput manner of up to 50,000 events per second. However, shorter sorting times often come at the expense of purity and viability. FACS is a useful technique for sorting rare cell populations whilst minimising the number of sorting steps and can sort up to 6 populations in parallel.
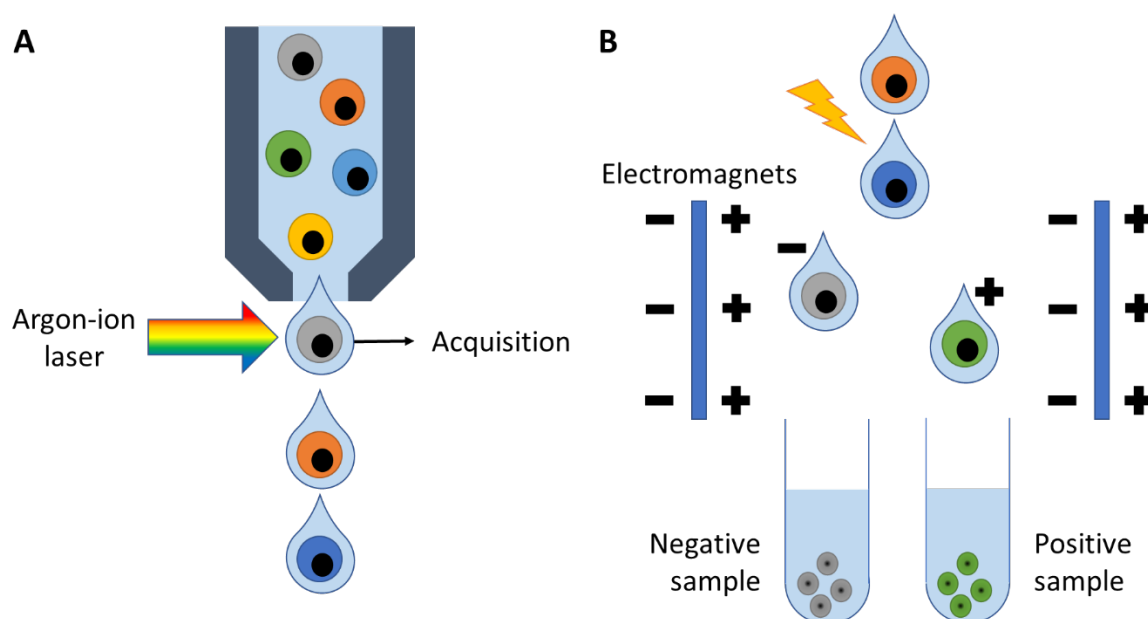
Figure 2.9   Components of the cell sorting system used for FACS showing (A) breakage of flow stream into droplets by vibration and (B) sorting of droplets into positive and negative populations following the application of charge to the droplet

The number of cells designated for sorting were placed into a 5ml PP tube. Cells were stained for cell surface markers as described in Section 2.5.1.1 Cell surface staining. Following staining cells were resuspended in FACS buffer at a density of 15million cells/ml for sorting. Details of the cell surface markers used for FACS are detailed within each experimental chapter. Samples were sorted by the SIgN Flow Cytometry Platform by Salanne Lee, Ivy Low and Seri Mustafah. Cells were sorted in 5ml PP tubes containing 500µl medium unless otherwise stated. Cells were left to rest overnight at 37˚C, 5% CO_2 prior to use in downstream assays.

2.5.3   Magnetic-activated cell sorting (MACS)

MACS sorts cells based on their expression of surface antigens. By staining cells with antibody-coated magnetic particles and passing them through a magnetic column cells can be sorted into positive and negative populations. MACS works as shown in Figure 2.10. Cells labelled with the antibody of interest are applied to the separation column within a magnetic field. Positively labelled cells are retained within the field whilst unlabelled cells are washed out of the column. Following removal from the magnetic field, labelled cells can then be washed out of the column. In this manner MACS can be used for both positive and negative sorting of cells. Compared to FACS, the MACS method has lower target cell purity due to the retention of unlabelled cells in the column, however MACS does not put as much stress on the cells as it does not require the high pressures involved in FACS.
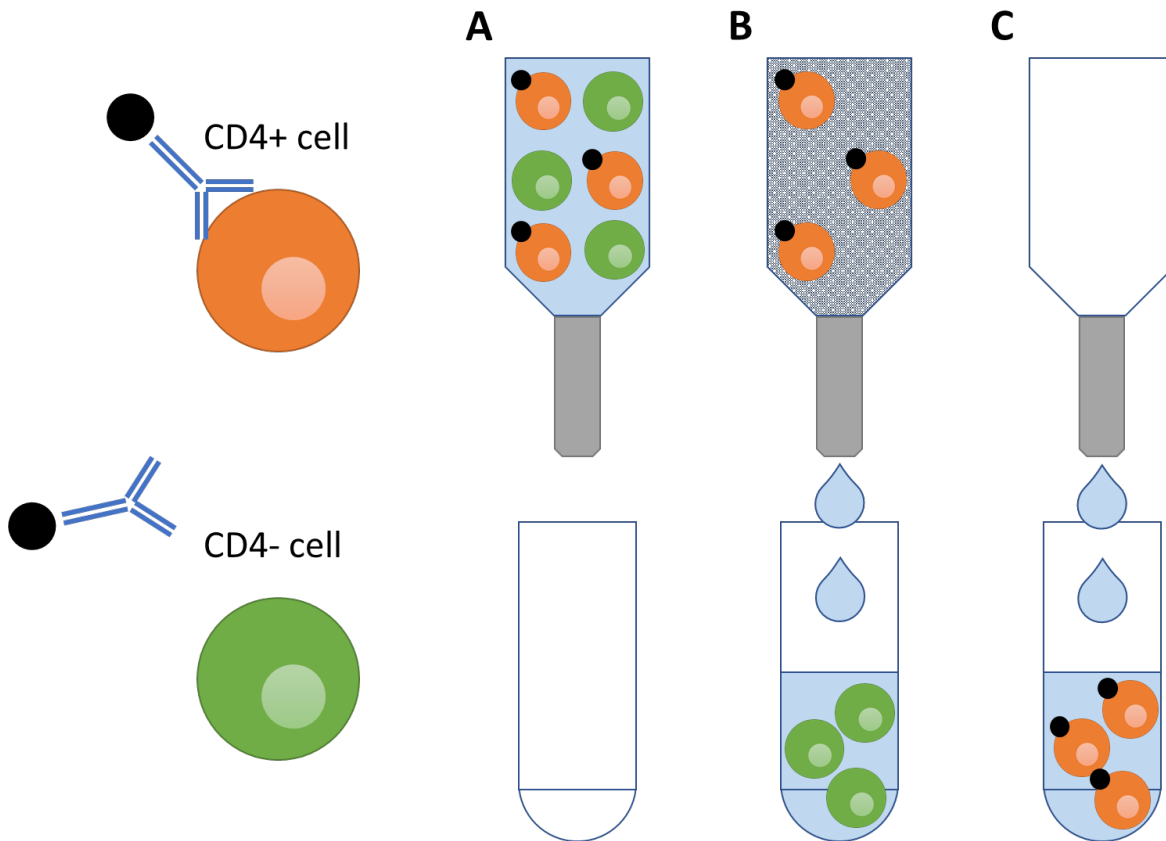
Figure 2.10 Magnetic-associated cell sorting from PBMCs showing labelling of CD4 positive and negative cells (A) application of cell suspension to the column (B) retention of CD4 positive cells in the magnetic field and expulsion of unlabelled cells and (C) collection of CD4 positive labelled cells following removal from the magnetic field

Cells were isolated by MACS® (Miltenyi Biotech, Germany) according to manufacturer's instructions. 50 million PBMCs from each donor were centrifuged at 300xg for 10 minutes at 4˚C and resuspended in 400µl MACS® buffer containing 0.5% bovine serum albumin (BSA) and 2mM EDTA in PBS. 100µl MicroBeads (Miltenyi Biotech, Germany) was added to the cell suspension and incubated for 15 minutes at 4˚C. Cells were washed by adding 5 ml of MACS® buffer and centrifugation at 300xg for 10 minutes at 4˚C before resuspending in 500µl MACS® buffer prior to magnetic separation. MACS® LS columns were placed in the magnetic field of a MACS® separator (Miltenyi Biotech, Germany) and rinsed with 3ml MACS® buffer before applying the cell suspension. Unlabelled cells passed through the column and were collected using three washes of 3ml MACS® buffer. After depleting unlabelled cells, the column was transferred to a 15ml Eppendorf collection tube and labelled cells collected by rinsing the column with 5ml MACS® buffer using the supplied plunger.

2.6   Live-cell metabolic analysis

Live-cell metabolic analysis is an extremely useful tool for metabolic research and can be applied to almost all cell types. Due to the creation of a transient microchamber Seahorse XF analysers require fewer cells for metabolic analysis compared to other live-cell methods such as the Oxygraph-2k (Oroborus Instruments, Austria). Therefore, the Seahorse XFe96 Analyser (Agilent Technologies, CA) is useful for studying the metabolism of precious samples and rare cell types. Within the Seahorse analyser measurements of oxygen consumption rate (OCR) and extracellular acidification rate (ECAR) are measured in a small volume (2µL) above a monolayer of cells as seen in Figure 2.11. Solid-state sensor probes for measuring OCR and ECAR are contained within the microchamber approximately 200µm above the monolayer. These two probes contain fluorophores which are quenched by oxygen (O_2) and protons (H^+) for measurement of OCR and ECAR respectively.
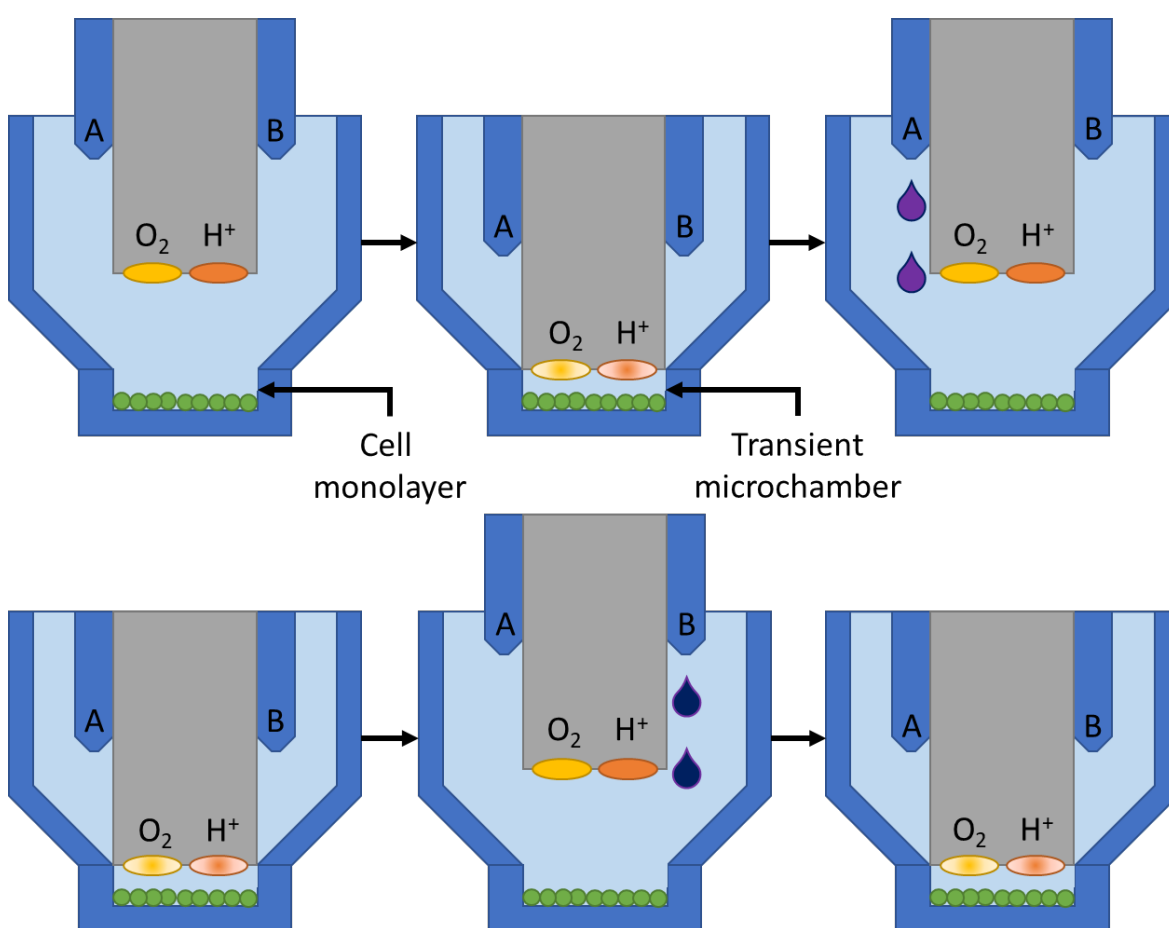
Figure 2.11   Transient microchamber and port injection in Seahorse assay showing seeding of cell monolayer, creation of transient microchamber and injection of port A compound (top panel) and subsequent measurement, injection of port B compound and final measurement (bottom panel) (O_2= oxygen consumption rate probe; H^+= extracellular acidification rate probe)

The sensor cartridge contains four injection ports to treat the cells with drugs to inhibit and stimulate metabolism or add in metabolic substrates. These injection ports can add drugs sequentially throughout the assay into each well as seen in Figure 2.11. As shown in Table 2.3, this study utilised the injection of four compounds to alter metabolism:

A. Oligomycin – inhibitor of ATP synthase by blocking the proton channel necessary for adenosine diphosphate (ADP) conversion to ATP. Used to measure ATP-linked respiration and proton leak.

B. 2-deoxy-D-glucose (2DG) – phosphorylated by hexokinase following cell entry which acts to competitively inhibit hexokinase and glycolysis. Used to measure reliance on glycolysis for metabolism.

C. Carbonyl cyanide-4-(trifluoromethoxy)phenylhydrazone (FCCP) – uncoupling agent which disrupts the transportation of hydrogen ions across the mitochondrial membrane. Used to measure maximal respiration rates and spare capacity.

D. Rotenone (Rot) & Antimycin A (AA) – inhibitors of complex I and cytochrome c respectively to shut down the electron transport chain and all mitochondrial respiration. Used to measure non-mitochondrial respiration.
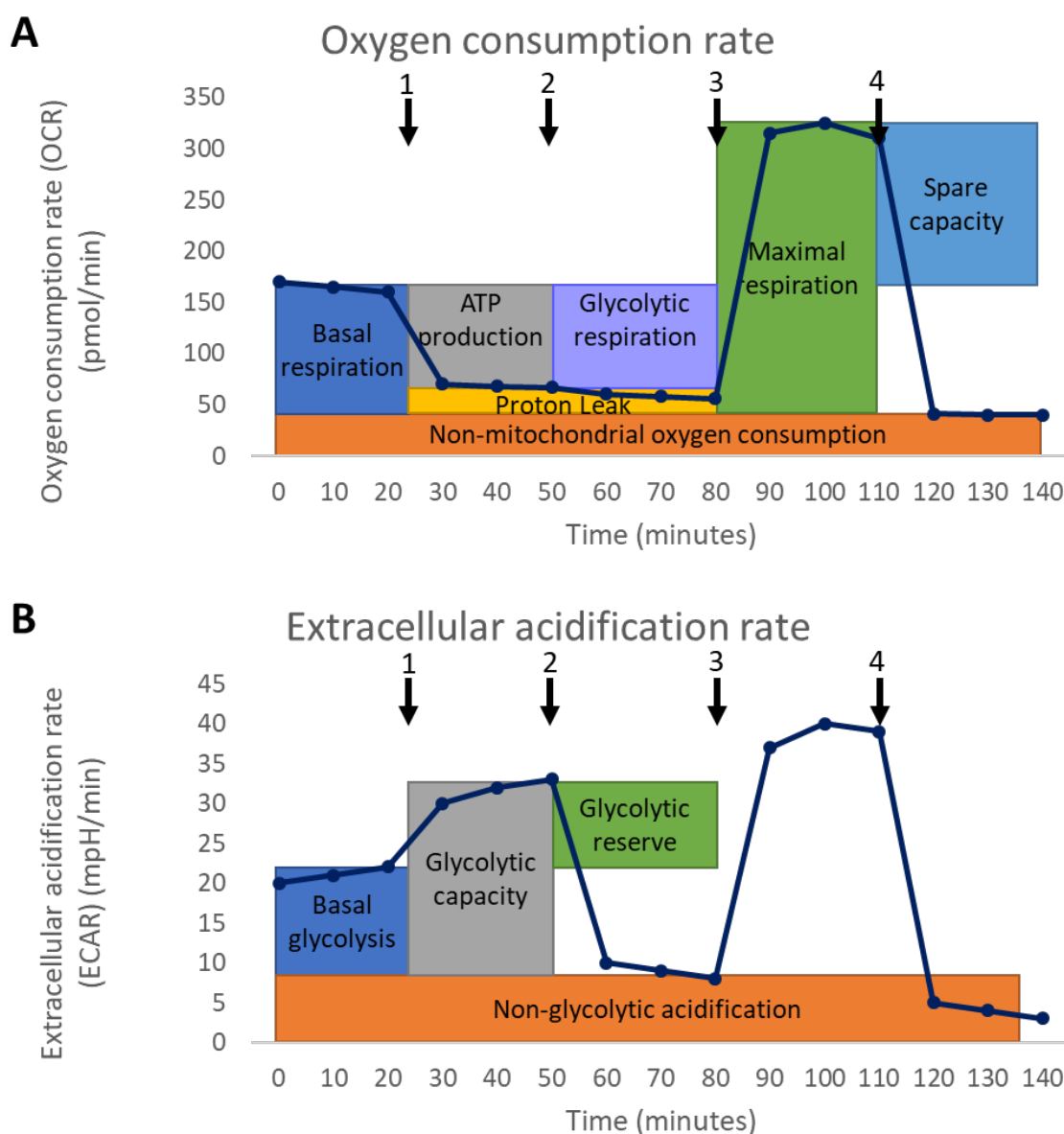
Figure 2.12 Analysis of mitochondrial metabolism during Agilent Seahorse assay showing (A) oxygen consumption rate (OCR) analysis with measurement of basal respiration, ATP production, glycolytic respiration, proton leak, maximal respiration, spare capacity and non-mitochondrial oxygen consumption and (B) extracellular acidification rate (ECAR) with measurement of basal glycolysis, glycolytic capacity, glycolytic reserve and non-glycolytic acidification following injection of (1) oligomycin, (2) 2DG, (3) FCCP and (4) Rot/AA

One day prior to the assay XF96 cell culture plates (Agilent Technologies, CA) were coated with 20µl of 100µg/ml poly-D-lysine (PDL) diluted in PBS and left to incubate overnight or for a minimum of 6 hours at 4˚C. Simultaneously XF96 sensor cartridges (Agilent Technologies, CA) were hydrated with 200µl XF Calibrant (Agilent Technologies, CA) and placed in a non-CO_2 37˚C incubator overnight or for a minimum of 6 hours. For each assay 100ml of XF Rosewell park memorial institute (RPMI)

Medium (Agilent Technologies, CA) containing 10mM glucose, 1mM pyruvate and 2mM L-Glutamine (seahorse assay medium; ThermoFisher, MA) was pre-warmed to 37˚C. Coated XF96 cell culture plates were washed twice with PBS. Cells were resuspended in 50µl seahorse assay medium at the density required for the assay and transferred to the wells of the XF96 cell culture plate. Cells were centrifuged at 200xg for 1 minute without brake and transferred to a non-CO_2 37˚C incubator for 30 minutes before the addition 130µl of seahorse assay medium per well. Cells were returned to the incubator for a further 15 minutes prior to the start of the assay. Compounds were loaded into the XF96 sensor cartridge according to Table 2.3. The assay was designed using Seahorse Wave software (Agilent Technologies, CA) and plates were loaded into the XFe96 Analyzer (Agilent Technologies, CA) according to manufacturer's instructions. Results were analysed using Wave software.

Table 2.3   Injection strategy for seahorse assay

PORT	COMPOUND	VOLUME	10X PORT CONCENTRATION	FINAL WELL CONCENTRATION
A	Oligomycin	20µl	20µM	2µM
B	2DG	22µl	500mM	50mM
C	FCCP	25µl	20µM	2µM
D	Rot/AA	28µl	5µM	500nM

2.7   Immune cell stimulation

2.7.1   CD3 (OKT3) stimulation

Sterile 96-well flat-bottom plates were used for CD3 (OKT3) stimulation of T cells. Wells were coated with 5µg/ml anti-CD3 (Clone: OKT3; ThermoFisher, MA) diluted in PBS overnight at 4˚C. Control wells were coated with PBS only. Following coating, wells were washed twice with PBS. PBMCs were plated at a density of 2 million cells per well in 200µl RPMI with 10% FBS (R-10) and left to incubate at 37˚C with 5% CO_2 for the duration of the experiment. PBS was used as a control for CD3 (OKT3) stimulation experiments. Cells were stimulated for either 4 or 24 hours prior to analysis.

2.7.2   Phorbol 12-myristate 13-acetate/Ionomycin stimulation

Lymphocytes were stimulated using Phorbol 12-myristate 13-acetate (PMA) and Ionomycin. Cells were treated with DMSO control or 10ng/ml PMA and 100ng/ml Ionomycin for six hours prior to use in downstream assays.

2.8   Enzyme-linked immunosorbent assay (ELISA)

ELISA was first developed by Engvall and Perlmann in 1972 (Engvall and Perlmann, 1972), to measure the concentration of a ligand in a sample. The ligand is measured using antibodies directed against the antigen of interest, such as a cytokine or protein. ELISAs can come in several formats including direct, indirect and sandwich capture assays as shown in Figure 2.13. Both the direct and indirect ELISA methods require the immobilisation of the antigen to the plate surface, which is then detected by enzyme-conjugated primary antibody or a set of unlabelled primary and conjugated secondary antibodies for the direct and indirect assays respectively. The sandwich ELISA uses a capture antibody bound to the plate surface to capture the antigen and detection by a set of unlabelled primary and conjugated secondary antibodies. The assay used within this project uses the sandwich ELISA method to measure the concentration of interferon gamma (IFNγ). Sandwich ELISAs do not require the antigen to be purified prior to the assay, making it a simple measurement with increased specificity and sensitivity over the other assay methods.
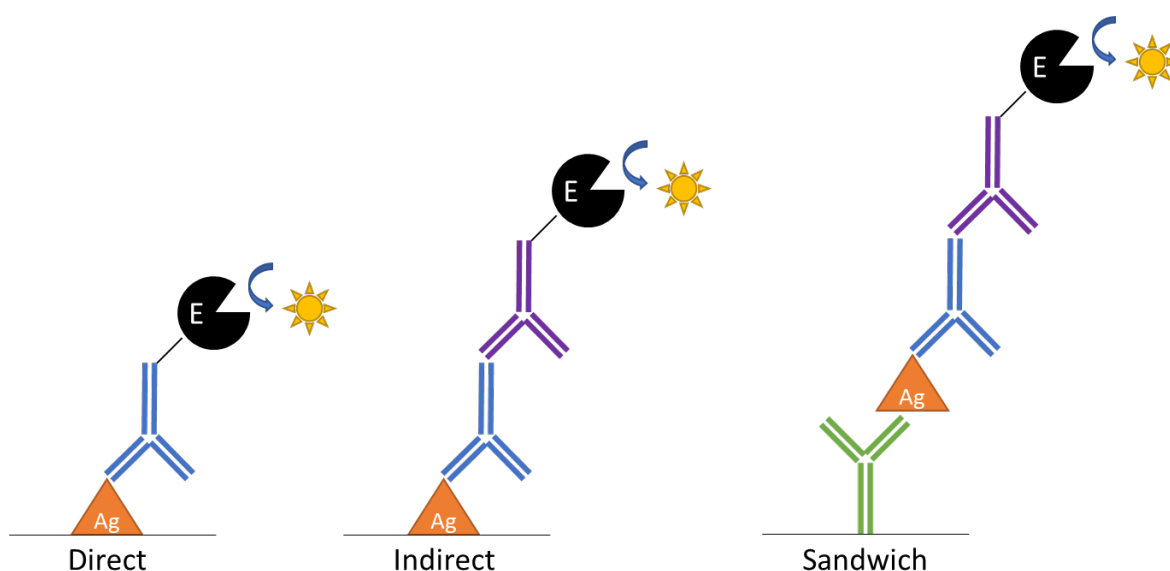
Figure 2.13   Comparison of common ELISA formats showing direct, indirect and sandwich antigen detection systems (Ag=antigen; E=enzyme)

Cells were plated at a density of 500,000 cells per well and treated as required for the experiment. Following treatment, cell culture medium was removed and stored at -20˚C until the day of the

assay. IFNγ was measured according to manufacturer's instructions using the Human IFNγ ELISA MAX™ deluxe set (BioLegend, CA). Seven IFNγ standards were produced by performing six two-fold serial dilutions of 500pg/ml IFNγ creating IFNγ standards of: 500pg/ml, 250pg/ml, 125pg/ml, 62.5pg/ml, 31.3pg/ml, 15.6pg/ml and 7.8pg/ml. The assay diluent served as a zero standard (0pg/ml). Dilution factors were determined in a preliminary experiment. Control samples were diluted 10x and stimulated samples 100x with assay diluent. One day prior to running the ELISA, the provided 96-well plates were coated with the IFNγ capture antibody, sealed and incubated overnight at 4˚C. Following coating the wells were washed three times with the provided wash buffer and blocked with assay diluent. After sealing the plate was incubated for 1 hour at room temperature on a plate shaker at 500rpm, before washing 4 times. 100µl of standard or diluted sample was added to each well and incubated for 2 hours at room temperature with shaking. Four further washes were followed by a 1 hour incubation with the detection antibody solution at room temperature before washing again. 100µl Avidin-horseradish peroxidase was added to each well, sealed and incubated at room temperature for 30 minutes with shaking. Finally, after washing the wells 5 times, 3,3',5,5'-Tetramethylbenzidine substrate solution was added to the wells and incubated in the dark for 20 minutes turning the wells blue, following this stop solution was added resulting in a yellow colour.

2.9   Statistical analysis

Data was assessed for normality using SPSS Statistics software (International Business Machine Corporation, NY). Sample groups of parametric data were analysed using either a Two-way analysis of variance (ANOVA) model or Three-way ANOVA model depending on the experiment design in GraphPad Prism (GraphPad Software, CA). Samples were paired within-subjects. *Post-hoc* analysis was performed using the Tukey method for unpaired and paired models and the Sidak method was utilised for mixed-model datasets. Non-parametric data was analysed using an unpaired Kruskal-Wallis model with Dunn's *post-hoc* analysis in SPSS Statistics. Statistical power was assessed using G*Power software (Faul et al., 2007, Faul et al., 2009). A *p* value of <0.05 was used to define significance. Details of the statistical tests used as part of this study can be found in each experimental chapter and in the figure legend. All graphs were created using GraphPad prism software. For graphical purposes p values are designated by *p<0.05, **p<0.01 and ***p<0.001.

Chapter 3 *Timp3*$^{-/-}$ (KO) and C57BL/6J (WT) mice show alterations in mitochondrial structure during ageing

3.1 Introduction

Previous research within the Pender group has shown that tissue inhibitor of metalloproteinase 3 (*Timp3*)$^{-/-}$ mice (KO) have reduced bodyweight compared to C57BL/6J (WT) controls. This effect occurs across the life course from 2 weeks to 72 weeks of age, with WT mice weighing ~30g at 50 weeks of age whilst KO mice weigh ~20g (Supplementary figure A.1; unpublished data). Within the literature, the effect of *Timp3* KO extends to animals placed on a high fat diet (HFD). Mavilio *et al.* (2016) found that on HFD KO mice gain significantly less weight than their WT counterparts in line with other published studies (Mavilio et al., 2016, Rossi et al., 2018). Cumulatively these results suggest that metabolism may be altered within *Timp3*$^{-/-}$ mice.

Whilst *Timp3*$^{-/-}$ mice do not gain weight on the induction of HFD to the extent of that observed in WT mice, these mice do develop glucose intolerance, reduced insulin responses and hepatic steatosis (Mavilio et al., 2016). The development of this phenotype and the link with *Timp3* expression has been extensively studied (Federici et al., 2005, Gao et al., 2015, Fiorentino et al., 2013a, Fiorentino et al., 2013b). Reduced expression of *TIMP3* has been linked to type 2 diabetes development in humans (Cardellini et al., 2011, Cardellini et al., 2009, Monroy et al., 2009).

Timp3 has been shown to regulate a metabolic switch within mice which leads to the development of this diabetic phenotype in KO mice. Previously, *Timp3*$^{-/-}$ mice on HFD have been shown to metabolise amino acids differently to that of WT mice, specifically branched chained amino acids (Mavilio et al., 2016). This is thought to occur through gut dysbiosis and alterations in the gut microbiome leading to increased numbers of circulating pro-inflammatory cells such as macrophages and dendritic cells (DCs) leading to an increased pro-inflammatory profile (Mavilio et al., 2016). This profile involves increased levels of serum cytokines such as interleukin (IL)-6, interferon-gamma (IFNγ) and tumour necrosis factor-α (TNF-α) driven by metabolic inflammation. Overexpression of *Timp3* in a monocyte-specific manner has been shown to improve metabolic dysfunction on HFD and decrease the pro-inflammatory profile (Casagrande et al., 2012, Menghini et al., 2012).

Studies have observed altered metabolic function in apolipoprotein E (*ApoE*)$^{-/-}$*Timp3*$^{-/-}$ double knock-out mice (Stöhr et al., 2015). *ApoE*$^{-/-}$*Timp3*$^{-/-}$ mice are characterised by impaired lipid oxidation and lipid deposition in the heart, and a marked decrease in fatty acid oxidation

intermediates present in serum. Decreased metabolic profiles of mitochondrial fatty acid oxidation have been observed in *Timp3$^{-/-}$* mice (Rossi et al., 2018). In a proteomic study of kidneys derived from *Timp3$^{-/-}$* mice, gene ontology terms of differentially expressed proteins were enriched for mitochondrial function, fatty acid oxidation (FAO) and catabolism, oxygen transporter activity and mitochondrial membrane permeability (Rossi et al., 2018). Overexpression of *Timp3* in a hepatocyte-specific manner was able to improve glucose metabolism and FAO parameters observed in WT mice fed HFD (Casagrande et al., 2017). This research suggests that KO mice have altered metabolism compared to that observed within WT mice. The TIMP3/TNF-α-converting enzyme (ADAM17) pathway has previously been implicated in glucose metabolism and inflammation in both murine models of obesity and human obesity-related diabetes (Menghini et al., 2012).

Alongside altered metabolism in *Timp3$^{-/-}$* mice, there is evidence to suggest that these mice are subject to a more inflammatory environment characterised by oxidative stress. Increased inflammation, reactive oxygen species (ROS) production and nicotinamide adenine dinucleotide phosphate (NADPH) oxidase activity are characteristic of KO mice (Basu et al., 2012) and a decrease in serum levels of cysteine-glutathione disulphide (GSH) and oxidised glutathione (GSSG) have been observed in *ApoE$^{-/-}$Timp3$^{-/-}$* double knock-out compared to *ApoE$^{-/-}$* single knock-out mice (Stöhr et al., 2015).

Alongside the increased presence of pro-inflammatory cells following HFD in KO mice, alterations in the number of immune cells have been detected within KO mice with age compared to WT (Martelli, 2017). Previously, this work within the Pender group has showed that natural killer (NK) cell numbers are reduced with age in both WT and KO mice whilst CD4+ and CD8+ T cell numbers remain stable. Reductions in NK cell numbers with age are more pronounced within KO mice at 50 weeks of age and associated with a switch from a mature (CD11b+, CD62L+, killer cell lectin-like receptor subfamily G member 1 (KLRG1)+, Ly49H+) to immature (CD27+, CD127+) NK cell phenotype. These phenotypic changes result in an upregulation of TNF-α and IL-6 secretion from 50 week old KO NK cells compared to WT. This same trend was observed for CD4+ and CD8+ T cells, which showed greater immaturity in KO animals with age (Martelli, 2017). Previous work within the Pender group has shown that female KO mice develop spinal curvature starting from 20 weeks of age (Supplementary figure A.2A; unpublished data). This phenotype is attributed to decreased bone mass within the thoracic vertebrae (Supplementary figure A.2B; unpublished data). As immune cells originate from the bone marrow and one of the hallmarks of ageing involves stem cell exhaustion, the *Timp3$^{-/-}$* mouse model was utilised for this study.

Although metabolic dysfunction has been well studied in KO mice placed on normal chow and HFD, there has been a lack of focus in studying the metabolism of mitochondria directly. The aims and objectives for the work carried out within this chapter are summarised in Figure 3.1. In brief, the metabolic and mitochondrial phenotypes of bone marrow and splenic cells from WT and KO mice were compared at 6 weeks, 15 weeks and 40 weeks of age. WT mice were also analysed at 72 weeks of age encompassing the full life course of both these models. It was hypothesised that KO mice would exhibit a greater extent of mitochondrial dysfunction compared to WT mice.

Aim:
To analyse mitochondrial dysfunction in the spleen and bone marrow immune cell compartments of C57BL/6J and *Timp3*$^{-/-}$ mice across the life course

Objectives:
- Examine isolated bone marrow cells from wild-type and *Timp3*$^{-/-}$ mice at 6, 15 and 40 weeks of age
- Perform additional observations of bone marrow cells at 72 weeks of age in wild-type mice
- Analyse mitochondrial ultrastructure using transmission electron microscopy (TEM)
- Confirm structural alterations by utilising serial block-face scanning electron microscopy (SBF-SEM)
- Measure ATP production from bone marrow cells, alongside the glutathione anti-oxidation system
- Confirm previous observations of altered maturation in NK and T cells
- Measure mitochondrial mass and membrane potential in NK cells, T cells and dendritic cells

Figure 3.1   Aims and objectives for analysing age-related mitochondrial dysfunction in C57BL/6J and *Timp3*$^{-/-}$ mice

3.2 Materials and methods

3.2.1 Animals

Details of the animals used within this chapter can be found in Section 2.1.1.1.1 *Timp3*$^{-/-}$ study. A total of 80 mice were used for this study. The spleens and bone marrow of these mice were isolated as described in Section 2.1.1.2 Isolation of cells for animal studies. Tissue was collected from mice across the life course as shown in Figure 3.2.
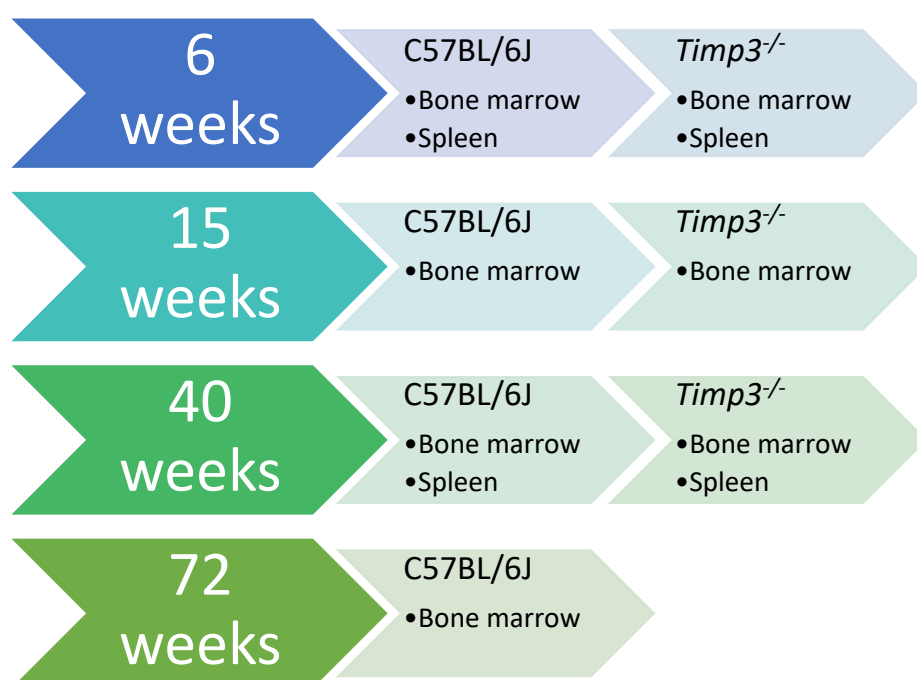
Figure 3.2   Schematic of tissue collection from C57BL/6J (WT) and *Timp3*$^{-/-}$ (KO) mice during the study n=8 for all test groups

3.2.2 Transmission electron microscopy (TEM)

Bone marrow cells isolated from *Timp3*$^{-/-}$ and C57BL/6J mice were stained for transmission electron microscopy as described in Section 2.2.1 Transmission electron microscopy (TEM). Mitochondria were imaged using a Technai F12 TEM at 26,500x magnification using a blinded un-biased selection method. Organelle cross-sectional length, width and area were analysed in ImageJ as shown in Figure 3.3A. Mitochondrial length was measured as the longest diameter through the organelle and the mitochondrial width measured perpendicular to this line. Mitochondrial cross-sectional surface area was measured by tracing the mitochondrial outer membrane. Mitochondrial cristae structure was analysed as described in Figure 3.3B. Up to 150 mitochondria were measured and averaged per mouse for this analysis.
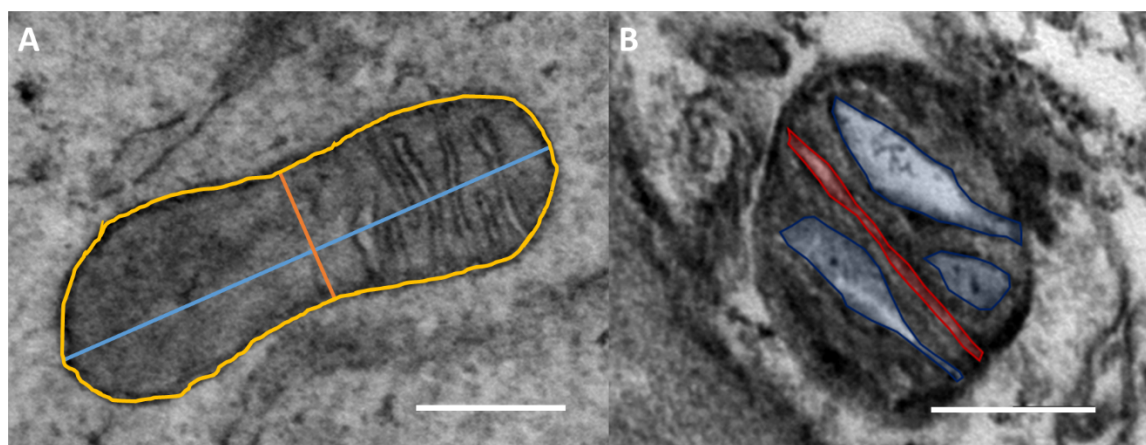
Figure 3.3   Analysis of bone marrow mitochondria in ImageJ (A) Measurement of mitochondrial length (blue), width (orange) and area (yellow) (B) Analysis of mitochondrial cristae structure as laminar (red) and tubular (blue) (Scale= 200nm)

3.2.3   Serial block face scanning electron microscopy (SBF-SEM)

Samples for SBF-SEM were prepared as described in Section 2.2.2 Serial block face scanning electron microscopy (SBF-SEM). Samples for SBF-SEM were passed to Patricia Goggin at the Biomedical Imaging Unit, University of Southampton and imaged using the Gatan 3view system mounted inside a FEI Quanta 250 Zeiss Sigma SEM (Gatan, CA). Images were transformed in FIJI (Version 1.52r). Mitochondria were reconstructed manually using the TrackEM2 plugin in FIJI developed by Cardona *et al* using a blind trial un-biased selection method (Cardona et al., 2012). Three dimensional reconstructions were generated using this software to analyse mitochondrial surface area and volume.

3.2.4   Reverse transcription real-time quantitative polymerase chain reaction (RT-qPCR)

Total ribonucleic acid (RNA) was isolated from the bone marrow of C57BL/6J and *Timp3$^{-/-}$* mice using the method described in Section 2.3 Reverse transcription real-time quantitative polymerase chain reaction (RT-qPCR). Primers for murine dynamin-related protein 1 (*Dnm1L*), fission protein 1 (*Fis1*), mitofusin 1 (*Mfn1*), mitofusin 2 (*Mfn2*), optic atrophy 1 (*Opa1*) and beta-actin (*β-actin*) were designed, optimised and validated by Primer Design, UK. The primer sequences are listed in Table 3.1. Upon delivery, primers were resuspended in 600µl RNAse/DNAse-free water to a concentration of 25µg/ml, before aliquoting and storage at -20˚C. RT-qPCR was measured using the Real-Time 7900HT Applied Biosystems polymerase chain reaction (PCR) machine (ThermoFisher, MA). The reaction was activated using the HotStart function for 2 minutes at 95˚C before cycling 40 times at 95˚C for 10 seconds and 60˚C for 20 seconds allowing for denaturation and SYBR green fluorescence

detection, respectively. Cycle threshold (Ct) values were analysed using a self-designed template in Microsoft Excel to calculate the relative gene expression values within each sample.

Table 3.1   Primer sequences used for RT-qPCR

GENE NAME	SENSE PRIMER SEQUENCE	ANTI-SENSE PRIMER SEQUENCE
Dnm1L	ATGCGGTGGTGCTAGGATT	CAGTCAGGATGTCAATAGTGTTAAG
Fis1	CTGGGGGACACTGGAAGAG	ATGGAGACTGTAGAGGTAGACTA
Mfn1	CTGGAAACTAATCTCTGTCACCTT	ACTGCTGCTTAAACGCTCTC
Mfn2	TTCCACCCATCCCCAGTTG	GCAGCGGTCAGACAGGTT
Opa1	CTCCTGGTGACACAGCCATT	CCTGACGCCTAGTTCAGACAT

3.2.5   Cell culture

Bone marrow cells were cultured in α-minimum essential medium (α-MEM) containing 1x Penicillin/Streptomycin (Pen/Strep; ThermoFisher, MA), 5% fetal bovine serum (FBS; Sigma-Aldrich, MO) and 200µl L-glutamine (ThermoFisher, MA) (complete α-MEM) at 37˚C. Cells were incubated in T25 cell culture flasks for 5 days in 10ml complete α-MEM at 37˚C with 5% CO_2. To passage, cells were washed twice with 5ml ice-cold PBS containing 1x Pen/Strep before incubating with 1% trypsin (Sigma-Aldrich, MO) for 10 minutes at 37˚C. Cell detachment was observed under the microscope and the enzyme activity stopped by the addition of 7ml complete α-MEM. Dissociated cells were collected in a 15ml conical tube and after centrifugation at 1,500rpm for 5 minutes at 4˚C, the pellet was resuspended in 1ml complete α-MEM. The spleens of WT and KO mice were cultured in complete α-MEM. Cells were incubated in T25 cell culture flasks overnight at 37˚C with 5% CO_2. To passage cells were collected in 15ml conical tube and centrifuged at 1,500rpm for 5 minutes at 4˚C before resuspending in 1ml complete α-MEM. Cells were counted manually with a haemocytometer and viability assessed by trypan blue exclusion.

3.2.6   Luciferase assays

Bone marrow cells were cultured for 4 days at 37˚C with 5% CO_2. Cellular adenosine triphosphate (ATP) production was measured using the CellTiter-Glo® Luminescent Cell Viability Assay (Promega, WI) as described in Section 2.4.1 Adenosine triphosphate production. Cellular total glutathione (GSH+GSSG) and oxidised glutathione (GSSG) production was measured using the GSH/GSSG-Glo®

Assay (Promega, WI) as described in Section 2.4.2 Glutathione anti-oxidation system. Glucose uptake was measured using the Glucose Uptake-Glo® Assay (Promega, WI) as described in Section 2.4.3 Glucose uptake. Luminescence was recorded using the FLUOstar Optima plate reader (BMG Labtech, Germany) with an adjusted gain for the best optical range. Samples were measured in triplicate for each treatment group and analysed as relative fluorescent values.

3.2.7   Fluorescence-associated cell sorting (FACS)

Following isolation, 5 million splenic cells were transferred to a 96-well U-bottom plate for staining. Staining was conducted as described in Section 2.5.2 Fluorescence-activated cell sorting (FACS). Flow cytometric analysis was performed on 1 million cells by following the staining protocol described in Section 2.5.1 Flow cytometry. NK cells were stained with the panel described in Table 3.2, CD4+ T cells with those in Table 3.3, CD8+ T cells with those in Table 3.4 and the panel listed in Table 3.5 for DCs. FACS and flow cytometry acquisition were performed using the BD FACSAria IIU system (Becton Dickson, NJ).

Table 3.2   Antibodies and metabolic dyes used for NK cell identification and analysis

SURFACE MARKER	FLUOROPHORE	CLONE	RETAILER	DILUTION
Propidium iodide	Phycoerythrin (PE)/Texas Red	n/a	ThermoFisher, MA	1:200
CD3	Allophycocyanin (Apc)/Cyanine (Cy)7	17A2	BioLegend, CA	100ng/million
NK-1.1	Pacific Blue	PK136	BioLegend, CA	100ng/million
CD27	PE/Cy7	LG.3A10	BioLegend, CA	100ng/million
CD11b	Apc	M1/70	BioLegend, CA	100ng/million
MitoTracker Green	Fluorescein (FITC)	n/a	ThermoFisher, MA	150nM
TMRE	PE	n/a	Sigma-Aldrich, MO	25nM

Table 3.3   Antibodies and metabolic dyes used for CD4+ T cell identification and analysis

SURFACE MARKER	FLUOROPHORE	CLONE	RETAILER	DILUTION
Propidium iodide	PE/Texas Red	n/a	ThermoFisher, MA	1:200
CD3	Apc/Cy7	17A2	BioLegend, CA	100ng/million
CD4	Pacific Blue	RM4-4	BioLegend, CA	100ng/million
CD62L	PE/Cy7	MEL-14	BioLegend, CA	100ng/million
CD44	Apc	IM7	BioLegend, CA	100ng/million
MitoTracker Green	FITC	n/a	ThermoFisher, MA	150nM
TMRE	PE	n/a	Sigma-Aldrich, MO	25nM

Table 3.4   Antibodies and metabolic dyes used for CD8+ T cell identification and analysis

SURFACE MARKER	FLUOROPHORE	CLONE	RETAILER	DILUTION
Propidium iodide	PE/Texas Red	n/a	ThermoFisher, MA	1:200
CD3	Apc/Cy7	17A2	BioLegend, CA	100ng/million
CD8a	Pacific Blue	53-6.7	BioLegend, CA	100ng/million
CD62L	PE/Cy7	MEL-14	BioLegend, CA	100ng/million
CD44	Apc	IM7	BioLegend, CA	100ng/million
MitoTracker Green	FITC	n/a	ThermoFisher, MA	150nM
TMRE	PE	n/a	Sigma-Aldrich, MO	25nM

Table 3.5   Antibodies and metabolic dyes used for DC identification and analysis

SURFACE MARKER	FLUOROPHORE	CLONE	RETAILER	DILUTION
Propidium iodide	PE/Texas Red	n/a	ThermoFisher, MA	1:200
CD3	Pacific Blue	17A2	BioLegend, CA	100ng/million
Ly-6G	Pacific Blue	1A8	BioLegend, CA	100ng/million
CD19	Pacific Blue	6D5	BioLegend, CA	100ng/million
NK-1.1	Pacific Blue	PK136	BioLegend, CA	100ng/million
CD11c	Apc/Cy7	N418	BioLegend, CA	100ng/million
I-A/I-E	Apc/Cy7	M5/114.15.2	BioLegend, CA	100ng/million
CD8a	Apc	53-6.7	BioLegend, CA	100ng/million
CD11b	PE/Cy7	M1/70	BioLegend, CA	100ng/million
MitoTracker Green	FITC	n/a	ThermoFisher, MA	150nM
TMRE	PE	n/a	Sigma-Aldrich, MO	25nM

3.2.8   Confocal microscopy

Sorted cells were stained for live-cell analysis of mitochondria as described in Section 2.2.3 Confocal microscopy. Cells were imaged using a Leica SP8 Confocal microscope system (Leica, Germany) contained within a 37°C incubator supplemented with 5% CO_2 for live-cell imaging. Images were analysed using Imaris software (Oxford Instruments, UK). Some images were analysed by Eileen Li as part of her research placement with Dr Sylvia Pender.

3.2.9   Statistical analysis

Data normality was tested using SPSS. Data generated from TEM and RT-qPCR experiments was analysed in SPSS using the Kruskal-Wallis test, a non-parametric equivalent of a one-way ANOVA on ranks. Genotypic and age-related analyses were conducted in unison. Dunn-Bonferroni *post-hoc* analysis was performed for identifying significance between groups. Unpaired students t-tests were used to analyse luciferase assay data in SPSS. Graphs were created using GraphPad Prism software by entering descriptive data obtained within SPSS. FACS and confocal microscopy data were analysed by two-way ANOVA in GraphPad. A *p* value of <0.05 was used to identify significance.

3.3   Results

3.3.1   Mitochondria increase in size with age in both WT and KO mice

In order to begin studying the mitochondrial landscape within *Timp3*$^{-/-}$ (KO) and C57BL/6J (WT) mice, mitochondrial structure was analysed using transmission electron microscopy (TEM). TEM has a greater resolution than traditional light microscopy techniques for identifying mitochondrial ultrastructure. Representative images of mitochondria in the bone marrow of WT and KO mice are shown in Figure 3.4.
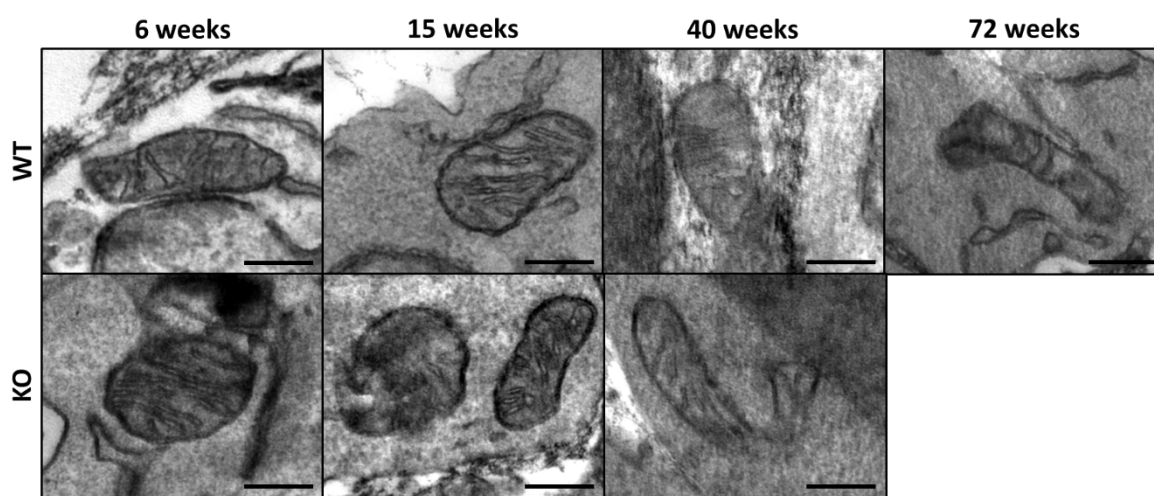
Figure 3.4   Structure of bone marrow mitochondria from WT and KO mice analysed by TEM (scale= 200nm)

By taking measurements of these mitochondria no significant changes in the cross-sectional length of mitochondria were observed with ageing in either KO or WT mice (Figure 3.5A). However, mitochondrial width was affected by ageing. Mitochondria in isolated bone marrow cells from 6 week old KO mice were significantly wider than those present in WT mice by ~19nm ($p < 0.05$; Figure 3.5B). This suggests that knock-out of *Timp3* affects mitochondrial structure. A significant increase in mitochondrial width was observed with age in the bone marrow of WT mice, increasing from 6 weeks of age to 40 weeks and 72 weeks of age by up to 24% ($p < 0.001$; Figure 3.5B). However, this increase was not observed with age in KO mice bone marrow. Finally, mitochondrial cross-sectional area was shown to significantly increase with age in both WT and KO mice bone marrow (Figure 3.5C). Whilst mitochondrial cross-sectional area was increased by 22% ($p < 0.05$) from 6 weeks to 72 weeks of age in WT mice, it was increased by 33% ($p < 0.05$) from 15 weeks to 40 weeks of age in KO mice. Together these results suggest that mitochondrial structure is regulated differently with age in the bone marrow of WT and KO mice.
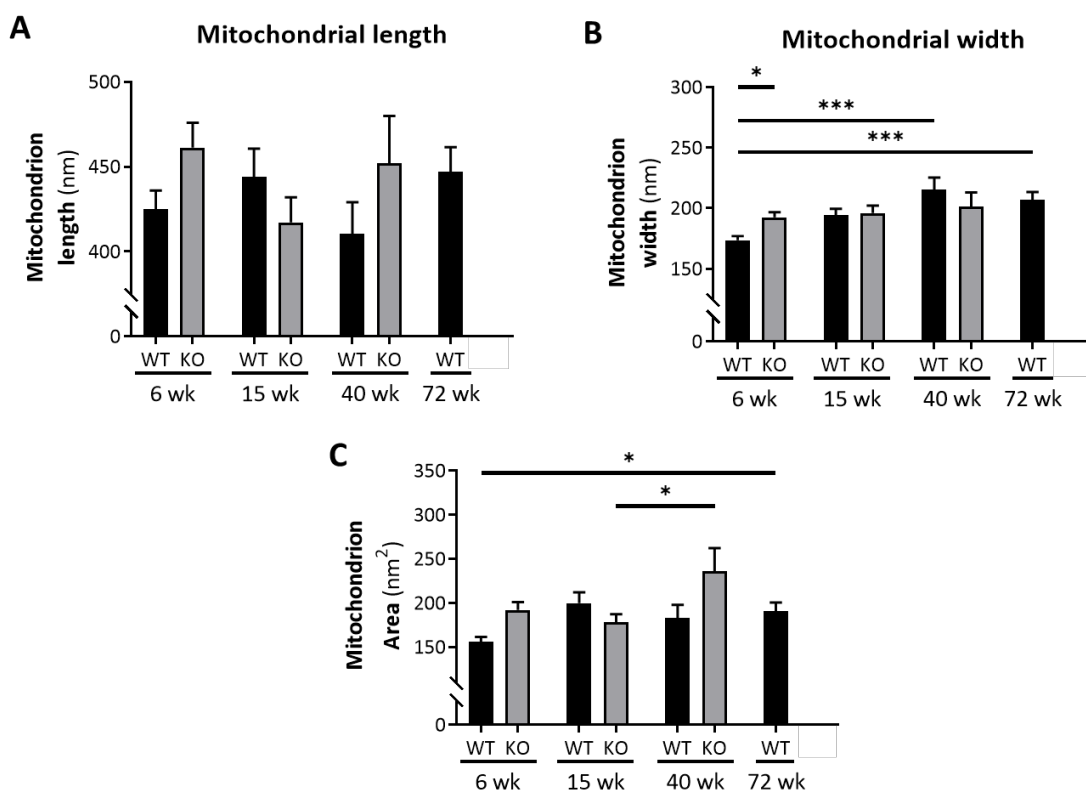
Figure 3.5   Measurement of bone marrow mitochondria structure showing (A) mitochondrial length (B) mitochondrial width and (C) mitochondrial cross-sectional area in WT and KO mice (mean+SEM; n=7; Kruskal-Wallis test by ranks; *p<0.05, ***p<0.001)

3.3.2   Mitochondrial volume and surface area are not altered with age in either WT or KO mice

3D reconstruction using TEM is limited by sample thickness of <100nm (Mannella, 2006). As mitochondria can be several microns in size, mitochondria within bone marrow cells was analysed using serial block-face scanning electron microscopy (SBF-SEM), also known as 3-view (Figure 3.6A). SBF-SEM allows for complete 3D reconstruction of the mitochondrial landscape with a slight loss in resolution compared to TEM. A total of 20 mitochondria were analysed using this method from a total of 5 cells within each sample. Due to the time-intensive nature of SBF-SEM image processing an *n* of 3 was used for each study group at 15 weeks and 40 weeks of age. In contrast to mitochondria measured by TEM, no significant changes in mitochondrial surface area or mitochondrial volume were observed with age in either WT or KO bone marrow (Figure 3.6B and C). Similarly, there was no effect of age on these parameters in either of the models studied due to the small sample size. Combined with findings using TEM, these results suggest that whilst mitochondrial cross-sectional structure is altered by ageing within WT and KO mice bone marrow, these changes may not affect mitochondrial volume or surface area in these cells. It should be noted that only samples from mice of 15 weeks and 40 weeks of age were included in this analysis due to

the labour intensive nature of SBF-SEM. Due to the small sample size the observed power of these experiments was reported as 0.114 and 0.129 for mitochondrial surface area and volume respectively, and therefore has a lack of power.
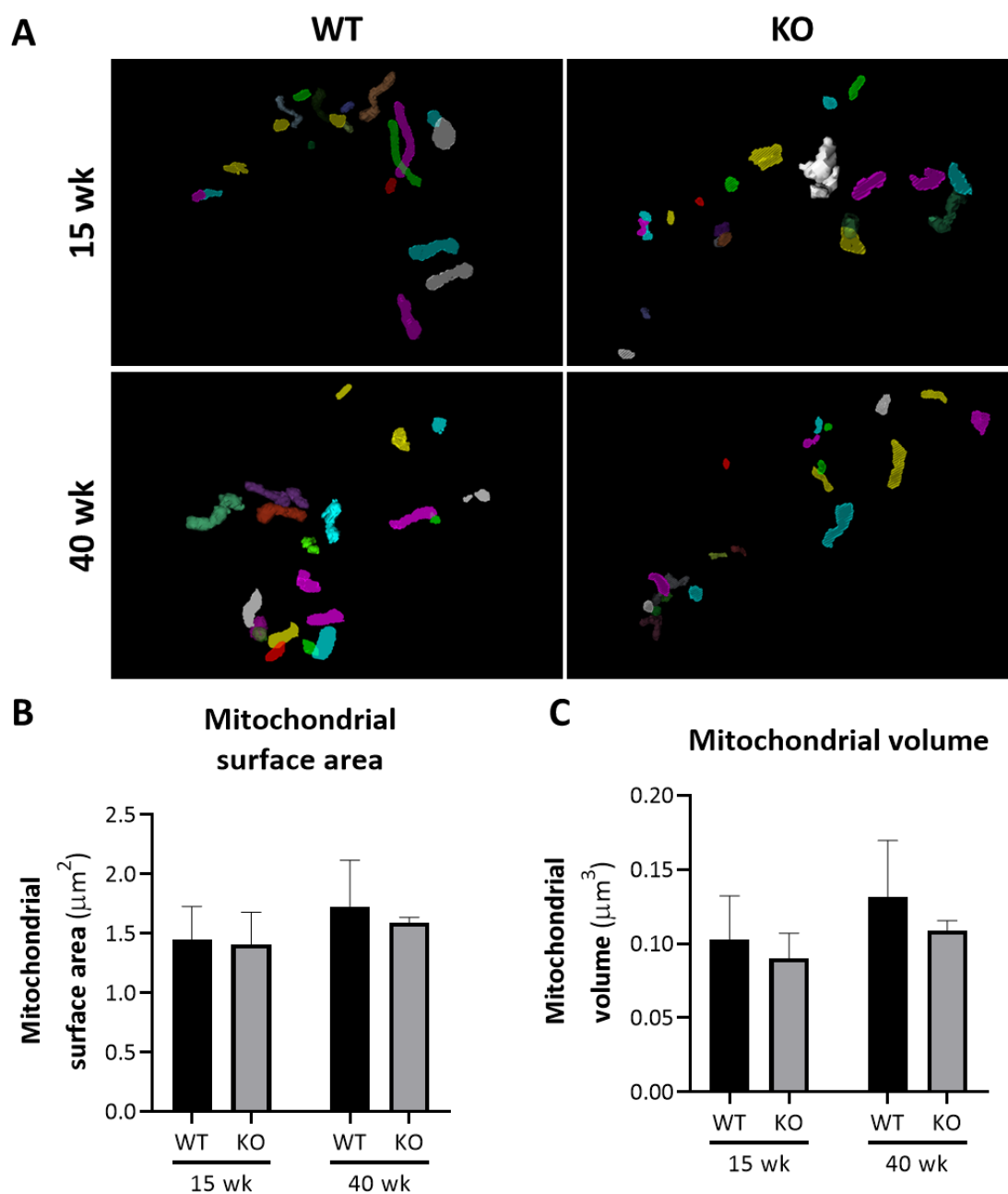
Figure 3.6   Volume and surface area of mitochondria in bone marrow cells showing (A) 3-dimensional rendering of 20 mitochondria from 5 cells per mouse using 3view, (B) mitochondrial volume and (C) mitochondrial surface area in WT and KO mice (mean+SEM; n=3; Two-way ANOVA)

3.3.3 Mitochondrial fission and fusion gene expression patterns are altered with age in WT mice but are not affected in KO mice

In order to confirm the findings from this TEM and SBF-SEM study, the expression of five mitochondrial fission and fusion genes was measured at the ribonucleic acid (RNA) level by reverse transcription polymerase chain reaction (RT-qPCR). The expression profiles of two mitochondrial fission genes *Dynamin-related protein 1L* (*Dnm1L*) and *Fission 1* (*Fis1*) and three mitochondrial fusion genes *Mitofusin 1* and *2* (*Mfn1* and *Mfn2*) and *Optic atrophy 1* (*Opa1*) were measured in this study.

No effect of genotype or age on the expression of mitochondrial fission genes *Dnm1L* or *Fis1* was found in bone marrow cells (Figure 3.7A and B). However, whilst *Mfn2* expression was unchanged, both the *Mfn1* and *Opa1* genes of the mitochondrial fusion machinery were affected by either age or genotype (Figure 3.7C-E). *Mfn1* expression was increased with age in the bone marrow of WT mice between both 6 weeks and 40 weeks of age (77%; $p < 0.01$) and 15 weeks to 40 weeks of age (2-fold; $p < 0.001$). However, these changes were not observed in KO mice bone marrow cells (Figure 3.7D). This increase may aid understanding on the differences in mitochondrial width observed within the bone marrow of WT mice with age and not KO mice.

Additionally, an effect of genotype on *Opa1* expression at 6 weeks and 15 weeks of age was observed between WT and KO mice bone marrow (Figure 3.7E). *Opa1* gene expression was increased by 34% ($p < 0.05$) and 88% ($p < 0.05$) at 6 weeks and 15 weeks of age respectively in the bone marrow of KO mice compared to WT. This difference in the expression of *Opa1* was not apparent at 40 weeks of age. These results suggest that alterations in mitochondrial structure of bone marrow cells in WT and KO mice may be due to changes in the expression of genes involved in the mitochondrial fusion process.
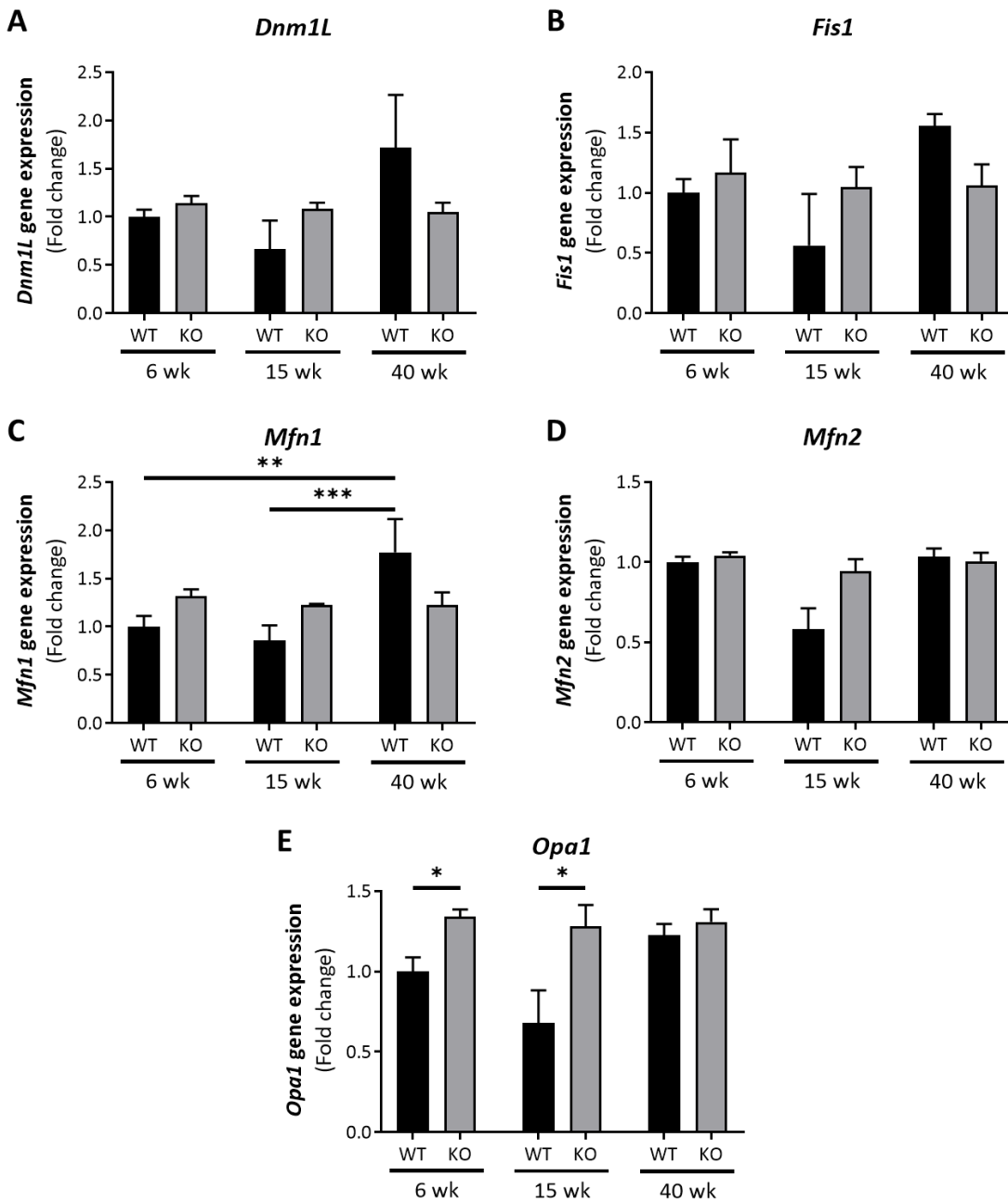
Figure 3.7   Gene expression analysis of mitochondrial fission and fusion genes in bone marrow cells showing (A) dynamin related protein 1L (*Dnm1L*) epxression (B) fission protein 1 (*Fis1*) expression (C) mitofusin 1 (*Mfn1*) expression (D) mitofusin 2 (*Mfn2*) expression and (E) optic atrophy 1 (*Opa1*) expression in WT and KO mice normalised to β-actin expression and relative to WT gene expression at 6 weeks of age (mean+SEM; n=5; Kruskal-Wallis test by ranks; *p<0.05 **p<0.01 ***p<0.001)

3.3.4   Altered cristae structure in WT bone marrow cells is associated with decreased ATP production

As mitochondrial fission and fusion gene expression is involved in the regulation of mitochondrial ultrastructure, particularly that of *Opa1*, the structure of cristae contained within the mitochondria of bone marrow cells from WT and KO mice was analysed across the life course. Several mitochondria with 'swollen' (tubular) cristae compared to the tight (laminar) structure were observed. The differences between the cristae can be observed in Figure 3.8A.

By quantifying the ratio of laminar and tubular cristae within each mitochondrion, a significant increase in the percentage of tubular cristae in bone marrow cells was observed with age in WT mice (Figure 3.8B). The percentage of tubular cristae in WT mice, increased from 13% at 6 weeks and 14% at 15 weeks to 22% at 72 weeks of age ($p < 0.05$). However, the percentage of tubular cristae observed in KO mouse bone marrow remained stable across the timepoints studied, ranging from 11-13% (Figure 3.8B).
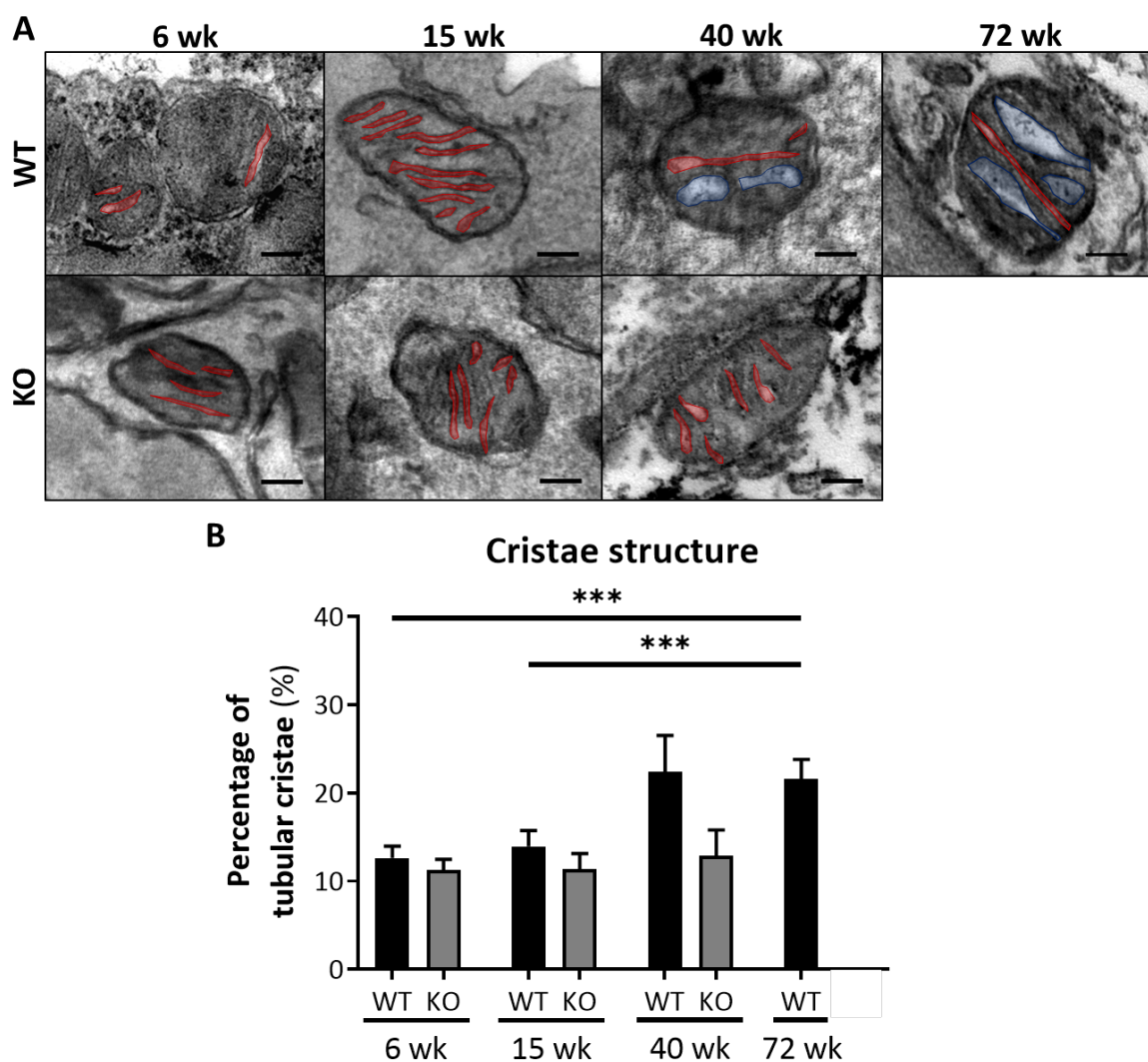
Figure 3.8   Mitochondrial cristae structure in bone marrow mitochondria showing (A) TEM of mitochondrial cristae with laminar (red) and tubular (blue) structure (scale= 100nm) and (B) percentage of tubular cristae per mitochondria in WT and KO mice (mean+SEM; n=5; Kruskal-Wallis test by ranks; ***p<0.001)

Further analysis of mitochondrial cristae structure at 40 weeks of age in WT and KO mice bone marrow, revealed a significant increase in the percentage of laminar cristae present in KO compared to WT mice at 87% and 78% respectively (p<0.01; Figure 3.9A). As the electron transport chain (ETC) machinery is situated on the inner mitochondrial membrane, it was tested whether adenosine triphosphate (ATP) production was affected by altered cristae structure within the bone marrow of WT and KO mice at 40 weeks of age. A significant increase in ATP production was observed in KO mice compared to WT bone marrow (Figure 3.9B) mirroring the percentage of laminar cristae present within the mitochondria. These results suggest that the retention of laminar cristae in older KO mice bone marrow is associated with increased ATP production within the animals. Conversely the loss of laminar cristae in WT bone marrow affects energy production within these cells.
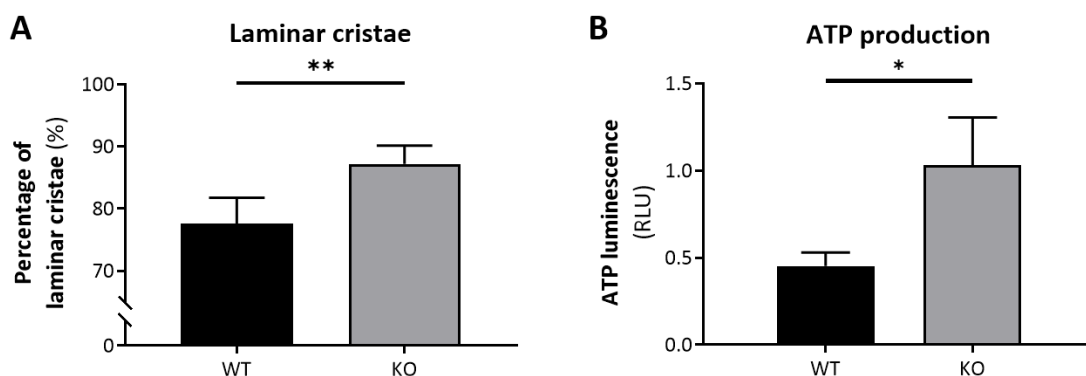
Figure 3.9   Comparison of cristae structure and ATP production in bone marrow cells showing (A) percentage of tubular cristae per mitochondria (mean+SEM; n=5; Unpaired t test; **p<0.001) and (B) ATP production measured by luciferase assay showing relative luminescent units (RLU) in WT and KO mice (mean+SEM; n=3; Unpaired t test; *p<0.05)

3.3.5   The glutathione anti-oxidative pathway shows alteration in KO mice with age whilst glucose uptake is increased in both WT and KO mice with age

Previous studies have suggested that KO mice may be characterised by increased oxidative stress, the glutathione anti-oxidation system in bone marrow cells from WT and KO mice was analysed at 6 weeks and 40 weeks of age. Total glutathione levels consist of both the reduced (GSH; glutathione) and oxidised (GSSG) forms of glutathione. No alterations in total glutathione level were observed between genotypes or with age in bone marrow cells (Figure 3.10A). However, the level of GSSG was significantly reduced at 40 weeks in KO bone marrow cells compared to WT (p<0.05; Figure 3.10B).

As ATP production was reduced in association with cristae structure in bone marrow cells from 40 week old WT mice, the glucose uptake of bone marrow cells from WT and KO mice at 6 weeks and 40 weeks of age was measured (Figure 3.10C). Whilst no changes in glucose uptake were detected between bone marrow cells from KO and WT mice at either 6 weeks or 40 weeks of age, a significant increase in glucose uptake was detected with age in bone marrow cells from both WT and KO mice. Whilst WT mice increased their glucose uptake by 3.5-fold (p<0.001), KO mice increased glucose uptake by 5.5-fold (p<0.001) with age in the bone marrow.
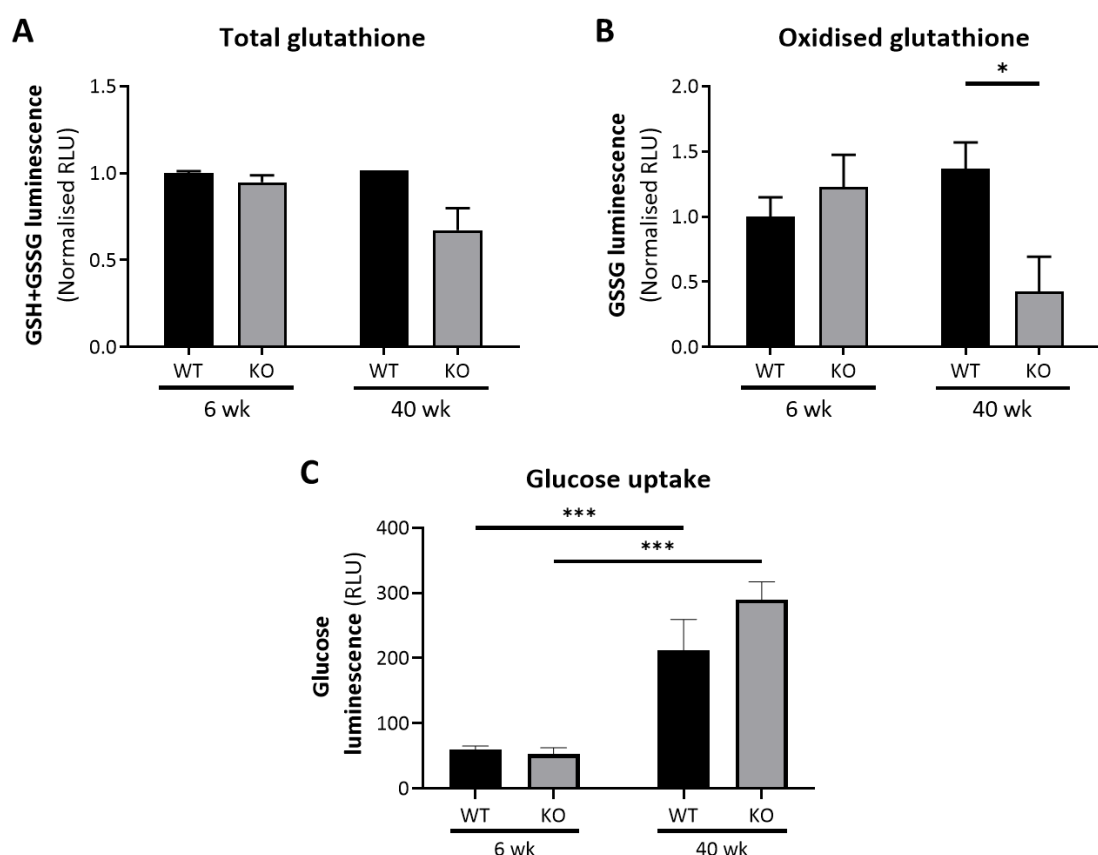
Figure 3.10 Glutathione anti-oxidant system and glucose uptake in bone marrow cells showing (A) total glutathione (GSH+GSSG) relative luminescent units (RLU) level (B) oxidised glutathione (GSSG) level (mean+SEM; n=3; Kruskal-Wallis by ranks; *p<0.05) and (C) glucose uptake in bone marrow cells from WT and KO mice (mean+SEM; n=5; Two-way ANOVA; ***p<0.001)

3.3.6 KO mice show maturation defects within the CD4+ T cell compartment with age whilst WT mice show alterations in DC populations

Previous research has suggested that immune cell populations are altered with age in KO mice (Martelli, 2017). Therefore, the percentage of CD4+ and CD8+ T cell, natural killer (NK) and dendritic cell (DC) subset compartmentalisation was analysed within the spleen of this cohort of WT and KO mice. A significant increase in the percentage of CD4+ naïve cells was observed with age in KO mice, rising from 8% to 27% of the CD4+ cell population between 6 weeks and 40 weeks of age (p<0.05; Figure 3.11). Concurrently, a significant decrease in the percentage of CD4+ effector memory (EM) cells was observed in these mice representing 36% and 15% of the CD4+ population at 6 weeks and 40 weeks of age respectively in KO mice (p<0.05; Figure 3.11A). The percentage of CD4+ central memory (CM) cells was unaltered by both genotype and age. Whilst a trend towards an increased

proportion of naïve and decreased proportion of EM cells was seen within the CD8+ T cell population, this did not reach significance for either WT or KO animals (Figure 3.11B).

Alterations in the compartmentalisation of NK cells along the maturation pathway was not observed to be changed by age in the spleen of either WT or KO mice (Figure 3.11C). However, a decrease in the percentage of CD11b+ DCs within the CD11c+ major histocompatibility complex (MHC) Class II (I-A/I-E)+ population was observed in response to both age and genotype (Figure 3.11D). Ageing within WT mice saw a reduction in CD11b+ DC proportion in the spleen from 36% at 6 weeks to 26% at 40 weeks of age (p<0.001). This reduction was not apparent within KO mice however, as KO mouse spleen showed a reduction in CD11b+ DC percentage to 24% at 6 weeks of age. The CD11b+ DC population was significantly reduced in KO mice spleen compared to WT mice at 6 weeks of age (p<0.01). Despite these changes, no differences in the proportion of CD8a+ DCs was observed between phenotypes or with age (Figure 3.11D). These results suggest that the CD4+ T cell and DC populations are altered within the spleen of KO mice.
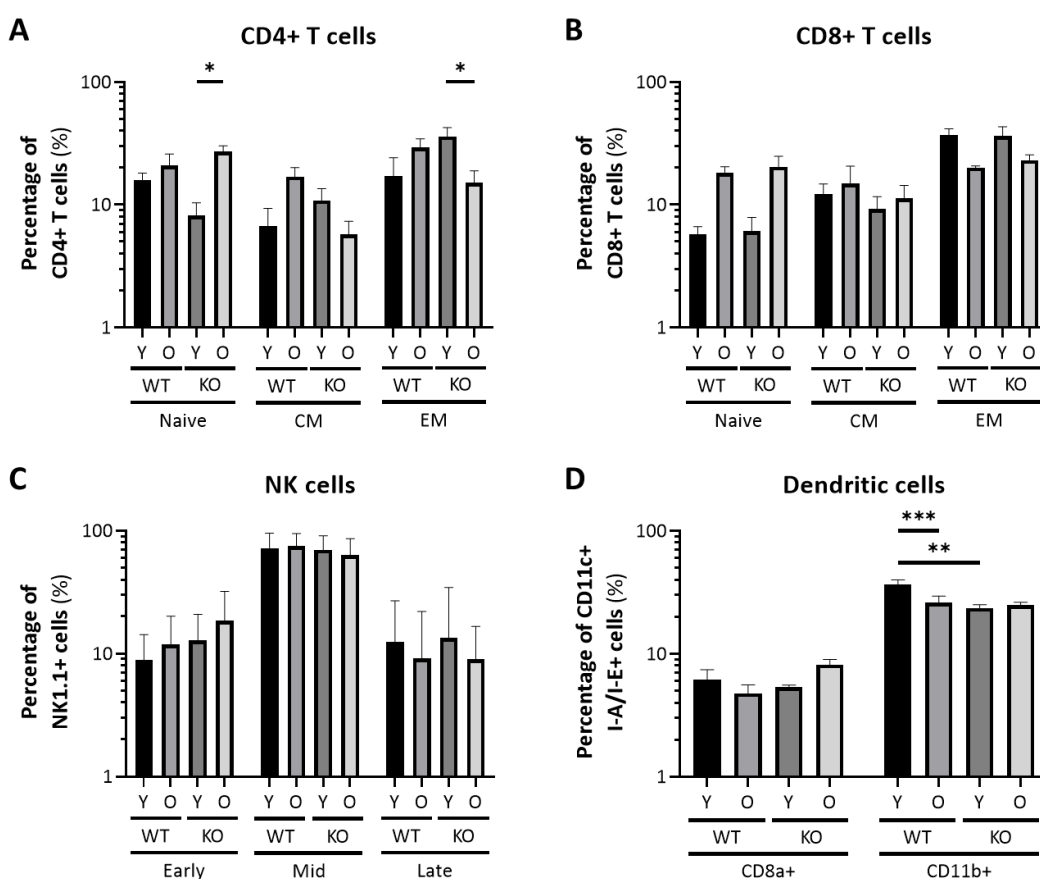
Figure 3.11 Analysis of immune cell populations in the spleen with age showing (A) CD4+ T cell subsets as a percentage of total CD4+ cells (B) CD8+ T cell subsets as a percentage of total CD8+ cells (C) NK cell subsets as a percentage of total NK1.1+ cells and (D) DC subsets as a percentage of total I-A/I-E+ cells in WT and KO mice (Y=6 week; O=40 week) (mean+ SEM; n=8; Three-way ANOVA; *p<0.05 **p<0.01 ***p<0.001)

3.3.7   CD4+ T cells show alterations in mitochondrial mass and membrane potential in old KO mice compared to WT

As defects in immune cell maturation have previously been described within KO mice, the mitochondrial mass and membrane potential of these subsets was analysed to identify any alterations in metabolism which may occur. MitoTracker Green (MTG) was used as a marker of mitochondrial mass, whilst tetramethylrhodamine ethyl ester (TMRE) normalised to MTG staining was used to as a marker of mitochondrial membrane potential.

Within naïve CD4+ T cells, a significant decrease in MTG staining was observed with age in WT mice (Figure 3.12A). Mitochondrial mass was reduced by approximately one-third in this instance ($p<0.05$), whilst no alterations were observed within naïve CD4+ T cells from KO mice. Surprisingly, an increase in mitochondrial membrane potential was observed with age in WT mice ($p<0.05$; Figure 3.12B), and a reduction in mitochondrial membrane potential was observed in KO mice compared to WT mice at 40 weeks of age ($p<0.01$). Similarly, these alterations were observed within CM and EM CD4+ T cells. Reduced mitochondrial mass was observed within 40 week old WT mice compared to their 6 week old counterparts for both CM ($p<0.05$; Figure 3.12C) and EM ($p<0.05$; Figure 3.12D) cells. Additionally, mitochondrial mass was reduced in KO mice at 6 weeks of age in comparison to WT mice by 76% ($p<0.05$; Figure 3.12C). Increased mitochondrial membrane potential with age was observed within WT mice for both CM ($p<0.01$; Figure 3.12D) and EM ($p<0.01$; Figure 3.12F) cells, resulting in reduced mitochondrial membrane potential in 40 week old KO mice compared to WT (CM $p<0.01$; EM $p<0.001$). These results suggest that mitochondrial mass and membrane potential with CD4+ T cells are regulated differently with age in WT and KO mice.
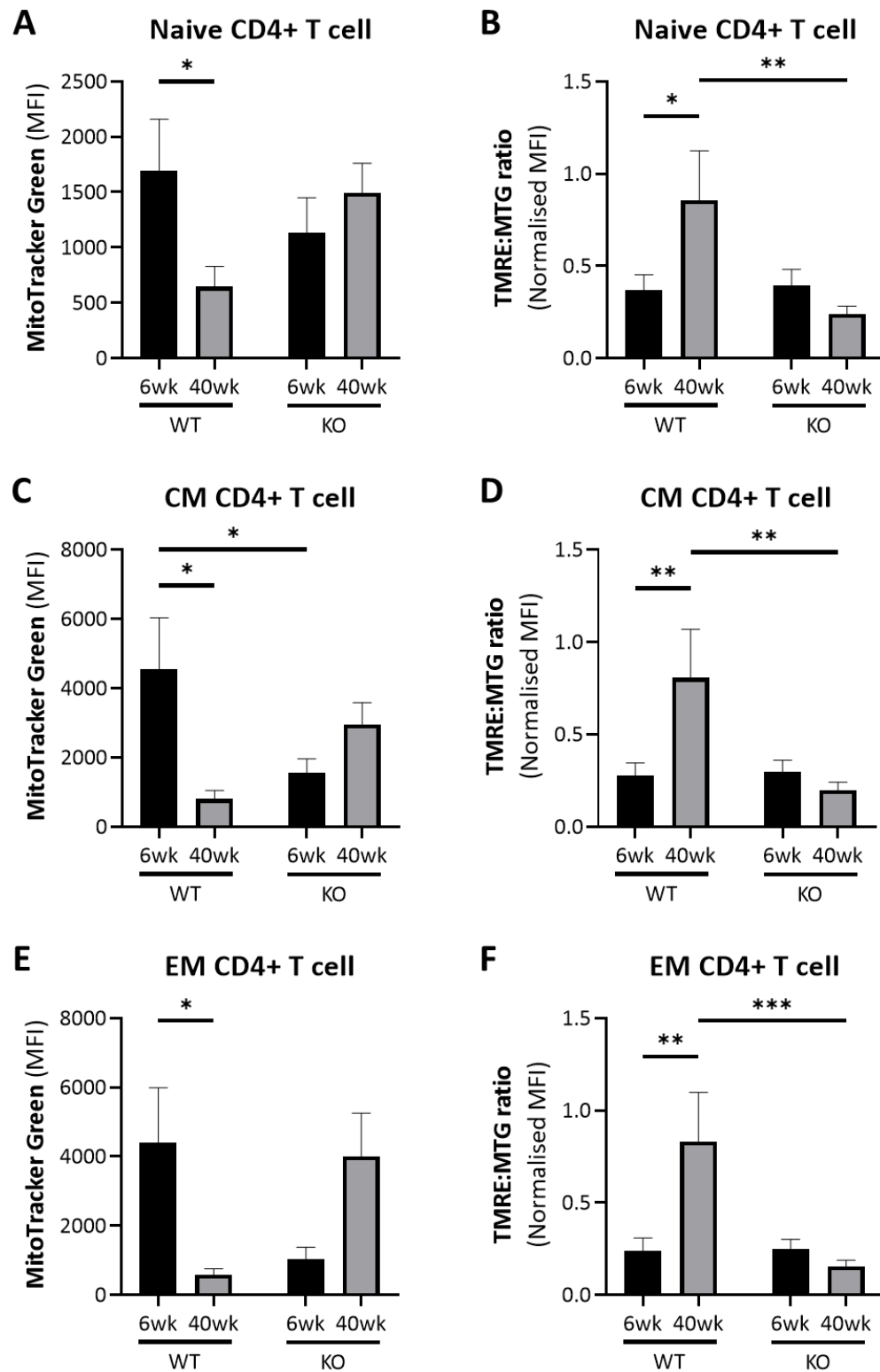
Figure 3.12 Mitochondrial mass and membrane potential in CD4+ T cell subsets showing (A) mitochondrial mass in naïve CD4+ cells (B) mitochondrial membrane potential in naïve CD4+ cells (C) mitochondrial mass in CD4+ CM cells (D) mitochondrial membrane potential in CD4+ CM cells (E) mitochondrial mass in CD4+ EM cells and (F) mitochondrial membrane potential in CD4+ EM cells from the spleen of WT and KO mice (mean+SEM; n=8; Two-way ANOVA; *p<0.05 **p<0.01 ***p<0.001)

Contrary to CD4+ T cells, an increase in mitochondrial mass with age in KO mice for naïve, CM and EM CD8+ T cells was observed (Figure 3.13A, C and E). MTG staining was increased 4.7-fold within naïve cells ($p<0.05$), 4-fold in CM cells ($p<0.05$) and 4.4-fold in EM cells ($p<0.05$). This resulted in increased mitochondrial mass in CD8+ T cells in KO mice at 40 weeks of age compared to WT within these subsets ($p<0.05$; Figure 3.13A, C and E). Measurement of mitochondrial membrane potential within these cells revealed a significant decrease in 40 week old KO mice compared to WT for naïve, CM and EM CD8+ T cells (Figure 3.13B, D and F). Mitochondrial membrane potential was reduced to approximately one-fifth of that observed within 40 week old WT CD8+ T cells. As with CD4+ T cells, this suggests that mitochondrial mass and membrane potential are regulated differently with age within CD8+ T cells. However, the way these parameters are regulated opposes that observed within CD4+ T cells, highlighting the differences between helper and cytotoxic T cells.
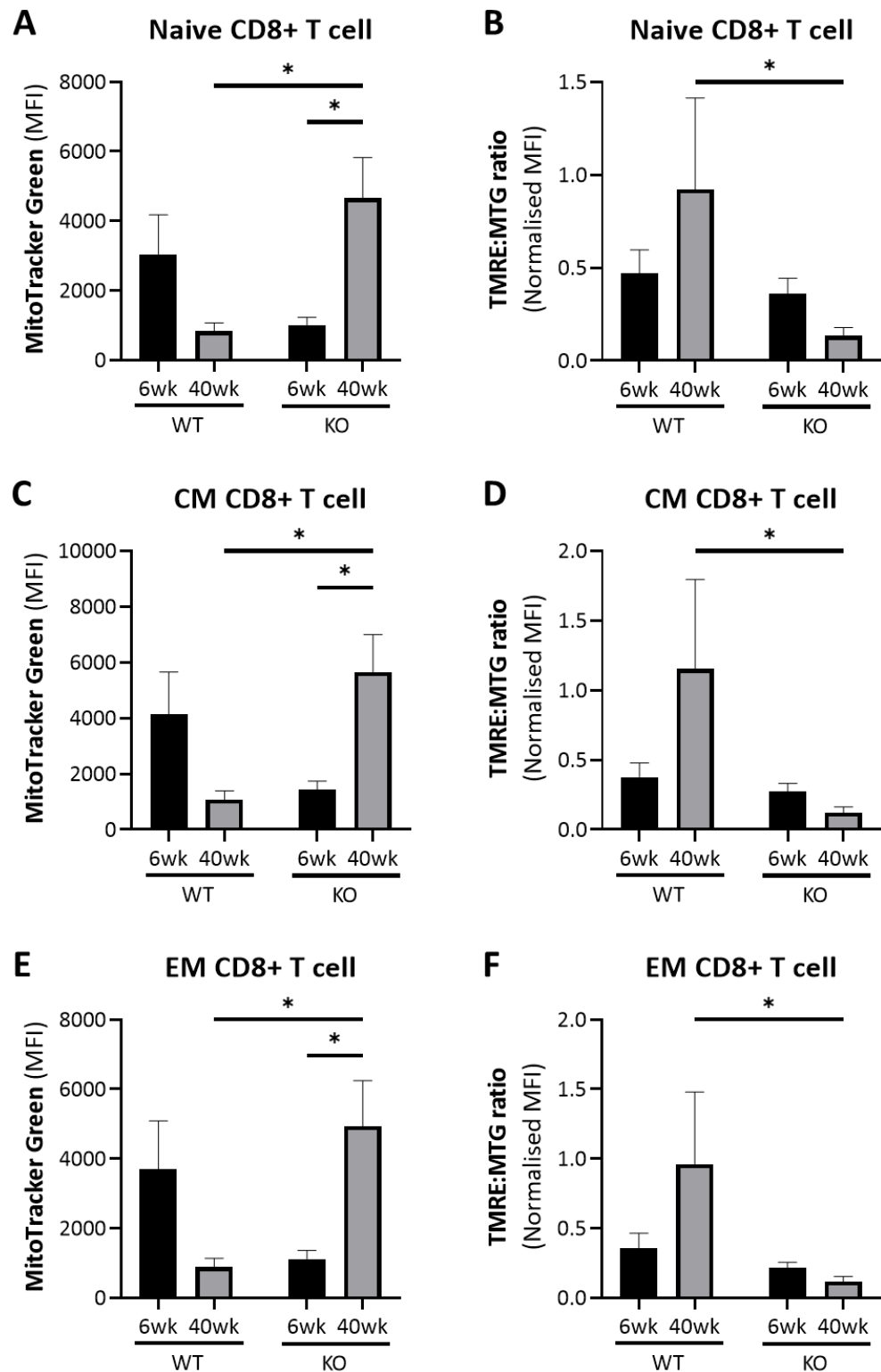
Figure 3.13 Mitochondrial mass and membrane potential in CD8+ T cell subsets showing (A) mitochondrial mass in CD8+ naïve cells (B) mitochondrial membrane potential in naïve CD8+ cells (C) mitochondrial mass in CD8+ CM cells (D) mitochondrial membrane potential in CD8+ CM cells (E) mitochondrial mass in CD8+ EM cells and (F) mitochondrial membrane potential in CD8+ EM cells from the spleen of WT and KO mice (mean+SEM; n=8; Two-way ANOVA; *p<0.05)

Due to previous observations of maturation defects in NK cells from the spleen of KO mice (Martelli, 2017), three subsets of NK cells along the maturation pathway were analysed by flow cytometry. A significant increase in mitochondrial mass was observed with age within KO mice within two of the subsets studied. MTG staining was tripled within early NK cells ($p<0.05$; Figure 3.14A) and mid NK cells ($p<0.05$; Figure 3.14C). Late NK cells were not subject to this increase, however all three subsets showed increased mitochondrial mass in 40 week old KO mice compared to WT controls ($p<0.05$; Figure 3.14E). This result was related to decreased mitochondrial membrane potential in 40 week old KO mice compared to WT mice for NK cells (Figure 3.14B, D and F). Membrane potential was reduced by 78% ($p<0.001$), 60% ($p<0.001$) and 30% ($p<0.001$) within early, mid and late NK cells respectively. Surprisingly, all three NK cell stages studied doubled their mitochondrial membrane potential staining with age in WT mice ($p<0.01$; Figure 3.14B, D and F). Similarly, to CD4+ and CD8+ T cells, this suggests that immune cells within KO mice regulate the mitochondrial landscape differently to that observed within WT mice.
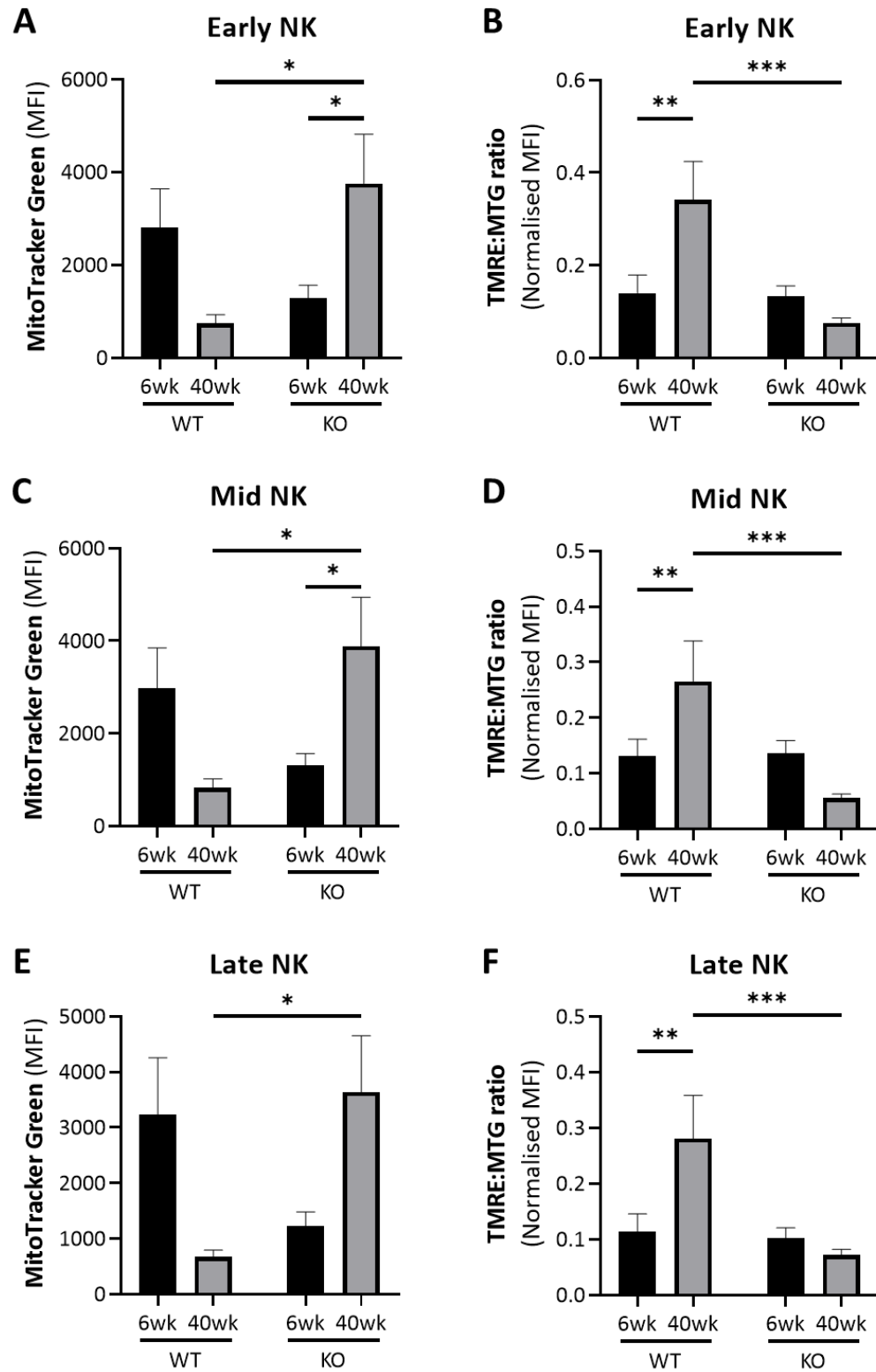
Figure 3.14 Mitochondrial mass and membrane potential in NK cell subsets showing (A) mitochondrial mass in early NK cells (B) mitochondrial membrane potential in early NK cells (C) mitochondrial mass in mid NK cells (D) mitochondrial membrane potential in mid NK cells (E) mitochondrial mass in late NK cells and (F) mitochondrial membrane potential in late NK cells along the maturation pathway in WT and KO mouse spleen (mean+SEM; n=8; Two-way ANOVA; *$p<0.05$ **$p<0.01$ ***$p<0.001$)

Finally, the mitochondrial landscape within CD8a+ and CD11b+ DCs was studied. Whilst CD8a+ DCs decreased mitochondrial mass with age in WT mice ($p<0.05$), the opposite effect was observed for KO mice which appeared to increase mitochondrial mass ($p<0.01$; Figure 3.15A). This resulted in a discrepancy between mitochondrial mass in WT and KO animals at both 6 weeks ($p<0.01$) and 40 weeks ($p<0.05$) of age. Surprisingly however, no alterations in mitochondrial membrane potential were observed for CD8a+ DCs (Figure 3.15B). CD11b+ DCs on the other hand regulated both mitochondrial mass and membrane potential differently to CD8a+ DCs. Whilst a decrease in mitochondrial mass with age was evident within CD11c+ DCs from WT mice ($p<0.05$), the increased in mitochondrial mass with age in KO mice did not reach significance (Figure 3.15C). Unlike CD8a+ DCs, CD11b+ DCs displayed a significant upregulation of mitochondrial membrane potential with age in WT mice ($p<0.01$; Figure 3.15D). Whilst this trend was observed with age for KO mice this increase did not reach significance.
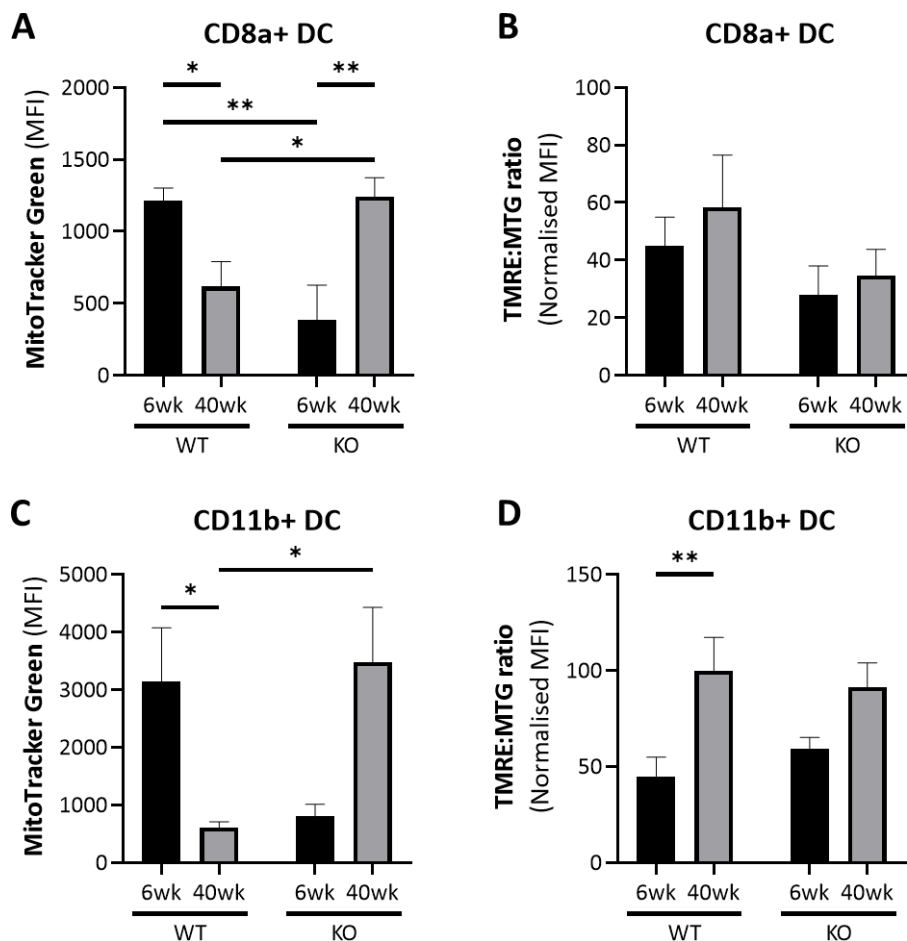
Figure 3.15 Mitochondrial mass and membrane potential in dendritic cell subsets showing (A) mitochondrial mass in CD8+ DC (B) mitochondrial membrane potential in CD8+ DC (C) mitochondrial mass in CD11b+ DC and (D) mitochondrial membrane potential in CD8+ DC from the spleen of WT and KO mice (mean+SEM; n=8; Two-way ANOVA; *$p<0.05$ **$p<0.01$ ***$p<0.001$)

3.4 Discussion: Mitochondrial structure in the bone marrow and periphery of ageing mice

Mitochondrial structure has been associated with ageing in several tissues (Senoo-Matsuda et al., 2003, Lesnefsky et al., 2001, López-Lluch et al., 2008). Mitochondrial ultrastructure has yet to be studied within TIMP3 KO mice, however here it is proposed that bone marrow mitochondria in KO mice are subject to different ageing effects compared to WT. Within WT mice, an increase in the cross-sectional measurements of bone marrow mitochondria with age but not gross volume or surface area was identified. Previous research has highlighted significant alterations in mitochondria during the ageing process within cardiac tissue (Cheng et al., 2013, Coleman et al., 1988). These results include widening of mitochondrial cross-sectional width as observed with this study utilising bone marrow cells. Whilst these alterations in mitochondrial structure are believed to be detrimental in the process of ageing, bone marrow from KO mice was not observed to be subject to the same effects. Thus, this suggests that ageing of the bone marrow in KO mice may not be due to mitochondrial dysfunction. In fact, CR which has been shown to increase life span retains mitochondrial organisation within male C57BL/6 mice (Lee et al., 2012).

Mfn1 protein expression increases with age in WT mice skeletal muscle (Joseph et al., 2013). It was found that *Mfn1* gene expression is increased with age in bone marrow cells, supporting this research. In rats however, Mfn1 has been shown to be reduced with age in muscle tissue, heart and liver (Zhao et al., 2014). This highlights the differing elements of mitochondrial dysfunction in differing ageing models. Previous studies have shown that *Opa1*-dependent modulation of cristae structure is essential for metabolic adaptation (Patten et al., 2014). Increased *Opa1* expression in the bone marrow of KO mice at 6 weeks and 15 weeks of age, may suggest that these cells are able to adapt to metabolic stress better than their WT counterparts. This further suggests that the bone marrow of KO mice is not subject to mitochondrial dysfunction during ageing to the extent of that observed within WT mice.

Perturbed *Opa1* expression has previously been shown to directly affect mitochondrial ultrastructure and ATPase activity within human skin fibroblasts and immortalised hepatocytes (Agier et al., 2012, Plecitá-Hlavatá et al., 2016). The structure of mitochondrial cristae affects mitochondrial activity by regulating the assembly and stability of the electron transport chain and ATPase activity (Cogliati et al., 2013). Here it is shown, that within bone marrow cells from 40 week old WT mice, mitochondrial cristae structure affects ATP production thus supporting previous research. It is shown that this mechanism is attributed to the ageing process in the bone marrow of WT mice. Daum *et al.* revealed an age-dependent loss of cristae structure previously within *Podospora anserine* fungus which affected ATPase dimerization (Daum et al., 2013). Evidence of

altered mitochondrial ultrastructure in *Drosophila* has been observed with age, as well as in Fisher rat cardiac muscle (Jiang et al., 2017, Hoppel et al., 2017). This research extends this finding into the bone marrow of the C57BL/6J murine model.

A significant reduction in the levels of GSSG in KO mice of 40 weeks of age compared to WT mice was observed, with a concomitant decrease in total GSH/GSSG levels in the bone marrow. This same phenomenon has been attributed to *Timp3* previously, whereby *ApoE$^{-/-}$Timp3$^{-/-}$* double knock-out mice show reduced levels of GSSG compared to single *ApoE$^{-/-}$* mice (Stöhr et al., 2015). This research supports the reduced levels of GSSG observed within these KO mice. However, a reduction in glutathione system with age as previously described for ageing mice and humans was not observed int his study (Lang et al., 1992, Samiec et al., 1998, Rebrin et al., 2007). However decreased plasma levels of glutathione have been detected in specific human studies (Hernanz et al., 2000).

A maturation defect in CD4+ T cells and the distribution of CD11b+ DCs was observed with age in the spleen of KO mice. Whilst this work supports that of Martelli in terms of CD4+ T cells, the same maturation defect within CD8+ T cell or NK cell populations was not observed (Martelli, 2017). Previous research conducted using a mammary cancer model in *Timp3$^{-/-}$* mice saw no differences in NK or CD8+ and CD4+ T cell infiltration into the mammary gland (Jackson et al., 2015). However, this study only looked at NK, CD4+ and CD8+ T cell populations and not the distribution of the subsets within them. Similarly, similar numbers of NK cells and CD4+ or CD8+ T cells have been noted in the splenocytes of KO and WT mice at 12 weeks of age (Murthy et al., 2012). Surprisingly, Timp3 has a role in the differentiation of DCs and their ability to polarise T cells (Shao et al., 2012). Within KO mice this effect was attributed to alterations in the CD11b+ (Type 2) DC population.

This study showed that although only CD4+ T cells experience an age-related maturation defect in KO mice, all the immune subsets studied showed an age-related defect in mitochondrial mass and membrane potential. Aloss of mitochondrial membrane potential was identifed in CD4+ and CD8+ T cell naïve, CM and EM populations as well as NK cells at early, mid and late points along their maturation pathway from KO mice at 40 weeks of age. These alterations were not observed for DCs however, which showed no significant change in mitochondrial membrane potential compared to WT mice at this age. This is one of the first studies of mitochondrial mass and membrane potential in immune cell populations derived from WT and KO mice at 6 weeks and 40 weeks of age. These alterations may affect immune cell functionality within these mice with age as described previously by Mavilio *et al.* and Martelli (Martelli, 2017, Mavilio et al., 2016).

3.4.1 Limitations

In effort to reduce the number of mice utilised for animal studies, this study was limited by the restricted number of mice. This smaller sample size may affect the statistical significance of some analyses. This is particularly the case for SBF-SEM data where a small number of mice (n=3) were utilised due to the labour-intensive nature of advanced microscopy techniques. As a result, this experiment exhibited a loss of power and did not reach significance. Future work could build upon this low n number within microscopy experiments by integrating high-throughput microscopy techniques such as imaging flow cytometry and imaging mass cytometry. These techniques allow for multi-parameter imaging of protein markers at subcellular resolution and would be useful for looking at global changes in mitochondrial structure with age. To date, no systems exist for high-throughput imaging of mitochondria at the ultrastructural level.

This study was unable to able to track animal ageing longitudinally and instead utilised a cross-sectional design for sampling timepoints due to the tissue type analysed. More definitive conclusions may have been reached utilising this alternative longitudinal study design and brought additional strength to the study and its conclusions. It was also not possible to fully follow the life course of WT mice due to home office licensing restrictions in place. C57BL/6J mice can live up to two years in the laboratory setting, however the oldest time point studied was 72 weeks of age. Following these mice up to 2 years of age would have helped to develop a clearer picture of ageing in both WT and KO mice and the differences which set them apart.

Techniques for studying the metabolism of live cells in small numbers are not routinely available at the University of Southampton, and as such this aspect of mitochondrial function was unable to studied. Platforms such as the Seahorse XF analyser could have been used for this research and would be useful for performing future work related to the findings of this study. These additional experiments could have been useful for looking at the impact of altered Opa1 expression and mitochondrial cristae structure on mitochondrial function which may impact the ageing process of $Timp3^{-/-}$ animals in comparison to wild-type mice.

3.5   Conclusion

Age-related differences in the cross-sectional measurements of bone marrow mitochondria within WT mice were detected which were not observed within KO mice. However, measurements of mitochondrial surface area and volume using 3-dimensional rendering suggested that these age-related differences were at the ultrastructural level. Confirmation of these findings by expression analysis of mitochondrial fission and fusion genes in bone marrow cells, revealed a relationship with *Mfn1* and *Opa1*. Further analysis of mitochondrial ultrastructure revealed the loss of laminar cristae structure with age in WT mice, which was associated with decreased ATP production within bone marrow cells. Analysis of the glutathione antioxidant system revealed a reduction in GSSG in 40 week old KO mice compared to WT, which may be influenced by the oxidative stress present within the bone marrow of these animals. KO mice exhibit alterations in the maturation status of the CD4+ T cell population and DC population within the spleen. Further analysis of these cell types by flow cytometry along with CD8+ T cells and NK cells, revealed that the mitochondrial landscape is affected differently by ageing within WT and KO mice. These findings are summarised in Figure 3.16. In summary, KO mice show elements of mitochondrial dysfunction within the bone marrow and immune system when compared to WT mice which may be associated with their diminished lifespan.
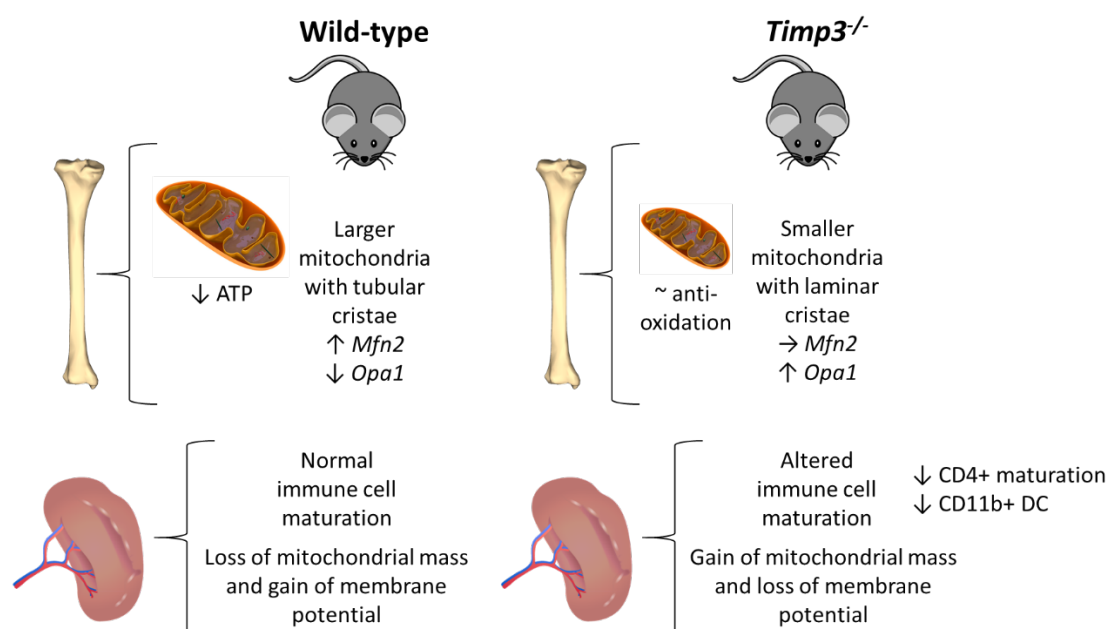
Figure 3.16   Summary of findings from ageing WT and KO mice showing altered ATP production in the bone marrow of ageing WT mice and altered immune cell maturation in the spleen of KO mice

Chapter 4   Metabolic alterations in senescence-accelerated mice (SAM) with age

4.1   Introduction

Mesenchymal stem cells from SAMP6 mice show reduced adenosine triphosphate (ATP):adenosine diphosphate (ADP) ratio compared to senescence-accelerated mice (SAM)R1 mice, alongside increased reactive oxygen species (ROS) production and increased average mitochondrial area (Lv et al., 2018). SAMP6 mice treated with 100mg/kg resveratrol, which is believed to mimic caloric restriction (CR), counteracted bone loss and reduced osteogenic decline (Lv et al., 2018). Resveratrol mimics CR by acting on similar downstream targets such as Sirtuin 1, peroxisome proliferator-activated receptor gamma coactivator 1-alpha and manganese-dependent superoxide dismutase (Lagouge et al., 2006). This was found to be the result of mitochondrial functionality restoration in mesenchymal stem cells. Resveratrol reorganised mitochondrial cristae structure within these cells, increased mitochondrial membrane potential and restored oxygen consumption. However, it should be noted that this study used a high concentration of resveratrol for treatment at 100mg/kg every other day. Human studies have used much lower resveratrol concentrations of 150mg.

SAMP8 are characterised by high levels of oxidative stress in muscle tissue compared to SAMR1 (Barquissau et al., 2017). Hydrogen peroxide (H_2O_2) production by nicotinamide adenine dinucleotide phosphate (NADPH) oxidase was found to be 70% higher in SAMP8. This affected mitochondrial function by lowering the respiratory control ratio in muscle cells, which is indicative of mitochondrial uncoupling and dysfunction. This study by Barquissau *et al.* found increased citrate synthase and complex II and IV activity within the muscle cells of SAMP8 mice, and lower complex I enzymatic activity (Barquissau et al., 2017). Lower respiratory control ratio was observed in SAMP8 liver and heart mitochondria after 12 months of age (Nakahara et al., 1998). SAMP11 show significantly higher levels of ROS compared to SAMR1 in murine dermal fibroblast-like cells and increased mitochondrial mass following extended cell culture (Chiba et al., 2005). Mitochondrial membrane potential appeared to be lower in SAMP11 fibroblasts, in line with mitochondrial ultrastructural changes including cristae swelling. Mitochondrial swelling was observed in several tissues including neurons, myocardium, hepatocytes and brown adipose tissue (Chiba et al., 2005). Similarly, reduced mitochondrial quality control in SAMP8 mice was observed in skeletal gastrocnemius muscle as measured by reduced mitochondrial biogenesis and autophagy (Chang et al., 2019).

Neurons from SAMP8 mice show lower mitochondrial membrane potential than SAMR1 neurons (Cristòfol et al., 2012), whilst mitochondrial mass remains stable. Decreased mitochondrial membrane potential in the brain of SAMP8 was confirmed by Eckert *et al.* in 2013, they observed decreased ATP concentrations and complex V protein expression within SAMP8 brain (Eckert et al., 2013). These alterations were associated with decreased expression of optic atrophy 1 (Opa1) compared to SAMR1 and increase mitofusin 1 (Mfn1) and dynamin related protein 1 (Drp1) expression.

SAMP8 mice have been shown to have mitochondrial defects in comparison to SAMR1 mice (Torregrosa-Muñumer et al., 2016). There is an age-related decrease in the expression of the mitochondrial deoxyribose nucleic acid (mtDNA) repair enzyme, apurinic/apyrimidinic endonuclease, in SAMP8 mice which is associated within increased levels of mtDNA oxidative damage in the brain. Increased levels of oxidative damage were observed in the liver of SAMP10 mice with age (Kawahara et al., 2018). However, other studies have shown that SAMP8 do not show any increase in H_2O_2 over that of SAMR1 mice at 12 months of age in the liver (Nakahara et al., 1998).

Very few studies have measured metabolism longitudinally with age in SAM. However, Nakahara *et al.* reported declines in uncoupled respiration with age alongside decreased calcium transport (Nakahara et al., 1998). Whilst uncoupled respiration was shown to increase with age in SAMR1, calcium transport decreased with age within these mice. The mitochondrial membrane potential and ATP content of platelets and hippocampi decreased at an earlier age with SAMP8 than SAMR1 mice (Xu et al., 2007). This implies that mitochondrial dysfunction occurs at an earlier age within these mice.

SAM mice represent an excellent opportunity to study immune-senescence, ageing and mitochondrial dysfunction in parallel. As the immune cells reside within both the bone marrow and spleen of mice, the SAM model was utilised to analyse mitochondrial dysfunction during ageing and senescence of the immune system. The aims and objectives for the work contained within this chapter are summarised in Figure 4.1. It was hypothesised that, in accordance with their physiology, SAMP8 mice would display dysfunction in splenic cell metabolism and SAMP6 would be subject to mitochondrial dysfunction in bone marrow cells with age.

Aim:
To investigate age-related immune cell dysfunction in the spleen and bone marrow of C57BL/6J, SAMP6 and SAMP8 mouse strains by analysing mitochondria and metabolism

Objectives:
- Analyse peripheral immune cells
  - Compare oxidative and glycolytic metabolism in C57BL/6J, SAMP6 and SAMP8 mouse strains
  - Measure ATP production and H_2O_2 production of cultured splenic cells
  - Confirm metabolic dysfunction by measuring mitochondrial mass and membrane potential in T cells, B cells, NK cells and monocytes
- Analyse immune cell compartment in bone marrow
  - Compare oxidative and glycolytic metabolism in C57BL/6J, SAMP6 and SAMP8 mouse strains
  - Measure ATP production, H_2O_2 production and glucose concentration of cultured bone marrow cells
  - Confirm metabolic dysfunction by measuring mitochondrial mass and membrane potential in eosinophils, monocytes, neutrophils and B cells

Figure 4.1   Aims and objectives for studying age-related mitochondrial dysfunction in C57BL/6J, SAMP6 and SAMP8 mouse strains

4.2 Materials and methods

4.2.1 Animals and cell culture

The animals used within this experimental chapter and ethical details are described in Section 2.1.1.1.2 Senescence-accelerated mouse (SAM) study. A total of 30 C57BL/6J mice, 30 SAMP6 and 30 SAMP8 were used for the purpose of this study. 15 mice within each group were less than 3 months of age (young) and 15 more than 12 months of age (old). Bone marrow was flushed into α-minimum essential medium (ThermoFisher, MA) containing 10% FBS (ThermoFisher, MA) (complete α-MEM) as described in Section 2.1.1.2 Isolation of cells for animal studies. Splenocytes were also collected in complete α-MEM. For long term storage cells were processed as described in Section 2.1.3 Cell culture and tissue storage. Tissue was collected from animals at the time points shown in Figure 4.2.

Young <3 months	C57BL/6J	SAMP6	SAMP8
	•Spleen	•Spleen	•Spleen
	•Bone marrow	•Bone marrow	•Bone marrow
Old >12 months	C57BL/6J	SAMP6	SAMP8
	•Spleen	•Spleen	•Spleen
	•Bone marrow	•Bone marrow	•Bone marrow
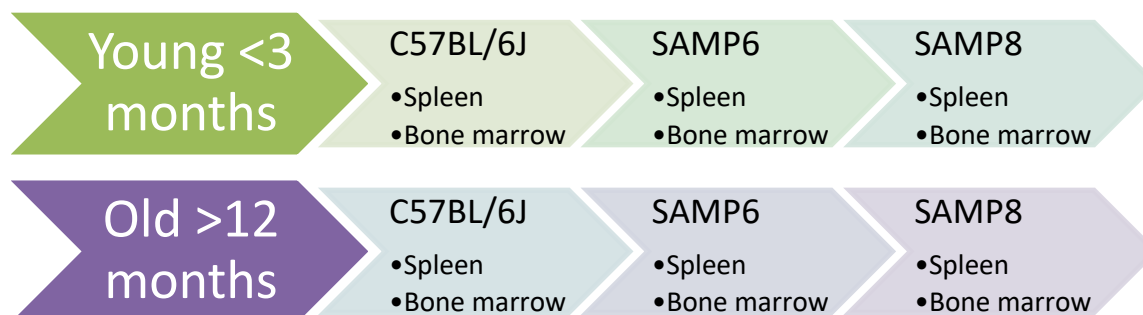
Figure 4.2   Schematic of tissue collection from C57BL/6J (C57), SAMP6 and SAMP8 mice during the study

4.2.2 Seahorse XF assay

Seahorse experiments were conducted as described in Section 2.6 Live-cell metabolic analysis. Mouse splenic and bone marrow cells were plated at a density of 250,000 cells per well and tested in triplicate for each sample.

4.2.3 Luciferase assay

The CellTiter-Glo® 2.0 Assay kit (Promega, WI) was used to measure ATP production in murine splenic and bone marrow cells as described in Section 2.4.1 Adenosine triphosphate production. Glucose concentration was measured using the Glucose-Glo™ Assay kit (Promega, WI) as described in Section 2.4.5 Glucose concentration. H_2O_2 production was measured at a density of 20,000 cells per well using the ROS-Glo™ H_2O_2 Assay kit (Promega, WI) as described in Section 2.4.4 Hydrogen

peroxide (H_2O_2) production. Luminescence was measured using the GloMax® Discover microplate reader (Promega, WI) using a fixed integration time of 0.5 seconds per well.

4.2.4   Flow cytometry

Cells were plated at a density of 1 million cells per well in 96-well U-bottom plates for the entirety of the flow cytometry experiment and stained as described in Sections 2.5.1.1 Cell surface staining and 2.5.1.2 Live cell mitochondrial staining. The surface staining and viability markers used for murine spleens are listed in Table 4.1. The surface staining and viability markers used for murine bone marrow are listed in Table 4.2. The dyes used for mitochondrial assessment of splenic and bone marrow cells are listed in Table 4.3. The gating strategy for murine spleen and bone marrow are shown in Figure 4.3 and Figure 4.4, respectively. The gating strategy for each cell type is defined in Table 4.4 for splenic cells and Table 4.5 for bone marrow cells.

Table 4.1   Cell surface markers for identifying immune cell populations resident in the mouse spleen

SURFACE MARKER	FLUOROPHORE	CLONE	RETAILER	DILUTION
Live-Dead	AmCyan	n/a	ThermoFisher, MA	1:200
CD3	Allophycocyanin (Apc)	17A2	BioLegend, CA	1µl
CD4	Pacific Blue	GK1.5	BioLegend, CA	1µl
CD8a	Apc/Cyanine (Cy)7	53-6.7	BioLegend, CA	1µl
CD44	Phycoerythrin (PE)/Cy7	IM7	BioLegend, CA	1µl
CD62L	Brilliant violet (BV)605	MEL-14	BioLegend, CA	1µl
CD335 (NKp46)	BV785	29A1.4	BioLegend, CA	1µl
CD11b	PE/Cy5	M1/70	BioLegend, CA	1µl
CD27	V650	LG.3A10	BioLegend, CA	1µl

Table 4.2   Cell surface markers for identifying immune cell populations resident in mouse bone marrow

SURFACE MARKER	FLUOROPHORE	CLONE	RETAILER	DILUTION
Live-Dead	AmCyan	n/a	ThermoFisher, MA	1:200
Ly6C	V605	AL-21	Becton Dickinson, NJ	1µl
CD11c	V650	HL3	Becton Dickinson, NJ	1µl
CD45R/B220	PE/Cy7	RA3-6B2	Becton Dickinson, NJ	1µl
Ly6G	Af700	1A8	Becton Dickinson, NJ	1µl
NK1.1	PerCP/Cy5.5	PK136	Becton Dickinson, NJ	1µl
Siglec-F (SigF)	PE/CF594	E50-2440	Becton Dickinson, NJ	1µl
CD11b	Apc/Cy7	M1/70	Becton Dickinson, NJ	1µl

Table 4.3   Dyes used for mitochondrial assessment of immune cells resident in the spleen and bone marrow

MITOCHONDRIAL DYE	FLUOROPHORE	RETAILER	DILUTION
MitoTracker Green	FITC	ThermoFisher, MA	150nM
TMRM	PE	SigmaAldrich, MO	25nM

Table 4.4   Gating strategy for identifying immune cells resident in the mouse spleen

CELL TYPE	GATING STRATEGY	FIGURE REFERENCE
Monocytes	CD11b+	Figure 4.3A
CD4+ naïve	CD3+, CD4+, CD8-, CD44lo	Figure 4.3B
CD4+ memory	CD3+, CD4+, CD8-, CD44hi	Figure 4.3C
CD8+ naive	CD3+, CD4-, CD8+, CD44lo	Figure 4.3D
CD8+ memory	CD3+, CD4-, CD8+, CD44hi	Figure 4.3E
B cells	CD3-, NKp46-	Figure 4.3F
Immature NK	CD3-, NKp46+, CD11b-, CD27hi	Figure 4.3G
Mature NK	CD3-, NKp46+, CD11b+, CD27lo	Figure 4.3H
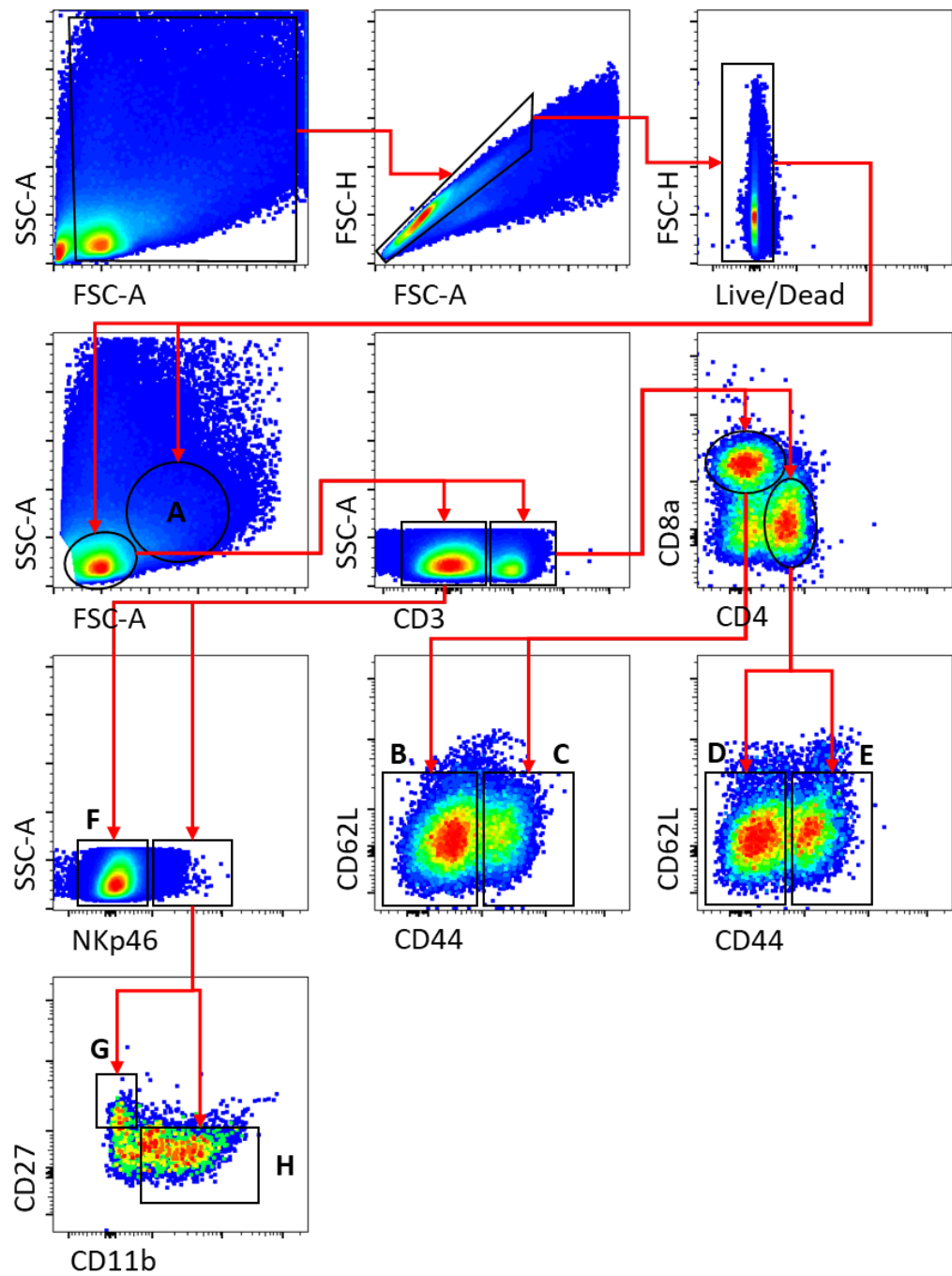
Figure 4.3   Gating strategy for identifying immune cells resident within the spleen of mice showing (A) Monocytes, (B) CD4+ naïve T cells, (C) CD4+ memory T cells, (D) CD8+ naïve T cells, (E) CD8+ memory T cells, (F) B cells, (G) immature NK cells and (H) mature NK cells

Table 4.5   Gating strategy for identifying immune cells resident in mouse bone marrow

CELL TYPE	GATING STRATEGY	FIGURE REFERENCE
Naïve B cell	CD11b-, CD45R+	Figure 4.4A
Memory B cell	CD11b+, CD45R+	Figure 4.4B
Neutrophils	CD11b+, CD45R-, NK1.1-, CD11c-, Ly6G+	Figure 4.4C
Ly6C- monocytes	CD11b+, CD45R-, NK1.1-, CD11c-, Ly6G-, SSC-Alo, Ly6C-	Figure 4.4D
Ly6C+ monocytes	CD11b+, CD45R-, NK1.1-, CD11c-, Ly6G-, SSC-Alo, Ly6C+	Figure 4.4E
Eosinophils	CD11b+, CD45R-, NK1.1-, CD11c-, Ly6G-, SSC-Ahi, SigF+	Figure 4.4F
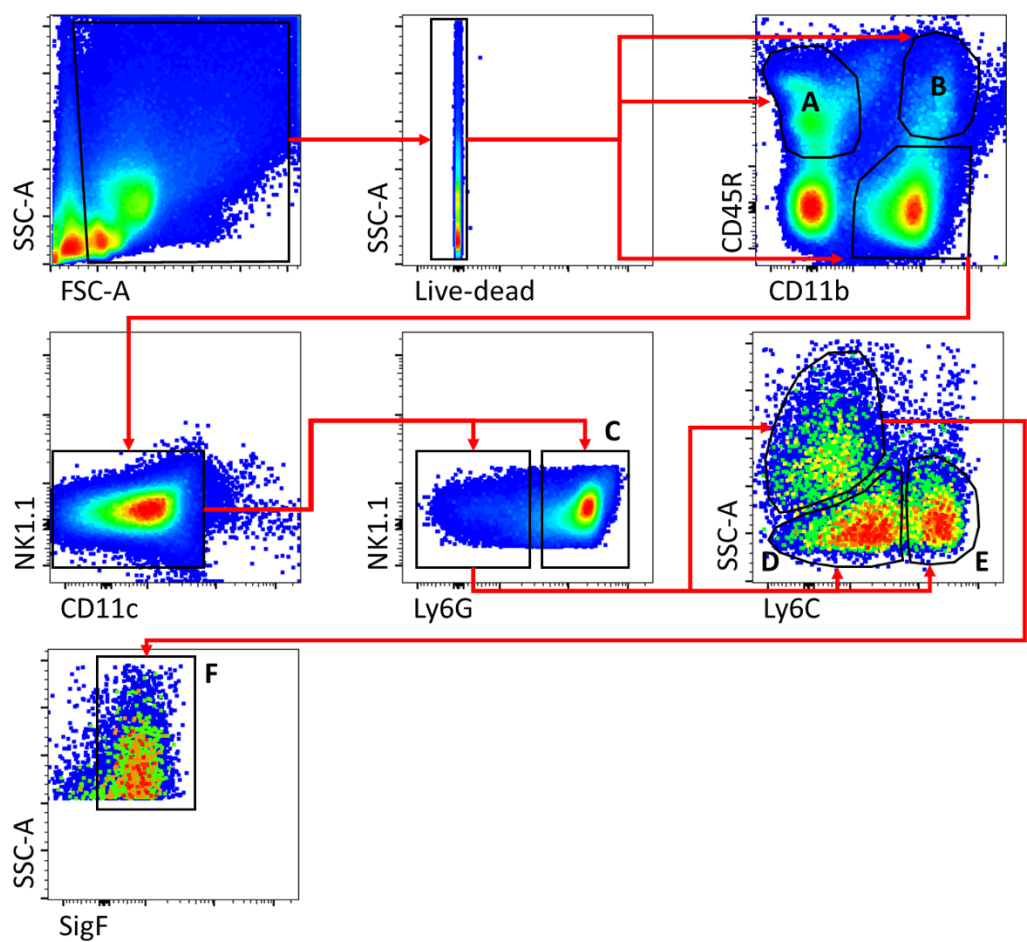
Figure 4.4   Gating strategy for identifying immune cells resident in mouse bone marrow showing (A) Naïve B cells, (B) Memory B cells, (C) Neutrophils, (D) Ly6C- monocytes, (E) Ly6C+ monocytes and (F) Eosinophils

4.2.5   Statistical analysis

Statistical analysis for all experiments was performed using an unpaired two-way ANOVA model unless otherwise stated, for parametric assessment of data. *Post-hoc* analysis was performed using Tukey's multiple comparison test. Flow cytometry data was analysed using FlowJo software. Statistical analysis was performed using GraphPad Prism software. GraphPad was used to create graphs. A p value of <0.05 was used to identify significance.

4.3   Results

4.3.1   Mitochondrial respiration is altered with age in C57 and SAMP8 mouse strains

The oxygen consumption rate (OCR) and extracellular acidification rate (ECAR) of spleen cells from young and old C57BL/6J (C57), SAMP6 and SAMP8 mice was measured using the Seahorse XF96 metabolic flux analyser (Figure 4.5A-E and Figure 4.6A-D). Whilst no reduction or increase in basal OCR was observed with age in either C57, SAMP6 or SAMP8 spleen, cells from SAMP8 spleens in young mice showed increased basal oxidation compared to C57 and SAMP6 mice. Basal respiration in SAMP8 spleens was increased by 2.3-fold compared to C57 mice (p=0.001) and 1.7-fold compared to SAMP6 mice (p=0.028; Figure 4.5B). Basal respiration was increased in cells from old SAMP8 spleens compared to those from SAMP6 by 2.1-fold (p=0.009).

A significant effect of age on spare capacity, the ability of cells to respond to increased demands on metabolism, was observed in splenic cells following analysis by Two-way ANOVA (p<0.001; $F_{(1,24)}=27.21$). Following *post-hoc* analysis a significant 90% reduction in spare capacity was observed in splenic cells derived from old C57 mice compared to young (p=0.009; Figure 4.5C). Although similar reductions in spare capacity of splenic cells from SAMP6 and SAMP8 mice were observed with age, this reduction did not reach significance due to the increased variability in spare capacity within these mice (p=0.15 for SAMP6, p=0.13 for SAMP8). Whilst this was believed to be attributed to a lack of experimental power the observed power of this experiment was 97.5% suggesting that sample size was adequate.

Alongside reductions in the spare capacity of splenic cells from old mice, a significant effect of age on maximal respiration was also observed (Figure 4.5D; p<0.001; $F_{(1,24)}=14.42$) alongside a genotypic effect (p=0.015; $F_{(2,24)}=4.99$). However, *post-hoc* analysis revealed no significant differences between splenic cells from young and old mice of the same genotype or between genotypes in mice of the same age. Due to alterations in ATP production observed in the bone marrow of C57 mice in Southampton (Chapter 3), ATP-linked respiration of splenic cells was measured within C57, SAMP6 and SAMP8 mice in Singapore. ATP-linked respiration accounts for oxygen utilised to drive the ATPase machinery during normal metabolism. Cells derived from SAMP8 spleens were observed to have a greater level of ATP-linked respiration than SAMP6 and C57 mice (Figure 4.5E). Splenic cells from young SAMP8 mice showed a 4.2-fold increase in ATP-linked respiration compared to young C57 mice (p<0.001). This trend was observed for old SAMP8 splenic cells which showed a 2-fold increase compared to old C57 mice (p=0.038), and 2.7-fold increase compared to old SAMP6 mice (p=0.006).
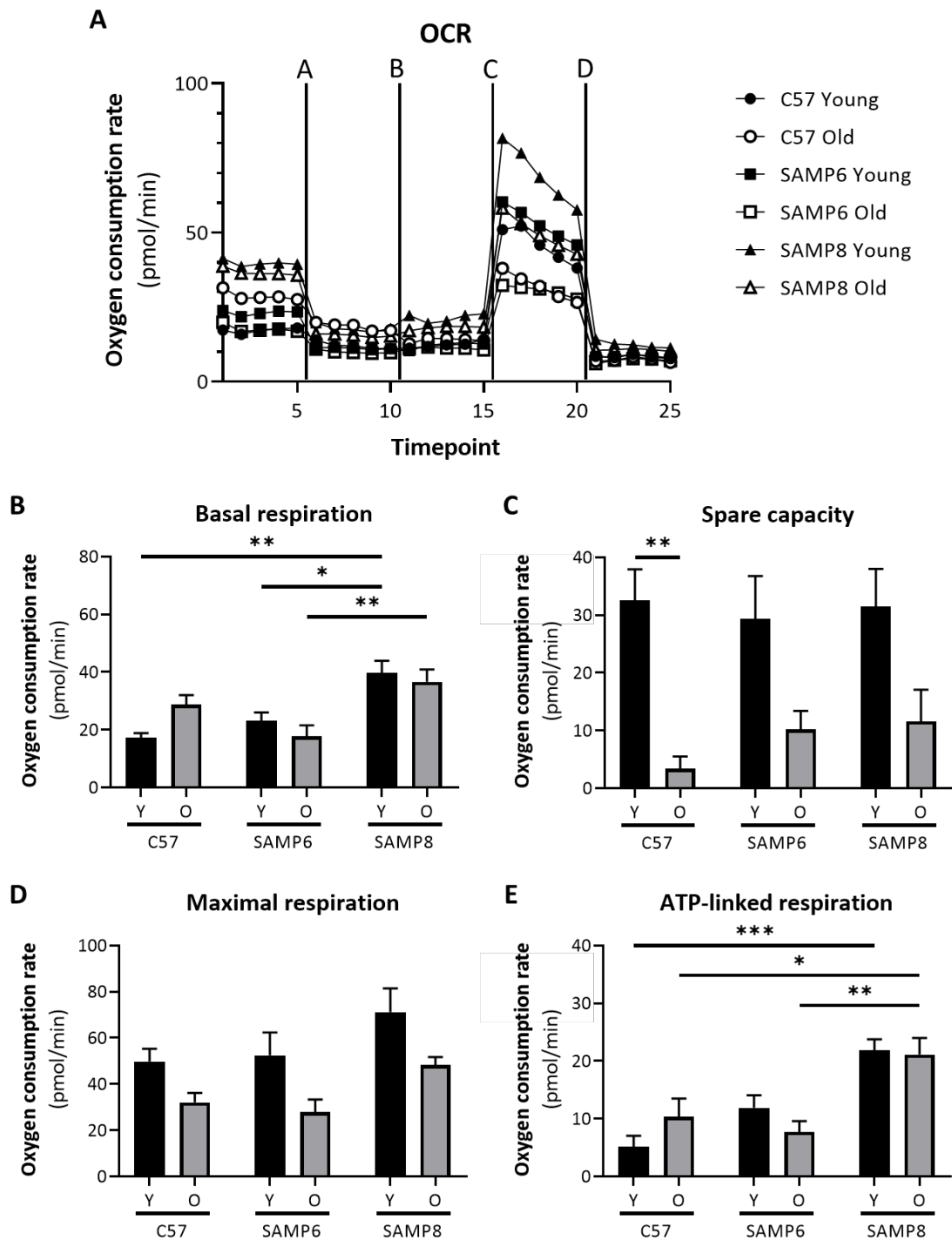
Figure 4.5   Oxygen consumption rate analysis of cells derived from the spleen with age showing (A) OCR of cells treated with (a) 2μM Oligomycin (b) 50mM 2DG (c) 2μM FCCP and (d) 500nM Rot/AA (mean; n=5) and (B) basal respiration (C) spare capacity (D) maximal respiration and (E) ATP-linked respiration of spleen cells from C57, SAMP6 and SAMP8 mice (mean+SEM; n=5; Ordinary two-way ANOVA; *p<0.05, **p<0.01, ***p<0.001)

Despite changes in oxidative metabolism, no significant differences were observed in glycolytic metabolism with age or between the three genotypes in splenic cells following analysis by Two-way ANOVA. This finding extended to rates of basal glycolysis, glycolytic reserve and glycolytic capacity of splenic cells derived from these mice (Figure 4.6B-D).
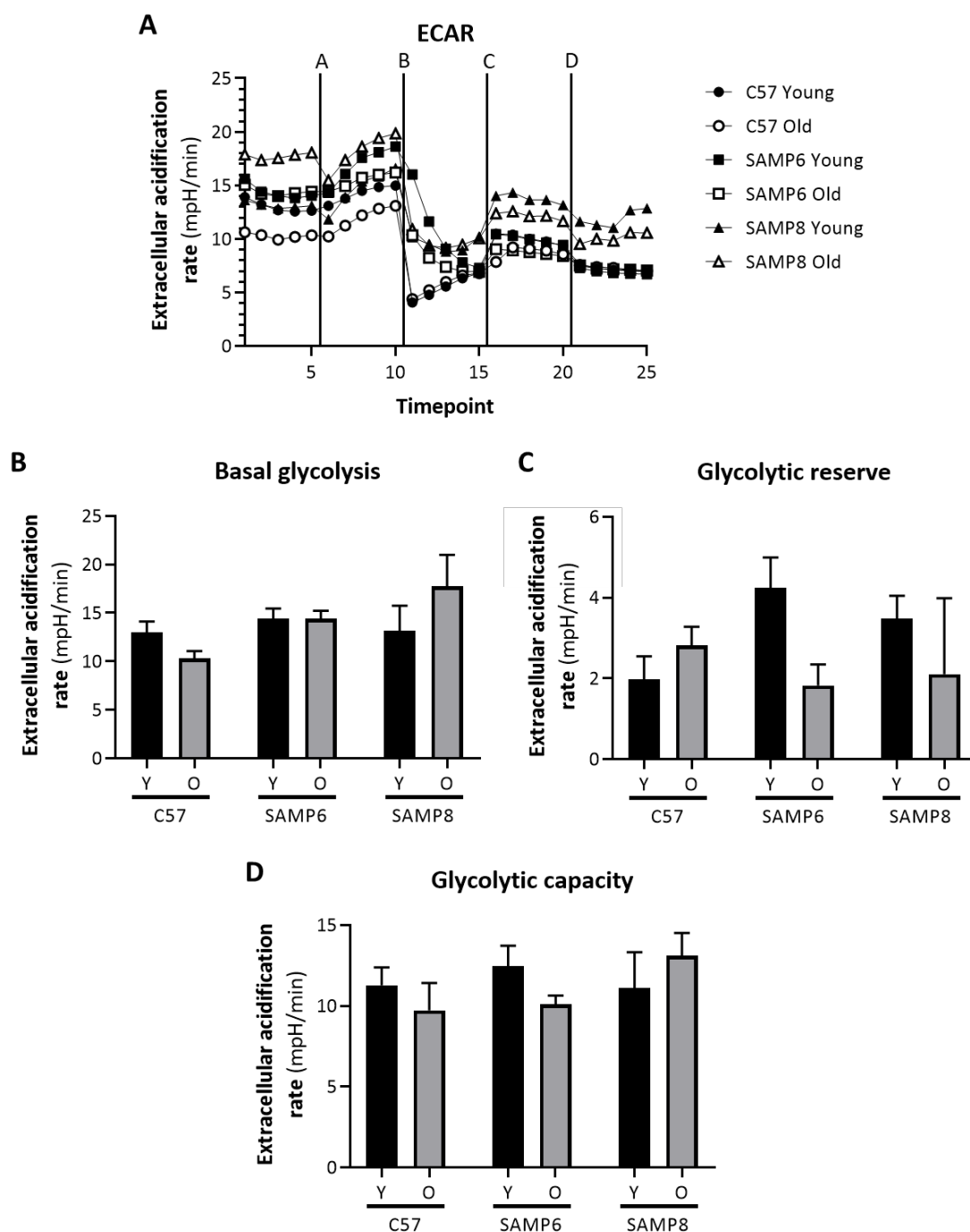
Figure 4.6   Extracellular acidification rate analysis of spleen cells with age showing (A) extracellular acidification rate of cells treated with (a) 2μM Oligomycin (b) 50mM 2DG (c) 2μM FCCP and (d) 500nM Rot/AA (mean; n=5) and (B) basal glycolysis (C) glycolytic reserve and (D) glycolytic capacity of spleen cells from C57, SAMP6 and SAMP8 mice (mean+SEM; n=5; Ordinary two-way ANOVA)

4.3.2   No alterations are observed in ATP or ROS production in C57, SAMP6 or SAMP8 mice with age

Despite the reduction in ATP production previously observed in bone marrow cells from C57 mice with age in Southampton (Chapter 3) this finding did not extend to splenic cells derived from ageing C57 mice bred in Singapore (Figure 4.7A). Despite a reduction in spare capacity, ATP production was not altered with age in cells from C57 mouse spleens bred in Singapore, which suggests this previous finding may be tissue specific. In line with this, no alterations in ATP production of splenic cells derived from SAMP6 and SAMP8 mice were observed with age (Figure 4.7A). ROS levels were analysed in splenic cells from young and old C57, SAMP6 and SAMP8 using luciferase detection of H_2O_2 production (Figure 4.7B). No alterations in ROS production from C57, SAMP6 or SAMP8 mice with age or any differences in H_2O_2 production between each of the strains were observed, despite SAMP8 mice showing increased basal respiration and ATP-linked respiration rates in the spleen.
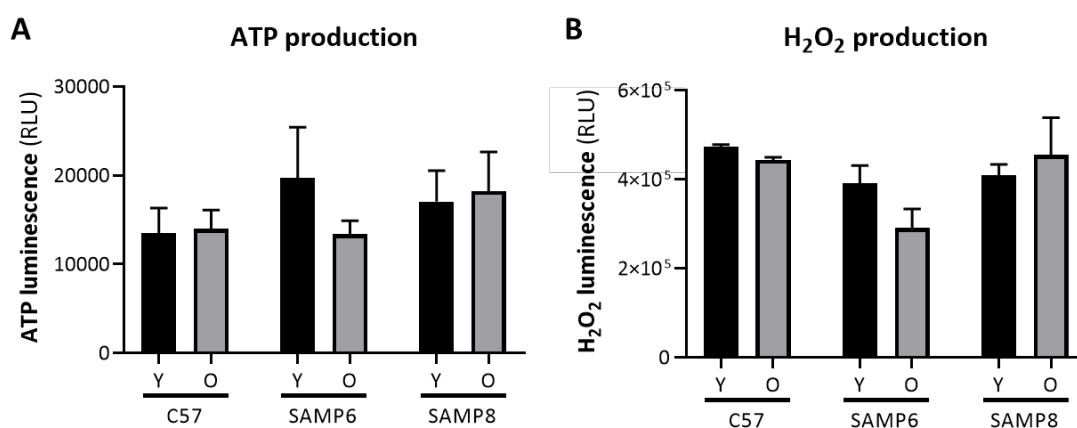
Figure 4.7   ATP production and ROS levels with age in cultured spleen cells showing relative luminescent units (RLU) of (A) ATP production and (B) H_2O_2 production in spleen cells from C57, SAMP6 and SAMP8 mice (mean+SEM; n=5; Ordinary two-way ANOVA)

4.3.3 T cells and B cells from SAMP8 are not subject to the same alterations in mitochondrial mass and membrane potential with age as those from SAMP6 and C57 mice

As the oxidative metabolism of splenic cells showed alterations between the mouse strains studied and the spare capacity of cells from C57 mice was reduced with age, mitochondrial mass and membrane potential were analysed by flow cytometry. CD4+ and CD8+ memory and naïve T cells, B cells, immature and mature NK cells and monocytes were studied.

Within CD4+ T cells a significant reduction in the mitochondrial mass of memory cells was observed for C57 and SAMP6 mice. Mitochondrial mass, analysed by MitoTracker Green (MTG) staining mean fluorescent index (MFI), was reduced by 28% in C57 mice and 22% in SAMP6 mice with age ($p<0.001$ for C57 and $p=0.005$ for SAMP6; Figure 4.8A). This finding did not extend to the SAMP8 strain which showed no alterations in mitochondrial mass with age in CD4+ memory T cells. Mitochondrial mass in CD4+ naïve T cells was not affected by age in any of the mouse strains studied (Figure 4.8B), revealing that age only affects the memory subtype of CD4+ T cells within C57 and SAMP6 mice. In line with reductions in mitochondrial mass the MFI of TMRM as a marker of mitochondrial membrane potential was reduced by 29% with age in CD4+ memory cells from SAMP6 mice ($p=0.042$; Figure 4.8C). Surprisingly, this reduction in SAMP6 mice extended to CD4+ naïve cells (26% $p=0.027$; Figure 4.8D). However, when these changes in mitochondrial membrane potential were normalised to mitochondrial mass no significant alterations in TMRM:MTG ratio were observed with age in CD4+ memory and naïve T cells from C57, SAMP6 or SAMP8 mice (Figure 4.8E and F).
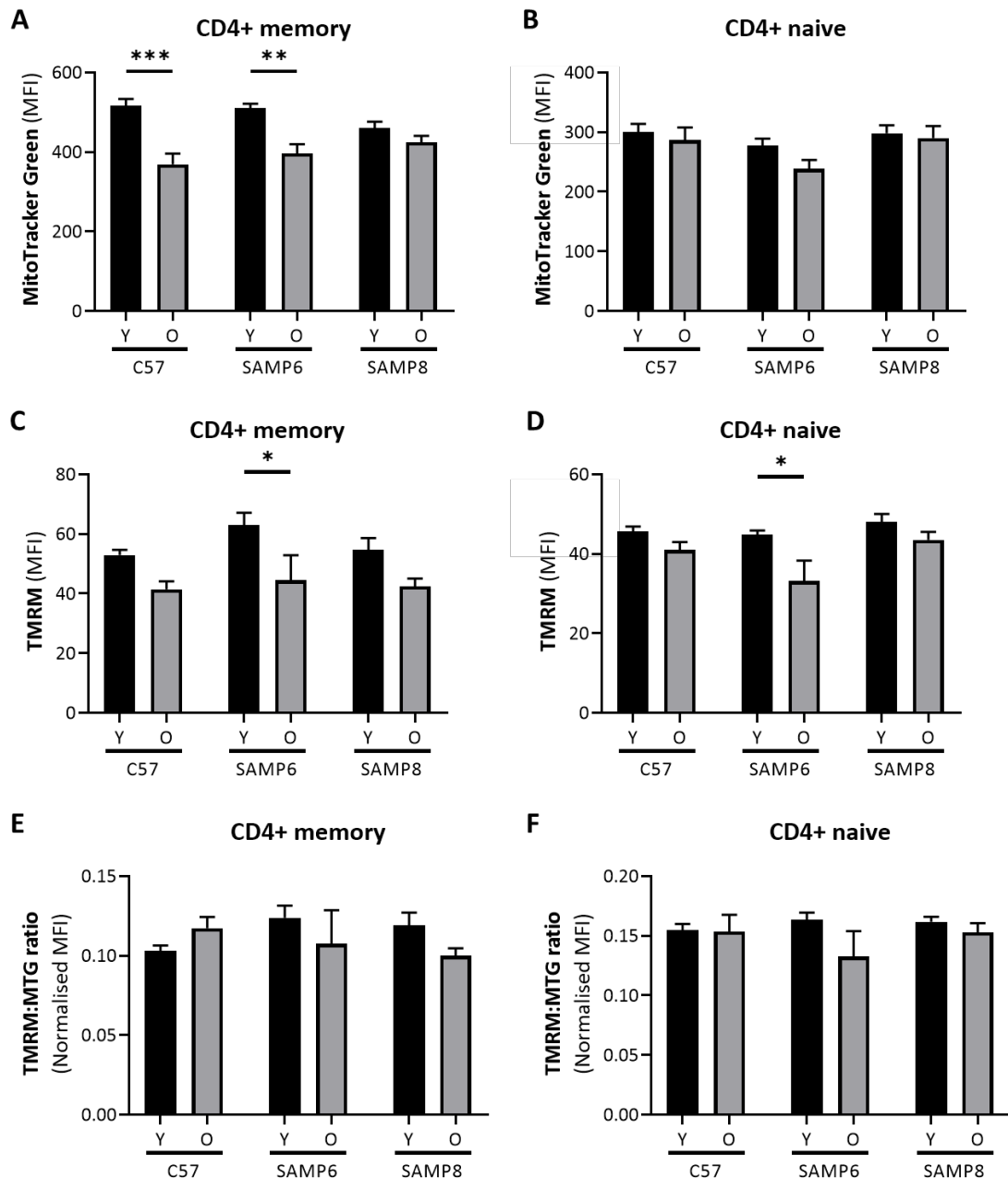
Figure 4.8   Mitochondrial mass and membrane potential in CD4+ memory and naïve T cells resident in the spleen showing (A) MTG staining in CD4+ memory cells (B) MTG staining in CD4+ naïve cells (C) TMRM staining in CD4+ memory cells (D) TMRM staining in CD4+ naïve cells (E) TMRM:MTG staining ratio in CD4+ memory cells and (F) TMRM:MTG staining ratio in CD4+ naïve cells from C57, SAMP6 and SAMP8 mice (mean+SEM; n=10; Ordinary two-way ANOVA; *p<0.05, **p<0.01, ***p<0.001)

Similar alterations were observed within the CD8+ T cell compartment. Mitochondrial mass in CD8+ memory T cells was reduced with age in C57 mice (Figure 4.9A). MTG MFI was reduced by 22% with age within these cells (p=0.002). Surprisingly, mitochondrial mass in CD8+ memory T cells was not altered with age in either SAMP6 or SAMP8 mice. MTG staining remained unaltered within CD8+

naïve cells from C57, SAMP6 and SAMP8 mice with age (Figure 4.9B). This was true of mitochondrial membrane potential of CD8+ memory cells with MTG MFI remaining unaltered with age in all the mouse strains (Figure 4.9C). On the other hand, CD8+ naïve T cells were subject to more dynamic changes in mitochondrial membrane potential (Figure 4.9D). As with CD4+ memory cells, CD8+ naïve T cell TMRM MFI was reduced by 28% with age in SAMP6 mice (p=0.032) whilst no alterations were observed within C57 or SAMP8 mice. This resulted in a significant reduction in TMRM staining in CD8+ naïve T cells in old SAMP6 mice compared to C57 and SAMP8 mice (p=0.044 and p=0.006, respectively). Similarly, to CD4+ T cells, TMRM:MTG ratio remained unaltered with age for both CD8+ memory and naïve T cells (Figure 4.9E and F).

These findings suggest that alterations in the oxidative metabolism of spleen cells derived from SAMP8 mice may be due to sustained mitochondrial mass and membrane potential of CD4+ and CD8+ T cells with age. This effect is not present in SAMP6 and C57 on the other hand, which show lower rates of oxidative metabolism in comparison to SAMP8 mice at all ages.
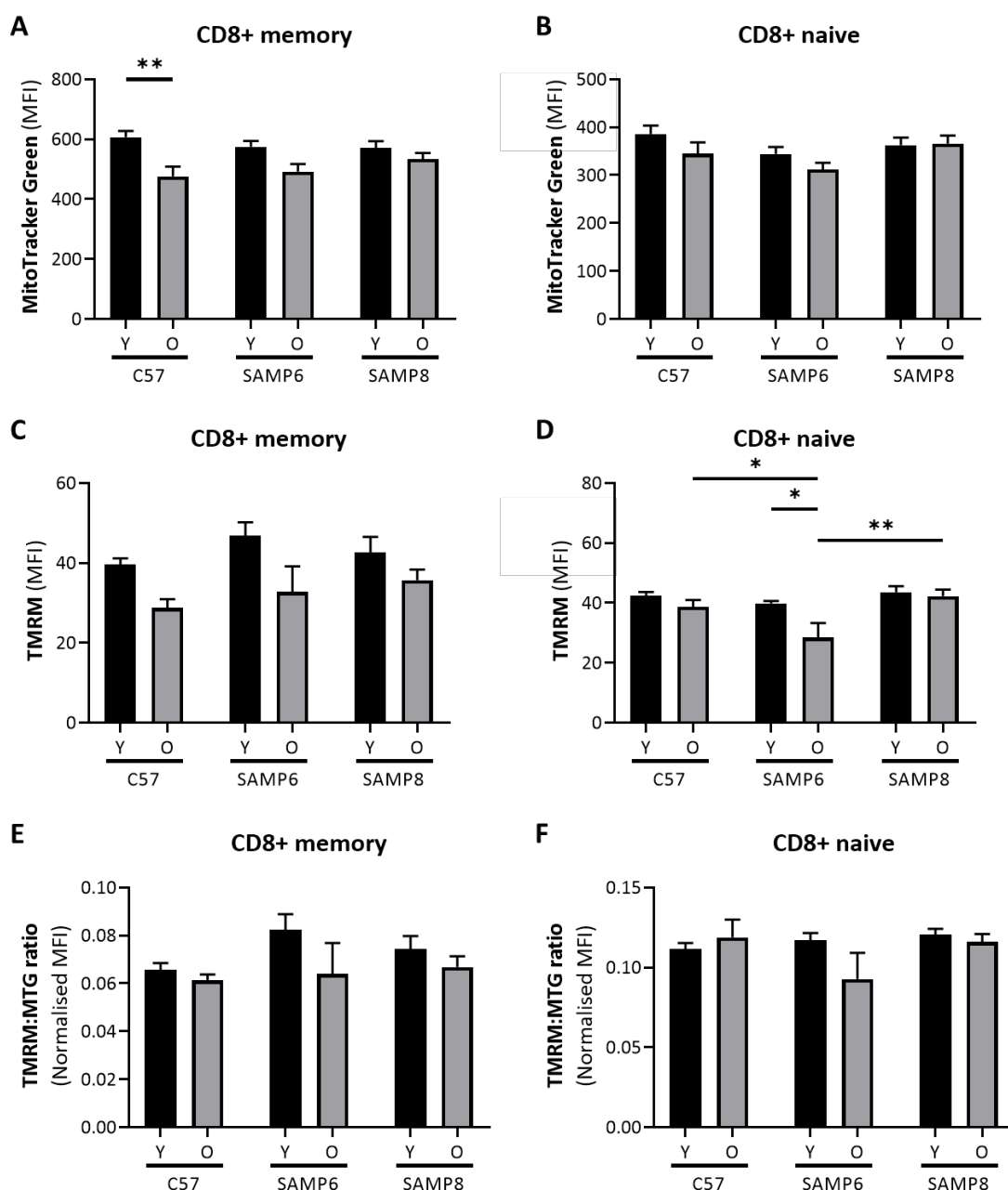
Figure 4.9   Mitochondrial mass and membrane potential in CD8+ memory and naïve T cells resident in the spleen showing (A) MTG staining in CD8+ memory cells (B) MTG staining in CD8+ naïve cells (C) TMRM staining in CD8+ memory cells (D) TMRM staining in CD8+ naïve cells (E) TMRM:MTG staining ratio in CD8+ memory cells and (F) TMRM:MTG staining ratio in CD8+ naïve cells from C57, SAMP6 and SAMP8 mice (mean+SEM; n=10; Ordinary two-way ANOVA; *p<0.05, **p<0.01)

The mitochondrial mass in B cells contained within the splenic cell population was decreased with age in C57 and SAMP6 mice (Figure 4.10A). MTG staining was reduced by 25% and 28% within these mice with age, respectively (p=0.004 for C57, p=0.009 for SAMP6). This resulted in a significant reduction of mitochondrial mass within old C57 (p<0.001) and SAMP6 (p<0.001) mice compared to

SAMP8 mice. Similarly, mitochondrial membrane potential was reduced within B cells contained within the spleen of SAMP6 mice with age (Figure 4.10B). TMRM MFI was reduced by 27% with age in these animals (p=0.037), resulting in a significant reduced in mitochondrial membrane potential compared to SAMP8 mice (p=0.034). Despite these alterations TMRM:MTG ratio remained unchanged with age within all the mouse strains studied (Figure 4.10C). However, the sustained mitochondrial mass observed with age in SAMP8 mice which is increased in comparison to SAMP6 and C57 mice, may aid in explaining the increased metabolic rates observed within SAMP8 mice.

Figure 4.10   Mitochondrial mass and membrane potential in B cells resident in the spleen showing (A) MTG staining (B) TMRM staining and (C) TMRM:MTG staining ratio in B cells from C57, SAMP6 and SAMP8 mice (mean+SEM; n=10; Ordinary two-way ANOVA; *p<0.05, **p<0.01, ***p<0.001)

4.3.4   NK cells and monocytes from SAMP6 spleens show increased mitochondrial mass and membrane potential

Despite cells from the spleens of SAMP8 mice showing increased oxidative metabolism compared to the other mouse strains studied, SAMP6 mice surprisingly showed increased mitochondrial mass in immature NK cells compared to SAMP8 and C57 mice (Figure 4.11A). MTG MFI was increased 3-fold ($p<0.001$) in young SAMP6 mice compared to C57 and by 7-fold ($p<0.001$) compared to SAMP8. This effect was maintained within old SAMP6 mice (2-fold increase; $p=0.024$), regardless of the 41% decrease observed in MTG staining with age ($p<0.001$). SAMP6 mice showed increased TMRM staining compared to SAMP8 and C57 mice (Figure 4.11C). Mitochondrial membrane potential was increased by approximately 3-fold in SAMP6 mice ($p<0.001$). When normalised to mitochondrial mass, SAMP8 mice showed a significant reduction in TMRM:MTG ratio with age (Figure 4.11E). TMRM:MTG ratio was reduced by 56% with age in these cells ($p=0.028$). This decrease did not result in a significant reduction in TMRM:MTG ratio compared to the other strains studied, as young SAMP8 mice showed significantly increased TMRM:MTG ratio compared to young SAMP6 mice ($p=0.047$).

Similar observations were made within mature NK cells (Figure 4.11B). Mature NK cells from SAMP6 spleens showed significantly increased MTG MFI compared to C57 mice at both young (77%; $p<0.001$) and old ages (75%; $p<0.001$). Similarly, mitochondrial mass was increased by 64% in SAMP6 compared to SAMP8 in young mice ($p<0.001$). MTG staining was increased by 53% with age in SAMP8 mice ($p=0.005$) which resulted in a significant increase over that observed in old C57 mice (61%; $p<0.001$). When mitochondrial membrane potential was measured only young SAMP6 mice showed a significant increase in TMRM MFI compared to C57 mice (2.5-fold; $p=0.005$; Figure 4.11E). Despite these alterations, TMRM:MTG ratio was not increased with age or between any of the strains studied (Figure 4.11F). This result suggests that mature NK cells from SAMP8 mice are not subject to alterations in mitochondrial landscape, whilst immature NK cells show reductions in mitochondrial membrane potential with age. SAMP8 NK cells are therefore not involved with the increased oxidative metabolism observed in the spleen of these animals.
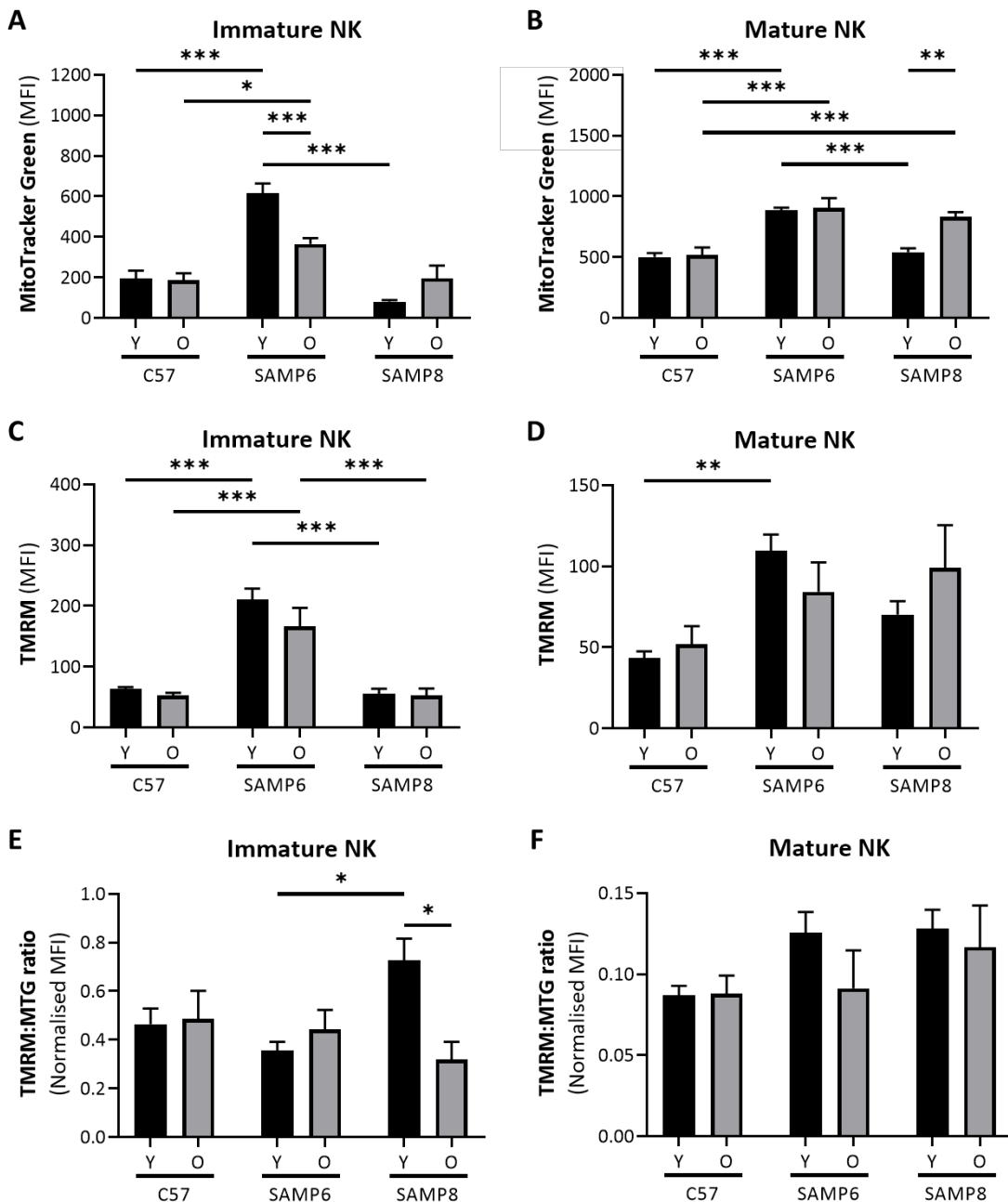
Figure 4.11 Mitochondrial mass and membrane potential in immature and mature NK cells resident in the spleen showing (A) MTG staining in immature NK cells (B) MTG staining in mature NK cells (C) TMRM staining in immature NK cells (D) TMRM staining in mature NK cells (E) TMRM:MTG staining ratio in immature NK cells and (F) TMRM:MTG staining ratio in mature NK cells from C57, SAMP6 and SAMP8 mice (mean+SEM; n=10; Ordinary two-way ANOVA; *p<0.05, **p<0.01, ***p<0.001)

In a similar manner to NK cells, a significant increase in MTG staining was observed in old SAMP6 mice compared to C57 for monocytes (Figure 4.12A). Mitochondrial mass was increased by 37% within these cells (p=0.002). Alongside this increase a 2.5-fold upregulation of TMRM staining in monocytes from young SAMP6 mice was observed compared to C57 (p<0.001; Figure 4.12B).

However, this increased mitochondrial membrane potential was lost with age, as SAMP6 displayed a 54% decrease in TMRM MFI (p=0.004). This same trend was observed when TMRM staining was normalised to mitochondrial mass (Figure 4.12C). TMRM:MTG ratio was reduced to half of that observed in monocytes from young SAMP6 mice with age (p=0.004). This decrease did not result in a significant reduction in TMRM:MTG ratio compared to the other strains studied, as young SAMP6 mice showed significantly increased TMRM:MTG ratio compared to young C57 mice (p<0.001). This result suggests that monocytes from SAMP8 mice are not responsible for the increased oxidative metabolism observed in the spleen of these animals.
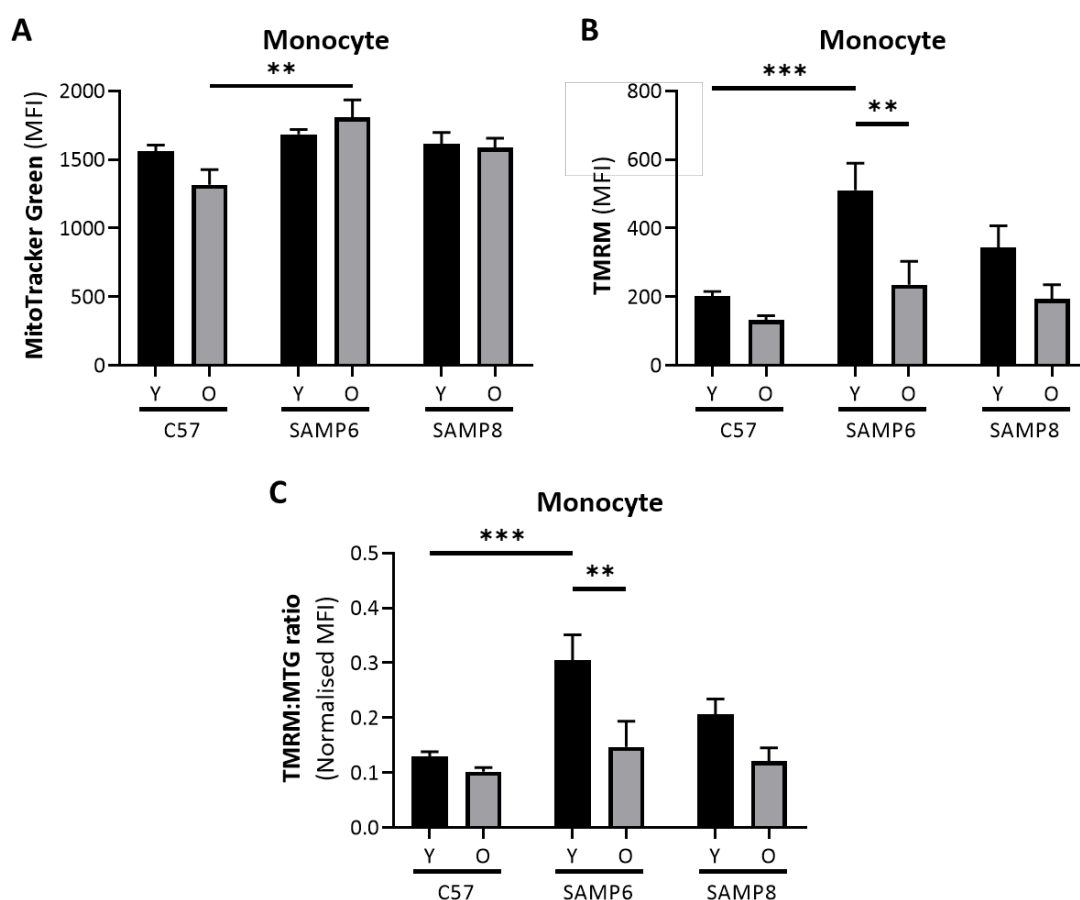
Figure 4.12 Mitochondrial mass and membrane potential in monocytes resident in the spleen showing (A) MTG staining (B) TMRM staining and (C) TMRM:MTG staining ratio in monocytes from C57, SAMP6 and SAMP8 mice (mean+SEM; n=10; Ordinary two-way ANOVA; **p<0.01, ***p<0.001)

4.3.5   **Bone marrow cells from SAMP8 mice show alterations in oxidative metabolism whilst SAMP6 cells display decreased glycolytic reserve and increased glycolytic capacity**

As the metabolism of bone marrow cells derived from C57 and *Timp3*$^{-/-}$ mice bred in Southampton was shown to be altered with age, the metabolism of bone marrow cells from C57, SAMP6 and SAMP8 mice bred in Singapore was measured. Both oxidative and glycolytic metabolism were measured simultaneously (Figure 4.13A and Figure 4.14A). A significant downregulation of basal metabolism in the bone marrow was observed in old SAMP6 mice when compared to old C57 mice (Figure 4.13B). Basal OCR of bone marrow cells was reduced by 75% within these mice (p=0.003). No differences were observed within the bone marrow of young and old SAMP8 mice in terms of their basal respiration. However, the maximal respiration of SAMP8 bone marrow cells from young mice was significantly lower in comparison to the other mouse strains (Figure 4.13C). Maximal respiration was decreased to 38% and 37% of that observed in the bone marrow of young C57 (p=0.002) and SAMP6 mice (p<0.001), respectively. Additionally, a significant increase in ATP-linked respiration was observed in SAMP8 bone marrow with age (Figure 4.13D). Oxygen consumption utilised for driving the ATPase machinery was increased 6-fold in bone marrow cells derived from SAMP8 mice (p=0.002). This resulted in a significant increase in ATP-linked respiration in old SAMP8 bone marrow when compared to old SAMP6 bone marrow (p=0.001). Therefore, whilst basal respiration is affected in bone marrow of SAMP6 mice, SAMP8 show alterations in maximal respiration and the oxidative requirements ATPase activity.
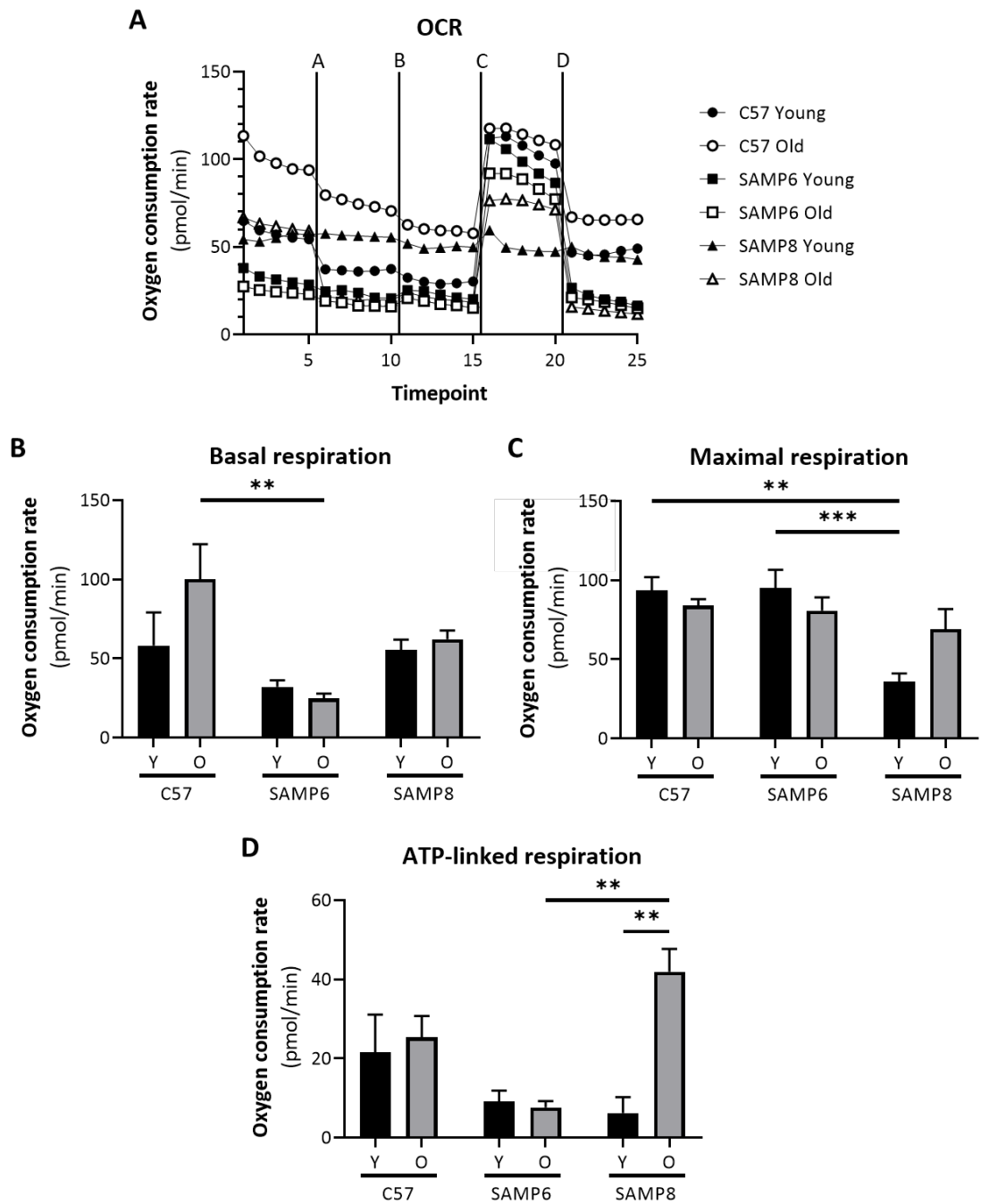
Figure 4.13 Oxygen consumption rate analysis of mouse bone marrow cells with age showing (A) OCR of cells treated with (a) 2μM Oligomycin (b) 50mM 2DG (c) 2μM FCCP and (d) 500nM Rot/AA (mean; n=5) and (B) basal respiration (C) maximal respiration and (D) ATP-linked respiration of bone marrow cells from C57, SAMP6 and SAMP8 mice (mean+SEM; n=5; Ordinary two-way ANOVA; **$p<0.01$, ***$p<0.001$)

In line with the increased reliance on glycolysis for ATP production in C57 mice bred in Southampton with age, an increase in the basal glycolysis of bone marrow cells was observed (Figure 4.14A). Basal glycolysis almost doubled in bone marrow cells from aged mice (81% increase; p=0.043). This resulted in old C57 mouse bone marrow cells having increased basal glycolysis in comparison to old SAMP8 cells (p<0.001). This low-level basal glycolysis was found to be significantly lower than that observed in SAMP6 bone marrow cells (p=0.012). Despite showing a decreased glycolytic reserve in comparison to SAMP8 mice, bone marrow cells from SAMP6 mice showed an increased glycolytic capacity (Figure 4.14C and D). Glycolytic reserve was reduced by 74% (p=0.03) and 88% (p=0.034) within young and old SAMP6 bone marrow, respectively. A 2-fold increase was observed in the glycolytic capacity of SAMP6 bone marrow cells from young and old mice compared to SAMP8 (p=0.03 in young; p=0.02 in old). Bone marrow cells from SAMP8 mice showed reduced glycolytic capacity in comparison to C57 mice with age, which was reduced to 40% of that observed in old C57 mice (p=0.001). Bone marrow cells from SAMP6 mice show aberrant glycolytic reserve and capacity in comparison to SAMP8 mice, which may be due to their osteoporotic pathology.
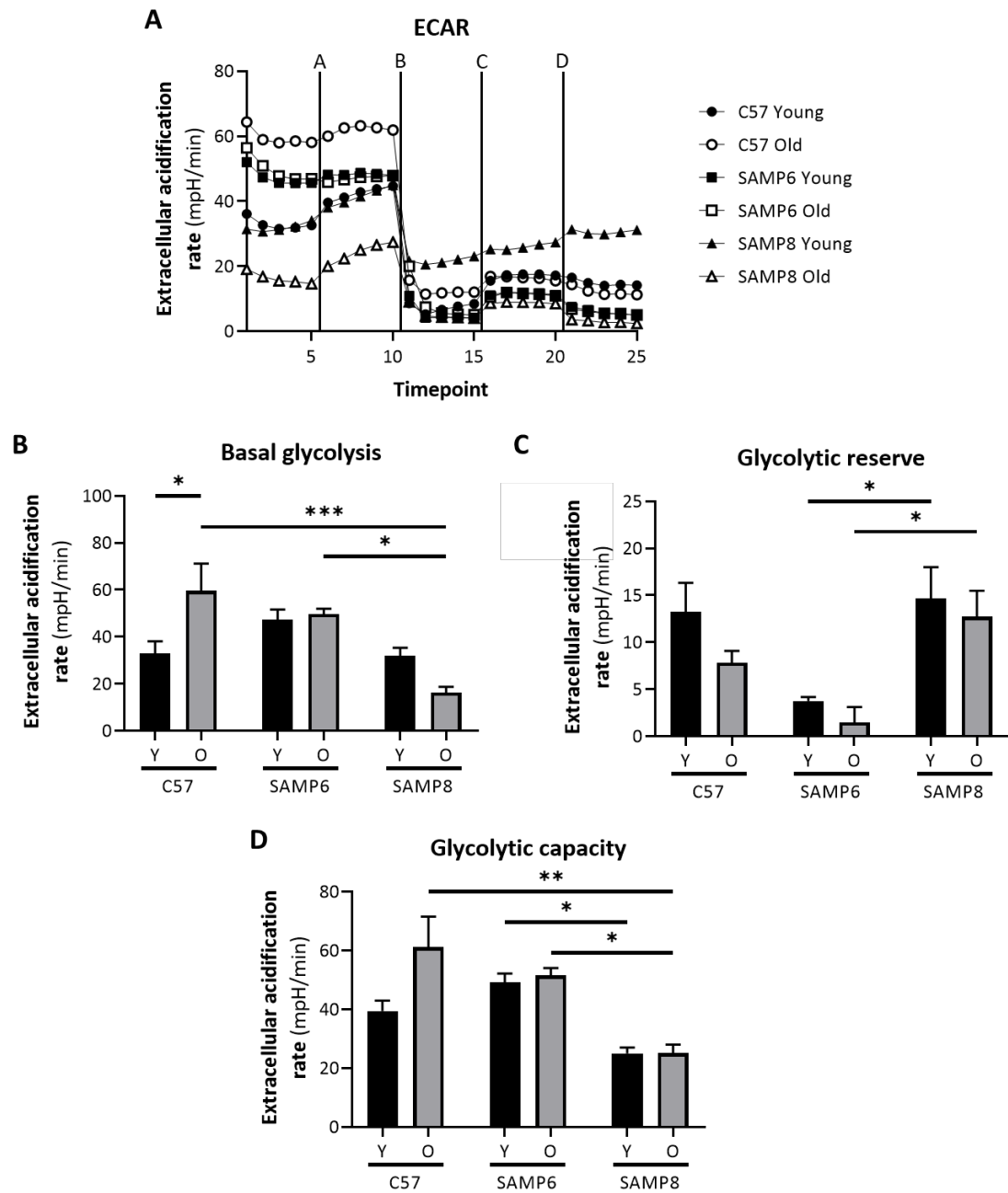
Figure 4.14 Extracellular acidification rate analysis of bone marrow cells with age showing (A) ECAR of cells treated with (a) 2μM Oligomycin (b) 50mM 2DG (c) 2μM FCCP and (d) 500nM Rot/AA (mean; n=5) and (B) basal glycolysis (C) glycolytic reserve and (D) glycolytic capacity of bone marrow cells from C57, SAMP6 and SAMP8 mice (mean+SEM; n=5; Ordinary two-way ANOVA; *p<0.05, **p<0.01, ***p<0.001)

4.3.6 SAMP6 and SAMP8 bone marrow cells show increase glucose utilisation and SAMP6 mice display increased ATP production with age

As alterations in both oxidative and glycolytic metabolism were seen in bone marrow cells, changes in ATP, H_2O_2 and glucose concentrations were measured using luciferase reporter assays. Whilst the bone marrow of C57 mice bred in Southampton showed a reduction in ATP production with age (Chapter 3), this effect was not observed within mice bred in Singapore (Figure 4.15A). However, an increase in ATP production within SAMP6 bone marrow cells with age was observed. The relative luminescence was doubled compared that measured in young mice ($p=0.035$). This increase was reiterated as a significant increase in ATP production within these cells as compared to C57 and SAMP8 bone marrow cells from old mice ($p=0.02$ for C57; $p=0.01$ for SAMP8). Previous reports have suggested that oxidative stress is increased with age in SAMP8 mice, however no significant up- or down-regulation of H_2O_2 production was observed within bone marrow cells (Figure 4.15B). As with splenic cells, H_2O_2 production remained stable with age and was not significantly altered in bone marrow cells between the three mouse strains. Finally, the glucose concentration within the cell culture medium used for maintaining bone marrow cells was measured (Figure 4.15C). The concentration of glucose within the cell culture medium was not altered with age in any of the mouse strains studied, however a significant reduction in glucose concentration was observed for SAMP6 (50% in young $p<0.001$; 47% in old $p=0.003$) and SAMP8 (38% in young $p=0.009$; 39% in old $p=0.018$) bone marrow cells when compared to C57 cells. Glucose concentration was reduced by half within the cell culture medium, suggesting that SAMP6 and SAMP8 bone marrow cells uptake twice the amount of glucose. However, unaltered rates of glycolytic metabolism, as measured by lactate output, within bone marrow cells suggests that this glucose may be utilised for alternative metabolic pathways.
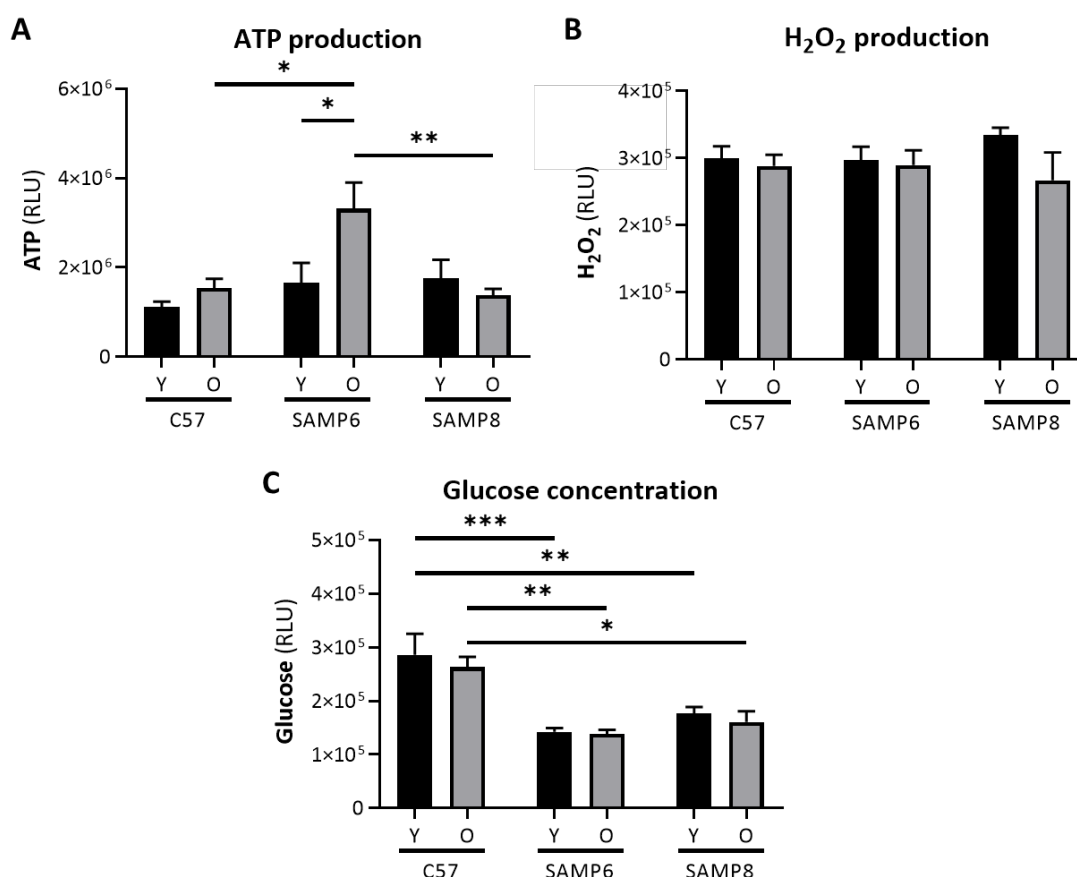
Figure 4.15 ATP production, ROS levels and glucose concentration with age in cultured bone marrow cells showing luciferase analysis of (A) ATP production (B) H_2O_2 production and (C) glucose concentration in bone marrow cells from C57, SAMP6 and SAMP8 mice (mean+SEM; n=5; Ordinary two-way ANOVA; *p<0.05, **p<0.01, ***p<0.001)

4.3.7 Eosinophils, monocytes and neutrophils from the SAMP6 strain show reduced mitochondrial membrane potential compared to SAMP8 mice

As the oxidative metabolism and glycolytic metabolism of bone marrow cells showed alterations between the mouse strains studied and with age, mitochondrial mass and membrane potential was analysed by flow cytometry. When mitochondrial mass was measured within eosinophils only old SAMP6 mice showed a significant increase in MTG staining compared to C57 mice (22%; p=0.026; Figure 4.16). Despite this alteration, TMRM MFI was not increased in parallel with mitochondrial mass within these cells (Figure 4.16B). However, TMRM staining within eosinophils derived from young SAMP6 mice was reduced to half of that observed in eosinophils derived from SAMP8 (p=0.006). Taken together a significant reduction in TMRM:MTG ratio within SAMP6 eosinophils was observed (Figure 4.16C). TMRM:MTG ratio was reduced in eosinophils from both young and old SAMP6 bone marrow compared to C57 (61% for young p<0.001; 40% for old p=0.003) and SAMP8 (64% for young p<0.001; 43% for old p<0.001) mice. This reduction in TMRM:MTG ratio may

represent the appearance of dysfunctional mitochondria within the bone marrow of SAMP6 mice. Dysfunctional mitochondrial metabolism may aid in understanding the increased glycolytic capacity but decreased glycolytic reserve observed within bone marrow cells.
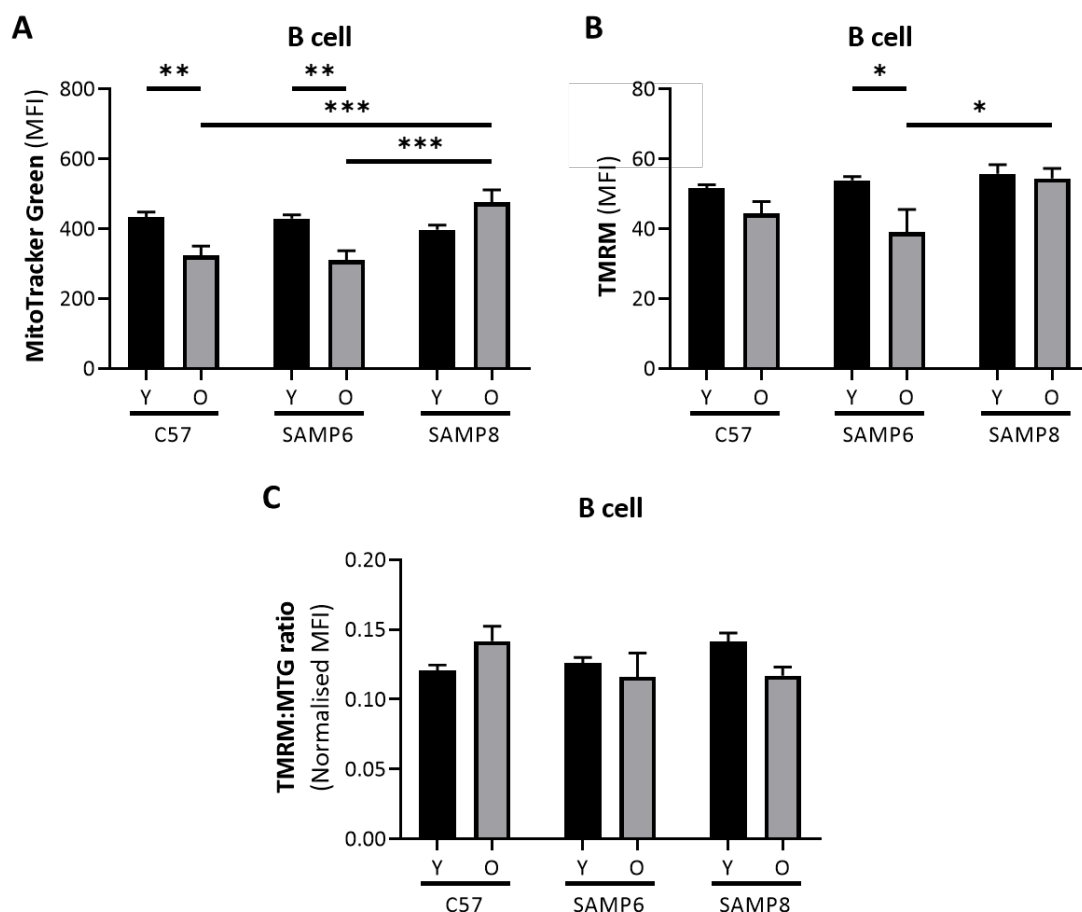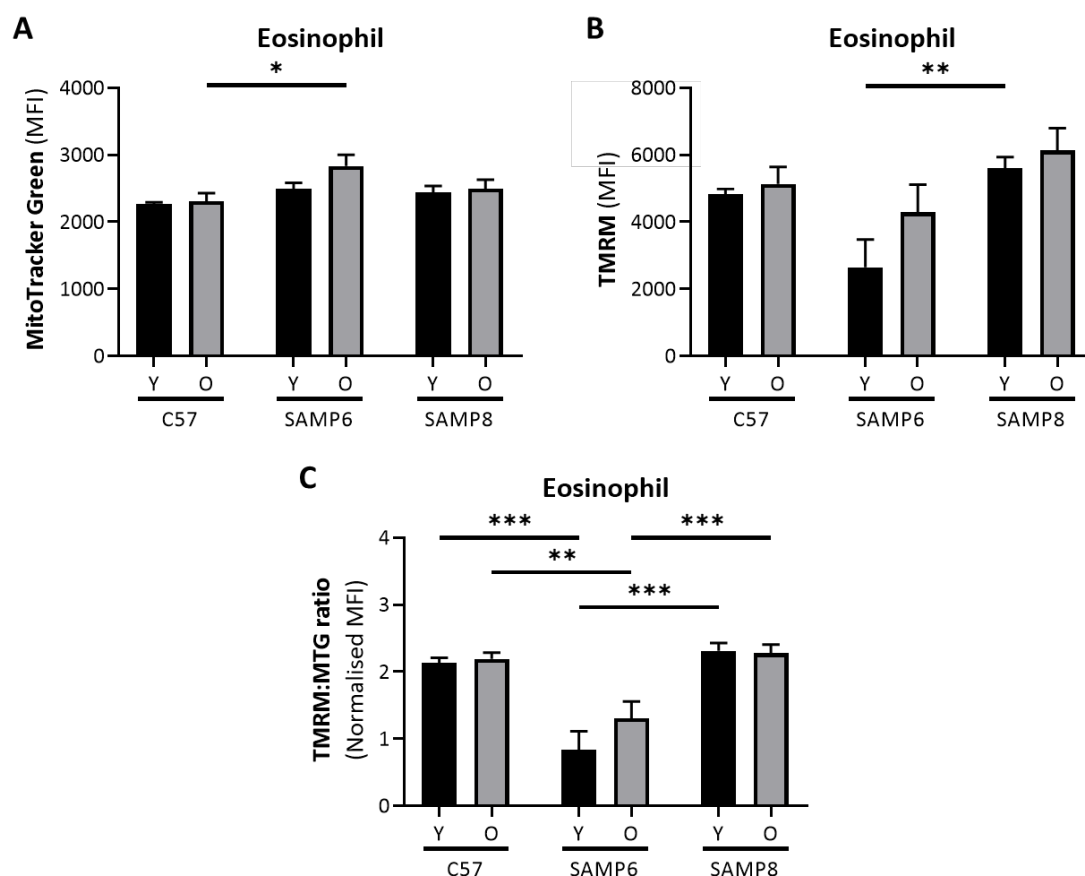

Figure 4.16 Mitochondrial mass and membrane potential in eosinophils resident in bone marrow showing (A) MTG staining (B) TMRM staining and (C) TMRM:MTG staining ratio in eosinophils from C57, SAMP6 and SAMP8 mice (mean+SEM; n=10; Ordinary two-way ANOVA; *p<0.05, **p<0.01, ***p<0.001)

Mitochondrial mass was increased in both Ly6C+ and Ly6C- monocytes with age in the bone marrow of SAMP6 mice (Figure 4.17A and B). MTG MFI increased by 44% (p=0.02) and 37% (p=0.029) within Ly6C+ and Ly6C- monocytes, respectively. This resulted in a significant upregulation of mitochondrial mass in old SAMP6 monocytes as compared to old C57 monocytes (p<0.001 for Ly6C+; p=0.011 for Ly6C-). Ly6C+ monocytes from old SAMP8 displayed increased mitochondrial mass than old C57, despite no significant upregulation of mitochondrial mass with age (p=0.023). In terms of mitochondrial membrane potential, TMRM staining was increased in Ly6C+ monocytes contained within both young and old SAMP8 bone marrow compared to C57 (2.8-fold for young p<0.001; 3-fold for old p<0.001) and SAMP6 (2-fold for young p=0.04; 3-fold for old p<0.001) mice (Figure 4.17C). These findings were extended to TMRM:MTG ratio, where SAMP8 mice showed

increased mitochondrial membrane potential compared to C57 mice at both ages (p<0.001 in young and old; Figure 4.17E). The TMRM:MTG ratio was significantly decreased in SAMP6 mice in comparison to SAMP8. TMRM:MTG ratio was reduced by 69% (p<0.001) and 81% (p<0.001) in young and old SAMP6 Ly6C+ monocytes, respectively.

Despite these alterations in Ly6C+ monocytes, TMRM staining was not affected in the same manner within Ly6C- monocytes (Figure 4.17D). TMRM staining was only observed to be increased by 63% in SAMP8 Ly6C- monocytes in comparison to those derived from young SAMP6 bone marrow (p=0.011). However, similar observations were made for TMRM:MTG ratio within these cells (Figure 4.17F). TMRM:MTG ratio was reduced in Ly6C- monocytes from both young and old SAMP6 bone marrow compared to C57 (39% for young p=0.03; 47% for old p=0.001) and SAMP8 (59% for young p<0.001; 56% for old p<0.001) mice. This reduction in TMRM:MTG ratio in Ly6C+ and Ly6C- monocytes may represent the appearance of dysfunctional mitochondria within the bone marrow of SAMP6 mice. Dysfunctional mitochondrial metabolism may aid in understanding the increased glycolytic capacity but decreased glycolytic reserve observed within bone marrow cells.
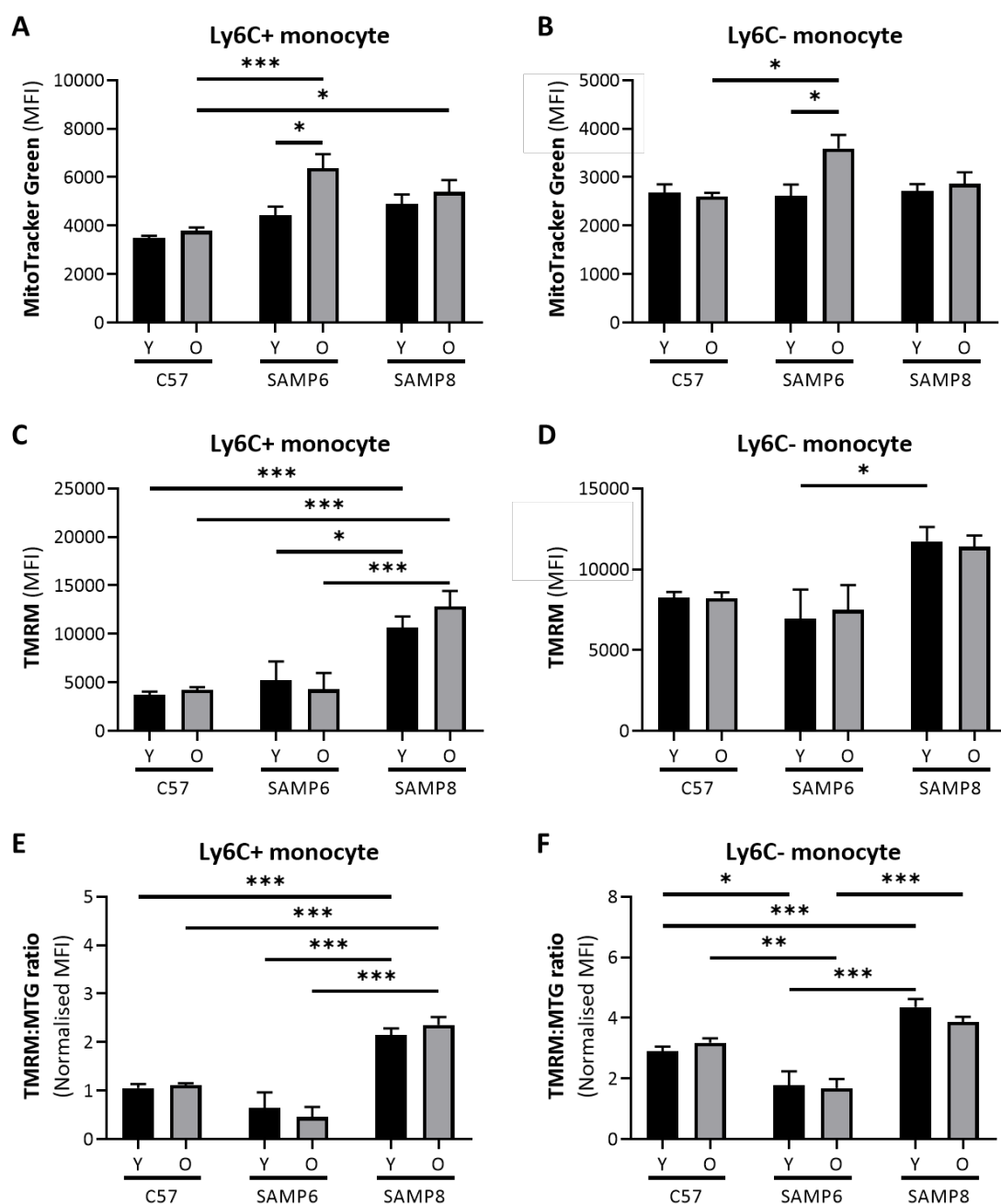
Figure 4.17 Mitochondrial mass and membrane potential in Ly6C+ and Ly6C- monocytes resident in the bone marrow showing MitoTracker Green (MTG) mean fluorescent index (MFI) in (A) Ly6C+ and (B) Ly6C- monocytes, TMRM MFI in (C) Ly6C+ and (D) Ly6C- monocytes and TMRM:MTG ratio in (E) Ly6C+ and (F) Ly6C- monocytes from C57, SAMP6 and SAMP8 mice (mean+SEM; n=10; Ordinary two-way ANOVA; *p<0.05, **p<0.01, ***p<0.001)

Surprisingly, no alterations were observed in MTG staining with age within the neutrophil population (Figure 4.18A). This was the case for mitochondrial mass between each of the mouse strains studied and for TMRM staining (Figure 4.18B). Alterations in the mitochondrial dynamics of these cells were revealed when TMRM staining was normalised to mitochondrial mass. As with the eosinophil population and monocyte subsets contained within the bone marrow population, SAMP6 mice showed reduced TMRM:MTG ratio within neutrophils (Figure 4.18C). TMRM:MTG ratio was reduced in Ly6C- monocytes from both young and old SAMP6 bone marrow compared to C57 (44% p<0.001 in young; 37% p=0.005 in old) and SAMP8 (51% p<0.001 in young; 52% p<0.001 in old) mice. This suggests that this cell population may be involved in the altered glycolytic metabolism observed within the bone marrow of SAMP6 mice.
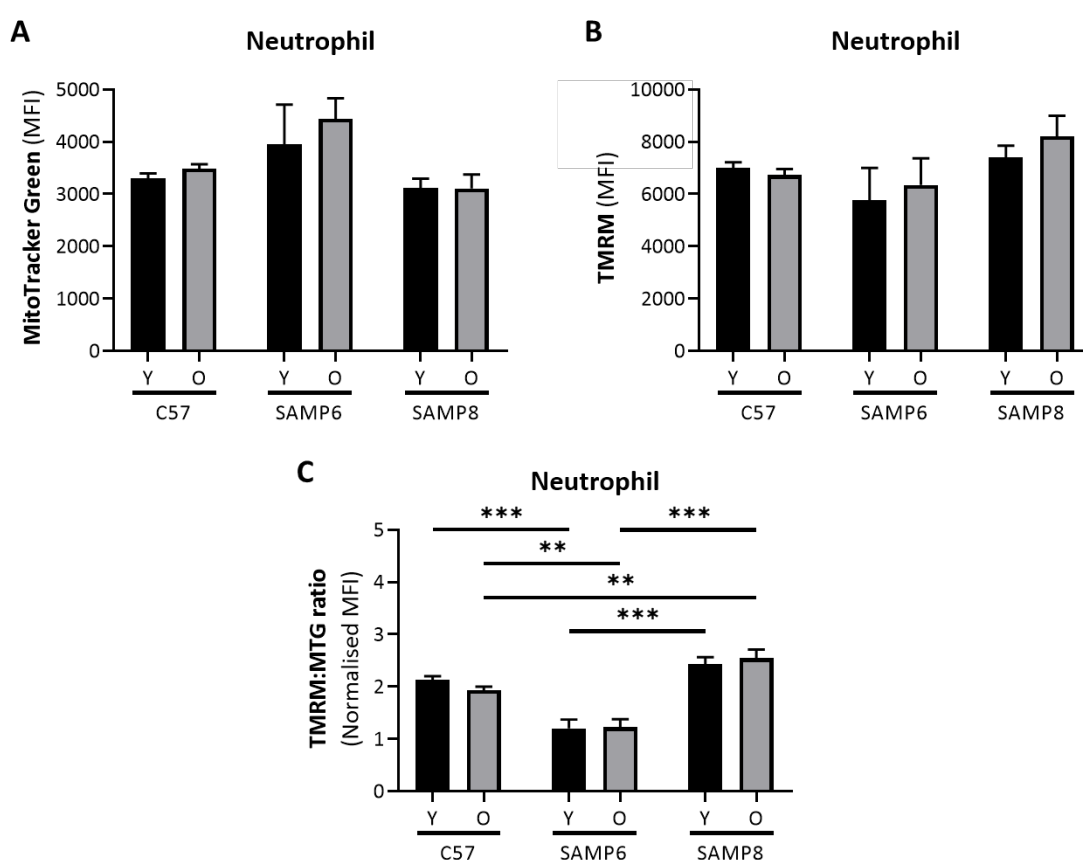
Figure 4.18 Mitochondrial mass and membrane potential in neutrophils resident in the bone marrow showing (A) MTG staining (B) TMRM staining and (C) TMRM:MTG staining ratio in neutrophils from C57, SAMP6 and SAMP8 mice (mean+SEM; n=10; Ordinary two-way ANOVA; **p<0.01, ***p<0.001)

Despite alterations in the mitochondrial landscape of eosinophils, monocytes and neutrophils contained within the bone marrow of SAMP6 mice, B cells were not subject to such changes. Naïve B cells saw no changes in MTG and TMRM staining or TMRM:MTG ratio with age within C57, SAMP6 and SAMP8 mice or between any of the strains studied (Figure 4.19A, C and E). Memory B cells on

the other hand, did show some alterations between the mouse strains. MTG staining (p=0.001 in young; p<0.001 in old), TMRM staining (p<0.001 in young and old) and TMRM:MTG ratio (p=0.042 in young; p<0.001 in old) was found to be increased in SAMP8 mice compared to C57 (Figure 4.19B, D and F). Whilst TMRM MFI was found to be decreased in both young (p=0.004) and old (p=0.025) SAMP6 memory B cells in comparison to SAMP8, this did not translate to TMRM:MTG ratio where a reduction was observed within young mice (34% decrease; p=0.009).
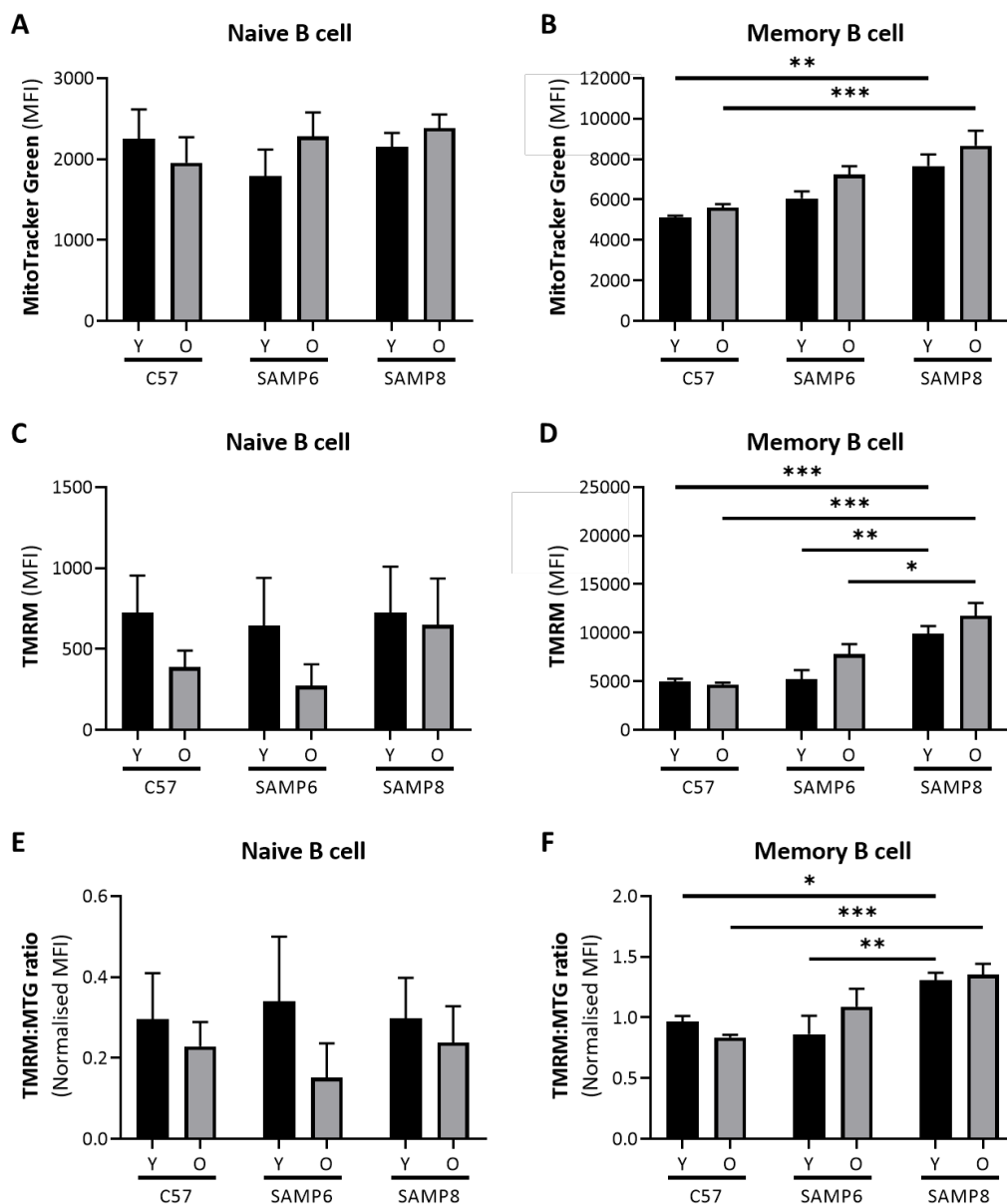
Figure 4.19 Mitochondrial mass and membrane potential in naïve and memory B cells resident in bone marrow showing (A) MTG staining in naïve B cells (B) MTG staining in memory B cells (C) TMRM staining in naïve B cells (D) TMRM staining in memory B cells (E) TMRM:MTG staining ratio in naïve B cells and (F) TMRM:MTG staining ratio in memory B cells from C57, SAMP6 and SAMP8 mice (mean+SEM; n=10; Ordinary two-way ANOVA; *p<0.05, **p<0.01, ***p<0.001)

4.4 Discussion: Metabolic efficiency in the bone marrow and periphery of ageing mice

Whilst mitochondrial dysfunction has been well characterised within the brain and liver of SAMP8 mice, relatively few studies have focused on other tissues or other SAM strains for mitochondrial and metabolic analysis. Therefore, the metabolism and the mitochondrial landscape within cells from the bone marrow and spleen of both the SAMP6 and SAMP8 strains and C57BL/6J mice was studied. A summary of flow cytometry results from this chapter presenting mitochondrial mass and membrane potential in immune cells derived from the spleen and bone marrow can be found in Table 4.6.

Table 4.6   Summary of mitochondrial mass and membrane potential of immune cells in spleen and bone marrow of C57, SAMP6 and SAMP8 mouse strains

TISSUE	CELL TYPE	MITOCHONDRIAL MASS			MITOCHONDRIAL MEMBRANE POTENTIAL			NORMALISED MEMBRANE POTENTIAL		
		C57	SAMP6	SAMP8	C57	SAMP6	SAMP8	C57	SAMP6	SAMP8
SPLEEN	CD4+ naïve T cell	→	→	→	→	↓	→	→	→	→
	CD4+ memory T cell	↓	↓	→	→	↓	→	→	→	→
	CD8+ naïve T cell	→	→	→	→	↓	→	→	→	→
	CD8+ memory T cell	↓	→	→	→	→	→	→	→	→
	B cell	↓	↓	→	→	↓	→	→	→	→
	Immature NK	→	↓	→	→	→	→	→	→	↓
	Mature NK	→	→	↑	→	→	→	→	→	→
	Monocyte	→	→	→	→	↓	→	→	↓	→
BONE MARROW	Eosinophil	→	→	→	→	→	→	→	→	→
	Ly6C+ monocyte	→	↑	→	→	→	→	→	→	→
	Ly6C- monocyte	→	↑	→	→	→	→	→	→	→
	Neutrophil	→	→	→	→	→	→	→	→	→
	Naïve B cell	→	→	→	→	→	→	→	→	→
	Memory B cell	→	→	→	→	→	→	→	→	→

SAMP6 mice are characterised by senile osteoporosis whilst SAMP8 mice are subject to deficits in learning and memory and impaired immune responses (Takeda, 1999). Oxidative damage and oxidative stress have been well described within SAMP8 mice. Nakahara *et al.* and Liu *et al.* proposed that this oxidative damage affects the efficiency of ATP synthesis in liver mitochondria (Nakahara et al., 1998, Liu et al., 2008, Huang et al., 2019). Within this study, this finding did not extend to splenic cells. However, a significant reduction in the ATP production from bone marrow cells of old SAMP8 mice was observed compared to SAMP6 which may be related to decreased ATPase efficiency, although ATP production was not altered with age within these mice. Similarly, it has been proposed that the oxidative defence system is reduced in SAMP8 mice, as they show lower activity of superoxide dismutase (SOD) and glutathione (GSH) within the liver and brain (Mori et al., 1998, Liu and Mori, 1993). Despite this decrease in oxidative defence, no significant difference in H_2O_2 production from bone marrow cells was observed between SAMP8 and SAMP6 or C57 mice. This suggests that increased oxidative stress as a result of reduced defence systems may be tissue specific as previously described (Rebrin et al., 2005).

Increased expression of inflammatory markers has previously been reported in the brains of SAMP8 mice. At 10 months of age, a significant increase in the messenger RNA (mRNA) level of TNF-α, IL-6 and IL-1β was observed in the hippocampus, cerebral cortex and hypothalamus of SAMP8 mice over that of SAMR1 (Tha et al., 2000). Increased TNF-α and IL-6 levels have also been reported in the peripheral blood of SAMP8 mice (Kobayashi et al., 2018). This is thought to be as a result of chronic activation of immune cells. In terms of immune cell metabolism, sustained mitochondrial mass was observed within splenic T cells and B cells in comparison to SAMP6 and C57 mice, which showed a loss of mitochondrial mass with age. Simultaneously, increased mitochondrial membrane potential was observed within eosinophils, monocytes and neutrophils within the bone marrow compared to SAMP6 mice. These findings may sustain the production of pro-inflammatory markers within SAMP8 mice, however without further study this cannot be confirmed.

NMR analysis of plasma metabolites has shown reduced glucose and pyruvate and increased lactate in the sera of SAMP8 mice compared to SAMR1 (Jiang et al., 2008). This finding suggested perturbed glucose and lipid metabolism within SAMP8 mice and was found to be more pronounced within females which show greater development of Alzheimer's disease. In line with these findings increases in the basal respiration and ATP-linked respiration of SAMP8 splenic cells was observed within this study, which may alter serum metabolites levels. Increased ATP-linked respiration was observed within bone marrow cells alongside decreased glycolysis and glycolytic capacity. Whilst decreased Complex I activity has been observed in SAMP8 mice compared to SAMR1, and

concomitant increase in Complex II and IV respiration and activity have previously been observed in muscle, and mirrors the bioenergetic capacity observed in spleen (Barquissau et al., 2017).

Previous research has found mesenchymal stem cells (MSCs) from SAMP6 mice to have reduced ATP:ADP ratio, increased ROS production and decreased mitochondrial membrane potential in comparison to SAMR1 mice (Lv et al., 2018). These changes result in reduced oxygen consumption rates as a result of increased inner membrane to outer membrane ratio of the mitochondria. However these changes within the bone marrow compartment were not observed in this study. A significant increase in ATP production, but no changes in H_2O_2 production with age were observed within these cells. However, a significant reduction in the mitochondrial membrane potential of eosinophils, monocytes and neutrophils within the bone marrow of SAMP6 mice was seen, like that observed within MSCs. Whilst decreased mitochondrial membrane potential within MSCs was due to decreased oxidative metabolism, a switch towards glycolytic metabolism in bone marrow immune cells was observed (Lv et al., 2018).

Within SAMP1 mice, increased mortality as a result of influenza A infection, has been found to result from impaired NK cell and CD8+ T cell activity and partial CD4+ T cell deficiency (Dong et al., 2000). Disruption of immune cells resident within the spleen and bone marrow of SAMP8 and SAMP6 mice was observed. Immune-modulation has previously been described within both SAMP6 and SAMP8 mice (Molina et al., 2016, Tsuji et al., 2018, Liu et al., 2019, Kuo et al., 2017). This study confirms that immune cells are affected within these mice. The mitochondrial landscape involving mitochondrial mass and membrane potential, affects the global metabolism of the splenic and bone marrow cell populations.

4.4.1 Limitations

The introduction of more mice into the study design could have brought more strength to the conclusions drawn. Whilst the Seahorse XF experiments did not show a lack of power, increasing the n number may have extended the number of statistically significant results. This is particularly the case for where experiments showed a trend towards reduced spare capacity in splenic cells with age which did not quite reach significance.

The study design may also have been impacted by the varying ages of the mice utilised for this study. Mice were grouped as young (<3 months of age) or old (>12 months of age). Due to the small litter size and reduced breeding activity of SAMP mice within the laboratory setting used for this project, it was impractical to collect tissues from mice of the exact same age. This introduced a degree of variability within the age groups which may have impacted statistically relevant findings.

The SAMR1 mouse strain, which would have been the ideal control for this study, was not available at A*STAR. The SAMR1 strain is costly to maintain and not as widely used by researchers. Therefore, C57BL/6J mice were integrated into this study as a control. Previous reports have suggested that SAM mice typically live until approximately 60 weeks of age. However, the SAM strains used within this experiment had a life span of up to 120 weeks of age. Whilst this may be due to the SPF housing environment of the mice, it may also be a result of less selective in-breeding of SAM strains. This may account for the differences observed between the mice used within this study and those used within previous research. Future work should focus on characterising the SAM strains contained within the biological research facility at A*STAR to establish their relevance to other SAMP6 and SAMP8 strains.

4.5   Conclusion

Basal oxidative metabolism and ATP-linked respiration were increased in splenic cells derived from SAMP8 mice in comparison to SAMP6 and C57 mice. A significant reduction in spare oxidative capacity was also observed with age in C57 mice, however this finding was not significant in SAMP6 and SAMP8 mice. Despite changes in oxidative metabolism, no changes in the glycolytic metabolism of these cells was observed with age or between genotypes. Despite SAMP8 cells showing increased ATP-linked respiration, no increase in the ATP production of the cells was observed. Similarly, no changes in H_2O_2 production were observed with age despite previous findings. It is proposed that differences in the regulation of mitochondrial mass and membrane potential are observed in SAMP8 mice with age, which may contribute to the increased oxidative metabolism observed in splenic cells. NK cells and monocytes resident within the spleen have a limited role within this effect, however.

When analysing bone marrow cells, alterations in the oxidative metabolism of SAMP8 mice and glycolytic metabolism of SAMP6 mice were observed. Whilst SAMP8 bone marrow cells displayed decreased maximal respiration in young mice and increased ATP-linked respiration with age, SAMP6 cells surprisingly showed increased glycolytic capacity with a concurrent decrease in glycolytic reserve. It is proposed that these modifications in glycolytic metabolism may be linked to the development of osteoporosis within SAMP6 mice. Changes in the ATP production and glucose uptake by bone marrow cells within these mice were also observed, therefore it was sought to identify which cell types may influence these alterations. Eosinophils, neutrophils and monocytes from SAMP6 mice all showed reduced TMRM:MTG ratio compared to C57 and SAMP8 mice. This reduction in mitochondrial membrane potential may force these cells to rely more heavily on glycolytic metabolism to sustain energy production, resulting in the increased glycolytic capacity but decreased glycolytic reserve observed within SAMP6 bone marrow. This increased reliance on glycolysis may contribute to the development of osteoporosis within these mice.

A summary of these findings in shown in Figure 4.20. In summary, it was shown that SAMP6 mice exhibit alterations in oxidative metabolism within the bone marrow which may be linked to the osteoporosis observed within these mice. This decreased oxidative metabolism is associated with decreased mitochondrial membrane potential of immune cells contained in the bone marrow of SAMP6 mice. These mice showed an altered mitochondrial landscape of immune cells in the spleen. SAMP8 mice showed increased oxidative metabolism in the spleen, however this finding did not appear to affect the mitochondrial content of immune cells obtained from these mice.

C57BL/6J   **SAMP6**   **SAMP8**

	C57BL/6J	SAMP6	SAMP8
(bone)	Normal metabolism	↓ Basal oxygen consumption rate = Osteoporosis (↑ ATP production)	↑ Glycolytic metabolism
	↑ Mitochondrial membrane potential in immune cells	↓ Mitochondrial membrane potential in immune cells	↑ Mitochondrial membrane potential in immune cells
(spleen)	Normal metabolism	Normal metabolism	↑ Oxidative metabolism = dysregulated immunity
	Normal immune cell profile	↑ Mitochondrial mass and membrane potential of immune cells	Normal immune cell profile

Figure 4.20 Summary of findings during ageing of C57BL/6J, SAMP6 and SAMP8 mouse strains showing altered oxidative metabolism in the bone marrow of SAMP6 mice and spleen of SAMP8 mice with age

Chapter 5   Investigating the metabolism of CD4+ effector memory T cells re-expressing CD45RA (TEMRA)

5.1   Introduction

With age there is a dramatic shift within the CD4+ and CD8+ T cell pools from naïve cells in the young to memory cells in elderly mice and humans (Trzonkowski et al., 2010). This natural process is thought to result from involution of the thymus and lifetime exposure to pathogens. Naylor *et al.* found a significant reduction in the number of recent thymic emergents over the age of 55 years in a cohort of 156 donors of varying ages (Naylor et al., 2005). However, previous studies have shown that T cell receptor (TCR) diversity can be maintained until 65 years of age in humans (Naylor et al., 2005). Memory cells show a ten-fold reduction in the diversity of their TCR repertoire than naïve cells (Naylor et al., 2005). Whilst mice do not increase homeostatic proliferation with age, they instead show increased longevity of naïve T cells which come with their own functional defects (Tsukamoto et al., 2009).

In humans, Koch *et al.* reported numerous differences in the frequency of CD8+ naïve and memory T cell subsets with age, whilst differences within the CD4+ population were less pronounced between young and elderly individuals (Koch et al., 2008). Whilst they found only a significant increase within the CD4+ central memory (CM) cell subset with age, naïve and T effector memory cells re-expressing CD45RA (TEMRA) were subject to reduced and increased frequency respectively within the CD8+ T cell compartment (Koch et al., 2008, Fülöp et al., 2013). The CD4+ T cell compartment showed a much-reduced frequency of TEMRA cells compared to the CD8+ compartment between the young and elderly, instead the bulk of memory lay within CM cells. Poor responses to infection and poor vaccine efficiency in the elderly are just two of the major health concerns of today. Ageing of the CD4+ T cell compartment has been associated with these issues but has not been attributed to one specific CD4+ T cell subset (Deng et al., 2004, Lorenzo et al., 2018, Scollay et al., 1980).

Persistent viral infections such as cytomegalovirus (CMV) and dengue virus (DENV) are associated with the development of TEMRA cells within both the CD8+ and CD4+ T cell compartments (Tian et al., 2017, Libri et al., 2011, Gordon et al., 2017). The accumulation of TEMRA cells has been described within human immunodeficiency virus (HIV) patients on antiretroviral therapy and in patients with osteoporosis and increased frailty scores (McElhaney and Effros, 2009, Booiman et al., 2017). This accumulation is thought to occur through extensive and prolonged TCR stimulation

over time during the ageing process resulting in T cell exhaustion. TEMRA cells have previously been shown to have characteristics of terminal differentiation and senescence associated with increased programmed cell death receptor 1 (PD-1) expression (Booiman et al., 2017, Bengsch et al., 2016). Both CD8+ and CD4+ TEMRA cells have been shown to express high levels of senescence markers CD57 and killer cell lectin-like receptor subfamily G member 1 (KLRG1), with roughly 60% of cells expressing these markers compared to <10% of naïve and CM cells (Koch et al., 2008, Tian et al., 2017). The loss of functionality in the CD4+ T cell compartment with age is exemplified by reduced rates of transplant rejections in the elderly (Bradley, 2002, Trzonkowski et al., 2010). This phenomenon was found to be associated with reduced telomere length, reduced proliferative capacity of T cells and reduced naïve CD4+ T cell numbers (Trzonkowski et al., 2010). As they age CD4+ T cells lose their proliferative capacity and telomerase activity and increase their production of interferon-gamma (IFNγ) leading to the immunosenescent and inflamm-ageing phenotypes described in Chapter 1 (Trzonkowski et al., 2010).

However, CD8+ TEMRA cells have previously been found to express high levels of TNFα, IFNγ, granzyme B (GZB) and perforin, resulting in potent cytotoxic activity (Henson et al., 2014, Tian et al., 2017). Consequently, recent studies have shown that high numbers of CD8+ TEMRA are associated with an increased immune response, ie. kidney graft rejection and multiple sclerosis (Yap et al., 2014, De Biasi et al., 2019). Whilst TEMRA cells account for ~22% of CD8+ cells, the TEMRA cell population within the CD4+ T cell compartment can vary drastically between individuals from <0.3% to 18% (Tian et al., 2017, Henson et al., 2014). Therefore, it is unknown whether CD4+ TEMRA cells contribute to this phenomenon.

Differences between memory and naïve T cells within the CD8+ T cell compartment have already been studied. Van der Windt *et al.* found that memory cells have 2-fold higher ratio of mitochondrial deoxyribose nucleic acid (DNA) (mtDNA) to nuclear DNA compared to naïve cells indicating a significantly higher mitochondrial mass (van der Windt et al., 2013). This trend was found within the CD4+ T cell compartment, with naïve cells showing significantly lower mitochondrial mass than effector memory (EM) cells. This result was confirmed by translocase outer mitochondrial membrane 20 (TOM20) staining in sorted cells (De Biasi et al., 2019). This increase in mitochondrial mass made memory cells able to proliferate faster and generate more IFNγ during secondary effector cell formation compared to primary effector cells derived from naïve T cells. Previous studies have suggested that the terminal differentiation of T cells requires aerobic glycolysis (Gaber et al., 2015). Increased oxygen consumption rate (OCR) and increased extracellular acidification rate (ECAR) were noted within memory cells following stimulation with anti-CD3/28 (van der Windt et al., 2013). Within the CD4+ T cell compartment EM cells have been found to have higher ECAR than naïve cells within the context of primary progressive and secondary progressive

forms of multiple sclerosis and a greater tendency to shift from oxidative phosphorylation (OXPHOS) to glycolysis (De Biasi et al., 2019).

Studies focusing on CD8+ TEMRA cell metabolism have revealed that TEMRA cells have profound metabolic instability described by decreased spare respiratory capacity, decreased mitochondrial mass and membrane potential and increased reactive oxygen species (ROS) production (Henson et al., 2014, Callender et al., 2019). Prior to stimulation TEMRA cells have similar levels of mitochondrial mass to naïve cells, which is reduced in comparison to that of EM cells (Tilly et al., 2017). This is reflected in their response to a mitochondrial uncoupling agent, whereby EM cells have greatly increased maximal respiration rates compared to naïve and TEMRA cells. Whilst prior to stimulation TEMRA cells do not show significantly increased adenosine triphosphate (ATP)-linked respiration, they do have a significantly larger ATP reservoir compared to naïve cells which is rapidly utilised upon interleukin (IL)-15 stimulation (Tilly et al., 2017). Surprisingly, CD8+ TEMRA cells showed upregulated expression of genes involved in glycolysis, fatty acid oxidation and the pentose phosphate pathway compared to both naïve and EM cells, pathways which are further upregulated upon stimulation (Tilly et al., 2017). This increase in glycolysis has been shown to support CD8+ TEMRA cell effector function (Henson et al., 2014). Upon polyclonal phorbol 12-myristate 13-acetate (PMA)/Ionomycin stimulation, TEMRA cells exhibited similar and sustained increases in OCR and ECAR to EM cells whilst naïve cells only increased OCR transiently. Additionally, it has been shown that mitochondrial membrane potential is reduced upon CD3/CD28 stimulation in CD4+ naïve, CM, EM and TEMRA cells by approximately 30%, 12%, 24% and 39% respectively (De Biasi et al., 2019).

Whilst studies on the metabolism of CD4+ TEMRA cells are limited, Callender *et al.* noted that CD4+ TEMRA cells have 2-fold more mitochondrial mass than CD8+ TEMRA cells which causes them to become senescent at a slower rate (Callender et al., 2019). This study showed that CD4+ TEMRA cell mitochondria are more hyperpolarised and have increased OCR and spare respiratory capacity (SRC) than CD8+ TEMRA, resulting in greater ATP production. However, the results of this study performed in Caucasians has yet to be confirmed by others or within different populations.

In this chapter, the aim was to compare mitochondrial regulation and the metabolic phenotype of the four CD4+ T cell subsets (naïve, CM, EM and TEMRA) in response to CD3 (clone: OKT3) stimulation. It was hypothesised that all four subsets would have similar rates of mitochondrial regulation and metabolism prior to stimulation but different responses to stimulation. It was expected that CM and EM cells would show the largest response to stimulation, whilst TEMRA cells would show the smallest. The aims and objectives for the work conducted within this chapter are summarised in Figure 5.1.

Aim:
To determine mitochondrial programming in CD4+ T cell subsets during senescence including naïve, CM, EM and TEMRA cells

Objectives:
- Analyse mitochondrial dysfunction following CD3 (OKT3) stimulation
  - Analyse mitochondrial mass and membrane potential
  - Confirm expression of glucose transporter 1 (Glut1)
  - Analyse mitochondrial fission and fusion dynamics
  - Explore optic atrophy 1 (Opa1) protein expression
- Sort CD4+ naïve, central memory (CM), effector memory (EM) and terminal effector memory T cells re-expressing CD45RA (TEMRA) cells
- Analyse mitochondrial mass within these subsets to confirm flow cytometry findings
- Perform live-cell metabolic analysis of CD4+ T cells to confirm mitochondrial dysfunction in senescent cells

Figure 5.1   Aims and objectives for studying mitochondrial dysfunction in CD4+ TEMRA cells in comparison to other CD4+ T cell subsets

5.2   Materials and methods

5.2.1   Donors and blood processing

Details of the donors and blood processing protocol can be found in Section 2.1.2.1.1 CD4+ T cell study. A total of 30 blood cones were used for the purpose of this study.

5.2.2   PBMC and isolated T cell culture

Cells were cultured in Rosewell park memorial institute (RPMI)-1640 medium (ThermoFisher, MA) containing 10% FBS (ThermoFisher, MA) (R-10) for all experiments as described in Section 2.1.3 Cell culture and tissue storage. Cultured cells were incubated at 37˚C with 5% CO_2 for the duration of the experiment. Cells were processed for long term storage as described in Section 2.1.3 Cell culture and tissue storage. After thawing, cells were incubated overnight using the above conditions before use in subsequent experiments.

5.2.3   CD3 (OKT3) stimulation

Cells were stimulated with CD3 (Clone: OKT3) as described in Section 2.7.1 CD3 (OKT3) stimulation for downstream analysis.

5.2.4   Flow cytometry for mitochondrial assessment

PBMCs were stained with the cell surface markers listed in Table 5.1 as described in Section 2.5.1.1 Cell surface staining. For intracellular protein staining cells were stained with the primary antibodies listed in Table 5.2 as described in Section 2.5.1.3 Intracellular protein staining. The secondary antibodies used are listed in Table 5.3. Fluorescence was acquired on a BD LSR-Fortessa flow cytometry system (Becton Dickson, MJ) at a flow rate of ~6,000 events per second for a total of 1 million events. The gating strategy for each subset is defined in Table 5.4 and shown in Figure 5.2.

Chapter 5

Table 5.1   Surface staining antibodies for T cell subsets

SURFACE MARKER	FLUOROPHORE	CLONE	RETAILER	DILUTION
Live-Dead	AmCyan	n/a	ThermoFisher, MA	1:200
CD3	PE	UCHT1	BioLegend, CA	1µl
CD4	Pacific Blue	OKT4	BioLegend, CA/Becton Dickson, NJ	1µl
CD27	Bv650	O323	BioLegend, CA	2µl
CD28	PE/Cy7	CD28.2	BioLegend, CA	1µl
CD45RO	Bv785	UCHL1	BioLegend, CA	1µl
CD45RA	Bv605	HI100	BioLegend, CA	1µl

Table 5.2   Primary antibodies for mitochondrial analysis in T cell subsets

PRIMARY ANTIBODY	FLUOROPHORE	SPECIFICITY/HOST SPECIES	RETAILER	DILUTION
Glut1	FITC	Rabbit	Abcam, UK	1µl
Opa1	n/a	Mouse IgG1	Abcam, UK	1µl
Mfn2[1]	n/a	Mouse IgG2α	Abcam, UK	1µl
Drp1	n/a	Mouse IgG2β	Abcam, UK	1µl

Table 5.3   Secondary antibodies for mitochondrial analysis in T cell subsets

SECONDARY ANTIBODY	FLUOROPHORE	HOST SPECIES	RETAILER	DILUTION
Anti-mouse IgG1	FITC	Goat	Abcam, UK	1µl
Anti-mouse IgG2β	Apc	Rat	R&D Systems, MN	1µl

---

[1] Mfn2 primary antibody was not detected by anti-mouse IgG2α secondary antibody but was detected by anti-mouse IgG2β therefore this secondary antibody was used instead

Table 5.4   T cell subset gating strategy using cell surface markers

T CELL SUBSET	GATING STRATEGY
Naïve	CD3+, CD4+, CD27hi, CD28+, CD45RA+
Central memory	CD3+, CD4+, CD27hi, CD28+, CD45RA-
Effector memory	CD3+, CD4+, CD27lo, CD28+, CD45RA-, CD45RA+
TEMRA	CD3+, CD4+, CD27lo, CD28+, CD45RA+, CD45RO-
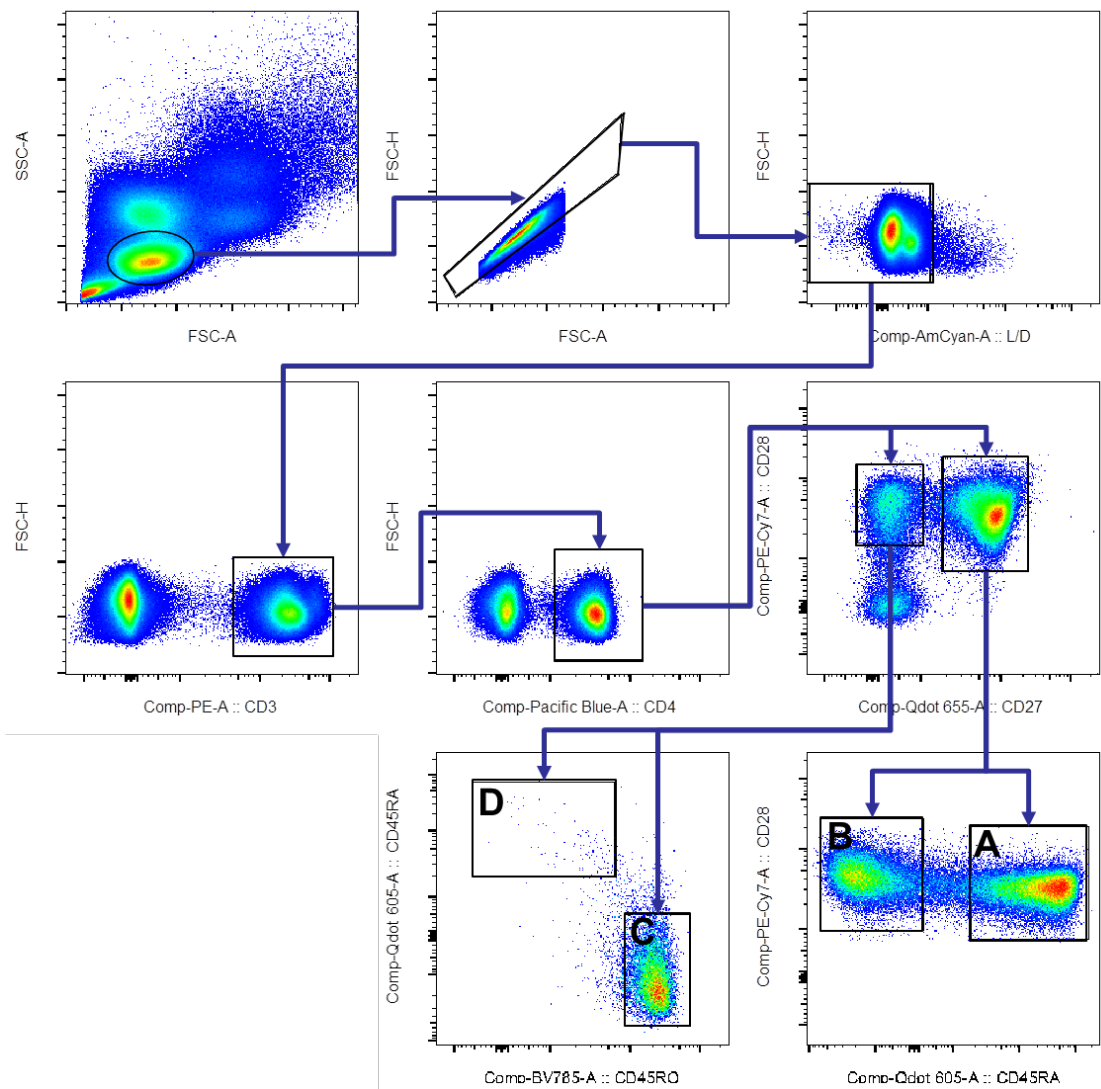
Figure 5.2   Gating strategy for identifying human CD4+ T cell subsets gated for cell size, singlets, live cells, CD3+ then CD4+ (A) Naïve cells gated as CD28+CD27hi then CD45RA+, (B) Central memory cells gated as CD28+CD27hi then CD45RA- (C) Effector memory cells gated as CD28+CD27lo then CD45RO+CD45RA- and (D) TEMRA cells gated as CD28+CD27lo then CD45RO-CD45RA+

5.2.5   CD4+ T cell subset sorting

5.2.5.1   Magnetic (MACS®) CD4+ T cell sorting

CD4+ cells were isolated from PBMCs by MACS® (Miltenyi Biotech, Germany) according to manufacturer's instructions. The procedure for MACS® separation is detailed in Section 2.5.3 Magnetic-activated cell sorting (MACS). For the purpose of this study cells were separated based on CD4 expression to isolate CD4+ T cells prior to fluorescence-activated cell sorting (FACS) for live-cell metabolic analysis.

5.2.5.2   Fluorescence (FACS) cell sorting of T cell subsets

CD4+ cells were stained for FACS in 5ml PP tubes using the staining procedure described in Section 2.5.2 Fluorescence-activated cell sorting (FACS). The surface staining antibodies used are listed in Table 5.5. Stained cells were passed to Ivy Low, Salanne Lee and Seri Mustafa at the A*STAR Flow cytometry core-facility and sorted using the BD FACS Aria II system. Following staining cells were washed twice with R-10 and cultured in 96-well U-bottom plates overnight at 37˚C with 5% CO_2 at density of 500,000 cells per well in 200µl R-10.

Table 5.5   Surface staining antibodies used for sorting CD4+ T cell subsets

SURFACE MARKER	FLUOROPHORE	CLONE	RETAILER	DILUTION
LIVE/DEAD	AmCyan	n/a	ThermoFisher, MA	1:200
CD3	PE	OKT3	BioLegend, CA	0.5µl/million
CD4	Pacific Blue	OKT4	BioLegend, CA	0.5µl/million
CD8	Apc/Cy7	SK1	BioLegend, CA	0.5µl/million
CD27	Bv650	O323	BioLegend, CA	1µl/million
CD28	PE/Cy7	CD28.2	BioLegend, CA	0.5µl/million
CD45RO	Apc	UCHL1	BioLegend, CA	0.5µl/million
CD45RA	Bv605	HI100	BioLegend, CA	0.5µl/million

5.2.6   Super-resolution microscopy

Sorted CD4+ and CD8+ T cell subsets (naïve, CM, EM and TEMRA) were used for super-resolution microscopy of mitochondria. Cells were stained, prepared and imaged as described in Section 2.2.4 Super-resolution microscopy. A total of 20 cells were imaged for each T cell subset from each of 2 donors. Images were analysed and mitochondria reconstructed using Imaris software (Oxford Instruments, UK).

5.2.7   CD4+ T cell seahorse analysis

The oxygen consumption rate (OCR) and extracellular acidification rate (ECAR) of T cell subsets was analysed using Seahorse XF technology (Agilent Technologies, CA). The assay was set-up as described in Section 2.6 Live-cell metabolic analysis. Sorted CD4+ T cell subsets (naïve, CM, EM and TEMRA) were plated at a density of 500,000 cells per well for the purposes of the assay.

5.2.8   Statistical analysis

Statistical analysis for all experiments was performed using a paired two-way ANOVA model, for parametric assessment of paired samples within donors. Tukey's multiple comparisons test was used for *post-hoc* analysis. Analysis of seahorse data was performed using a paired one-way ANOVA model with Tukey's multiple comparisons test *post-hoc* analysis. Flow cytometry data was analysed using FlowJo software. Statistical analysis was performed using GraphPad Prism software. GraphPad was used to create graphs. A p value of <0.05 was used to identify significance.

5.3   Results

5.3.1   Mitochondrial mass and membrane potential staining are unchanged between CD4+ T cell subsets, but the mitochondrial mass to membrane potential ratio is reduced in CD4+ TEMRA

In order to clarify whether mitochondrial mass and mitochondrial membrane potential were affected by OKT3 stimulation, MitoTracker Green (MTG) and tetramethylrhodamine methyl ester (TMRM) staining were analysed by flow cytometry in CD4+ T cells. A significant effect of CD4+ T cell subset was observed on mitochondrial mass (Figure 5.3A; $p=0.001$, $F(2.13,14.93)=9.519$). However, no differences between MTG staining were observed between the time points studied for each subset. Similar observations of a significant effect of CD4+ T cell subset were made for TMRM staining as an indicator of mitochondrial membrane potential ($p=0.004$; $F(1.95,13.66)=8.635$) with time-dependent effects of no significance as shown in Figure 5.3B. However, when TMRM staining was normalised to MTG staining significant differences between subsets were observed. Whilst there were no significant differences observed prior to stimulation CM cells displayed higher normalised mitochondrial membrane potential than both naïve and TEMRA cells (Figure 5.3C). Continued OKT3 stimulation for 24 hours maintained significantly increased normalised mitochondrial membrane potential within CM cells compared to naïve cells. This trend was continued within EM and TEMRA cells following 4 hours and 24 hours of stimulation, which both showed an increased mitochondrial membrane potential to mitochondrial mass ratio than naïve cells. At 24 hours TEMRA cells also showed significantly reduced normalised membrane potential than EM cells (Figure 5.3C), suggesting that TEMRA cells have different mitochondrial membrane maintenance to both naïve and EM cells following prolonged OKT3 stimulation.
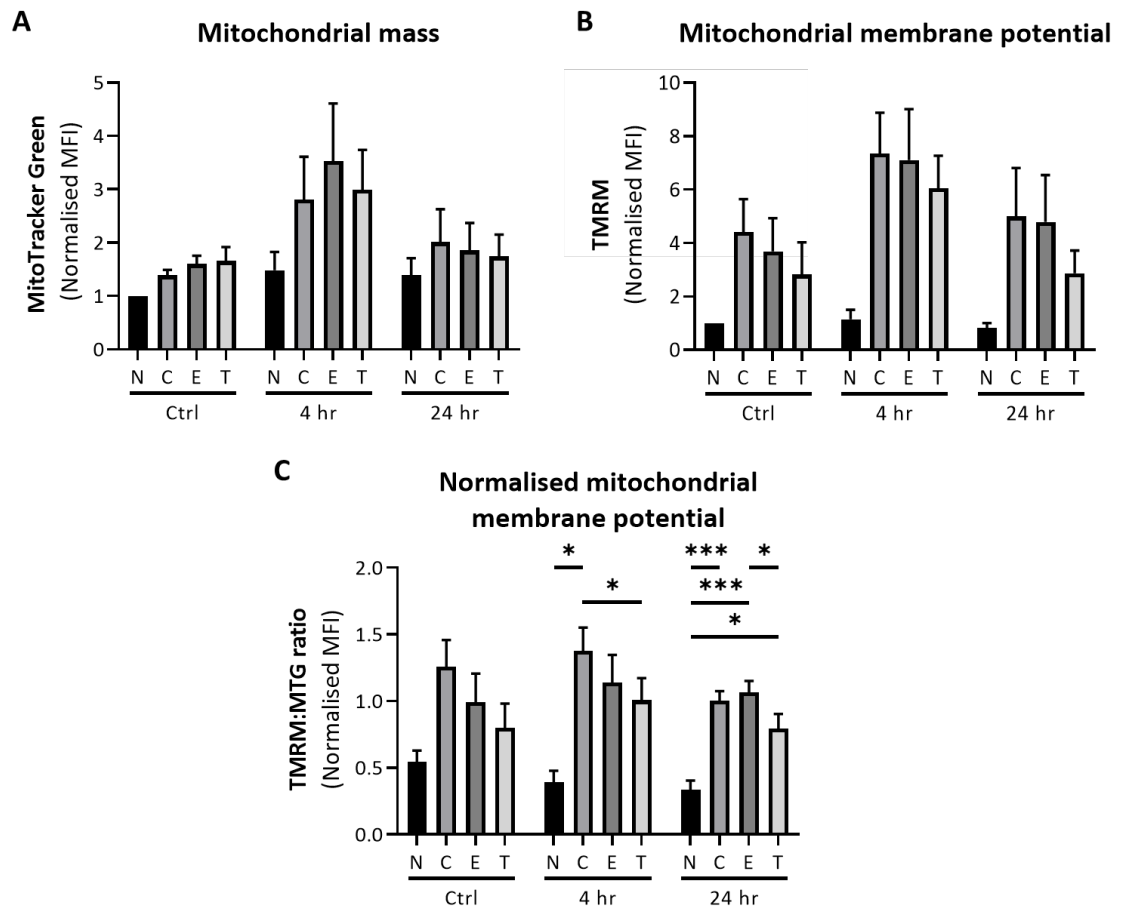
Figure 5.3 Mitochondrial mass and membrane potential in CD4+ T cells following OKT3 stimulation compared to control unstimulated cells (Ctrl) showing (A) MTG staining (B) TMRM staining and (C) TMRM:MTG staining ratio in each subset normalised to unstimulated naïve cells (N=naïve, C=central memory, E=effector memory, T=TEMRA) (mean+SEM; n=8; Two-way repeated measures ANOVA; *p<0.05 ***p<0.001)

5.3.2   Expression of Glucose transporter 1 (Glut1) is increased in CD4+ effector memory and TEMRA cells

Upregulation of glycolysis is an important part of engageing T cell effector function following stimulation. Therefore the extracellular surface expression of glucose transporter protein 1 (Glut1) was analysed by flow cytometry in unstimulated and stimulated cells following 4 hours and 24 hours of OKT3 stimulation. All four subsets (naïve, CM, EM and TEMRA) significantly upregulated Glut1 surface expression following 24 hours of stimulation (Figure 5.4A). No significant changes in extracellular Glut1 expression were observed during the first 4 hours of stimulation. The increase in Glut1 expression following 24 hours stimulation is exemplified by the shift in Glut1 fluorescence observed in Figure 5.4B.

Prior to stimulation memory CD4+ T cell subsets (CM, EM and TEMRA) displayed an increased level of Glut1 expression compared to cells contained within the naïve cell subset (Figure 5.4C). This increase was observed following 4 hours of OKT3 stimulation. At this time point significantly greater surface expression of Glut1 was observed within the EM cell subset compared to CM cells. Following 24 hours of stimulation the upregulation of Glut1 in memory subsets compared to naïve cells had diminished following the upregulation of Glut1 in all four subsets (Figure 5.4C and D).
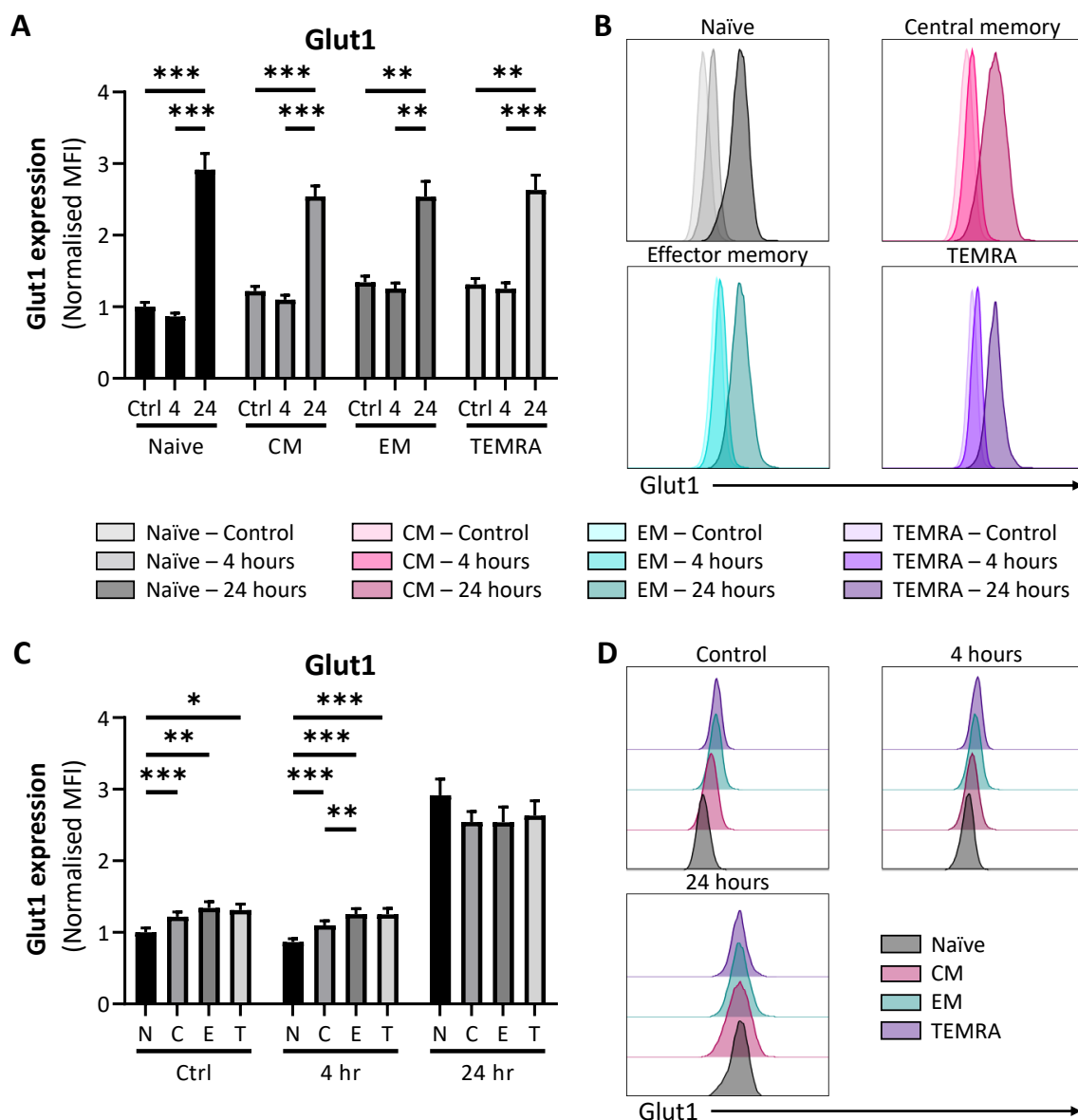
Figure 5.4   Glucose transporter 1 expression in CD4+ T cell subsets following OKT3 stimulation compared to unstimulated control cells (Ctrl) showing (A) Glut1 expression in subsets by stimulation time B) Histogram of Glut1 fluorescence in each subset (C) Glut1 expression following stimulation by subset (D) Histogram of Glut1 fluorescence at each stimulation timepoint normalised to unstimulated naïve cells (N=naïve, C=central memory, E=effector memory, T=TEMRA) (mean+SEM; n=19; Two-way repeated measures ANOVA; *p<0.05 **p<0.01 ***p<0.001)

5.3.3   Mitochondrial fission and fusion dynamics remain stable in CD4+ TEMRA cells

In order to confirm the upregulation of mitochondrial fission (dynamin related protein 1; Drp1) and fusion (mitofusin 2; Mfn2) upon OKT3 stimulation, the expression level of these proteins was measured by flow cytometry. Upon 4 hours of stimulation Drp1 expression was significantly increased within the CM, EM and TEMRA T cell subsets (Figure 5.5A and B). CM and EM cells have significantly higher expression of Drp1 following 24 hours of OKT3 stimulation (Figure 5.5C). Prior to stimulation EM cells showed significantly higher levels of Drp1 expression compared to naïve T cells. TEMRA cells showed similar levels of Drp1 expression to naïve cells at all time points observed in Figure 5.5D.

Interestingly, a significant effect of CD4+ T cell subset on Mfn2 expression was reported following analysis by two-way repeated measures ANOVA (Figure 5.6A-D; p=0.004, $F_{(1.054,10.54)}=13.04$). Whilst no specific interactions were identified by *post-hoc* analysis, CM and EM cells showed a trend towards higher expression levels than naïve T cells at all time points studied but this was not found to be significant. It is interesting to note that naïve T cells and TEMRA cells showed a great deal of Mfn2 expression variability after 24 hours of OKT3 stimulation as shown in Figure 5.6C compared to CM and EM cell subsets.
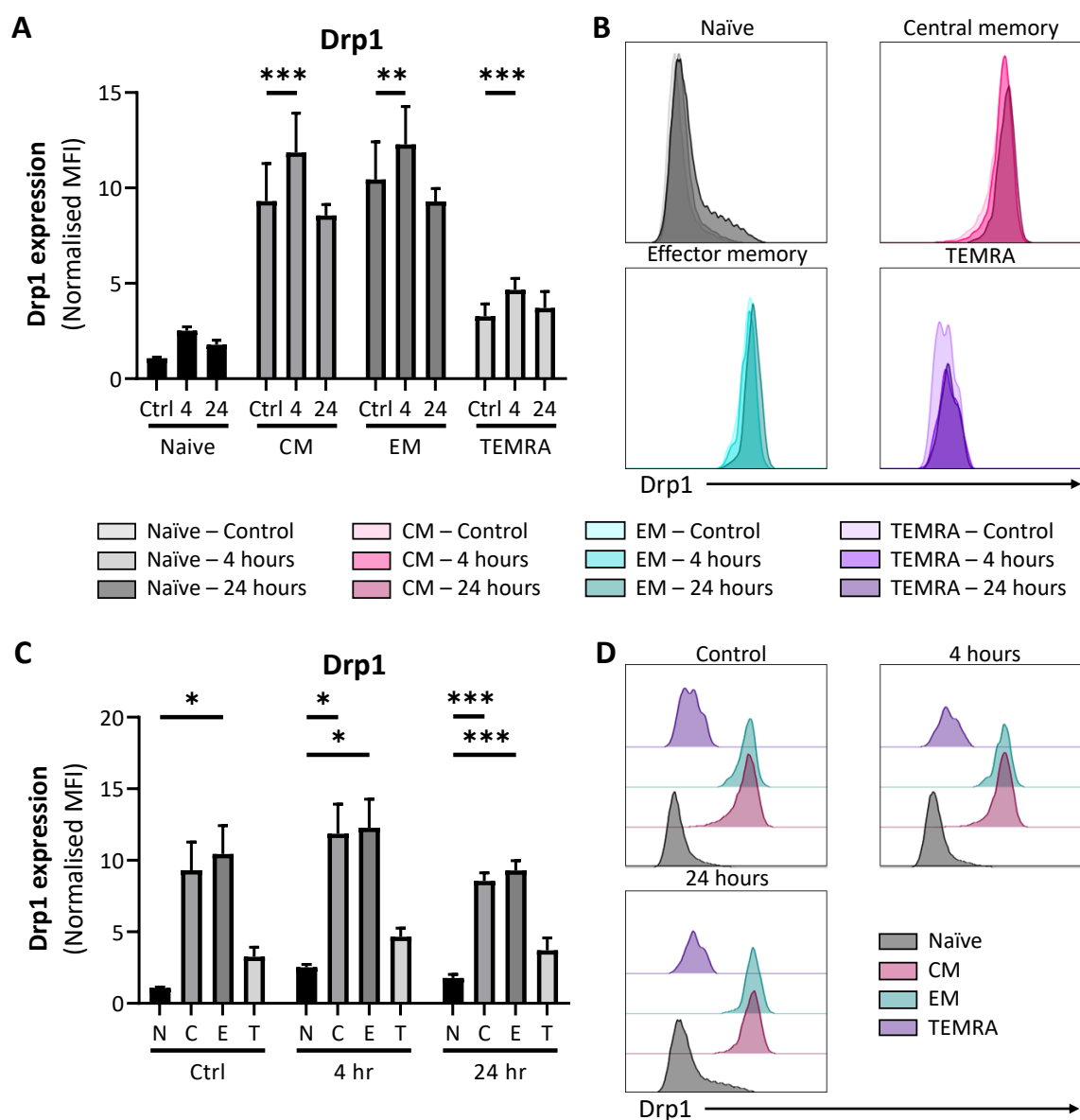
Figure 5.5   Dynamin related protein 1 expression in CD4+ T cell subsets following OKT3 stimulation compared to unstimulated control cells (Ctrl) showing (A) Drp1 expression in subsets by stimulation time (B) Drp1 fluorescence in each subset (C) Drp1 expression following stimulation by subset (D) Drp1 fluorescence at each stimulation timepoint normalised to unstimulated naïve cells (N=naïve, C=central memory, E=effector memory, T=TEMRA) (mean+SEM; n=17; Two-way repeated measures ANOVA; *$p < 0.05$ **$p < 0.01$ ***$p < 0.001$)
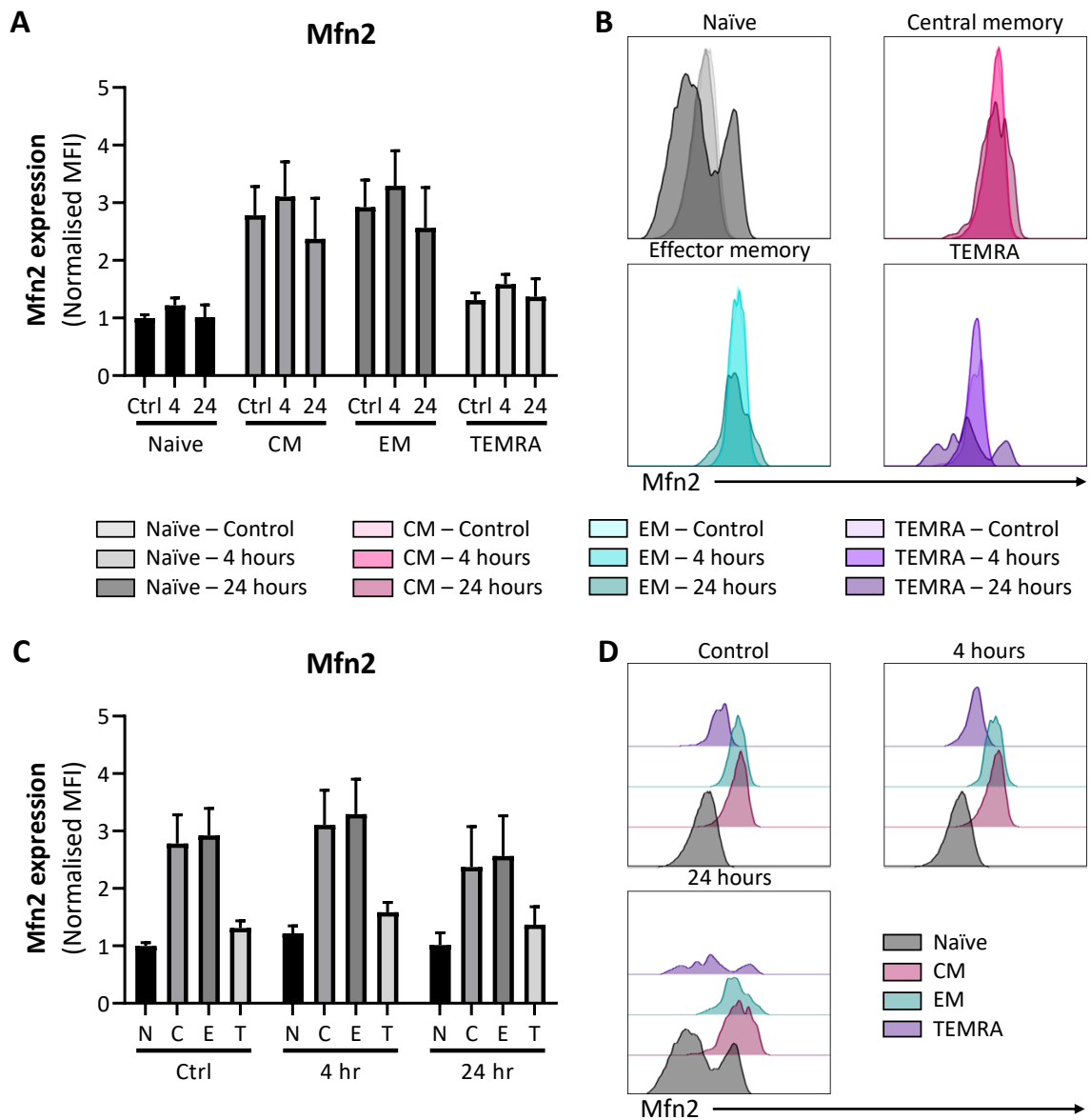
Figure 5.6   Mitofusin 2 expression in CD4+ T cell subsets following OKT3 stimulation compared to unstimulated control cells (Ctrl) showing (A) Mfn2 expression in subsets by stimulation time (h) (B) Histogram of Mfn2 fluorescence in each subset (C) Mfn2 expression following stimulation by subset (D) Histogram of Mfn2 fluorescence at each stimulation timepoint normalised to unstimulated naïve cells (N=naïve, C=central memory, E=effector memory, T=TEMRA) (mean+SEM; n=17; Two-way repeated measures ANOVA)

As Drp1 and Mfn2 expression levels should be in equilibrium prior to stimulation, expression levels of Drp1 and Mfn2 were tracked during the 24 hour time course of OKT3 stimulation. Only naïve T cells appeared to show a significant upregulation of Drp1 expression above Mfn2 expression following 4 hours of stimulation (Figure 5.7A). The CM, EM and TEMRA cell subsets did not appear

to show any upregulation of Drp1 or Mfn2 in comparison to the other over the time course of stimulation (Figure 5.7B-D).
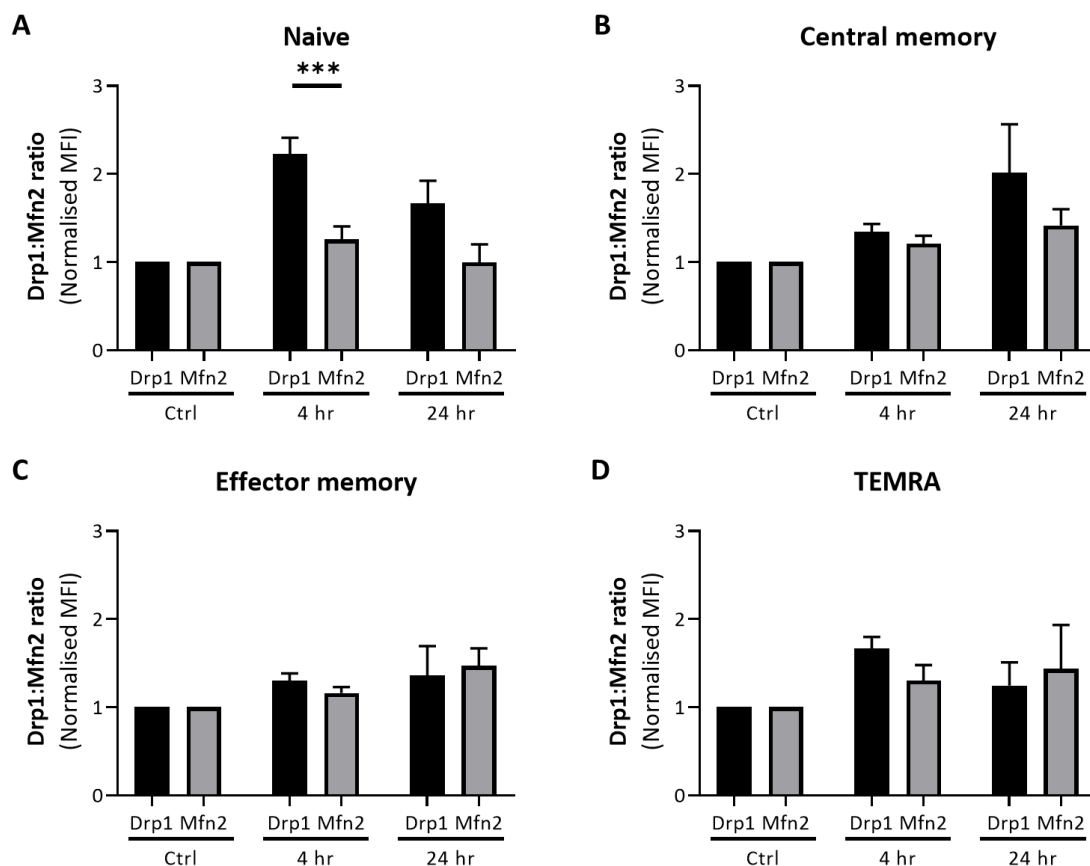
Figure 5.7   Balance of dynamin related protein 1 and mitofusin 2 expression in CD4+ T cell subsets following OKT3 stimulation compared to unstimulated control cells (Ctrl) showing (A) naïve cells (B) central memory cells (C) effector memory cells and (D) TEMRA cells normalised to mean fluorescent index (MFI) without stimulation (mean+SEM; n=17; Two-way repeated measures ANOVA; ***p<0.001)

5.3.4   Optic atrophy protein 1 (Opa1) expression is reduced in CD4+ effector memory and TEMRA cells following stimulation

As cristae remodelling has previously been observed between the T cell subsets and upon stimulation within naïve cells, the expression of Opa1 upon stimulation within these subsets was analysed by flow cytometry. A significant decrease in Opa1 expression was observed following 24 hours of OKT3 stimulation in all four CD4+ subsets, resulting in a shift in Opa1 fluorescence intensity (Figure 5.8A and B). No significant changes in Opa1 expression were observed during the first 4 hours of stimulation (Figure 5.8A).

No differences between the subsets in terms of their Opa1 expression were observed prior to OKT3 stimulation (Figure 5.8C). Following 4 hours and 24 hours of stimulation however, a significant reduction in Opa1 expression was observed within EM and TEMRA cells compared to CM cells. This reduction was observed following 24 hours when comparing EM and TEMRA cells to naïve T cells. This changing pattern of Opa1 expression within the four subsets is exemplified by a shift in Opa1 expression observed in Figure 5.8D following 24 hours of stimulation.
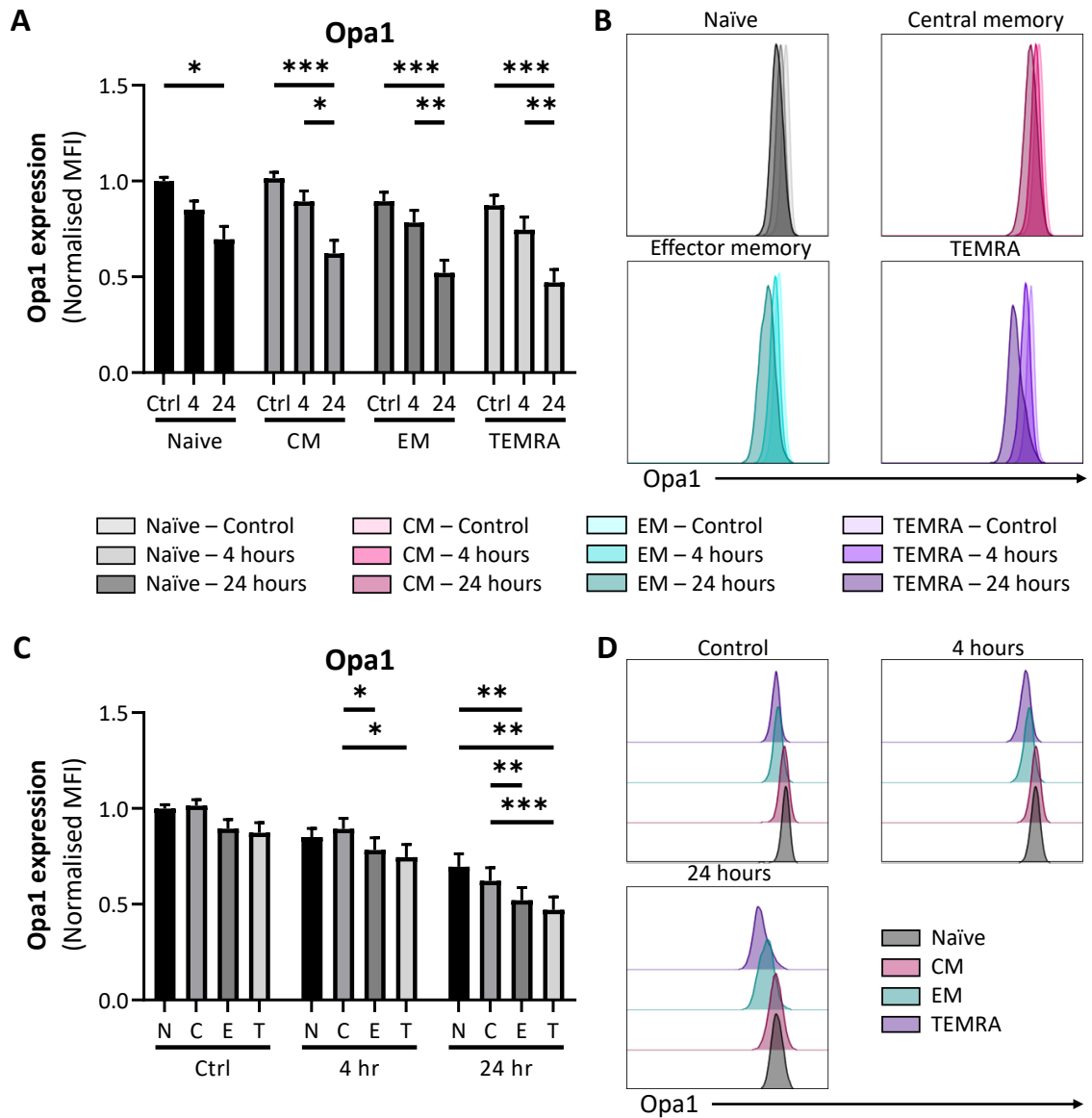
Figure 5.8   Optic atrophy 1 expression in CD4+ T cell subsets following OKT3 stimulation compared to unstimulated control cells (Ctrl) showing (A) Opa1 expression in subsets by stimulation time (B) Histogram of Opa1 fluorescence in each subset (C) normalised Opa1 expression following stimulation by subset (D) Histogram of Opa1 fluorescence at each stimulation timepoint normalised to unstimulated naïve cells (N=naïve, C=central memory, E=effector memory, T=TEMRA) (mean+SEM; n=18; Two-way repeated measures ANOVA; *p<0.05 **p<0.01 ***p<0.001)

5.3.5 Super-resolution microscopy of CD8+ and CD4+ T cells reveals differences in mitochondrial structure

In order to observe the mitochondrial landscape within CD4+ and CD8+ T cell subsets cells were sorted by FACS from each of 2 donors and analysed using super-resolution microscopy as seen in Figure 5.9. Using translocase outer mitochondrial membrane 20 (TOM20) a translocase present on the outer mitochondrial membrane as a marker, mitochondrial membranes were rendered and compared. Increased mitochondrial surface area and mitochondrial volume were observed in CM cells compared to naïve cells within the CD4+ T cell but not the CD8+ T cell compartment (Figure 5.10A and B). However, mitochondrial volume was significantly decreased in CD4+ CM cells compared to CD4+ EM cells.

Within the CD8+ T cell compartment increased mitochondrial surface area and increased mitochondrial volume were observed in EM cells compared to naïve T cells (Figure 5.10A and B). However, mitochondrial surface area was decreased in CD8+ TEMRA cells compared to EM cells, and mitochondrial volume decreased in CM cells compared to EM cells. Additionally, mitochondrial surface area and mitochondrial volume was significantly decreased in CD4+ EM cells compared to CD8+ EM cells (Figure 5.10A and B).

When calculating the number of distinct mitochondrial nodes, a reduction in the number of nodes was observed in CD4+ CM cells and CD4+ EM cells when compared to their CD8+ CM cell and CD8+ EM cell counterparts, respectively (Figure 5.10C). When comparing the number of mitochondrial nodes within the CD4+ T cell and CD8+ T cell compartments, CD4+ EM cells showed reduced mitochondrial numbers compared to CD4+ naïve cells. A reduced number of mitochondrial nodes were observed in CD8+ TEMRA cells compared to CD8+ CM cells (Figure 5.10C).
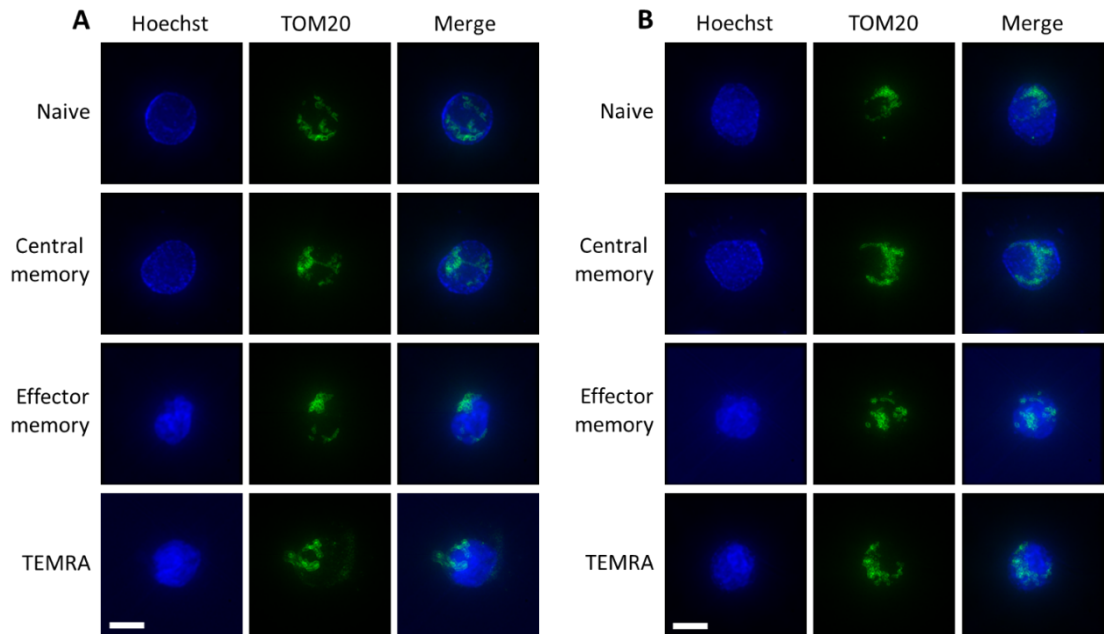
Figure 5.9   Super-resolution microscopy of T cell subsets within the (A) CD4+ T cell and (B) CD8+ T cell compartment with widefield Hoechst and SIM TOM20 imaging. Images are representative of one sample (scale = 5µm)
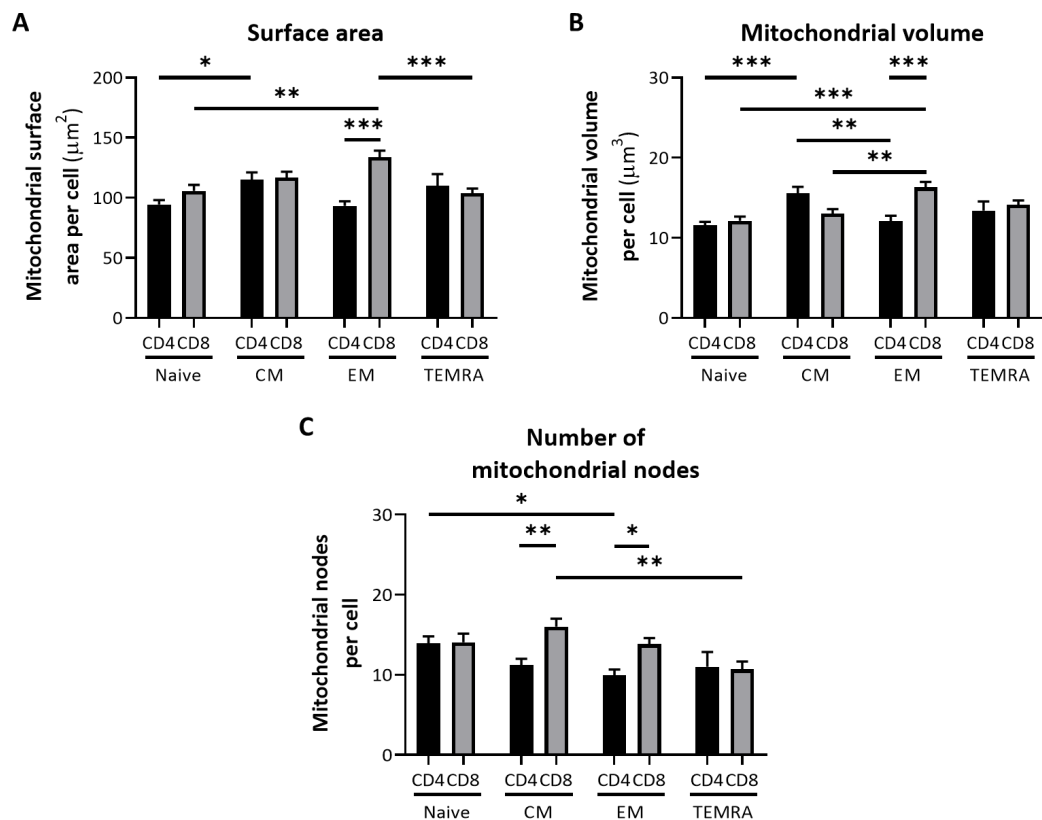
Figure 5.10 Super-resolution microscopy analysis of CD4+ and CD8+ T cell subsets showing (A) mitochondrial surface area (B) mitochondrial volume and (C) number of mitochondrial nodes per cell (mean+SEM; n=40 cells from 2 donors; Two-way repeated measured ANOVA; *p<0.05 **p<0.01 ***p<0.001)

5.3.6   Seahorse XF analysis does not reveal alterations in metabolism of CD4+ TEMRA cells

As mitochondrial fission and fusion dynamics and the expression of Glut1 were altered in TEMRA cells, seahorse analysis was carried to out to examine the metabolic profile of CD4+ T cell subsets. Due to the limited cell numbers available for TEMRA cells, samples from different donors were pooled to maintain the assay within the dynamic range required. Oxygen consumption rate (OCR) and extracellular acidification rate (ECAR) were measured using Seahorse XFe96 technology resulting in the metabolic traces observed in Figure 5.11A and B.
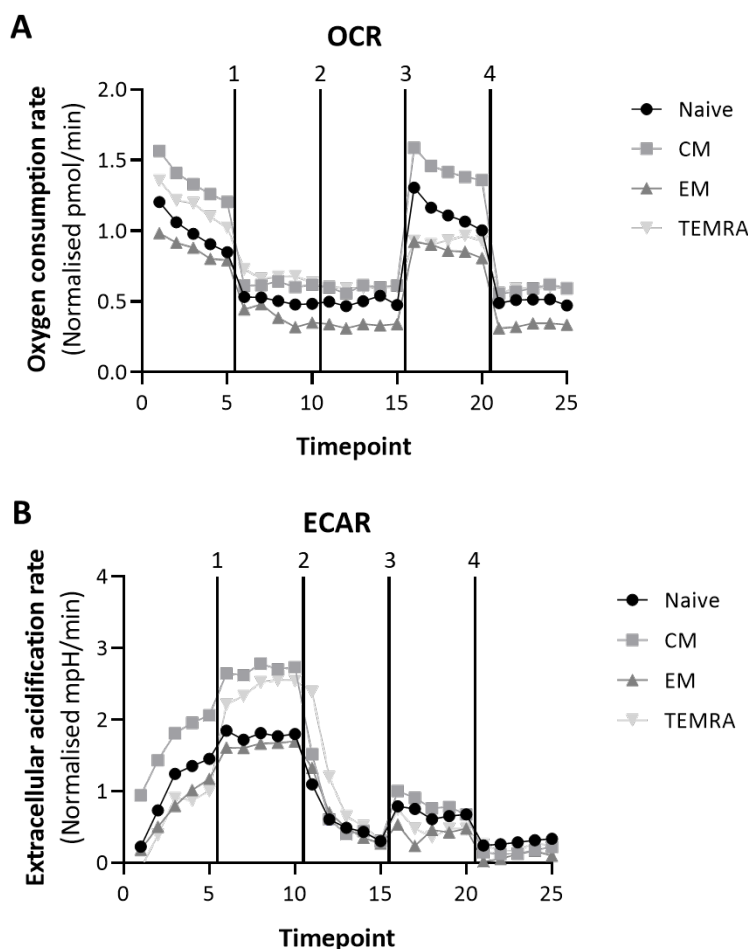
Figure 5.11   Oxygen consumption and extracellular acidification rate of CD4+ T cell subsets showing (A) oxygen consumption rate and (B) extracellular acidification rate of naïve (n=21), central memory (n=19), effector memory (n=15) and TEMRA (n=8) cells treated with (1) 2µM Oligomycin (2) 50mM 2DG (3) 2µM FCCP and (4) 500nM Rot/AA normalised to naïve T cells (mean only)

Due to the large variability in the metabolism of T cell subsets derived from different donors a large standard deviation was observed within all experiments (Figure 5.12A-C; Figure 5.13A-C). A significantly higher basal OCR was noted in CM cells compared EM cells prior to the injection of port compounds (Figure 5.12A). No significant differences were observed between the T cell subsets for their basal glycolytic rates, ability to engage glycolysis upon inhibition of ATPase activity (glycolytic reserve) and their glycolytic capacity (Figure 5.13A-C). Due to the lower number of CD4+ TEMRA cells is was not possible to perform Seahorse analysis on stimulated CD4+ T cells.
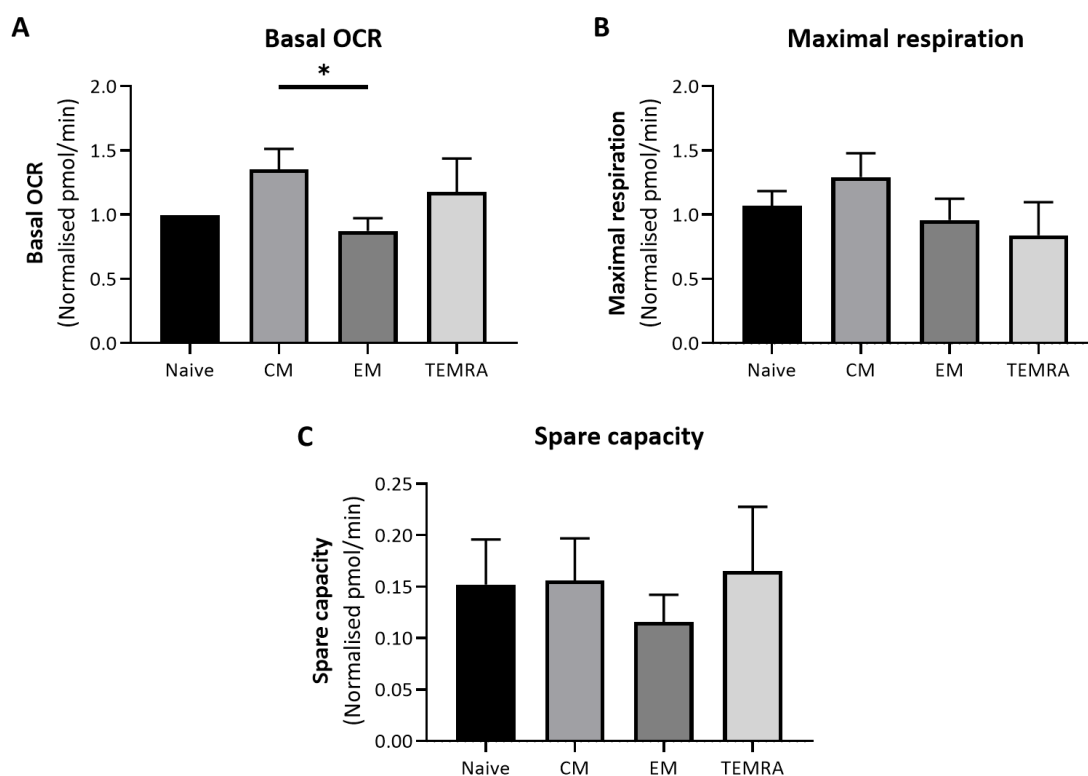
Figure 5.12   Oxygen consumption rate analysis of CD4+ T cell subsets showing (A) baseline OCR (B) maximal respiration and (C) spare capacity of naïve (n=21), central memory (n=19), effector memory (n=15) and TEMRA cells (n=8) normalised to baseline OCR of naïve T cells (mean+SEM; Ordinary one-way ANOVA; *p<0.05)
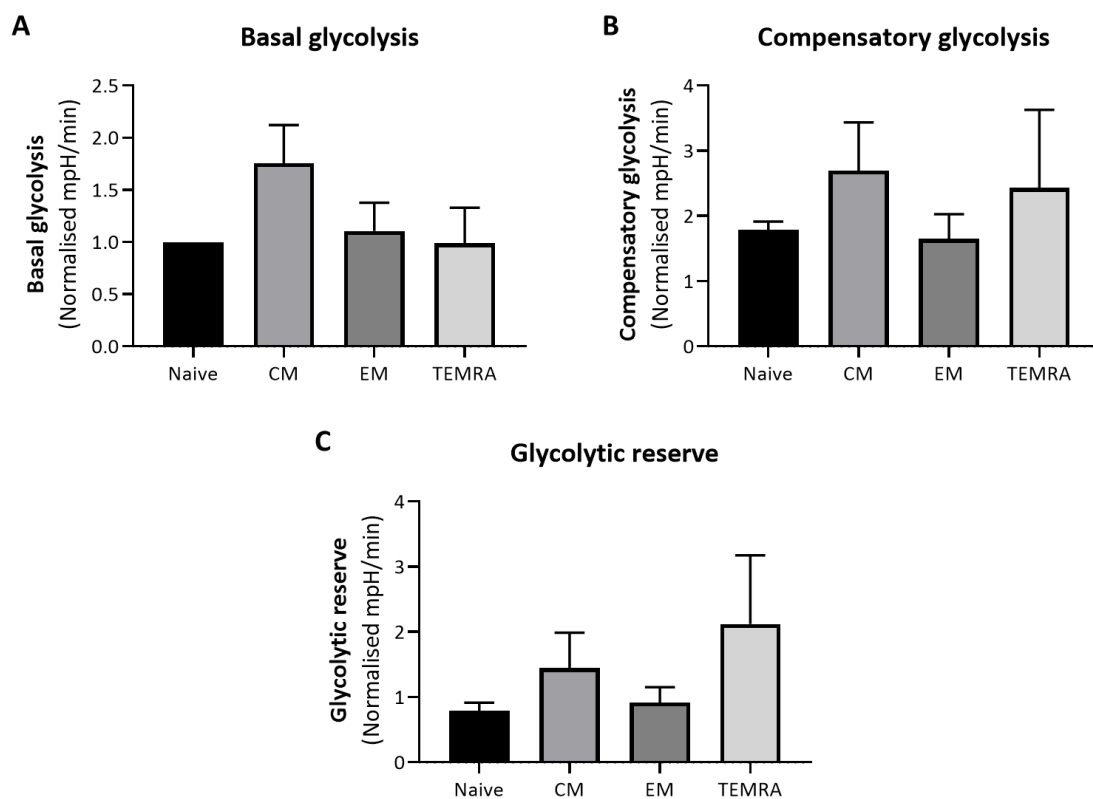
Figure 5.13 Extracellular acidification rate analysis of CD4+ T cell populations showing (A) baseline ECAR (B) compensatory glycolysis and (C) glycolytic reserve of naïve (n=21), central memory (n=19), effector memory (n=15) and TEMRA subsets (n=8) normalised to baseline ECAR of naïve T cells (mean+SEM; Ordinary one-way ANOVA)

5.4   Discussion: Mitochondrial regulation and metabolic efficiency in the immune-senescence of human T cells

As shown here and in other literature TEMRA cells have altered mitochondrial control (Henson et al., 2014, Callender et al., 2019, Tilly et al., 2017, De Biasi et al., 2019). Previous studies have shown that CD8+ TEMRA cells have reduced mitochondrial mass compared to CD8+ EM cells, resulting in a lower mDNA:nDNA ratio and reduced MitoTracker Green MFI (Henson et al., 2014). The results presented within this thesis do not represent this however, as no differences in mitochondrial mass were observed prior to or following OKT3 stimulation. A reduction in the membrane potential of the mitochondria within CD8+ TEMRA cells has previously been described (Henson et al., 2014). Whilst this trend was previously observed between naïve and TEMRA cells without stimulation, the results presented within thesis show that CD4+ TEMRA cells have a reduced mitochondrial membrane potential to mitochondrial mass ratio compared to the other memory subsets following 4 hours and 24 hours of OKT3 stimulation. An increased MTG:TMRM ratio was observed in TEMRA cells compared to naïve cells within this study. These results may reflect the differential control of mitochondrial mass and membrane potential with CD4+ T cell subsets in comparison to CD8+ T cells, as has been shown in previous studies (Callender et al., 2019). Whilst the effect of reduced MTG:TMRM ratio within CD4+ TEMRA cells is unknown, it may be plausible that reduced mitochondrial membrane potential may affect the ability of CD4+ TEMRA cells to produce IL-21 and IL-4 as a result of IL-6 signalling, reducing the differentiation of Th2 and effector function following secondary stimulation (Yang et al., 2015). Decreased IL-4 and IL-21 expression has been observed in elderly humans, where TEMRA cells accumulate, impairing memory CD4+ T cell responses to infection and vaccination (Yu et al., 2012). A reduced mitochondrial membrane potential has been observed within apoptotic lymphocytes in mice and thymocytes in rats, suggesting that CD4+ TEMRA cells may be more susceptible to apoptosis than the other memory cell subsets following OKT3 stimulation (Zamzami et al., 1995, Cossarizza et al., 1994). However, CD4+ TEMRA cells and EM cells have previously been observed to be more resistant to apoptosis induced by TNF-α (Gupta and Gollapudi, 2005).

When observing mitochondrial structure using super-resolution microscopy, decreased mitochondrial surface area was detected between CD8+ EM and TEMRA cells, supporting the findings of reduced mitochondrial mass in CD8+ TEMRA cells compared to EM cells by Henson *et al.* (Henson et al., 2014). However, in line with the findings seen when analysing flow cytometry analysis of MTG staining no significant differences were observed between these subsets within the CD4+ T cell compartment. Additionally, whilst a decrease in the number of mitochondria was observed between CD4+ naïve and EM cell subsets, previous research has shown an opposite trend

in CD4+ naïve and EM cells isolated from Swiss donors and CD8+ naïve and memory cells isolated from C57BL/6 mice (Dimeloe et al., 2016, van der Windt et al., 2012). Once again this suggests that mitochondrial regulation differs between CD4+ and CD8+ memory T cells.

Whilst CD4+ T cells express four of the thirteen Glut family members (Glut1, 3, 6 and 8), Glut1 is the most highly expressed glucose transporter following activation (Macintyre et al., 2014). Previous studies have revealed that the metabolism and function of CD4+ T cells is impaired by selective inhibition of Glut1 (Macintyre et al., 2014). Therefore, this study focused on Glut1 over other Glut family members. Increased expression of Glut1 was observed in naïve, CM, EM and TEMRA cells following prolonged (24 hour) OKT3 stimulation within this study. It is interesting to note that De Biasi *et al.* reported no significant upregulation of Glut1 following CD3/CD28 stimulation for 16 hours in CD4+ T cells (De Biasi et al., 2019). Whilst this result conflicts with the data in this study, the surface expression of Glut1 may not be upregulated until 16 hours following co-stimulation with CD3/CD28 (De Biasi et al., 2019). Other reports utilising murine T cells have suggested that intracellular Glut1 is upregulated as soon as 2 hours following CD3/CD28 stimulation, whilst extracellular expression increases following 4 hours of CD3/CD28 stimulation and becomes maximal following 24 hours stimulation (Macintyre et al., 2014). Nevertheless, it is proposed that CD4+ TEMRA cells exhibit no defects in their ability to upregulate Glut1 expression following CD3 stimulation.

Whilst no defects in the ability of TEMRA cells to upregulate Glut1 were observed, increased expression of Glut1 was observed within CM, EM and TEMRA cells prior to and during the early stages of OKT3 stimulation. Whilst Henson *et al.* reported that CD8+ TEMRA cells have reduced expression of Glut1 TEMRA cells contained with the CD4+ T cell compartment may not have this defect, showing better access to extracellular glucose (Henson et al., 2014). Examining T cell phenotypes within Glut1 high and Glut1 low populations has revealed that CD4+ and CD8+ EM cells typically pool within the Glut1 high population representing 60-78% and 60-68% of the Glut1 high population respectively. This same trend is observed for CD4+ naïve (9-13%) and CM (34-46%) cells which pool within the Glut1 low population (Cretenet et al., 2016). Whilst Cretenet *et al.* did not observe pooling of TEMRA cells within either the 10% of lymphocytes expressing the lowest and highest levels of Glut1, the data collected within this study suggests that CD4+ TEMRA cells are likely to be contained within a population of cells expressing mid to high levels of Glut1. Additionally cells expressing high levels of surface Glut1 were found to contain an increased percentage of IFNγ producing cells, tying Glut1 expression in with increased levels of IFNγ production in TEMRA cells (Cretenet et al., 2016, Henson et al., 2014, Tian et al., 2017).

Buck *et al.* compared the levels of Mfn2 and Drp1 in CD8+ T cells derived from C57BL/6 mice, using IL-2 and IL-15 to support the maintenance of effector and memory T cells respectively (Buck et al., 2016). Following 6 days of culture they revealed that expression of the mitochondrial fusion protein Mfn2 was increased in memory cells alongside decreased phosphorylation of Drp1. Whilst Buck *et al.* used effector CD8+ T cells as a control, this study utilised naïve CD4+ T cells and observed the opposite trend, increased expression of Drp1 within memory cells whilst Mfn2 expression was unaffected. Whilst it is difficult to compare these two studies based on the different control populations used and their application within different models (mice vs. human), studies comparing Drp1 and Mfn2 expression within T cells are limited and non-existent for TEMRA cells. No significant upregulation of Drp1 was observed within TEMRA cells. One study found that Drp1 expression supports metabolic reprogramming of effector cells upon activation though cMyc-dependent upregulation of metabolic genes, this may suggest that CM and EM cells are primed upon re-stimulation to promote secondary effector cell development (Simula et al., 2018). Whilst this upregulation of Drp1 is not observed in TEMRA cells compared to naïve cells, there is no significant downregulation compared to CM and EM cells suggesting that TEMRA cells may be primed for re-stimulation but to a lesser extent. Additionally, Drp1 has been shown to support T cell clonal expansion and migration (reviewed in (Simula et al., 2019)). Mfn2 on the other hand has been shown to support proliferation, IL-2 and IFNγ production of Jurkat cells following stimulation with PMA/Ionomycin (Xu et al., 2018). Despite being upregulated within CM and EM cells, Mfn2 was not significantly up/down-regulated in one subtype versus the other.

Opa1 is necessary for the development of memory T cells, and T cells lacking Opa1 show deformed and disorganised cristae structure (Buck et al., 2016). As discussed previously, Opa1 controls cristae structure and the efficiency of the electron transport chain. During this study a downregulation of Opa1 was observed for naïve, CM, EM and TEMRA CD4+ T cells with OKT3 stimulation, in line with the simultaneous upregulation of Glut1. This change in Opa1 to Glut1 ratio may reflect the engagement of glycolysis with OKT3 stimulation with the simultaneous disengagement of oxidative phosphorylation mediated by Opa1, reflecting change in the metabolic requirements of effector T cells (Tilly et al., 2017, Henson et al., 2014, Chang et al., 2013). Interestingly Opa1 expression was down-regulated within EM and TEMRA CD4+ T cells compared to naïve and CM cells during the latter stages of CD3 stimulation. Previous studies have observed a downregulation of Opa1 within exhausted CD8+ T cells as a result of HBV infection (Fisicaro et al., 2017).

Seahorse experiments within the CD8+ T cell compartment have noted a higher basal metabolic rate within CM and EM cells than naïve and TEMRA cells, with ECAR higher in EM and TEMRA cells (Henson et al., 2014). The results presented within this thesis however do not support this. No detectable differences were observed in oxidative and glycolytic parameters between naïve and

memory subsets. The only evident difference between CM and EM CD4+ T cells was in basal OCR, due to the high variability in OCR and ECAR between donors. Previous studies comparing CD8+ T cell subset metabolism have observed higher basal metabolic rates and spare respiratory capacity in CM and EM cells (Henson et al., 2014). As with the results presented here no significant differences were observed between naïve and TEMRA cell OCR. However, a higher rate of ECAR was observed within EM and TEMRA cells which was not observable within this study despite increased expression of Glut1 within CD4+ EM and TEMRA cells (Henson et al., 2014, Callender et al., 2019). Bengsch *et al.* showed that exhausted CD8+ T cells expressing high levels of PD-1 exhibit repressed glycolytic and mitochondrial metabolism following lymphocytic choriomeningitis mammarenavirus infection in C57BL/6 mice (Bengsch et al., 2016). Whilst a decrease in mitochondrial and glycolytic metabolism were not observed within this study, exhaustion of EM and TEMRA cells may aid explaining their inability to match CM metabolic rates.

5.4.1 Limitations

Due to the nature of apheresis blood donation, the clinical features and age of the donors used are unknown. Whilst a cellular model of T cell senescence was utilised within this chapter, the age of individuals may influence the results alongside exposure to other infections such as CMV. Future studies could utilise samples such as those contained within the Singapore Longitudinal Ageing Study (SLAS), where clinical features and the age of participants are known in order to minimise the influence of these variables.

Working with rare cell populations, such as that of CD4+ TEMRA cells, limits the number of experiments which can be done. Whilst most of the experiments were not affected by this low cell number, samples had to be pooled for live-cell metabolic analysis using the Seahorse analyser. This drastically affected the n number for the experiment and the ability to pair samples when conducting statistical analysis. This may account for the lack of statistical significance observed for this experiment. Additionally, a high level of variability between samples was observed particularly when conducting Seahorse analysis. Future work should focus on increasing the n number for this experiment and using samples from individuals where more information is available.

5.5   Conclusion

In conclusion, this study showed that CD4+ TEMRA cells have some defects in mitochondrial control but not to the same extent as that described for CD8+ TEMRA cells. A summary of these findings is shown in Figure 5.14. The results presented within this study describe CD4+ TEMRA cells as like CM and EM cells as they show increased basal expression of Glut1 and increased TMRM:MTG ratio during prolonged OKT3 stimulation in comparison to naïve cells. However, TEMRA cells did show differences to CM and EM cells in terms of their expression of mitochondrial fission and fusion proteins, which was confirmed using super-resolution microscopy, and decreased expression of Opa1. Whilst it was hypothesised that TEMRA cells would show slow responses to CD3 stimulation, TEMRA cells were fully able to respond to activation in line with the other subsets. Similarly, EM cells responded no faster to stimulation than CM cells at the time points studied.
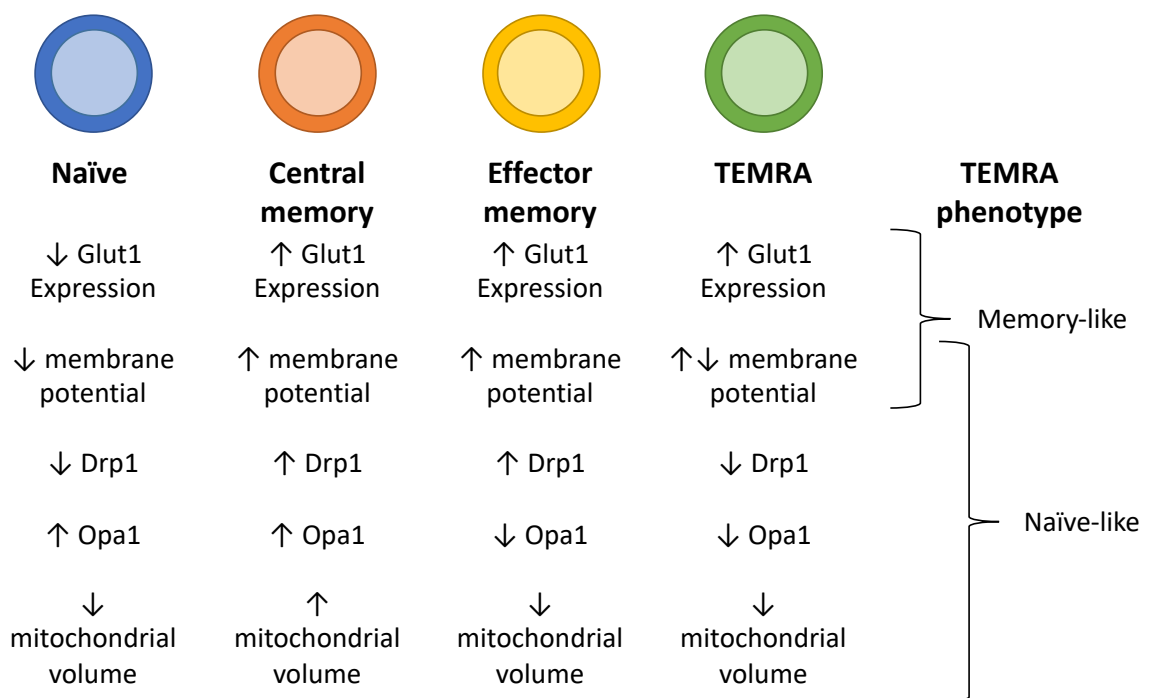
Figure 5.14 Summary of mitochondrial dysfunction in CD4+ T cell senescence showing the memory-like and naïve-like mitochondrial phenotypes of TEMRA cells

Chapter 6   Circulating human immune cells show altered metabolism in ageing

6.1   Introduction

Immune cells contained within the peripheral blood mononuclear cell (PBMC) compartment form the first line of defence against infection. In humans, PBMCs consist primarily of lymphocytes which include T cells, B cells and natural killer (NK) cells. PBMCs also contain many monocytes and a small percentage of dendritic cells (DC). Due to this, PBMCs are an ideal material for studying changes in both the adaptive and innate immune systems.

Analysis of PBMCs and human plasma has been utilised in the discovery of biomarkers for a variety of age-related diseases. These include: isoaspartyl residues in Alzheimer's disease (Yang et al., 2011) and miR-34b in Huntington's disease (Gaughwin et al., 2011) in humans, and microRNA (miR)-34a as a marker of brain ageing (Li et al., 2011) in mice. More striking changes in blood viscosity have also been observed during ageing, independently of coronary heart disease risk (Carallo et al., 2011). These findings suggest that blood components are readily altered with age, and this may also be true for metabolic factors.

Metabolic analysis of whole PBMC populations has been reported previously. For example, Alonso *et al* (Alonso et al., 2004) saw an acute and reversible inhibition of mitochondrial complex IV in PBMCs after smoking and within chronic smokers (Miró et al., 1998). Other studies have also suggested that mammalian target of rapamycin (mTOR) protein levels may be reduced in PBMCs derived from old patients through increased levels of miR-496 (Rubie et al., 2016). However, the distribution of mTOR within immune cells contained within the PBMC population and the effect of this decline on immune cell activation remains unclear.

Age-related declines in sirtuin 1 (SIRT1) expression have been detected in PBMCs (Owczarz et al., 2017). Although this gene had a minimal effect on longevity, as shown through analysis of centenarians, it was hypothesised that SIRT1 dysregulation may be involved in immune system decline and the appearance of immune-senescence in the elderly. Other studies focusing on age-related declines in metabolism have generally used skeletal muscle, however PBMCs represent a much easier tool for studying these changes. They can be isolated much easier from humans and do not require invasive procedures such as tissue biopsy.

Chapter 6

In this chapter, the regulation of metabolism in PBMCs derived from young (<35 years) and old (>60 years) blood donors was compared. It was hypothesised that PBMCs from old donors would exhibit defects in both oxidative and glycolytic metabolism resulting in reduced adenosine triphosphate (ATP) production and glucose uptake. When studying metabolic parameters of immune cell subsets through flow cytometry, it was hypothesised that T cells and NK cells would show the greatest defects into mitochondrial control following stimulation. The aims and objectives for this chapter are summarised in Figure 6.1.

Aim:
To examine mitochondrial dysfunction in PBMCs derived from young and old donors by analysing mitochondrial parameters in PBMCs and immune cells

Objectives:
- Conduct live-cell metabolic analysis on PBMCs from young and old donors at baseline and following stimulation
- Measure ATP production, hydrogen peroxide (H_2O_2) production and glucose concentration within cultured PBMCs from this cohort
- Confirm increased inflammation in old donors by measuring interferon-gamma (IFN-γ) production
- Analyse metabolic parameters in immune cells isolated from young and old donors at baseline and following stimulation
- Measure mitochondrial mass and membrane potential and attribute to mitochondrial dysfunction
- Analyse mitochondrial fission and fusion dynamics
- Compare expression of optic atrophy (Opa1) and glucose transporter 1 (Glut1) between groups
- Measure phosphorylation of mTOR - a central regulator of metabolism

Figure 6.1   Aim and objectives for studying mitochondrial dysfunction in PBMCs and immune cells from young and old donors

6.2   Materials and methods

6.2.1   Blood donors and PBMC isolation

The donors used within this study are detailed in Section 2.1.2.3 Isolation of cells for Singapore Longitudinal Ageing Study (SLAS). The isolation of peripheral blood mononuclear cells (PBMCs) from CPT tubes is also detailed in Section 2.1.2.3 Isolation of cells for Singapore Longitudinal Ageing Study (SLAS). A total of 20 young (<30 years) and 20 old (>60 years; Average: 68±5.63 years) donors were used for the purpose of this study. The clinical features of SLAS participants utilised within this study can be found in Table 6.1.

Table 6.1   Clinical data of participants from the Singapore Longitudinal Ageing Study

Sample ID	Age	Gender	Ethnicity	Frailty category	Frailty score	Cholesterol (mmol/L)	Triglyceride (mmol/L)	High density lipoprotein (mmol/L)	Low density lipoprotein (mmol/L)	Blood Pressure	Diabetes	Body mass index
0230	71	Male	Chinese	Robust	0	6.49	3.16	1.18	3.87	152/93	No	28.89
0275	69	Female	Chinese	Pre-frail	2	4.86	1.48	1.14	3.05	125/71	No	25.22
0434	71	Male	Chinese	Pre-frail	2	3.98	0.64	1.38	2.31	123/79	No	23.24
0442	73	Male	Indian	NA	NA	NA	NA	1.46	2.37	100/61	Yes	24.28
0635	73	Male	Malay	NA	NA	6.95	0.97	2.27	4.24	NA	NA	NA
0848	77	Male	Chinese	Robust	0	NA	NA	NA	NA	138/83	Yes	22.34
1050	78	Female	Malay	Pre-frail	1	4.77	0.93	1.15	3.20	151/104	No	30.25
1100	61	Male	Chinese	NA	NA	5.03	1.75	0.80	3.43	142/86	Yes	22.83
1127	68	Male	Chinese	Pre-frail	1	4.96	1.61	1.30	2.93	107/74	No	23.54
1157	70	Male	Chinese	Pre-frail	2	6.30	1.67	1.32	4.22	119/76	No	28.03

Sample ID	Age	Gender	Ethnicity	Frailty category	Frailty score	Cholesterol (mmol/L)	Triglyceride (mmol/L)	High density lipoprotein (mmol/L)	Low density lipoprotein (mmol/L)	Blood Pressure	Diabetes	Body mass index
1224	69	Male	Chinese	Pre-frail	1	4.42	0.87	1.69	2.33	166/80	Yes	28.25
1908	61	Female	Chinese	Robust	0	NA	NA	NA	NA	154/97	No	20.22
1936	73	Female	Chinese	Pre-frail	2	NA	NA	NA	NA	140/88	No	27.78
1945	59	Female	Indian	Robust	0	3.89	2.30	0.78	2.06	120/83	No	21.35
1990	62	Female	Chinese	Pre-frail	1	NA	NA	NA	NA	116/75	No	23.60
1999	60	Female	Chinese	Pre-frail	1	NA	NA	NA	NA	123/83	No	23.75
5496	62	Female	Malay	Pre-frail	2	NA	NA	NA	NA	115/66	No	22.86
6268	68	Male	Chinese	Pre-frail	1	NA	NA	NA	NA	120/62	No	19.26
6298	68	Female	Chinese	Pre-frail	1	4.67	3.50	1.00	2.08	130/73	Yes	39.37
7020	71	Male	Chinese	Pre-frail	2	NA	NA	NA	NA	147/76	No	26.20

6.2.2 Agilent Seahorse analysis

Aglient Seahorse experiments were set-up as described in Section 2.6 Live-cell metabolic analysis. PBMCs were plated at a density of 250,000 cells per well in R-10 and treated with DMSO control or treated with 10ng/ml Phorbol 12-myristate 13-acetate (PMA) and 100ng/ml Ionomycin for six hours prior to the experiment as described in Section 2.7.2 Phorbol 12-myristate 13-acetate/Ionomycin stimulation. A total of four repeats were performed for each sample within both treatment groups.

6.2.3 Luciferase assays

PBMCs were stimulated as described in Section 2.7.2 Phorbol 12-myristate 13-acetate/Ionomycin stimulation. ATP production was measured using the CellTiter-Glo™ 2.0 Assay (Promega, WI) as described in Section 2.4.1 Adenosine triphosphate production. Glucose concentration was measured using the Glucose-Glo® Assay (Promega, WI) as described in Section 2.4.5 Glucose concentration. H_2O_2 production was measured using the ROS-Glo® H_2O_2 Assay (Promega, WI) as described in Section 2.4.4 Hydrogen peroxide (H_2O_2) production. Luminescence was measured using the GloMax®- Multi+ plate reader system (Promega, WI).

6.2.4 ELISA of interferon gamma (IFNγ) production

Cells were plated at a density of 500,000 cells per well in 96-well plates and as described in Section 2.7.2 Phorbol 12-myristate 13-acetate/Ionomycin stimulation for 6 hours in a 37°C incubator with 5% CO_2. IFNγ production was analysed by ELISA as described in Section 2.8 Enzyme-linked immunosorbent assay (ELISA). Absorbance was read within 15 minutes at 450nm and 570nm using the 2104 EnVision® multilabel plate reader platform (PerkinElmer, MA).

6.2.5 Flow cytometry

Prior to staining, PBMCs were stimulated as described in Section 2.7.2 Phorbol 12-myristate 13-acetate/Ionomycin stimulation. Cells were stained as described in Section 2.5.1 Flow cytometry. The surface staining and viability markers used to distinguish PBMC immune cells are listed in Table 6.2. Measurement of mitochondrial mass and membrane potential in live cells are listed in Table 6.3. A list of primary antibodies is listed in Table 6.4. Secondary antibodies are listed in Table 6.5. Gating strategy for each cell type is defined in Table 6.6 and displayed in Figure 6.2.

Table 6.2   Surface staining antibodies used identifying immune cell populations in human PBMCs

SURFACE MARKER	FLUOROPHORE	CLONE	RETAILER	DILUTION
Live-Dead	AmCyan	n/a	ThermoFisher, MA	1:200
CD3	Af700	UCHT1	Becton Dickinson, NJ	2µl
CD4	Pacific Blue	OKT4	BioLegend, CA	1µl
CD8	Apc/Cy7	SK1	Becton Dickinson, NJ	2µl
CD27	V650	L128	Becton Dickinson, NJ	2µl
CD28	PE/Cy7	CD28.2	Becton Dickinson, NJ	1µl
CD45RO	PE/Cy5	UCHL1	Becton Dickinson, NJ	5µl
CD45RA	V605	5H9	Becton Dickinson, NJ	1µl
CD56	BUV563	NCAM16.2	Becton Dickinson, NJ	1µl
CD16	BUV737	3G8	Becton Dickinson, NJ	1µl
CD14	PE-CF594	MφP9	Becton Dickinson, NJ	1µl
HLA-DR	V786	G46-6	Becton Dickinson, NJ	1µl
CD66b	PerCP/Cy5.5	G10F5	Becton Dickinson, NJ	1µl
CD1c	BUV395	F10/21A3	Becton Dickinson, NJ	1µl
CD141	BV711	1A4	Becton Dickinson, NJ	1µl

Table 6.3   Dyes for live-cell mitochondrial assessment of human immune cell populations

MITOCHONDRIAL DYE	FLUOROPHORE	RETAILER	DILUTION
MitoTracker Green	FITC	ThermoFisher, MA	150nM
TMRM	PE	SigmaAldrich, MO	25nM

Table 6.4   Primary antibodies for mitochondrial assessment of human immune cell populations

PRIMARY ANTIBODY	FLUOROPHORE	CLONE	SPECIFICITY/ HOST SPECIES	RETAILER	DILUTION
Glut1	FITC	EPR3915	Rabbit	Abcam, UK	1µl
Opa1	n/a	1E81D9	Mouse IgG1	Abcam, UK	1µl
Mfn2[2]	n/a	6A8	Mouse IgG2α	Abcam, UK	1µl
Drp1	n/a	n/a	Mouse IgG2β	Abcam, UK	1µl
Phospho-mTOR (S2448)	PE	O21-404	Mouse	Becton Dickinson, NJ	5 µl

Table 6.5   Secondary antibodies for mitochondrial assessment of human immune cell populations

SECONDARY ANTIBODY	FLUOROPHORE	HOST SPECIES	RETAILER	DILUTION
Anti-mouse IgG1	FITC	Goat	Abcam, UK	1µl
Anti-mouse IgG2β	Apc	Rat	R&D Systems, MN	1µl

---

[2] Mfn2 primary antibody was not detected by anti-mouse IgG2α secondary antibody but was detected by anti-mouse IgG2β therefore this secondary antibody was used instead

Table 6.6   Gating strategy for immune cell populations in PBMC compartment of young and old donors

CELL TYPE	GATING STRATEGY	FIGURE REFERENCE
CD4+ naïve	CD3+ CD4+ CD8- CD27+ CD28+ CD45RA+	Figure 6.2A
CD4+ central memory	CD3+ CD4+ CD8- CD27+ CD27+ CD45RA-	Figure 6.2B
CD4+ effector memory	CD3+ CD4+ CD8- CD27- CD28+ CD45RO+ CD45RA-	Figure 6.2C
CD4+ TEMRA	CD3+ CD4+ CD8- CD27- CD28+ CD45RO- CD45RA+	Figure 6.2D
CD8+ naïve	CD3+ CD4- CD8+ CD27+ CD28+ CD45RA+	Figure 6.2E
CD8+ central memory	CD3+ CD4- CD8+ CD27+ CD27+ CD45RA-	Figure 6.2F
CD8+ effector memory	CD3+ CD4- CD8+ CD27- CD28+ CD45RO+ CD45RA-	Figure 6.2G
CD8+ TEMRA	CD3+ CD4- CD8+ CD27- CD28+ CD45RO- CD45RA+	Figure 6.2H
Cytotoxic NK	CD3- CD16- CD56+	Figure 6.2I
Inflammatory NK	CD3- CD16+ CD56+	Figure 6.2J
Regulatory NK	CD3- CD16+ CD56-	Figure 6.2K
Non-classical monocyte	HLA-DR+ CD14- CD16+	Figure 6.2L
Intermediate monocyte	HLA-DR+ CD14+ CD16+	Figure 6.2M
Classical monocyte	HLA-DR+ CD14+ CD16-	Figure 6.2N
CD141+ DC	HLA-DR+ CD14- CD16- CD141+	Figure 6.2O
CD1c+ DC	HLA-DR+ CD14- CD16- CD141- CD1c+	Figure 6.2P
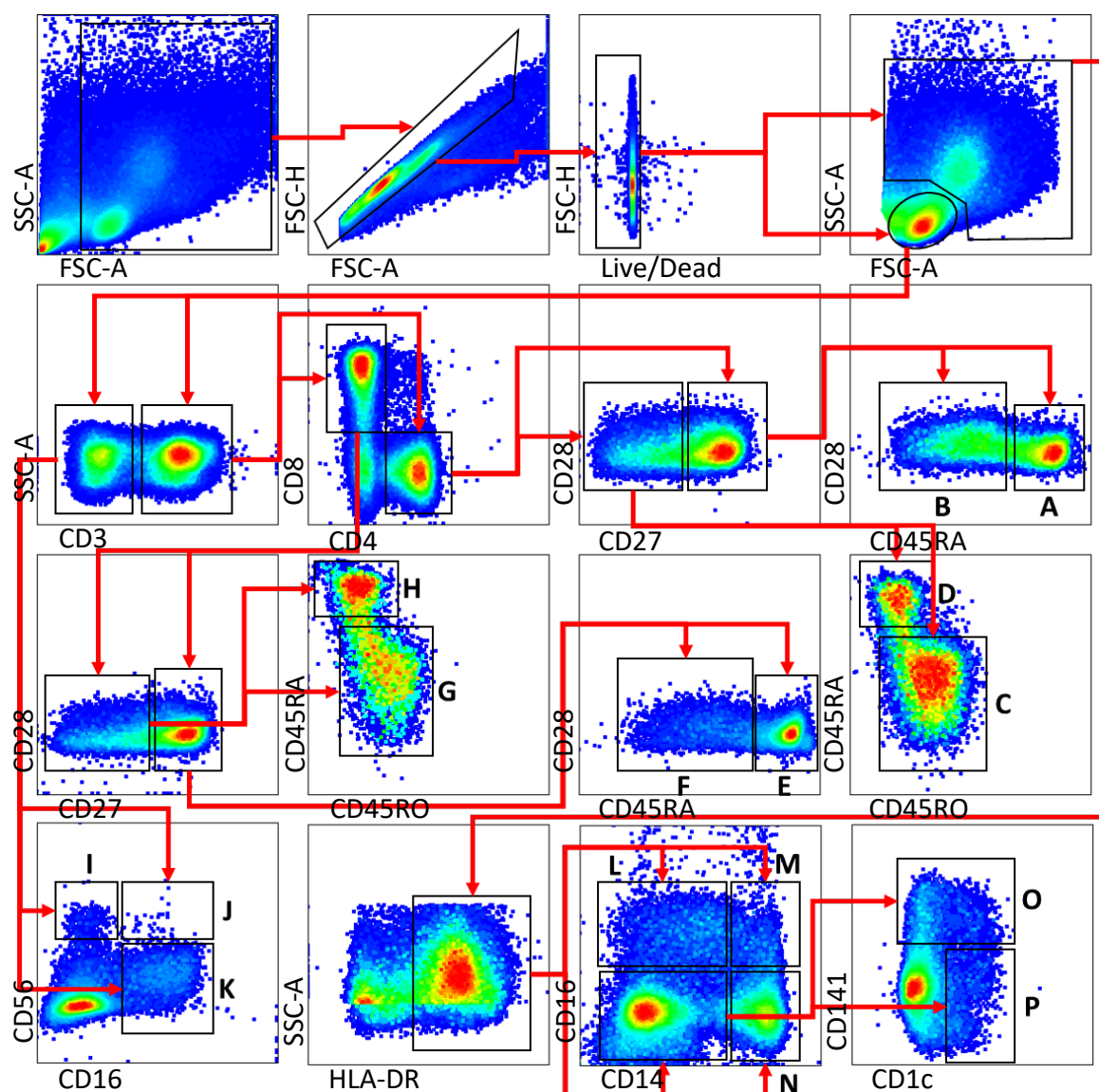
Figure 6.2   Gating strategy for identification of immune cell populations in PBMCs from young and old donors showing CD4+ naïve (A), central memory (B), effector memory (C) and TEMRA (D) cells, CD8+ naïve (E), central memory (F), effector memory (G) and TEMRA (H) cells, regulatory (I), cytotoxic (J) and inflammatory (K) NK cells, non-classical (L), intermediate (M) and classical (N) monocytes and CD141+ (O) and CD1c+ (P) dendritic cells

6.2.6   Statistical analysis

Statistical analysis for all experiments was performed using a two-way mixed-model ANOVA unless otherwise stated, samples were unpaired for age-related analysis and paired for stimulation-related analysis. *Post-hoc* analysis was performed using Sidak's multiple comparisons test. Flow cytometry data was analysed using FlowJo software. Statistical analysis was performed using GraphPad Prism software. GraphPad was also used to create graphs. A p value of <0.05 was used to identify significance.

6.3 Results

6.3.1 PBMCs from old donors display defects in oxidative but not glycolytic metabolism

In order to investigate the metabolism of PBMCs derived from young (<35 years) and old (>60 years) donors, Seahorse XF analysis was performed to study oxygen consumption rate (OCR) and extracellular acidification rate (ECAR) between samples. Stimulation of samples using 10ng/ml PMA and 100ng/ml Ionomycin was also performed to differentiate responses to stimulation between the donor groups.

Basal metabolism was observed to be unchanged in PBMCs from young and old donors either before or following 6 hours of PMA/Ionomycin stimulation (Figure 6.3A and B). However, a significant decline in maximal respiration was observed in unstimulated cells from old donors compared to those from young donors (Figure 6.3A and C). This may suggest that PBMCs from old donors have a decreased capacity to respond to energetic demands when required. This result was not observed in stimulated PBMCs however as young donors see a decrease in maximal respiration following 6 hours of PMA/Ionomycin to match that of old donors (Figure 6.3A and C). This decrease in maximal respiration may be due to the switch to glycolytic metabolism upon stimulation, therefore ECAR was also measured using Seahorse XF Technology.
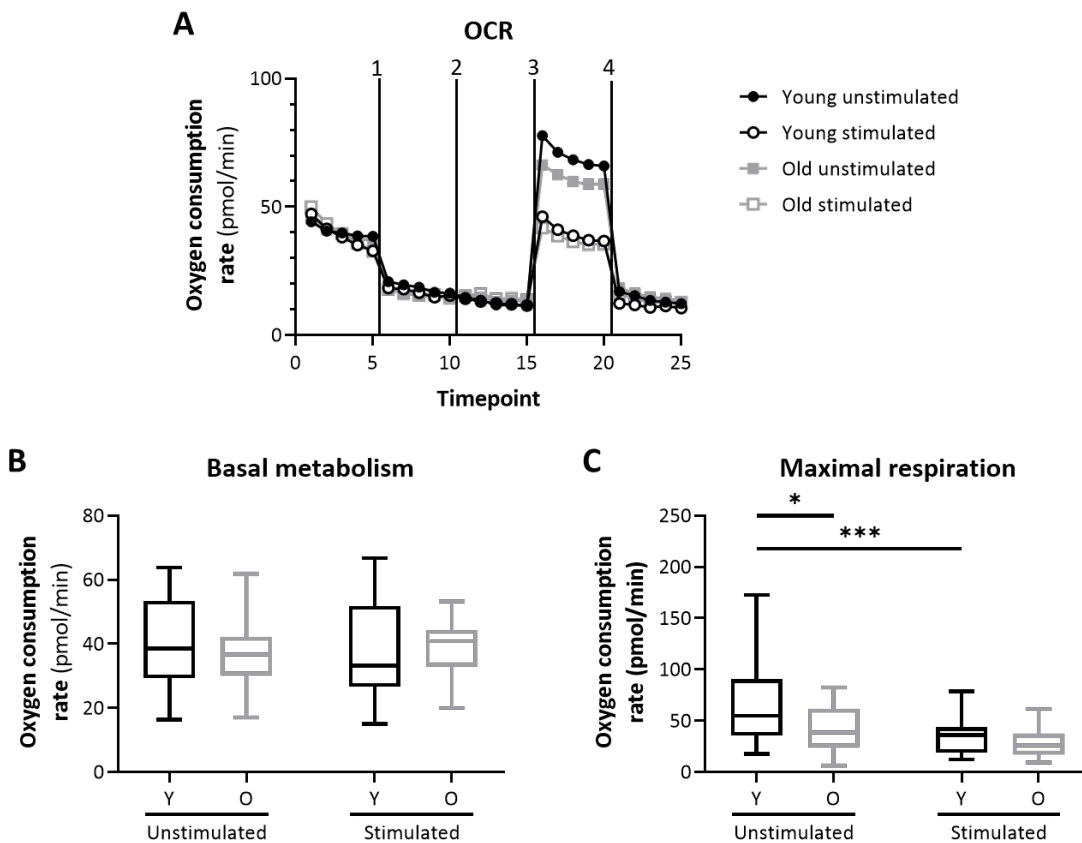
Figure 6.3   Oxygen consumption rate analysis of PBMCs from young and old donors showing (A) OCR of cells treated with (1) 2µM Oligomycin (2) 50mM 2DG (3) 2µM FCCP and (4) 500nM Rot/AA and (B) basal metabolism and (C) maximal respiration of cells unstimulated or stimulated with PMA/Ionomycin (Y=young donor, O=old donor) (Box and whisker plot; n=20; Two-way mixed-model ANOVA; *p<0.05 ***p<0.001)

A significant upregulation of basal glycolysis was observed in PBMCs from both young and old donors following 6 hours of PMA/Ionomycin stimulation (Figure 6.4A and B). This result was also detected for glycolytic capacity which showed an upregulation in both young and old PBMCs following PMA/Ionomycin stimulation (Figure 6.4C). This highlights the switch towards glycolytic metabolism following stimulation in PBMCs whilst oxidative metabolism remains unaffected. Glycolytic capacity is increased in young donors following stimulation decreases in line with capacity for maximal oxidative respiration (Figure 6.3C and Figure 6.4C). However, old donors show decreased capacity for maximal respiration prior to stimulation which is not counteracted by increased glycolytic metabolism at baseline or glycolytic capacity (Figure 6.3C and Figure 6.4B and C). Therefore, PBMCs from old donors display defects in oxidative metabolism but not glycolytic metabolism.
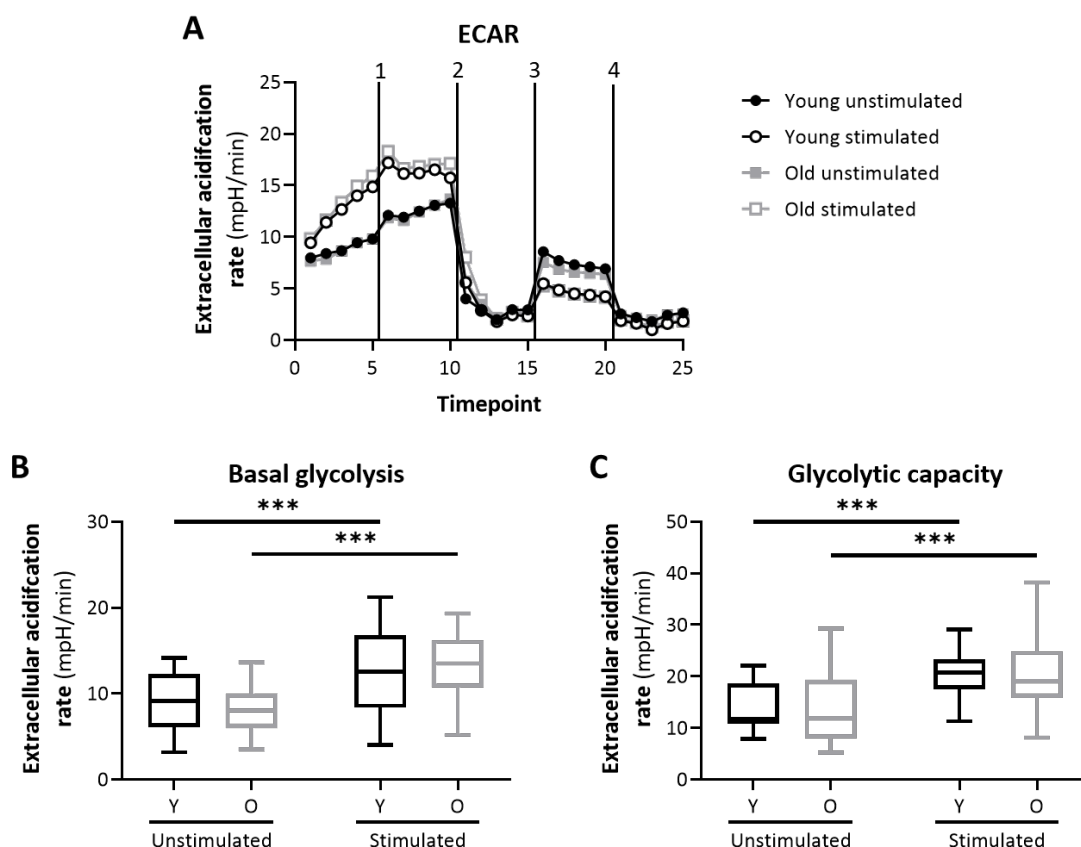
Figure 6.4   Extracellular acidification rate analysis of PBMCs from young and old donors showing (A) ECAR (n=20; mean) of cells treated with (1) 2µM Oligomycin (2) 50mM 2DG (3) 2µM FCCP and (4) 500nM Rot/AA and (B) basal glycolysis and (C) glycolytic capacity of cells unstimulated or stimulated with PMA/Ionomycin (Y=young donor, O=old donor) (Box and whisker plot; n=20; Two-way mixed-model ANOVA; ***$p<0.001$)

6.3.2   PBMCs from old donors show ability to maintain ATP production and increase glucose uptake following stimulation

Despite the defects in oxidative metabolism observed in PBMCs derived from old donors, no significant difference in the production of ATP from these cells was observed either before or after PMA/Ionomycin stimulation (Figure 6.5A). This suggests that PBMCs from old donors may upregulate other pathways of metabolism to maintain their ATP production. Therefore, glucose concentration within the cell culture medium was also measured. No significant difference in the ECAR of PBMCs derived from young and old donors was confirmed by no significant difference in the glucose concentration contained in the cell culture medium of unstimulated cells (Figure 6.5B). Whilst no significant decrease in media glucose concentration was observed following stimulation of young PBMCs, a significant reduction was observed for stimulated PBMCs (Figure 6.5B). This suggests that PBMCs derived from old donors may have an increased surface expression of glucose

Chapter 6

transporters and are able to increase their uptake of glucose more rapidly than PBMCs from young donors.
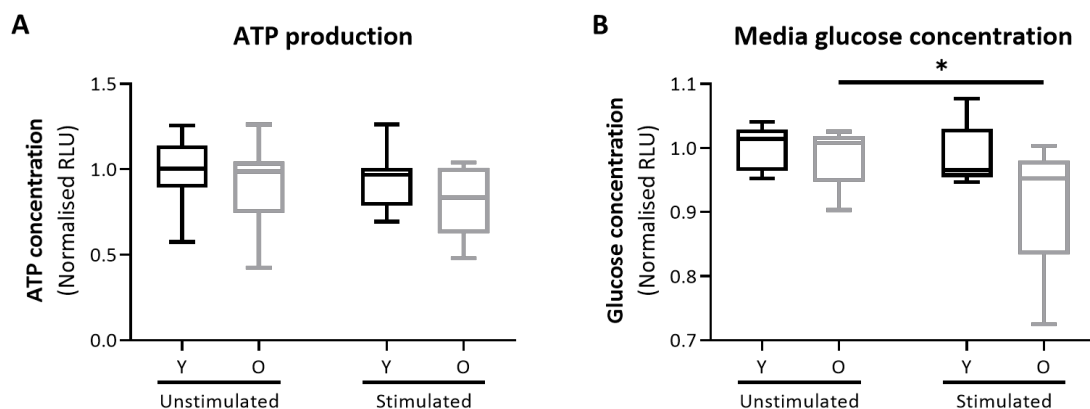
Figure 6.5   Luciferase reporter assay of ATP production and media glucose concentration from PBMCs in young and old donors showing (A) ATP production (n=15) and (B) media glucose concentration (n=5) in cells stimulated with PMA/Ionomycin. Results normalised to young unstimulated PBMCs (Y=young donor, O=old donor) (Box and whisker plot; Two-way mixed-model ANOVA; *p<0.05)

6.3.3   ROS production is increased whilst IFNγ production is not altered in PBMCs derived from old donors

Inflamm-ageing is currently a hot topic in the area of geriatric research. Therefore, the production of reactive oxygen species and the pro-inflammatory marker IFNγ were measured in PBMCs derived from young and old donors. Whilst no increase in H_2O_2 production was observed in young PBMCs upon stimulation, old PBMCs significantly increased their production of this ROS (Figure 6.6A). As ROS and inflammation are linked this may explain the increased levels of inflammation in the elderly. An increase in IFNγ production was observed from both young and old PBMCs following 6 hours of PMA/Ionomycin stimulation (Figure 6.6B). This result suggests that PBMCs from old donors retain their capacity to produce IFNγ following stimulation, however ROS production which is linked to inflammation is increased in the elderly upon PBMC stimulation.
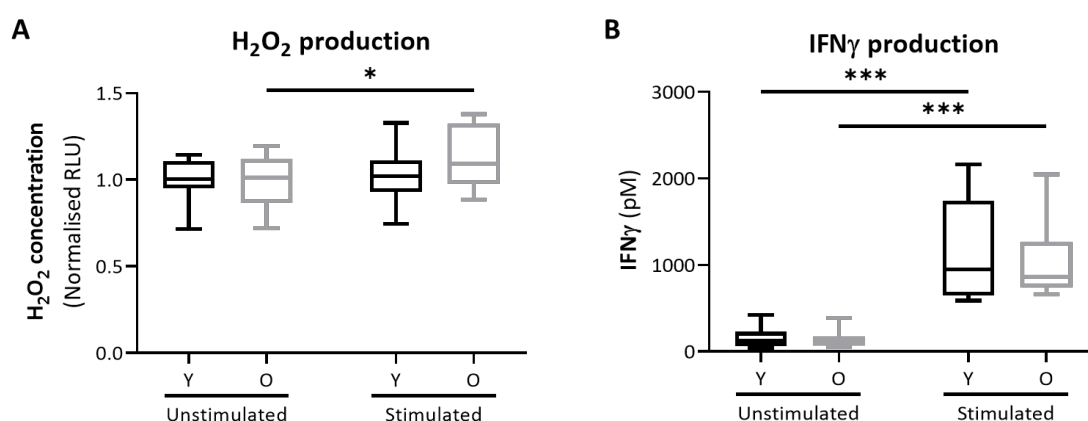
Figure 6.6   ROS levels and IFNγ production from PBMCs in young and old donors showing (A) H_2O_2 production (n=10) measured by luciferase reporter assay normalised to young unstimulated PBMCs and (B) IFNγ production (n=5) measured by ELISA in cells stimulated with PMA/Ionomycin (Y=young donor, O=old donor) (Box and whisker plot; Two-way mixed-model ANOVA; *p<0.05 ***P<0.001)

6.3.4   Immune cell compartmentalisation is altered with ageing

It is well established that immune cell compartmentalisation is altered with ageing. The compartmentalisation of immune cells within the study group used here was therefore studied. A significant reduction in the percentage of CD27+ CD45RA+ (naïve) cells was observed within the CD4+ compartment (Figure 6.7A and B). CD4+ naïve cells accounted for 48.2% and 34.3% (p<0.001) of CD4+ cells within young and old donors respectively. A reduction in CD27+ CD45RA+ cells was also observed from 57.9% in old to 42.1% (p=0.004) in young subjects (Figure 6.7C and D). Within the memory compartment, a significant increase in the proportion of CD27+ CD45RA- (CM) cells was observed within the CD8+ population from 22.6% to 32.3% (p=0.024) (Figure 6.7C and D). Whilst a significant difference was not seen within the CD4+ population for CM cells, there was a trend towards an increased proportion of CM (p=0.072) and CD27- CD45RA- cells (EM; p=0.057). Surprisingly diverging trends in the proportion of CD27- CD45RA+ (TEMRA) cells were noted within the CD4+ and CD8+ populations. Whilst the percentage of CD8+ TEMRA cells was increased from 5.5% to 9.9% in the elderly (p=0.009), the percentage of CD4+ TEMRA was reduced from 3% to 1.8% with age in the samples used for this study (p=0.001) (Figure 6.7A and C).
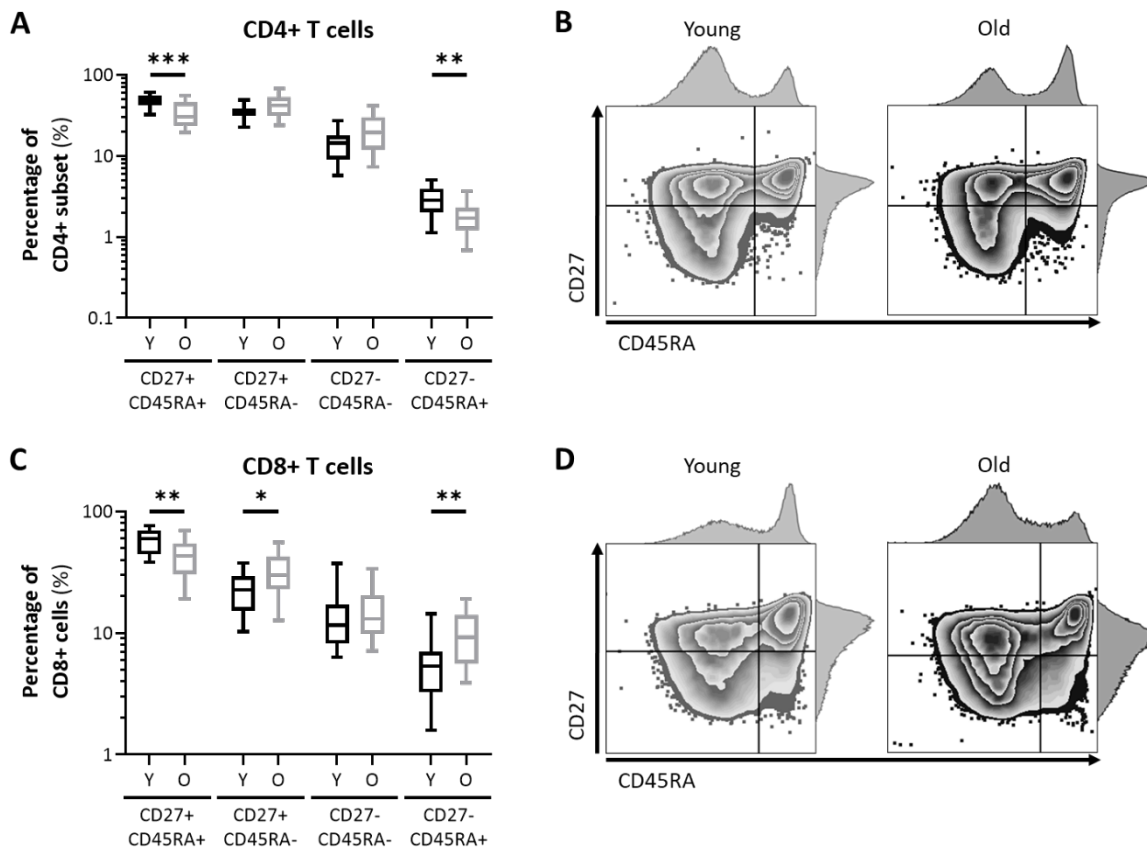
Figure 6.7 Levels of CD4+ T cell and CD8+ T cell subsets in young and elderly individuals showing (A) CD4+ T cell subsets as a percentage of total CD4+ cells (B) zebra plot of CD4+ T cell subsets in young and old subjects (C) CD8+ T cell subsets as a percentage of total CD8+ cells and (D) zebra plot of CD8+ T cell subsets in young and old subjects (Y=young donor, O=old donor) (Box and whisker plot; n=20; Three-way mixed-model ANOVA; *p<0.05 **p<0.01 ***p<0.001)

When comparing NK cell subset distribution within CD3- cells, no significant changes within the CD56+ CD16- (regulatory) or CD56+ CD16+ (cytotoxic) populations were observed (Figure 6.8A and B). A significant increase in CD56- CD16+ (inflammatory) NK cells was observed between the young and old subjects, accounting for 13.6% and 31.2% of the CD3- population respectively (p<0.001; Figure 6.8A and B). A similar pattern was also observed for the distribution of monocytes within the HLA-DR+ population. Whilst no significant differences were seen for CD16+ CD14- (non-classical) and CD16+ CD14+ (intermediate) monocyte subsets, and significant increase in CD16- CD14+ (classical) monocytes was observed (Figure 6.8C and D). Non-classical monocytes accounted for 45.5% and 56.5% of human leukocyte antigen DR isotype (HLA-DR)+ cells within young and elderly subjects respectively (p=0.035). The compartmentalisation of dendritic cells was also studied within this cohort; however, no significant changes were seen within the CD141+ or CD1c+ dendritic cell population with age.
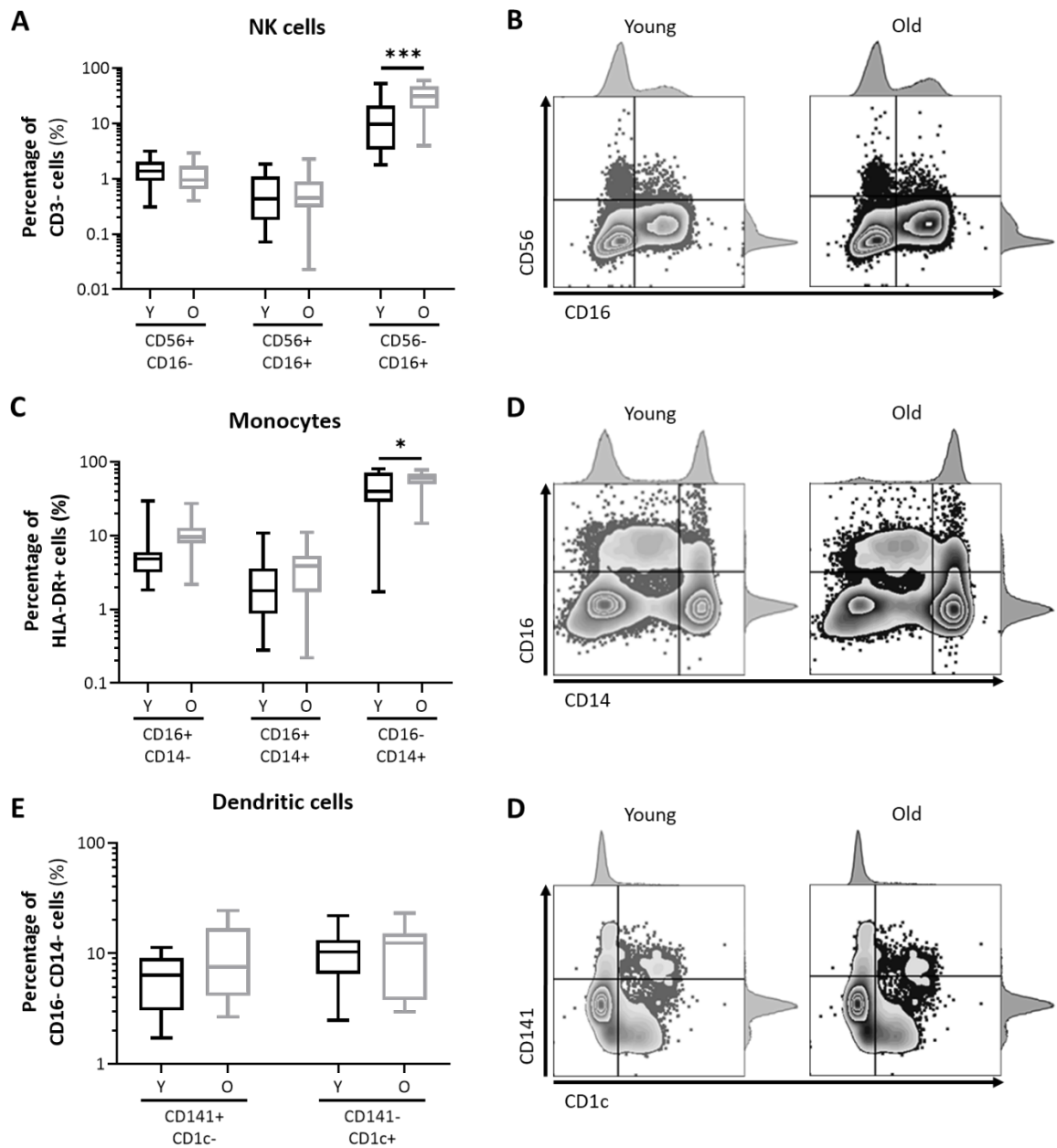
Figure 6.8   Levels of NK cell, monocyte and dendritic cell subsets in young and elderly individuals showing (A) NK cell subsets as a percentage of total CD3- cells (B) zebra plot of NK cell subsets (C) monocyte subsets as percentage of total HLA-DR+ cells (D) zebra plot of monocyte subsets (E) dendritic cell subsets as a percentage of total CD16-CD14- cells (F) zebra plot of dendritic cell subsets in young and old subjects (Y=young donor, O=old donor) (Box and whisker plot; n=20; Three-way mixed-model ANOVA; *p<0.05 ***p<0.001)

6.3.5 Mitochondrial mass is increased in old donors within T cells, NK cells and dendritic cells

A significant increase in the extent of MitoTracker Green (MTG) staining was observed in old donors within CD4+ naïve, effector memory and TEMRA cells, but not central memory cells (Figure 6.9A-B, D-E). Mitochondrial mass was increased by 1.6-fold (p=0.003), 1.8-fold (p<0.001) and 1.6-fold (p<0.001) within naïve, effector memory and TEMRA cells respectively. There was a trend towards increased mitochondrial mass within central memory cells also, whereby MTG staining was increased 1.1-fold within old donors (p=0.066). The shift in MTG staining can be seen in Figure 6.9C and F. A significant decrease in MTG staining, and therefore mitochondrial mass, was observed following 6 hours of PMA/Ionomycin stimulation within cells from both young and old donors. Within young donors, mitochondrial mass was decreased by approximately 20.7% (p=0.019), 37.5% (p<0.001) and 31.2% (p=0.022) within CD4+ naïve, central memory and effector memory respectively (Figure 6.9A, B and D). CD4+ TEMRA cells from young donors also decreased their mitochondrial mass by 24.1% however this was found to be not significant (p=0.0717; Figure 6.9E). Decreases in MTG staining observed upon stimulation were less pronounced within old donors for naïve and central memory cells: naïve cells decreased their mitochondrial mass by 18.6% (p=0.001) and central memory cells by 23.3% (p<0.001), maintaining increased mitochondrial mass in old donors compared to young donors following stimulation (p=0.012; p=0.001). CD4+ Effector memory and TEMRA cells were subject to more pronounced decreases in mitochondrial mass, by 55.4% (p<0.001) and 50.6% (p<0.001) respectively, bringing mitochondrial mass in line with cells from young donors upon stimulation.
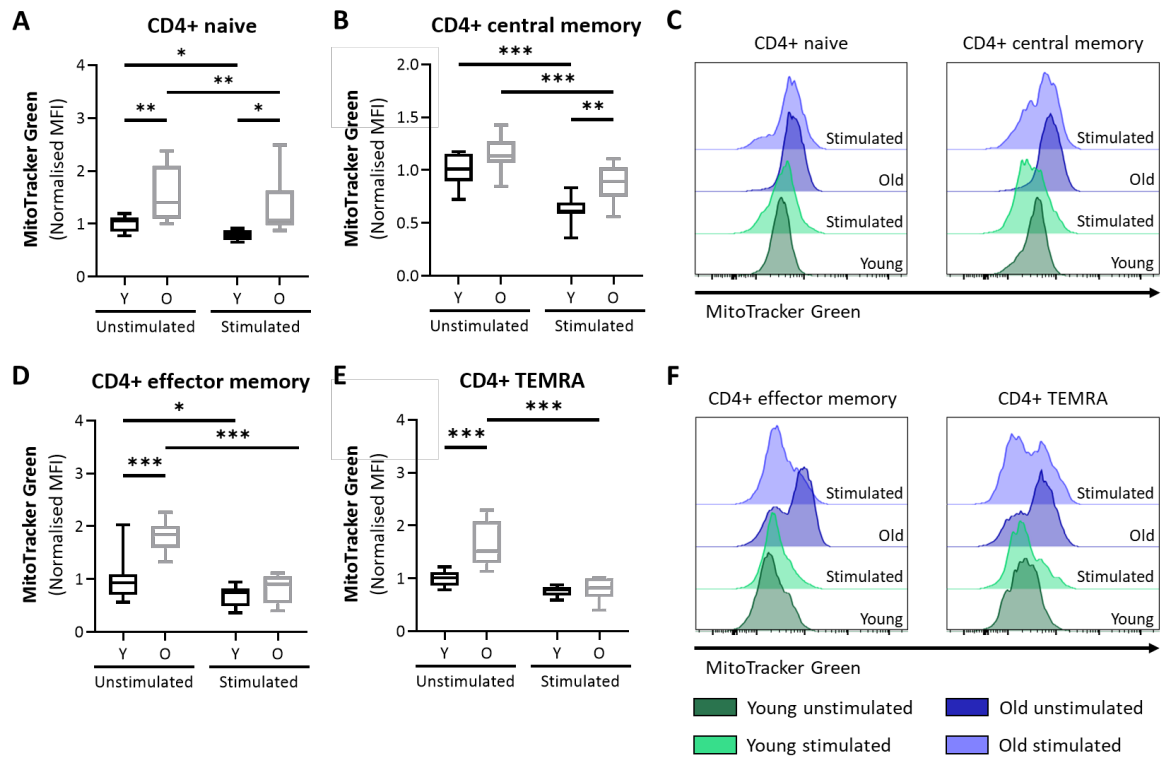
Figure 6.9   Mitochondrial mass of CD4+ T cell subsets from young and old donors with PMA/Ionomycin stimulation showing (A) MTG staining CD4+ naïve cells (B) MTG staining in CD4+ central memory cells (C) Histogram of MTG staining in CD4+ naïve and CD4+ central memory cells (D) MTG staining in CD4+ effector memory cells (E) MTG staining in CD4+ TEMRA cells and (F) Histogram of MTG staining in CD4+ effector memory and CD4+ TEMRA cells normalised to young unstimulated control cells (Y=young donor, O=old donor) (Box and whisker plot; n=10; Two-way mixed-model ANOVA; *p<0.05 ***p<0.001)

Within the CD8+ T cell compartment, old donors were also observed to have increased mitochondrial mass compared to young donors prior to stimulation which was mitigated following stimulation. On average MTG staining was increased 1.6-fold within naïve cells (p=0.044; Figure 6.10A), 1.9-fold within central memory cells (p=0.006; Figure 6.10B), 2.6-fold within effector memory cells (p<0.001; Figure 6.10D) and 1.6-fold within TEMRA (p<0.001; Figure 6.10E). This resulted in a shift in MTG MFI as seen in Figure 6.10C and F. Whilst CD8+ T cells from young donors did not change their mitochondrial mass following PMA/Ionomycin stimulation, cells from old donors saw drastic decreases in MFI (Figure 6.10C and F). Decreases in mitochondrial mass upon stimulation were most pronounced within CD8+ TEMRA (48.1%; p<0.001; Figure 6.10E), followed by CD8+ EM (42.7%; p<0.001; Figure 6.10D), naïve (33.6%; p=0.02; Figure 6.10A) and CM (30.5%; p=0.001; Figure 6.10B).

Figure 6.10 Mitochondrial mass in CD8+ T cell subsets from young and old donors with PMA/Ionomycin stimulation showing (A) MTG staining CD8+ naïve cells (B) MTG staining in CD8+ central memory cells (C) Histogram of MTG staining in CD8+ naïve and CD8+ central memory cells (D) MTG staining in CD8+ effector memory cells (E) MTG staining in CD8+ TEMRA cells and (F) Histogram of MTG staining in CD8+ effector memory and CD8+ TEMRA cells normalised to young unstimulated control cells (Y=young donor, O=old donor) (Box and whisker plot; n=10; Two-way mixed-model ANOVA; *p<0.05 ***p<0.001)

A significant increase in mitochondrial mass was also observed in cytotoxic and regulatory NK cells with age (Figure 6.11A-F). On the other hand, no significant changes in mitochondrial mass were observed in inflammatory NK cells (p=0.154; Figure 6.11B and E). MTG staining MFI was increased by 1.6-fold (p=0.011) and 1.8-fold (p=0.001) with age in cytotoxic and regulatory NK cells respectively. Differing trends in control of mitochondrial mass was observed upon PMA/Ionomycin stimulation with these NK cell subsets. Whilst cytotoxic NK cells from young donors increased their mitochondrial mass following stimulation by 1.4-fold (p=0.006), old donors were not able to increase mitochondrial biogenesis (p=0.762; Figure 6.11A and D). The opposite was observed within regulatory NK cells whereby cells from young donors did not alter their mitochondrial mass upon stimulation (p=0.854) but cells from old donors saw a significant decrease in MTG MFI by 37% (p=0.004; Figure 6.11C and F).
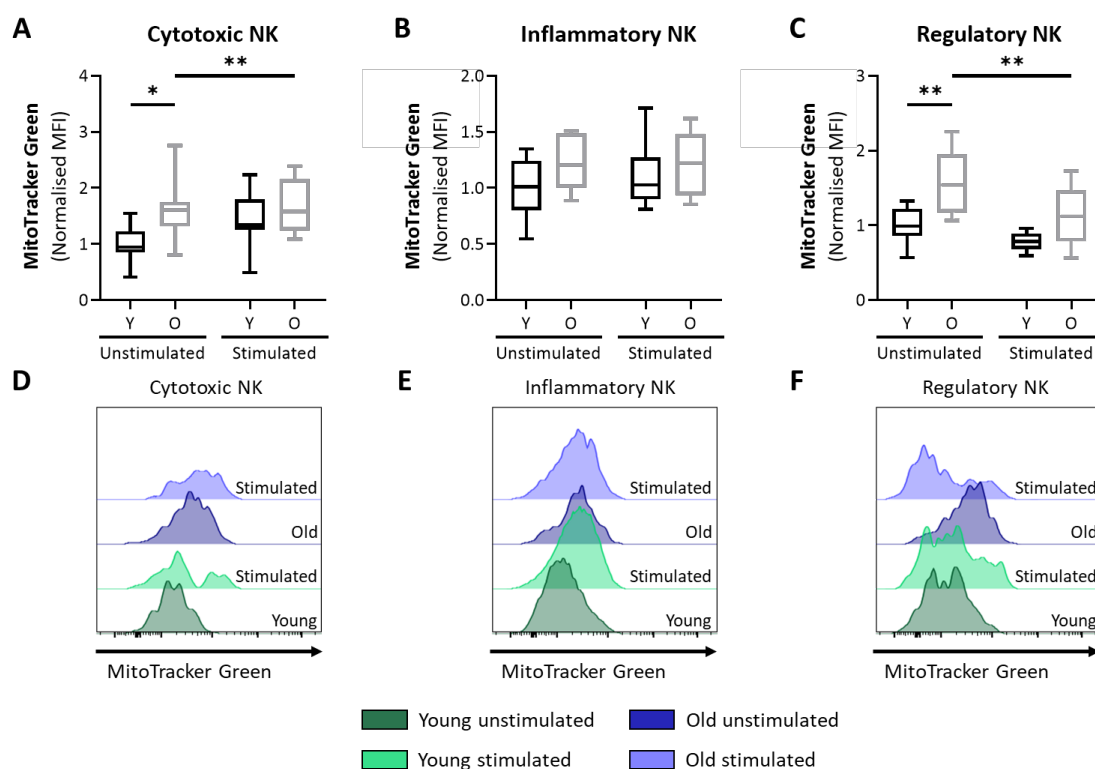
Figure 6.11 Mitochondrial mass in NK cell subsets from young and old donors with PMA/Ionomycin stimulation showing MTG staining in (A) Cytotoxic (B) Inflammatory and (C) Regulatory NK cells normalised to young unstimulated control cells and histogram of MitoTracker Green staining in (D) Cytotoxic (E) Inflammatory and (F) Regulatory NK cells (Y=young donor, O=old donor) (Box and whisker plot; n=10; Two-way mixed-model ANOVA; *p<0.05 **p<0.01)

However, no changes in mitochondrial mass with age were observed within this cohort for three subsets of monocytes: classical, intermediate and non-classical (Figure 6.12A-F). Whilst classical monocytes from both young and old donors decreased their mitochondrial mass upon stimulation by 35% (p=0.01) and 39% (p=0.003) respectively (Figure 6.12A and D), non-classical monocytes did not show any changes in MTG staining in response to PMA/Ionomycin (Figure 6.12C and F). Additionally, no changes in MTG MFI were observed upon stimulation in intermediate monocytes from young donors (p=0.117), those from old donors on the other hand displayed a significant reduction in mitochondrial mass by 31% (p=0.043; Figure 6.12B and E).
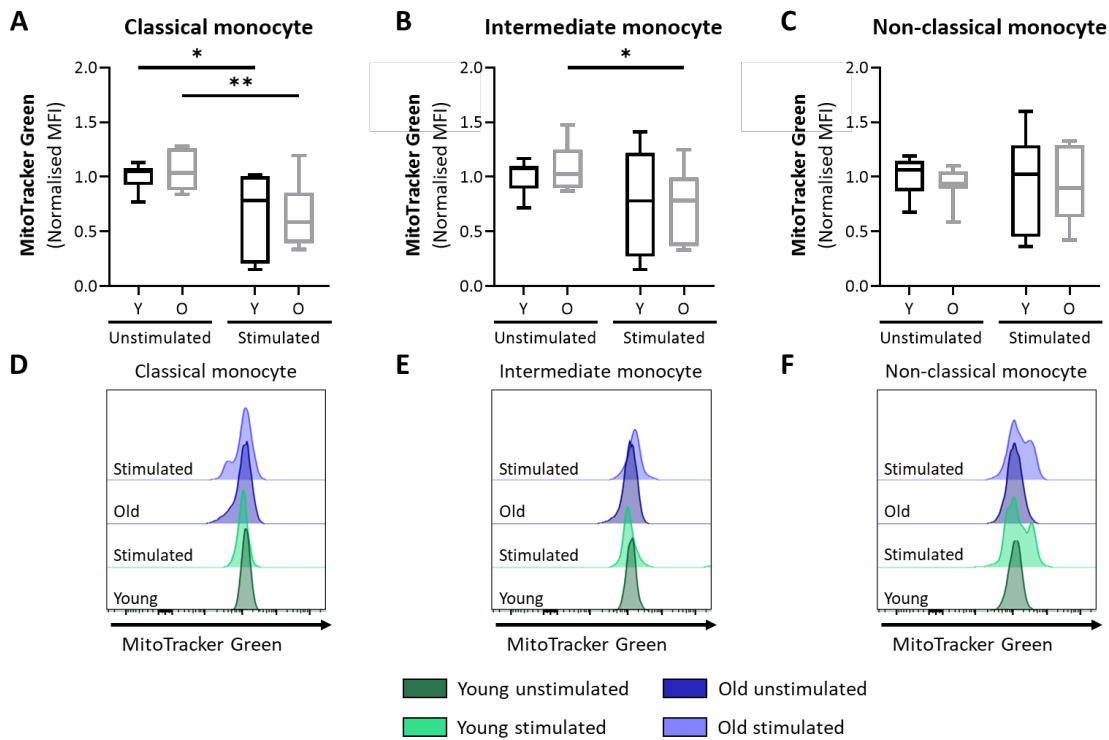
Figure 6.12 Mitochondrial mass in monocyte subsets from young and old donors with PMA/Ionomycin stimulation showing MTG staining in (A) Classical (B) Intermediate and (C) Non-classical monocytes normalised to young unstimulated control cells and histogram of MitoTracker Green staining in (D) Classical (E) Intermediate and (F) Non-classical monocytes (Y=young donor, O=old donor) (Box and whisker plot; n=10; Two-way mixed-model ANOVA; *p<0.05 **p<0.01)

CD141+ dendritic cells appeared to act similarly within both young and old donors. No significant differences in MTG MFI were observed prior to and following 6 hours of PMA/Ionomycin stimulation between CD141+ dendritic cells in young and old donors (Figure 6.13A and C). Mitochondrial mass was reduced similarly in CD141+ cells from young and old donors following PMA/Ionomycin stimulation, where MTG MFI was reduced by 31% in both young (p=0.003) and old (p<0.001) donors. A similar trend was observed with CD1c+ dendritic cells whereby mitochondrial mass was reduced within both young (28%, p<0.001) and old (28%, p<0.001) donors following stimulation (Figure 6.13B and D). However, within the cohort studied CD1c+ dendritic cells from old donors were observed to have 1.3-fold (p=0.006) increased mitochondrial mass compared to those from young donors (Figure 6.13B and D).
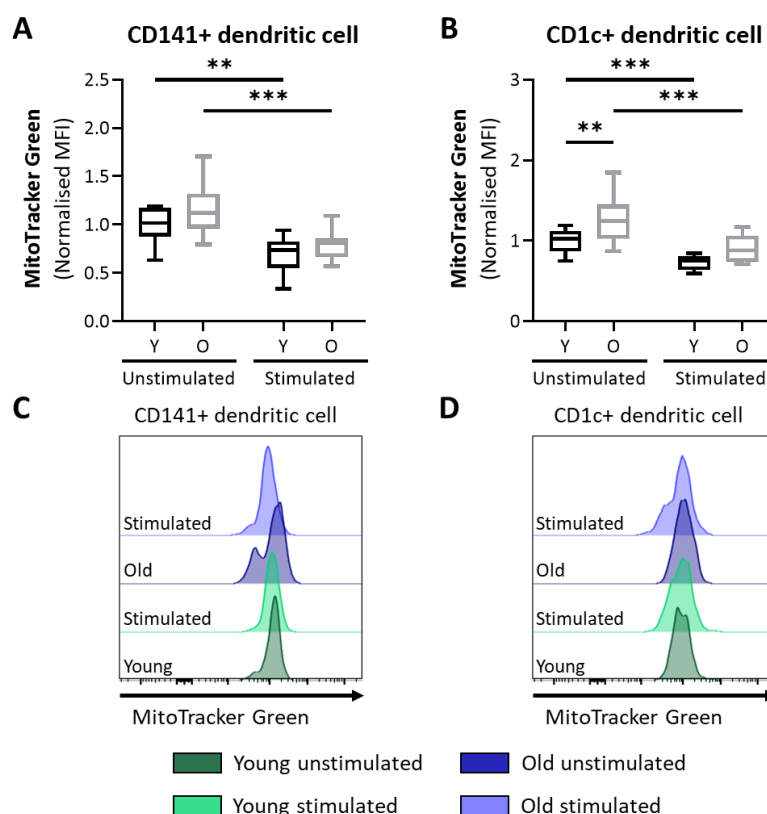
Figure 6.13 Mitochondrial mass in dendritic cell subsets from young and old donors with PMA/Ionomycin stimulation showing MTG staining in (A) CD141+ and (B) CD1c+ dendritic cells normalised to young unstimulated control cells and histogram of MitoTracker Green staining in (C) CD141+ and (D) CD1c+ dendritic cells (Y=young donor, O=old donor) (Box and whisker plot; n=10; Two-way mixed-model ANOVA; **p<0.01 ***p<0.001)

6.3.6   CD4+ TEMRA cells and classical and non-classical monocytes display defects in mitochondrial membrane potential with age

Prior to stimulation no significant difference between normalised mitochondrial membrane potential in young and old donors was detected within any of the CD4+ or CD8+ subsets studied: naïve, central memory, effector memory and TEMRA (Figure 6.14A-H). Whilst all CD8+ subsets and CD4+ naïve and effector cells saw no significant increase or decrease in mitochondrial membrane potential following PMA/Ionomycin stimulation, a significant increase in CD4+ central memory membrane potential was observed upon stimulation. These cells increased their membrane potential 1.6-fold (p=0.01; Figure 6.14B). The opposite trend was observed within CD4+ TEMRA cells where a 30% decrease in membrane potential was detected (p=0.034; Figure 6.14D). This decrease was not observed within old donors for CD4+ TEMRA and therefore following stimulation old

donors displayed significantly increased membrane potential compared to young donors by 66% (p=0.014).
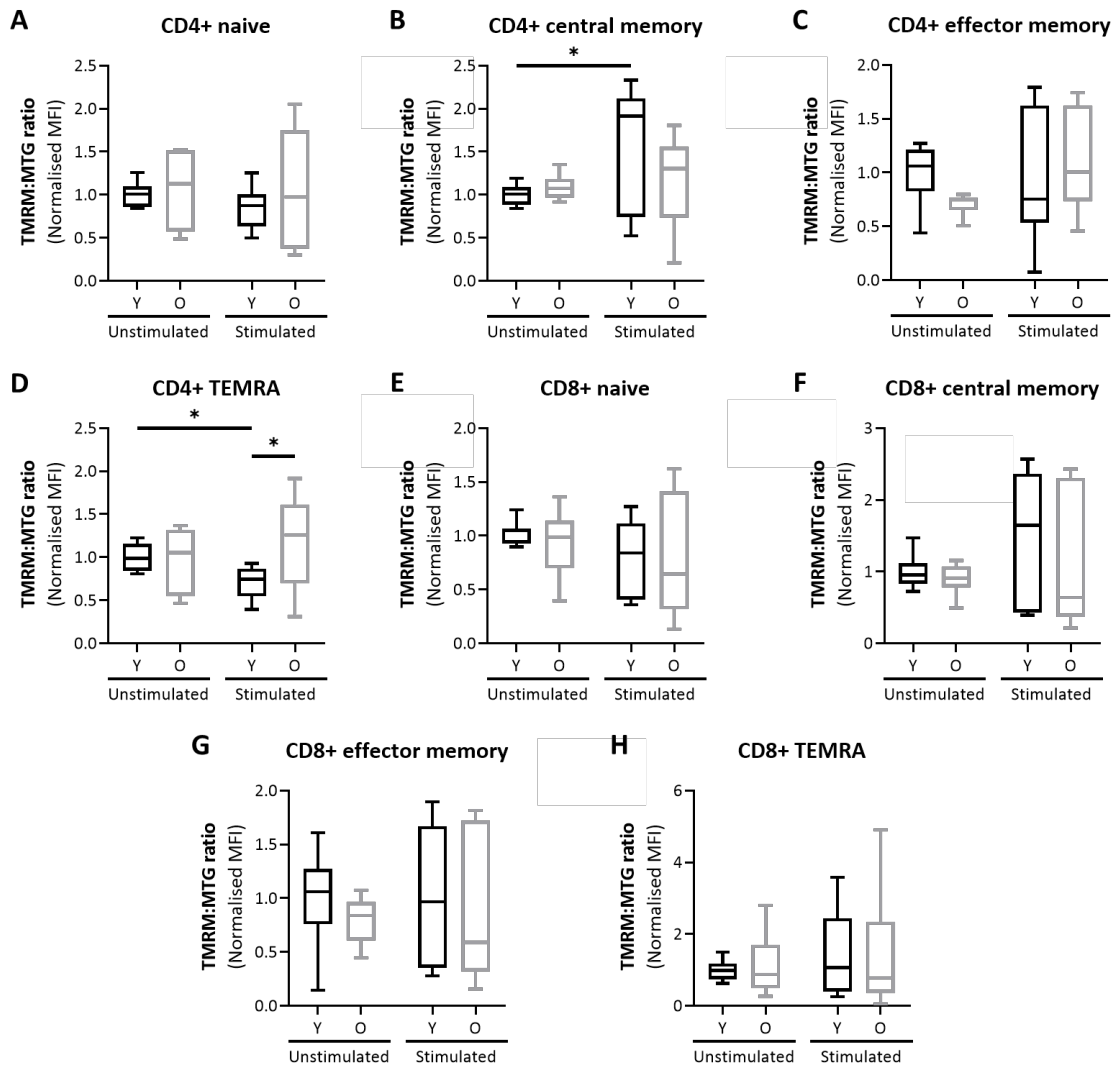
Figure 6.14 Mitochondrial membrane potential in CD4+ and CD8+ T cell subsets normalised to mitochondrial mass showing MTG:TMRM ratio in (A) CD4+ naïve cells (B) CD4+ central memory cells (C) CD4+ effector memory cells (D) CD4+ TEMRA cells (E) CD8+ naïve cells (F) CD8+ central memory cells (G) CD8+ effector memory cells and (H) CD8+ TEMRA cells normalised to young unstimulated control cells (Y=young donor, O=old donor) (Box and whisker plot; n=10; Two-way mixed-model ANOVA; *p<0.05)

Responses to stimulation in terms of mitochondrial membrane potential were more dynamic in response to PMA/Ionomycin stimulation than those of CD4+ and CD8+ T cells. Both young and old donors reduced mitochondrial membrane potential following stimulation in cytotoxic and inflammatory NK cells by over 50% (p<0.001) and 40% (p<0.009) respectively (Figure 6.15A and B). No differences between young and old donors were detected in mitochondrial membrane potential either prior to or following stimulation for all NK cells (Figure 6.15A-C). Whilst a significant decrease

in MTG:TMRM ratio was observed within young regulatory NK cells of 36% (p=0.001), no such tendency was observed for these cells in old donors (p=0.079; Figure 6.15C).

Within the three monocyte subsets studied here: classical, intermediate and non-classical, a significant increase in non-classical monocyte membrane potential was observed in old donors prior to stimulation. Membrane potential was increased 1.5-fold within these cells (p<0.001; Figure 6.15F). Whilst a loss of membrane potential was seen in classical (30%; p=0.035), intermediate (37%; p=0.019) and non-classical (72%; p<0.001) monocyte subsets from old donors following stimulation, the same trend was only observed for young donors in the non-classical subset (66%, p<0.001; Figure 6.15D-F). Following stimulation these changes resulted in a significantly reduced mitochondrial membrane potential in classical monocytes from old donors to 69% of that observed in young donors (p=0.031; Figure 6.15D).

Finally, mitochondrial membrane potential was also measured in dendritic cells and normalised to mitochondrial mass. Both CD141+ and CD1c+ dendritic cells from young donors reduced their MTG:TMRM ratio upon PMA/Ionomycin stimulation, by 32% (p=0.011) and 29% (p=0.01) respectively (Figure 6.15G and H). Membrane potential was also reduced within these cells from old donors but to a larger extent, 52% (p<0.001) and 51% (p<0.001) respectively. As with NK cells, no significant differences in the membrane potential of CD141+ or CD1c+ were observed between young and old donors prior to or following PMA/Ionomycin stimulation.
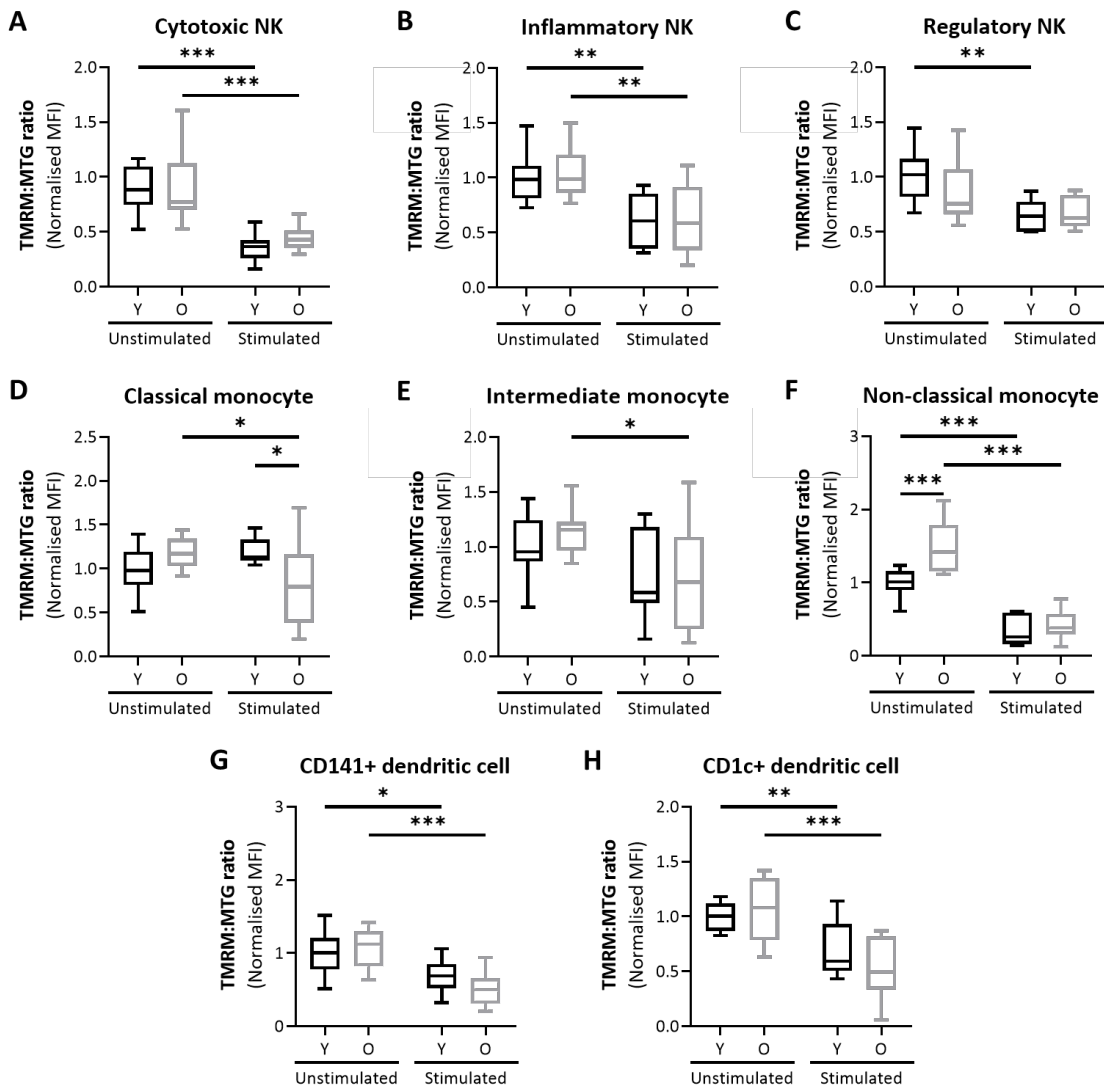
Figure 6.15 Mitochondrial membrane potential in NK, monocyte and dendritic cell subsets from young and old donors normalised to mitochondrial mass showing MTG:TMRM ratio in (A) cytotoxic NK cells (B) inflammatory NK cells (C) regulatory NK cells (D) classical monocytes (E) intermediate monocytes (F) non-classical monocytes (G) CD141+ dendritic cells and (H) CD1c+ dendritic cells normalised to young unstimulated control cells (Y=young donor, O=old donor) (Box and whisker plot; n=10; Two-way mixed-model ANOVA; *p<0.05 **p<0.01 ***p<0.001)

6.3.7   Immune cells subsets from old donors are subject to altered control of mitochondrial fission and fusion dynamics

Drp1 expression was significantly increased in CD4+ naïve and TEMRA cells following PMA/Ionomycin stimulation in both young and old donors (Figure 6.16A, C-D and E). Drp1 expression within young donors was increased by 16% (p=0.001) and 20% (p<0.001) within CD4+ naïve and TEMRA cells respectively, whilst in old donors it was increased by 19% (p<0.001) and 12%

(p=0.024) following stimulation. However, due to a greater level of variability between donors no significant upregulation of Drp1 expression was observed in CD4+ central memory and effector memory cells following stimulation in either young or old donors (Figure 6.16B, D and F).
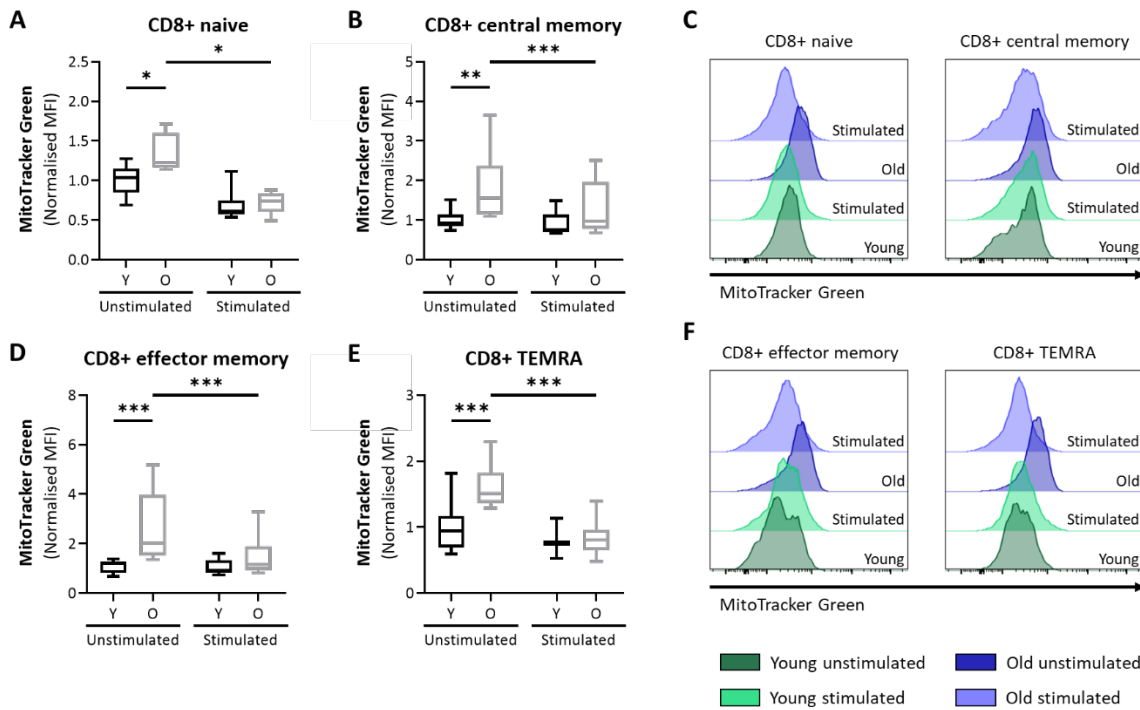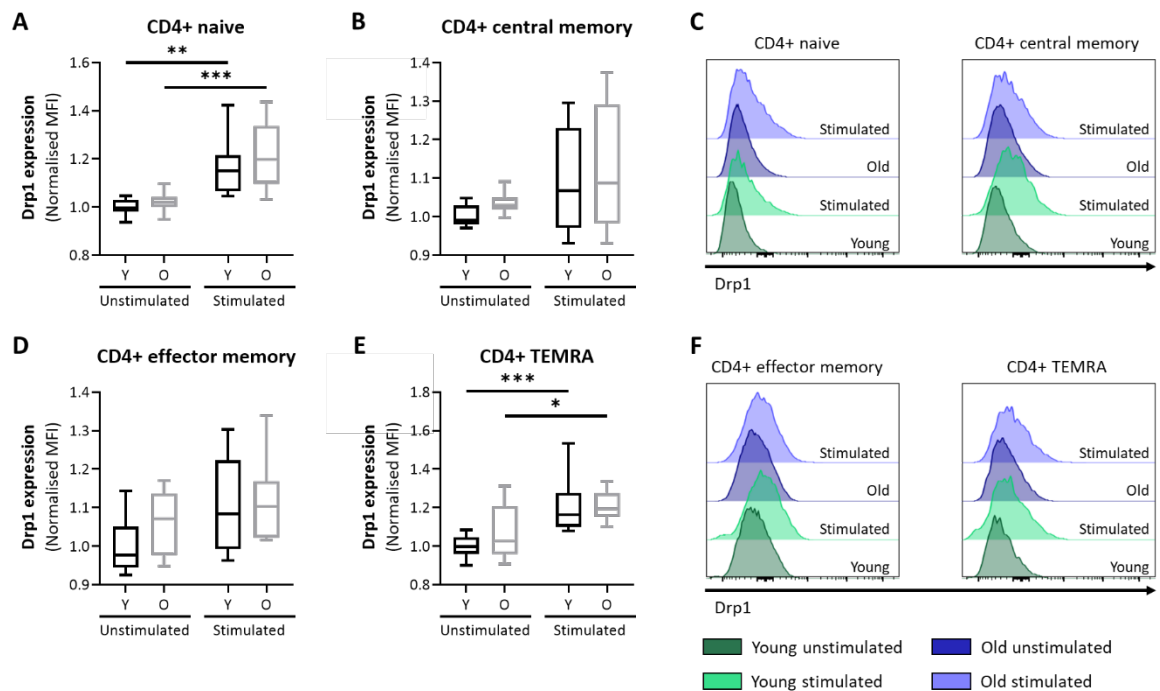

Figure 6.16 Drp1 expression in CD4+ T cell subsets from young and old donors with PMA/Ionomycin stimulation showing (A) Drp1 staining CD4+ naïve cells (B) Drp1 staining in CD4+ central memory cells (C) Histogram of Drp1 staining in CD4+ naïve and CD4+ central memory cells (D) Drp1 staining in CD4+ effector memory cells (E) Drp1 staining in CD4+ TEMRA cells and (F) Histogram of Drp1 staining in CD4+ effector memory and CD4+ TEMRA cells normalised to young unstimulated control cells (Y=young donor, O=old donor) (Box and whisker plot; n=10; Two-way mixed-model ANOVA; *p<0.05 **p<0.01 ***p<0.001)

A similar trend was also observed for Mfn2 expression. Mfn2 expression was significantly increased in CD4+ naïve and TEMRA cells following stimulation in both young and old donors (Figure 6.17A, C-D and E). Mfn2 expression within young donors was increased by 17% (p<0.001) and 10% (p=0.034) within CD4+ naïve and TEMRA cells respectively, whilst in old donors it was increased by 16% (p<0.001) and 10% (p=0.016) following stimulation. However, due to a greater level of variability between donors no significant upregulation of Mfn2 expression was observed in CD4+ central memory and effector memory cells following stimulation in either young or old donors (Figure 6.17B, D and F).
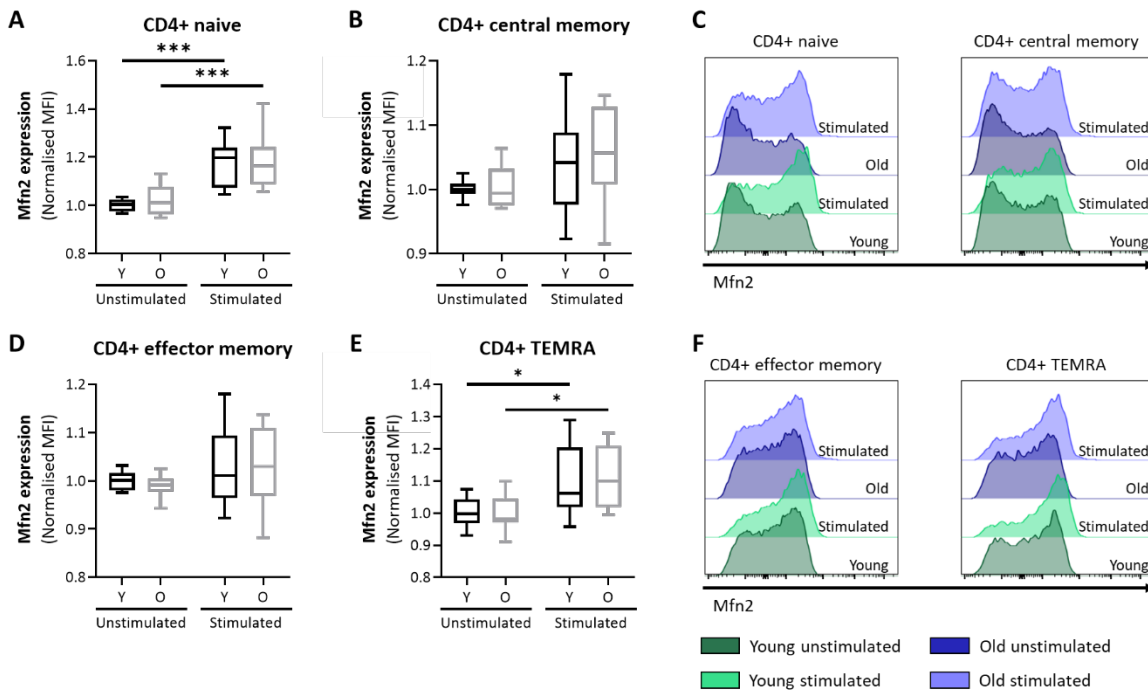
Figure 6.17 Mfn2 expression in CD4+ T cell subsets from young and old donors with PMA/Ionomycin stimulation showing (A) Mfn2 staining CD4+ naïve cells (B) Mfn2 staining in CD4+ central memory cells (C) Histogram of Mfn2 staining in CD4+ naïve and CD4+ central memory cells (D) Mfn2 staining in CD4+ effector memory cells (E) Mfn2 staining in CD4+ TEMRA cells and (F) Histogram of Mfn2 staining in CD4+ effector memory and CD4+ TEMRA cells normalised to young unstimulated control cells (Y=young donor, O=old donor) (Box and whisker plot; n=10; Two-way mixed-model ANOVA; *p<0.05 ***p<0.001)

All CD8+ subsets studied responded to stimulation by upregulating Drp1 and Mfn2 expression (Figure 6.18 and Figure 6.19). The shift in Drp1 and Mfn2 fluorescence with increasing protein expression is evident in Figure 6.18C and F and Figure 6.19C and F. Upon stimulation CD8+ naïve cells saw a 4.6- (p<0.001) and 4-fold (p<0.001) increase in Drp1 and Mfn2 expression in young donors, whilst old donors upregulated the expression of these proteins by 3.4- (p=0.013) and 3.3-fold (p<0.001) respectively (Figure 6.18A and Figure 6.19A). Within CD8+ central memory cells Drp1 MFI increased 2.2- (p=0.015) and 2.3-fold (p=0.002) following stimulation in young and old donors, whilst within the CD8+ effector memory subset Drp1 MFI was increased by 1.8-fold for both young (p=0.007) and old (p=0.002) donors (Figure 6.18B and D). A similar trend was observed for Mfn2 expression which was increased by 2.5- (p=0.009) and 2.6-fold (p=0.002) in CD8+ central memory cells and 1.9- (p=0.008) and 2-fold (p=0.002) in effector memory cells, in young and old donors respectively. CD8+ TEMRA from young and old donors also significantly increased Drp1 expression following stimulation by 2.5- (p<0.001) and 1.9-fold (p=0.003) respectively (Figure 6.18E). The same was true for Mfn2 expression which was increased by 3.9- and 2.3-fold in young and old CD8+

TEMRA (Figure 6.19E). However, this discrepancy between the fold-change in regulation of Mfn2 in young and old donors resulted in old donors showing significantly reduced expression following stimulation. Mfn2 expression in old donors was reduced by 36% compared to old donors (p=0.024; Figure 6.19E).

Figure 6.18 Drp1 expression in CD8+ T cell subsets from young and old donors with PMA/Ionomycin stimulation showing (A) Drp1 staining CD8+ naïve cells (B) Drp1 staining in CD8+ central memory cells (C) Histogram of Drp1 staining in CD8+ naïve and CD8+ central memory cells (D) Drp1 staining in CD8+ effector memory cells (E) Drp1 staining in CD8+ TEMRA cells and (F) Histogram of Drp1 staining in CD8+ effector memory and CD8+ TEMRA cells normalised to young unstimulated control cells (Y=young donor, O=old donor) (Box and whisker plot; n=10; Two-way mixed-model ANOVA; *p<0.05 **p<0.01 ***p<0.001)

Figure 6.19 Mfn2 expression in CD8+ T cell subsets from young and old donors with PMA/Ionomycin stimulation showing (A) Mfn2 staining CD8+ naïve cells (B) Mfn2 staining in CD8+ central memory cells (C) Histogram of Mfn2 staining in CD8+ naïve and CD8+ central memory cells (D) Mfn2 staining in CD8+ effector memory cells (E) Mfn2 staining in CD8+ TEMRA cells and (F) Histogram of Mfn2 staining in CD8+ effector memory and CD8+ TEMRA cells normalised to young unstimulated control cells (Y=young donor, O=old donor) (Box and whisker plot; n=10; Two-way mixed-model ANOVA; *p<0.05 **p<0.01 ***p<0.001)

Cytotoxic NK cells from young and old donors showed differential upregulation of Drp1 and Mfn2 upon stimulation. Whilst cells from young donors saw a large upregulation of Mfn2 expression by 62% (p=0.027) compared to Drp1 (24%; p=0.129), old donors upregulated Drp1 expression by 36% (p=0.006) compared to only a 6% (p=0.934) increase in Mfn2 expression (Figure 6.20A and D, Figure 6.21A and D). This shows that following stimulation cytotoxic NK cells undergo mitochondrial fusion in young donors and mitochondrial fission with age.

Inflammatory and regulatory NK cells are not subject to these changes, however. Drp1 expression is upregulated upon stimulation in inflammatory NK cells from both young and old donors (16% p=0.001 in young, 11% p=0.013 in old; Figure 6.20B and E). The same is true for Mfn2 expression within the inflammatory subset, upregulated by 17% (p=0.015) in young and 16% (p=0.023) in old donors (Figure 6.21B and E). Within regulatory NK cells Drp1 expression is upregulated similarly in young and old donors following stimulation (16% p=0.023 for young, 18% p=0.01 for old donors; Figure 6.20C and F). However, whilst both young and old donors significantly increase expression

of Mfn2 following stimulation, young donors increase Mfn2 expression by 28% (p<0.001) whilst Mfn2 is increased by 40% (p<0.001) in old donors (Figure 6.21C and F). As a result, following stimulation Mfn2 expression is increased by 15% in old donors over that of young donors (p=0.001). This suggests that upon stimulation regulatory NK in old donors may be subject to more mitochondrial fusion than those of young donors. These results suggest that mitochondrial fission and fusion in response to stimulation is regulated differently with age within cytotoxic and regulatory NK cells.

Figure 6.20 Drp1 expression in NK cell subsets from young and old donors with PMA/Ionomycin stimulation showing Drp1 expression in (A) cytotoxic (B) inflammatory and (C) regulatory NK cells normalised to young unstimulated control cells and histograms of Drp1 staining in (D) cytotoxic (E) inflammatory and (F) regulatory NK cells (Y=young donor, O=old donor) (Box and whisker plot; n=10; Two-way mixed-model ANOVA; *p<0.05 **p<0.01)

Figure 6.21 Mfn2 expression in NK cell subsets from young and old donors with PMA/Ionomycin stimulation showing Mfn2 expression in (A) cytotoxic (B) inflammatory and (C) regulatory NK cells normalised to young unstimulated control cells and histograms of Mfn2 staining in (D) cytotoxic (E) inflammatory and (F) regulatory NK cells (Y=young donor, O=old donor) (Box and whisker plot; n=10; Two-way mixed-model ANOVA; *p<0.05 **p<0.01 ***p<0.001)

Drp1 expression is downregulated similarly within classical monocytes from both young and old donors following stimulation (28% in young p<0.001, 34% in old p<0.001; Figure 6.22A and C). However, with stimulation Drp1 expression remains unchanged in intermediate monocytes from young donors whilst a significant reduction is observed in those from old donors (20% p=0.008; Figure 6.22B and E). Whilst both young and old donors significantly increase expression of Drp1 following stimulation in non-classical monocytes, young donors increase Drp1 expression by 79% (p<0.001) whilst Drp1 is increased by 40% (p<0.001) in old donors (Figure 6.22C and F). As a result, following stimulation Drp1 expression is decreased by 18% in old donors below that of young donors (p=0.012). This suggests that upon stimulation non-classical and intermediate monocytes in old donors are subject to decreased mitochondrial fission than those of young donors.

Figure 6.22   Drp1 expression in monocyte subsets from young and old donors with PMA/Ionomycin stimulation showing Drp1 expression in (A) classical (B) intermediate and (C) non-classical monocytes normalised to young unstimulated control cells and histograms of Drp1 staining in (D) classical (E) intermediate and (F) non-classical monocytes (Y=young donor, O=old donor) (Box and whisker plot; n=10; Two-way mixed-model ANOVA; *p<0.05 **p<0.01 ***p<0.001)

Despite changes in Drp1 expression, Mfn2 expression remains unchanged in classical monocytes upon stimulation in both young and old donors (Figure 6.23A and D). This same trend is true within the intermediate and non-classical monocytes subsets for young donors (Figure 6.23B-C and E-F). However, within old donors Mfn2 expression increases following PMA/Ionomycin stimulation by 1.3- and 1.5-fold within intermediate (p=0.027) and non-classical (p=0.006) monocytes respectively. When considering Mfn2 expression upon stimulation it can be clearly seen that classical monocyte mitochondrial dynamics are controlled differently to that of intermediate and non-classical monocytes with age. Overall, classical monocytes from both young and old donors down regulate mitochondrial fission upon stimulation. Intermediate monocytes do not change their mitochondrial dynamics in response to stimulation in young donors, however old donors upregulate both mitochondrial fission and mitochondrial fusion. Finally, non-classical monocytes from young and old donors both upregulate mitochondrial fission following stimulation but to a greater extent within young cells, whilst mitochondrial fusion is only upregulated in old donors. These results

suggest that mitochondrial fission and fusion in response to stimulation is regulated differently with age for intermediate and non-classical monocyte subsets.
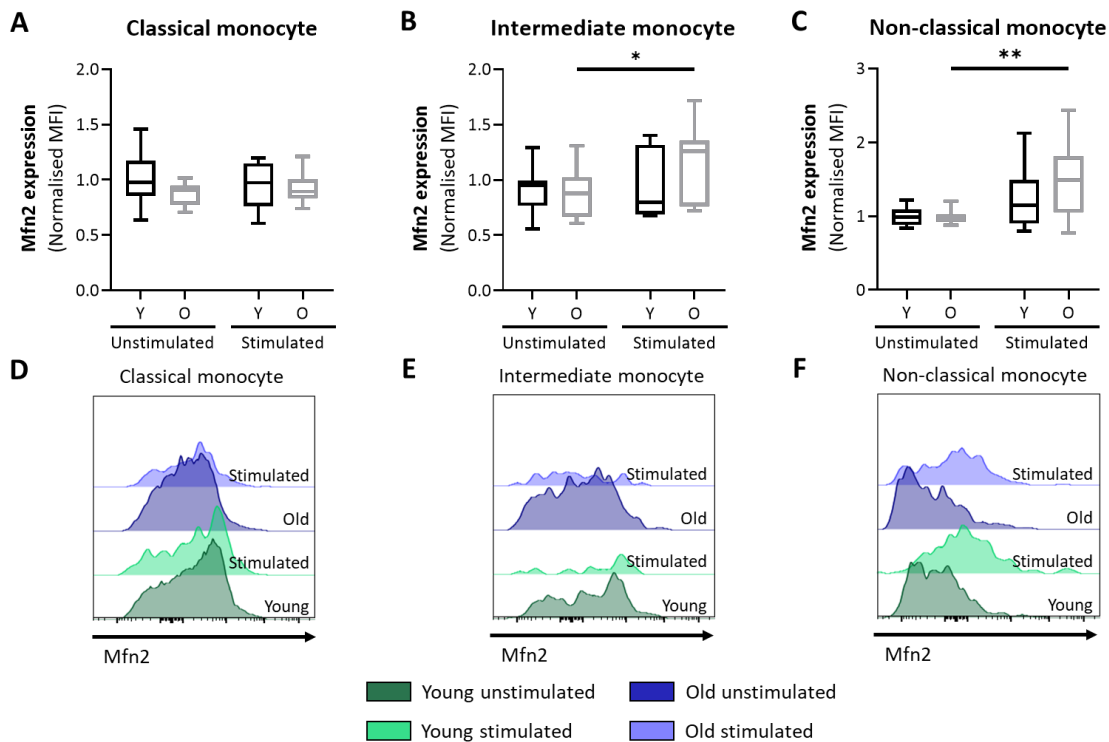
Figure 6.23 Mfn2 expression in monocyte subsets from young and old donors with PMA/Ionomycin stimulation showing Mfn2 expression in (A) classical (B) intermediate and (C) non-classical monocytes normalised to young unstimulated control cells and histograms of Mfn2 staining in (D) classical (E) intermediate and (F) non-classical monocytes (Y=young donor, O=old donor) (Box and whisker plot; n=10; Two-way mixed-model ANOVA; *p<0.05 **p<0.01)

Finally, within dendritic cells Drp1 staining is increased following stimulation. Within the CD141+ subset of dendritic cells Drp1 expression is increased upon stimulation in both young and old donors by 2- and 1.8-fold respectively (p=0.001 in young and p<0.001 in old; Figure 6.24A and C). Similarly, there is a 1.3- and 1.2-fold increase in Drp1 expression in young and old donors respectively within CD1c+ dendritic cells following stimulation (p<0.001 for young, p=0.015 for old; Figure 6.24B and D).
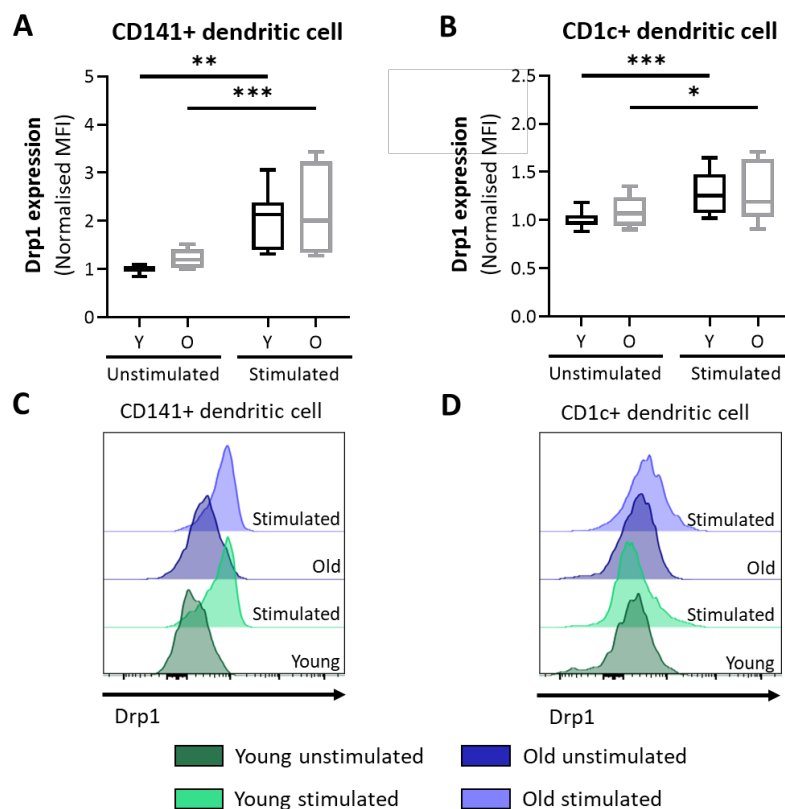
Figure 6.24 Drp1 expression in dendritic cell subsets from young and old donors with PMA/Ionomycin stimulation showing Drp1 expression in (A) CD141+ and (B) CD1c+ dendritic cells normalised to young unstimulated control cells and histograms of Drp1 staining in (C) CD141+ and (D) CD1c+ dendritic cells (Y=young donor, O=old donor) (Box and whisker plot; n=10; Two-way mixed-model ANOVA; *p<0.05 **p<0.01 ***p<0.001)

Increases in Mfn2 expression were also observed within this cohort following stimulation. Within young donors Mfn2 expression was increased by 1.4-fold (p<0.001) and 1.3-fold (p<0.001) in CD141+ and CD1c+ dendritic cell subsets respectively (Figure 6.25A-D). Similarly, 1.5- and 1.3-fold increases were detected in Mfn2 expression in CD141+ (p<0.001) and CD1c+ (p<0.001) dendritic cells for old donors. Therefore, no differences in the regulation of mitochondrial fission and fusion dynamics were observed in dendritic cells with age.

Figure 6.25 Mfn2 expression in dendritic cell subsets from young and old donors with PMA/Ionomycin stimulation showing Mfn2 expression in (A) CD141+ and (B) CD1c+ dendritic cells normalised to young unstimulated control cells and histograms of Mfn2 staining in (C) CD141+ and (D) CD1c+ dendritic cells (Y=young donor, O=old donor) (Box and whisker plot; n=10; Two-way mixed-model ANOVA; ***p<0.001)

6.3.8   Changes in Opa1 expression following stimulation with are dissimilar to those observed in young immune cells

In line with the results from Section 5.3.4, no up- or downregulation of Opa1 expression following stimulation in CD4+ T cells from young donors was observed (Figure 6.26A-F). Of the four CD4+ T cell subsets studied: naïve, central, memory, effector memory and TEMRA, a significant increase in Opa1 staining following stimulation was only observed within old donors (Figure 6.26E and F). Opa1 expression was increased by 14% within this group (p=0.033). This suggests that within CD4+ TEMRA there is a disparity between the control of Opa1 expression in young and old donors.
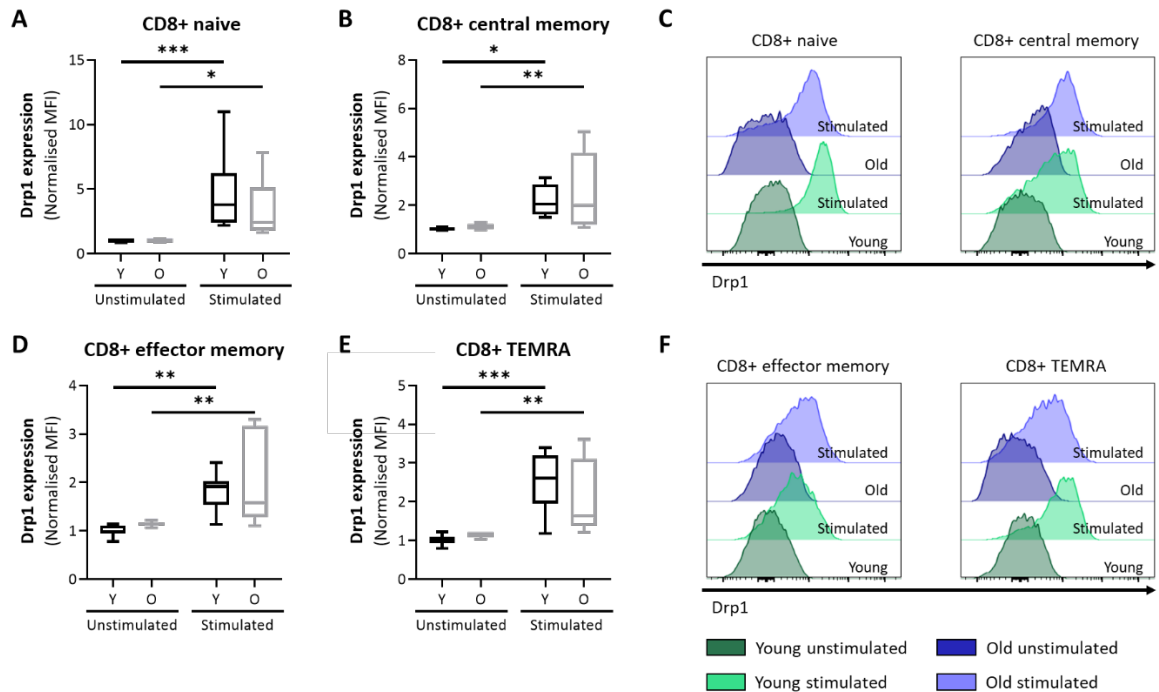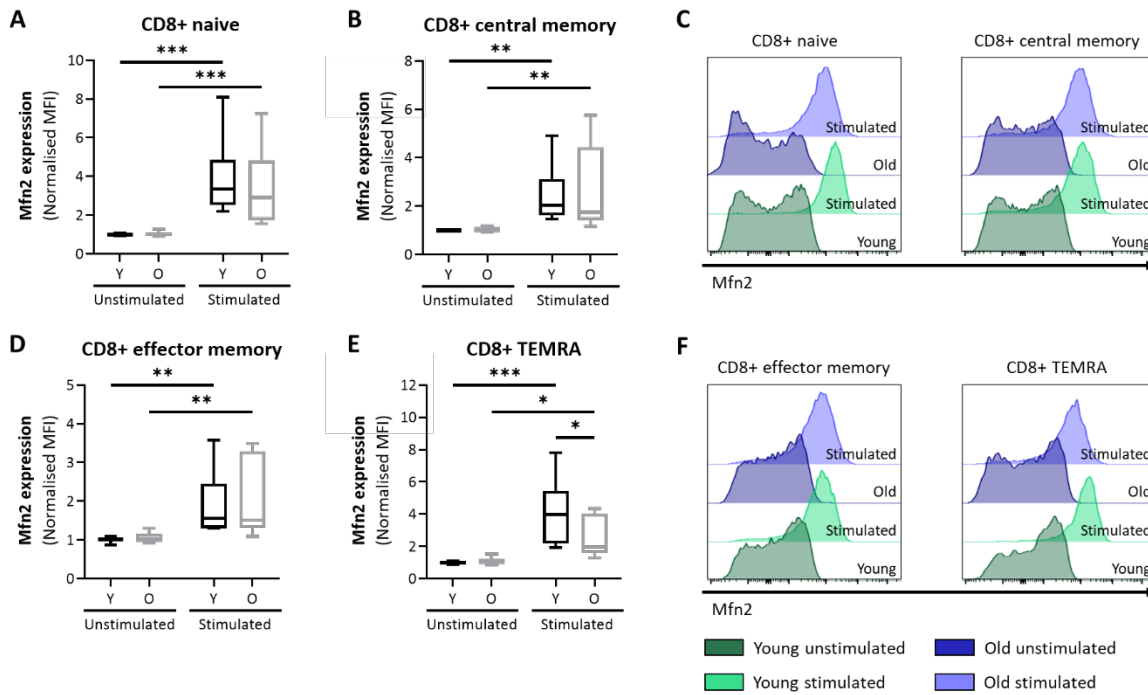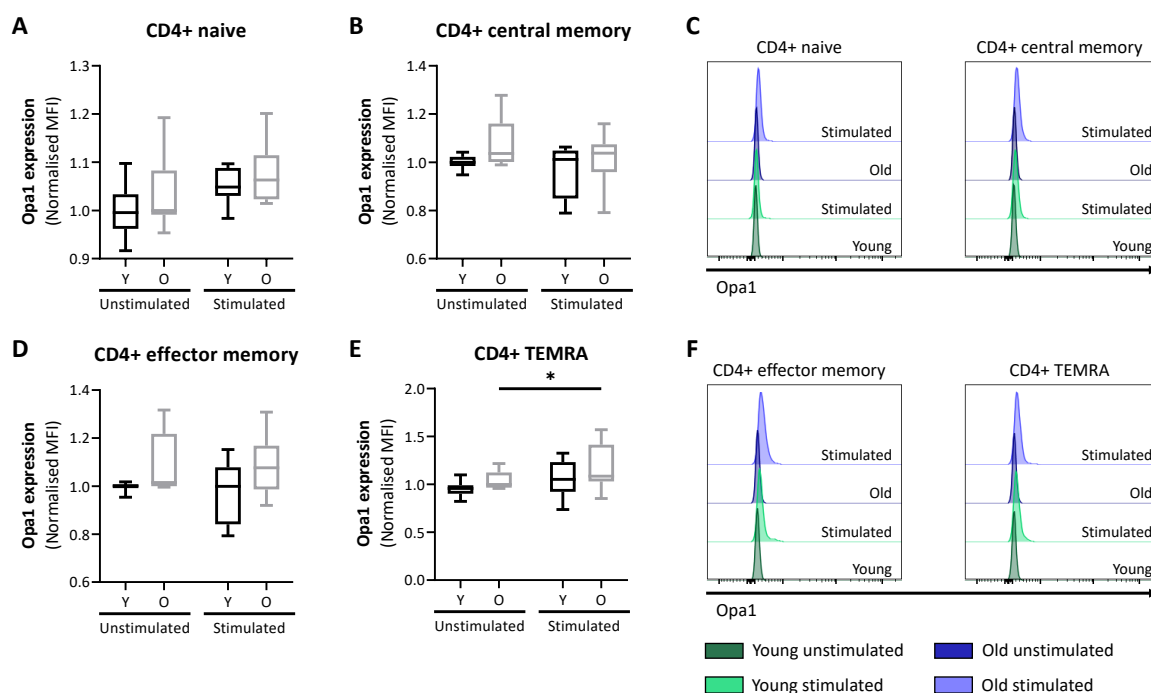
Figure 6.26 Opa1 expression in CD4+ T cell subsets from young and old donors with PMA/Ionomycin stimulation showing (A) Opa1 staining CD4+ naïve cells (B) Opa1 staining in CD4+ central memory cells (C) Histogram of Opa1 staining in CD4+ naïve and CD4+ central memory cells (D) Opa1 staining in CD4+ effector memory cells (E) Opa1 staining in CD4+ TEMRA cells and (F) Histogram of Opa1 staining in CD4+ effector memory and CD4+ TEMRA cells normalised to young unstimulated control cells (Y=young donor, O=old donor) (Box and whisker plot; n=10; Two-way mixed-model ANOVA)

When measuring Opa1 expression in CD8+ T cells, no changes were observed within cells from young donors upon stimulation (Figure 6.27A-F). However, a baseline increase in Opa1 expression was observed in CD8+ TEMRA from old donors. Old donors showed a 1.2-fold increase in Opa1 expression compared to young donors prior to stimulation (p=0.007; Figure 6.27E and F), however this difference was negated following treatment with PMA/Ionomycin. Following stimulation, a decrease in Opa1 staining of 18% was observed in old donor CD8+ effector memory cells (p=0.022; Figure 6.27D and F). However, this did not result in a significant difference in Opa1 levels between young and old donors following stimulation. In a similar manner to CD4+ TEMRA, this suggests that CD8+ TEMRA have altered Opa1 expression with age alongside CD8+ effector memory cells.
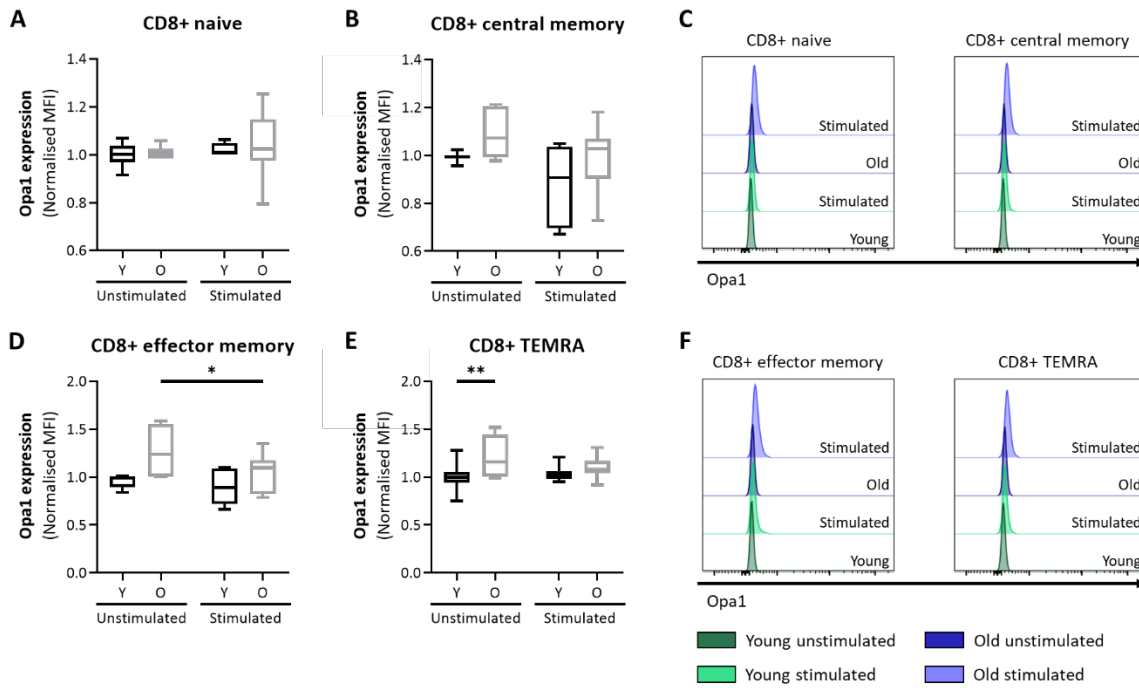
Figure 6.27 Opa1 expression in CD8+ T cell subsets from young and old donors with PMA/Ionomycin stimulation showing (A) Opa1 staining CD8+ naïve cells (B) Opa1 staining in CD8+ central memory cells (C) Histogram of Opa1 staining in CD8+ naïve and CD8+ central memory cells (D) Opa1 staining in CD8+ effector memory cells (E) Opa1 staining in CD8+ TEMRA cells and (F) Histogram of Opa1 staining in CD8+ effector memory and CD8+ TEMRA cells normalised to young unstimulated control cells (Y=young donor, O=old donor) (Box and whisker plot; n=10; Two-way mixed-model ANOVA; *p<0.05 **p<0.01)

Due to a significant upregulation of Opa1 upon stimulation in cytotoxic NK cells from old donors (1.6-fold p=0.003; Figure 6.28A and D), a significant increase in Opa1 staining was observed in old donors following stimulation in comparison to young donors. Cytotoxic NK cells from old donors showed a 76% increase in expression compared to young donors (p<0.001). However, this trend was not observed within inflammatory NK cells (Figure 6.28B and E). Whilst a significant upregulation of Opa1 expression following stimulation was observed within regulatory NK cells from old donors, this increase was also seen in cells from young donors. Young and old donors increased expression of Opa1 by 83% and 87%, respectively (p<0.001 for young, p<0.001 for old; Figure 6.28C and F). These results suggest that cytotoxic NK cells from old donors show Opa1 expression with age which may affect mitochondrial function.
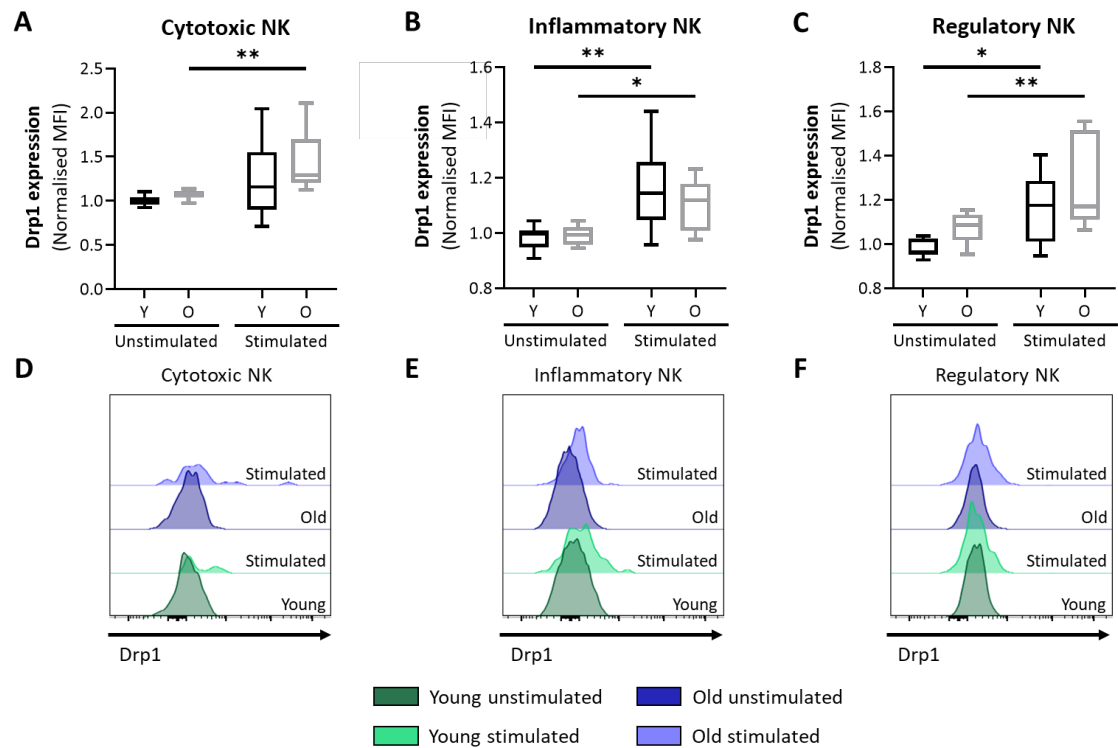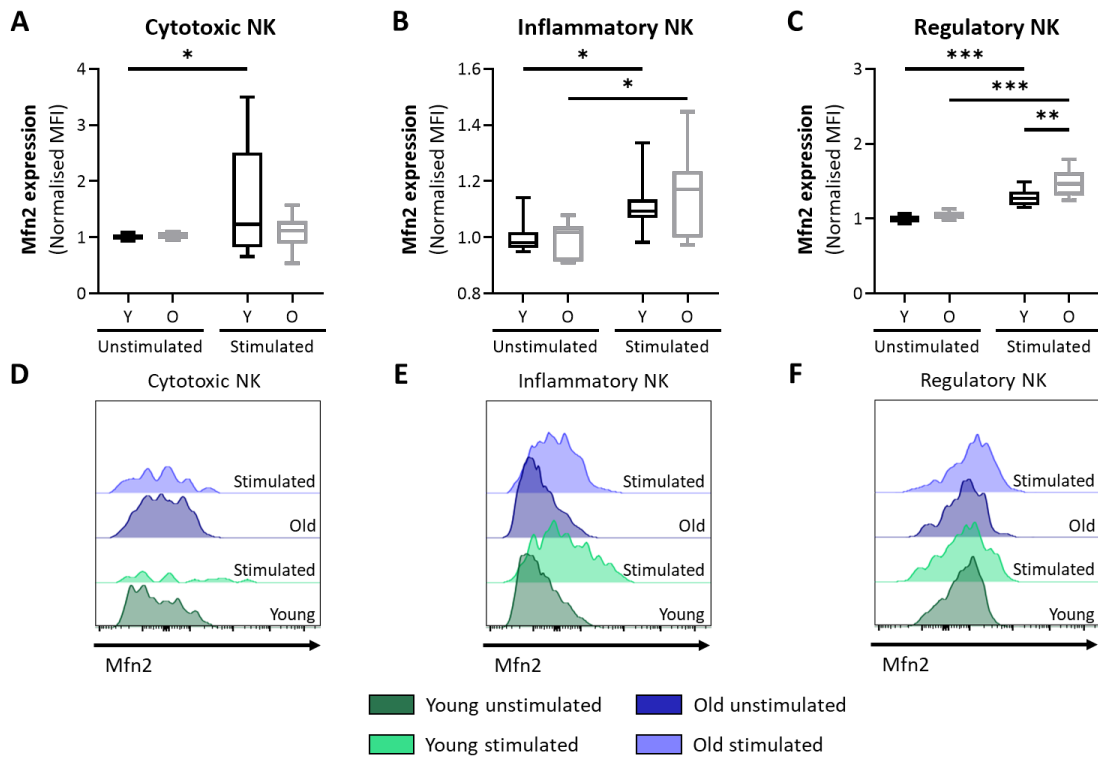
Figure 6.28 Opa1 expression in NK cell subsets from young and old donors with PMA/Ionomycin stimulation showing Opa1 expression in (A) cytotoxic (B) inflammatory and (C) regulatory NK cells normalised to young unstimulated control cells and histograms of Opa1 staining in (D) cytotoxic (E) inflammatory and (F) regulatory NK cells (Y=young donor, O=old donor) (Box and whisker plot; n=10; Two-way mixed-model ANOVA; **p<0.01 ***p<0.001)

Whilst a significant upregulation of Opa1 expression following stimulation was observed within classical monocytes from young donors, this increase was also seen in cells from old donors. Young and old donors increased expression of Opa1 by 18% and 16%, respectively (p=0.011 for young, p=0.008 for old; Figure 6.29A and D). Due to a significant upregulation of Opa1 upon PMA/Ionomycin stimulation in intermediate monocytes from old donors (1.2-fold p=0.006; Figure 6.29B and E), a significant increase in Opa1 staining was observed in old donors following stimulation in comparison to young donors. Intermediate monocytes from old donors displayed a 26% increase in expression compared to young donors (p=0.02). However, this increase was not observed within non-classical monocytes (Figure 6.29C and F). These results suggest that intermediate monocytes may be subject to altered mitochondrial cristae remodelling with age and stimulation.
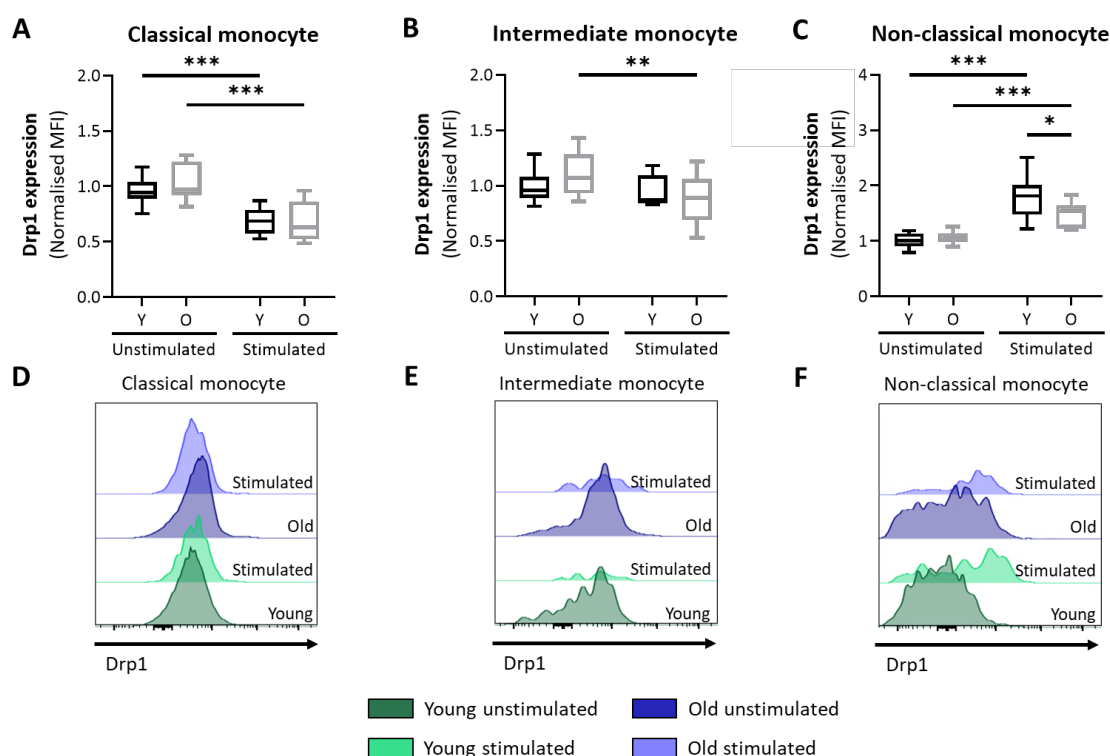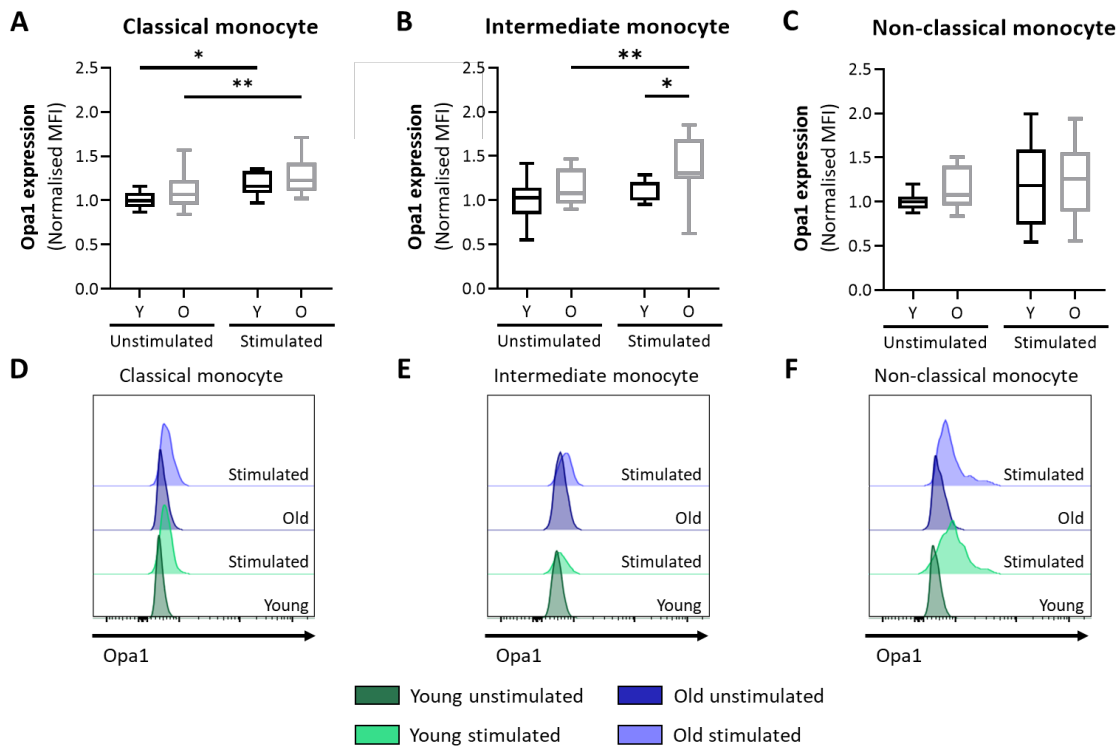
Figure 6.29 Opa1 expression in monocyte subsets from young and old donors with PMA/Ionomycin stimulation showing Opa1 expression in (A) classical (B) intermediate and (C) non-classical monocytes normalised to young unstimulated control cells and histograms of Opa1 staining in (D) classical (E) intermediate and (F) non-classical monocytes (Y=young donor, O=old donor) (Box and whisker plot; n=10; Two-way mixed-model ANOVA; *p<0.05 **p<0.01)

Finally, within dendritic cells a significant upregulation of Opa1 staining was seen in CD141+ dendritic cells upon stimulation in young donors. Opa1 was upregulated 1.7-fold within the cells from young donors (p=0.033), whereas no significant increase was detected in old donors (p=0.11; Figure 6.30A and C). Within, CD1c+ dendritic cells on the other hand, no significant differences were observed in the regulation of Opa1 either prior to or following stimulation between young and old donors (Figure 6.29B and D).
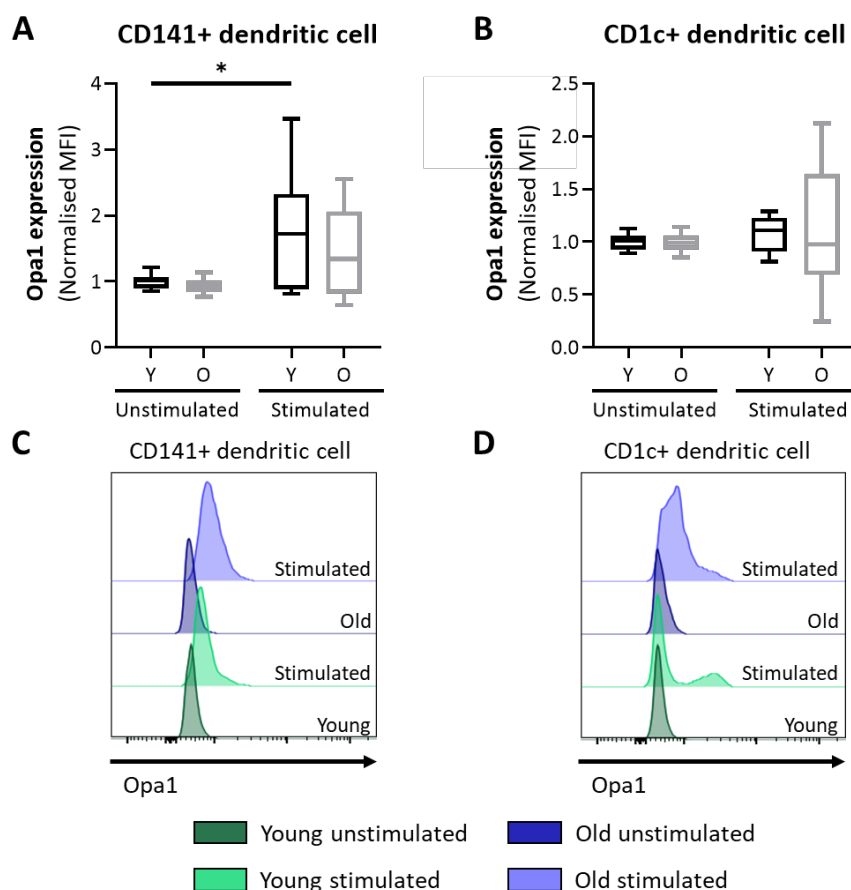
Figure 6.30 Opa1 expression in dendritic cell subsets from young and old donors with PMA/Ionomycin stimulation showing Opa1 expression in (A) CD141+ and (B) CD1c+ dendritic cells normalised to young unstimulated control cells and histograms of Opa1 staining in (C) CD141+ and (D) CD1c+ dendritic cells (Y=young donor, O=old donor) (Box and whisker plot; n=10; Two-way mixed-model ANOVA; *p<0.05)

6.3.9 Effector memory cells within the CD4+ and CD8+ T cell compartments and CD141+ dendritic cells show changes in surface Glut1 staining

As discussed in Chapter 4, Glut1 is an important factor in upregulating T cell glycolysis following stimulation. Therefore, the surface expression of Glut1 was measured prior to and following 6 hours of PMA/Ionomycin to identify any differences in Glut1 regulation with age in these cells. It was observed that CD4+ naïve T cells and TEMRA, do not upregulate Glut1 expression over the time course studied here (Figure 6.31A, C, E and F). This finding was maintained within CD4+ naïve and CD4+ TEMRA from young and old donors. A significant upregulation of surface Glut1 was measured within CD4+ central memory cells, however. Glut1 expression was increased by 28% within young donors and by 17% in old donors (p<0.001 for young and p=0.015 for old; Figure 6.31B and C). For CD4+ effector memory cells on the other hand, whilst Glut1 expression was decreased by 17% in young donors (p=0.003) there was only a trend towards decreased expression in old donors

(p=0.068; Figure 6.31D and F). Whilst this inconsistency did not result in significantly altered Glut1 expression in the elderly, it may suggest that there is a small difference in the control of Glut1 expression following stimulation in old donors.
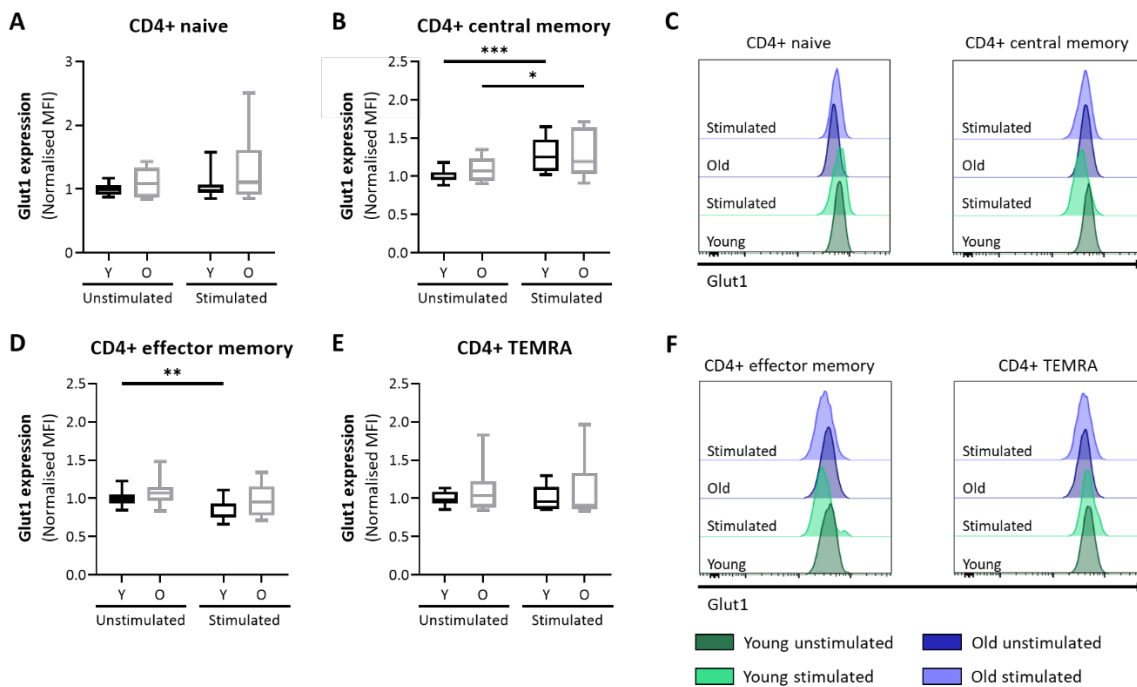
Figure 6.31 Glut1 expression in CD4+ T cell subsets from young and old donors with PMA/Ionomycin stimulation showing (A) Glut1 staining CD4+ naïve cells (B) Glut1 staining in CD4+ central memory cells (C) Histogram of Glut1 staining in CD4+ naïve and CD4+ central memory cells (D) Glut1 staining in CD4+ effector memory cells (E) Glut1 staining in CD4+ TEMRA cells and (F) Histogram of Glut1 staining in CD4+ effector memory and CD4+ TEMRA cells normalised to young unstimulated control cells (Y=young donor, O=old donor) (Box and whisker plot; n=10; Two-way mixed-model ANOVA; *p<0.05 **p<0.01 ***p<0.001)

Within CD8+ T cells from young donors no changes in Glut1 expression were observed in the naïve, central memory or TEMRA subsets (Figure 6.32A-C, E and F). This finding was maintained within old donors. Surprisingly however, as with CD4+ effector memory, a significant decrease in Glut1 expression was observed following stimulation in cells from young donors. These cells decreased Glut1 expression by 16% over 6 hours (p=0.021; Figure 6.32D and F). CD8+ effector memory cells from old donors on the other hand, maintained their expression of Glut1 upon treatment with PMA/Ionomycin (p=0.177). As a result, this may suggest that Glut1 may be regulated differently in CD8+ effector memory cells with stimulation in the elderly.
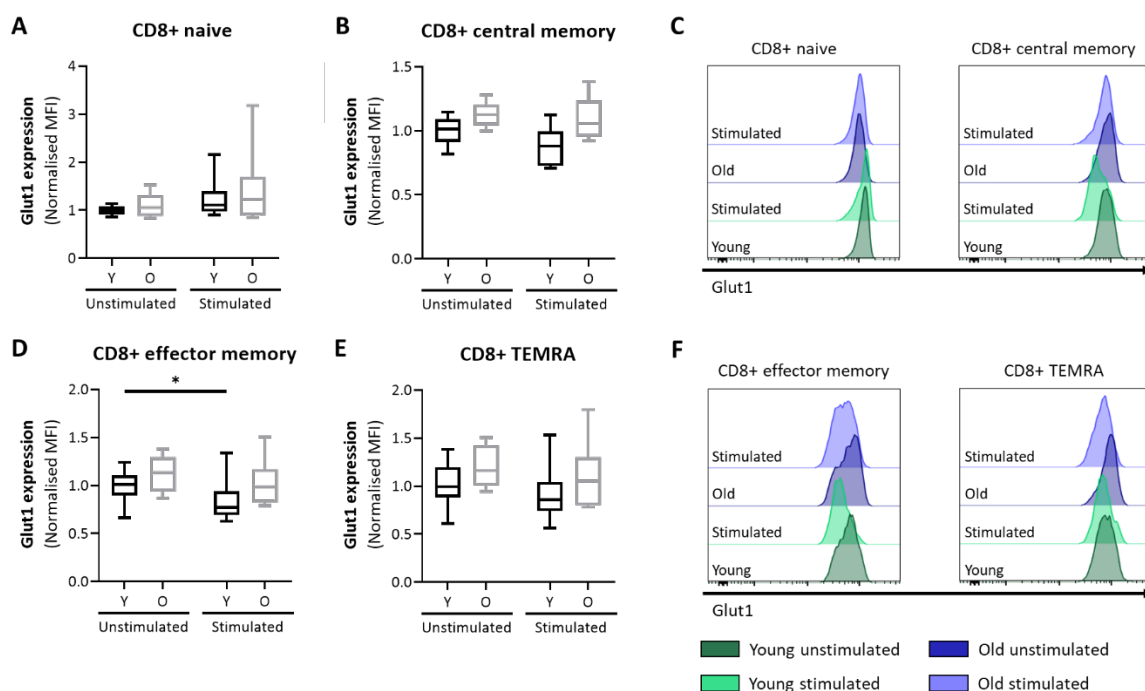
Figure 6.32 Glut1 expression in CD8+ T cell subsets from young and old donors with PMA/Ionomycin stimulation showing (A) Glut1 staining CD8+ naïve cells (B) Glut1 staining in CD8+ central memory cells (C) Histogram of Glut1 staining in CD8+ naïve and CD8+ central memory cells (D) Glut1 staining in CD8+ effector memory cells (E) Glut1 staining in CD8+ TEMRA cells and (F) Histogram of Glut1 staining in CD8+ effector memory and CD8+ TEMRA cells normalised to young unstimulated control cells (Y=young donor, O=old donor) (Box and whisker plot; n=10; Two-way mixed-model ANOVA; *$p<0.05$)

Surprisingly, despite changes in other mitochondrial and metabolic parameters with stimulation, no changes in Glut1 surface staining were observed within NK cells. All three subsets studied: cytotoxic, inflammatory and regulatory did not increase or decreased Glut1 expression following treatment (Figure 6.33A-F). Interestingly, no differences between the surface expression of Glut1 were seen between young and old donors either prior to or following stimulation. Therefore, these results suggest that Glut1 expression is not altered in NK cells with age and Glut1 may not be an important factor in NK cell stimulation.
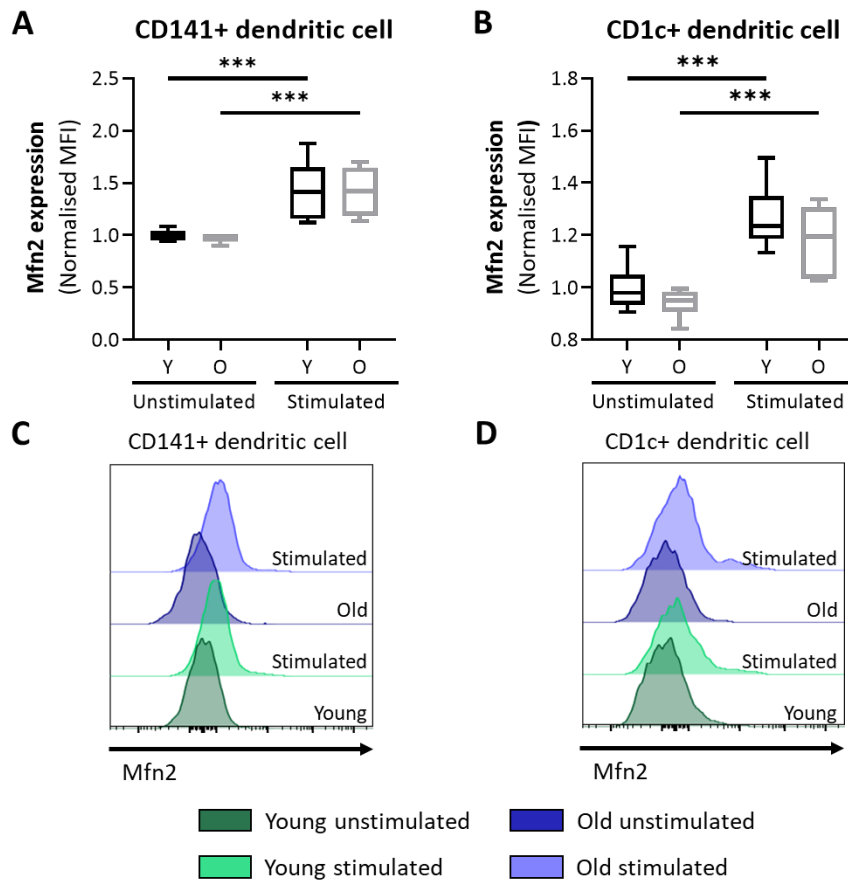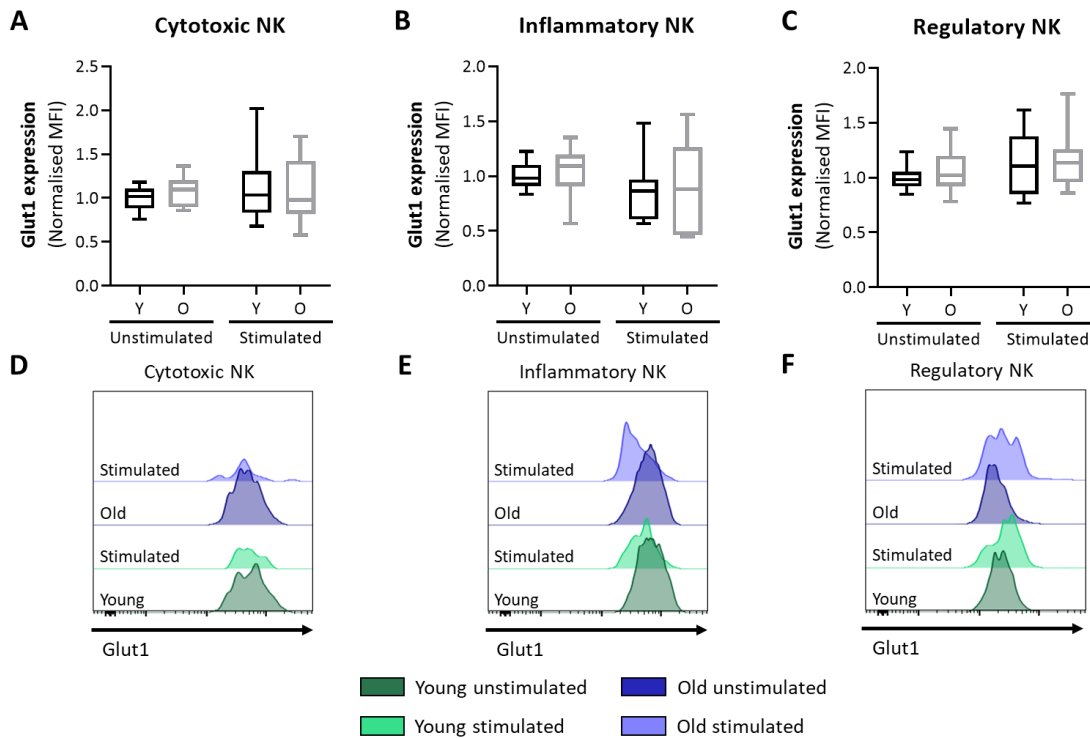
Figure 6.33 Glut1 expression in NK cell subsets from young and old donors with PMA/Ionomycin stimulation showing Glut1 expression in (A) cytotoxic (B) inflammatory and (C) regulatory NK cells normalised to young unstimulated control cells and histograms of Glut1 staining in (D) cytotoxic (E) inflammatory and (F) regulatory NK cells (Y=young donor, O=old donor) (Box and whisker plot; n=10; Two-way mixed-model ANOVA)

Similarly, no changes in Glut1 surface staining were observed within three monocyte subsets studied here: classical, intermediate or non-classical. All monocyte subsets did not increase or decreased Glut1 expression following stimulation (Figure 6.34A-F). Interestingly, no differences between the surface expression of Glut1 were seen between young and old donors either prior to or following stimulation. Therefore, these results suggest that Glut1 expression is not altered in monocytes with age and Glut1 expression is not involved in the first 6 hours of monocyte stimulation.
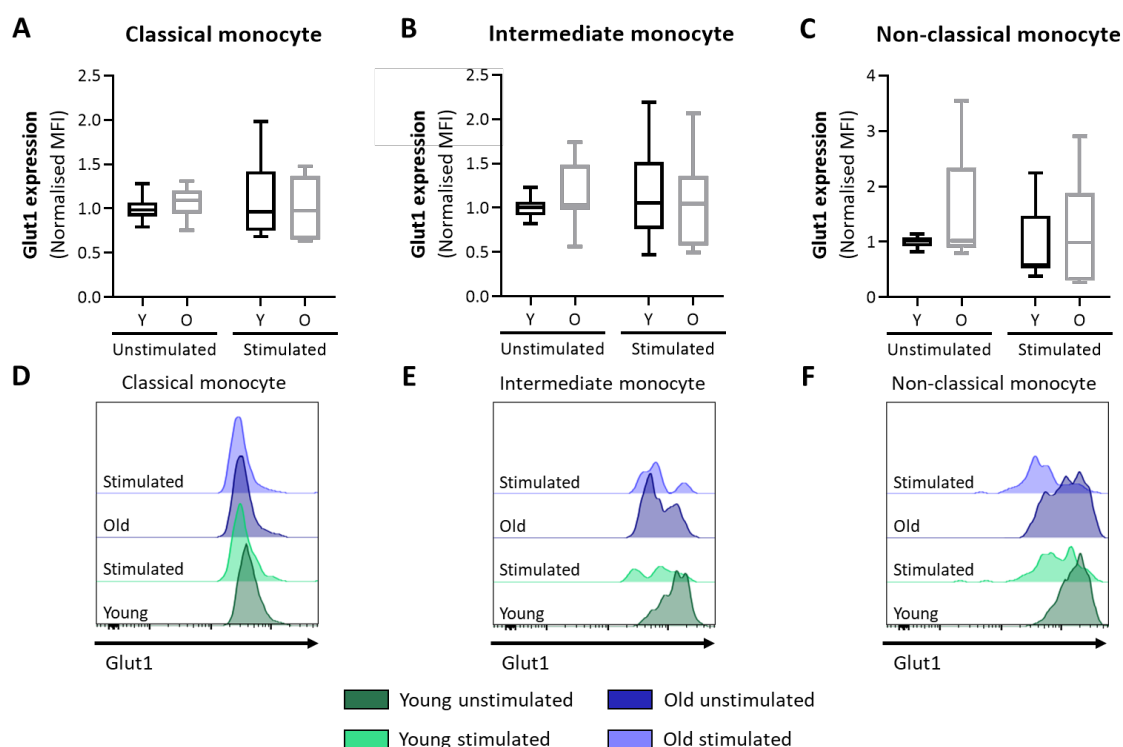
Figure 6.34 Glut1 expression in monocyte subsets from young and old donors with PMA/Ionomycin stimulation showing Glut1 expression in (A) classical (B) intermediate and (C) non-classical monocytes normalised to young unstimulated control cells and histograms of Glut1 staining in (D) classical (E) intermediate and (F) non-classical monocytes (Y=young donor, O=old donor) (Box and whisker plot; n=10; Two-way mixed-model ANOVA)

Finally, changes in Glut1 expression prior and following stimulation were studied in dendritic cells. CD141+ dendritic cells within old donors showed a significantly reduced level of Glut1 staining compared to those in young donors (Figure 6.35A and C). Glut1 staining was reduced to 80% of that observed in young donors (p=0.01). Whilst this difference was observed at baseline, this effect was lost following stimulation as Glut1 expression was decreased in both young and old donors. Upon stimulation Glut1 staining was reduced by 46% (p<0.001) and 39% (p<0.001) in young and old donors, respectively. CD1c+ dendritic cells did not show any differences in Glut1 expression between young and old donors (Figure 6.35B and D). Glut1 staining was significantly reduced upon stimulation in cells from both young and elderly donors to 77% (p=0.005) and 82% (p=0.028) of that observed prior to stimulation, respectively. Taking these results into account, it would appear that CD141+ dendritic cells are more susceptible to age-related changes in Glut1 expression than the CD1c+ subset.
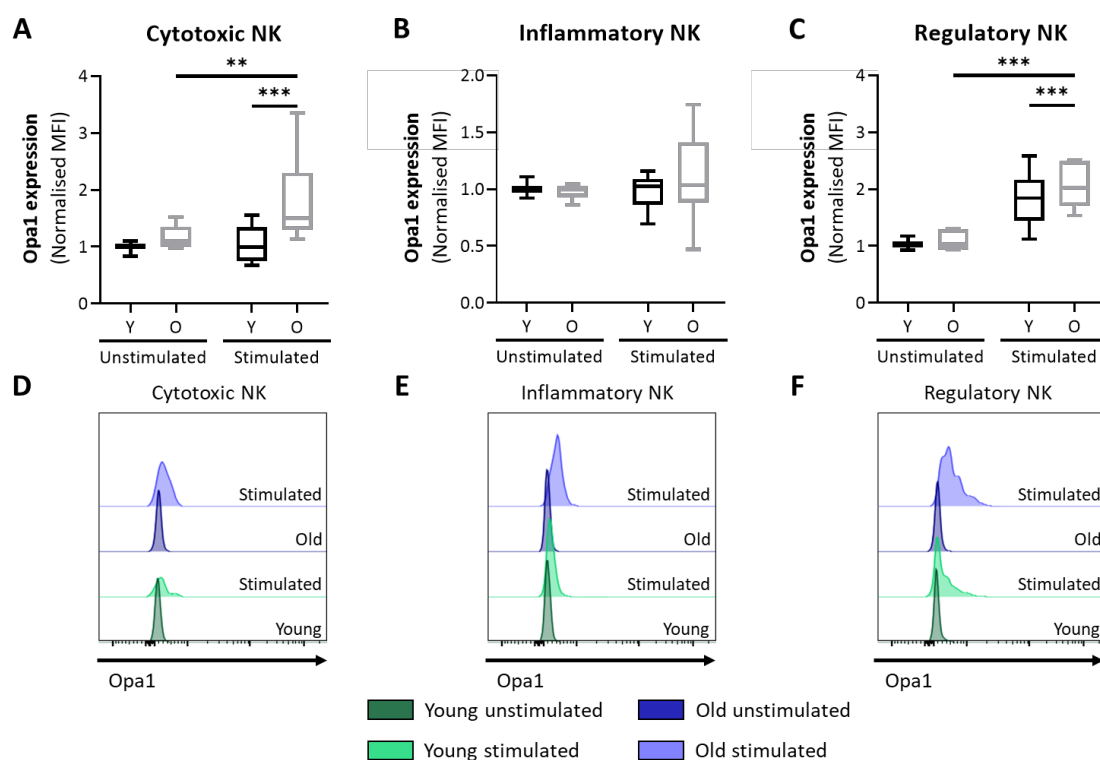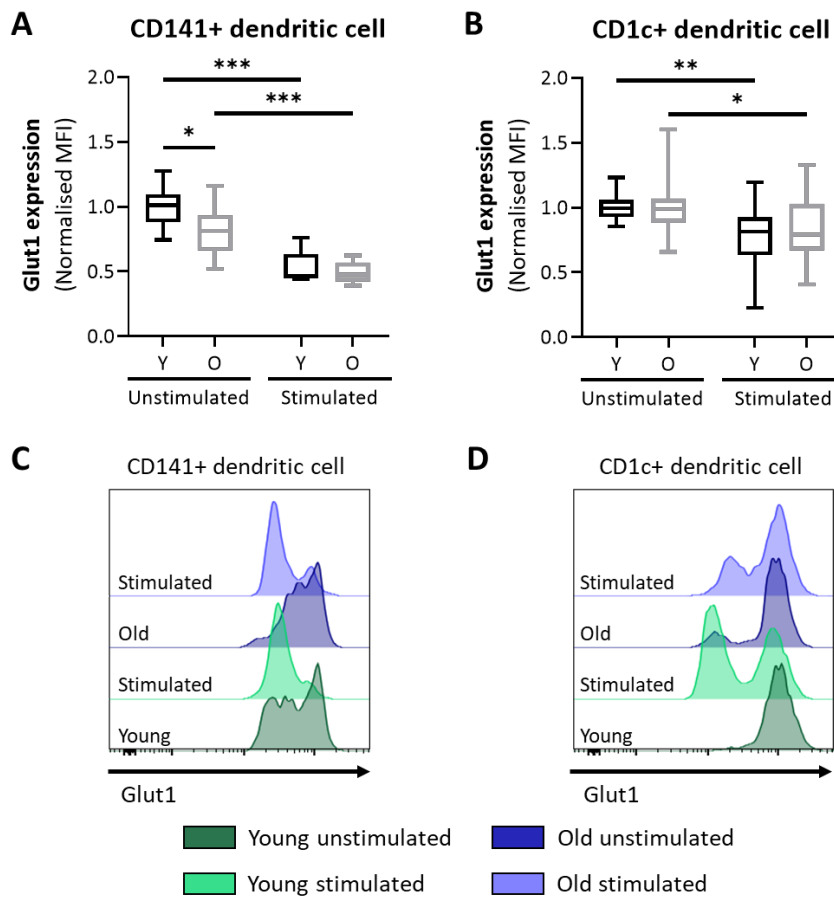
Figure 6.35 Glut1 expression in dendritic cell subsets from young and old donors with PMA/Ionomycin stimulation showing Glut1 expression in (A) CD141+ and (B) CD1c+ dendritic cells normalised to young unstimulated control cells and histograms of Glut1 staining in (C) CD141+ and (D) CD1c+ dendritic cells (Y=young donor, O=old donor) (Box and whisker plot; n=10; Two-way mixed-model ANOVA; *p<0.05 **p<0.01 ***p<0.001)

6.3.10   mTOR (S2448) phosphorylation following stimulation is delayed in CD4+ and CD8+ TEMRA as well as CD1c+ dendritic cells

Phosphorylation of the mammalian target of rapamycin (mTOR) protein at S2448, is a primary event which occurs following stimulation of immune cells. As discussed in the Introduction, mTOR controls the switch between oxidative and glycolytic metabolism within immune cells. Therefore, the level of mTOR S2448 phosphorylation was measured within immune cell subsets from young and old donors, to see whether the response is altered with age.

Within CD4+ T cells an increase in mTOR phosphorylation was observed following stimulation in young donors (Figure 6.36A-F). This increase occurred within all four subsets: naïve increased mTOR S2448 phosphorylation 1.4-fold (p=0.004), central memory 1.3-fold (p=0.001), effector memory

1.2-fold (p=0.023) and TEMRA 1.2-fold (p=0.046). This increase following stimulation was also observed in old donors within CD4+ naïve, central memory and effector memory cells which increased phosphorylation 1.4 fold (p<0.001), 1.3-fold (p=0.004) and 1.2-fold (p=0.005) respectively (Figure 6.36A-D and F). Whilst a trend towards increased mTOR phosphorylation was observed in CD4+ TEMRA from old donors, this was found to be insignificant (p=0.073; Figure 6.36E and F). This did not result in a significant difference between mTOR phosphorylation in young and old donors following stimulation within this cell type, however this does suggest that CD4+ TEMRA may not induce mTOR phosphorylation as robustly in elderly patients.
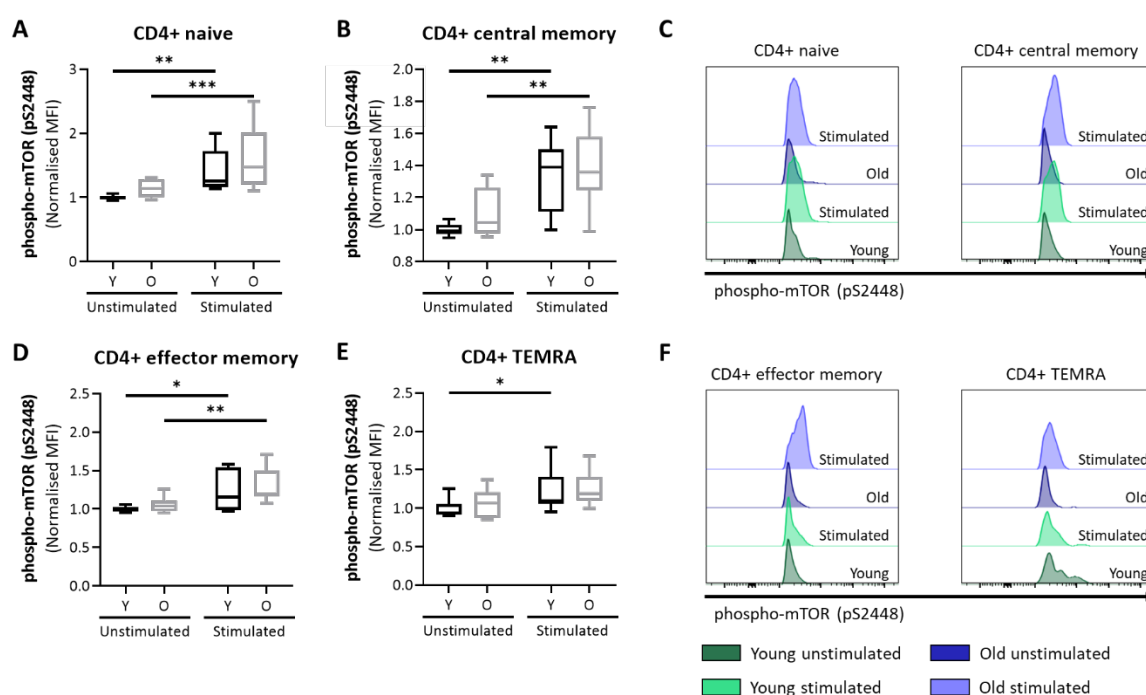
Figure 6.36   mTOR (pS2448) phosphorylation in CD4+ T cell subsets from young and old donors with PMA/Ionomycin stimulation showing (A) mTOR-pS2448 staining CD4+ naïve cells (B) mTOR-pS2448 staining in CD4+ central memory cells (C) Histogram of mTOR-pS2448 staining in CD4+ naïve and CD4+ central memory cells (D) mTOR-pS2448 staining in CD4+ effector memory cells (E) mTOR-pS2448 staining in CD4+ TEMRA cells and (F) Histogram of mTOR-pS2448 staining in CD4+ effector memory and CD4+ TEMRA cells normalised to young unstimulated control cells (Y=young donor, O=old donor) (Box and whisker plot; n=10; Two-way mixed-model ANOVA; *p<0.05 **p<0.01 ***p<0.001)

Measurement of mTOR S2448 phosphorylation was also performed within CD8+ T cells. A significant increase in mTOR phosphorylation was observed in CD8+ naïve T cells from young and old donors (Figure 6.37A-C). This cell type saw a 39% increase in mTOR phosphorylation in young donors (p<0.001) and a 27% increase in old donors (p<0.001). Increases in mTOR phosphorylation

following stimulation were also seen in young and old donors in CD8+ central memory cells (36% for young p=0.004 and 31% for old p=0.004). However, significant increases in mTOR phosphorylation were not observed in CD8+ effector memory cells from either young or old donors with PMA/Ionomycin treatment (Figure 6.37D and F). A significant increase in mTOR phosphorylation was observed within CD8+ TEMRA from young donors however, which showed a 1.2-fold increase in pS2448 staining (p=0.015; Figure 6.37E and F). On the other hand, CD8+ TEMRA from old donors did not show any increase following stimulation (p=0.887). Whilst this did not result in a significant difference between mTOR phosphorylation in young and old donors following stimulation, this does suggest that CD8+ TEMRA may not be able to induce mTOR phosphorylation as robustly in elderly patients.
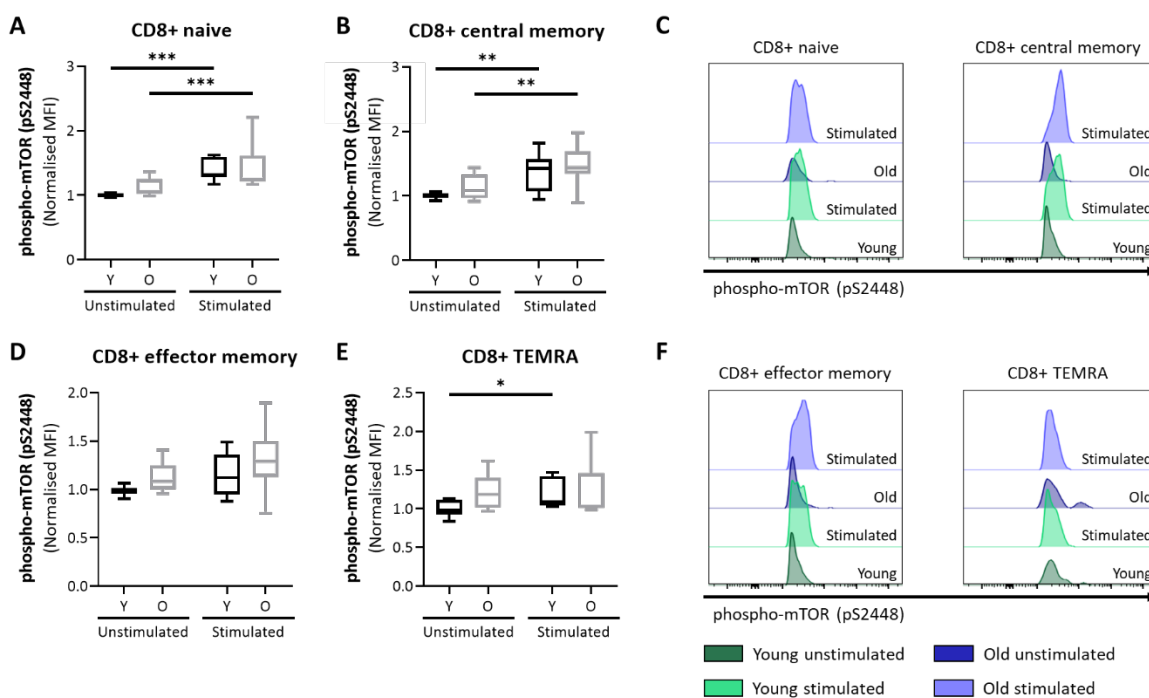
Figure 6.37 mTOR (pS2448) phosphorylation in CD8+ T cell subsets from young and old donors with PMA/Ionomycin stimulation showing (A) mTOR-pS2448 staining CD8+ naïve cells (B) mTOR-pS2448 staining in CD8+ central memory cells (C) Histogram of mTOR-pS2448 staining in CD8+ naïve and CD8+ central memory cells (D) mTOR-pS2448 staining in CD8+ effector memory cells (E) mTOR-pS2448 staining in CD8+ TEMRA cells and (F) Histogram of mTOR-pS2448 staining in CD8+ effector memory and CD8+ TEMRA cells normalised to young unstimulated control cells (Y=young donor, O=old donor) (Box and whisker plot; n=10; Two-way mixed-model ANOVA; *p<0.05 **p<0.01 ***p<0.001)

Surprisingly, despite changes in other mitochondrial and metabolic parameters with stimulation, no changes in mTOR phosphorylation were observed within NK cells. All three subsets studied: cytotoxic, inflammatory and regulatory did not increase or decreased phosphorylation of mTOR

S2448 following PMA/Ionomycin treatment (Figure 6.38A-F). Interestingly, no differences between the phosphorylation status of mTOR were seen between young and old donors either prior to or following stimulation. Therefore, these results suggest that mTOR phosphorylation is not altered in NK cells with age.
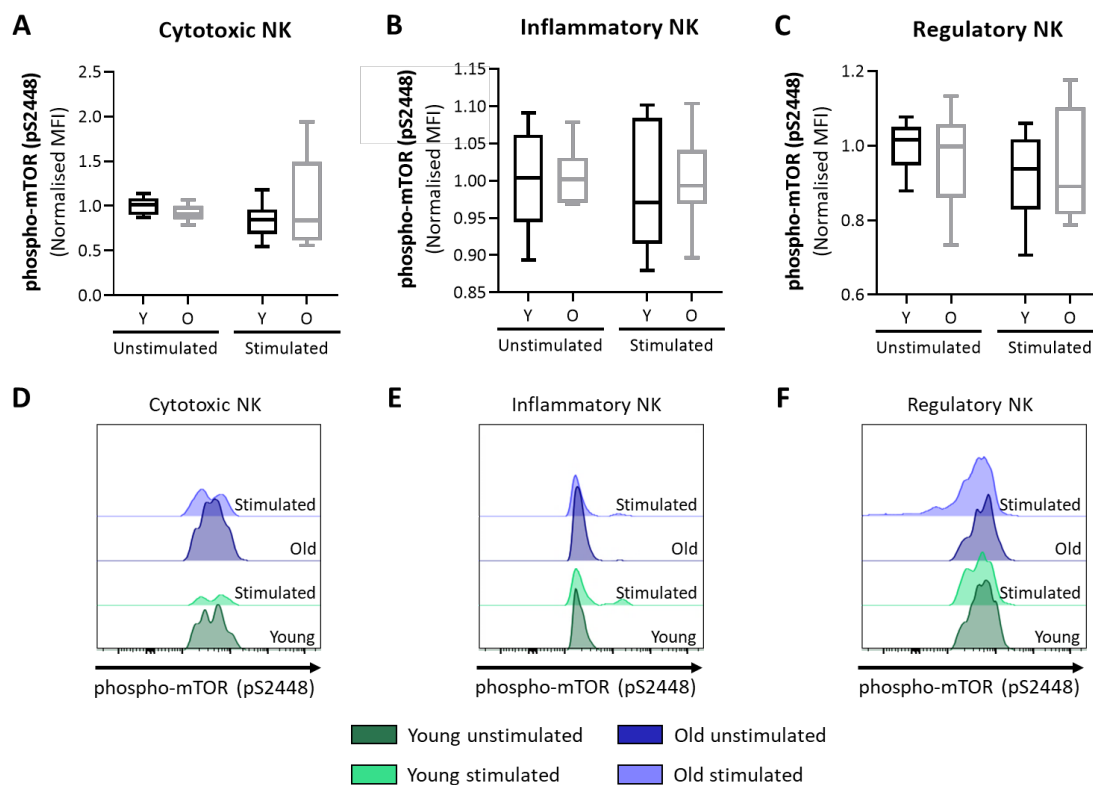
Figure 6.38 mTOR (pS2448) phosphorylation in NK cell subsets from young and old donors with PMA/Ionomycin stimulation showing mTOR-pS2448 staining in (A) cytotoxic (B) inflammatory and (C) regulatory NK cells normalised to young unstimulated control cells and histograms of mTOR-pS2448 staining in (D) cytotoxic (E) inflammatory and (F) regulatory NK cells (Y=young donor, O=old donor) (Box and whisker plot; n=10; Two-way mixed-model ANOVA)

The phosphorylation status of mTOR was also studied within three monocytes subsets: classical, intermediate and non-classical. A significant increase in mTOR phosphorylation was observed in classical monocytes from young and old donors (Figure 6.39A and D). This cell type saw a 10% increase in mTOR phosphorylation in young donors (p=0.005) and an 8% increase in old donors (p=0.019). Increases in mTOR phosphorylation following stimulation were also seen in young and old donors in non-classical monocytes (50% for young p<0.001 and 27% for old p<0.001; Figure 6.40C and F). However, significant increases in mTOR phosphorylation were not observed in intermediate monocytes from either young or old donors with PMA/Ionomycin treatment (Figure 6.39B and E). Whilst the control of mTOR phosphorylation is clearly regulated differently between the three monocyte subsets, age did not have any effect on this control.
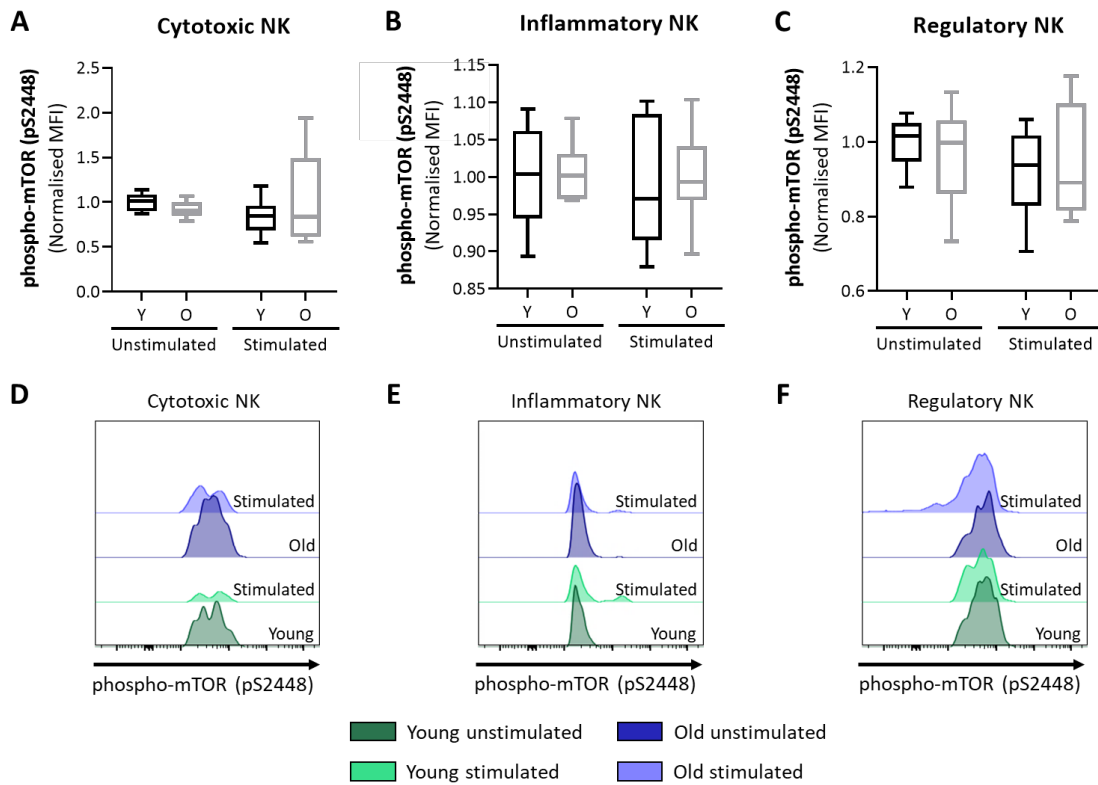
Figure 6.39 mTOR (pS2448) phosphorylation in monocyte subsets from young and old donors with PMA/Ionomycin stimulation showing mTOR-pS2448 staining in (A) classical (B) intermediate and (C) non-classical monocytes normalised to young unstimulated control cells and histograms of mTOR-pS2448 staining in (D) classical (E) intermediate and (F) non-classical monocytes (Y=young donor, O=old donor) (Box and whisker plot; n=10; Two-way mixed-model ANOVA; *p<0.05 **p<0.01 ***p<0.001)

Within CD141+ dendritic cells, mTOR S2448 phosphorylation was increased following stimulation in both young and old donors. Whilst young donors increased phosphorylation by 60% (p=0.004), old donors increased mTOR phosphorylation by 52% (p=0.009; Figure 6.40A and C). A significant increase in mTOR phosphorylation was also observed within CD1c+ dendritic cells from young donors, which showed a 1.2-fold increase in pS2448 staining (p=0.027; Figure 6.40B and D). Whilst a trend towards increased mTOR phosphorylation was observed in CD1c+ dendritic cells from old donors, this was found to be insignificant (p=0.062; Figure 6.40B and D). Whilst this did not result in a significant difference between mTOR phosphorylation in young and old donors following stimulation within this cell type, this finding does suggest that CD1c+ dendritic cells may not induce mTOR phosphorylation as robustly in old donors.
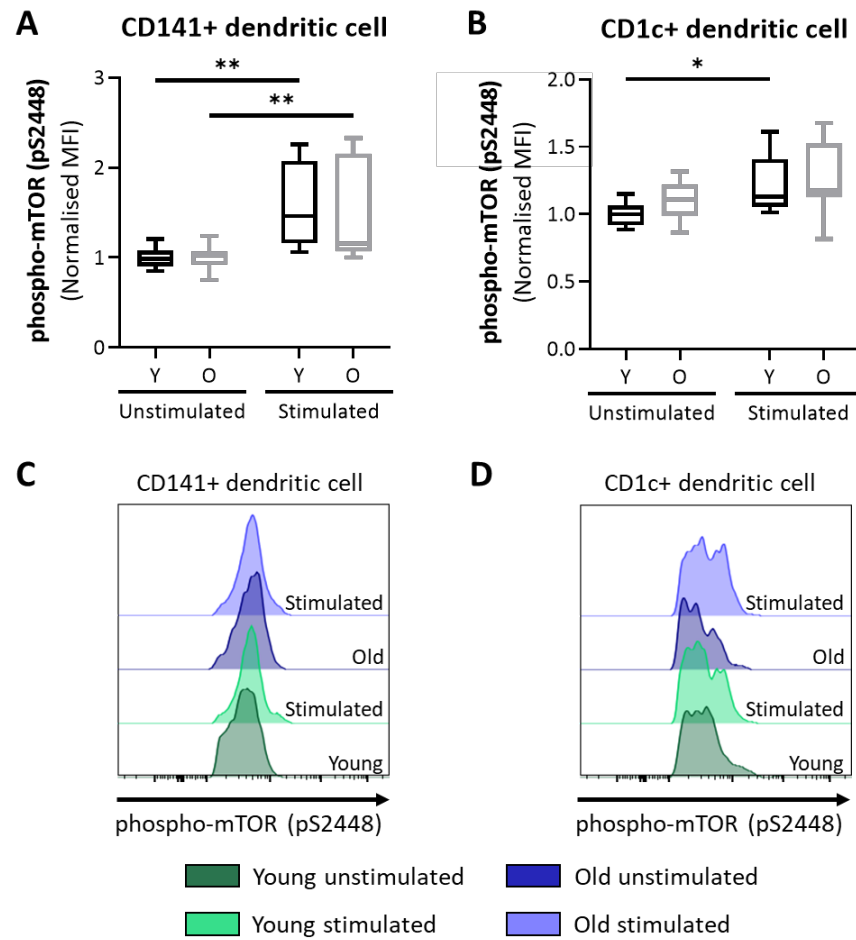
Figure 6.40 mTOR (pS2448) phosphorylation in dendritic cell subsets from young and old donors with PMA/Ionomycin stimulation showing mTOR-pS2448 staining in (A) CD141+ and (B) CD1c+ dendritic cells normalised to young unstimulated control cells and histograms of mTOR-pS2448 staining in (C) CD141+ and (D) CD1c+ dendritic cells (Y=young donor, O=old donor) (Box and whisker plot; n=10; Two-way mixed-model ANOVA; *p<0.05 **p<0.01)

6.4 Discussion: Mitochondrial structure and metabolic efficiency in the periphery of ageing humans

A significant decrease in mTOR phosphorylation has previously been observed in PBMCs from old donors (Rubie et al., 2016), whilst mTOR mRNA levels remained stable. This finding was found to be related to upregulation of miR-496 with age which interacts with the 3'UTR region of mTOR mRNA (Rubie et al., 2016). Although mitochondrial bioenergetics have yet to be studied in PBMCs from young and old donors elsewhere, previous studies have suggested that bioenergetics are reduced with age-related factors. For example, Tyrrell *et al.* reported that PBMC mitochondrial bioenergetics were correlated with grip strength and gait speed which are often used as markers of frailty (Tyrrell et al., 2015a, Tyrrell et al., 2015b). Individuals with a lower grip strength and gait speed showed reduced spare respiratory capacity, maximal respiration and basal respiration. Additionally, IL-6 levels were found to inversely correlated with these metabolic parameters (Tyrrell et al., 2015b). Due to the relationships between age, frailty and inflammation this suggests that mitochondria may have reduced bioenergetic capacity with age.

Taken together these findings suggest that mitochondrial bioenergetics may be reduced with age. Therefore, the metabolism of PBMCs within this cohort was tested both prior to and following PMA/Ionomycin stimulation. It was found that PBMCs display reduced maximal respiratory capacity with age. This ties in with previous observations of reduced mitochondrial function with ageing in skeletal muscle (Short et al., 2005, Hiona et al., 2010, Waters et al., 2003) and heart (Gong et al., 2003, Hill et al., 2009). Gene set enrichment analysis of monocytes and T cells previously found 61 mitochondrial and oxidative phosphorylation genes to be negatively regulated with age (Reynolds et al., 2015). A similar trend was also observed with age in the skeletal muscle of rhesus monkeys (Kayo et al., 2001), alongside the upregulation of inflammatory and oxidative stress transcripts. Reduced mitochondrial respiration has also been observed in age-related diseases, including: type 2 diabetes (Avila et al., 2012, Larsen et al., 2011, Hartman et al., 2014), congestive heart failure (Gong et al., 2003) and sarcopenia (Hiona et al., 2010). Although the implications of reduced mitochondrial capacity are unknown, research has suggested that bioenergetic failure may play a role in the pathogenesis of sepsis (Japiassu et al., 2011) and may affect responses to other infections in the elderly.

Alongside these results showing no changes in basal glycolytic and oxidative metabolism with age, no significant defects were observed in ATP production from PBMCs in old donors. Analysis of ATP production in Fischer-344 rats *in vivo* also showed no changes in ATP content or ATP production with age in brain and liver, mirroring the results from this study (Drew and Leeuwenburgh, 2003). However, previous reports have noted that ATP-producing capacity is reduced by 8% per decade in

human skeletal muscle, although this only occurs alongside reductions in muscle oxidative capacity (Short et al., 2005). Other research has suggested that this finding is applicable to some muscles *in vivo*, such as the first dorsal interosseus but not the tibialis anterior muscle (Amara et al., 2007). This suggests that whilst limitations in ATP production are observed in some muscles with age, the same phenomenon does not occur within the PBMC compartment.

Following stimulation, a significant increase in glucose uptake by PBMCs from old donors was observed, whereas glucose uptake from young donors remained unchanged. Typically, human ageing is characterised by loss of glycolytic metabolism in brain tissue as measured by positron-emission tomography (Goyal et al., 2017). On the other hand, elderly subjects show increased glucose uptake into muscles during walking (Shimada et al., 2009). This suggests that changes in glucose-uptake with age are tissue-specific and would suggest that PBMCs show alterations in glucose uptake with age which manifests during immune cell stimulation. In order to test which immune cells are subject to these changes, the expression of Glut1 in different populations was anlysed. Through this changes in the surface expression of Glut1 in CD4+ effector memory and CD8+ effector memory T cells were observed. Whilst Glut1 expression was decreased following six hours of PMA/Ionomycin stimulation in young donors, expression remained unchanged in old donors. This maintenance of Glut1 expression may aid in explaining the increased glucose uptake observed in PBMCs from old donors following stimulation. Similarly, in ageing-related lung fibrosis Glut1-dependent glycolysis is increased in both humans and mice through an AMPK-dependent mechanism (Cho et al., 2017).

As discussed in Chapter 1, there is conflicting evidence over whether ROS production increases with age. Within this study it was found that H_2O_2 production does not differ with age in PBMCs, but PBMCs from old donors induce H_2O_2 production during stimulation whereas those from young donors do not. Within immune cells, ROS play an integral role in macrophage polarisation, T and B cell activation and Nod-like receptor family pyrin domain containing 3 (NLRP3) inflammasome activation (Angajala et al., 2018, Yang et al., 2013). Surprisingly, PBMCs from old donors did not show increased IFNγ production at baseline. This suggests that PBMCs are not responsible for increased serum IFNγ levels observed in other studies. However, the production of IFNγ from PBMCs has scarcely been studied within the context of ageing. Studies which have tested PBMCs report increased IFNγ production from T cells with age, but this effect is gender specific and only reported within females (Pietschmann et al., 2003). Therefore, the results of this study may be confounded by this issue and the fact that different immune cells express different pro-inflammatory factors. For example, monocytes express IL-6 and TNF-α whilst T cells express IFNγ and IL-10 and as a result changes in IFNγ may be lost when studying whole PBMC cultures. Previous

studies have noted that cytokine release from monocytes does not differ with age prior to or following LPS stimulation (Seidler et al., 2010).

Next, any changes in immune cell compartmentalisation which may be contributing to these results were assessed. The proportion of CD4+ and CD8+ T cells, NK cell, monocytes and dendritic cells were measured by flow cytometry. Loss of CD28 expression with age has been well documented within both CD4+ and CD8+ T cells (Czesnikiewicz-Guzik et al., 2008). A significant decrease in the number of naïve CD4+ and CD8+ T cells has previously been observed with age, in line with decreased CD28 expression (Czesnikiewicz-Guzik et al., 2008). This trend is mirrored within this cohort, despite recent research suggesting that naïve T cells may be able to increase their ability to persist in the circulation with age (Rane et al., 2018). Whilst Czesnikiewicz-Guzik *et al.* and Koch *et al.* reported no alterations in the number of CD4+ CM, EM and TEMRA cells with age, a significant decrease in the percentage of CD4+ TEMRA cells was observed (Czesnikiewicz-Guzik et al., 2008, Koch et al., 2008). Trends towards a reduction in the percentage of CD4+ TEMRA with age have been described within other tissues, such as lung and mesenteric lymph node (Thome et al., 2014). This is one of the first reports of reduced CD4+ TEMRA cell frequency in blood with age.

CD8+ T cells are also subject to alterations in compartmentalisation with age. An increase in the proportion of CD8+ TEMRA cells was observed with age in line with other reports (Thome et al., 2014, Koch et al., 2008, Czesnikiewicz-Guzik et al., 2008). Surprisingly, despite observing an increase in the proportion of CD8+ CM with age, other studies have suggested that their numbers may in fact decrease or remain stable (Czesnikiewicz-Guzik et al., 2008, Koch et al., 2008). This effect may be due to increased rates of apoptosis within these cells with age (Gupta and Gollapudi, 2008). These reasons for an increased proportion of CD8+ CM within this cohort are unknown, however Thome *et al.* also found a small but insignificant correlation between increased CD8+ CM numbers and age (Thome et al., 2014).

Previous research within the Pender group has suggested that the proportion of NK cells is altered with age. Specifically, decreases in the percentage of regulatory NK cells and the expansion of inflammatory NK cells was detected (Martelli, 2017). Whilst a significant decrease in the percentage of regulatory NK cells was not observed, this cohort reflected the increase in inflammatory NK percentage observed previously. Increases in the percentage and absolute number of CD56dim cells have been reported previously by Boreggo *et al.* and further support this data (Borrego et al., 1999).

A significant increase in the proportion of classical monocytes was observed with age within this cohort. Whilst other data has revealed significant increases in the percentage of both classical and intermediate monocytes (Nyugen et al., 2010), an increase was only observed in the percentage of classical monocytes. No change in the proportion of non-classical monocytes was seen within this

study or that of Nyugen *et al.* in 2010 (Nyugen et al., 2010). Hearps *et al.* have previously reported an inverse trend in the distribution of monocytes with age. They reported an increase in the percentage of non-classical and intermediate monocytes and a decrease in the number of classical monocytes (Hearps et al., 2012). However, studies within mice have supported an increase in the classical monocyte population with age (Strohacker et al., 2012).

Previous research has suggested that the total number of myeloid DCs (CD141+ and CD1c+) present in the blood is not altered with age (Agrawal et al., 2007, Jing et al., 2009). However, data taken from studies on DC compartmentalisation are conflicting. In 2016, Agrawal *et al.* reported that CD141+ dendritic cells are lost with age and CD1c+ numbers remain stable, whilst Metcalf *et al.* reported no change in the percentage of CD141+ and CD1c+ DCs (Metcalf et al., 2015, Agrawal et al., 2016). The data in this study supports the findings of Metcalf *et al.* whereby both CD141+ and CD1c+ DC compartmentalisation is not altered with age.

Changes in immune cell function with age have been known for some time. However, studies investigating immunometabolic changes in line with ageing are lacking. Here, one of the first studies investing mitochondrial function in ageing immune cells is presented. Lymphocytes from elderly subjects have previously been found to exist in an activated state (Le Page et al., 2018). This involves increased basal lymphocyte-specific protein tyrosine kinase (Lck) and Src homology region 2 domain-containing phosphatase-1 (SHP-1) phosphorylation within both CD4+ and CD8+ T cells, which are usually phosphorylated downstream of TCR/CD28 activation. Le Page *et al.* revealed a basal upregulation in mTOR S2448 phosphorylation in naïve, EM and TEMRA CD4+ and naïve, CM and EM CD8+ T cells (Le Page et al., 2018). An age-related decline in Janus kinase (JAK)- signal transducer and activator of transcription (STAT) pathway signalling has also been reported in T cells (Longo et al., 2014). Increased mitochondrial mass in all CD4+ and CD8+ T cell subsets was observed with age, all well as subset specific alterations in mitochondrial membrane potential and Mfn2, Opa1, Glut1 and phospho-mTOR responses to stimulation. Mitochondrial biogenesis occurs during T cell stimulation and increases glucose uptake through metabolic reprograming (Ron-Harel et al., 2016). This re-capitulates the mitochondrial state observed within these donors, although increased Glut1 expression was not observed. Ron-Harel *et al.* also observed increased spare respiratory capacity and maximal respiration following stimulation (Ron-Harel et al., 2016), whilst reduced maximal respiration was observed within this cohort with age. This may suggest that whilst mitochondrial mass is increased, these mitochondria may not work as well within old donors. Subset specific alterations in mitochondrial fission/fusion dynamics, Glut1 expression and mTOR phosphorylation following stimulation may also suggest further alterations in the metabolism of T cells in the elderly. These findings aid in understanding deficient T cell responses to influenza, vaccination and cancer in the elderly (Scharping et al., 2016). Mitochondrial mass has also been

shown to support cytokine production during stimulation (Fischer et al., 2018). The increased mitochondrial mass in T lymphocytes with age may be involved in maintaining their activated state in the elderly. The changes are similar to those seen during HIV infection, which has been shown to recapitulate T cell ageing (Yu et al., 2017, Pathai et al., 2014).

Previous research has revealed that NK cell proliferation declines with age (Gounder et al., 2018). Additionally, NK cell maturation and functionality has previously been shown to be affected by age within the Pender research group (Martelli, 2017). Whilst inflammatory NK cells showed no alterations in the mitochondrial markers measured within this study, increased mitochondrial mass was observed with age in cytotoxic and regulatory NK cells alongside alterations in the mitochondrial membrane potential response to stimulation. Changes in the regulation of Drp1, Mfn2 and Opa1 were also observed in response to stimulation in old donors. Certain aspects of metabolism are essential for NK cell functionality (Assmann et al., 2017, Loftus et al., 2018, Donnelly et al., 2014). It is interesting that metabolic control during ageing is only maintained in inflammatory NK cells, which increase in proportion with age, whilst cytotoxic and regulatory NK which are maintained and lost with age respectively show metabolic changes. Mature NK cells rely less on glucose metabolism whilst fatty acid oxidation (FAO) and aerobic metabolism are upregulated, in line with mTOR signalling (Marçais et al., 2014). Whilst no differences in mTOR S2448 phosphorylation were observed with age in NK cells, increases in mitochondrial mass in cytotoxic and regulatory NK cells were seen which may represent increased aerobic metabolism with age. No increases were observed in inflammatory NK cells which may reflect their immaturity with increasing age. Dysfunctional NK cell responses have previously been linked to chronic inflammation, decreased viral clearance and cancer (Oliviero et al., 2009, O'Shea et al., 2010, Gardiner, 2015, Donnelly et al., 2014).

Studies unveiling age-related changes in monocyte functionality have shown alterations. Whilst Metcalf *et al.* did not reveal any significant alterations prior to toll-like receptor (TLR)4/7/8 or retinoic acid-inducible gene I (RIG-I) stimulation, a reduction in the production of IFNα, IFNγ. IL-1β, CC chemokine ligand (CCL)20 and CCL8 was observed following activation in cells from elderly donors (Metcalf et al., 2017). Ageing has previously been shown to reduce mitochondrial respiratory capacity in classical monocytes (Pence and Yarbro, 2018). Using seahorse analysis, classical monocytes showed changes in oxidative and glycolytic metabolism like those observed within this study; reduced maximal respiration and unchanged ECAR profiles. Alterations in the regulation of mitochondrial mass, membrane potential and Drp1, Mfn2 and Opa1 expression in response to stimulation were observed within intermediate monocytes. Changes in mitochondrial membrane responses and mitochondrial dynamics were also observed in classical and non-classical monocytes, which may be responsible for the reduced maximal respiration rates observed in old

donors. These findings may aid in explaining the impaired phagocytosis and IFNγ production observed in aged monocytes (Hearps et al., 2012, Molony et al., 2017).

CD141+ DCs were observed to have reduced Glut1 expression with age and an altered Opa1 response to stimulation. CD1c+ DCs on the other hand, showed increased mitochondrial mass with age and altered mTOR S2448 phosphorylation response to stimulation. The production of pro-inflammatory markers from DCs from aged donors has been argued for some time. Whilst Lung *et al.* reported no difference in secretion between young and old donors in 2000, more recent reports have observed increased production of basal cytokines including IFNα, IL-6 and TNFα from DCs (Lung et al., 2000, Agrawal et al., 2009, Panda et al., 2010). These later studies also noted increased reactivity to self-antigens and poor immunisation responses in aged DCs (Agrawal et al., 2009, Panda et al., 2010). These alterations appeared to be due to basal nuclear factor kappa B (NF-κB) activation and altered TLR expression, respectively. These observations of increased mitochondrial mass in CD1c+ DCs and decreased Glut1 expression in CD141+ DCs may affect the function of DCs and immune responses in the elderly (Thwe et al., 2017).

6.4.1 Limitations

Whilst flow cytometry offers a good method for studying protein expression within rare cell populations, more experimentation should be undertaken to confirm the results from this analysis. Future should focus on performing western blot experiments and RNA sequencing to confirm the up- or down-regulation of proteins in the experimental groups used within this study. This would help to confirm this data at both the proteomic and genomic levels.

The samples used within this study were cryo-preserved prior to use due to timing issues when gathering samples from such many individuals. Often PBMCs from young donors were processed and stored separately to those isolated from old individuals which may increase the variability observed between groups. This effect was minimised wherever possible by standardising sample preparation reagents and storing samples within the same liquid nitrogen tanks. Cryo-preservation may also have affected the functionality of the immune cells studied here. Future research should focus on using freshly isolated PBMCs to conduct these experiments.

The results observed within this study may also be impacted by other age-related disease present within the older population. Whilst it is possible to recruit an entirely healthy of elderly individuals who have no evidence of medical intervention, this is beyond the scope of this study. Several chronic conditions are present within our cohort, such as hypertension, high cholesterol, frailty and diabetes. Whilst efforts were made to reduce the effect of these parameters on the results of this study, future research should improve on minimising these effects further. Additionally, the

utilisation of a longitudinal study design may also minimise the effects of age-related disease development as parameters can be compared within rather than between subjects.

6.5 Conclusion

A summary of the findings observed during ageing of the periphery is shown in Figure 6.41. In conclusion, this study showed that PBMCs derived from old donors have reduced rates of maximal oxidative respiration. This reduction in maximal respiration does not affect ATP production at baseline or following stimulation but may be related to increased glucose uptake following stimulation. Surprisingly ageing did not increase reactive oxygen species production, in the form of H_2O_2, or the production of IFNγ from these cells. However, in line with other studies, alteration in immune cell compartmentalisation were observed including a decreased proportion of naïve T cells and increased ratios of memory T cells, regulatory NK cells and non-classical monocytes. These changes appeared alongside increased mitochondrial mass in most immune cell subsets and alterations in mitochondrial membrane potential in CD4+ TEMRA and classical and non-classical monocytes. Changes in the expression of mitochondrial fission and fusion proteins, Drp1 and Mfn2 were also observed, alongside differences in Opa1 response to stimulation. Finally, effector memory T cells and CD141+ dendritic cells showed altered surface expression of Glut1, whilst TEMRA cells and CD1c+ dendritic cells showed reduced phosphorylation of mTOR S2448 following stimulation. Therefore, mitochondrial and metabolic control of PBMCs is altered with age.

Whilst it was shown that one aspect of oxidative metabolism, maximal respiration, was reduced with age this finding was not supported by additional alterations in glycolytic metabolism. However, PBMCs from old donors did show increased glucose uptake following stimulation. Through detailed analysis of PBMC immune cell subsets, changes in metabolic parameters occur in all five cell types studied: CD4+ and CD8+ T cells, NK cells, monocytes and dendritic cells. Contrary to the hypothesis these changes were not confined to T cells and NK cells.

MEASUREMENT	CD4+ T cell				CD8+ T cell				NK cell			Monocyte			DC	
	N	CM	EM	T	N	CM	EM	T	Cyt	Inf	Reg	Cla	Int	Non	CD141	CD1c
Number	↓	→	→	↓	↓	↑	→	↑	→	→	↑	→	→	↑	→	→
Mitochondrial mass	↑	↑	↑	↑	↑	↑	↑	↑	↑	→	↑	→	↓	→	→	↑
Membrane potential	→	↓	→	↑	→	→	→	→	→	→	↓	↓	↓	↑	→	→
Drp1	→	→	→	→	→	→	→	→	↑	→	→	→	↓	↓	→	→
Mfn2	→	→	→	→	→	→	→	↓	↑	→	↑	→	↑	↑	→	→
Opa1	→	→	→	→	→	→	↓	↑	↑	→	↑	→	↑	→	↓	→
Glut1	→	→	↑	→	→	→	↑	→	→	→	→	→	→	→	↓	→
mTOR phosphorylation	→	→	→	↓	→	→	→	↓	→	→	→	→	→	→	→	↓

Figure 6.41 Summary of findings in human PBMCs and circulating immune cells from young (<35 years) and old (>60 years) individuals detailing metabolic dysfunction at baseline and following immune cell stimulation with emphasis on age-related alterations in maximal respiration of PBMCs and mitochondrial mass in immune cell subsets (↑ = increase, ↓ = decrease, → = no change)

Chapter 7   Conclusions and perspective

7.1   General discussion and concluding remarks

In conclusion, this study identified a relationship between mitochondrial dysfunction and ageing of immune cells in four different murine and human models. Within C57BL/6J mice mitochondrial dysfunction was observed with ageing which was characterised by an increased presence of tubular cristae structure alongside reduced adenosine (ATP) production within bone marrow cells. Simultaneously alterations in mitochondrial structure in tissue inhibitor of matrix metalloproteinase 3 (Timp3) knock-out mice were observed in comparison to C57BL/6J mice alongside alterations in the glutathione anti-oxidation system with age in bone marrow. Analysis of immune cells in the spleen of these animals revealed alterations in mitochondrial mass and membrane potential which occur with age. These findings affected both the CD8+ and CD4+ T cell populations, as well as natural killer and dendritic cells.

The *Timp3*$^{-/-}$ mouse is useful for conducting ageing research as these animals exhibit a drastically reduced lifespan compared to wild-type mice. However, whilst the *Timp3*$^{-/-}$ mouse model does have a shortened lifespan, humans with reduced expression of the same gene do not exhibit this same phenomenon. This reduces the ability to translate the findings of this study to human ageing. Therefore, the following aspect of this study utilised the senescence-accelerated mouse prone (SAMP) model to study which factors may be at play during the ageing process. Rather than being attributed to one singular genetic mutation, the SAMP models are in-bred based on their characteristics of senescence. This means that a number of genetic and epigenetic alterations contribute to shortening their lifespan and increasing the development of disease with age. Therefore, the SAMP model would appear to better recapitulate the characteristics of human ageing and age-related disease development.

When analysing mitochondria and their function in C57BL/6J, SAMP6 and SAMP8 mouse strains, evidence of mitochondrial dysfunction was observed across the life course. SAMP8 mice appeared to show decreased oxidative metabolism within splenocytes whilst SAMP6 mice showed alterations in glycolytic metabolism of bone marrow cells. These changes lie in accordance with the phenotypic changes observed in these mice of immune cell dysfunction and osteoporosis respectively. Alterations in the mitochondrial mass and membrane potential of immune cells contained in the splenic and bone marrow compartments were observed. Decreased mitochondrial membrane potential was observed within eosinophils, neutrophils and monocytes resident within the bone marrow of SAMP6 mice.

Through using the *Timp3^{-/-}* and SAMP mouse models for ageing research, a number of similarities and differences in the ageing of the immune system were observed. A decrease in the mitochondrial mass within CD4+ and CD8+ T cells was observed for both C57BL/6J mice bred in Southampton and Singapore. This suggests that dysregulation of the immune system with age is prevalent in C57BL/6J regardless of their environment. Similarly, this trend was observed in SAMP mice but not *Timp3^{-/-}* mice, suggesting that these models are subject to differences in immune system ageing in line with their different genetic backgrounds. Within the bone marrow, SAMP8 mice were shown to have increased ATP production compared to C57BL/6J mice similar to that observed for bone marrow cells obtained from *Timp3^{-/-}* mice. In SAMP8 mice this finding correlated with increased ATP-linked respiration, whilst in *Timp3^{-/-}* mouse this was related to preservation of mitochondrial cristae structure.

In order to draw comparisons between immune cell ageing in murine and human models, CD4+ T cell subsets were first utilised as a model of ageing. This model tracked these CD4+ T cell subsets along the memory cell development pathway from naïve to central memory, effector memory and terminal effector memory T cell re-expressing CD45RA (TEMRA). Within this human model, differences in metabolism between TEMRA cells and other memory cell subsets were observed. TEMRA cells were designated as naïve-like in terms of their expression of mitochondrial fission and fusion proteins and memory-like in terms of their mitochondrial membrane potential and glucose transporter 1 expression. As with C57BL/6J mice, defective optic atrophy 1 (Opa1) signalling was observed within these cells which may alter their function.

The findings of mitochondrial dysfunction in T cells from murine samples and human donors are difficult to compare as mice do not have a TEMRA cell population. However, some common features were shared. Utilising TEMRA cells as a model of exhausted T cells a significant reduction in mitochondrial membrane potential was observed compared to the other memory T cell subtypes, suggesting that these cells may be exhausted and unable to act as efficiently as central and effector memory T cells. Similarly, a reduction in the expression of Opa1 was observed within these cells, reminiscent of the reduction of Opa1 expression observed in C57BL/6J bone marrow cells with age. Loss of Opa1 may have affected the mitochondrial membrane potential within these cells, as was observed for CD4+ T cells in the spleen of *Timp3^{-/-}* mice. This finding did not extend to the oxygen consumption and extracellular acidification rates of these cells despite findings of reduced oxygen consumption of splenic cells in SAMP6 mice. However, the use of CD4+ TEMRA cells as model of immune cell ageing is somewhat flawed as this study did not take into account the age of the subject and these cells show both naïve- and memory-like properties. Therefore, this aspect of the study was followed by analysis of immune cell metabolism in the blood of young and old human donors.

Finally, decreased rates of maximal respiration were observed within PBMCs derived from human donors over the age of 60 years. These changes were attributed to alterations in glucose uptake rates and altered immune cell compartmentalisation with age, involving increased percentages of memory T cell subsets and regulatory natural killer (NK) cells and non-classical monocytes. Increasing alterations in mitochondrial mass and membrane potential were observed within these cells, alongside dysregulation of mitochondrial parameters in old donors. This dysregulation involved the dynamin-related protein 1, mitofusin 2 and Opa1 mitochondrial fission and fusion proteins, whilst the expression of highly conserved proteins and processes such as Glut1 and mammalian target of rapamycin phosphorylation (mTOR-S2448) are not affected by ageing.

This final part of the study helped to draw together conclusions from each of the ageing models studied. There was a significant effect of age on maximal respiration in both human PBMCs and in immune cell-containing splenocytes from C57BL/6J and SAMP mouse strains. This finding within human and murine models of ageing would suggest that the maximal respiration of immune cells is decreased with age. However, whilst a significant increase in mitochondrial mass was observed in specific immune cell subsets with age in humans, the murine models used for this study often showed reduced mitochondrial mass with age in these same immune cells. This finding does correlate with the increased mitochondrial mass observed in memory CD4+ T cells compared to their naïve counterparts and may represent a shift in the immune cell repertoire. This is highlighted by the increased numbers of memory T cells and regulatory NK cells observed with age in this cohort with T cells and NK cells showing increased mitochondrial mass with age. In similarity to the other models, alterations in the expression of mitochondrial fission and fusion protein and Opa1 expression was observed in immune cells from old donors compared to their young counterparts, which may have affected the respiration of these cells.

Consulting the findings from the study, integrating both the SAMP mouse model and utilising human subjects would be beneficial for designing future studies involving ageing research. As discussed above the SAMP model is not created by a single genetic mutation and instead represents an in-bred strain with multiple genetic and epigenetic factors which contribute to the ageing process. This means that these mouse strains more closely recapitulate the ageing process observed in humans which is also based on a number of genetic, epigenetic and environmental factors. On the same note human subjects are best used for ageing research, although come with their own issues. The model used within this study utilises an unmatched design comparing the immune cell compartments in young and old donors. Future studies would benefit from integrating a matched and longitudinal study design where possible to minimise genetic and environmental effects. Whilst this is difficult to obtain a number of studies such as the Singapore Longitudinal Ageing Study have begun following participants over the course of several years in order to give

more insight into the biology of ageing and factors which influence the development of age-related disease.

A summary of findings from this study is shown in Figure 7.1. Overall, mitochondrial dysfunction in the immune system during ageing is attributed to alterations in mitochondrial mass and membrane potential as well as Opa1 expression within the murine and human models used within this study. Therefore, it is proposed that immune cell mitochondrial dysfunction is involved in the ageing process and excessive mitochondrial dysfunction may be associated with the shortened lifespan observed as a result of low-grade chronic inflammation and increased senescence in mice. Similarly accumulating mitochondrial dysfunction in human immune cells with age may contribute in part to increased susceptibility to infection and cancer development, alongside decreased responses to vaccination. These findings represent potential avenues for curtailing mitochondrial dysfunction in immune cells throughout the ageing process in order to minimise the development of age-related disease and promote healthy ageing.

Mouse			Human	
Wild-type	**Chronic inflammation**	**Senescence**	**T cell senescence**	**Ageing**
↑ tubular cristae ↓ ATP production of bone marrow cells	~ Mitochondrial structure ~ Glutathione anti-oxidation	↓ oxidative metabolism in spleen and bone marrow	Naïve-like expression of fission and fusion proteins	↓ maximal respiration ↑ glucose uptake ↑ ROS
~Opa1 signalling	↑ mitochondrial mass ↓ membrane potential of immune cells	~ mitochondrial mass and membrane potential of immune cells	Memory-like membrane potential and Glut1 expression ~Opa1 signalling	~ mitochondrial mass and membrane potential of immune cells

Figure 7.1   Summary of findings showing the appearance of mitochondrial dysfunction in the immune system of ageing mice and humans

7.2   Future directions

This is not the end of the road for analysis of mitochondrial dysfunction and immune-senescence in the context of ageing by far. Ageing is still a very complex issue which requires a wealth of future

work to unravel. The work conducted within this thesis identifies a number of areas in which future work could develop understanding even further:

- **How do alterations in immune cell mitochondrial dynamics affect their function?** It has been extensively described that both mitochondrial dysfunction and immune-senescence occur with age. Whilst this research examines the changes which occur in the regulation of metabolism and mitochondrial structure with age, how these changes relate to immune cell function was not studied. Future studies should look at what effects increased mitochondrial mass and decreases in mitochondrial membrane potential have on immune cells in both their resting and activated state. Whilst previous research has studied the role of metabolism in regulating immune cell function (reviewed in (Ganeshan and Chawla, 2014), the time has come to put this in the context of healthy ageing and age-related disease.

- **What mechanisms underly these metabolic alterations?** The descriptive work conducted within this thesis does not examine the mechanisms which underlie the development of metabolic dysfunction with age. Many theories have suggested that ROS species are involved in the development of mitochondrial dysfunction with age, however these results concerning increased ROS production from these cells were mixed. Therefore, future research should focus on how these metabolic alterations occur with age. For example, how does lack of *Timp3* decrease mitochondrial membrane potential and sustain tubular cristae structure with age whilst wild-type mice are not subject to these effects and live a longer life span. Why do EM and TEMRA cells experience a lack of Opa1 expression and what are the advantages/disadvantages for these cells.

- **How does the mitochondrial dysfunction-immunosenescence-ageing axis contribute to the development of age-related disease?** There is a wealth of research concerning the individual roles of mitochondrial dysfunction and immune-senescence in the development of age-related disease. However, research looking at the role of both these factors simultaneously is lacking. Evidence would point towards mitochondrial dysfunction causing immune cell dysfunction with age with results in the development of disease, however no research has linked these concepts to date. The work conducted within this thesis links mitochondrial dysfunction and immune cell dysfunction during ageing and highlights the need to look at this axis in the development of age-related disease. By studying these issues in concert, alongside other theories of ageing, researchers may be able to unravel the serious complexity which surrounds ageing research making the creation of evidence-based

strategies for improving healthy ageing difficult. It is proposed to first study aspects of mitochondrial and immune cell dysfunction in the context of reduced vaccine efficiency and increased susceptibility to infections as these processes have previously been linked.

Appendix A   Preliminary data of *Timp3⁻/⁻* (KO) mice
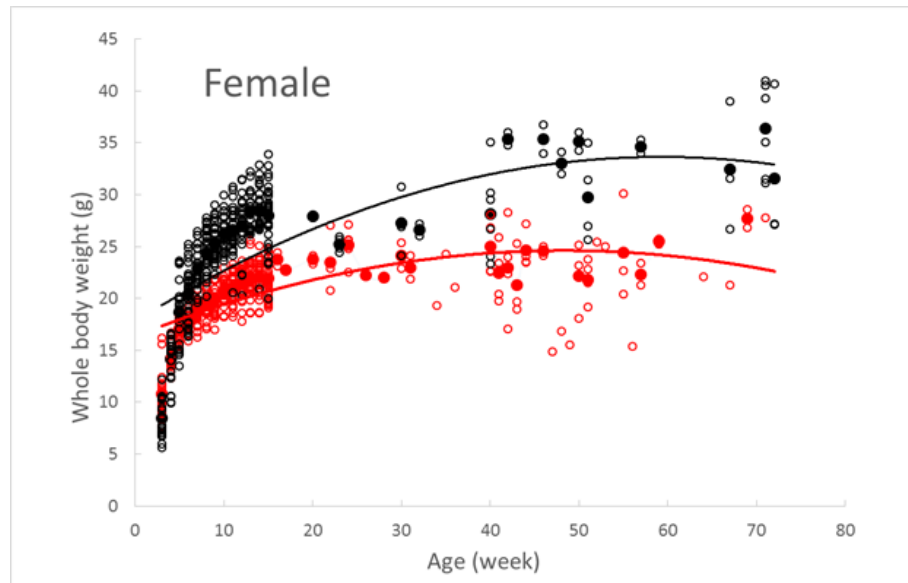
Figure A.1   Body weight analysis of female *Timp3⁻/⁻* and C57BL/6J mice from 3 weeks to 72 weeks of age (*Timp3⁻/⁻* = red; C57BL/6J= black)
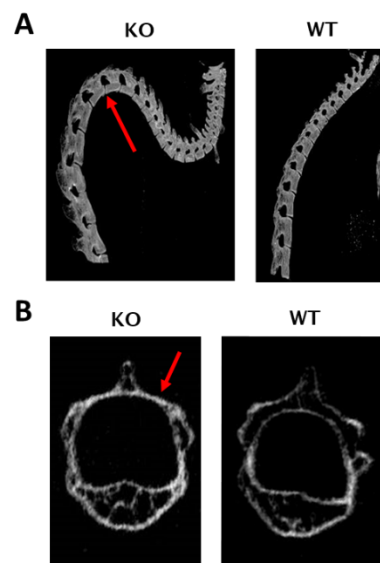
Figure A.2   Computed tomography (CT) scan of *Timp3⁻/⁻* (KO) and C57BL/6J (WT) mouse spine showing (A) spine curvature and (B) decreased bone density in KO mice compared to WT mice (red arrows point to regions of interest)

List of References

ABID, M. R. & SELLKE, F. W. 2016. Subcellular ROS Signaling in Cardiovascular Disease. *Free Radicals and Diseases.* InTech.

ABOU-SLEIMAN, P. M., MUQIT, M. M. K. & WOOD, N. W. 2006. Expanding insights of mitochondrial dysfunction in Parkinson's disease. *Nature Reviews Neuroscience,* 7**,** 207.

ACUTO, O. & MICHEL, F. 2003. CD28-mediated co-stimulation: a quantitative support for TCR signalling. *Nat Rev Immunol,* 3**,** 939-51.

AGE UK 2019. Breifing: Health and Care of Older People in England 2019.

AGIER, V., OLIVIERO, P., LAINÉ, J., L'HERMITTE-STEAD, C., GIRARD, S., FILLAUT, S., JARDEL, C., BOUILLAUD, F., BULTEAU, A. L. & LOMBÈS, A. 2012. Defective mitochondrial fusion, altered respiratory function, and distorted cristae structure in skin fibroblasts with heterozygous OPA1 mutations. *Biochimica et Biophysica Acta (BBA) - Molecular Basis of Disease,* 1822**,** 1570-1580.

AGRAWAL, A., AGRAWAL, S., CAO, J.-N., SU, H., OSANN, K. & GUPTA, S. 2007. Altered Innate Immune Functioning of Dendritic Cells in Elderly Humans: A Role of Phosphoinositide 3-Kinase-Signaling Pathway. *The Journal of Immunology,* 178**,** 6912.

AGRAWAL, A., AGRAWAL, S. & GUPTA, S. 2017. Role of Dendritic Cells in Inflammation and Loss of Tolerance in the Elderly. *Frontiers in Immunology,* 8.

AGRAWAL, A., TAY, J., TON, S., AGRAWAL, S. & GUPTA, S. 2009. Increased Reactivity of Dendritic Cells from Aged Subjects to Self-Antigen, the Human DNA. *The Journal of Immunology,* 182**,** 1138.

AGRAWAL, S., GANGULY, S., TRAN, A., SUNDARAM, P. & AGRAWAL, A. 2016. Retinoic acid treated human dendritic cells induce T regulatory cells via the expression of CD141 and GARP which is impaired with age. *Aging,* 8**,** 1223-1235.

AHMAD, F., SINGH, K., DAS, D., GOWAIKAR, R., SHAW, E., RAMACHANDRAN, A., RUPANAGUDI, K. V., KOMMADDI, R. P., BENNETT, D. A. & RAVINDRANATH, V. 2017. Reactive Oxygen Species-Mediated Loss of Synaptic Akt1 Signaling Leads to Deficient Activity-Dependent Protein Translation Early in Alzheimer's Disease. *Antioxidants & Redox Signaling,* 27**,** 1269-1280.

AIELLO, A., FARZANEH, F., CANDORE, G., CARUSO, C., DAVINELLI, S., GAMBINO, C. M., LIGOTTI, M. E., ZAREIAN, N. & ACCARDI, G. 2019. Immunosenescence and Its Hallmarks: How to Oppose Aging Strategically? A Review of Potential Options for Therapeutic Intervention. *Frontiers in Immunology,* 10.

AKIGUCHI, I., PALLÀS, M., BUDKA, H., AKIYAMA, H., UENO, M., HAN, J., YAGI, H., NISHIKAWA, T., CHIBA, Y. & SUGIYAMA, H. 2017. SAMP8 mice as a neuropathological model of accelerated brain aging and dementia: Toshio Takeda's legacy and future directions. *Neuropathology,* 37**,** 293-305.

AKKAYA, M., TRABA, J., ROESLER, A. S., MIOZZO, P., AKKAYA, B., THEALL, B. P., SOHN, H., PENA, M., SMELKINSON, M., KABAT, J., DAHLSTROM, E., DORWARD, D. W., SKINNER, J., SACK, M. N. & PIERCE, S. K. 2018. Second signals rescue B cells from activation-induced mitochondrial dysfunction and death. *Nat Immunol,* 19**,** 871-884.

List of References

AKRAM, M. 2014. Citric acid cycle and role of its intermediates in metabolism. *Cell Biochem Biophys,* 68**,** 475-8.

ALDER, J. K., CHEN, J. J.-L., LANCASTER, L., DANOFF, S., SU, S.-C., COGAN, J. D., VULTO, I., XIE, M., QI, X., TUDER, R. M., PHILLIPS, J. A., LANSDORP, P. M., LOYD, J. E. & ARMANIOS, M. Y. 2008. Short telomeres are a risk factor for idiopathic pulmonary fibrosis. *Proceedings of the National Academy of Sciences,* 105**,** 13051-13056.

ALLSOPP, R. C., VAZIRI, H., PATTERSON, C., GOLDSTEIN, S., YOUNGLAI, E. V., FUTCHER, A. B., GREIDER, C. W. & HARLEY, C. B. 1992. Telomere length predicts replicative capacity of human fibroblasts. *Proceedings of the National Academy of Sciences,* 89**,** 10114-10118.

ALONSO, J. R., CARDELLACH, F., CASADEMONT, J. & MIRÓ, Ò. 2004. Reversible inhibition of mitochondrial complex IV activity in PBMC following acute smoking. *European Respiratory Journal,* 23**,** 214.

ALVES-LOPES, R., NEVES, K. B., MONTEZANO, A. C., HARVEY, A., CARNEIRO, F. S., TOUYZ, R. M. & TOSTES, R. C. 2016. Internal Pudendal Artery Dysfunction in Diabetes Mellitus Is Mediated by NOX1-Derived ROS-, Nrf2-, and Rho Kinase–Dependent MechanismsNovelty and Significance. *Hypertension,* 68**,** 1056-1064.

AMARA, C. E., SHANKLAND, E. G., JUBRIAS, S. A., MARCINEK, D. J., KUSHMERICK, M. J. & CONLEY, K. E. 2007. Mild mitochondrial uncoupling impacts cellular aging in human muscles <em>in vivo</em&gt. *Proceedings of the National Academy of Sciences,* 104**,** 1057.

ANGAJALA, A., LIM, S., PHILLIPS, J. B., KIM, J.-H., YATES, C., YOU, Z. & TAN, M. 2018. Diverse Roles of Mitochondria in Immune Responses: Novel Insights Into Immuno-Metabolism. *Frontiers in immunology,* 9**,** 1605-1605.

ANISIMOV, V. N. 2003. Insulin/IGF-1 signaling pathway driving aging and cancer as a target for pharmacological intervention. *Experimental Gerontology,* 38**,** 1041-1049.

ARITA, M. 2016. Eosinophil polyunsaturated fatty acid metabolism and its potential control of inflammation and allergy. *Allergology International,* 65**,** 2-5.

ARKING, R., BUCK, S., BERRIOS, A., DWYER, S. & BAKER, G. T., 3RD 1991. Elevated paraquat resistance can be used as a bioassay for longevity in a genetically based long-lived strain of Drosophila. *Dev Genet,* 12**,** 362-70.

ARNOLD, L., HENRY, A., PORON, F., BABA-AMER, Y., VAN ROOIJEN, N., PLONQUET, A., GHERARDI, R. K. & CHAZAUD, B. 2007. Inflammatory monocytes recruited after skeletal muscle injury switch into antiinflammatory macrophages to support myogenesis. *J Exp Med,* 204**,** 1057-69.

ARNOULT, D., CARNEIRO, L., TATTOLI, I. & GIRARDIN, S. E. 2009. The role of mitochondria in cellular defense against microbial infection. *Semin Immunol,* 21**,** 223-32.

ARTIS, D. & SPITS, H. 2015. The biology of innate lymphoid cells. *Nature,* 517**,** 293-301.

ASSMANN, N., O'BRIEN, K. L., DONNELLY, R. P., DYCK, L., ZAIATZ-BITTENCOURT, V., LOFTUS, R. M., HEINRICH, P., OEFNER, P. J., LYNCH, L., GARDINER, C. M., DETTMER, K. & FINLAY, D. K. 2017. Srebp-controlled glucose metabolism is essential for NK cell functional responses. *Nat Immunol,* 18**,** 1197-1206.

AVILA, C., HUANG, R. J., STEVENS, M. V., APONTE, A. M., TRIPODI, D., KIM, K. Y. & SACK, M. N. 2012. Platelet mitochondrial dysfunction is evident in type 2 diabetes in association with

modifications of mitochondrial anti-oxidant stress proteins. *Exp Clin Endocrinol Diabetes,* 120**,** 248-51.

AW, D., SILVA, A. B. & PALMER, D. B. 2007. Immunosenescence: emerging challenges for an ageing population. *Immunology,* 120**,** 435-446.

AZEVEDO, E. P., ROCHAEL, N. C., GUIMARÃES-COSTA, A. B., DE SOUZA-VIEIRA, T. S., GANILHO, J., SARAIVA, E. M., PALHANO, F. L. & FOGUEL, D. 2015. A metabolic shift toward pentose phosphate pathway is necessary for amyloid fibril-and phorbol 12-myristate 13-acetate-induced neutrophil extracellular trap (NET) formation. *Journal of Biological Chemistry,* 290**,** 22174-22183.

AZUMA, K., ZHOU, Q. & KUBO, K.-Y. 2018. Morphological and molecular characterization of the senile osteoporosis in senescence-accelerated mouse prone 6 (SAMP6). *Medical molecular morphology,* 51**,** 139-146.

BAEK, J. H., SON, H., JEONG, Y.-H., PARK, S. W. & KIM, H. J. 2019. Chronological Aging Standard Curves of Telomere Length and Mitochondrial DNA Copy Number in Twelve Tissues of C57BL/6 Male Mouse. *Cells,* 8**,** 247.

BAINS, I., THIEBAUT, R., YATES, A. J. & CALLARD, R. 2009. Quantifying thymic export: combining models of naive T cell proliferation and TCR excision circle dynamics gives an explicit measure of thymic output. *J Immunol,* 183**,** 4329-36.

BALTES, P. B. & MAYER, K. U. 2001. *The Berlin aging study: Aging from 70 to 100*, Cambridge University Press.

BANCHEREAU, J., BRIERE, F., CAUX, C., DAVOUST, J., LEBECQUE, S., LIU, Y.-J., PULENDRAN, B. & PALUCKA, K. 2000. Immunobiology of dendritic cells. *Annual review of immunology,* 18**,** 767-811.

BARBER, D. L., WHERRY, E. J., MASOPUST, D., ZHU, B., ALLISON, J. P., SHARPE, A. H., FREEMAN, G. J. & AHMED, R. 2006. Restoring function in exhausted CD8 T cells during chronic viral infection. *Nature,* 439**,** 682-7.

BARQUISSAU, V., CAPEL, F., DARDEVET, D., FEILLET-COUDRAY, C., GALLINIER, A., CHAUVIN, M.-A., RIEUSSET, J. & MORIO, B. 2017. Reactive oxygen species enhance mitochondrial function, insulin sensitivity and glucose uptake in skeletal muscle of senescence accelerated prone mice SAMP8. *Free Radical Biology and Medicine,* 113**,** 267-279.

BASU, R., LEE, J., WANG, Z., PATEL, V. B., FAN, D., DAS, S. K., LIU, G. C., JOHN, R., SCHOLEY, J. W., OUDIT, G. Y. & KASSIRI, Z. 2012. Loss of TIMP3 selectively exacerbates diabetic nephropathy. *American Journal of Physiology-Renal Physiology,* 303**,** F1341-F1352.

BELI, E., DURIANCIK, D. M., CLINTHORNE, J. F., LEE, T., KIM, S. & GARDNER, E. M. 2014. Natural killer cell development and maturation in aged mice. *Mechanisms of ageing and development,* 135**,** 33-40.

BELL, B., ROSE, C. L. & DAMON, A. 1972. The Normative Aging Study: an interdisciplinary and longitudinal study of health and aging. *Aging and Human Development,* 3**,** 5-17.

BELLEZZA, I. 2018. Oxidative stress in age-related macular degeneration: Nrf2 as therapeutic target. *Frontiers in pharmacology,* 9**,** 1280.

BEN-ZVI, A., MILLER, E. A. & MORIMOTO, R. I. 2009. Collapse of proteostasis represents an early molecular event in Caenorhabditis elegans aging. *Proceedings of the National Academy of Sciences,* 106**,** 14914-14919.

List of References

BENGSCH, B., JOHNSON, A. L., KURACHI, M., ODORIZZI, P. M., PAUKEN, K. E., ATTANASIO, J., STELEKATI, E., MCLANE, L. M., PALEY, M. A., DELGOFFE, G. M. & WHERRY, E. J. 2016. Bioenergetic Insufficiencies Due to Metabolic Alterations Regulated by the Inhibitory Receptor PD-1 Are an Early Driver of CD8(+) T Cell Exhaustion. *Immunity,* 45**,** 358-73.

BERNARDES DE JESUS, B., VERA, E., SCHNEEBERGER, K., TEJERA, A. M., AYUSO, E., BOSCH, F. & BLASCO, M. A. 2012. Telomerase gene therapy in adult and old mice delays aging and increases longevity without increasing cancer. *EMBO Molecular Medicine,* 4**,** 691-704.

BERRYMAN, D. E., CHRISTIANSEN, J. S., JOHANNSSON, G., THORNER, M. O. & KOPCHICK, J. J. 2008. Role of the GH/IGF-1 axis in lifespan and healthspan: Lessons from animal models. *Growth Hormone & IGF Research,* 18**,** 455-471.

BIRCH, J., BARNES, P. J. & PASSOS, J. F. 2018. Mitochondria, telomeres and cell senescence: implications for lung ageing and disease. *Pharmacology & therapeutics,* 183**,** 34-49.

BISCHOFF, C., PETERSEN, H. C., GRAAKJAER, J., ANDERSEN-RANBERG, K., VAUPEL, J. W., BOHR, V. A., KØLVRAA, S. & CHRISTENSEN, K. 2006. No Association Between Telomere Length and Survival Among the Elderly and Oldest Old. *Epidemiology,* 17**,** 190-194.

BLACKBURN, S. D., SHIN, H., HAINING, W. N., ZOU, T., WORKMAN, C. J., POLLEY, A., BETTS, M. R., FREEMAN, G. J., VIGNALI, D. A. & WHERRY, E. J. 2009. Coregulation of CD8+ T cell exhaustion by multiple inhibitory receptors during chronic viral infection. *Nat Immunol,* 10**,** 29-37.

BLANCO, E., PEREZ-ANDRES, M., ARRIBA-MENDEZ, S., CONTRERAS-SANFELICIANO, T., CRIADO, I., PELAK, O., SERRA-CAETANO, A., ROMERO, A., PUIG, N., REMESAL, A., TORRES CANIZALES, J., LOPEZ-GRANADOS, E., KALINA, T., SOUSA, A. E., VAN ZELM, M., VAN DER BURG, M., VAN DONGEN, J. J. M. & ORFAO, A. 2018. Age-associated distribution of normal B-cell and plasma cell subsets in peripheral blood. *J Allergy Clin Immunol,* 141**,** 2208-2219.e16.

BOCHNER, B. S., MCKELVEY, A. A., STERBINSKY, S. A., HILDRETH, J., DERSE, C. P., KLUNK, D. A., LICHTENSTEIN, L. M. & SCHLEIMER, R. P. 1990. IL-3 augments adhesiveness for endothelium and CD11b expression in human basophils but not neutrophils. *The Journal of Immunology,* 145**,** 1832-1837.

BOOIMAN, T., WIT, F. W., GIRIGORIE, A. F., MAURER, I., DE FRANCESCO, D., SABIN, C. A., HARSKAMP, A. M., PRINS, M., FRANCESCHI, C., DEEKS, S. G., WINSTON, A., REISS, P. & KOOTSTRA, N. A. 2017. Terminal differentiation of T cells is strongly associated with CMV infection and increased in HIV-positive individuals on ART and lifestyle matched controls. *PLoS One,* 12**,** e0183357.

BORREGO, F., ALONSO, M. C., GALIANI, M. D., CARRACEDO, J., RAMIREZ, R., OSTOS, B., PEÑA, J. & SOLANA, R. 1999. NK phenotypic markers and IL2 response in NK cells from elderly people. *Experimental Gerontology,* 34**,** 253-265.

BOSCO, D. A., LAVOIE, M. J., PETSKO, G. A. & RINGE, D. 2011. Proteostasis and Movement Disorders: Parkinson's Disease and Amyotrophic Lateral Sclerosis. *Cold Spring Harbor Perspectives in Biology,* 3.

BOUSQUET, P. A., MELTZER, S., SØNSTEVOLD, L., ESBENSEN, Y., LYCKANDER, L. G., DUELAND, S., FLATMARK, K., REDALEN, K. R., EIDE, L. & REE, A. H. 2017. Reactive oxygen species (ROS) and mitochondrial DNA (mtDNA) damage in tumor hypoxia, poor radiotherapy response, and metastatic progression of rectal cancer. AACR.

BOYLE, M., WONG, C., ROCHA, M. & JONES, D. L. 2007. Decline in Self-Renewal Factors Contributes to Aging of the Stem Cell Niche in the Drosophila Testis. *Cell Stem Cell,* 1**,** 470-478.

BRADLEY, B. A. 2002. Rejection and recipient age. *Transplant Immunology,* 10**,** 125-132.

BRENNER, S. 1974. The genetics of Caenorhabditis elegans. *Genetics,* 77**,** 71-94.

BRICEÑO, O., LISSINA, A., WANKE, K., AFONSO, G., VON BRAUN, A., RAGON, K., MIQUEL, T., GOSTICK, E., PAPAGNO, L. & STIASNY, K. 2016. Reduced naïve CD 8+ T-cell priming efficacy in elderly adults. *Aging Cell,* 15**,** 14-21.

BRUUNSGAARD, H., LADELUND, S., PEDERSEN, A. N., SCHROLL, M., JØRGENSEN, T. & PEDERSEN, B. 2003. Predicting death from tumour necrosis factor-alpha and interleukin-6 in 80-year-old people. *Clinical & Experimental Immunology,* 132**,** 24-31.

BUCK, MICHAEL D., O'SULLIVAN, D., KLEIN GELTINK, RAMON I., CURTIS, JONATHAN D., CHANG, C.-H., SANIN, DAVID E., QIU, J., KRETZ, O., BRAAS, D., VAN DER WINDT, GERRITJE J. W., CHEN, Q., HUANG, STANLEY C.-C., O'NEILL, CHRISTINA M., EDELSON, BRIAN T., PEARCE, EDWARD J., SESAKI, H., HUBER, TOBIAS B., RAMBOLD, ANGELIKA S. & PEARCE, ERIKA L. 2016. Mitochondrial Dynamics Controls T Cell Fate through Metabolic Programming. *Cell,* 166**,** 63-76.

BULTERIJS, S., HULL, R. S., BJÖRK, V. C. E. & ROY, A. G. 2015. It is time to classify biological aging as a disease. *Frontiers in genetics,* 6**,** 205-205.

BURD, C. E., JECK, W. R., LIU, Y., SANOFF, H. K., WANG, Z. & SHARPLESS, N. E. 2010. Expression of Linear and Novel Circular Forms of an INK4/ARF-Associated Non-Coding RNA Correlates with Atherosclerosis Risk. *PLOS Genetics,* 6**,** e1001233.

BUSSE, P. J., BIRMINGHAM, J. M., CALATRONI, A., MANZI, J., GORYACHOKOVSKY, A., FONTELA, G., FEDERMAN, A. D. & WISNIVESKY, J. P. 2017. Effect of aging on sputum inflammation and asthma control. *Journal of Allergy and Clinical Immunology,* 139**,** 1808-1818.e6.

BUSSE, P. J. & MATHUR, S. K. 2010. Age-related changes in immune function: effect on airway inflammation. *J Allergy Clin Immunol,* 126**,** 690-9; quiz 700-1.

CAHU, J., BUSTANY, S. & SOLA, B. 2012. Senescence-associated secretory phenotype favors the emergence of cancer stem-like cells. *Cell Death &Amp; Disease,* 3**,** e446.

CALLENDER, L. A., CARROLL, E. C., BOBER, E. A., AKBAR, A. N., SOLITO, E. & HENSON, S. M. 2019. Mitochondrial mass governs the extent of T cell senescence. *bioRxiv***,** 627240.

CAMPOLO, M., CASILI, G., BIUNDO, F., CRUPI, R., CORDARO, M., CUZZOCREA, S. & ESPOSITO, E. 2016. The Neuroprotective Effect of Dimethyl Fumarate in an MPTP-Mouse Model of Parkinson's Disease: Involvement of Reactive Oxygen Species/Nuclear Factor-κB/Nuclear Transcription Factor Related to NF-E2. *Antioxidants & Redox Signaling,* 27**,** 453-471.

CAMPOS, C., PERA, A., SANCHEZ-CORREA, B., ALONSO, C., LOPEZ-FERNANDEZ, I., MORGADO, S., TARAZONA, R. & SOLANA, R. 2014. Effect of age and CMV on NK cell subpopulations. *Exp Gerontol,* 54**,** 130-7.

CARALLO, C., IRACE, C., DE FRANCESCHI, M. S., COPPOLETTA, F., TIRIOLO, R., SCICCHITANO, C., SCAVELLI, F. & GNASSO, A. 2011. The effect of aging on blood and plasma viscosity. An 11.6 years follow-up study. *Clin Hemorheol Microcirc,* 47**,** 67-74.

CARDELLINI, M., MENGHINI, R., LUZI, A., DAVATO, F., CARDOLINI, I., D'ALFONSO, R., GENTILESCHI, P., RIZZA, S., MARINI, M. A. & PORZIO, O. 2011. Decreased IRS2 and TIMP3 expression in monocytes from offspring of type 2 diabetic patients is correlated with insulin resistance and increased intima-media thickness. *Diabetes,* 60**,** 3265-3270.

List of References

CARDELLINI, M., MENGHINI, R., MARTELLI, E., CASAGRANDE, V., MARINO, A., RIZZA, S., PORZIO, O., MAURIELLO, A., SOLINI, A. & IPPOLITI, A. 2009. TIMP3 is reduced in atherosclerotic plaques from subjects with type 2 diabetes and increased by SirT1. *Diabetes,* 58**,** 2396-2401.

CARDONA, A., SAALFELD, S., SCHINDELIN, J., ARGANDA-CARRERAS, I., PREIBISCH, S., LONGAIR, M., TOMANCAK, P., HARTENSTEIN, V. & DOUGLAS, R. J. 2012. TrakEM2 Software for Neural Circuit Reconstruction. *PLOS ONE,* 7**,** e38011.

CARO-MALDONADO, A., WANG, R., NICHOLS, A. G., KURAOKA, M., MILASTA, S., SUN, L. D., GAVIN, A. L., ABEL, E. D., KELSOE, G., GREEN, D. R. & RATHMELL, J. C. 2014. Metabolic reprogramming is required for antibody production that is suppressed in anergic but exaggerated in chronically BAFF-exposed B cells. *J Immunol,* 192**,** 3626-36.

CARRARD, G., BULTEAU, A.-L., PETROPOULOS, I. & FRIGUET, B. 2002. Impairment of proteasome structure and function in aging. *The International Journal of Biochemistry & Cell Biology,* 34**,** 1461-1474.

CASAGRANDE, V., MAURIELLO, A., BISCHETTI, S., MAVILIO, M., FEDERICI, M. & MENGHINI, R. 2017. Hepatocyte specific TIMP3 expression prevents diet dependent fatty liver disease and hepatocellular carcinoma. *Scientific Reports,* 7**,** 6747.

CASAGRANDE, V., MENGHINI, R., MENINI, S., MARINO, A., MARCHETTI, V., CAVALERA, M., FABRIZI, M., HRIBAL, M. L., PUGLIESE, G. & GENTILESCHI, P. 2012. Overexpression of tissue inhibitor of metalloproteinase 3 in macrophages reduces atherosclerosis in low-density lipoprotein receptor knockout mice. *Arteriosclerosis, thrombosis, and vascular biology,* 32**,** 74-81.

CASILI, G., CAMPOLO, M., BIUNDO, F., CRUPI, R., CORDARO, M., CUZZOCREA, S. & ESPOSITO, E. 2017. The Neuroprotective Effect of Dimethyl Fumarate in MPTP-mouse Model of Parkinson's Disease via ROS/NF-κB/Nrf-2. *The FASEB Journal,* 31**,** 1061.7-1061.7.

CASTILHO, R. M., SQUARIZE, C. H., CHODOSH, L. A., WILLIAMS, B. O. & GUTKIND, J. S. 2009. mTOR Mediates Wnt-Induced Epidermal Stem Cell Exhaustion and Aging. *Cell Stem Cell,* 5**,** 279-289.

CHAM, C. M., DRIESSENS, G., O'KEEFE, J. P. & GAJEWSKI, T. F. 2008. Glucose deprivation inhibits multiple key gene expression events and effector functions in CD8+ T cells. *European Journal of Immunology,* 38**,** 2438-2450.

CHAMBERS, S. M., SHAW, C. A., GATZA, C., FISK, C. J., DONEHOWER, L. A. & GOODELL, M. A. 2007. Aging Hematopoietic Stem Cells Decline in Function and Exhibit Epigenetic Dysregulation. *PLOS Biology,* 5**,** e201.

CHANG, C.-H., CURTIS, J. D., MAGGI JR, L. B., FAUBERT, B., VILLARINO, A. V., O'SULLIVAN, D., HUANG, S. C.-C., VAN DER WINDT, G. J., BLAGIH, J. & QIU, J. 2013. Posttranscriptional control of T cell effector function by aerobic glycolysis. *Cell,* 153**,** 1239-1251.

CHANG, Y.-C., CHEN, Y.-T., LIU, H.-W., CHAN, Y.-C., LIU, M.-Y., HU, S.-H., TSENG, W.-T., WU, H.-L., WANG, M.-F. & CHANG, S.-J. 2019. Oligonol Alleviates Sarcopenia by Regulation of Signaling Pathways Involved in Protein Turnover and Mitochondrial Quality. *Molecular Nutrition & Food Research,* 63**,** 1801102.

CHARLES, N., HARDWICK, D., DAUGAS, E., ILLEI, G. G. & RIVERA, J. 2010. Basophils and the T helper 2 environment can promote the development of lupus nephritis. *Nature medicine,* 16**,** 701.

CHEIGNON, C., JONES, M., ATRIÁN-BLASCO, E., KIEFFER, I., FALLER, P., COLLIN, F. & HUREAU, C. 2017. Identification of key structural features of the elusive Cu–Aβ complex that generates ROS in Alzheimer's disease. *Chemical Science*.

CHEN, J., ASTLE, C. M. & HARRISON, D. E. 1999. Development and aging of primitive hematopoietic stem cells in BALB/cBy mice. *Experimental Hematology,* 27**,** 928-935.

CHEN, J., ASTLE, C. M. & HARRISON, D. E. 2003. Hematopoietic senescence is postponed and hematopoietic stem cell function is enhanced by dietary restriction. *Experimental Hematology,* 31**,** 1097-1103.

CHEN, K., XU, W., WILSON, M., HE, B., MILLER, N. W., BENGTEN, E., EDHOLM, E.-S., SANTINI, P. A., RATH, P. & CHIU, A. 2009. Immunoglobulin D enhances immune surveillance by activating antimicrobial, proinflammatory and B cell–stimulating programs in basophils. *Nature immunology,* 10**,** 889.

CHEN, S., ZHOU, Y., ZHOU, L., GUAN, Y., ZHANG, Y. & HAN, X. 2018. Anti-neovascularization effects of DMBT in age-related macular degeneration by inhibition of VEGF secretion through ROS-dependent signaling pathway. *Molecular and cellular biochemistry,* 448**,** 225-235.

CHENG, Z., ITO, S., NISHIO, N., THANASEGARAN, S., FANG, H. & ISOBE, K.-I. 2013. Characteristics of cardiac aging in C57BL/6 mice. *Experimental Gerontology,* 48**,** 341-348.

CHEONG, C., MATOS, I., CHOI, J. H., DANDAMUDI, D. B., SHRESTHA, E., LONGHI, M. P., JEFFREY, K. L., ANTHONY, R. M., KLUGER, C., NCHINDA, G., KOH, H., RODRIGUEZ, A., IDOYAGA, J., PACK, M., VELINZON, K., PARK, C. G. & STEINMAN, R. M. 2010. Microbial stimulation fully differentiates monocytes to DC-SIGN/CD209(+) dendritic cells for immune T cell areas. *Cell,* 143**,** 416-29.

CHEONG, C. Y., NYUNT, M. S. Z., GAO, Q., GWEE, X., CHOO, R. W. M., YAP, K. B., WEE, S. L. & NG, T.-P. 2019. Risk Factors of Progression to Frailty: Findings from the Singapore Longitudinal Ageing Study. *The journal of nutrition, health & aging*.

CHIBA, Y., YAMASHITA, Y., UENO, M., FUJISAWA, H., HIRAYOSHI, K., HOHMURA, K.-I., TOMIMOTO, H., AKIGUCHI, I., SATOH, M., SHIMADA, A. & HOSOKAWA, M. 2005. Cultured Murine Dermal Fibroblast-Like Cells From Senescence-Accelerated Mice as In Vitro Models for Higher Oxidative Stress Due to Mitochondrial Alterations. *The Journals of Gerontology: Series A,* 60**,** 1087-1098.

CHIU, B.-C., MARTIN, B. E., STOLBERG, V. R. & CHENSUE, S. W. 2013. The host environment is responsible for aging-related functional NK cell deficiency. *Journal of immunology (Baltimore, Md. : 1950),* 191**,** 4688-4698.

CHO, S. J., MOON, J. S., LEE, C. M., CHOI, A. M. & STOUT-DELGADO, H. W. 2017. Glucose Transporter 1-Dependent Glycolysis Is Increased during Aging-Related Lung Fibrosis, and Phloretin Inhibits Lung Fibrosis. *Am J Respir Cell Mol Biol,* 56**,** 521-531.

CHOUGNET, C. A., THACKER, R. I., SHEHATA, H. M., HENNIES, C. M., LEHN, M. A., LAGES, C. S. & JANSSEN, E. M. 2015. Loss of phagocytic and antigen cross-presenting capacity in aging dendritic cells is associated with mitochondrial dysfunction. *The Journal of Immunology,* 195**,** 2624-2632.

CLANCY, D. J., GEMS, D., HARSHMAN, L. G., OLDHAM, S., STOCKER, H., HAFEN, E., LEEVERS, S. J. & PARTRIDGE, L. 2001. Extension of life-span by loss of CHICO, a Drosophila insulin receptor substrate protein. *Science,* 292**,** 104-6.

COGLIATI, S., FREZZA, C., SORIANO, M. E., VARANITA, T., QUINTANA-CABRERA, R., CORRADO, M., CIPOLAT, S., COSTA, V., CASARIN, A., GOMES, L. C., PERALES-CLEMENTE, E., SALVIATI, L., FERNANDEZ-SILVA, P., ENRIQUEZ, J. A. & SCORRANO, L. 2013. Mitochondrial cristae shape determines respiratory chain supercomplexes assembly and respiratory efficiency. *Cell,* 155**,** 160-71.

List of References

COLEMAN, R., WEISS, A., FINKELBRAND, S. & SILBERMANN, M. 1988. Age and exercise-related changes in myocardial mitochondria in mice. *Acta Histochemica,* 83**,** 81-90.

COLMAN, R. J., ANDERSON, R. M., JOHNSON, S. C., KASTMAN, E. K., KOSMATKA, K. J., BEASLEY, T. M., ALLISON, D. B., CRUZEN, C., SIMMONS, H. A., KEMNITZ, J. W. & WEINDRUCH, R. 2009. Caloric restriction delays disease onset and mortality in rhesus monkeys. *Science,* 325**,** 201-4.

COLONNA-ROMANO, G., BULATI, M., AQUINO, A., PELLICANO, M., VITELLO, S., LIO, D., CANDORE, G. & CARUSO, C. 2009. A double-negative (IgD-CD27-) B cell population is increased in the peripheral blood of elderly people. *Mech Ageing Dev,* 130**,** 681-90.

COOPER, M. D. 2015. The early history of B cells. *Nat Rev Immunol,* 15**,** 191-7.

COPELAND, J. M., CHO, J., LO, T., JR., HUR, J. H., BAHADORANI, S., ARABYAN, T., RABIE, J., SOH, J. & WALKER, D. W. 2009. Extension of Drosophila life span by RNAi of the mitochondrial respiratory chain. *Curr Biol,* 19**,** 1591-8.

COPPE, J. P., DESPREZ, P. Y., KRTOLICA, A. & CAMPISI, J. 2010. The senescence-associated secretory phenotype: the dark side of tumor suppression. *Annu Rev Pathol,* 5**,** 99-118.

CORTEGANO, I., RODRÍGUEZ, M., MARTÍN, I., PRADO, M. C., RUÍZ, C., HORTIGÜELA, R., ALÍA, M., VILAR, M., MIRA, H. & CANO, E. 2017. Altered marginal zone and innate-like B cells in aged senescence-accelerated SAMP8 mice with defective IgG1 responses. *Cell death & disease,* 8**,** e3000.

COSSARIZZA, A., KALASHNIKOVA, G., GRASSILLI, E., CHIAPPELLI, F., SALVIOLI, S., CAPRI, M., BARBIERI, D., TROIANO, L., MONTI, D. & FRANCESCHI, C. 1994. Mitochondrial Modifications during Rat Thymocyte Apoptosis: A Study at the Single Cell Level. *Experimental Cell Research,* 214**,** 323-330.

CRETENET, G., CLERC, I., MATIAS, M., LOISEL, S., CRAVEIRO, M., OBUROGLU, L., KINET, S., MONGELLAZ, C., DARDALHON, V. & TAYLOR, N. 2016. Cell surface Glut1 levels distinguish human CD4 and CD8 T lymphocyte subsets with distinct effector functions. *Scientific Reports,* 6**,** 24129.

CRISTÒFOL, R., PORQUET, D., CORPAS, R., COTO-MONTES, A., SERRET, J., CAMINS, A., PALLÀS, M. & SANFELIU, C. 2012. Neurons from senescence-accelerated SAMP8 mice are protected against frailty by the sirtuin 1 promoting agents melatonin and resveratrol. *Journal of Pineal Research,* 52**,** 271-281.

CROS, J., CAGNARD, N., WOOLLARD, K., PATEY, N., ZHANG, S.-Y., SENECHAL, B., PUEL, A., BISWAS, S. K., MOSHOUS, D. & PICARD, C. 2010. Human CD14dim monocytes patrol and sense nucleic acids and viruses via TLR7 and TLR8 receptors. *Immunity,* 33**,** 375-386.

CUERVO, A. M., BERGAMINI, E., BRUNK, U. T., DRÖGE, W., FFRENCH, M. & TERMAN, A. 2005. Autophagy and Aging: The Importance of Maintaining "Clean" Cells. *Autophagy,* 1**,** 131-140.

CZESNIKIEWICZ-GUZIK, M., LEE, W.-W., CUI, D., HIRUMA, Y., LAMAR, D. L., YANG, Z.-Z., OUSLANDER, J. G., WEYAND, C. M. & GORONZY, J. J. 2008. T cell subset-specific susceptibility to aging. *Clinical Immunology,* 127**,** 107-118.

D'AQUILA, P., ROSE, G., BELLIZZI, D. & PASSARINO, G. 2013. Epigenetics and aging. *Maturitas,* 74**,** 130-136.

DAIGNEAULT, M., PRESTON, J. A., MARRIOTT, H. M., WHYTE, M. K. & DOCKRELL, D. H. 2010. The identification of markers of macrophage differentiation in PMA-stimulated THP-1 cells and monocyte-derived macrophages. *PloS one,* 5**,** e8668.

DANCEY, J. T., DEUBELBEISS, K. A., HARKER, L. A. & FINCH, C. A. 1976. Neutrophil kinetics in man. *J Clin Invest,* 58**,** 705-15.

DANG, W., STEFFEN, K. K., PERRY, R., DORSEY, J. A., JOHNSON, F. B., SHILATIFARD, A., KAEBERLEIN, M., KENNEDY, B. K. & BERGER, S. L. 2009. Histone H4 lysine 16 acetylation regulates cellular lifespan. *Nature,* 459**,** 802-807.

DAUM, B., WALTER, A., HORST, A., OSIEWACZ, H. D. & KÜHLBRANDT, W. 2013. Age-dependent dissociation of ATP synthase dimers and loss of inner-membrane cristae in mitochondria. *Proceedings of the National Academy of Sciences,* 110**,** 15301.

DE BIASI, S., SIMONE, A. M., BIANCHINI, E., LO TARTARO, D., PECORINI, S., NASI, M., PATERGNANI, S., CARNEVALE, G., GIBELLINI, L., FERRARO, D., VITETTA, F., PINTON, P., SOLA, P., COSSARIZZA, A. & PINTI, M. 2019. Mitochondrial functionality and metabolism in T cells from progressive multiple sclerosis patients. *European Journal of Immunology,* 0.

DE GREY AUBREY, D. N. J. 2007. Life Span Extension Research and Public Debate: Societal Considerations. *Studies in Ethics, Law, and Technology.*

DE LIMA THOMAZ, L., PERON, G., OLIVEIRA, J., DA ROSA, L. C., THOME, R. & VERINAUD, L. 2018. The impact of metabolic reprogramming on dendritic cell function. *International immunopharmacology,* 63**,** 84-93.

DEELEN, J., UH, H.-W., MONAJEMI, R., VAN HEEMST, D., THIJSSEN, P. E., BÖHRINGER, S., VAN DEN AKKER, E. B., DE CRAEN, A. J. M., RIVADENEIRA, F., UITTERLINDEN, A. G., WESTENDORP, R. G. J., GOEMAN, J. J., SLAGBOOM, P. E., HOUWING-DUISTERMAAT, J. J. & BEEKMAN, M. 2013. Gene set analysis of GWAS data for human longevity highlights the relevance of the insulin/IGF-1 signaling and telomere maintenance pathways. *AGE,* 35**,** 235-249.

DELLA BELLA, S., BIERTI, L., PRESICCE, P., ARIENTI, R., VALENTI, M., SARESELLA, M., VERGANI, C. & VILLA, M. L. 2007. Peripheral blood dendritic cells and monocytes are differently regulated in the elderly. *Clinical immunology,* 122**,** 220-228.

DEMONTIS, F. & PERRIMON, N. 2010. FOXO/4E-BP Signaling in Drosophila Muscles Regulates Organism-wide Proteostasis during Aging. *Cell,* 143**,** 813-825.

DENG, Y., JING, Y., CAMPBELL, A. E. & GRAVENSTEIN, S. 2004. Age-Related Impaired Type 1 T Cell Responses to Influenza: Reduced Activation Ex Vivo, Decreased Expansion in CTL Culture In Vitro, and Blunted Response to Influenza Vaccination In Vivo in the Elderly. *The Journal of Immunology,* 172**,** 3437.

DENZEL, A., MAUS, U. A., GOMEZ, M. R., MOLL, C., NIEDERMEIER, M., WINTER, C., MAUS, R., HOLLINGSHEAD, S., BRILES, D. E. & KUNZ-SCHUGHART, L. A. 2008. Basophils enhance immunological memory responses. *Nature immunology,* 9**,** 733.

DERLET, A., RASPER, T., ROY CHOUDHURY, A., BOTHUR, S., RIEGER, M. A., NAMGALADZE, D., FISCHER, A., SCHÜRMANN, C., BRANDES, R. P., TSCHULENA, U., STEPPAN, S., ASSMUS, B., DIMMELER, S., ZEIHER, A. M. & SEEGER, F. H. 2016. Metabolism Regulates Cellular Functions of Bone Marrow-Derived Cells used for Cardiac Therapy. *STEM CELLS,* 34**,** 2236-2248.

DESLER, C., FREDERIKSEN, J. H., ANGLEYS, M., MAYNARD, S., KEIJZERS, G., FAGERLUND, B., MORTENSEN, E. L., OSLER, M., LAURITZEN, M., BOHR, V. A. & RASMUSSEN, L. J. 2015.

Increased deoxythymidine triphosphate levels is a feature of relative cognitive decline. *Mitochondrion,* 25**,** 34-37.

DI MICCO, R., FUMAGALLI, M., CICALESE, A., PICCININ, S., GASPARINI, P., LUISE, C., SCHURRA, C., GARRE, M., GIOVANNI NUCIFORO, P., BENSIMON, A., MAESTRO, R., GIUSEPPE PELICCI, P. & D/'ADDA DI FAGAGNA, F. 2006. Oncogene-induced senescence is a DNA damage response triggered by DNA hyper-replication. *Nature,* 444**,** 638-642.

DILLIN, A., HSU, A. L., ARANTES-OLIVEIRA, N., LEHRER-GRAIWER, J., HSIN, H., FRASER, A. G., KAMATH, R. S., AHRINGER, J. & KENYON, C. 2002. Rates of behavior and aging specified by mitochondrial function during development. *Science,* 298**,** 2398-401.

DIMELOE, S., MEHLING, M., FRICK, C., LOELIGER, J., BANTUG, G. R., SAUDER, U., FISCHER, M., BELLE, R., DEVELIOGLU, L., TAY, S., LANGENKAMP, A. & HESS, C. 2016. The Immune-Metabolic Basis of Effector Memory CD4<sup>+</sup> T Cell Function under Hypoxic Conditions. *The Journal of Immunology,* 196**,** 106.

DONG, K., NI, H., WU, M., TANG, Z., HALIM, M. & SHI, D. 2016. ROS-mediated glucose metabolic reprogram induces insulin resistance in type 2 diabetes. *Biochemical and biophysical research communications,* 476**,** 204-211.

DONG, L., MORI, I., HOSSAIN, M. J. & KIMURA, Y. 2000. The Senescence-Accelerated Mouse Shows Aging-Related Defects in Cellular but Not Humoral Immunity against Influenza Virus Infection. *The Journal of Infectious Diseases,* 182**,** 391-396.

DONNELLY, R. P., LOFTUS, R. M., KEATING, S. E., LIOU, K. T., BIRON, C. A., GARDINER, C. M. & FINLAY, D. K. 2014. mTORC1-dependent metabolic reprogramming is a prerequisite for NK cell effector function. *J Immunol,* 193**,** 4477-84.

DORIGHELLO, G. G., PAIM, B. A., LEITE, A. C. R., VERCESI, A. E. & OLIVEIRA, H. C. F. 2017. Spontaneous experimental atherosclerosis in hypercholesterolemic mice advances with ageing and correlates with mitochondrial reactive oxygen species. *Experimental Gerontology*.

DREW, B. & LEEUWENBURGH, C. 2003. Method for measuring ATP production in isolated mitochondria: ATP production in brain and liver mitochondria of Fischer-344 rats with age and caloric restriction. *Am J Physiol Regul Integr Comp Physiol,* 285**,** R1259-67.

DUDEK, A. M., MARTIN, S., GARG, A. D. & AGOSTINIS, P. 2013. Immature, semi-mature, and fully mature dendritic cells: toward a DC-cancer cells interface that augments anticancer immunity. *Frontiers in immunology,* 4**,** 438.

DURAND, N. & STORZ, P. 2017. Targeting reactive oxygen species in development and progression of pancreatic cancer. *Expert Review of Anticancer Therapy,* 17**,** 19-31.

ECKERT, G. P., SCHIBORR, C., HAGL, S., ABDEL-KADER, R., MÜLLER, W. E., RIMBACH, G. & FRANK, J. 2013. Curcumin prevents mitochondrial dysfunction in the brain of the senescence-accelerated mouse-prone 8. *Neurochemistry International,* 62**,** 595-602.

ENGVALL, E. & PERLMANN, P. 1972. Enzyme-linked immunosorbent assay, Elisa. 3. Quantitation of specific antibodies by enzyme-labeled anti-immunoglobulin in antigen-coated tubes. *J Immunol,* 109**,** 129-35.

EVERTS, B., AMIEL, E., HUANG, S. C.-C., SMITH, A. M., CHANG, C.-H., LAM, W. Y., REDMANN, V., FREITAS, T. C., BLAGIH, J. & VAN DER WINDT, G. J. 2014. TLR-driven early glycolytic reprogramming via the kinases TBK1-IKKε supports the anabolic demands of dendritic cell activation. *Nature immunology,* 15**,** 323.

EVERTS, B., AMIEL, E., VAN DER WINDT, G. J., FREITAS, T. C., CHOTT, R., YARASHESKI, K. E., PEARCE, E. L. & PEARCE, E. J. 2012. Commitment to glycolysis sustains survival of NO-producing inflammatory dendritic cells. *Blood,* 120**,** 1422-1431.

FAUL, F., ERDFELDER, E., BUCHNER, A. & LANG, A.-G. 2009. Statistical power analyses using G*Power 3.1: Tests for correlation and regression analyses. *Behavior Research Methods,* 41**,** 1149-1160.

FAUL, F., ERDFELDER, E., LANG, A.-G. & BUCHNER, A. 2007. G* Power 3: A flexible statistical power analysis program for the social, behavioral, and biomedical sciences. *Behavior research methods,* 39**,** 175-191.

FEDERICI, M., HRIBAL, M. L., MENGHINI, R., KANNO, H., MARCHETTI, V., PORZIO, O., SUNNARBORG, S. W., RIZZA, S., SERINO, M. & CUNSOLO, V. 2005. Timp3 deficiency in insulin receptor–haploinsufficient mice promotes diabetes and vascular inflammation via increased TNF-α. *The Journal of clinical investigation,* 115**,** 3494-3505.

FENG, L., CHONG, M. S., LIM, W. S., LEE, T. S., COLLINSON, S. L., YAP, P. & NG, T. P. 2013. Metabolic syndrome and amnestic mild cognitive impairment: Singapore Longitudinal Ageing Study-2 findings. *Journal of Alzheimer's Disease,* 34**,** 649-657.

FIORENTINO, L., CAVALERA, M., MAVILIO, M., CONSERVA, F., MENGHINI, R., GESUALDO, L. & FEDERICI, M. 2013a. Regulation of TIMP3 in diabetic nephropathy: a role for microRNAs. *Acta diabetologica,* 50**,** 965-969.

FIORENTINO, L., CAVALERA, M., MENINI, S., MARCHETTI, V., MAVILIO, M., FABRIZI, M., CONSERVA, F., CASAGRANDE, V., MENGHINI, R. & PONTRELLI, P. 2013b. Loss of TIMP3 underlies diabetic nephropathy via FoxO1/STAT1 interplay. *EMBO molecular medicine,* 5**,** 441-455.

FISCHER, M., BANTUG, G. R., DIMELOE, S., GUBSER, P. M., BURGENER, A. V., GRAHLERT, J., BALMER, M. L., DEVELIOGLU, L., STEINER, R., UNTERSTAB, G., SAUDER, U., HOENGER, G. & HESS, C. 2018. Early effector maturation of naive human CD8(+) T cells requires mitochondrial biogenesis. *Eur J Immunol,* 48**,** 1632-1643.

FISICARO, P., BARILI, V., MONTANINI, B., ACERBI, G., FERRACIN, M., GUERRIERI, F., SALERNO, D., BONI, C., MASSARI, M., CAVALLO, M. C., GROSSI, G., GIUBERTI, T., LAMPERTICO, P., MISSALE, G., LEVRERO, M., OTTONELLO, S. & FERRARI, C. 2017. Targeting mitochondrial dysfunction can restore antiviral activity of exhausted HBV-specific CD8 T cells in chronic hepatitis B. *Nature Medicine,* 23**,** 327.

FLEISCHER, J. G., SCHULTE, R., TSAI, H. H., TYAGI, S., IBARRA, A., SHOKHIREV, M. N., HUANG, L., HETZER, M. W. & NAVLAKHA, S. 2018. Predicting age from the transcriptome of human dermal fibroblasts. *Genome biology,* 19**,** 221.

FLORES-LANGARICA, A., MARSHALL, J. L., BOBAT, S., MOHR, E., HITCHCOCK, J., ROSS, E. A., COUGHLAN, R. E., KHAN, M., VAN ROOIJEN, N., HENDERSON, I. R., MACLENNAN, I. C. & CUNNINGHAM, A. F. 2011. T-zone localized monocyte-derived dendritic cells promote Th1 priming to Salmonella. *Eur J Immunol,* 41**,** 2654-65.

FONTANA, L., WEISS, E. P., VILLAREAL, D. T., KLEIN, S. & HOLLOSZY, J. O. 2008. Long-term effects of calorie or protein restriction on serum IGF-1 and IGFBP-3 concentration in humans. *Aging Cell,* 7**,** 681-687.

FORCE, A. G., STAPLES, T., SOLIMAN, S. & ARKING, R. 1995. Comparative biochemical and stress analysis of genetically selected Drosophila strains with different longevities. *Dev Genet,* 17**,** 340-51.

List of References

FRANCESCHI, C. & CAMPISI, J. 2014. Chronic Inflammation (Inflammaging) and Its Potential Contribution to Age-Associated Diseases. *The Journals of Gerontology: Series A,* 69**,** S4-S9.

FRANCESCHI, C., CAPRI, M., MONTI, D., GIUNTA, S., OLIVIERI, F., SEVINI, F., PANOURGIA, M. P., INVIDIA, L., CELANI, L., SCURTI, M., CEVENINI, E., CASTELLANI, G. C. & SALVIOLI, S. 2007. Inflammaging and anti-inflammaging: A systemic perspective on aging and longevity emerged from studies in humans. *Mechanisms of Ageing and Development,* 128**,** 92-105.

FRASCA, D., DIAZ, A., ROMERO, M. & BLOMBERG, B. B. 2017. Human peripheral late/exhausted memory B cells express a senescent-associated secretory phenotype and preferentially utilize metabolic signaling pathways. *Exp Gerontol,* 87**,** 113-120.

FRASCA, D., DIAZ, A., ROMERO, M., THALLER, S. & BLOMBERG, B. B. 2019. Metabolic requirements of human pro-inflammatory B cells in aging and obesity. *PLOS ONE,* 14**,** e0219545.

FRIEDMAN, D. B. & JOHNSON, T. E. 1988. A mutation in the age-1 gene in Caenorhabditis elegans lengthens life and reduces hermaphrodite fertility. *Genetics,* 118**,** 75-86.

FÜLÖP, T., LARBI, A. & PAWELEC, G. 2013. Human T cell aging and the impact of persistent viral infections. *Frontiers in immunology,* 4**,** 271-271.

GABER, T., STREHL, C., SAWITZKI, B., HOFF, P. & BUTTGEREIT, F. 2015. Cellular Energy Metabolism in T-Lymphocytes. *International Reviews of Immunology,* 34**,** 34-49.

GALOCHKINA, T., CHONG, M. N. F., CHALLALI, L., ABBAR, S. & ETCHEBEST, C. 2019. New insights into GluT1 mechanics during glucose transfer. *Scientific reports,* 9**,** 998.

GANESHAN, K. & CHAWLA, A. 2014. Metabolic regulation of immune responses. *Annual review of immunology,* 32**,** 609-634.

GAO, F., DU, W., ZAFAR, M. I., SHAFQAT, R. A., JIAN, L., CAI, Q. & LU, F. 2015. 4-Hydroxyisoleucine ameliorates an insulin resistant-like state in 3T3-L1 adipocytes by regulating TACE/TIMP3 expression. *Drug design, development and therapy,* 9**,** 5727.

GAO, Q., CAMOUS, X., LU, Y.-X., LIM, M.-L., LARBI, A. & NG, T.-P. 2016. Novel inflammatory markers associated with cognitive performance: Singapore Longitudinal Ageing Studies. *Neurobiology of aging,* 39**,** 140-146.

GARDINER, C. M. 2015. NK cell function and receptor diversity in the context of HCV infection. *Front Microbiol,* 6**,** 1061.

GAUGHWIN, P. M., CIESLA, M., LAHIRI, N., TABRIZI, S. J., BRUNDIN, P. & BJORKQVIST, M. 2011. Hsa-miR-34b is a plasma-stable microRNA that is elevated in pre-manifest Huntington's disease. *Hum Mol Genet,* 20**,** 2225-37.

GENEVA: WORLD HEALTH ORGANIZATION 2015. World report on ageing and health.

GENEVA: WORLD HEALTH ORGANIZATION 2017. Global strategy and action plan on ageing and health.

GIFONDORWA, D. J., ROBINSON, M. B., HAYES, C. D., TAYLOR, A. R., PREVETTE, D. M., OPPENHEIM, R. W., CARESS, J. & MILLIGAN, C. E. 2007. Exogenous Delivery of Heat Shock Protein 70 Increases Lifespan in a Mouse Model of Amyotrophic Lateral Sclerosis. *The Journal of Neuroscience,* 27**,** 13173-13180.

GODFREY, D. I., KENNEDY, J., MOMBAERTS, P., TONEGAWA, S. & ZLOTNIK, A. 1994. Onset of TCR-beta gene rearrangement and role of TCR-beta expression during CD3-CD4-CD8- thymocyte differentiation. *J Immunol,* 152**,** 4783-92.

248

GOGOLAK, P., RETHI, B., SZATMARI, I., LANYI, A., DEZSO, B., NAGY, L. & RAJNAVOLGYI, E. 2006. Differentiation of CD1a– and CD1a+ monocyte-derived dendritic cells is biased by lipid environment and PPARγ. *Blood,* 109**,** 643-652.

GOLDSTEIN, S., STOTLAND, D. & CORDEIRO, R. 1976. Decreased proteolysis and increased amino acid efflux in aging human fibroblasts. *Mechanisms of ageing and development,* 5**,** 221-233.

GONG, G., LIU, J., LIANG, P., GUO, T., HU, Q., OCHIAI, K., HOU, M., YE, Y., WU, X., MANSOOR, A., FROM, A. H., UGURBIL, K., BACHE, R. J. & ZHANG, J. 2003. Oxidative capacity in failing hearts. *Am J Physiol Heart Circ Physiol,* 285**,** H541-8.

GONZÁLEZ-NAVARRO, H., VINUÉ, Á., SANZ, M. J., DELGADO, M., POZO, M. A., SERRANO, M., BURKS, D. J. & ANDRÉS, V. 2013. Increased dosage of Ink4/Arf protects against glucose intolerance and insulin resistance associated with aging. *Aging Cell,* 12**,** 102-111.

GOPING, I. S., BARRY, M., LISTON, P., SAWCHUK, T., CONSTANTINESCU, G., MICHALAK, K. M., SHOSTAK, I., ROBERTS, D. L., HUNTER, A. M., KORNELUK, R. & BLEACKLEY, R. C. 2003. Granzyme B-induced apoptosis requires both direct caspase activation and relief of caspase inhibition. *Immunity,* 18**,** 355-65.

GORDON, C. L., MIRON, M., THOME, J. J. C., MATSUOKA, N., WEINER, J., RAK, M. A., IGARASHI, S., GRANOT, T., LERNER, H., GOODRUM, F. & FARBER, D. L. 2017. Tissue reservoirs of antiviral T cell immunity in persistent human CMV infection. *The Journal of Experimental Medicine,* 214**,** 651.

GORONZY, J. J. & WEYAND, C. M. 2019. Mechanisms underlying T cell ageing. *Nat Rev Immunol,* 19**,** 573-583.

GOUNDER, S. S., ABDULLAH, B. J. J., RADZUANB, N., ZAIN, F., SAIT, N. B. M., CHUA, C. & SUBRAMANI, B. 2018. Effect of Aging on NK Cell Population and Their Proliferation at Ex Vivo Culture Condition. *Anal Cell Pathol (Amst),* 2018**,** 7871814.

GOYAL, M. S., VLASSENKO, A. G., BLAZEY, T. M., SU, Y., COUTURE, L. E., DURBIN, T. J., BATEMAN, R. J., BENZINGER, T. L., MORRIS, J. C. & RAICHLE, M. E. 2017. Loss of Brain Aerobic Glycolysis in Normal Human Aging. *Cell Metab,* 26**,** 353-360.e3.

GRAY, D. A., TSIRIGOTIS, M. & WOULFE, J. 2003. Ubiquitin, Proteasomes, and the Aging Brain. *Sci. Aging Knowl. Environ.,* 2003**,** re6-.

GREENLEE-WACKER, M. C. 2016. Clearance of apoptotic neutrophils and resolution of inflammation. *Immunol Rev,* 273**,** 357-70.

GREER, E. L., MAURES, T. J., HAUSWIRTH, A. G., GREEN, E. M., LEEMAN, D. S., MARO, G. S., HAN, S., BANKO, M. R., GOZANI, O. & BRUNET, A. 2010. Members of the H3K4 trimethylation complex regulate lifespan in a germline-dependent manner in C. elegans. *Nature,* 466**,** 383-387.

GREER, E. L. & SHI, Y. 2012. Histone methylation: a dynamic mark in health, disease and inheritance. 13**,** 343.

GRUBECK-LOEBENSTEIN, B., DELLA BELLA, S., IORIO, A. M., MICHEL, J.-P., PAWELEC, G. & SOLANA, R. 2009. Immunosenescence and vaccine failure in the elderly. *Aging Clinical and Experimental Research,* 21**,** 201-209.

GUILLIAMS, M., DUTERTRE, C.-A., SCOTT, CHARLOTTE L., MCGOVERN, N., SICHIEN, D., CHAKAROV, S., VAN GASSEN, S., CHEN, J., POIDINGER, M., DE PRIJCK, S., TAVERNIER, SIMON J., LOW, I., IRAC, SERGIO E., MATTAR, CITRA N., SUMATOH, HERMI R., LOW, GILLIAN HUI L., CHUNG,

TAM JOHN K., CHAN, DEDRICK KOK H., TAN, KER K., HON, TONY LIM K., FOSSUM, E., BOGEN, B., CHOOLANI, M., CHAN, JERRY KOK Y., LARBI, A., LUCHE, H., HENRI, S., SAEYS, Y., NEWELL, EVAN W., LAMBRECHT, BART N., MALISSEN, B. & GINHOUX, F. 2016. Unsupervised High-Dimensional Analysis Aligns Dendritic Cells across Tissues and Species. *Immunity,* 45**,** 669-684.

GUO, L., KARPAC, J., TRAN, S. L. & JASPER, H. 2014. PGRP-SC2 promotes gut immune homeostasis to limit commensal dysbiosis and extend lifespan. *Cell,* 156**,** 109-22.

GUO, R., GU, J., ZONG, S., WU, M. & YANG, M. 2018. Structure and mechanism of mitochondrial electron transport chain. *Biomedical Journal,* 41**,** 9-20.

GUPTA, S. & GOLLAPUDI, S. 2005. Molecular mechanisms of TNF-α-induced apoptosis in aging human T cell subsets. *The international journal of biochemistry & cell biology,* 37**,** 1034-1042.

GUPTA, S. & GOLLAPUDI, S. 2008. CD95-mediated apoptosis in naïve, central and effector memory subsets of CD4+ and CD8+ T cells in aged humans. *Experimental Gerontology,* 43**,** 266-274.

HAGER, M., COWLAND, J. B. & BORREGAARD, N. 2010. Neutrophil granules in health and disease. *J Intern Med,* 268**,** 25-34.

HAJISHENGALLIS, G. & CHAVAKIS, T. 2013. Endogenous modulators of inflammatory cell recruitment. *Trends Immunol,* 34**,** 1-6.

HAMER, M., LAVOIE, K. L. & BACON, S. L. 2014. Taking up physical activity in later life and healthy ageing: the English longitudinal study of ageing. *Br J Sports Med,* 48**,** 239-243.

HAN, Y., HAN, D., YAN, Z., BOYD-KIRKUP, J. D., GREEN, C. D., KHAITOVICH, P. & HAN, J.-D. J. 2012. Stress-associated H3K4 methylation accumulates during postnatal development and aging of rhesus macaque brain. *Aging Cell,* 11**,** 1055-1064.

HARLEY, C. B., FUTCHER, A. B. & GREIDER, C. W. 1990. Telomeres shorten during ageing of human fibroblasts. *Nature,* 345**,** 458-460.

HARRINGTON, L. 2003. Biochemical aspects of telomerase function. *Cancer Letters,* 194**,** 139-154.

HARTMAN, M. L., SHIRIHAI, O. S., HOLBROOK, M., XU, G., KOCHERLA, M., SHAH, A., FETTERMAN, J. L., KLUGE, M. A., FRAME, A. A., HAMBURG, N. M. & VITA, J. A. 2014. Relation of mitochondrial oxygen consumption in peripheral blood mononuclear cells to vascular function in type 2 diabetes mellitus. *Vasc Med,* 19**,** 67-74.

HASEGAWA-ISHII, S., INABA, M., LI, M., SHI, M., UMEGAKI, H., IKEHARA, S. & SHIMADA, A. 2016. Increased recruitment of bone marrow-derived cells into the brain associated with altered brain cytokine profile in senescence-accelerated mice. *Brain Structure and Function,* 221**,** 1513-1531.

HAYFLICK, L. & MOORHEAD, P. S. 1961. The serial cultivation of human diploid cell strains. *Experimental Cell Research,* 25**,** 585-621.

HAYHOE, R. P., HENSON, S. M., AKBAR, A. N. & PALMER, D. B. 2010. Variation of human natural killer cell phenotypes with age: identification of a unique KLRG1-negative subset. *Hum Immunol,* 71**,** 676-81.

HAZELDINE, J. & LORD, J. M. 2013. The impact of ageing on natural killer cell function and potential consequences for health in older adults. *Ageing Res Rev,* 12**,** 1069-78.

HEARPS, A. C., MARTIN, G. E., ANGELOVICH, T. A., CHENG, W.-J., MAISA, A., LANDAY, A. L., JAWOROWSKI, A. & CROWE, S. M. 2012. Aging is associated with chronic innate immune activation and dysregulation of monocyte phenotype and function. *Aging Cell,* 11**,** 867-875.

HENSON, S. M., LANNA, A., RIDDELL, N. E., FRANZESE, O., MACAULAY, R., GRIFFITHS, S. J., PULESTON, D. J., WATSON, A. S., SIMON, A. K., TOOZE, S. A. & AKBAR, A. N. 2014. p38 signaling inhibits mTORC1-independent autophagy in senescent human CD8+ T cells. *The Journal of Clinical Investigation,* 124**,** 4004-4016.

HERNANZ, A., FERNANDEZ-VIVANCOS, E., MONTIEL, C., VAZQUEZ, J. & ARNALICH, F. 2000. Changes in the intracellular homocysteine and glutathione content associated with aging. *Life sciences,* 67**,** 1317-1324.

HILL, B. G., DRANKA, B. P., ZOU, L., CHATHAM, J. C. & DARLEY-USMAR, V. M. 2009. Importance of the bioenergetic reserve capacity in response to cardiomyocyte stress induced by 4-hydroxynonenal. *Biochem J,* 424**,** 99-107.

HIONA, A., SANZ, A., KUJOTH, G. C., PAMPLONA, R., SEO, A. Y., HOFER, T., SOMEYA, S., MIYAKAWA, T., NAKAYAMA, C., SAMHAN-ARIAS, A. K., SERVAIS, S., BARGER, J. L., PORTERO-OTIN, M., TANOKURA, M., PROLLA, T. A. & LEEUWENBURGH, C. 2010. Mitochondrial DNA mutations induce mitochondrial dysfunction, apoptosis and sarcopenia in skeletal muscle of mitochondrial DNA mutator mice. *PLoS One,* 5**,** e11468.

HIROSUE, A., ISHIHARA, K., TOKUNAGA, K., WATANABE, T., SAITOH, N., NAKAMOTO, M., CHANDRA, T., NARITA, M., SHINOHARA, M. & NAKAO, M. 2012. Quantitative assessment of higher-order chromatin structure of the INK4/ARF locus in human senescent cells. *Aging Cell,* 11**,** 553-556.

HO, R. C., NITI, M., YAP, K. B., KUA, E. H. & NG, T.-P. 2008. Metabolic syndrome and cognitive decline in Chinese older adults: results from the Singapore longitudinal ageing studies. *The American Journal of Geriatric Psychiatry,* 16**,** 519-522.

HOFFMAN, W., LAKKIS, F. G. & CHALASANI, G. 2016. B Cells, Antibodies, and More. *Clinical journal of the American Society of Nephrology : CJASN,* 11**,** 137-154.

HOPPEL, C. L., LESNEFSKY, E. J., CHEN, Q. & TANDLER, B. 2017. Mitochondrial Dysfunction in Cardiovascular Aging. *In:* SANTULLI, G. (ed.) *Mitochondrial Dynamics in Cardiovascular Medicine.* Cham: Springer International Publishing.

HUANG, H.-Y., HUANG, Y.-X., CHEN, Y.-W., CHOU, N.-W., CHEN, Y.-R., LEE, H.-C. & LEE, Y.-J. 2019. Lactobacillus paracasei PS23 modulated the age-related inflammation in Senescence Accelerated Mouse Prone 8 (SAMP8) mice. *The FASEB Journal,* 33**,** 651.11-651.11.

ILIADI, K. G. & BOULIANNE, G. L. 2010. Age-related behavioral changes in Drosophila. *Ann N Y Acad Sci,* 1197**,** 9-18.

INGERSOLL, M. A., SPANBROEK, R., LOTTAZ, C., GAUTIER, E. L., FRANKENBERGER, M., HOFFMANN, R., LANG, R., HANIFFA, M., COLLIN, M., TACKE, F., HABENICHT, A. J., ZIEGLER-HEITBROCK, L. & RANDOLPH, G. J. 2010. Comparison of gene expression profiles between human and mouse monocyte subsets. *Blood,* 115**,** e10-9.

ISHIZAKA, K., TOMIOKA, H. & ISHIZAKA, T. 1970. Mechanisms of passive sensitization: I. Presence of IgE and IgG molecules on human leukocytes. *The Journal of Immunology,* 105**,** 1459-1467.

JACKSON, H. W., HOJILLA, C. V., WEISS, A., SANCHEZ, O. H., WOOD, G. A. & KHOKHA, R. 2015. Timp3 Deficient Mice Show Resistance to Developing Breast Cancer. *PLOS ONE,* 10**,** e0120107.

List of References

JACOBS, S. R., HERMAN, C. E., MACIVER, N. J., WOFFORD, J. A., WIEMAN, H. L., HAMMEN, J. J. & RATHMELL, J. C. 2008. Glucose Uptake Is Limiting in T Cell Activation and Requires CD28-Mediated Akt-Dependent and Independent Pathways. *The Journal of Immunology,* 180**,** 4476.

JACOBSEN, E. A., OCHKUR, S. I., PERO, R. S., TARANOVA, A. G., PROTHEROE, C. A., COLBERT, D. C., LEE, N. A. & LEE, J. J. 2008. Allergic pulmonary inflammation in mice is dependent on eosinophil-induced recruitment of effector T cells. *J Exp Med,* 205**,** 699-710.

JAKUBZICK, C., GAUTIER, E. L., GIBBINGS, S. L., SOJKA, D. K., SCHLITZER, A., JOHNSON, T. E., IVANOV, S., DUAN, Q., BALA, S., CONDON, T., VAN ROOIJEN, N., GRAINGER, J. R., BELKAID, Y., MA'AYAN, A., RICHES, D. W., YOKOYAMA, W. M., GINHOUX, F., HENSON, P. M. & RANDOLPH, G. J. 2013. Minimal differentiation of classical monocytes as they survey steady-state tissues and transport antigen to lymph nodes. *Immunity,* 39**,** 599-610.

JAKUBZICK, C. V., RANDOLPH, G. J. & HENSON, P. M. 2017. Monocyte differentiation and antigen-presenting functions. *Nature Reviews Immunology,* 17**,** 349-362.

JAPIASSU, A. M., SANTIAGO, A. P., D'AVILA, J. C., GARCIA-SOUZA, L. F., GALINA, A., CASTRO FARIA-NETO, H. C., BOZZA, F. A. & OLIVEIRA, M. F. 2011. Bioenergetic failure of human peripheral blood monocytes in patients with septic shock is mediated by reduced F1Fo adenosine-5'-triphosphate synthase activity. *Crit Care Med,* 39**,** 1056-63.

JIANG, N., YAN, X., ZHOU, W., ZHANG, Q., CHEN, H., ZHANG, Y. & ZHANG, X. 2008. NMR-Based Metabonomic Investigations into the Metabolic Profile of the Senescence-Accelerated Mouse. *Journal of Proteome Research,* 7**,** 3678-3686.

JIANG, T., YU, J.-T., ZHU, X.-C., TAN, M.-S., GU, L.-Z., ZHANG, Y.-D. & TAN, L. 2014. Triggering receptor expressed on myeloid cells 2 knockdown exacerbates aging-related neuroinflammation and cognitive deficiency in senescence-accelerated mouse prone 8 mice. *Neurobiology of aging,* 35**,** 1243-1251.

JIANG, Y.-F., LIN, S.-S., CHEN, J.-M., TSAI, H.-Z., HSIEH, T.-S. & FU, C.-Y. 2017. Electron tomographic analysis reveals ultrastructural features of mitochondrial cristae architecture which reflect energetic state and aging. *Scientific Reports,* 7**,** 45474.

JIN, C., LI, J., GREEN, CHRISTOPHER D., YU, X., TANG, X., HAN, D., XIAN, B., WANG, D., HUANG, X., CAO, X., YAN, Z., HOU, L., LIU, J., SHUKEIR, N., KHAITOVICH, P., CHEN, CHARLIE D., ZHANG, H., JENUWEIN, T. & HAN, J.-DONG J. 2011. Histone Demethylase UTX-1 Regulates C. elegans Life Span by Targeting the Insulin/IGF-1 Signaling Pathway. *Cell Metabolism,* 14**,** 161-172.

JING, Y., SHAHEEN, E., DRAKE, R. R., CHEN, N., GRAVENSTEIN, S. & DENG, Y. 2009. Aging is associated with a numerical and functional decline in plasmacytoid dendritic cells, whereas myeloid dendritic cells are relatively unaltered in human peripheral blood. *Human immunology,* 70**,** 777-784.

JOLLES, J., HOUX, P., VAN BOXTEL, M. & PONDS, R. 1995. The Maastricht Aging Study. *Determinants of cognitive aging. Maastricht: Neuropsych Publishers***,** 192.

JOSEPH, A.-M., ADHIHETTY, P. J., WAWRZYNIAK, N. R., WOHLGEMUTH, S. E., PICCA, A., KUJOTH, G. C., PROLLA, T. A. & LEEUWENBURGH, C. 2013. Dysregulation of Mitochondrial Quality Control Processes Contribute to Sarcopenia in a Mouse Model of Premature Aging. *PLOS ONE,* 8**,** e69327.

JUNG, J., ZENG, H. & HORNG, T. 2019. Metabolism as a guiding force for immunity. *Nature Cell Biology,* 21**,** 85-93.

JUNNILA, R. K., LIST, E. O., BERRYMAN, D. E., MURREY, J. W. & KOPCHICK, J. J. 2013. The GH/IGF-1 axis in ageing and longevity. 9**,** 366.

KAARNIRANTA, K., PAWLOWSKA, E., SZCZEPANSKA, J., JABLKOWSKA, A. & BLASIAK, J. 2019. Role of mitochondrial DNA damage in ROS-mediated pathogenesis of age-related macular degeneration (AMD). *International journal of molecular sciences,* 20**,** 2374.

KAMEI, M. & HOLLYFIELD, J. G. 1999. TIMP-3 in Bruch's Membrane: Changes during Aging and Age-related Macular Degeneration. *Investigate opthalmology & visual science,* 40**,** 2367-2375.

KARLMARK, K. R., TACKE, F. & DUNAY, I. R. 2012. Monocytes in health and disease - Minireview. *European journal of microbiology & immunology,* 2**,** 97-102.

KARUPPAGOUNDER, V., GIRIDHARAN, V. V., ARUMUGAM, S., SREEDHAR, R., PALANIYANDI, S. S., KRISHNAMURTHY, P., QUEVEDO, J., WATANABE, K., KONISHI, T. & THANDAVARAYAN, R. A. 2016. Modulation of macrophage polarization and HMGB1-TLR2/TLR4 cascade plays a crucial role for cardiac remodeling in senescence-accelerated prone mice. *PLoS One,* 11**,** e0152922.

KATSIMPARDI, L., LITTERMAN, N. K., SCHEIN, P. A., MILLER, C. M., LOFFREDO, F. S., WOJTKIEWICZ, G. R., CHEN, J. W., LEE, R. T., WAGERS, A. J. & RUBIN, L. L. 2014. Vascular and Neurogenic Rejuvenation of the Aging Mouse Brain by Young Systemic Factors. *Science,* 344**,** 630-634.

KAWAHARA, T., KITA, T., UENO, Y., YAMASAKI, S., KIMURA, G., NAKANISHI, M., HOSOKAWA, T., KURASAKI, M., SIKDER, T. & SAITO, T. 2018. Elucidation of the mechanism of changes in the antioxidant function with the aging in the liver of the senescence-accelerated mouse P10 (SAMP10). *Experimental Gerontology,* 106**,** 46-53.

KAWAKAMI, K., NAKAMURA, A., ISHIGAMI, A., GOTO, S. & TAKAHASHI, R. 2009. Age-related difference of site-specific histone modifications in rat liver. *Biogerontology,* 10**,** 415-421.

KAYO, T., ALLISON, D. B., WEINDRUCH, R. & PROLLA, T. A. 2001. Influences of aging and caloric restriction on the transcriptional profile of skeletal muscle from rhesus monkeys. *Proc Natl Acad Sci U S A,* 98**,** 5093-8.

KENYON, C., CHANG, J., GENSCH, E., RUDNER, A. & TABTIANG, R. 1993. A C. elegans mutant that lives twice as long as wild type. *Nature,* 366**,** 461-4.

KEPLEY, C. L., WILSON, B. S. & OLIVER, J. M. 1998. Identification of the FcεRI-activated tyrosine kinases Lyn, Syk, and Zap-70 in human basophils. *Journal of allergy and clinical immunology,* 102**,** 304-315.

KIETZMANN, T., PETRY, A., SHVETSOVA, A., GERHOLD, J. M. & GÖRLACH, A. 2017. The epigenetic landscape related to reactive oxygen species formation in the cardiovascular system. *British Journal of Pharmacology,* 174**,** 1533-1554.

KIM, Y. G., KAMADA, N., SHAW, M. H., WARNER, N., CHEN, G. Y., FRANCHI, L. & NUNEZ, G. 2011. The Nod2 sensor promotes intestinal pathogen eradication via the chemokine CCL2-dependent recruitment of inflammatory monocytes. *Immunity,* 34**,** 769-80.

KIRCHMAN, P. A., KIM, S., LAI, C. Y. & JAZWINSKI, S. M. 1999. Interorganelle signaling is a determinant of longevity in Saccharomyces cerevisiae. *Genetics,* 152**,** 179-90.

KLASS, M. R. 1977. Aging in the nematode Caenorhabditis elegans: major biological and environmental factors influencing life span. *Mech Ageing Dev,* 6**,** 413-29.

List of References

KOBAYASHI, Y., INAGAWA, H., KOHCHI, C., KAZUMURA, K., TSUCHIYA, H., MIWA, T., OKAZAKI, K. & SOMA, G.-I. 2018. Oral administration of Pantoea agglomerans-derived lipopolysaccharide prevents metabolic dysfunction and Alzheimer's disease-related memory loss in senescence-accelerated prone 8 (SAMP8) mice fed a high-fat diet. *PLOS ONE,* 13**,** e0198493.

KOCH, S., LARBI, A., DERHOVANESSIAN, E., ÖZCELIK, D., NAUMOVA, E. & PAWELEC, G. 2008. Multiparameter flow cytometric analysis of CD4 and CD8 T cell subsets in young and old people. *Immunity & Ageing,* 5**,** 6.

KORNBERG, H. 2000. Krebs and his trinity of cycles. *Nature Reviews Molecular Cell Biology,* 1**,** 225-228.

KOWALTOWSKI, A. J. & VERCESI, A. E. 1999. Mitochondrial damage induced by conditions of oxidative stress. *Free Radical Biology and Medicine,* 26**,** 463-471.

KRATCHMAROV, R., VIRAGOVA, S., KIM, M. J., ROTHMAN, N. J., LIU, K., REIZIS, B. & REINER, S. L. 2018. Metabolic control of cell fate bifurcations in a hematopoietic progenitor population. *Immunology and cell biology,* 96**,** 863-871.

KRAWCZYK, C. M., HOLOWKA, T., SUN, J., BLAGIH, J., AMIEL, E., DEBERARDINIS, R. J., CROSS, J. R., JUNG, E., THOMPSON, C. B. & JONES, R. G. 2010. Toll-like receptor–induced changes in glycolytic metabolism regulate dendritic cell activation. *Blood,* 115**,** 4742-4749.

KREBS, H. A. & JOHNSON, W. A. 1937. The role of citric acid in intermediate metabolism in animal tissues. *Enzymologia,* 4**,** 148-156.

KRIETE, A., MAYO, K. L., YALAMANCHILI, N., BEGGS, W., BENDER, P., KARI, C. & RODECK, U. 2008. Cell autonomous expression of inflammatory genes in biologically aged fibroblasts associated with elevated NF-kappaB activity. *Immunity & Ageing,* 5**,** 5.

KUHN, S., YANG, J. & RONCHESE, F. 2015. Monocyte-Derived Dendritic Cells Are Essential for CD8(+) T Cell Activation and Antitumor Responses After Local Immunotherapy. *Frontiers in immunology,* 6**,** 584-584.

KUJOTH, G. C., HIONA, A., PUGH, T. D., SOMEYA, S., PANZER, K., WOHLGEMUTH, S. E., HOFER, T., SEO, A. Y., SULLIVAN, R., JOBLING, W. A., MORROW, J. D., VAN REMMEN, H., SEDIVY, J. M., YAMASOBA, T., TANOKURA, M., WEINDRUCH, R., LEEUWENBURGH, C. & PROLLA, T. A. 2005. Mitochondrial DNA Mutations, Oxidative Stress, and Apoptosis in Mammalian Aging. *Science,* 309**,** 481-484.

KUO, C.-Y., CHAN, C.-H., LI, L.-A., CHEN, W.-L., KU, H.-H., LIAN, Y.-Z. & HUANG, H.-Y. 2017. Long Term Probiotics Administration Alleviates Immunosenescence in Senescence-accelerated Mouse Prone 8 (SAMP8). *The FASEB Journal,* 31**,** 645.19-645.19.

KURZ, D. J., DECARY, S., HONG, Y. & ERUSALIMSKY, J. D. 2000. Senescence-associated (beta)-galactosidase reflects an increase in lysosomal mass during replicative ageing of human endothelial cells. *Journal of Cell Science,* 113**,** 3613-3622.

KURZ, D. J., DECARY, S., HONG, Y., TRIVIER, E., AKHMEDOV, A. & ERUSALIMSKY, J. D. 2004. Chronic oxidative stress compromises telomere integrity and accelerates the onset of senescence in human endothelial cells. *Journal of Cell Science,* 117**,** 2417-2426.

KUZUMAKI, N., IKEGAMI, D., TAMURA, R., SASAKI, T., NIIKURA, K., NARITA, M., MIYASHITA, K., IMAI, S., TAKESHIMA, H., ANDO, T., IGARASHI, K., KANNO, J., USHIJIMA, T., SUZUKI, T. & NARITA, M. 2010. Hippocampal epigenetic modification at the doublecortin gene is involved in the impairment of neurogenesis with aging. *Synapse,* 64**,** 611-616.

LACHMANDAS, E., BEIGIER-BOMPADRE, M., CHENG, S.-C., KUMAR, V., VAN LAARHOVEN, A., WANG, X., AMMERDORFFER, A., BOUTENS, L., DE JONG, D., KANNEGANTI, T.-D., GRESNIGT, M. S., OTTENHOFF, T. H. M., JOOSTEN, L. A. B., STIENSTRA, R., WIJMENGA, C., KAUFMANN, S. H. E., VAN CREVEL, R. & NETEA, M. G. 2016. Rewiring cellular metabolism via the AKT/mTOR pathway contributes to host defence against Mycobacterium tuberculosis in human and murine cells. *European Journal of Immunology,* 46**,** 2574-2586.

LAGOUGE, M., ARGMANN, C., GERHART-HINES, Z., MEZIANE, H., LERIN, C., DAUSSIN, F., MESSADEQ, N., MILNE, J., LAMBERT, P., ELLIOTT, P., GENY, B., LAAKSO, M., PUIGSERVER, P. & AUWERX, J. 2006. Resveratrol Improves Mitochondrial Function and Protects against Metabolic Disease by Activating SIRT1 and PGC-1α. *Cell,* 127**,** 1109-1122.

LANG, C. A., NARYSHKIN, S., SCHNEIDER, D. L., MILLS, B. J. & LINDEMAN, R. D. 1992. Low blood glutathione levels in healthy aging adults. *The Journal of laboratory and clinical medicine,* 120**,** 720-725.

LANGLET, C., TAMOUTOUNOUR, S., HENRI, S., LUCHE, H., ARDOUIN, L., GREGOIRE, C., MALISSEN, B. & GUILLIAMS, M. 2012. CD64 expression distinguishes monocyte-derived and conventional dendritic cells and reveals their distinct role during intramuscular immunization. *J Immunol,* 188**,** 1751-60.

LARSEN, S., STRIDE, N., HEY-MOGENSEN, M., HANSEN, C. N., ANDERSEN, J. L., MADSBAD, S., WORM, D., HELGE, J. W. & DELA, F. 2011. Increased mitochondrial substrate sensitivity in skeletal muscle of patients with type 2 diabetes. *Diabetologia,* 54**,** 1427-36.

LAVRIK, I., GOLKS, A. & KRAMMER, P. H. 2005. Death receptor signaling. *J Cell Sci,* 118**,** 265-7.

LE PAGE, A., DUPUIS, G., LARBI, A., WITKOWSKI, J. M. & FULOP, T. 2018. Signal transduction changes in CD4(+) and CD8(+) T cell subpopulations with aging. *Exp Gerontol,* 105**,** 128-139.

LECO, K. J., WATERHOUSE, P., SANCHEZ, O. H., GOWING, K. L., POOLE, A. R., WAKEHAM, A., MAK, T. W. & KHOKHA, R. 2001. Spontaneous air space enlargement in the lungs of mice lacking tissue inhibitor of metalloproteinases-3 (TIMP-3). *The Journal of clinical investigation,* 108**,** 817-829.

LEE, H.-C., LIM, M. L., LU, C.-Y., LIU, V. W., FAHN, H.-J., ZHANG, C., NAGLEY, P. & WEI, Y.-H. 1999. Concurrent increase of oxidative DNA damage and lipid peroxidation together with mitochondrial DNA mutation in human lung tissues during aging—smoking enhances oxidative stress on the aged tissues. *Archives of biochemistry and biophysics,* 362**,** 309-316.

LEE, J.-S., PARK, A. H., LEE, S.-H., LEE, S.-H., KIM, J.-H., YANG, S.-J., YEOM, Y. I., KWAK, T. H., LEE, D., LEE, S.-J., LEE, C.-H., KIM, J. M. & KIM, D. 2012. Beta-Lapachone, a Modulator of NAD Metabolism, Prevents Health Declines in Aged Mice. *PLOS ONE,* 7**,** e47122.

LEE, S.-J., HWANG, A. B. & KENYON, C. 2010. Inhibition of Respiration Extends C. elegans Life Span via Reactive Oxygen Species that Increase HIF-1 Activity. *Current Biology,* 20**,** 2131-2136.

LEESON, G. W. 2014. Future prospects for longevity. *Post Reproductive Health,* 20**,** 11-15.

LEMIEUX, M. E., YANG, X., JARDINE, K., HE, X., JACOBSEN, K. X., STAINES, W. A., HARPER, M. E. & MCBURNEY, M. W. 2005. The Sirt1 deacetylase modulates the insulin-like growth factor signaling pathway in mammals. *Mech Ageing Dev,* 126**,** 1097-105.

LENG, S. X., TIAN, X., MATTEINI, A., LI, H., HUGHES, J., JAIN, A., WALSTON, J. D. & FEDARKO, N. S. 2011. IL-6-independent association of elevated serum neopterin levels with prevalent frailty in community-dwelling older adults. *Age and ageing,* 40**,** 475-481.

List of References

LEON, B., LOPEZ-BRAVO, M. & ARDAVIN, C. 2007. Monocyte-derived dendritic cells formed at the infection site control the induction of protective T helper 1 responses against Leishmania. *Immunity,* 26**,** 519-31.

LESNEFSKY, E. J., MOGHADDAS, S., TANDLER, B., KERNER, J. & HOPPEL, C. L. 2001. Mitochondrial Dysfunction in Cardiac Disease: Ischemia–Reperfusion, Aging, and Heart Failure. *Journal of Molecular and Cellular Cardiology,* 33**,** 1065-1089.

LEY, K., HOFFMAN, H. M., KUBES, P., CASSATELLA, M. A., ZYCHLINSKY, A., HEDRICK, C. C. & CATZ, S. D. 2018. Neutrophils: New insights and open questions. *Science immunology,* 3**,** eaat4579.

LI, M., GUO, K., ADACHI, Y. & IKEHARA, S. 2016. Immune dysfunction associated with abnormal bone marrow-derived mesenchymal stroma cells in senescence accelerated mice. *International journal of molecular sciences,* 17**,** 183.

LI, X., KHANNA, A., LI, N. & WANG, E. 2011. Circulatory miR34a as an RNAbased, noninvasive biomarker for brain aging. *Aging,* 3**,** 985-1002.

LIANG, ZHANG, INSERRA, JIANG, LEE, GARZA, MARCHALONIS & WATSON 1998. Injection of T-cell receptor peptide reduces immunosenescence in aged C57BL/6 mice. *Immunology,* 93**,** 462-468.

LIBERT, S., CHAO, Y., CHU, X. & PLETCHER, S. D. 2006. Trade-offs between longevity and pathogen resistance in Drosophila melanogaster are mediated by NFkappaB signaling. *Aging Cell,* 5**,** 533-43.

LIBRI, V., AZEVEDO, R. I., JACKSON, S. E., DI MITRI, D., LACHMANN, R., FUHRMANN, S., VUKMANOVIC-STEJIC, M., YONG, K., BATTISTINI, L., KERN, F., SOARES, M. V. & AKBAR, A. N. 2011. Cytomegalovirus infection induces the accumulation of short-lived, multifunctional CD4+CD45RA+CD27+ T cells: the potential involvement of interleukin-7 in this process. *Immunology,* 132**,** 326-39.

LIU, B., WANG, J., CHAN, K. M., TJIA, W. M., DENG, W., GUAN, X., HUANG, J.-D., LI, K. M., CHAU, P. Y. & CHEN, D. J. 2005a. Genomic instability in laminopathy-based premature aging. *Nature medicine,* 11**,** 780.

LIU, H.-W., CHAN, Y.-C., WEI, C.-C., CHEN, Y.-A., WANG, M.-F. & CHANG, S.-J. 2017. An alternative model for studying age-associated metabolic complications: Senescence-accelerated mouse prone 8. *Experimental Gerontology,* 99**,** 61-68.

LIU, J., LIU, J., WANG, J., XIAO, L., LI, H., YANG, S. & TU, P. 2019. Electroacupuncture improved immunocompetence of DCs and CIKs from peripheral blood in SAMP8 mice. *Int J Clin Exp Med,* 12**,** 4949-4959.

LIU, J. & MORI, A. 1993. Age-associated changes in superoxide dismutase activity, thiobarbituric acid reactivity and reduced glutathione level in the brain and liver in senescence accelerated mice (SAM): a comparison with ddY mice. *Mechanisms of Ageing and Development,* 71**,** 23-30.

LIU, L., TRIMARCHI, J. R., SMITH, P. J. S. & KEEFE, D. L. 2002. Mitochondrial dysfunction leads to telomere attrition and genomic instability. *Aging Cell,* 1**,** 40-46.

LIU, X., JIANG, N., HUGHES, B., BIGRAS, E., SHOUBRIDGE, E. & HEKIMI, S. 2005b. Evolutionary conservation of the clk-1-dependent mechanism of longevity: loss of mclk1 increases cellular fitness and lifespan in mice. *Genes Dev,* 19**,** 2424-34.

LIU, Y., HE, J., JI, S., WANG, Q., PU, H., JIANG, T., MENG, L., YANG, X. & JI, J. 2008. Comparative Studies of Early Liver Dysfunction in Senescence-accelerated Mouse Using Mitochondrial Proteomics Approaches. *Molecular &amp; Cellular Proteomics,* 7**,** 1737.

LIU, Y., JOHNSON, S. M., FEDORIW, Y., ROGERS, A. B., YUAN, H., KRISHNAMURTHY, J. & SHARPLESS, N. E. 2011. Expression of p16^{INK4a} prevents cancer and promotes aging in lymphocytes. *Blood,* 117**,** 3257-3267.

LIU, Y., SANOFF, H. K., CHO, H., BURD, C. E., TORRICE, C., IBRAHIM, J. G., THOMAS, N. E. & SHARPLESS, N. E. 2009. Expression of p16(INK4a) in peripheral blood T-cells is a biomarker of human aging. *Aging Cell,* 8**,** 439-48.

LOFTUS, R. M., ASSMANN, N., KEDIA-MEHTA, N., O'BRIEN, K. L., GARCIA, A., GILLESPIE, C., HUKELMANN, J. L., OEFNER, P. J., LAMOND, A. I., GARDINER, C. M., DETTMER, K., CANTRELL, D. A., SINCLAIR, L. V. & FINLAY, D. K. 2018. Amino acid-dependent cMyc expression is essential for NK cell metabolic and functional responses in mice. *Nat Commun,* 9**,** 2341.

LOK, K., ZHAO, H., SHEN, H., WANG, Z., GAO, X., ZHAO, W. & YIN, M. 2013. Characterization of the APP/PS1 mouse model of Alzheimer's disease in senescence accelerated background. *Neuroscience Letters,* 557**,** 84-89.

LONGO, D. M., LOUIE, B., PTACEK, J., FRIEDLAND, G., EVENSEN, E., PUTTA, S., ATALLAH, M., SPELLMEYER, D., WANG, E., POS, Z., MARINCOLA, F. M., SCHAEFFER, A., LUKAC, S., RAILKAR, R., BEALS, C. R., CESANO, A., CARAYANNOPOULOS, L. N. & HAWTIN, R. E. 2014. High-dimensional analysis of the aging immune system: Verification of age-associated differences in immune signaling responses in healthy donors. *Journal of Translational Medicine,* 12**,** 178.

LÓPEZ-LLUCH, G., IRUSTA, P. M., NAVAS, P. & DE CABO, R. 2008. Mitochondrial biogenesis and healthy aging. *Experimental gerontology,* 43**,** 813-819.

LÓPEZ-OTÍN, C., BLASCO, M. A., PARTRIDGE, L., SERRANO, M. & KROEMER, G. 2013. The Hallmarks of Aging. *Cell,* 153**,** 1194-1217.

LORENZO, E. C., BARTLEY, J. M. & HAYNES, L. 2018. The impact of aging on CD4(+) T cell responses to influenza infection. *Biogerontology,* 19**,** 437-446.

LU, Y., TAN, C. T. Y., NYUNT, M. S. Z., MOK, E. W. H., CAMOUS, X., KARED, H., FULOP, T., FENG, L., NG, T. P. & LARBI, A. 2016. Inflammatory and immune markers associated with physical frailty syndrome: findings from Singapore longitudinal aging studies. *Oncotarget,* 7**,** 28783.

LUNG, T. L., SAURWEIN-TEISSL, M., PARSON, W., SCHÖNITZER, D. & GRUBECK-LOEBENSTEIN, B. 2000. Unimpaired dendritic cells can be derived from monocytes in old age and can mobilize residual function in senescent T cells. *Vaccine,* 18**,** 1606-1612.

LUO, L., TULLY, T. & WHITE, K. 1992. Human amyloid precursor protein ameliorates behavioral deficit of flies deleted for Appl gene. *Neuron,* 9**,** 595-605.

LV, Y.-J., YANG, Y., SUI, B.-D., HU, C.-H., ZHAO, P., LIAO, L., CHEN, J., ZHANG, L.-Q., YANG, T.-T., ZHANG, S.-F. & JIN, Y. 2018. Resveratrol counteracts bone loss via mitofilin-mediated osteogenic improvement of mesenchymal stem cells in senescence-accelerated mice. *Theranostics,* 8**,** 2387-2406.

MA, Q., QIANG, J., GU, P., WANG, Y., GENG, Y. & WANG, M. 2011. Age-related autophagy alterations in the brain of senescence accelerated mouse prone 8 (SAMP8) mice. *Experimental gerontology,* 46**,** 533-541.

List of References

MA, S., WANG, C., MAO, X. & HAO, Y. 2019. B Cell Dysfunction Associated With Aging and Autoimmune Diseases. *Frontiers in Immunology,* 10.

MACGREGOR, A. M., EBERHART, C. G., FRAIG, M., LU, J. & HALUSHKA, M. K. 2009. Tissue inhibitor of matrix metalloproteinase-3 levels in the extracellular matrix of lung, kidney, and eye increase with age. *Journal of Histochemistry & Cytochemistry,* 57**,** 207-213.

MACINTYRE, A. N., GERRIETS, V. A., NICHOLS, A. G., MICHALEK, R. D., RUDOLPH, M. C., DEOLIVEIRA, D., ANDERSON, S. M., ABEL, E. D., CHEN, B. J., HALE, L. P. & RATHMELL, J. C. 2014. The glucose transporter Glut1 is selectively essential for CD4 T cell activation and effector function. *Cell Metabolism,* 20**,** 61-72.

MANNELLA, C. A. 2006. The relevance of mitochondrial membrane topology to mitochondrial function. *Biochimica et Biophysica Acta (BBA) - Molecular Basis of Disease,* 1762**,** 140-147.

MARÇAIS, A., CHERFILS-VICINI, J., VIANT, C., DEGOUVE, S., VIEL, S., FENIS, A., RABILLOUD, J., MAYOL, K., TAVARES, A., BIENVENU, J., GANGLOFF, Y.-G., GILSON, E., VIVIER, E. & WALZER, T. 2014. The metabolic checkpoint kinase mTOR is essential for IL-15 signaling during the development and activation of NK cells. *Nature Immunology,* 15**,** 749.

MARQUES-MEJIAS, M. A., RODRIGUEZ, R. I., JEONG, B. M., CODEN, M. E. & BERDNIKOVS, S. 2019. Glucose metabolism dictates murine eosinophil differentiation, chemotaxis, and IL-4 expression. *Journal of Allergy and Clinical Immunology,* 143**,** AB307.

MARTELLI, S. 2017. *Maturation and function of natural killer cells during aging.* Universty of Southampton.

MASORO, E. J. 2005. Overview of caloric restriction and ageing. *Mechanisms of Ageing and Development,* 126**,** 913-922.

MATHEU, A., MARAVER, A., COLLADO, M., GARCIA-CAO, I., CAÑAMERO, M., BORRAS, C., FLORES, J. M., KLATT, P., VIÑA, J. & SERRANO, M. 2009. Anti-aging activity of the Ink4/Arf locus. *Aging Cell,* 8**,** 152-161.

MAVILIO, M., MARCHETTI, V., FABRIZI, M., STÖHR, R., MARINO, A., CASAGRANDE, V., FIORENTINO, L., CARDELLINI, M., KAPPEL, B., MONTELEONE, I., GARRET, C., MAURIELLO, A., MONTELEONE, G., FARCOMENI, A., BURCELIN, R., MENGHINI, R. & FEDERICI, M. 2016. A Role for Timp3 in Microbiota-Driven Hepatic Steatosis and Metabolic Dysfunction. *Cell Reports,* 16**,** 731-743.

MAZUCANTI, C. H., CABRAL-COSTA, J. V., VASCONCELOS, A. R., ANDREOTTI, D. Z., SCAVONE, C. & KAWAMOTO, E. M. 2015. Longevity Pathways (mTOR, SIRT, Insulin/IGF-1) as Key Modulatory Targets on Aging and Neurodegeneration. *Curr Top Med Chem,* 15**,** 2116-38.

MCCARROLL, S. A., MURPHY, C. T., ZOU, S., PLETCHER, S. D., CHIN, C. S., JAN, Y. N., KENYON, C., BARGMANN, C. I. & LI, H. 2004. Comparing genomic expression patterns across species identifies shared transcriptional profile in aging. *Nat Genet,* 36**,** 197-204.

MCCORD, R. P., NAZARIO-TOOLE, A., ZHANG, H., CHINES, P. S., ZHAN, Y., ERDOS, M. R., COLLINS, F. S., DEKKER, J. & CAO, K. 2013. Correlated alterations in genome organization, histone methylation, and DNA–lamin A/C interactions in Hutchinson-Gilford progeria syndrome. *Genome research,* 23**,** 260-269.

MCELHANEY, J. E. & EFFROS, R. B. 2009. Immunosenescence: what does it mean to health outcomes in older adults? *Curr Opin Immunol,* 21**,** 418-24.

MCINTURFF, A. M., CODY, M. J., ELLIOTT, E. A., GLENN, J. W., ROWLEY, J. W., RONDINA, M. T. & YOST, C. C. 2012. Mammalian target of rapamycin regulates neutrophil extracellular trap formation via induction of hypoxia-inducible factor 1 α. *Blood,* 120**,** 3118-3125.

MCKIERNAN, S. H., COLMAN, R. J., AIKEN, E., EVANS, T. D., BEASLEY, T. M., AIKEN, J. M., WEINDRUCH, R. & ANDERSON, R. M. 2012. Cellular adaptation contributes to calorie restriction-induced preservation of skeletal muscle in aged rhesus monkeys. *Exp Gerontol,* 47**,** 229-36.

MCKIERNAN, S. H., COLMAN, R. J., LOPEZ, M., BEASLEY, T. M., AIKEN, J. M., ANDERSON, R. M. & WEINDRUCH, R. 2011. Caloric restriction delays aging-induced cellular phenotypes in rhesus monkey skeletal muscle. *Exp Gerontol,* 46**,** 23-9.

MCWILLIAM, A. S., NAPOLI, S., MARSH, A. M., PEMPER, F. L., NELSON, D. J., PIMM, C. L., STUMBLES, P. A., WELLS, T. N. & HOLT, P. G. 1996. Dendritic cells are recruited into the airway epithelium during the inflammatory response to a broad spectrum of stimuli. *J Exp Med,* 184**,** 2429-32.

MCWILLIAM, A. S., NELSON, D., THOMAS, J. A. & HOLT, P. G. 1994. Rapid dendritic cell recruitment is a hallmark of the acute inflammatory response at mucosal surfaces. *J Exp Med,* 179**,** 1331-6.

MENGHINI, R., CASAGRANDE, V., MENINI, S., MARINO, A., MARZANO, V., HRIBAL, M. L., GENTILESCHI, P., LAURO, D., SCHILLACI, O. & PUGLIESE, G. 2012. TIMP3 overexpression in macrophages protects from insulin resistance, adipose inflammation, and nonalcoholic fatty liver disease in mice. *Diabetes,* 61**,** 454-462.

METCALF, D. 2007. On Hematopoietic Stem Cell Fate. *Immunity,* 26**,** 669-673.

METCALF, T. U., CUBAS, R. A., GHNEIM, K., CARTWRIGHT, M. J., GREVENYNGHE, J. V., RICHNER, J. M., OLAGNIER, D. P., WILKINSON, P. A., CAMERON, M. J., PARK, B. S., HISCOTT, J. B., DIAMOND, M. S., WERTHEIMER, A. M., NIKOLICH-ZUGICH, J. & HADDAD, E. K. 2015. Global analyses revealed age-related alterations in innate immune responses after stimulation of pathogen recognition receptors. *Aging cell,* 14**,** 421-432.

METCALF, T. U., WILKINSON, P. A., CAMERON, M. J., GHNEIM, K., CHIANG, C., WERTHEIMER, A. M., HISCOTT, J. B., NIKOLICH-ZUGICH, J. & HADDAD, E. K. 2017. Human Monocyte Subsets Are Transcriptionally and Functionally Altered in Aging in Response to Pattern Recognition Receptor Agonists. *Journal of immunology (Baltimore, Md. : 1950),* 199**,** 1405-1417.

MILLET, P., VACHHARAJANI, V., MCPHAIL, L., YOZA, B. & MCCALL, C. E. 2016. GAPDH Binding to TNF-α mRNA Contributes to Posttranscriptional Repression in Monocytes: A Novel Mechanism of Communication between Inflammation and Metabolism. *The Journal of Immunology,* 196**,** 2541-2551.

MILLS, E. L. & O'NEILL, L. A. 2016. Reprogramming mitochondrial metabolism in macrophages as an anti-inflammatory signal. *European Journal of Immunology,* 46**,** 13-21.

MIN, B. 2018. Spontaneous T Cell Proliferation: A Physiologic Process to Create and Maintain Homeostatic Balance and Diversity of the Immune System. *Frontiers in Immunology,* 9.

MINISTRY OF HEALTH 2016. Action Plan for Successful Ageing.

MIRÓ MARTÍ, M., GARCIA JUST, A., AMAT, C., POLO, J., MORETÓ, M. & PÉREZ BOSQUE, A. 2017. Dietary animal plasma proteins improve the intestinal immune response in senescent mice. *Nutrients, 2017, vol. 9, num. 12*.

List of References

MIRÓ, Ò., CASADEMONT, J., BARRIENTOS, A., URBANO–MÁRQUEZ, Á. & CARDELLACH, F. 1998. Mitochondrial cytochrome c oxidase inhibition during acute carbon monoxide poisoning. *Pharmacology & toxicology,* 82**,** 199-202.

MOHAMMED, F. F., SMOOKLER, D. S., TAYLOR, S. E., FINGLETON, B., KASSIRI, Z., SANCHEZ, O. H., ENGLISH, J. L., MATRISIAN, L. M., AU, B., YEH, W. C. & KHOKHA, R. 2004. Abnormal TNF activity in Timp3-/- mice leads to chronic hepatic inflammation and failure of liver regeneration. *Nat Genet,* 36**,** 969-77.

MOLINA, V. C., MEDICI, M. G., VILLENA, J. C., FONT, G. M. & TARANTO, M. P. 2016. Dietary Supplementation with Probiotic Strain Improves Immune-Health in Aged Mice.

MOLONY, R. D., NGUYEN, J. T., KONG, Y., MONTGOMERY, R. R., SHAW, A. C. & IWASAKI, A. 2017. Aging impairs both primary and secondary RIG-I signaling for interferon induction in human monocytes. *Sci Signal,* 10.

MONROY, A., KAMATH, S., CHAVEZ, A., CENTONZE, V., VEERASAMY, M., BARRENTINE, A., WEWER, J., COLETTA, D., JENKINSON, C. & JHINGAN, R. 2009. Impaired regulation of the TNF-α converting enzyme/tissue inhibitor of metalloproteinase 3 proteolytic system in skeletal muscle of obese type 2 diabetic patients: a new mechanism of insulin resistance in humans. *Diabetologia,* 52**,** 2169-2181.

MOORE, M. L., NEWCOMB, D. C., PAREKH, V. V., VAN KAER, L., COLLINS, R. D., ZHOU, W., GOLENIEWSKA, K., CHI, M. H., MITCHELL, D. & BOYCE, J. A. 2009. STAT1 negatively regulates lung basophil IL-4 expression induced by respiratory syncytial virus infection. *The Journal of Immunology,* 183**,** 2016-2026.

MORAWE, T., HIEBEL, C., KERN, A. & BEHL, C. 2012. Protein Homeostasis, Aging and Alzheimer's Disease. *Molecular Neurobiology,* 46**,** 41-54.

MORI, A., UTSUMI, K., LIU, J. & HOSOKAWA, M. 1998. Oxidative Damage in the Senescence-accelerated Mouse. *Annals of the New York Academy of Sciences,* 854**,** 239-250.

MORLEY, J. E., ARMBRECHT, H. J., FARR, S. A. & KUMAR, V. B. 2012. The senescence accelerated mouse (SAMP8) as a model for oxidative stress and Alzheimer's disease. *Biochimica et Biophysica Acta (BBA)-Molecular Basis of Disease,* 1822**,** 650-656.

MUECKLER, M., CARUSO, C., BALDWIN, S. A., PANICO, M., BLENCH, I., MORRIS, H. R., ALLARD, W. J., LIENHARD, G. E. & LODISH, H. F. 1985. Sequence and structure of a human glucose transporter. *Science,* 229**,** 941.

MUKAI, K., MATSUOKA, K., TAYA, C., SUZUKI, H., YOKOZEKI, H., NISHIOKA, K., HIROKAWA, K., ETORI, M., YAMASHITA, M. & KUBOTA, T. 2005. Basophils play a critical role in the development of IgE-mediated chronic allergic inflammation independently of T cells and mast cells. *Immunity,* 23**,** 191-202.

MUNITZ, A., BRANDT, E. B., MINGLER, M., FINKELMAN, F. D. & ROTHENBERG, M. E. 2008. Distinct roles for IL-13 and IL-4 via IL-13 receptor alpha1 and the type II IL-4 receptor in asthma pathogenesis. *Proc Natl Acad Sci U S A,* 105**,** 7240-5.

MUNRO, H. N. 2012. *Mammalian protein metabolism*, Elsevier.

MURTHY, A., SHAO, Y. W., DEFAMIE, V., WEDELES, C., SMOOKLER, D. & KHOKHA, R. 2012. Stromal TIMP3 Regulates Liver Lymphocyte Populations and Provides Protection against Th1 T Cell-Driven Autoimmune Hepatitis. *The Journal of Immunology,* 188**,** 2876.

NAIR, S., FANG, M. & SIGAL, L. J. 2015. The natural killer cell dysfunction of aged mice is due to the bone marrow stroma and is not restored by IL-15/IL-15Ralpha treatment. *Aging Cell,* 14**,** 180-90.

NAKAHARA, H., KANNO, T., INAI, Y., UTSUMI, K., HIRAMATSU, M., MORI, A. & PACKER, L. 1998. Mitochondrial Dysfunction in the Senescence Accelerated Mouse (SAM). *Free Radical Biology and Medicine,* 24**,** 85-92.

NARASIMHAN, P. B., MARCOVECCHIO, P., HAMERS, A. A. J. & HEDRICK, C. C. 2019. Nonclassical Monocytes in Health and Disease. *Annual Review of Immunology,* 37**,** 439-456.

NASCIMENTO, M. P. P. D., PINKE, K. H., PENITENTI, M., IKOMA, M. R. V. & LARA, V. S. 2015. Aging does not affect the ability of human monocyte-derived dendritic cells to phagocytose Candida albicans. *Aging Clinical and Experimental Research,* 27**,** 785-789.

NAUSEEF, W. M. & BORREGAARD, N. 2014. Neutrophils at work. *Nat Immunol,* 15**,** 602-11.

NAYLOR, K., LI, G., VALLEJO, A. N., LEE, W.-W., KOETZ, K., BRYL, E., WITKOWSKI, J., FULBRIGHT, J., WEYAND, C. M. & GORONZY, J. J. 2005. The Influence of Age on T Cell Generation and TCR Diversity. *The Journal of Immunology,* 174**,** 7446.

NEWSHOLME, P., CRUZAT, V. F., KEANE, K. N., CARLESSI, R. & DE BITTENCOURT, P. I. H. 2016. Molecular mechanisms of ROS production and oxidative stress in diabetes. *Biochemical Journal,* 473**,** 4527-4550.

NEWSHOLME, P., CURI, R., GORDON, S. & NEWSHOLME, E. A. 1986. Metabolism of glucose, glutamine, long-chain fatty acids and ketone bodies by murine macrophages. *Biochemical Journal,* 239**,** 121-125.

NG, T. P., CAMOUS, X., NYUNT, M. S. Z., VASUDEV, A., TAN, C. T. Y., FENG, L., FULOP, T., YAP, K. B. & LARBI, A. 2015a. Markers of T-cell senescence and physical frailty: insights from Singapore Longitudinal Ageing Studies. *npj Aging and Mechanisms of Disease,* 1**,** 15005.

NG, T. P., FENG, L., NYUNT, M. S. Z., FENG, L., GAO, Q., LIM, M. L., COLLINSON, S. L., CHONG, M. S., LIM, W. S. & LEE, T. S. 2016. Metabolic syndrome and the risk of mild cognitive impairment and progression to dementia: follow-up of the Singapore longitudinal ageing study cohort. *JAMA neurology,* 73**,** 456-463.

NG, T. P., JIN, A., FENG, L., NYUNT, M. S. Z., CHOW, K. Y., FENG, L. & FONG, N. P. 2015b. Mortality of older persons living alone: Singapore Longitudinal Ageing Studies. *BMC geriatrics,* 15**,** 126.

NG, T. P., NITI, M., YAP, K. B. & TAN, W. C. 2014. Dietary and supplemental antioxidant and anti-inflammatory nutrient intakes and pulmonary function. *Public health nutrition,* 17**,** 2081-2086.

NOGUEIRA-NETO, J., CARDOSO, A. S. C., MONTEIRO, H. P., FONSECA, F. L. A., RAMOS, L. R., JUNQUEIRA, V. B. C. & SIMON, K. A. 2016. Basal neutrophil function in human aging: Implications in endothelial cell adhesion. *Cell Biology International,* 40**,** 796-802.

NOWAK, W. N., DENG, J., RUAN, X. Z. & XU, Q. 2017. Reactive Oxygen Species Generation and Atherosclerosis. *Arteriosclerosis, Thrombosis, and Vascular Biology,* 37**,** e41-e52.

NYUGEN, J., AGRAWAL, S., GOLLAPUDI, S. & GUPTA, S. 2010. Impaired Functions of Peripheral Blood Monocyte Subpopulations in Aged Humans. *Journal of Clinical Immunology,* 30**,** 806-813.

List of References

O'SHEA, D., CAWOOD, T. J., O'FARRELLY, C. & LYNCH, L. 2010. Natural killer cells in obesity: impaired function and increased susceptibility to the effects of cigarette smoke. *PLoS One,* 5**,** e8660.

O'NEILL, L. A. & PEARCE, E. J. 2016. Immunometabolism governs dendritic cell and macrophage function. *Journal of Experimental Medicine,* 213**,** 15-23.

OCHKUR, S. I., NAZAROFF, C. D., FOLMES, C. D., LESUER, W. E., LEE, J. J., WRIGHT, B. L., RANK, M. A. & JACOBSEN, E. A. 2019. Eosinophils Display Subtype-specific Metabolic Profiles. *Journal of Allergy and Clinical Immunology,* 143**,** AB308.

ODEGAARD, J. I., RICARDO-GONZALEZ, R. R., GOFORTH, M. H., MOREL, C. R., SUBRAMANIAN, V., MUKUNDAN, L., RED EAGLE, A., VATS, D., BROMBACHER, F., FERRANTE, A. W. & CHAWLA, A. 2007. Macrophage-specific PPARgamma controls alternative activation and improves insulin resistance. *Nature,* 447**,** 1116-20.

OFFICE FOR NATIONAL STATISTICS 2018. *Overview of the UK population: July 2018.*

OLIVIERO, B., VARCHETTA, S., PAUDICE, E., MICHELONE, G., ZARAMELLA, M., MAVILIO, D., DE FILIPPI, F., BRUNO, S. & MONDELLI, M. U. 2009. Natural killer cell functional dichotomy in chronic hepatitis B and chronic hepatitis C virus infections. *Gastroenterology,* 137**,** 1151-60, 1160.e1-7.

ONG, S.-M., HADADI, E., DANG, T.-M., YEAP, W.-H., TAN, C. T.-Y., NG, T.-P., LARBI, A. & WONG, S.-C. 2018. The pro-inflammatory phenotype of the human non-classical monocyte subset is attributed to senescence. *Cell death & disease,* 9**,** 266.

OWCZARZ, M., BUDZINSKA, M., DOMASZEWSKA-SZOSTEK, A., BORKOWSKA, J., POLOSAK, J., GEWARTOWSKA, M., SLUSARCZYK, P. & PUZIANOWSKA-KUZNICKA, M. 2017. miR-34a and miR-9 are overexpressed and SIRT genes are downregulated in peripheral blood mononuclear cells of aging humans. *Experimental Biology and Medicine,* 242**,** 1453-1461.

OWUSU-ANSAH, E., SONG, W. & PERRIMON, N. 2013. Muscle mitohormesis promotes longevity via systemic repression of insulin signaling. *Cell,* 155**,** 699-712.

PANDA, A., QIAN, F., MOHANTY, S., VAN DUIN, D., NEWMAN, F. K., ZHANG, L., CHEN, S., TOWLE, V., BELSHE, R. B., FIKRIG, E., ALLORE, H. G., MONTGOMERY, R. R. & SHAW, A. C. 2010. Age-Associated Decrease in TLR Function in Primary Human Dendritic Cells Predicts Influenza Vaccine Response. *The Journal of Immunology,* 184**,** 2518.

PANTEL, A., TEIXEIRA, A., HADDAD, E., WOOD, E. G., STEINMAN, R. M. & LONGHI, M. P. 2014. Direct type I IFN but not MDA5/TLR3 activation of dendritic cells is required for maturation and metabolic shift to glycolysis after poly IC stimulation. *PLoS biology,* 12**,** e1001759.

PARISH, S. T., WU, J. E. & EFFROS, R. B. 2009. Modulation of T Lymphocyte Replicative Senescence via TNF-α Inhibition: Role of Caspase-3. *The Journal of Immunology,* 182**,** 4237-4243.

PATHAI, S., BAJILLAN, H., LANDAY, A. L. & HIGH, K. P. 2014. Is HIV a model of accelerated or accentuated aging? *J Gerontol A Biol Sci Med Sci,* 69**,** 833-42.

PATTEN, D. A., WONG, J., KHACHO, M., SOUBANNIER, V., MAILLOUX, R. J., PILON-LAROSE, K., MACLAURIN, J. G., PARK, D. S., MCBRIDE, H. M., TRINKLE-MULCAHY, L., HARPER, M.-E., GERMAIN, M. & SLACK, R. S. 2014. OPA1-dependent cristae modulation is essential for cellular adaptation to metabolic demand. *The EMBO Journal,* 33**,** 2676-2691.

PAVSHINTCEV, V., PODSHIVALOVA, L., AVERINA, O., EGOROV, M. & LOVAT, M. 2017. Mitochondria-targeted antioxidant SkQ1 reduces the death of dopaminergic neurons in the model of Parkinson's disease in mice. *European Neuropsychopharmacology,* 27**,** S1031-S1032.

PENCE, B. D. & YARBRO, J. R. 2018. Aging impairs mitochondrial respiratory capacity in classical monocytes. *Experimental Gerontology,* 108**,** 112-117.

PÉREZ, V. I., VAN REMMEN, H., BOKOV, A., EPSTEIN, C. J., VIJG, J. & RICHARDSON, A. 2009. The overexpression of major antioxidant enzymes does not extend the lifespan of mice. *Aging Cell,* 8**,** 73-75.

PETROSILLO, G., MATERA, M., MORO, N., RUGGIERO, F. M. & PARADIES, G. 2009. Mitochondrial complex I dysfunction in rat heart with aging: critical role of reactive oxygen species and cardiolipin. *Free Radical Biology and Medicine,* 46**,** 88-94.

PIETSCHMANN, P., GOLLOB, E., BROSCH, S., HAHN, P., KUDLACEK, S., WILLHEIM, M., WOLOSZCZUK, W., PETERLIK, M. & TRAGL, K. H. 2003. The effect of age and gender on cytokine production by human peripheral blood mononuclear cells and markers of bone metabolism. *Experimental Gerontology,* 38**,** 1119-1127.

PLECITÁ-HLAVATÁ, L., ENGSTOVÁ, H., ALÁN, L., ŠPAČEK, T., DLASKOVÁ, A., SMOLKOVÁ, K., ŠPAČKOVÁ, J., TAUBER, J., STRÁDALOVÁ, V., MALÍNSKÝ, J., LESSARD, M., BEWERSDORF, J. & JEŽEK, P. 2016. Hypoxic HepG2 cell adaptation decreases ATP synthase dimers and ATP production in inflated cristae by mitofilin down-regulation concomitant to MICOS clustering. *The FASEB Journal,* 30**,** 1941-1957.

POPOV, N. & GIL, J. 2010. Epigenetic regulation of the INK4b-ARF-INK4a locus. *Epigenetics,* 5**,** 685-690.

PRAKASH, S., AGRAWAL, S., MA, D., GUPTA, S., PETERSON, E. M. & AGRAWAL, A. 2014. Dendritic cells from aged subjects display enhanced inflammatory responses to Chlamydophila pneumoniae. *Mediators of inflammation,* 2014.

PUGH, T. D., CONKLIN, M. W., EVANS, T. D., POLEWSKI, M. A., BARBIAN, H. J., PASS, R., ANDERSON, B. D., COLMAN, R. J., ELICEIRI, K. W., KEELY, P. J., WEINDRUCH, R., BEASLEY, T. M. & ANDERSON, R. M. 2013. A shift in energy metabolism anticipates the onset of sarcopenia in rhesus monkeys. *Aging Cell,* 12**,** 672-681.

QI, H., CASALENA, G., SHI, S., YU, L., EBEFORS, K., SUN, Y., ZHANG, W., D'AGATI, V., SCHLONDORFF, D., HARALDSSON, B., BÖTTINGER, E. & DAEHN, I. 2017. Glomerular Endothelial Mitochondrial Dysfunction Is Essential and Characteristic of Diabetic Kidney Disease Susceptibility. *Diabetes,* 66**,** 763-778.

QI, J. H., EBRAHEM, Q., MOORE, N., MURPHY, G., CLAESSON-WELSH, L., BOND, M., BAKER, A. & ANAND-APTE, B. 2003. A novel function for tissue inhibitor of metalloproteinases-3 (TIMP3): inhibition of angiogenesis by blockage of VEGF binding to VEGF receptor-2. *Nature Medicine,* 9**,** 407-415.

QIAN, F., WANG, X., ZHANG, L., LIN, A., ZHAO, H., FIKRIG, E. & MONTGOMERY, R. R. 2011. Impaired interferon signaling in dendritic cells from older donors infected in vitro with West Nile virus. *Journal of Infectious Diseases,* 203**,** 1415-1424.

RAMACHANDRAN, A., AHMAD, F., SHAW, E., SINGH, K., DAS, D., RUPANAGUDI, K. V., KOMMADDI, R. & RAVINDRANATH, V. 2016. 393-ROS-Mediated Loss of Synaptic Akt1 Signaling Leads to Deficient Activity-Dependent Protein Translation Early in Alzheimer's Disease. *Free Radical Biology and Medicine,* 100**,** S165.

RANA, A., OLIVEIRA, M. P., KHAMOUI, A. V., APARICIO, R., RERA, M., ROSSITER, H. B. & WALKER, D. W. 2017. Promoting Drp1-mediated mitochondrial fission in midlife prolongs healthy lifespan of Drosophila melanogaster. *Nature Communications,* 8**,** 448.

List of References

RANE, S., HOGAN, T., SEDDON, B. & YATES, A. J. 2018. Age is not just a number: Naive T cells increase their ability to persist in the circulation over time. *PLoS Biol,* 16**,** e2003949.

RATTAN, S. I., DEMIROVIC, D. & NIZARD, C. 2018. A preliminary attempt to establish multiple stress response profiles of human skin fibroblasts exposed to mild or severe stress during ageing in vitro. *Mechanisms of ageing and development,* 170**,** 92-97.

REBRIN, I., FORSTER, M. J. & SOHAL, R. S. 2007. Effects of age and caloric intake on glutathione redox state in different brain regions of C57BL/6 and DBA/2 mice. *Brain research,* 1127**,** 10-18.

REBRIN, I., ZICKER, S., WEDEKIND, K. J., PAETAU-ROBINSON, I., PACKER, L. & SOHAL, R. S. 2005. Effect of antioxidant-enriched diets on glutathione redox status in tissue homogenates and mitochondria of the senescence-accelerated mouse. *Free Radical Biology and Medicine,* 39**,** 549-557.

REDDY, P. H. & BEAL, M. F. 2008. Amyloid beta, mitochondrial dysfunction and synaptic damage: implications for cognitive decline in aging and Alzheimer's disease. *Trends in Molecular Medicine,* 14**,** 45-53.

REITER, L. T., POTOCKI, L., CHIEN, S., GRIBSKOV, M. & BIER, E. 2001. A systematic analysis of human disease-associated gene sequences in Drosophila melanogaster. *Genome Res,* 11**,** 1114-25.

REY, S., SCHITO, L., KORITZINSKY, M. & WOUTERS, B. G. 2016. ADP-dependent glucokinase enhances hypoxia-inducible factor-α target gene transactivation through modulation of ROS levels in hypoxic human cancer cells. AACR.

REYNOLDS, L. M., DING, J., TAYLOR, J. R., LOHMAN, K., SORANZO, N., DE LA FUENTE, A., LIU, T. F., JOHNSON, C., BARR, R. G., REGISTER, T. C., DONOHUE, K. M., TALOR, M. V., CIHAKOVA, D., GU, C., DIVERS, J., SISCOVICK, D., BURKE, G., POST, W., SHEA, S., JACOBS, D. R., HOESCHELE, I., MCCALL, C. E., KRITCHEVSKY, S. B., HERRINGTON, D., TRACY, R. P. & LIU, Y. 2015. Transcriptomic profiles of aging in purified human immune cells. *BMC Genomics,* 16**,** 333.

RIFFELMACHER, T., CLARKE, A., RICHTER, F. C., STRANKS, A., PANDEY, S., DANIELLI, S., HUBLITZ, P., YU, Z., JOHNSON, E., SCHWERD, T., MCCULLAGH, J., UHLIG, H., JACOBSEN, S. E. W. & SIMON, A. K. 2017. Autophagy-Dependent Generation of Free Fatty Acids Is Critical for Normal Neutrophil Differentiation. *Immunity,* 47**,** 466-480.e5.

RISTOW, M. 2014. Unraveling the Truth About Antioxidants: Mitohormesis explains ROS-induced health benefits. *Nature Medicine,* 20**,** 709.

RODRÍGUEZ-ESPINOSA, O., ROJAS-ESPINOSA, O., MORENO-ALTAMIRANO, M. M. B., LÓPEZ-VILLEGAS, E. O. & SÁNCHEZ-GARCÍA, F. J. 2015. Metabolic requirements for neutrophil extracellular traps formation. *Immunology,* 145**,** 213-224.

RON-HAREL, N., SANTOS, D., GHERGUROVICH, J. M., SAGE, P. T., REDDY, A., LOVITCH, S. B., DEPHOURE, N., SATTERSTROM, F. K., SHEFFER, M., SPINELLI, J. B., GYGI, S., RABINOWITZ, J. D., SHARPE, A. H. & HAIGIS, M. C. 2016. Mitochondrial Biogenesis and Proteome Remodeling Promote One-Carbon Metabolism for T Cell Activation. *Cell metabolism,* 24**,** 104-117.

ROSALES, C. 2018. Neutrophil: A Cell with Many Roles in Inflammation or Several Cell Types? *Frontiers in physiology,* 9**,** 113-113.

ROSSI, C., MARZANO, V., CONSALVO, A., ZUCCHELLI, M., LEVI MORTERA, S., CASAGRANDE, V., MAVILIO, M., SACCHETTA, P., FEDERICI, M., MENGHINI, R., URBANI, A. & CIAVARDELLI, D.

2018. Proteomic and metabolomic characterization of streptozotocin-induced diabetic nephropathy in TIMP3-deficient mice. *Acta Diabetologica,* 55**,** 121-129.

ROSSI, D. J., SEITA, J., CZECHOWICZ, A., BHATTACHARYA, D., BRYDER, D. & WEISSMAN, I. L. 2007. Hematopoietic Stem Cell Quiescence Attenuates DNA Damage Response and Permits DNA Damage Accumulation During Aging. *Cell Cycle,* 6**,** 2371-2376.

RUBIE, C., KÖLSCH, K., HALAJDA, B., EICHLER, H., WAGENPFEIL, S., ROEMER, K. & GLANEMANN, M. 2016. microRNA-496 – A new, potentially aging-relevant regulator of mTOR. *Cell Cycle,* 15**,** 1108-1116.

RUDOLPH, K. L., CHANG, S., LEE, H.-W., BLASCO, M., GOTTLIEB, G. J., GREIDER, C. & DEPINHO, R. A. 1999. Longevity, Stress Response, and Cancer in Aging Telomerase-Deficient Mice. *Cell,* 96**,** 701-712.

RYAN, D. G. & O'NEILL, L. A. 2017. Krebs cycle rewired for macrophage and dendritic cell effector functions. *FEBS letters,* 591**,** 2992-3006.

SABROE, I., JONES, E. C., USHER, L. R., WHYTE, M. K. & DOWER, S. K. 2002. Toll-like receptor (TLR) 2 and TLR4 in human peripheral blood granulocytes: a critical role for monocytes in leukocyte lipopolysaccharide responses. *The Journal of Immunology,* 168**,** 4701-4710.

SAHEBJAM, S., KHOKHA, R. & MORT, J. S. 2007. Increased collagen and aggrecan degradation with age in the joints of Timp3(-/-) mice. *Arthritis Rheum,* 56**,** 905-9.

SAKUISHI, K., APETOH, L., SULLIVAN, J. M., BLAZAR, B. R., KUCHROO, V. K. & ANDERSON, A. C. 2010. Targeting Tim-3 and PD-1 pathways to reverse T cell exhaustion and restore anti-tumor immunity. *J Exp Med,* 207**,** 2187-94.

SALAM, N., RANE, S., DAS, R., FAULKNER, M., GUND, R., KANDPAL, U., LEWIS, V., MATTOO, H., PRABHU, S., RANGANATHAN, V., DURDIK, J., GEORGE, A., RATH, S. & BAL, V. 2013. T cell ageing: effects of age on development, survival & function. *The Indian journal of medical research,* 138**,** 595-608.

SALLUSTO, F., GEGINAT, J. & LANZAVECCHIA, A. 2004. Central memory and effector memory T cell subsets: function, generation, and maintenance. *Annu Rev Immunol,* 22**,** 745-63.

SALMINEN, A., HUUSKONEN, J., OJALA, J., KAUPPINEN, A., KAARNIRANTA, K. & SUURONEN, T. 2008. Activation of innate immunity system during aging: NF-kB signaling is the molecular culprit of inflamm-aging. *Ageing Research Reviews,* 7**,** 83-105.

SALMINEN, A., OJALA, J., KAARNIRANTA, K., HAAPASALO, A., HILTUNEN, M. & SOININEN, H. 2011. Astrocytes in the aging brain express characteristics of senescence-associated secretory phenotype. *European Journal of Neuroscience,* 34**,** 3-11.

SAMIEC, P. S., DREWS-BOTSCH, C., FLAGG, E. W., KURTZ, J. C., STERNBERG JR, P., REED, R. L. & JONES, D. P. 1998. Glutathione in human plasma: decline in association with aging, age-related macular degeneration, and diabetes. *Free Radical Biology and Medicine,* 24**,** 699-704.

SANDERSON, S. L. & SIMON, A. K. 2017. In aged primary T cells, mitochondrial stress contributes to telomere attrition measured by a novel imaging flow cytometry assay. *Aging cell,* 16**,** 1234-1243.

SATHALIYAWALA, T., O'GORMAN, W. E., GRETER, M., BOGUNOVIC, M., KONJUFCA, V., HOU, Z. E., NOLAN, G. P., MILLER, M. J., MERAD, M. & REIZIS, B. 2010. Mammalian target of rapamycin

controls dendritic cell development downstream of Flt3 ligand signaling. *Immunity,* 33**,** 597-606.

SCHARPING, N. E., MENK, A. V., MORECI, R. S., WHETSTONE, R. D., DADEY, R. E., WATKINS, S. C., FERRIS, R. L. & DELGOFFE, G. M. 2016. The Tumor Microenvironment Represses T Cell Mitochondrial Biogenesis to Drive Intratumoral T Cell Metabolic Insufficiency and Dysfunction. *Immunity,* 45**,** 374-88.

SCHEFFLER, J. M., SPARBER, F., TRIPP, C. H., HERRMANN, C., HUMENBERGER, A., BLITZ, J., ROMANI, N., STOITZNER, P. & HUBER, L. A. 2014. LAMTOR2 regulates dendritic cell homeostasis through FLT3-dependent mTOR signalling. *Nature communications,* 5**,** 5138.

SCHLAEPFER, I. R., RIDER, L., RODRIGUES, L. U., GIJÓN, M. A., PAC, C. T., ROMERO, L., CIMIC, A., SIRINTRAPUN, S. J., GLODÉ, L. M. & ECKEL, R. H. 2014. Lipid catabolism via CPT1 as a therapeutic target for prostate cancer. *Molecular cancer therapeutics,* 13**,** 2361-2371.

SCHNEIDER, J. L., VILLARROYA, J., DIAZ-CARRETERO, A., PATEL, B., URBANSKA, A. M., THI, M. M., VILLARROYA, F., SANTAMBROGIO, L. & CUERVO, A. M. 2015. Loss of hepatic chaperone-mediated autophagy accelerates proteostasis failure in aging. *Aging Cell,* 14**,** 249-264.

SCHRINER, S. E., LINFORD, N. J., MARTIN, G. M., TREUTING, P., OGBURN, C. E., EMOND, M., COSKUN, P. E., LADIGES, W., WOLF, N., VAN REMMEN, H., WALLACE, D. C. & RABINOVITCH, P. S. 2005. Extension of Murine Life Span by Overexpression of Catalase Targeted to Mitochondria. *Science,* 308**,** 1909-1911.

SCHULZ, H. 1991. Beta oxidation of fatty acids. *Biochimica et Biophysica Acta (BBA)-Lipids and Lipid Metabolism,* 1081**,** 109-120.

SCOLLAY, R. G., BUTCHER, E. C. & WEISSMAN, I. L. 1980. Thymus cell migration. Quantitative aspects of cellular traffic from the thymus to the periphery in mice. *Eur J Immunol,* 10**,** 210-8.

SEIDLER, S., ZIMMERMANN, H. W., BARTNECK, M., TRAUTWEIN, C. & TACKE, F. 2010. Age-dependent alterations of monocyte subsets and monocyte-related chemokine pathways in healthy adults. *BMC Immunology,* 11**,** 30.

SENOO-MATSUDA, N., HARTMAN, P. S., AKATSUKA, A., YOSHIMURA, S. & ISHII, N. 2003. A complex II defect affects mitochondrial structure, leading to ced-3-and ced-4-dependent apoptosis and aging. *Journal of Biological Chemistry,* 278**,** 22031-22036.

SERBINA, N. V., SALAZAR-MATHER, T. P., BIRON, C. A., KUZIEL, W. A. & PAMER, E. G. 2003. TNF/iNOS-producing dendritic cells mediate innate immune defense against bacterial infection. *Immunity,* 19**,** 59-70.

SHANKAR, A., HAMER, M., MCMUNN, A. & STEPTOE, A. 2013. Social isolation and loneliness: relationships with cognitive function during 4 years of follow-up in the English Longitudinal Study of Ageing. *Psychosomatic medicine,* 75**,** 161-170.

SHANTSILA, E., WRIGLEY, B., TAPP, L., APOSTOLAKIS, S., MONTORO-GARCIA, S., DRAYSON, M. & LIP, G. 2011. Immunophenotypic characterization of human monocyte subsets: possible implications for cardiovascular disease pathophysiology. *Journal of Thrombosis and Haemostasis,* 9**,** 1056-1066.

SHAO, Q., NING, H., LV, J., LIU, Y., ZHAO, X., REN, G., FENG, A., XIE, Q., SUN, J., SONG, B., YANG, Y., GAO, W., DING, K., YANG, M., HOU, M., PENG, J. & QU, X. 2012. Regulation of Th1/Th2 polarization by tissue inhibitor of metalloproteinase-3 via modulating dendritic cells. *Blood,* 119**,** 4636-4644.

SHAPIRO, H. M. 2005. *Practical flow cytometry*, John Wiley & Sons.

SHARMA, H. W., SOKOLOSKI, J. A., PEREZ, J. R., MALTESE, J. Y., SARTORELLI, A. C., STEIN, C. A., NICHOLS, G., KHALED, Z., TELANG, N. T. & NARAYANAN, R. 1995. Differentiation of immortal cells inhibits telomerase activity. *Proceedings of the National Academy of Sciences,* 92**,** 12343-12346.

SHEN, H. H., OCHKUR, S. I., MCGARRY, M. P., CROSBY, J. R., HINES, E. M., BORCHERS, M. T., WANG, H., BIECHELLE, T. L., O'NEILL, K. R., ANSAY, T. L., COLBERT, D. C., CORMIER, S. A., JUSTICE, J. P., LEE, N. A. & LEE, J. J. 2003. A causative relationship exists between eosinophils and the development of allergic pulmonary pathologies in the mouse. *J Immunol,* 170**,** 3296-305.

SHERR, C. J. 2012. Ink4-Arf Locus in Cancer and Aging. *Wiley interdisciplinary reviews. Developmental biology,* 1**,** 731-741.

SHI, C. & PAMER, E. G. 2011. Monocyte recruitment during infection and inflammation. *Nat Rev Immunol,* 11**,** 762-74.

SHI, H. Z., HUMBLES, A., GERARD, C., JIN, Z. & WELLER, P. F. 2000. Lymph node trafficking and antigen presentation by endobronchial eosinophils. *J Clin Invest,* 105**,** 945-53.

SHIMADA, H., KIMURA, Y., LORD, S. R., ODA, K., ISHII, K., SUZUKI, T. & ISHIWATA, K. 2009. Comparison of regional lower limb glucose metabolism in older adults during walking. *Scand J Med Sci Sports,* 19**,** 389-97.

SHORT, K. R., BIGELOW, M. L., KAHL, J., SINGH, R., COENEN-SCHIMKE, J., RAGHAVAKAIMAL, S. & NAIR, K. S. 2005. Decline in skeletal muscle mitochondrial function with aging in humans. *Proc Natl Acad Sci U S A,* 102**,** 5618-23.

SHUMAKER, D. K., DECHAT, T., KOHLMAIER, A., ADAM, S. A., BOZOVSKY, M. R., ERDOS, M. R., ERIKSSON, M., GOLDMAN, A. E., KHUON, S., COLLINS, F. S., JENUWEIN, T. & GOLDMAN, R. D. 2006. Mutant nuclear lamin A leads to progressive alterations of epigenetic control in premature aging. *Proceedings of the National Academy of Sciences,* 103**,** 8703-8708.

SIMULA, L., CAMPANELLA, M. & CAMPELLO, S. 2019. Targeting Drp1 and mitochondrial fission for therapeutic immune modulation. *Pharmacological Research,* 146**,** 104317.

SIMULA, L., PACELLA, I., COLAMATTEO, A., PROCACCINI, C., CANCILA, V., BORDI, M., TREGNAGO, C., CORRADO, M., PIGAZZI, M., BARNABA, V., TRIPODO, C., MATARESE, G., PICONESE, S. & CAMPELLO, S. 2018. Drp1 Controls Effective T Cell Immune-Surveillance by Regulating T Cell Migration, Proliferation, and cMyc-Dependent Metabolic Reprogramming. *Cell Reports,* 25**,** 3059-3073.e10.

SMOOKLER, D. S., MOHAMMED, F. F., KASSIRI, Z., DUNCAN, G. S., MAK, T. W. & KHOKHA, R. 2006. Tissue inhibitor of metalloproteinase 3 regulates TNF-dependent systemic inflammation. *J Immunol,* 176**,** 721-5.

SMYTH, M. J., CRETNEY, E., KELLY, J. M., WESTWOOD, J. A., STREET, S. E., YAGITA, H., TAKEDA, K., VAN DOMMELEN, S. L., DEGLI-ESPOSTI, M. A. & HAYAKAWA, Y. 2005. Activation of NK cell cytotoxicity. *Mol Immunol,* 42**,** 501-10.

SOHAL, R. S., AGARWAL, S., CANDAS, M., FORSTER, M. J. & LAL, H. 1994. Effect of age and caloric restriction on DNA oxidative damage in different tissues of C57BL/6 mice. *Mech Ageing Dev,* 76**,** 215-24.

SOLANA, R., PAWELEC, G. & TARAZONA, R. 2006. Aging and innate immunity. *Immunity,* 24**,** 491-4.

List of References

SOLANA, R., TARAZONA, R., GAYOSO, I., LESUR, O., DUPUIS, G. & FULOP, T. 2012. Innate immunosenescence: effect of aging on cells and receptors of the innate immune system in humans. *Semin Immunol,* 24**,** 331-41.

SONODA, J., LAGANIÈRE, J., MEHL, I. R., BARISH, G. D., CHONG, L.-W., LI, X., SCHEFFLER, I. E., MOCK, D. C., BATAILLE, A. R., ROBERT, F., LEE, C.-H., GIGUÈRE, V. & EVANS, R. M. 2007. Nuclear receptor ERR alpha and coactivator PGC-1 beta are effectors of IFN-gamma-induced host defense. *Genes & development,* 21**,** 1909-1920.

SOULTOUKIS, G. A. & PARTRIDGE, L. 2016. Dietary Protein, Metabolism, and Aging. *Annual Review of Biochemistry,* 85**,** 5-34.

SPONAAS, A. M., FREITAS DO ROSARIO, A. P., VOISINE, C., MASTELIC, B., THOMPSON, J., KOERNIG, S., JARRA, W., RENIA, L., MAUDUIT, M., POTOCNIK, A. J. & LANGHORNE, J. 2009. Migrating monocytes recruited to the spleen play an important role in control of blood stage malaria. *Blood,* 114**,** 5522-31.

SRIDHARAN, A., ESPOSO, M., KAUSHAL, K., TAY, J., OSANN, K., AGRAWAL, S., GUPTA, S. & AGRAWAL, A. 2011. Age-associated impaired plasmacytoid dendritic cell functions lead to decreased CD4 and CD8 T cell immunity. *Age,* 33**,** 363-376.

STARK, M. A., HUO, Y., BURCIN, T. L., MORRIS, M. A., OLSON, T. S. & LEY, K. 2005. Phagocytosis of apoptotic neutrophils regulates granulopoiesis via IL-23 and IL-17. *Immunity,* 22**,** 285-94.

STEINER, M., HUBER, S., HARRER, A. & HIMLY, M. 2016. The evolution of human basophil biology from neglect towards understanding of their immune functions. *BioMed research international,* 2016.

STEINMAN, R. M., INABA, K., TURLEY, S., PIERRE, P. & MELLMAN, I. 1999. Antigen capture, processing, and presentation by dendritic cells: recent cell biological studies. *Human immunology,* 60**,** 562-567.

STEPTOE, A., BREEZE, E., BANKS, J. & NAZROO, J. 2012. Cohort profile: the English longitudinal study of ageing. *International journal of epidemiology,* 42**,** 1640-1648.

STÖHR, R., KAPPEL, B. A., CARNEVALE, D., CAVALERA, M., MAVILIO, M., ARISI, I., FARDELLA, V., CIFELLI, G., CASAGRANDE, V., RIZZA, S., CATTANEO, A., MAURIELLO, A., MENGHINI, R., LEMBO, G. & FEDERICI, M. 2015. TIMP3 interplays with apelin to regulate cardiovascular metabolism in hypercholesterolemic mice. *Molecular Metabolism,* 4**,** 741-752.

STROHACKER, K., BRESLIN, W. L., CARPENTER, K. C. & MCFARLIN, B. K. 2012. Aged mice have increased inflammatory monocyte concentration and altered expression of cell-surface functional receptors. *Journal of Biosciences,* 37**,** 55-62.

SUMBAYEV, V. V., NICHOLAS, S. A., STREATFIELD, C. L. & GIBBS, B. F. 2009. Involvement of hypoxia-inducible factor-1 HiF(1α) in IgE-mediated primary human basophil responses. *European Journal of Immunology,* 39**,** 3511-3519.

SUMBAYEV, V. V., YASINSKA, I., ONIKU, A. E., STREATFIELD, C. L. & GIBBS, B. F. 2012. Involvement of hypoxia-inducible factor-1 in the inflammatory responses of human LAD2 mast cells and basophils. *PloS one,* 7**,** e34259-e34259.

SWIRSKI, F. K., NAHRENDORF, M., ETZRODT, M., WILDGRUBER, M., CORTEZ-RETAMOZO, V., PANIZZI, P., FIGUEIREDO, J. L., KOHLER, R. H., CHUDNOVSKIY, A., WATERMAN, P., AIKAWA, E., MEMPEL, T. R., LIBBY, P., WEISSLEDER, R. & PITTET, M. J. 2009. Identification of splenic reservoir monocytes and their deployment to inflammatory sites. *Science,* 325**,** 612-6.

SZATMARI, I., TÖRÖCSIK, D., AGOSTINI, M., NAGY, T., GURNELL, M., BARTA, E., CHATTERJEE, K. & NAGY, L. 2007. PPARγ regulates the function of human dendritic cells primarily by altering lipid metabolism. *Blood,* 110**,** 3271-3280.

TAI, J. 2016. Elderly health costs to rise tenfold by 2030: Report. *Straits Times*, Aug 25.

TAKEDA, T. 1999. Senescence-accelerated mouse (SAM): a biogerontological resource in aging research. *Neurobiology of Aging,* 20**,** 105-110.

TAKEDA, T., HIGUCHI, K. & HOSOKAWA, M. 1997. Senescence-accelerated Mouse (SAM): With Special Reference to Development and Pathobiological Phenotypes. *ILAR Journal,* 38**,** 109-118.

TAKEDA, T., HOSOKAWA, M., HIGUCHI, K., HOSONO, M., AKIGUCHI, I. & KATOH, H. 1994. A novel murine model of aging, Senescence-Accelerated Mouse (SAM). *Archives of Gerontology and Geriatrics,* 19**,** 185-192.

TAKEDA, T., HOSOKAWA, M., TAKESHITA, S., IRINO, M., HIGUCHI, K., MATSUSHITA, T., TOMITA, Y., YASUHIRA, K., HAMAMOTO, H., SHIMIZU, K., ISHII, M. & YAMAMURO, T. 1981. A new murine model of accelerated senescence. *Mechanisms of Ageing and Development,* 17**,** 183-194.

TAMOUTOUNOUR, S., GUILLIAMS, M., MONTANANA SANCHIS, F., LIU, H., TERHORST, D., MALOSSE, C., POLLET, E., ARDOUIN, L., LUCHE, H., SANCHEZ, C., DALOD, M., MALISSEN, B. & HENRI, S. 2013. Origins and functional specialization of macrophages and of conventional and monocyte-derived dendritic cells in mouse skin. *Immunity,* 39**,** 925-38.

TAN, J.-K., JAAFAR, F. & MAKPOL, S. 2018. Proteomic profiling of senescent human diploid fibroblasts treated with gamma-tocotrienol. *BMC complementary and alternative medicine,* 18**,** 314.

TATAR, M., KOPELMAN, A., EPSTEIN, D., TU, M.-P., YIN, C.-M. & GAROFALO, R. 2001. A mutant Drosophila insulin receptor homolog that extends life-span and impairs neuroendocrine function. *Science,* 292**,** 107-110.

TECCHIO, C. & CASSATELLA, M. A. 2016. Neutrophil-derived chemokines on the road to immunity. *Semin Immunol,* 28**,** 119-28.

TERAMOTO, S., FUKUCHI, Y., UEJIMA, Y., TERAMOTO, K. & ORIMO, H. 1995. Biochemical characteristics of lungs in senescence-accelerated mouse (SAM). *Eur Respir J,* 8**,** 450-6.

THA, K. K., OKUMA, Y., MIYAZAKI, H., MURAYAMA, T., UEHARA, T., HATAKEYAMA, R., HAYASHI, Y. & NOMURA, Y. 2000. Changes in expressions of proinflammatory cytokines IL-1β, TNF-α and IL-6 in the brain of senescence accelerated mouse (SAM) P8. *Brain Research,* 885**,** 25-31.

THIERY, J., KEEFE, D., BOULANT, S., BOUCROT, E., WALCH, M., MARTINVALET, D., GOPING, I. S., BLEACKLEY, R. C., KIRCHHAUSEN, T. & LIEBERMAN, J. 2011. Perforin pores in the endosomal membrane trigger the release of endocytosed granzyme B into the cytosol of target cells. *Nat Immunol,* 12**,** 770-7.

THOME, JOSEPH J. C., YUDANIN, N., OHMURA, Y., KUBOTA, M., GRINSHPUN, B., SATHALIYAWALA, T., KATO, T., LERNER, H., SHEN, Y. & FARBER, DONNA L. 2014. Spatial Map of Human T Cell Compartmentalization and Maintenance over Decades of Life. *Cell,* 159**,** 814-828.

THWE, P. M., PELGROM, L., COOPER, R., BEAUCHAMP, S., REISZ, J. A., D'ALESSANDRO, A., EVERTS, B. & AMIEL, E. 2017. Cell-intrinsic glycogen metabolism supports early glycolytic

reprogramming required for dendritic cell immune responses. *Cell metabolism,* 26**,** 558-567. e5.

TIAN, Y., BABOR, M., LANE, J., SCHULTEN, V., PATIL, V. S., SEUMOIS, G., ROSALES, S. L., FU, Z., PICARDA, G., BUREL, J., ZAPARDIEL-GONZALO, J., TENNEKOON, R. N., DE SILVA, A. D., PREMAWANSA, S., PREMAWANSA, G., WIJEWICKRAMA, A., GREENBAUM, J. A., VIJAYANAND, P., WEISKOPF, D., SETTE, A. & PETERS, B. 2017. Unique phenotypes and clonal expansions of human CD4 effector memory T cells re-expressing CD45RA. *Nat Commun,* 8**,** 1473.

TILLY, G., DOAN-NGOC, T.-M., YAP, M., CARISTAN, A., JACQUEMONT, L., DANGER, R., CADOUX, M., BRUNEAU, S., GIRAL, M., GUERIF, P., NICOL, B., GARCIA, A., LAPLAUD, D.-A., BROUARD, S., PECQUEUR HELLMAN, C. & DEGAUQUE, N. 2017. IL-15 Harnesses Pro-inflammatory Function of TEMRA CD8 in Kidney-Transplant Recipients. *Frontiers in Immunology,* 8.

TORREGROSA-MUÑUMER, R., GÓMEZ, A., VARA, E., KIREEV, R., BARJA, G., TRESGUERRES, J. A. F. & GREDILLA, R. 2016. Reduced apurinic/apyrimidinic endonuclease 1 activity and increased DNA damage in mitochondria are related to enhanced apoptosis and inflammation in the brain of senescence- accelerated P8 mice (SAMP8). *Biogerontology,* 17**,** 325-335.

TRIFUNOVIC, A., WREDENBERG, A., FALKENBERG, M., SPELBRINK, J. N., ROVIO, A. T., BRUDER, C. E., BOHLOOLY-Y, M., GIDLOF, S., OLDFORS, A., WIBOM, R., TORNELL, J., JACOBS, H. T. & LARSSON, N.-G. 2004. Premature ageing in mice expressing defective mitochondrial DNA polymerase. *Nature,* 429**,** 417-423.

TRZONKOWSKI, P., DĘBSKA-ŚLIZIEŃ, A., JANKOWSKA, M., WARDOWSKA, A., CARVALHO-GASPAR, M., HAK, Ł., MOSZKOWSKA, G., BZOMA, B., MILLS, N., WOOD, K. J., MYŚLIWSKA, J. & RUTKOWSKI, B. 2010. Immunosenescence increases the rate of acceptance of kidney allotransplants in elderly recipients through exhaustion of CD4+ T-cells. *Mechanisms of Ageing and Development,* 131**,** 96-104.

TSUDA, Y., TAKAHASHI, H., KOBAYASHI, M., HANAFUSA, T., HERNDON, D. N. & SUZUKI, F. 2004. Three different neutrophil subsets exhibited in mice with different susceptibilities to infection by methicillin-resistant Staphylococcus aureus. *Immunity,* 21**,** 215-26.

TSUJI, R., KOMANO, Y., OHSHIO, K., ISHII, N. & KANAUCHI, O. 2018. Long-term administration of pDC stimulative lactic acid bacteria, Lactococcus lactis strain Plasma, prevents immune-senescence and decelerates individual senescence. *Experimental gerontology,* 111**,** 10-16.

TSUKAMOTO, H., CLISE-DWYER, K., HUSTON, G. E., DUSO, D. K., BUCK, A. L., JOHNSON, L. L., HAYNES, L. & SWAIN, S. L. 2009. Age-associated increase in lifespan of naive CD4 T cells contributes to T-cell homeostasis but facilitates development of functional defects. *Proceedings of the National Academy of Sciences of the United States of America,* 106**,** 18333-18338.

TSUKAMOTO, M., SETA, N., YOSHIMOTO, K., SUZUKI, K., YAMAOKA, K. & TAKEUCHI, T. 2017. CD14 bright CD16+ intermediate monocytes are induced by interleukin-10 and positively correlate with disease activity in rheumatoid arthritis. *Arthritis research & therapy,* 19**,** 28.

TYRRELL, D. J., BHARADWAJ, M. S., VAN HORN, C. G., KRITCHEVSKY, S. B., NICKLAS, B. J. & MOLINA, A. J. A. 2015a. Respirometric Profiling of Muscle Mitochondria and Blood Cells Are Associated With Differences in Gait Speed Among Community-Dwelling Older Adults. *The journals of gerontology. Series A, Biological sciences and medical sciences,* 70**,** 1394-1399.

TYRRELL, D. J., BHARADWAJ, M. S., VAN HORN, C. G., MARSH, A. P., NICKLAS, B. J. & MOLINA, A. J. A. 2015b. Blood-cell bioenergetics are associated with physical function and inflammation in overweight/obese older adults. *Experimental gerontology,* 70**,** 84-91.

UCIECHOWSKI, P. & RINK, L. 2018. Neutrophil, basophil, and eosinophil granulocyte functions in the elderly. *Handbook of Immunosenescence: Basic Understanding and Clinical Implications***,** 1-27.

UNITED NATIONS, D. O. E. A. S. A., POPULATION DIVISION, 2019. World Population Prospects 2019.

VALERIO, A., CARDILE, A., COZZI, V., BRACALE, R., TEDESCO, L., PISCONTI, A., PALOMBA, L., CANTONI, O., CLEMENTI, E., MONCADA, S., CARRUBA, M. O. & NISOLI, E. 2006. TNF-alpha downregulates eNOS expression and mitochondrial biogenesis in fat and muscle of obese rodents. *J Clin Invest,* 116**,** 2791-8.

VALTORTA, N. K., KANAAN, M., GILBODY, S. & HANRATTY, B. 2018. Loneliness, social isolation and risk of cardiovascular disease in the English Longitudinal Study of Ageing. *European journal of preventive cardiology,* 25**,** 1387-1396.

VAN BEEK, A. A., FRANSEN, F., MEIJER, B., DE VOS, P., KNOL, E. F. & SAVELKOUL, H. F. 2018. Aged mice display altered numbers and phenotype of basophils, and bone marrow-derived basophil activation, with a limited role for aging-associated microbiota. *Immunity & Ageing,* 15**,** 32.

VAN BEEK, A. A., KNOL, E., DE VOS, P., SMELT, M., SAVELKOUL, H. & VAN NEERVEN, R. 2013. Recent developments in basophil research: do basophils initiate and perpetuate type 2 T-helper cell responses? *International archives of allergy and immunology,* 160**,** 7-17.

VAN DE VEN, R. A., SANTOS, D. & HAIGIS, M. C. 2017. Mitochondrial sirtuins and molecular mechanisms of aging. *Trends in molecular medicine,* 23**,** 320-331.

VAN DER GEEST, K. S., ABDULAHAD, W. H., TETELOSHVILI, N., TETE, S. M., PETERS, J. H., HORST, G., LORENCETTI, P. G., BOS, N. A., LAMBECK, A., ROOZENDAAL, C., KROESEN, B. J., KOENEN, H. J., JOOSTEN, I., BROUWER, E. & BOOTS, A. M. 2015. Low-affinity TCR engagement drives IL-2-dependent post-thymic maintenance of naive CD4+ T cells in aged humans. *Aging Cell,* 14**,** 744-53.

VAN DER WINDT, GERRITJE J. W., EVERTS, B., CHANG, C.-H., CURTIS, JONATHAN D., FREITAS, TORI C., AMIEL, E., PEARCE, EDWARD J. & PEARCE, ERIKA L. 2012. Mitochondrial Respiratory Capacity Is a Critical Regulator of CD8+ T Cell Memory Development. *Immunity,* 36**,** 68-78.

VAN DER WINDT, G. J. W., O'SULLIVAN, D., EVERTS, B., HUANG, S. C.-C., BUCK, M. D., CURTIS, J. D., CHANG, C.-H., SMITH, A. M., AI, T., FAUBERT, B., JONES, R. G., PEARCE, E. J. & PEARCE, E. L. 2013. CD8 memory T cells have a bioenergetic advantage that underlies their rapid recall ability. *Proceedings of the National Academy of Sciences,* 110**,** 14336.

VAN DEURSEN, J. M. 2014. The role of senescent cells in ageing. *Nature,* 509**,** 439-446.

VAN DUIN, D., MOHANTY, S., THOMAS, V., GINTER, S., MONTGOMERY, R. R., FIKRIG, E., ALLORE, H. G., MEDZHITOV, R. & SHAW, A. C. 2007. Age-associated defect in human TLR-1/2 function. *The Journal of Immunology,* 178**,** 970-975.

VATS, D., MUKUNDAN, L., ODEGAARD, J. I., ZHANG, L., SMITH, K. L., MOREL, C. R., WAGNER, R. A., GREAVES, D. R., MURRAY, P. J. & CHAWLA, A. 2006. Oxidative metabolism and PGC-1beta attenuate macrophage-mediated inflammation. *Cell Metab,* 4**,** 13-24.

VERMULST, M., WANAGAT, J., KUJOTH, G. C., BIELAS, J. H., RABINOVITCH, P. S., PROLLA, T. A. & LOEB, L. A. 2008. DNA deletions and clonal mutations drive premature aging in mitochondrial mutator mice. *Nat Genet,* 40**,** 392-394.

VERSCHOOR, C. P., LOUKOV, D., NAIDOO, A., PUCHTA, A., JOHNSTONE, J., MILLAR, J., LELIC, A., NOVAKOWSKI, K. E., DORRINGTON, M. G., LOEB, M., BRAMSON, J. L. & BOWDISH, D. M. E. 2015. Circulating TNF and mitochondrial DNA are major determinants of neutrophil phenotype in the advanced-age, frail elderly. *Molecular Immunology,* 65**,** 148-156.

VILLANI, A.-C., SATIJA, R., REYNOLDS, G., SARKIZOVA, S., SHEKHAR, K., FLETCHER, J., GRIESBECK, M., BUTLER, A., ZHENG, S. & LAZO, S. 2017. Single-cell RNA-seq reveals new types of human blood dendritic cells, monocytes, and progenitors. *Science,* 356**,** eaah4573.

VITALE, M., DELLA CHIESA, M., CARLOMAGNO, S., PENDE, D., ARICO, M., MORETTA, L. & MORETTA, A. 2005. NK-dependent DC maturation is mediated by TNFalpha and IFNgamma released upon engagement of the NKp30 triggering receptor. *Blood,* 106**,** 566-71.

WAGNER, W., BORK, S., HORN, P., KRUNIC, D., WALENDA, T., DIEHLMANN, A., BENES, V., BLAKE, J., HUBER, F.-X. & ECKSTEIN, V. 2009. Aging and replicative senescence have related effects on human stem and progenitor cells. *PloS one,* 4**,** e5846.

WALKER, G. A. & LITHGOW, G. J. 2003. Lifespan extension in C. elegans by a molecular chaperone dependent upon insulin-like signals. *Aging Cell,* 2**,** 131-139.

WANG, J., CHENG, X., ZHANG, X., CHENG, J., XU, Y., ZENG, J., ZHOU, W. & ZHANG, Y. 2016. The anti-aging effects of LW-AFC via correcting immune dysfunctions in senescence accelerated mouse resistant 1 (SAMR1) strain. *Oncotarget,* 7**,** 26949-26965.

WANG, M. C., BOHMANN, D. & JASPER, H. 2003. JNK Signaling Confers Tolerance to Oxidative Stress and Extends Lifespan in Drosophila. *Developmental Cell,* 5**,** 811-816.

WANG, Y., WANG, W., WANG, N., TALL, A. R. & TABAS, I. 2017. Mitochondrial oxidative stress promotes atherosclerosis and neutrophil extracellular traps in aged mice. *Arteriosclerosis, thrombosis, and vascular biology,* 37**,** e99-e107.

WANG, Y., XU, W., YAN, Z., ZHAO, W., MI, J., LI, J. & YAN, H. 2018. Metformin induces autophagy and G0/G1 phase cell cycle arrest in myeloma by targeting the AMPK/mTORC1 and mTORC2 pathways. *Journal of Experimental & Clinical Cancer Research,* 37**,** 63.

WARBURG, O. 1956. On the origin of cancer cells. *Science,* 123**,** 309-14.

WARDE, N. 2010. Activated basophils exacerbate lupus nephritis by amplifying production of autoreactive IgE. *Nat Rev Rheumatol,* 6**,** 438.

WATERS, D. L., BROOKS, W. M., QUALLS, C. R. & BAUMGARTNER, R. N. 2003. Skeletal muscle mitochondrial function and lean body mass in healthy exercising elderly. *Mech Ageing Dev,* 124**,** 301-9.

WCULEK, S. K., KHOUILI, S. C., PRIEGO, E., HERAS-MURILLO, I. & SANCHO, D. 2019. Metabolic Control of Dendritic Cell Functions: Digesting Information. *Frontiers in Immunology,* 10.

WEN, T. & ROTHENBERG, M. E. 2016. The Regulatory Function of Eosinophils. *Microbiology spectrum,* 4**,** 10.1128/microbiolspec.MCHD-0020-2015.

WENG, N. P., AKBAR, A. N. & GORONZY, J. 2009. CD28(-) T cells: their role in the age-associated decline of immune function. *Trends Immunol,* 30**,** 306-12.

WEST, A. P., BRODSKY, I. E., RAHNER, C., WOO, D. K., ERDJUMENT-BROMAGE, H., TEMPST, P., WALSH, M. C., CHOI, Y., SHADEL, G. S. & GHOSH, S. 2011. TLR signalling augments macrophage bactericidal activity through mitochondrial ROS. *Nature,* 472**,** 476-80.

WHITE, J. G., AMOS, W. B. & FORDHAM, M. 1987. An evaluation of confocal versus conventional imaging of biological structures by fluorescence light microscopy. *The Journal of cell biology,* 105**,** 41-48.

WHITING, C. C., SIEBERT, J., NEWMAN, A. M., DU, H. W., ALIZADEH, A. A., GORONZY, J., WEYAND, C. M., KRISHNAN, E., FATHMAN, C. G. & MAECKER, H. T. 2015. Large-Scale and Comprehensive Immune Profiling and Functional Analysis of Normal Human Aging. *PLoS One,* 10**,** e0133627.

WICK, M., BÜRGER, C., BRÜSSELBACH, S., LUCIBELLO, F. C. & MÜLLER, R. 1994. A novel member of human tissue inhibitor of metalloproteinases (TIMP) gene family is regulated during G1 progression, mitogenic stimulation, differentiation, and senescence. *Journal of Biological Chemistry,* 269**,** 18953-18960.

WILLIAMS-GRAY, C. H., WIJEYEKOON, R. S., SCOTT, K. M., HAYAT, S., BARKER, R. A. & JONES, J. L. 2018. Abnormalities of age-related T cell senescence in Parkinson's disease. *J Neuroinflammation,* 15**,** 166.

WILSON, A., LAURENTI, E., OSER, G., VAN DER WATH, R. C., BLANCO-BOSE, W., JAWORSKI, M., OFFNER, S., DUNANT, C. F., ESHKIND, L., BOCKAMP, E., LIÓ, P., MACDONALD, H. R. & TRUMPP, A. 2008. Hematopoietic Stem Cells Reversibly Switch from Dormancy to Self-Renewal during Homeostasis and Repair. *Cell,* 135**,** 1118-1129.

WORLD HEALTH ORGANIZATION 2015. *World report on ageing and health*, World Health Organization.

WORLD HEALTH ORGANIZATION 2016. *World health statistics 2016: monitoring health for the SDGs sustainable development goals*, World Health Organization.

XIA, N., FÖRSTERMANN, U. & LI, H. 2017. Implication of eNOS Uncoupling in Cardiovascular Disease. *Reactive Oxygen Species***,** 38–46%V 3.

XU, J., SHI, C., LI, Q., WU, J., FORSTER, E. L. & YEW, D. T. 2007. Mitochondrial dysfunction in platelets and hippocampi of senescence-accelerated mice. *J Bioenerg Biomembr,* 39**,** 195-202.

XU, M., TCHKONIA, T., DING, H., OGRODNIK, M., LUBBERS, E. R., PIRTSKHALAVA, T., WHITE, T. A., JOHNSON, K. O., STOUT, M. B., MEZERA, V., GIORGADZE, N., JENSEN, M. D., LEBRASSEUR, N. K. & KIRKLAND, J. L. 2015. JAK inhibition alleviates the cellular senescence-associated secretory phenotype and frailty in old age. *Proceedings of the National Academy of Sciences,* 112**,** E6301-E6310.

XU, X.-P., YAO, Y.-M., ZHAO, G.-J., WU, Z.-S., LI, J.-C., JIANG, Y.-L., LU, Z.-Q. & HONG, G.-L. 2018. Role of the Ca(2+)-Calcineurin-Nuclear Factor of Activated T cell Pathway in Mitofusin-2-Mediated Immune Function of Jurkat Cells. *Chinese medical journal,* 131**,** 330-338.

YAMAGATA, K., KATO, J.-I., SHIMAMOTO, A., GOTO, M., FURUICHI, Y. & IKEDA, H. 1998. Bloom's and Werner's syndrome genes suppress hyperrecombination in yeast sgs1 mutant: implication for genomic instability in human diseases. *Proceedings of the National Academy of Sciences,* 95**,** 8733-8738.

YAMAGUCHI, H., CALADO, R. T., LY, H., KAJIGAYA, S., BAERLOCHER, G. M., CHANOCK, S. J., LANSDORP, P. M. & YOUNG, N. S. 2005. Mutations in TERT, the Gene for Telomerase

Reverse Transcriptase, in Aplastic Anemia. *New England Journal of Medicine,* 352**,** 1413-1424.

YANG, H., LYUTVINSKIY, Y., SOININEN, H. & ZUBAREV, R. A. 2011. Alzheimer's disease and mild cognitive impairment are associated with elevated levels of isoaspartyl residues in blood plasma proteins. *J Alzheimers Dis,* 27**,** 113-8.

YANG, R., LIRUSSI, D., THORNTON, T. M., JELLEY-GIBBS, D. M., DIEHL, S. A., CASE, L. K., MADESH, M., TAATJES, D. J., TEUSCHER, C. & HAYNES, L. 2015. Mitochondrial Ca2+ and membrane potential, an alternative pathway for Interleukin 6 to regulate CD4 cell effector function. *Elife,* 4**,** e06376.

YANG, X.-F., LI, X., SHA, X., SHAO, Y., KUO, Y.-M., ANDREWS, A. J., PASCUAL, D. W. & WANG, H. 2017. IL-35, a Newly Proposed Homeostasis-Associated Molecular Pattern, Suppresses Aortic Endothelial Cell Activation and Atherosclerosis by Inhibiting Mitochondrial ROS-Mediated Site-Specific Acetylation of H3K14. Am Heart Assoc.

YANG, Y., BAZHIN, A. V., WERNER, J. & KARAKHANOVA, S. 2013. Reactive Oxygen Species in the Immune System. *International Reviews of Immunology,* 32**,** 249-270.

YAP, M., BOEFFARD, F., CLAVE, E., PALLIER, A., DANGER, R., GIRAL, M., DANTAL, J., FOUCHER, Y., GUILLOT-GUEGUEN, C., TOUBERT, A., SOULILLOU, J.-P., BROUARD, S. & DEGAUQUE, N. 2014. Expansion of Highly Differentiated Cytotoxic Terminally Differentiated Effector Memory CD8<sup>+</sup> T Cells in a Subset of Clinically Stable Kidney Transplant Recipients: A Potential Marker for Late Graft Dysfunction. *Journal of the American Society of Nephrology,* 25**,** 1856.

YEHUDA, A. B., GLOBERSON, A., KRICHEVSKY, S., ON, H. B., KIDRON, M., FRIEDLANDER, Y., FRIEDMAN, G. & YEHUDA, D. B. 2001. Ageing and the mismatch repair system. *Mechanisms of ageing and development,* 121**,** 173-179.

YOSHIDA, K., COLOGNE, J. B., CORDOVA, K., MISUMI, M., YAMAOKA, M., KYOIZUMI, S., HAYASHI, T., ROBINS, H. & KUSUNOKI, Y. 2017. Aging-related changes in human T-cell repertoire over 20years delineated by deep sequencing of peripheral T-cell receptors. *Exp Gerontol,* 96**,** 29-37.

YU, F., HAO, Y., ZHAO, H., XIAO, J., HAN, N., ZHANG, Y., DAI, G., CHONG, X., ZENG, H. & ZHANG, F. 2017. Distinct Mitochondrial Disturbance in CD4+T and CD8+T Cells From HIV-Infected Patients. *J Acquir Immune Defic Syndr,* 74**,** 206-212.

YU, M., LI, G., LEE, W.-W., YUAN, M., CUI, D., WEYAND, C. M. & GORONZY, J. J. 2012. Signal inhibition by the dual-specific phosphatase 4 impairs T cell-dependent B-cell responses with age. *Proceedings of the National Academy of Sciences of the United States of America,* 109**,** E879-E888.

ZACCAGNINO, P., SALTARELLA, M., MAIORANO, S., GABALLO, A., SANTORO, G., NICO, B., LORUSSO, M. & DEL PRETE, A. 2012. An active mitochondrial biogenesis occurs during dendritic cell differentiation. *The international journal of biochemistry & cell biology,* 44**,** 1962-1969.

ZAMZAMI, N., MARCHETTI, P., CASTEDO, M., ZANIN, C., VAYSSIÈRE, J. L., PETIT, P. X. & KROEMER, G. 1995. Reduction in mitochondrial potential constitutes an early irreversible step of programmed lymphocyte death in vivo. *The Journal of Experimental Medicine,* 181**,** 1661.

ZANINOTTO, P., FALASCHETTI, E. & SACKER, A. 2009. Age trajectories of quality of life among older adults: results from the English Longitudinal Study of Ageing. *Quality of Life Research,* 18**,** 1301-1309.

ZHANG, B., ASADI, S., WENG, Z., SISMANOPOULOS, N. & THEOHARIDES, T. C. 2012. Stimulated Human Mast Cells Secrete Mitochondrial Components That Have Autocrine and Paracrine Inflammatory Actions. *PLOS ONE,* 7**,** e49767.

ZHANG, C. & CUERVO, A. M. 2008. Restoration of chaperone-mediated autophagy in aging liver improves cellular maintenance and hepatic function. *Nat Med,* 14**,** 959-65.

ZHAO, L., ZOU, X., FENG, Z., LUO, C., LIU, J., LI, H., CHANG, L., WANG, H., LI, Y., LONG, J., GAO, F. & LIU, J. 2014. Evidence for association of mitochondrial metabolism alteration with lipid accumulation in aging rats. *Experimental Gerontology,* 56**,** 3-12.

ZHAO, R. Z., JIANG, S., ZHANG, L. & YU, Z. B. 2019. Mitochondrial electron transport chain, ROS generation and uncoupling. *International journal of molecular medicine,* 44**,** 3-15.

ZHARHARY, D. 1988. Age-related changes in the capability of the bone marrow to generate B cells. *J Immunol,* 141**,** 1863-9.

ZHOU, R., YAZDI, A. S., MENU, P. & TSCHOPP, J. 2011. A role for mitochondria in NLRP3 inflammasome activation. *Nature,* 469**,** 221-5.

ZIGMOND, E., VAROL, C., FARACHE, J., ELMALIAH, E., SATPATHY, A. T., FRIEDLANDER, G., MACK, M., SHPIGEL, N., BONECA, I. G., MURPHY, K. M., SHAKHAR, G., HALPERN, Z. & JUNG, S. 2012. Ly6C hi monocytes in the inflamed colon give rise to proinflammatory effector cells and migratory antigen-presenting cells. *Immunity,* 37**,** 1076-90.

ZOROV, D. B., FILBURN, C. R., KLOTZ, L.-O., ZWEIER, J. L. & SOLLOTT, S. J. 2000. Reactive Oxygen Species (Ros-Induced) Ros Release. *A New Phenomenon Accompanying Induction of the Mitochondrial Permeability Transition in Cardiac Myocytes,* 192**,** 1001-1014.